Mines and Minerals Division

Ontario Geological Survey
Miscellaneous Paper 136

Geoscience Research Grant Program
Summary of Research 1986-1987

edited by
V.G. Milne

1987

Ontario
Ministry of
Northern Development
and Mines
Sean Conway, Minister of Mines

©Queen's Printer for Ontario, 1987
ISSN 0704-2752
Printed in Ontario, Canada
ISSN 0225-5316(Sub-series)

Publications of the Ontario Geological Survey, Ministry of Northern Development and Mines, are available from the following sources. Orders for publications should be accompanied by cheque or money order payable to the *Treasurer of Ontario.*

Reports, maps, and price lists (personal shopping or mail order):

Public Information Centre, Ministry of Natural Resources
Room 1640, Whitney Block, Queen's Park
Toronto, Ontario M7A 1W3

Reports and accompanying maps only (personal shopping):

Ontario Government Bookstore
Main Floor, 880 Bay Street
Toronto, Ontario M7A 1N8

Reports and accompanying maps (mail order or telephone orders):

Publications Services Section, Ministry of Government Services
5th Floor, 880 Bay Street
Toronto, Ontario M7A 1N8
Telephone (local calls) 965-6015
Toll-free long distance 1-800-268-7540
Toll-free from Area Code 807 0-ZENITH-67200

Every possible effort is made to ensure the accuracy of the information contained in this report, but the Ministry of Northern Development and Mines does not assume any liability for errors that may occur. Source references are included in the report and users may wish to verify critical information.

Parts of this publication may be quoted if credit is given. It is recommended that reference be made in the following form:

Layer, Paul W., McMaster, N. Dawn, and York, Derek
1987: The Dating of Ontario's Gold Deposits; Grant 233, p.27-34 *in* Geoscience Research Grant Program, Summary of Research, 1986-1987, edited by V.G. Milne, Ontario Geological Survey, Miscellaneous Paper 136, 241p.

If you wish to reproduce any of the text, tables or illustrations in this report, please write for permission to the Director, Ontario Geological Survey, Ministry of Northern Development and Mines, 11th floor, 77 Grenville Street, Toronto, Ontario, M7A 1W4.

Scientific Editor: Guy Kendrick
1250-87-Lowe-Martin

Contents

Introductory Remarks, *V.G. Milne* 2

Grant 230 Petrologic, Chemical, Isotopic, and Economic-Potential Studies of the Nipissing Diabase, *P.C. Lightfoot, D. Conrod, A.J. Naldrett, and N.M. Evensen* 4

Grant 233 The Dating of Ontario's Gold Deposits, *Paul W. Layer, N. Dawn McMaster, and Derek York* 27

Grant 236 Au–Quartz Vein and Cu–Au–Ag–Mo–Anhydrite Mineralization, Hollinger–McIntyre Mines, Timmins, Ontario: $\delta^{13}C$ Values (McIntyre), Fluid Inclusion Gas Chemistry, Pressure (Depth) Estimation, and H_2O-CO_2 Phase Separation as a Precipitation and Dilation Mechanism, *E.T.C. Spooner, C.J. Bray, P.C. Wood, D.R. Burrows, and N.J. Callan* 35

Grant 249 Geochemical Studies of Formation Waters From Paleozoic Strata, Southwestern Ontario, *P. Dollar, S.K. Frape, R.H. McNutt, P. Fritz, and R.W. Macqueen* 57

Grant 262 Geology, Geochemistry, and Economic Significance of Carbonaceous Host Rocks in Gold Deposits of the Timmins Area, *Graham C. Wilson and John C. Rucklidge* 66

Grant 265 Bacteria as Nucleation Sites for Mineral Authigenesis, *F.G. Ferris, W.S Fyfe, and T.J. Beveridge* 77

Grant 266 Anomalous Carbonate Till, Hemlo and Geraldton Area, Ontario: Origin and Applications, *Stephen R. Hicock* 84

Grant 275 Deformation of the Sudbury Structure and its Footwall, *W.S. Shanks and W.M. Schwerdtner* 92

Grant 276 Platinum Group Element Abundances in Mafic and Ultramafic Rocks: Preliminary Geochemical Studies at the Lac des Iles Complex, District of Thunder Bay, *A.J. Naldrett and G.E. Brügmann* 96

Grant 280 Lead Isotope Study of Gold Mineralization in the Dome Mine Quartz–Fuchsite Vein, *R.P. Moritz, J.H. Crocket, and A.P. Dickin* 115

Grant 284 Paleomagnetism and Rock Magnetism of the Mulcahy Lake Gabbro and the Lac des Iles Complex, *H.C. Palmer* 126

Grant 286 The Geochemistry, Origin, and Economic Potential of Platinum Group Element Bearing Rocks of the Lac des Iles Complex, Northwestern Ontario, *J.M. Sweeny and A.D. Edgar* 140

Grant 288 Gneissose Trondhjemite/Tonalite Hosted Au-Quartz Vein Mineralization, Renabie Mine Area, Wawa: Geological Characteristics and Shear Zone Control, *N.J. Callan and E.T.C. Spooner* 153

Grant 290 Improved Computer Interpretation of Gravity and Magnetic Data, *R.C. Bailey and S.W. Reford* 176

Grant 291 Remote Sensing and Geobotany as an Aid to Mineral Exploration in Northern Terrains, *A.E. Beswick, P.J. Beckett, G.M. Courtin, and G.O. Tapper* 183

Grant 294 Quaternary Geology and Geochemical Exploration in the Matheson Area, *M.B. McClenaghan, O.P. Lavin, I. Nichol, and J. Shaw* 200

Grant 298A The Geological Setting of Gold Deposits in the Porcupine Mining Camp, *R. Mason and D.I. Brisbin* 215

Grant 298B Geology of the North Zone of the Delnite Mine at Timmins, Ontario, *D.I. Brisbin, F. Speidel, and R. Mason* 224

Grant 300 The Genesis of Silver Vein Deposits in the Thunder Bay Area, Northwestern Ontario, *S.A. Kissin and E.A. Jennings* 230

CONVERSION FACTORS FOR MEASUREMENTS IN ONTARIO GEOLOGICAL SURVEY PUBLICATIONS.

CONVERSION FROM SI TO IMPERIAL			CONVERSION FROM IMPERIAL TO SI		
SI Unit	*Multiplied by*	*Gives*	*Imperial Unit*	*Multiplied by*	*Gives*
			LENGTH		
1 mm	0.039 37	inches	1 inch	**25.4**	mm
1 cm	0.393 70	inches	1 inch	**2.54**	cm
1 m	3.280 84	feet	1 foot	**0.304 8**	m
1 m	0.049 709 7	chains	1 chain	20.116 8	m
1 km	0.621 371	miles (statute)	1 mile (statute)	**1.609 344**	km
			AREA		
1 cm^2	0.155 0	square inches	1 square inch	**6.451 6**	cm^2
1 m^2	10.763 9	square feet	1 square foot	**0.092 903 04**	m^2
1 km^2	0.386 10	square miles	1 square mile	2.589 988	km^2
1 ha	2.471 054	acres	1 acre	0.404 685 6	ha
			VOLUME		
1 cm^3	0.061 02	cubic inches	1 cubic inch	**16.387 064**	cm^3
1 m^3	35.314 7	cubic feet	1 cubic foot	0.028 316 85	m^3
1 m^3	1.308 0	cubic yards	1 cubic yard	0.764 555	m^3
			CAPACITY		
1 L	1.759 755	pints	1 pint	0.568 261	L
1 L	0.879 877	quarts	1 quart	1.136 522	L
1 L	0.219 969	gallons	1 gallon	**4.546 090**	L
			MASS		
1 g	0.035 273 96	ounces (avdp)	1 ounce (avdp)	28.349 523	g
1 g	0.032 150 75	ounces (troy)	1 ounce (troy)	**31.103 476 8**	g
1 kg	2.204 62	pounds (avdp)	1 pound (avdp)	**0.453 592 37**	kg
1 kg	0.001 102 3	tons (short)	1 ton (short)	**907.184 74**	kg
1 t	1.103 311	tons (short)	1 ton (short)	**0.907 184 74**	t
1 kg	0.000 984 21	tons (long)	1 ton (long)	**1016.046 908 8**	kg
1 t	0.984 206 5	tons (long)	1 ton (long)	**1.016 046 908 8**	t
			CONCENTRATION		
1 g/t	0.029 166 6	ounce (troy)/ ton (short)	1 ounce (troy)/ ton (short)	34.285 714 2	g/t
1 g/t	0.583 333 33	pennyweights/ ton (short)	1 pennyweight/ ton (short)	1.714 285 7	g/t

OTHER USEFUL CONVERSION FACTORS

1 ounce (troy) per ton (short)	20.0	pennyweights per ton (short)
1 pennyweight perton (short)	0.05	ounces (troy) per ton (short)

Note. Conversion factors which are in bold type are exact. The conversion factors have been taken from or have been derived from factors given in the Metric Practice Guide for the Canadian Mining and Metallurgical Industries, published by the Mining Association of Canada in cooperation with the Coal Association of Canada.

Geoscience Research Grant Program
Summary of Research 1986-1987

---

edited by
V.G. Milne

Director, Ontario Geological Survey

INTRODUCTORY REMARKS

The Ontario Geoscience Research Grants Program was initiated in 1978 to encourage geoscience research at Ontario universities. By supporting mission-oriented geological projects, a program of research was established which would complement the work of the Ontario Geological Survey through its mandate:

> To stimulate exploration for, and facilitate sound planning in, all matters related to, mineral and other earth resources by providing an inventory and analysis of the geology and mineral deposits of Ontario.

The program supports applied studies of up to three years duration towards: mineral deposit characterization involving studies of specific occurrences or groups of occurrences within Ontario; petrology, rock geochemistry, structural geology, stratigraphy, and geochronology studies; field and laboratory studies leading to the development of new geophysical or geochemical concepts and techniques; engineering and environmental geology studies; and methods for improving automated or manual processing, and facilitating the interpretation of geoscience data.

In order to receive funding, applications must be forwarded to the Ontario Geological Survey prior to November 15. Project proposals are subject to review by a committee which reports to the Director of the Ontario Geological Survey. This committee advises the Minister of Northern Development and Mines concerning geoscience research priorities at Ontario universities and of the scientific merit and relevance of proposals submitted to the Ontario Geoscience Research Grants Program. The committee consists of four representatives of the mineral industry, four representatives of the university community, and four representatives of the Survey. Members of the 1986-87 committee include:

Dr. D.J. Misener, Chairman; Paterson, Grant and Watson Limited
Dr. A.E. Beswick; Laurentian University
Dr. G. Cargill; Utah Mines Ltd.
Dr. M.E. Cherry; Ontario Geological Survey
Dr. W. Coker; Kidd Creek Mines Limited
Dr. J.A. Donaldson; Carleton University
Dr. V.K. Gupta; Ontario Geological Survey
Dr. C.J. Hodgson; Queen's University
Dr. R. Mitchell; Lakehead University
Mr. E.V. Sado; Ontario Geological Survey
Mr. J. Stewart; Selco Division BP-Resources Canada Limited
Mr. H. Wallace; Ontario Geological Survey

Successful grant recipients are expected to submit reports for publication in the annual Summary of Research and participate in the OGS Geoscience Research Seminar held annually in December.

Publication in other scientific journals is encouraged and a final report summarizing the research will be released as an Ontario Geological Survey Open File Report. Open File Reports concerning the Ontario Geoscience Research Grant Program are released from time to time and are available at the Mines Library, 77 Grenville Street, Toronto, or at Ministry of Northern Development and Mines regional offices. The following research projects partially or wholly funded by this Program during 1986-87 are due for release as Open File Reports (only principal applicant's name listed):

Grant 216: Sedimentology of the Long Rapids Formation; M.J. Risk, McMaster University.

Grant 225: Genesis of Pegmatites in the Quetico Gneiss Belt of Northwestern Ontario; S.A. Kissin, Lakehead University.

Grant 227: The Structural and Lithological Environment of the Kirkland - Larder Lakes; C.J. Hodgson, Queen's University.

Grant 230: Petrologic, Chemical, Isotopic and Economic Potential Studies of the Nipissing Diabase; A.J. Naldrett, University of Toronto.

Grant 233: Dating of Ontario's Gold Deposits; D. York, University of Toronto.

Grant 236: Quartz Vein Related Au (-W; scheelite) and Monzonite-hosted Cu-Au Mineralization, Hollinger (Timmins) and McIntyre (Schumacher) Mines; E.T.C. Spooner, University of Toronto.

Grant 242: Structural Studies of Shear Zones in the Quetico and Wabigoon Subprovinces; H.R. Williams, Brock University.

Grant 254: Exploration for Buried Granular Aggregates by Remote Sensing Techniques; M.B. Dusseault, University of Waterloo.

Grant 262: The Role of Carbonaceaus Materials in Precious Metal Deposits; J.C. Rucklidge, University of Toronto.

Grant 266: Anomalous Carbonate Till, Hemlo Area, Ontario: Origin and Applications; S.R. Hicock, University of Western Ontario.

Grant 276: PGE Studies of Mafic and Ultramafic Rocks; A.J. Naldrett, University of Toronto.

Grant 284: Paleomagnetism and Rock Magnetism of the Mulcahy Lake and Lac des Iles Gabbros; H.C. Palmer, University of Western Ontario.

During 1986-87, 24 projects were funded under the program. Of these, 12 were renewal projects:

University	**Value of Grants**	**No. of Grants**
Brock	$ 19,990	1
Lakehead	21,925	2
Laurentian	23,150	1
McMaster	13,000	2
Queen's	96,283	4
Toronto	178,824	8
Waterloo	60,166*	2
Western	86,662	4
TOTAL	$500,000	24

*A grant of $22,816 to the University of Waterloo involved staff from McMaster University.

The undersigned would like to thank Dr. D.J. Misener, who acted as Committee Chairman, and the Review Committee Members who gave freely of their time. The efforts of the researchers are of course fundamental and are acknowledged. Mr. R.B. Watson, who served as Grants Administrator and Secretary to the Committee, and Mr. Guy Kendrick, who acted as scientific editor for this publication, also deserve thanks.

V.G. Milne

Director

Ontario Geological Survey

Grant 230 Petrologic, Chemical, Isotopic, and Economic-Potential Studies of the Nipissing Diabase

P.C. Lightfoot, D. Conrod, A.J. Naldrett, and N.M. Evensen

Department of Geology, University of Toronto, Toronto

ABSTRACT

The Nipissing Diabase consists of a suite of tholeiitic rocks and associated differentiated rocks that extends from Cobalt to Sault Ste. Marie, Ontario, in the form of undulating sills, cone sheets, and dikes. It represents a major intrusive event at around 2220 Ma which most likely forms the intrusive part of an eroded Continental Flood Basalt (CFB), where the magmas rose as dikes which cut the Archean granitoid rocks, and spread out laterally within the metasediments of the Huronian basin.

Mafic intrusions associated with CFBs and rifting environments often contain significant concentrations of magmatic sulphide minerals rich in Ni, Cu, Co, and platinum group elements (PGE). The possibility that contamination of mafic magmas by silica-rich crustal material may have triggered sulphide segregation, as at Sudbury, has been investigated using combined petrographic, mineralogical, and geochemical techniques.

Geochemical data are presented in this paper which suggest that the chilled margins of the intrusions are equivalent in composition to the parental magma. Tight curved trends on chemical-variation diagrams show strong enrichment in the large large-ion lithophile elements (LIL) with respect to Zr content, and depletion in the hygromagmatophile elements (HYG) relative to Zr. The trends of compatible and incompatible trace elements are consistent with the petrographic evidence for a component of fractional crystallization of plagioclase, orthopyroxene, clinopyroxene, and olivine, even though this phase extract does not entirely explain the strong enrichment in LIL and depletion in HYG elements. Interelement-ratio variations, such as Th/Yb versus La/Yb, define trends which pass through the average chilled margin and the average Huronian hanging-wall metasediment compositions. It is suggested that this reflects contamination of a homogenous, trace-element-enriched, mantle-derived magma (with epsilon-Nd at 2.2 Ga ranging from -2 to -5) by Huronian metasediments which have higher LIL/Zr and lower HYG/Zr than the Nipissing Diabase and epsilon-Nd at 2.2 Ga ranging from -5 to -6. Contamination appears to be dominant in the arch zones of the intrusions close to the roof. Fractionation and assimilation (AFC) appear to be at least partially coupled in the diabases and granophyres. The aplites appear to have originated from wide-scale melting of the Huronian sediments. Observations, made by other workers, that double-diffusive interfaces within the magma column may effectively hinder chemical transfer whilst allowing heat transfer may be consistent with the petrogenesis of the aplites, which appear not to have mixed to any significant extent with the Nipissing magma.

Total PGE abundances appear to be low (<50 ppb total PGE) in diabase samples. Olivines are undepleted in nickel compared to olivines with similar forsterite contents from other intrusions. Geochemical parameters suggest that contamination by country rock with a high silica content occurred in the arch zones close to the roof of the intrusions, and is most clearly developed in the evolved, varied-textured diabases and granophyres. Early pyroxene and olivine fractionation is likely to have depleted the magma in nickel, whilst the remaining liquid became broadly enriched in Cu.

Assimilation and fractionation appears to be superimposed on a magma with broadly similar geochemical fingerprints to the Sudbury Igneous Complex. The origin of the regionally uniform parent magma (as defined by chilled-margin samples) appears to rest in a homogenous, subcontinental mantle which has either undergone trace-element enrichment, or has interacted with a recycled, Archean, crustal component.

In-situ contamination is unlikely to have promoted significant amounts of sulphide segregation. The uniform composition of the parental magma suggests that limited contamination occurred en route through the crust. This in turn suggests that magmatic sulphide segregation triggered by contamination in the crust is unlikely.

INTRODUCTION

This research project is primarily concerned with the problem of understanding the petrology and geochemistry of the Nipissing Diabase, and assessing the potential of the diabase as a host to sulphide minerals enriched in Ni, Cu, and Platinum Group Elements (PGE). To study this problem, trace element and Sm- Nd isotopic analyses combined with PGE studies have been employed in conjunction with field and petrographic observations, and studies of mineral chemistry.

Mafic intrusions associated with intraplate volcanism and rifting environments often contain significant concentrations of magmatic sulphide minerals rich in Ni-Cu-Co and PGE; examples include the Triassic-aged intrusions hosting the Noril'sk Deposit which feeds the Siberian flood basalts, and the Duluth Complex in Minnesota, which feeds the Keweenawan basalts. The Insizwa Complex, in Transkei, South Africa, which presumably represents the intrusive equivalent of the Lesotho volcanic edifice, also shows the development of a small amount of basal magmatic sulphide mineralization. In the case of the Duluth Complex, external sulphur appears to have been assimilated by the magma, enriched in Ni, Cu, and PGE from the magma, and segregated as a magmatic sulphide. At Sudbury, sulphur segregation appears to have been triggered by the incorporation of external silica.

The 2.2 Ga Nipissing Diabase outcrops over a wide tract of Central Ontario between Sault Ste. Marie in the west and Cobalt in the east. The close similarity of the Nipissing Diabase to other intrusive bodies

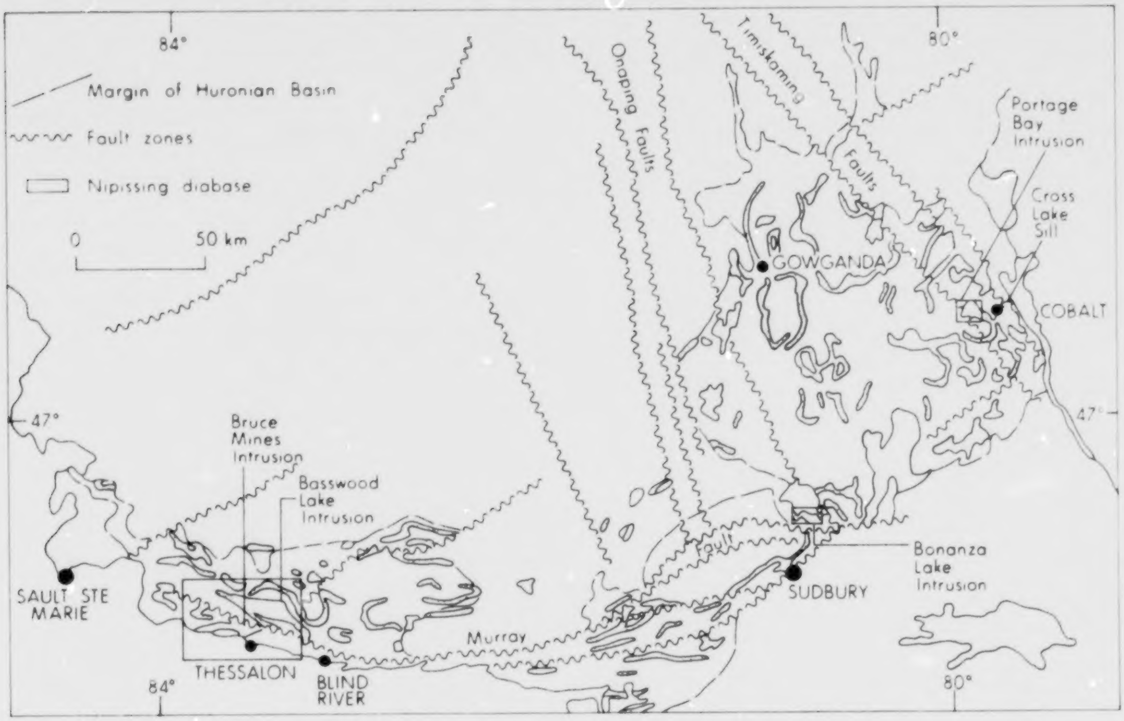

Figure 230.1a. *Location of the Nipissing Diabase.*

associated with continental flood basalts (CFB), and which host important magmatic sulphide mineralization, prompted the authors to undertake a detailed examination of several Nipissing Intrusions.

The emplacement of the Nipissing magma postdates both a major phase of folding (N- S axis) of the Huronian Supergroup, and the folding and faulting event (E- W axis) culminating in the Penokean Orogeny (Finn *et al.* 1982; Church 1966). The Nipissing Diabase outcrops largely within the Huronian metasedimentary basin as large, arcuate sheets derived by the erosion of undulating intrusions. This type of surface exposure is characteristic of many intrusive portions of CFB.

The diabase is generally in contact with Huronian metasediments, although some bodies cut the Archean basement. The contact of the diabase follows either the bedding planes or the Archean-Huronian unconformity in places, but also frequently cuts through the Huronian stratigraphy.

The sills are undulatory in nature with basinal zones occurring where the intrusions are thickest, and arch zones occurring where the intrusions are substantially thinner.

The diabase has been subdivided into a number of phases (Hriskevich 1968; Jambor 1971), the distribution of which is generally related to the configuration of the intrusion; basins contain a greater proportion of basic rocks, whereas arches have a higher proportion of silicic rocks. Whilst the lithologies tend to be ubiquitous to many of the intrusions, not all intrusions develop all the phases of the diabase (Hriskevich 1968). Generally speaking, a marginal layer of quartz diabase which shows chilling at the contact, is found at the base of the intrusions and the margins of dikes. This grades upwards, in the sills, through a thick zone of hypersthene diabase and gabbro. Overlying this is a transition zone into varied-textured diabase which consists of irregular schlieren, patches, and dikes of pegmatitic diabase in normal hypersthene diabase and gabbro. Granophyric diabase and aplitic dikes may occur within the varied-textured diabase, but generally, the varied-textured diabase grades into granophyric diabase, pegmatoidal diabase, granophyres, and aplites close to the roof of the intrusions in the arch regions. To place these rocks in the perspective of the intrusions as a whole, they constitute less than 5 percent of the exposed diabase. The dikes tend to grade from quartz diabase at the margins into varied-textured diabase and gabbro norites at the core.

Five intrusions from throughout the Nipissing Diabase Province (Figure 230.1a) have been studied: the Bruce Mines and Basswood Lake Intrusions in the western sector (Figures 230.1b and 230.1c), the Bonanza Lake Intrusion from the Wanapitei Lake district (*see* Lightfoot *et al.* 1986; Conrod in preparation), and the Portage Bay and Cross Lake Intrusions from the eastern part of the Province (*see* Lightfoot *et al.* 1986; Conrod in preparation).

Field, petrographic, and mineralogical studies have been reported elsewhere (Lightfoot *et al.* 1986). This report first summarizes the main conclusions from the earlier work, and then discusses major- and

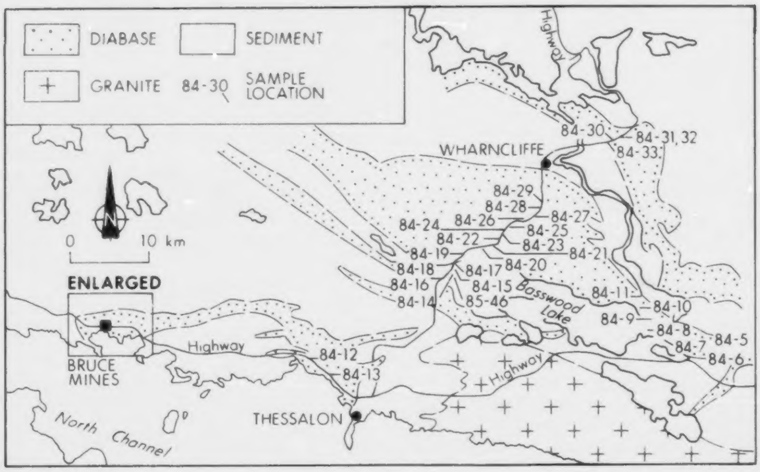

Figure 230.1b. *Location of the Basswood Lake and Bruce Mines Intrusions.*

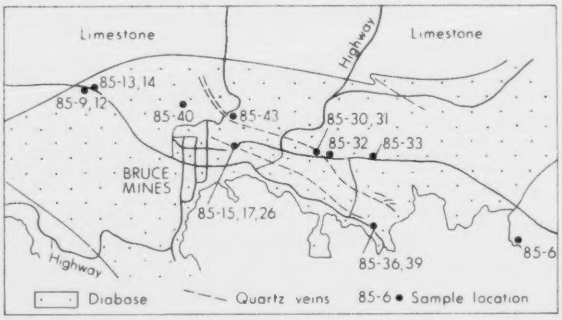

Figure 230.1c. *Detailed map of the Bruce Mines Intrusion.*

trace-element variations, Sm-Nd isotope studies, and PGE studies in the light of these observations.

GENERAL GEOLOGY, PETROGRAPHY, MINERALOGY, AND MINERAL CHEMISTRY

A general summary depicting the vertical and lateral distribution of the lithologies (after Hriskevich 1968) is shown in Figure 230.2a. Figure 230.2b shows detailed petrographic variations through the intrusions. Mapping and petrologic studies indicate that the Cross Lake, Bonanza Lake, Basswood Lake, and Bruce Mines Intrusions are all thick (up to 2 km in thickness), sill-like bodies, characterized by basal and capping quartz diabases in which plagioclase, augite, and inverted pigeonite are intergrown in a diabasic texture; a thick hypersthene gabbro and gabbro norite zone, in which hypersthene largely replaces inverted pigeonite, is present above the basal quartz diabase; a zone of varied-textured diabase containing pods of pegmatoidal gabbro is developed in the upper part of the intrusions; in the arch regions of the intrusions, the quartz diabase capping is not developed, but granophyres, pegmatoidal granites, and aplites are found. Petrographically, the transition from varied-textured diabase to granophyre is reflected in the increasing proportions of quartz and alkali-feldspar which are myrmekitically intergrown, and the replacement of pyroxene by hornblende. The Portage Bay Intrusion is dike-like in configuration and appears to be characterized by a core of varied-textured diabase and gabbro norite, and lacks hypersthene diabase. Similar lithological distributions have been described in Nipissing dikes from the Lake Temagami District (Lightfoot and Naldrett 1987).

Mineral-chemistry studies (Lightfoot *et al.* 1986; Conrod in preparation) reveal the following:

1. an increase of the anorthite (An) content in plagioclase through the Bonanza Lake and Cross Lake sills from the lower contact into the hypersthene diabase, followed by a decrease of the anorthite content towards the top of the intrusions
2. an apparent increase of the forsterite (Fo) content in olivine and of the Mg-number in orthopyroxene at the Cross Lake Sill away from the lower contact, followed by a decrease of the Mg-number in bronzite and Fo content in olivine towards the roof
3. an increase of the Ni-content in olivine at the Cross Lake Sill away from the lower contact, followed by a slight decrease at the sill's centre before olivine is wholly replaced

The upward tendency towards higher An contents in plagioclase, higher Fo contents in olivine, and higher Mg-numbers in orthopyroxene, followed by the reversal towards lower anorthite contents in plagioclase, Fo contents in olivine, and Mg-numbers in orthopyroxenes has been documented in other Nipissing intrusions (Finn *et al.* 1982), and within many layered intrusions and sills (for example , Lightfoot and Naldrett 1984, 1987). Various models have been proposed to explain this variation (e.g. Wilson and Engell-Sorensen 1986), and are discussed elsewhere (e.g. Conrod, in preparation).

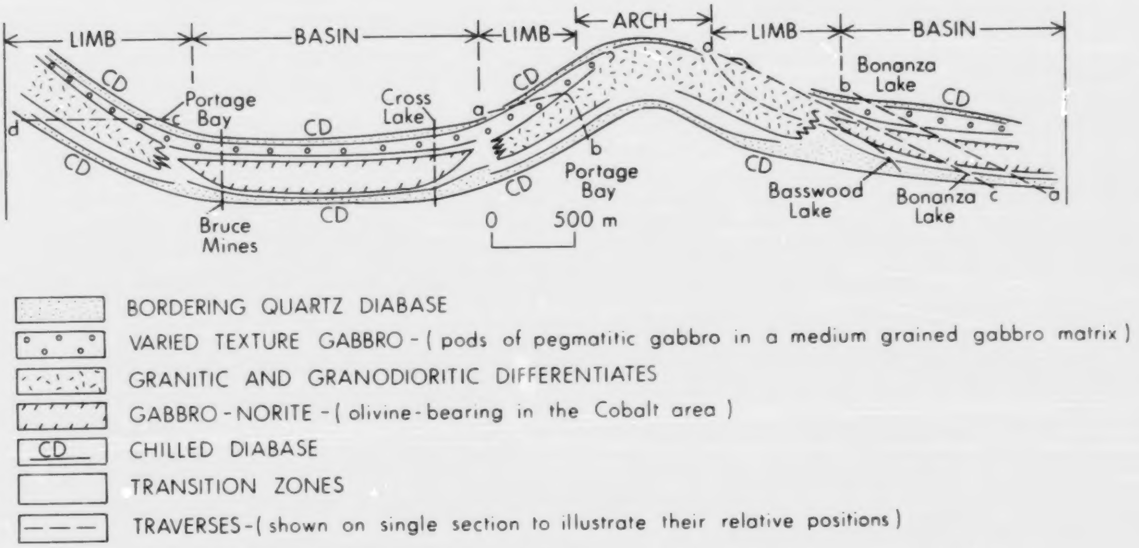
LIMB
BASIN
LIMB
ARCH
LIMB
BASIN
CD
Portage Bay
Cross Lake
Bonanza Lake
Portage Bay
Basswood Lake
Bonanza Lake
Bruce Mines
a
b
c
d
0
500 m
BORDERING QUARTZ DIABASE
VARIED TEXTURE GABBRO - (pods of pegmatitic gabbro in a medium grained gabbro matrix)
GRANITIC AND GRANODIORITIC DIFFERENTIATES
GABBRO - NORITE - (olivine - bearing in the Cobalt area)
CD CHILLED DIABASE
TRANSITION ZONES
TRAVERSES - (shown on single section to illustrate their relative positions)

Figure 230.2a. *Generalized hypothetical section through a typical Nipissing Intrusion, showing the distribution of the phases, and relative positions of the sample profiles.*

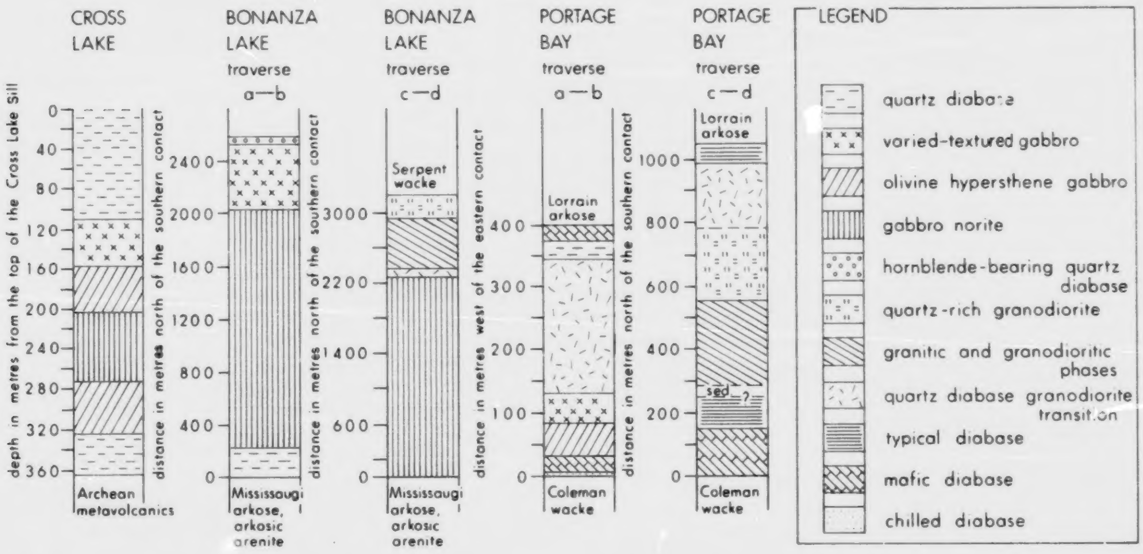
CROSS LAKE
BONANZA LAKE traverse a—b
BONANZA LAKE traverse c—d
PORTAGE BAY traverse a—b
PORTAGE BAY traverse c—d
depth in metres from the top of the Cross Lake Sill
distance in metres north of the southern contact
distance in metres north of the southern contact
distance in metres west of the eastern contact
distance in metres north of the southern contact
Archean metavolcanics
Mississaugi arkose, arkosic arenite
Serpent wacke
Mississaugi arkose, arkosic arenite
Lorrain arkose
Coleman wacke
Lorrain arkose
sed ?
Coleman wacke
LEGEND
quartz diabase
varied-textured gabbro
olivine hypersthene gabbro
gabbro norite
hornblende-bearing quartz diabase
quartz-rich granodiorite
granitic and granodioritic phases
quartz diabase granodiorite transition
typical diabase
mafic diabase
chilled diabase

Figure 230.2b. *Detailed petrographic sections through the intrusions.*

GEOCHEMICAL STUDIES

SAMPLE PREPARATION AND ANALYTICAL TECHNIQUES

Samples weighing in excess of 1 kg and being free of weathered surfaces were collected from five intrusions (Figure 230.1) and prepared using a steel-jaw crusher and an agate tema.

Whole-rock major and trace elements were determined on glass beads and pressed powder pellets by conventional X-ray flourescence (XRF) techniques. Results for UTB1 (University of Toronto in-house standard) are given in Table 230.1. Selected trace elements including Sc, Co, Th, Ta, Hf, U, and the Rare Earth Elements (REE) were determined on rock powders by instrumental neutron-activation analysis using both the SLOWPOKE reactor and counting facilities at the University of Toronto. Results for UTB1 and WHIN SILL (Open University irradiation standard) are presented in Table 230.1. Complete data for the major and trace elements are given elsewhere (Conrod, in preparation).

TABLE 230.1. ANALYTICAL DATA FOR ROCK STANDARDS DETERMINED DURING THE COURSE OF THIS STUDY.

Element	Mean UTB1	One standard deviation		Mean WHIN SILL	One standard deviation	
SiO_2	50.4	0.3	(50.5)			
TiO_2	3.06	0.06	(3.11)			
Al_2O_3	14.6	0.3	(13.2)			
Fe_2O_3	14.9	0.3	(15.2)			
MnO	0.22	0.00	(0.22)			
MgO	3.6	0.2	(4.39)			
CaO	8.6	0.2	(8.46)			
Na_2O	2.9	0.2	(2.47)			
K_2O	1.17	0.05	(1.33)			
P_2O_5	0.51	0.03	(0.65)			
Zr	205	2	(202)			
Y	46.4	1	(41)			
Nb	16.3	1.2				
Rb	35.2	1.6	(32)			
Sr	313	3	(312)			
Ba	593	49		419	48	
Th	4.21	0.06	(4.3)	2.75	0.26	(3.1)
Ta	0.96	0.06	(1.02)	1.6	0.9	(1.26)
Hf	5.06	0.96	(4.6)	4.92	0.48	(4.9)
U	1.02	0.18	(1.0)	0.45	0.14	(0.90)
La	26.4	1.6	(26.7)	24.7	0.5	(22.5)
Ce	62.1	2.8	(60.5)	60.4	3.8	(57.5)
Nd	33.6	2.0	(32.0)	28.4	5.2	(32.9)
Sm	7.98	0.18	(8.0)	7.02	0.26	(7.3)
Eu	2.30	0.22	(2.4)	2.04	0.10	(2.3)
Yb	4.05	0.42	(4.0)	2.51	0.14	(2.54)
Lu	0.64	0.06	(0.58)	0.35	0.02	(0.39)
Cr	123	46				
Ni	20	8	(25)			
Co	49.3	2.0		48.3	2.0	
Cu	30	6	(31)			
V	367	82				
Sc	40.0	1.3		30.4	0.8	

Footnotes

1. Oxides are in weight percent, elements are in ppm.
2. XRF data are presented, except where analyses for both UTB1 and WHIN SILL are shown - these are INAA data.
3. XRF (Mean UTB1) — major elements n = 2
   — minor elements n = 5

   INAA — $n_{UTB1} = 4$ $n_{WS} = 4$

   () Expected values for UTB1 and WHIN SILL (from Lightfoot 1985).

The platinum group elements were determined by a fire-assay and neutron-activation procedures (Hoffman *et al.* 1978).

Sm-Nd isotope data were determined by conventional chemical separation procedures in the University of Toronto's Sm-Nd isotope laboratory (Zindler 1980), and run, using a novel mass-spectrometric techique (Evensen and Turner, in preparation; Noble *et al.* in preparation; Lightfoot and Naldrett 1987), on a VG354 thermal-ionization mass spectrometer in the Jack Satterly Geochronology Laboratory at the Royal Ontario Museum. La Jolla gave 0.511863±13, and BCR1 gave 0.512605±7, normalized to $^{146}Nd/^{144}Nd = 0.7219$. Blanks for Sm and Nd are 1 ng or better.

BULK ROCK COMPOSITION

Major-element data obtained in this study reveal features similar to those documented by Finn *et al.* (1982) in the intrusion at Wanapitei Lake. A moderate iron-enrichment trend is observed, with a few of the samples from the arch zones falling within the calc-alkalic field of the AFM diagram.

Trace elements provide information of more intrinsic petrogenetic significance. To ensure that these results are free of the influence of weathering and alteration, fresh samples were used. Although all samples invariably showed some sign of low-grade metamorphism, this appears not to have influenced the majority of the elements. The exceptions are Rb and Sr which are extremely variable when compared to the tight variations defined by the rest of the trace elements (Lightfoot *et al.* 1986).

Trace-element variations may also be obscured by either local enrichment or depletion events occurring within the intrusions during or after cooling. This was investigated by Lightfoot and Naldrett (1987) in samples of diabase and varied-textured diabase from two outcrops where the distinct textural varieties were developed on the scale of from 50 cm to 3 m. The results suggested that the coarser diabase was enriched in the spectrum of incompatible elements when compared to the finer-grained diabase. Furthermore, Nd-isotopic data and Sm/Nd ratios were identical for both samples (see later). This suggested that pegmatoidal pods may have acted as traps for incompatible elements during the cooling and crystallization of the magma. Analogous depletion may be expected in cumulates as the trapped liquid is expelled into the overlying magma column; however, this process is also not well understood and is the subject of continuing work.

VARIATIONS WITHIN THE SILLS

Geochemical variations have been documented through the sills in a previous report (Lightfoot *et al.* 1986). Summarizing these findings, there appears to be a general depletion in the incompatible element concentrations away from the lower contact which is coupled with an increase in the Mg-number and the Ni and Cr content. Above the lower part of the hypersthene-diabase zone, there is an increase in incompatible-element concentration coupled with a decrease in the Mg-number and the Ni and Cr content. In the Portage Bay dike, trace-element enrichment occurs inwards away from the margins, and is coupled to a decrease in the Mg-number and the Ni and Cr contents. These variations appear to couple with the variations in mineral chemistry summarized earlier (i.e. the inflections in the mineral-chemistry trends occur at the same vertical levels in the sills as the major and trace-element inflections).

COMPOSITION OF THE PARENT MAGMA

Whether or not chilled margins are useful in the identification of parental magmas has been the subject of considerable speculation and debate (Wager and Brown 1968). More recently, geochemical techniques have been used in developing criteria by which parental magmas may be recognised (e.g. Lightfoot and Naldrett 1984). However, these criteria suggest that chilled-margin data should be treated with caution when they show signs of contamination by crustal material. The Nipissing Diabase chilled margins appear to be free of crustal material. A single sample from the Portage Bay Intrusion, and five samples from Lightfoot and Naldrett (1987) are analytically indistinguishable from each other (Table 230.2), with the exception of a slightly lower MgO content in the Portage Bay sample. The fact that two of these samples come from within a single intrusion, combined with the fact that the rest come from other intrusions covering a large area of the Nipissing Diabase Province, lends considerable support to the argument that they are indeed representative of the parent magma at the time of emplacement. Furthermore, this observation suggests that the magma was remarkably uniform in composition not only within each intrusion, but also between different intrusions, and may constitute a representative sample of the magma type of the Nipissing Diabase Province as a whole.

COMPOSITIONAL VARIATION IN THE HURONIAN METASEDIMENTS

Samples of Huronian metasediment from the footwalls and hanging walls of a number of intrusions were collected and analyzed. Representative data, together with an average, are given in Table 230.3.

TRACE-ELEMENT VARIATION DIAGRAMS

Representative samples from the Basswood Lake Intrusion are shown on MORB- (mid-ocean-ridge-basalt) and chondrite-normalized variation diagrams in Figure 230.3. Also documented in Figure 230.3 are the compositions of average chilled-margin samples, average footwall and hanging wall Huronian metasediment (Table 230.3), and average aplite from the roof regions of two intrusions from the eastern sector of the Province (Lightfoot and Naldrett 1987). A progressive depletion from the chill through the basal quartz diabase into the hypersthene diabase is confirmed for most of the incompatible elements (e.g sample numbers 84/15 and 84/20, Figure 230.3). Above this level, there is an overall enrichment in the incompatible elements (sample numbers 84/20 up to 84/27, Figure 230.3). The chilled-margin average is incompatible-element enriched relative to samples 84/15 and 84/20. The average Huronian metasediment is incompatible-element enriched compared to all of the samples, and overlaps with the average aplite (with the exception of TiO_2).

Figure 230.3 reveals the following additional points:

1. There is an overall enrichment in the large-ion lithophile (LIL) elements relative to the hygromagmatophile (HYG) elements. This is reflected in the steep chondrite-normalized plots and the high Th, K_2O, and Ba abundances relative to Zr, Y, and Yb on the MORB-normalized variation diagram.
2. The LIL/HYG-element ratio increases from the hypersthene diabases through the varied-textured diabase into the granophyres.
3. The patterns of the Huronian metasediment and aplite samples have higher LIL/HYG ratios than any of the Nipissing samples.
4. The Eu anomaly becomes progressively deeper as the incompatible-element abundances increase.

TABLE 230.2. COMPOSITIONAL DATA FOR CHILLED MARGIN SAMPLES.

Sample	86/148	86/141	86/136	86/100F	86/79	PB951	Mean (1-5)	One s.d.
	Lake Temagami					Portage Bay		
Mg*	0.66	0.68	0.64	0.70	0.60	0.58	0.65	0.04
SiO_2	53.0	49.8	53.1	50.8	50.6	52.4	51.5	1.7
TiO_2	0.61	0.63	0.72	0.55	0.66	0.78	0.63	0.06
Al_2O_3	13.0	11.9	12.2	13.4	13.0	14.3	12.7	0.6
Fe_2O_3	11.8	13.5	12.9	10.6	12.3	11.9	12.2	1.0
MgO	9.8	12.2	10.0	10.4	10.3	7.1	10.5	0.9
MnO	0.2	0.2	0.2	0.2	0.2	0.2	0.2	0.02
CaO	10.2	10.2	9.3	10.6	9.7	10.5	10.1	0.5
Na_2O	1.13	1.22	1.30	2.70	2.61	2.07	2.4	0.8
K_2O	0.18	0.34	n.a.	0.67	0.93	0.78	0.43	0.34
P_2O_5	0.03	0.08	0.10	0.11	0.11	0.07	0.09	0.03
Rb	10	17	3	25	49	23	21	18
Sr	200	129	242	197	199	166	193	41
Ba	11	76	45	113	199	120	88	72
Y	17	16	17	15	18	16	17	1
Zr	61	60	70	51	66	60	62	7
Nb	4	5	4	5	5	6	5	1
Th	1.5	1.2	1.5	1.2	1.4	1.6	1.4	0.2
Ta	0.1	0.2	0.2	0.2	0.2	0.3	0.2	0.1
Hf	1.2	1.2	2.0	1.3	1.2	1.2	1.4	0.3
U	0.57	0.33	0.49	0.32	0.37	0.50	0.39	0.03
La	5.4	4.6	5.8	5.2	5.4	5.6	5.3	0.4
Ce	11.9	10.6	12.2	12.2	12.5	13.4	11.8	0.8
Nd	6.8	6.2	6.1	6.9	5.9	7.3	6.4	0.5
Sm	1.8	2.0	2.3	2.1	2.2	2.2	2.1	0.2
Eu	0.55	0.58	0.67	0.69	0.67	0.75	0.63	0.06
Yb	1.58	1.30	1.55	1.33	1.47	1.42	1.45	0.12
Lu	0.25	0.19	0.27	0.21	0.24	0.23	0.23	0.03
Ni	138	n.a.	151	110	152	110	138	19
Cr	257	257	232	259	191	350	239	29
Cu	91	101	114	78	108	n.a.	98	14
Co	46	64	51	42	50	45	51	8
V	181	180	241	222	241	240	213	31
Sc	41	39	41	40	38	38	39	1

Mg* - Mg-number
n.a. - not available, s.d. - standard deviation

ELEMENT-Zr VARIATIONS

Geochemical variations within and between intrusions are best documented with reference to an index of enrichment or depletion having the following characteristics: it is readily determined with analytical accuracy and precision, is not influenced by alteration or metamorphism, is incompatible in a crystallizing phase extract (Pearce and Norry 1979; Watson and Ryerson 1986), and it has not significantly contributed to the magma during assimilation of crustal material. Zr has been chosen in preference to La (Lightfoot *et al.* 1986), as it has now become clear that simple Rayleigh Fractionation mechanisms may not account for all the geochemical variations, and, given the high abundance of La in crustal rocks, it would more likely reflect the magma composition rather than the contaminant composition. Zircon fractionation appears to be unimportant, given the constant Hf/Zr ratio (see later) of the rocks (DZr>>>DHf - Fujimaki 1986), and the low Zr abundance (<300 ppm) which would effectively preclude zircon saturation under normal conditions (Watson and Harrison 1983).

Figure 230.4 shows the variation in Mg-number versus Zr, and Figures 230.5a and 230.5b show the variations in TiO_2, P_2O_5, Ni, Cr, Sc, Co, La, Sm, Yb, Y, Th, and Hf versus Zr content. The data from each intrusion have been superimposed on the plots. The following points are evident both for individual intrusions, and for the Nipissing Diabase Province as a whole:

1. Mg-number, Ni, and Cr fall with increasing Zr content, whilst Th, Hf, Y, La, Sm, P_2O_5 and Yb increase. TiO_2, Co, and Sc appear to show an initial increase followed by a decline with increasing Zr content. This is consistent with a combination of pyroxene and olivine fractionation.
2. The trajectories are generally very tight and apparently curved.

TABLE 230.3. COMPOSITIONAL DATA FOR HURONIAN SEDIMENTARY ROCKS FROM THE FOOTWALL AND HANGING WALL OF NIPISSING DIABASE INTRUSIONS.

Sample	PB737	PB763	86.203	86.197F	86.197C	Average	One s.d.
Mg*	0.44	0.51	0.43	0.48	0.48	0.47	0.03
SiO_2	59.7	63.9	58.4	59.7	60.8	60.5	2.1
TiO_2	0.71	0.66	0.76	0.70	0.74	0.71	0.04
Al_2O_3	18.7	17.1	17.5	20.7	20.4	18.8	1.6
Fe_2O_3	8.0	5.5	11.7	7.3	7.5	8.0	2.3
MgO	2.7	2.5	3.8	3.2	3.3	3.1	0.5
MnO	0.04	0.03	1.7	0.02	0.02	0.36	0.75
CaO	3.70	0.36	2.30	0.40	0.40	1.4	1.5
Na_2O	4.1	5.9	1.2	2.7	2.9	3.4	1.8
K_2O	2.6	1.5	2.5	3.8	3.7	2.8	0.9
P_2O_5	0.19	0.12	0.20	0.26	0.29	0.21	0.07
Rb	96	63	123	131	143	111	32
Sr	33	68	108	42	42	59	31
Ba	503	278	388	401	401	394	80
Y	23	22	26	18	20	22	3
Zr	75	176	142	162	158	143	40
Nb	12	n.a.	11	10	10	11	1
Th	16.3	12.8	15.1	16.4	16.7	15.4	1.6
Ta	1.1	0.9	0.9	1.2	1.2	1.1	0.1
Hf	3.8	4.9	2.9	4.4	4.5	4.1	0.8
U	6.3	2.4	4.5	5.3	4.9	4.7	1.4
La	58.8	37.7	39.7	42.6	40.1	43	9
Ce	116.9	78.8	74.2	94.1	85.6	90	17
Nd	46.6	28.4	32.9	34.7	31.1	34.7	7
Sm	8.1	5.6	6.1	6.1	5.8	6.3	1
Eu	1.7	1.4	1.0	1.1	1.1	1.3	0.3
Yb	2.6	2.2	2.7	2.3	2.6	2.5	0.2
Lu	0.3	0.3	0.4	0.4	0.3	0.3	0.1
Ni	69	88	130	69	69	85	26
Cr	192	160	179	57	69	131	64
Cu	n.a.	n.a.	75	12	7	31	38
Co	29	16	50	20	20	27	14
V	n.a.	n.a.	137	137	94	123	25
Sc	20	17	22	21	22	20	2

3. The rate of increase of Th and La relative to Zr is greater than the rate of increase of Y and Yb, whereas Hf/Zr and Sm/Zr are almost constant in all the rocks. The 1:1 enrichment vectors originating at the composition of the chilled margin are plotted in Figures 230.5a and b. The trajectories of the Th and La data curve towards higher Th/Zr and La/Zr values in samples with highest Zr content, whereas the Y and Yb versus Zr plots reveal trajectories which deviate towards lower Y/Zr and Yb/Zr values at higher Zr contents.
4. Samples with lower Zr abundances than the chilled margin's values (<65 ppm) are hypersthene-rich diabases, and these appear to be enriched in pyroxene, but still contain a large proportion of trapped liquid (around 75 percent).
5. Samples from the eastern profile at Bonanza Lake have lower Mg-numbers, TiO_2, P_2O_5, CO, and Sc contents than samples with similar Zr contents from other intrusions. These samples also have higher La and Th contents.

Nd ISOTOPIC VARIATION

Nd-isotope data and Sm/Nd ratios were determined on a subset of samples from Basswood Lake and Bruce Mines. Results for these samples, in addition to other unpublished data, are given in Table 230.4. The $^{147}Sm/^{144}Nd$ and $^{143}Nd/^{144}Nd$ ratios were recalculated at 2.22 Ga (Corfu and Andrews 1986), along with epsilon-Nd values (calculated relative to a chondritic uniform-mantle reservoir (CHUR) at 2.22 Ga).

The variation in $^{143}Nd/^{144}Nd$ versus $^{147}Sm/^{144}Nd$ (present day) are shown in Figure 230.6 for samples from this study, and additional data (Lightfoot and Naldrett 1987 and unpublished data). The results define a wide range in present day $^{143}Nd/^{144}Nd$ and $^{147}Sm/^{144}Nd$ between 0.5109 to 0.5122 and 0.10 to 0.17 respectively. Samples of chilled diabase anchor the high $^{143}Nd/^{144}Nd$ extreme of the trend, and samples of quartz diabase and hypersthene diabase fall on a trend reaching $^{143}Nd/^{144}Nd = 0.5115$. The granophyres and pegmatoidal diabases fall on an extension of the diabase trend, but with a steeper slope reaching $^{143}Nd/^{144}Nd = 0.51145$. Samples of

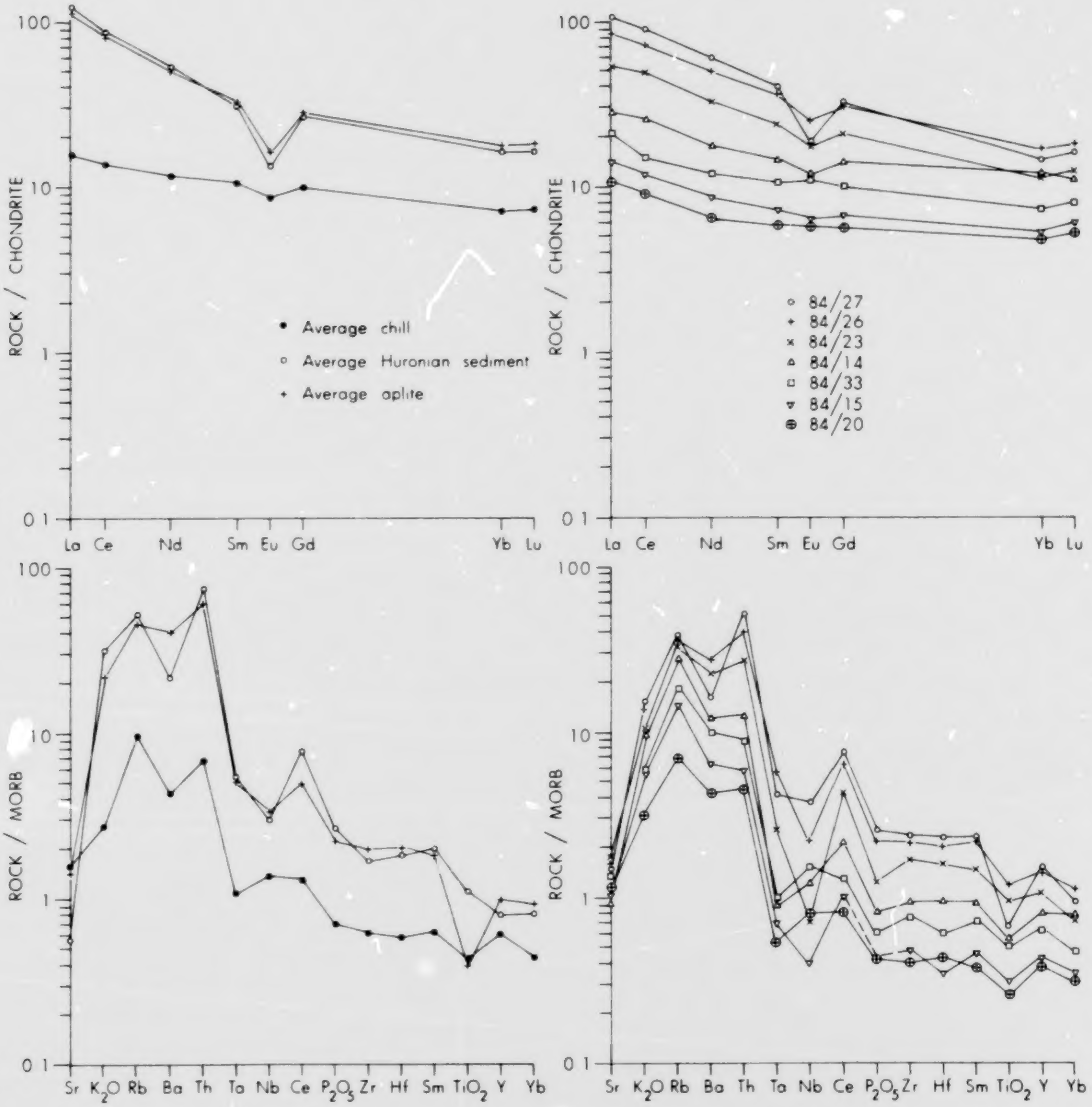

Figure 230.3. *Trace element variation diagrams for representative samples from the Basswood lake Intrusion. This diagram also shows the composition of the chilled margin (average), the Huronian sediments (average), and aplites (average).*

Huronian metasediment, from the footwall and hanging wall, and samples of aplite fall in the range $^{143}Nd/^{144}Nd = 0.5109$ to 0.5111 and $^{147}Sm/^{144}Nd = 0.10$ to 0.115. A series of 2.22 Ga reference lines with initial ratios of 0.5095 to 0.510 are superimposed on Figure 230.6. Most of the diabases fall close to the 2.22 Ga reference line with an initial ratio of ~0.5097. The granophyres are displaced below this reference line, whilst the aplites and Huronian metasediments show a stronger displacement.

A five-point isochron fitted by least-squares regression (samples with $^{143}Nd/^{144}Nd > 0.5116$), assuming constant blanket errors, yielded a line with a slope of 0.013369 and a $^{143}Nd/^{144}Nd$ intercept of 0.5098 for the Basswood Lake Intrusion. This corresponded to an age of 2.02 Ga assuming that the decay constant for Sm is $6.54810 \cdot 10^{-12}a^{-1}$. This could be interpreted to confirm the 2.2 Ga age. However, there is strong evidence that the system has been open with respect to the trace elements, and given this evidence, combined with the break in the trend at $^{143}Nd/^{144}Nd = 0.5116$ on the isochron plot, it would be premature to suggest that these data have any direct age significance for the Basswood Lake Intrusion.

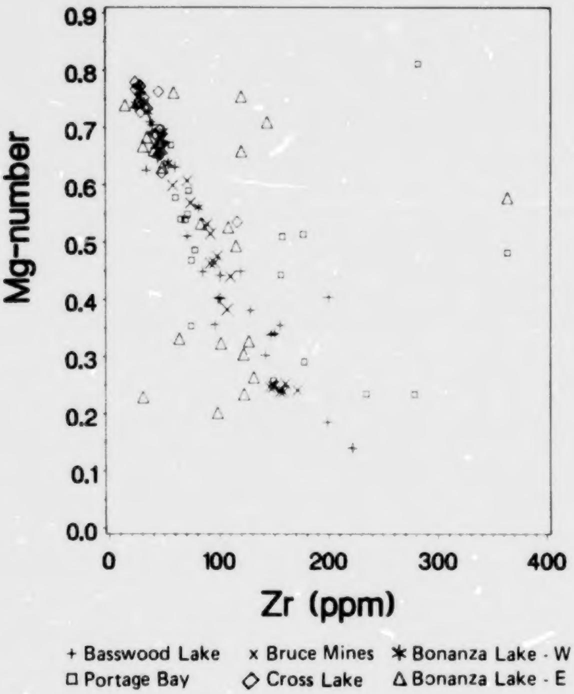

Figure 230.4. *Variation in Mg-number versus Zr content.*

TRACE-ELEMENT VARIATIONS AND Nd-ISOTOPIC COMPOSITION

Recalculation of the Nd-isotope data in epsilon format reveals a range of epsilon Nd between -2 and -6, with diabases (including chilled margins) falling between -2 and -5, and granophyres, aplites, and Huronian metasediments between -5 and -6. The error propagated from the Sm/Nd ratio, and used in age correcting the Nd-isotope data, makes a maximum analytical uncertainty of ±1 epsilon unit at 2.2 Ga inevitable, and therefore these data must be treated with caution. However, it can be said with a fair degree of confidence that the granophyres are analytically distinguishable from the diabases, and that they are not distinguished from either the Huronian metasediments or the aplites. The absence of a trend in the diabase samples is probably a reflection of the narrow range in initial Nd-isotope compositions (which are within analytical error).

It is now generally accepted that petrogenetic hypotheses should be based on a combination of isotope and trace-element data. Figure 230.7a shows the variation in epsilon Nd versus Th/Yb, whilst Figure 230.7b shows the variation in La/Yb and U/Yb values versus Th/Yb values. The epsilon-Nd versus Th/Yb plot confirms that the most radiogenic samples have the lowest Th/Yb value (i.e. the diabases), whilst the granophyres have least-radiogenic Nd-isotope signatures coupled with high Th/Yb values. This coupling is more clearly demonstrated on the trace-element-ratio plots (Figure 230.7b) which are not sensitive to the large uncertainty in initial Nd isotope ratio. On each plot, a trend is defined by the diabase data, which originates at low Th/Yb, La/Yb, and U/Yb values and points to high Th/Yb, La/Yb, and U/Yb values. Samples with lowest Th/Yb values include the chills, quartz diabases, and hypersthene diabases; samples with higher Th/Yb values include the varied-textured diabases, whilst samples with the highest Th/Yb values are the granophyres and pegmatoidal diabases. The Huronian-metasediment average plots on a linear extension of the trend of the Nipissing Diabase samples.

DISCUSSION

The geochemical variations documented above indicate that any geochemical model for the petrogenesis of the Nipissing Diabase must be consistent with several observations:

1. The parental magma, as indicated by the composition of chilled margin samples, must have been remarkably uniform in composition throughout the Province at the time of magma emplacement.
2. The geochemical data for the Nipissing Diabase samples define tight trends on variation diagrams, which pass through the composition of the chilled margin, and show a progressive increase in LIL/Zr and a decrease in HYG/Zr from the quartz diabases through the upper hypersthene diabases and into the varied-textured diabase, pegmatoidal diabase, and granophyre.
3. The trajectories on the element versus Zr plots never pass through the compositional average of the Huronian metasediments, but always curve towards this point. Significantly, however, the trajectories on the element-ratio plots (e.g. Th/Yb versus La/Yb) pass through the average composition of the Huronian metasediments, and mixing lines suggest that a maximum contribution of 50 percent crustal material could explain the relative distribution of samples on the interelement-ratio plots.
4. Samples from the lower part of the hypersthene diabase have lower Zr contents than the chilled margin samples, although the interelement ratios are indistinguishable from the basal quartz diabase and chill.
5. Field investigations conducted by Conrod (in preparation), and Lightfoot and Naldrett (1987) strongly suggest that the arch zones of the intrusions are regions of intense roof-rock melting. The production of aplites and granophyres appears to be intrinsically related to melting in the arch regions of the intrusions. The aplites appear to be compositionally similar to the Huronian metasediments, and are presumably derived by direct melting of them (the TiO_2 anomaly may be explained by ilmenite retention in the restite).

Collectively, these points provide strong evidence for a uniform parent magma which has interacted in situ with a variable amount of Huronian metasediment (up to 50 percent) during the crystallization of the magma. Furthermore, the tight trends in geochemical variation, combined with the presence of rocks with compositions depleted in incompatible

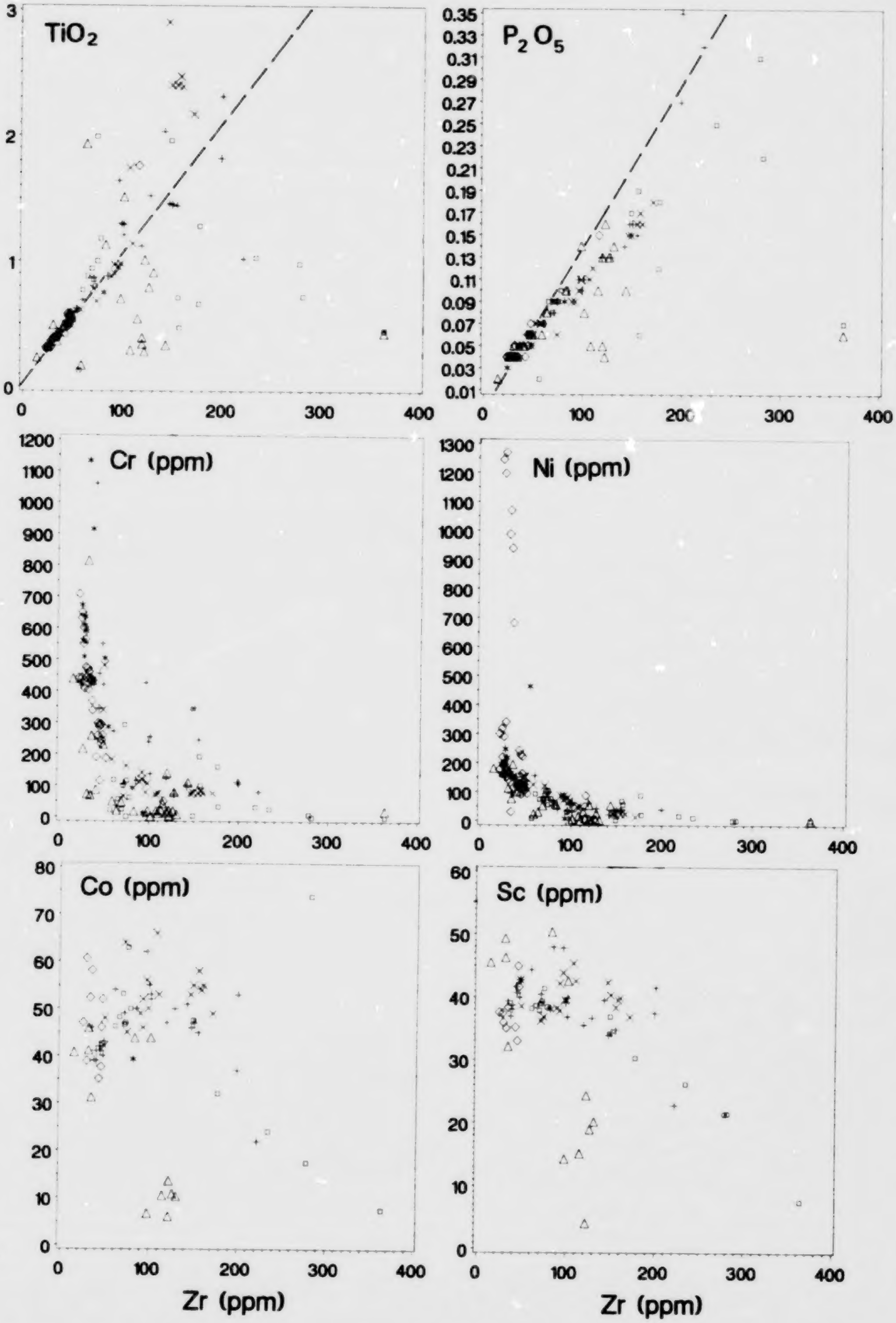

Figure 230.5a. *Variation in TiO$_2$, P$_2$O$_5$, Cr, Ni, Sc, and Co versus Zr.*

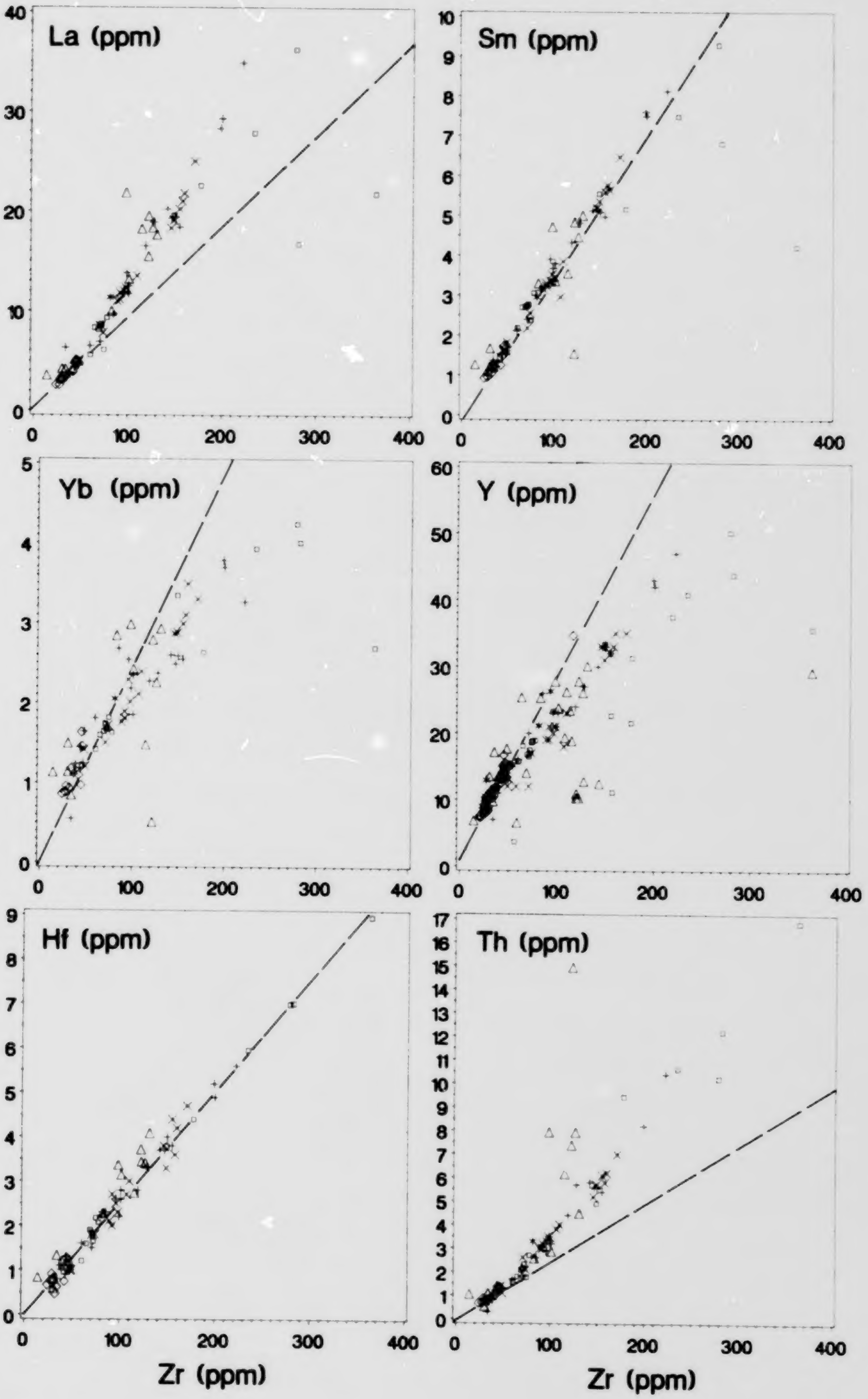

Figure 230.5b. Variation in La, Sm, Yb, Y, Th, and Hf versus Zr. Explanation of symbols are given in Figure 230.4.

TABLE 230.4. Sm/Nd ISOTOPE DATA FOR NIPISSING DIABASE SAMPLES.

Sample Location	$^{143}\text{Nd}/^{144}\text{Nd}$	Nd (ppm)	Sm (ppm)	$^{147}\text{Sm}/^{144}\text{Nd}$	$^{143}\text{Nd}/^{144}\text{Nd}$	Epsilon Nd (CHUR) at 2.2 Ga
		(PRESENT DAY VALUES)			(INITIAL)	
Portage Bay (PB):						
PB744 PB	0.511718	39.40	9.24	0.1418	0.50965	-2.32
PB745 PB	0.511449	25.39	5.62	0.1338	0.50949	-5.31
PB747 PB	0.511834	11.97	3.13	0.1580	0.50952	-4.72
PB743 PB	0.511739	30.45	7.45	0.1479	0.50958	-3.67
Basswood Lake (BS):						
84/23 BS	0.511770	23.30	5.74	0.1489	0.50959	-3.36
84/14 BS	0.511962	12.67	3.44	0.1641	0.50956	-3.96
84/22 BS	0.512051	5.89	1.65	0.1697	0.50957	3.70
84/18 BS	0.511990	5.63	1.54	0.1652	0.50957	-3.76
84/11 BS	0.511706	14.09	3.36	0.1442	0.50959	-3.25
84/21 BS	0.511559	35.10	7.98	0.1374	0.50955	-4.21
84/27 BS	0.511508	35.10	8.12	0.1398	0.50946	-5.89
Kerns and Hudson Township, Northwest of Cobalt (KH):						
86/169 KH	0.511828	20.07	5.06	0.1524	0.50960	-3.20
86/172 KH	0.511670	39.62	9.30	0.1419	0.50959	-3.30
86/189 KH	0.511520	46.18	10.53	0.1378	0.50951	-5.08
86F/197 KH	0.511096	47.08	7.82	0.1004	0.50949	-5.38
86/198 KH	0.511098	56.03	10.26	0.1107	0.50948	-5.56
86C/197 KH	0.510906	43.66	7.14	0.0988	0.50946	-5.93
86/186 KH	0.511606	12.61	3.04	0.1457	0.50948	-5.66
86/167 KH	0.512127	5.43	1.54	0.1710	0.50963	-2.69
Red Rock, Lake Temagami (RR):						
86/203 RR	0.511109	31.87	5.78	0.1096	0.50951	-5.05
86/73 RR	0.511120	30.58	5.74	0.1134	0.50946	-5.93
Portage Bay, Lake Temagami (PB-T):						
86/136 PB-T	0.512156	8.46	2.40	0.1714	0.50965	-2.26
West Coast, Lake Temagami (WC):						
86/104 WC	0.512048	8.75	2.47	0.1706	0.50955	-4.41
86/100 WC	0.512040	7.36	2.10	0.1725	0.50952	-4.82
Emerald Lake, West of Temagami (EL):						
86/155 EL	0.512028	8.57	2.35	0.1658	0.50960	-3.12
86/154 EL	0.512007	19.46	5.36	0.1665	0.50957	-3.75

PB - Portage Bay.
BA - Basswood Lake.
KH, RR, PB-T, WC, and El - Lightfoot and Naldrett (1987).

Blanks for Sm and Nd are <1 ng. Nd measured to better than 0.1%, SM to better than 0.7%. $^{143}\text{Nd}/^{144}\text{Nd}$ measured to 0.008% or better.

Present Day Bulk Earth (CHUR): $^{143}\text{Nd}/^{144}\text{Nd}=0.51246$, $^{147}\text{Sm}/^{144}\text{Nd}=0.1967$.

elements relative to the composition of the chilled margin, argue fairly strongly for a combination of assimilation and fractional crystallization, and the enrichment of the lower hypersthene diabase in pyroxene cumulates.

To test this model more rigorously, it is necessary to look in more detail at the element versus Zr plots. Figure 230.8 shows the variation in Th versus Zr (with an expanded portion depicting variations between 0 and 130 ppm Zr). The main diagram shows that a mixing line drawn between the average Huronian metasediments and the average chilled margin fails to reproduce the trend of the data. Furthermore, a 1:1 enrichment vector originating at the location of the chilled margin sample falls below the trend of the data. This suggests that neither simple mixing nor 1:1 enrichment is responsible for the observed variation. Assuming a phase extract consisting of plagioclase, orthopyroxene, clinopyroxene, and olivine (in the phase proportions 50:30:16:4, the approximate phase proportions observed in the hypersthene gabbro), and a parental magma similar in composition to the chilled margin, then Rayleigh Fractionation vectors can be constructed for different values of the bulk-distribution coefficients (Kd) of Th and Zr. For closed-system fractionation, Kd(Th) is suggested to be less than Kd(Zr), because the curve migrates towards higher Th/Zr values. Two curves have been shown in Figure 230.8a, one with Kd(Th) = 0.05 and Kd(Zr) = 0.25, and the other with Kd(Th) = 0.05 and Kd(Zr) = 0.5. The Kd value for Th

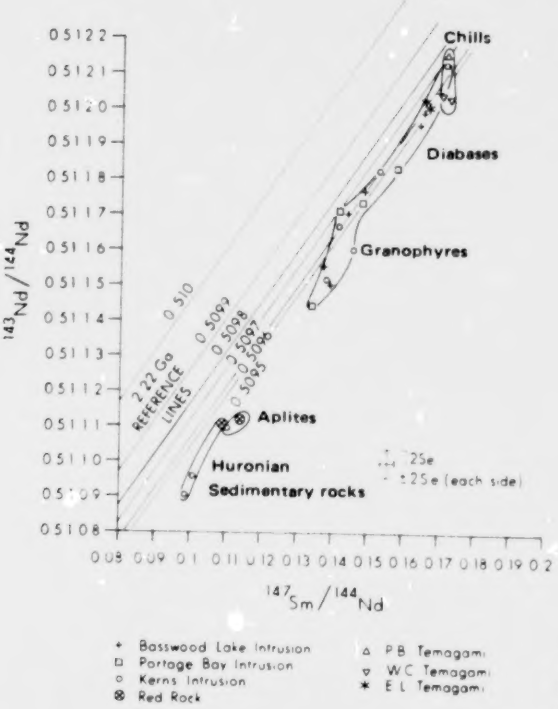

Figure 230.6. *Variation in present day ^{143}Nd/^{144}Nd versus ^{147}Sm/^{144}Nd.*

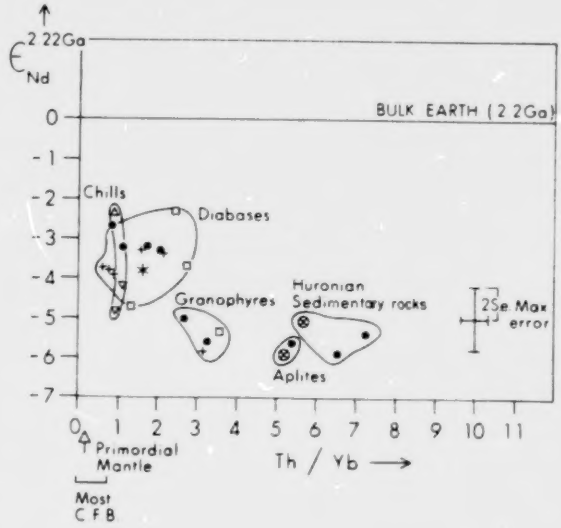

Figure 230.7a. *Variation in epsilon Nd (2.2 Ga) versus Th/Yb.*

is the minimum realistic value (see Table 5), whilst the Kd values for Zr are both high compared to an expected Kd(Zr)<0.1. Figure 8b shows a realistic fit for 100 percent crystallization with Kd(Zr) = 0.45, but the predicted composition of the equilibrium cumulates (plus trapped liquid) has higher Th/Zr values than the observed hypersthene-rich gabbros. Altering the phase extract or the proportions in which the phases participate in the fractionation process does not appear to improve the fit, and alternative phases such as amphibole and zircon can be ruled out (see above and Lightfoot *et al.* 1986).

Similar models can be constructed for the other incompatible trace elements, and reveal discrepancies in the observed bulk-distribution coefficients. Examination of the interelement-ratio plots (Figure 230.7b) reveals a wide range of Th/Yb, La/Yb, and U/Yb values which is not easily explained using available distribution-coefficient data. Furthermore, the variation in initial Nd-isotope composition suggests a component of open-system behaviour. Despite these poor fits, the Cr and Ni data are in good agreement with the phase extract used, as plots of Cr and Ni versus Zr tend not to be as sensitive to open-system processes as Th. This provides some support for the phase extract chosen (see Lightfoot *et al.* 1986).

Thus, there is strong evidence from the modeling that an additional component with high LIL/Zr and low HYG/Zr has been involved. Given the observation that the interelement-ratio-data trajectories point towards the composition of the average Huronian metasediment, and the field evidence for roof-rock melting, there is a strong suggestion that melting and assimilation of roof-rock material occurred during the crystallization of the magma. This appears to be most evident in the evolved rocks, and less evident in the most mafic rocks. Furthermore, this process appears not to have destroyed the tight trends on the element versus Zr variation diagrams. This observation lends support to the hypothesis stated by Bowen (1928) and more recently proposed by Taylor (1980) and DePaolo (1981, 1985); that is, that assimilation and fractionation are coupled (AFC), and the latent heat of crystallization of the magma releases heat which can produce a commensurate amount of melting of the roof rock. Although Campbell and Turner (1987) suggest that the processes may not be coupled if chemical interfaces are generated in the magma, this model merits further investigation.

Figure 230.9 shows the variation in Th and La versus Zr. AFC trajectories have been fitted assuming the phase extract used was that used in the Rayleigh models, with distribution coefficients from Table 230.5. The chilled margin was chosen as a parental magma composition, and the Huronian metasediment average was chosen as the contaminant. Two models are shown where the rate of change of mass assimilated to that crystallized is 0.15 and 0.2 (both of which are considered realistic figures in terms of mass and heat balance calculations). The composition of the equilibrium cumulate (with trapped liquid) is also shown. In these models, the maximum amount of fractionation recorded is 70 percent, compared with almost 100 percent for the Rayleigh models. Thus, the AFC models raise an important question about the extent to which these chambers were tapped during crystallization and the extent to which redistribution of material occurred in the sills during crystallization. Tapping of evolved magmas to

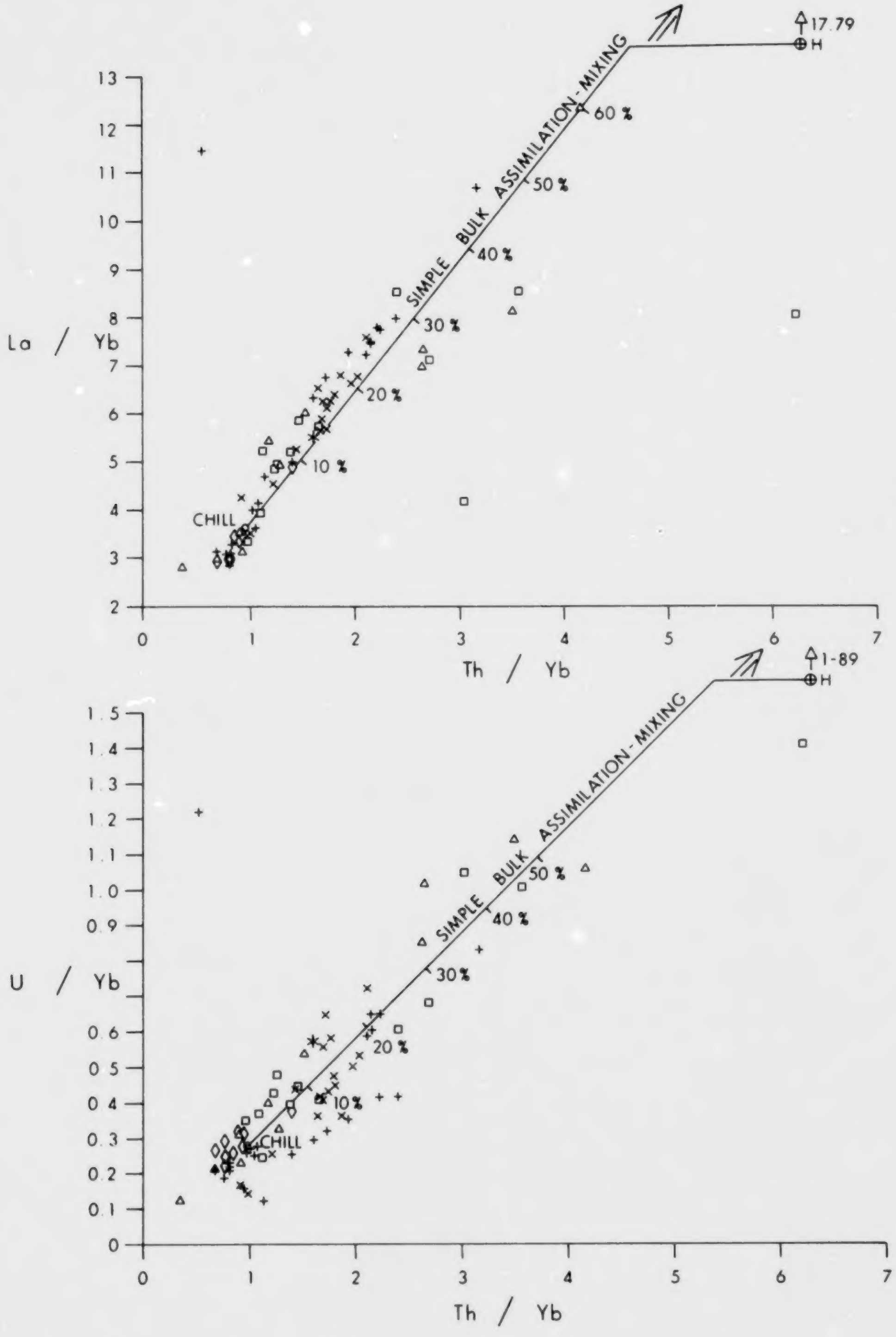

Figure 230.7b. *Variation in La/Yb and U/Yb versus Th/Yb.*

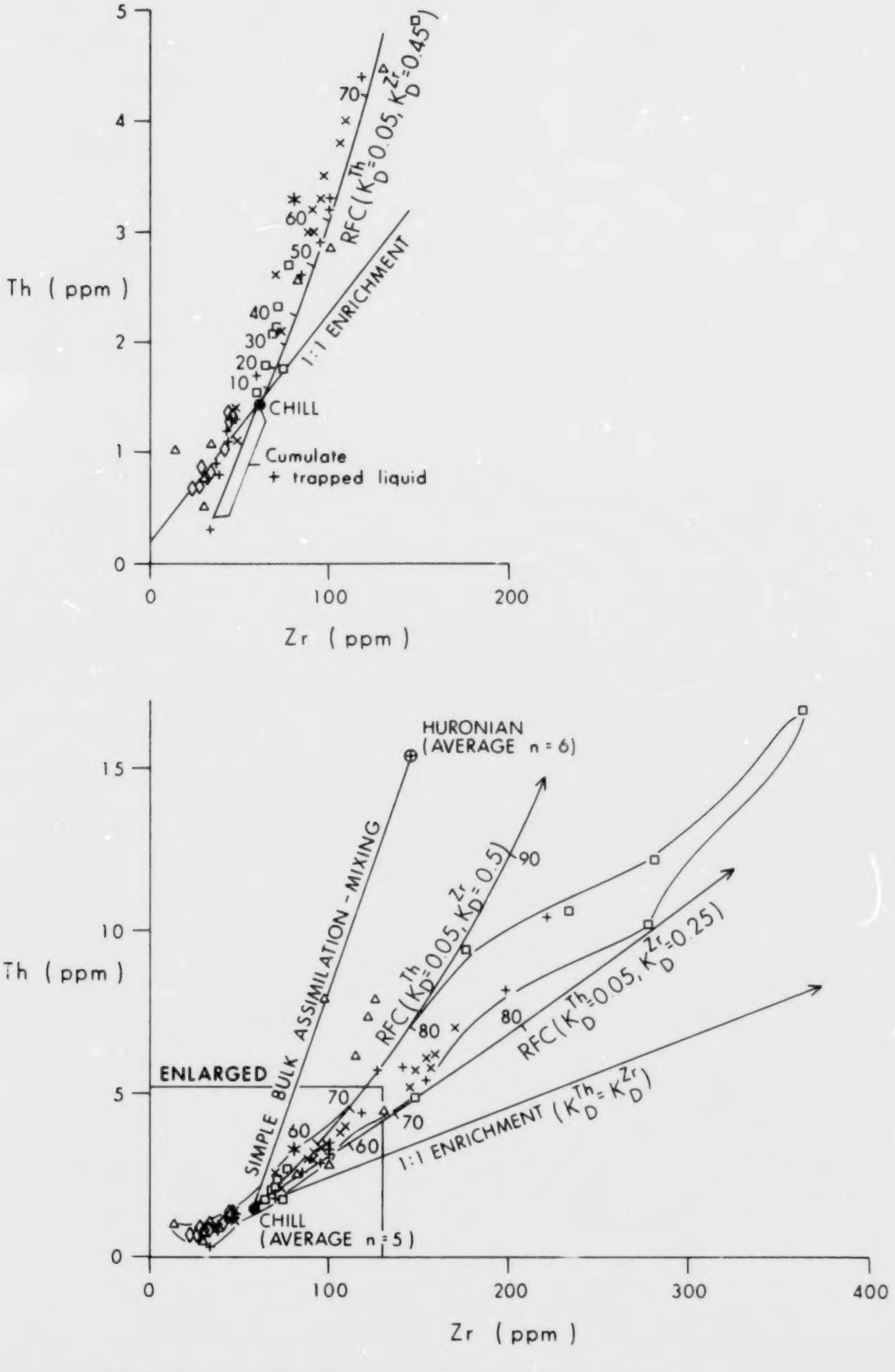

Figure 230.8. Rayleigh Fractionation vectors on a plot of Th versus Zr.

TABLE 230.5. DISTRIBUTION COEFFICIENTS FOR SELECTED TRACE ELEMENTS INTO OLIVINE, CLINOPYROXENE, AND ORTHOPYROXENE.

Element	Olivine	Ortho-pyroxene	Clino-pyroxene	Plagioclase
Extract	**4%**	**30%**	**16%**	**50%**
Cr	2.1	4.8	8.4	0
Ni	14	2.5	2.6	0.04
Th	0	0.15	0.02	0.02
Y	0.01	0.2	0.5	0.03
La	0.01	0.008	0.1	0.14
Sm	0.015	0.015	0.9	0.08
Yb	0.035	0.05	1.0	0.07
Hf	0	0.1	0.34	0.02
Zr	0.01	0.03	0.12	0.01
Ta	0	0.2	0.4	0.01
U	0.0024	0.008	0.04	0.009

Data sources: Henderson (1983, 1984), Pearce and Norry (1979), Irving (1978).

higher crustal levels has not been documented in the Nipissing Diabase Province, and, therefore, the AFC models presented here must be treated with some caution.

The extent to which assimilation and fractional crystallization are coupled may not be as simple as the AFC model predicts. Campbell and Turner (1987) suggest that roof material may melt and pond at the top of the intrusions, as a double-diffusive interface develops between the basic magma and the crustal melt. This interface may allow the diffusion of heat, but could prevent chemical transfer. Experimental observations made by Campbell and Turner (1987) on simple, binary, salt solutions suggest that such interfaces may commonly be developed at the roofs of large mafic-magma chambers. This observation suggests that assimilation and fractionation may only be coupled in a small portion of the magma chamber, with the ratio of the rate of assimilation to the rate of crystallization varying through the crystallization history of the intrusions. The genesis of the aplites appears to be a clear case in point where direct melting of Huronian metasediments produced liquids which crystallized without significant chemical interaction with the Nipissing magma. This is the subject of continuing work. Presently, the available data suggest that neither Rayleigh processes alone nor AFC alone can account for the entire range of observed variations in a fully satisfactory manner.

GEOCHEMICAL EVOLUTION OF THE HURONIAN MANTLE

Trace-element and Nd-isotope data for the chilled-margin samples confirm that the parental magma was both trace-element enriched and had evolved with a low Sm/Nd value to produce significantly unradiogenic Nd-isotope signatures (epsilon-Nd = -3) at 2.2 Ga. Given the large volume of homogenous magma produced over a wide area, it is suggested that this enrichment signature is more like a product of mantle than crustal processes. Jolly (in press) confirms that this trace-element signature is also recorded in Huronian volcanics, whilst data from Naldrett *et al.* (1985) confirm that a similar enrichment is present in samples from the Sudbury Igneous Complex.

Figure 230.10 shows the variation in Th/Yb versus Ta/Yb in Nipissing Diabase samples, and confirms that these rocks are enriched in Th relative to the primitive mantle, the present day MORB, and the Deccan Trap basalts (Lightfoot 1985), but similar to the Sudbury rocks.

A comparison of the observed Nd-isotope data with values derived from the Archean shield (Shirley and Hanson 1986; Machado and Brooks 1986) suggests that this trace-element enrichment event occurred after the production of Archean granite-greenstones, which all have epsilon-Nd values, at 2.7 Ga, of from +3.3 to -0.1—well above the range of Nipissing Diabase values (-2 to -5 for chilled margins).

Presently, further investigations are under way to determine whether this signature might reflect mantle or deep crustal processes, and whether any broad constraints can be placed on the role of crustal recycling in the Archean mantle.

ECONOMIC POTENTIAL

Since the discovery of the Cobalt ores and the recognition that mineralization is in close spatial association with the Nipissing Intrusions, and varies in type and style across the Southern Province (Card and Pattison 1973), the economic potential of the Nipissing Intrusions has been investigated. Card and Pattison (1973) record Ag, Co, and Ni as native metals and sulpharsenides within quartz-carbonate veins in the east of the Southern Province; in the central sector, they record predominantly Ni-Cu-sulphide minerals disseminated within the intrusions or occurring as pods; and in the western sector, they record Cu-rich sulphide minerals in quartz-carbonate vein systems.

The variation in type and style of mineralization appears unrelated to differences in the lithology, degree of metamorphism, or level of intrusion of the diabase. Thus, one of the key objectives in this study was to evaluate the potential of the Nipissing Intrusions as hosts to sulphide mineral ores enriched in Cu, Ni, and PGE. This investigation was conducted at three levels:

1. PGE data were determined for a suite of rocks.
2. Olivines were analyzed to determine whether any abnormal depletion in Ni relative to forsterite content was evident.
3. The major- and trace-element data documented above were utilized to investigate whether there was any evidence for large-scale contamination of the magma by crustal material, and whether this has any economic ramifications.

PLATINUM GROUP ELEMENTS

Selected samples of various lithologies from across the Portage Bay and Bonanza Lake Intrusions were analyzed for PGE. Samples included both barren samples and rocks containing disseminated sulphide

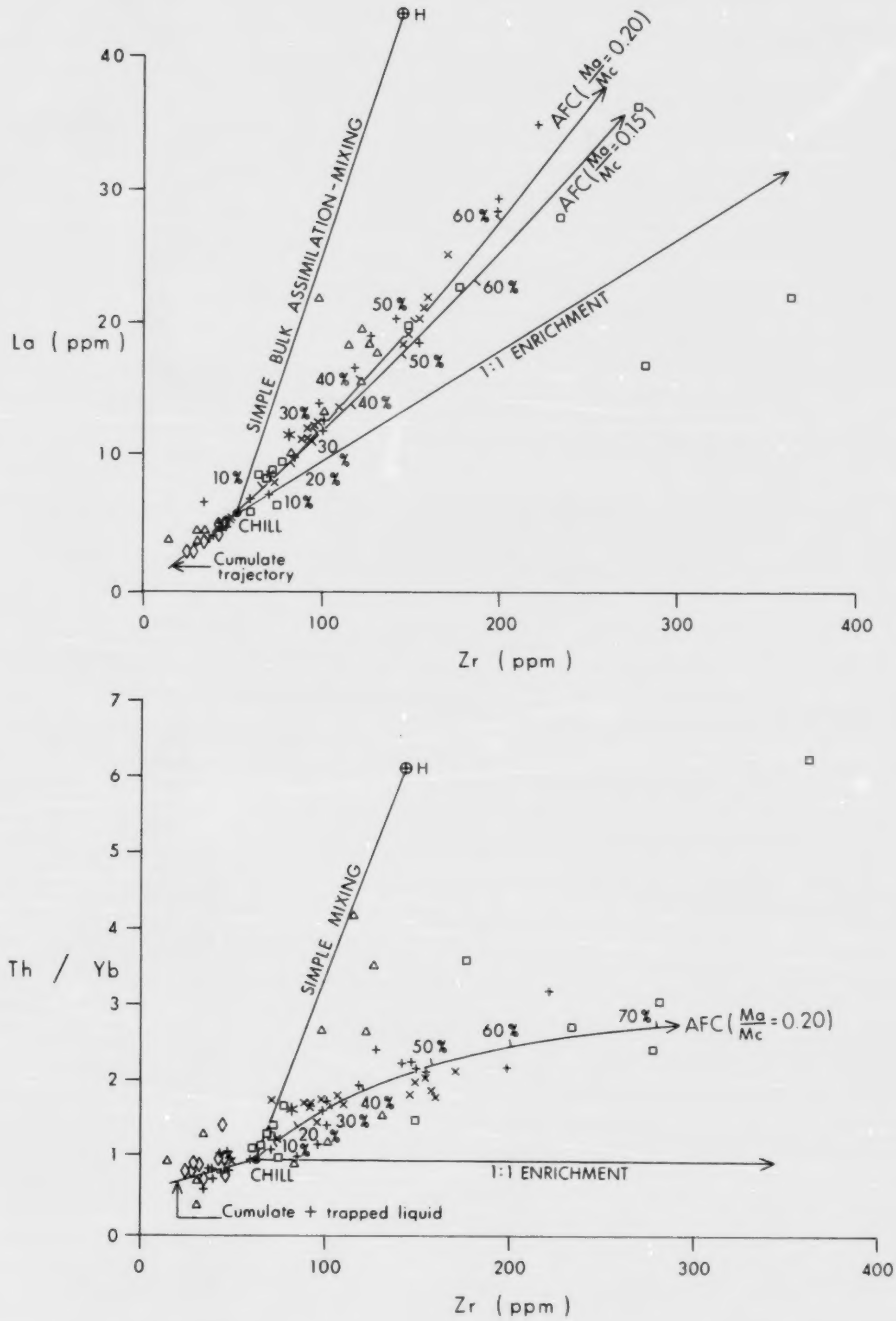

Figure 230.9. *AFC vectors for Th and La versus Zr.*

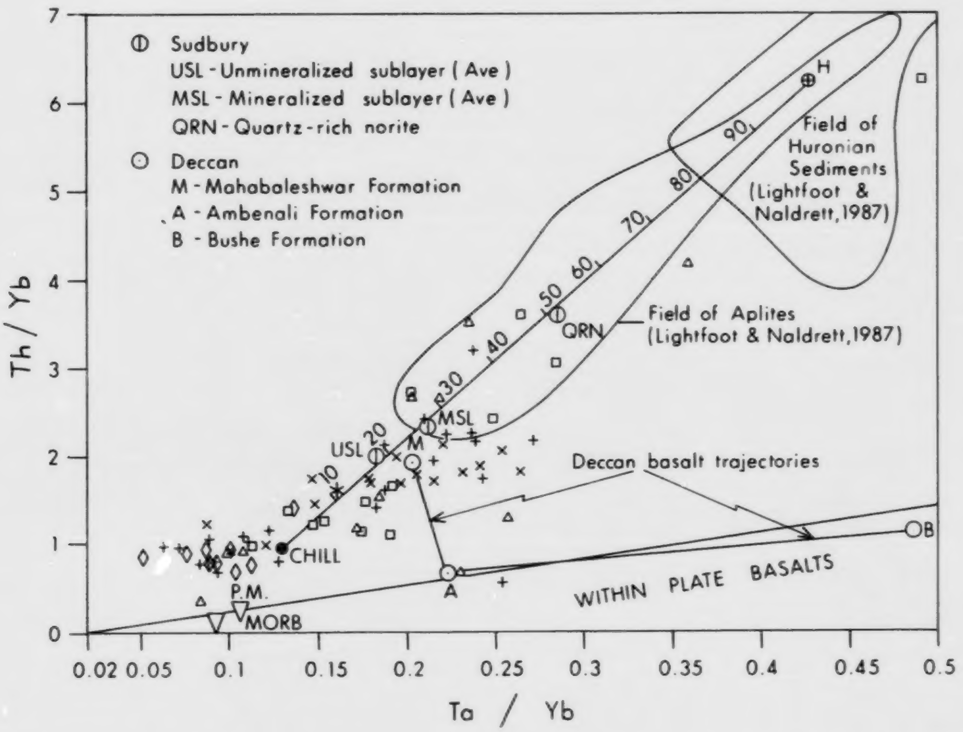

Figure 230.10. *Variation in Th/Yb versus Ta/Yb in the Nipissing Diabase, and comparison of data from other mafic igneous rocks from Sudbury and the Deccan.*

minerals. The results are listed in Table 230.6. The following observations can be made:

1. Concentrations of the PGE are generally low (<50 ppb total PGE).
2. Samples containing pyrrhotite are generally enriched relative to those free of this phase (Table 230.6).
3. The gabbro norites from the interiors of the intrusions are depleted in PGE relative to the basal quartz diabase.
4. The more-altered samples have higher PGE abundances.

A study of the Rathbun Lake occurrence (Rowell and Edgar 1986) suggests that higher values may be present in the sulphide mineralization. A hydrothermal origin for this mineralization is proposed (Rowell and Edgar 1986).

OLIVINE COMPOSITIONAL DATA

The extent to which magmas have interacted with sulphide liquid and the stage of this interaction may be recorded in the compositions of olivines crystallizing from the magma (e.g. Naldrett *et al.* 1984). Olivines from the Cross Lake Intrusion are slightly enriched in Ni relative to the Ni contents of olivines with similar forsterite contents from other basic intrusions (Figure 230.11). The high Ni-content of these olivines clearly argues against significant removal of Ni by a sulphide phase prior to the crystallization of the

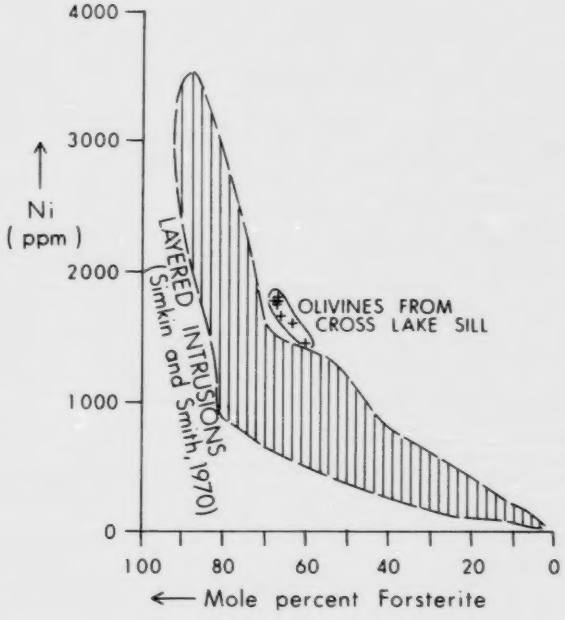

Figure 230.11. *Olivine compositional data for the Nipissing Diabase.*

TABLE 230.6. PETROGRAPHIC FEATURES AND PGE DATA FOR SELECTED SAMPLES.

Sample	Lithology	Sulphide bearing	S	Ni	Cu	Co	Cr	V
			%			ppm		
WL115	BQD	no	0.10	131	75	41	503	275
WL634	CQD	yes (1)	0.96	180	260	71	n.a.	n.a.
WL650	GN	no	0.11	113	160	46	72	248
WL659	PG-VTD	yes (2)	0.48	193	180	57	258	280
PB664	PG-VTD	no	0.13	77	160	50	62	304
PB672	G	yes (3)	0.26	41	3300	29	79	291
PB747	MD	no	0.10	104	120	47	293	275
PB761	QRG	yes (4)	0.14	6	65	36	18	113

BQD - basal quartz diabase, CQD - capping quartz diabase, GN - gabbronorite, PG-VTD pegmatoidal phase of varied-textured diabase, G - granodiorite, MD - mafic diabase, QRG - quartz-rich gabbro.

(1) Pyrrhotite replaced by marcasite.
(2) Pyrrhotite.
(3) Chalcopyrite rimmed by bornite, covellite, and digenite.
(4) Pyrite.

Sample	Ir (ppb)	Pt (ppb)	Pd (ppb)	Au (ppb)
WL115-1	0.08±0.01	12.92±10.87	n.d.	3.63±0.05
WL115-2	0.04±0.01	10.84±8.35	17.95± 9.67	2.39±0.04
WL650-1	0.01±0.01	n.d.	n.d.	1.62±0.02
WL650-2	0.02±0.01	n.d.	n.d.	0.66±0.05
WL634-1	0.12±0.01	9.77±8.86	n.d.	3.69±0.04
WL634-2	0.14±0.01	6.72±6.38	27.67±14.36	1.84±0.03
WL659-1	0.10±0.01	10.13±7.87	n.d.	2.81±0.03
WL659-2	0.13±0.01	10.13±7.87	n.d.	4.05±0.03
PB664-1	0.03±0.01	n.d.	n.d.	1.77±0.03
PB664-2	0.02±0.01	n.d.	n.d.	1.46±0.02
PB747-1	0.11±0.01	7.54±7.23	n.d.	3.46±0.04
PB747-2	0.12±0.01	19.33±10.25	25.16±8.39	3.76±0.04
PB761-1	0.04±0.01	n.d.	21.97±9.08	1.09±0.03
PB761-2	0.02±0.01	n.d.	n.d.	0.89±0.02
PB762-1	0.03±0.01	n.d.	n.d.	6.12±0.05
PB762-2	0.02±0.01	n.d.	14.81±11.89	2.00±0.04

n.d. - not detected. n.a. - not available. Errors are given at the 90% confidence level.

olivine in these rocks. Unfortunately, fresh olivine is largely absent from the Nipissing Diabases, and this hypothesis could not be tested at other locations. However, the observation that the olivines are not abnormally depleted in nickel strongly suggests that sulphide liquids have not produced an abnormal depletion in Ni, Cu, and some PGE in the magma. This could be interpreted to indicate that the magma becomes depleted in Ni during the fractionation of pyroxene and olivine, whilst Cu and possibly some PGE are enriched in the liquid. If sulphide saturation is achieved in the final stages of crystallization, then these sulphide minerals might be expected to be enriched in Cu and possibly PGE. This would be consistent with the observed higher tenors of some PGE in the varied-textured diabase and the presence of abundant chalcopyrite in the roof regions of the intrusions.

TRACE-ELEMENT EVIDENCE FOR CONTAMINATION

It has been suggested that the contamination of magma by siliceous country rocks has caused sulphide segregation at Sudbury (Irvine 1975; Naldrett *et al.* 1986). The available trace-element data suggest that contamination dominates the geochemical features of the arch regions of the intrusions. The enhanced silica content of these magmas could have induced sulphur saturation in the arch regions during the normal fractionation of the magma, and these sulphide minerals presumably provided a sink for Cu and any remaining PGE. These features appear to be common to most of the Nipissing Intrusions, and their value to exploration models has yet to be realized.

The geochemical data also suggest that the Nipissing diabase was enriched in LIL elements at the time of emplacement. However, it is interesting to observe that the trace-element-enrichment style, found in the Nipissing Diabase chilled margins, is common to the whole Nipissing Diabase Province, and it would require a remarkably uniform region of crustal material and degree of contamination to generate this signature in a crustal environment. Thus the possibility that contamination triggered sulphide saturation within the crust may be considered unlikely.

SUMMARY

The following conclusions may be drawn from this research:

1. The composition of the parental magma to the Nipissing Diabase was very uniform, and apparently originates in a region of mantle that has undergone considerable trace-element enrichment.
2. Chemical and mineralogical variations through a number of intrusions are similar; differences appear to reflect the lateral and vertical distribution of the samples in the sills and dikes.
3. The tight gecohemical trends argue for a combination of fractionation of plagioclase, orthopyroxene, clinopyroxene, and olivine, and the assimilation of crustal material which resembles average Huronian footwall and hanging wall metasediment. The extent to which assimilation and fractionation are coupled (AFC) remains open to question.
4. PGE data and compositional data for olivines suggest that the sampled intrusions do not host significant quantities of magmatic Ni-Cu-PGE mineralization, albeit that the trace-element data argue strongly in favour of a crustal-contamination signature in the upper portions of the intrusions.

ACKNOWLEDGMENTS

The authors would like to thank Ron Hancock (Department of Nuclear Engineering, University of Toronto) for use of the SLOWPOKE reactor and counting facilities. Phil Potts and John Watson (Department of Earth Sciences, The Open University, United Kingdom) are thanked for XRF analyses of some of the samples. Tom Krough (Royal Ontario Museum, Toronto) is thanked for access to the VG354 thermal-ionization mass spectrometer stationed in the Jack Satterly Age Laboratory, Royal Ontario Museum. Norm Evensen and Steve Noble (Department of Geology, University of Toronto) are thanked for assistance with Nd-isotope work. Bhodan Podstawskyj (Royal Ontario Museum, Toronto) provided technical assistance with VG software, and kept the 354 ticking over. Geof Norris (Department of Geology, University of Toronto) is thanked for his interest in the University of Toronto's isotope facility. Subash Shanhbag (Department of Geology, University of Toronto) is thanked for drafting the diagrams.

REFERENCES

Bowen, N.L.
1928: The Evolution of the Igneous Rocks. Dover, New York, N.Y. 332p.

Campbell, I.H., and Turner, J.S.
1987: A Laboratory Investigation of Assimilation at the Top of a Basaltic Magma Chamber. Journal of Geology, Volume 95, p.155-172.

Card, K.D., and Pattison, E.F.
1973: Nipissing Diabase of the Southern Province, Ontario; Geological Association of Canada, Special Paper 12, p.7-30.

Church, W.R.
1966: The Status of the Penokean Orogeny in Ontario (Abstract); Ninth Conference on Great Lakes Research, p.25.

Conrod, D.
In Prep.: Petrology, Geochemistry, and PGE Potential of the Nipissing Intrusions. University of Toronto MSc thesis.

Corfu, F., and Andrews, A.J.
1986: A U-Pb age for Mineralized Nipissing Diabase, Gowganda, Ontario. Canadian Journal of Earth Sciences, Volume 23, p.107-109.

DePaolo, D.J.
1981: Trace Element Effects of Combined Wall Rock Assimilation and Fractional Crystallization; Earth and Planetary Science Letters, Volume 53, p.189-202.

1985: Isotopic Studies of Processes in Mafic Magma Chambers: I. The Kiglapait Intrusion, Labrador. Journal of Petrology, Volume 26, Part 4, p.925-951.

Dressler, B.O.
1980: Geology of the Wanapitei Lake Area, District of Sudbury; Ontario Geological Survey, Open File Report 5287, 150p., 19 tables, 29 figures, 25 photos, and 3 maps.

Evensen, N.M., and Turner, P.
In Prep.: The Mathematical Basis of Multiple Collector Mass Spectrometry.

Finn, G.C., Edgar, A.D., and Rowell, W.F.
1982: Petrology, Geochemistry, and Economic Potential of the Nipissing Diabase; Grant 100, p.43-57 *in* Geoscience Research Grant Program, Summary of Research 1981-1982, edited by E.G. Pye, Ontario Geological Survey, Miscellaneous Paper 103, 219p.

Fujimaki, H.
1986: Partition coefficients of Hf, Zr, and REE between zircon, apatite, and liquid. Contributions to Mineralogy and Petrology, Volume 94, p.42-45.

Henderson, P.
1983: Inorganic Geochemistry, Pergamon International Press, 353p.
1984: Rare Earth Element Geochemistry, 2 vols.

Hoffman, E.L., Naldrett, A.J., Van Loon, J.C., Hancock, R.G.V., and Manson, A.
1978: The Determination of all the Platinum Group Elements and Gold in Rocks and Ores by Neutron Activation Analysis after Preconcentration by a nickel-sulphide Fire-Assay Technique on Large Samples; Analytica Chemica-Acta, Volume 102, p.157-166.

Hriskevich, M.E.
1968: Petrology of the Nipissing Diabase Sill of the Cobalt Area, Ontario, Canada. Geological Society of America Bulletin, Volume 79, p.1387-1404.

Irvine, T.N.
1975: Primary Precipitation of Concentrated Deposits of Magmatic Ores; Geological Survey of Canada, Paper 751B, p.73-79.

Irving, A.J.
1978: A Review of Experimental Studies on Crystal/Liquid Trace Element Partitioning; Geochimica Cosmochimica Acta, Volume 42, p.743-770.

Jambor, J.L.
1971: The Nipissing Diabase; Canadian Mineralogist, Volume 11, Part 1. p.34-75.

Jolly, W.T.
In Press: Geology and Geochemistry of Huronian Low-Ti Tholeiites and Calc-alkaline Rhyolites from the Thessalon Area, Central Ontario; Submitted to Canadian Journal of Earth Sciences.

Lightfoot, P.C.
1985: Isotope and Trace Element Geochemistry of the South Deccan Lavas, India; Unpublished PhD thesis, The Open University, Milton Keynes, United Kingdom, 589p.

Lightfoot, P.C., and Naldrett, A.J.
1984: Chemical Variation in the Insizwa Complex, Transkei, and the Nature of the Parent Magma; Canadian Mineralogist, Volume 22, p.111-123.
1987: Isotopic, Trace Element and Metallogenic Studies of the Nipissing Diabase, Sudbury-Cobalt Region, Ontario; Energy, Mines, and Resources Contract Report OST85-00422. Energy, Mines and Resources, Ottawa.

Lightfoot, P.C., Conrod, D., Naldrett, A.J., and Evensen, N.M.
1986: Petrologic, Chemical, Isotopic, and Economic Potential Studies of the Nipissing Diabase; Grant 230, p.87-106 *in* Geoscience Research Grant Program, Summary of Research 1985-1986, edited by V.G. Milne, Ontario Geological Survey, Miscellaneous Paper 130, 235p.

Machado, N., and Brooks, C.
1986: Determination of Initial $^{87}Sr/^{86}Sr$ and $^{143}Nd/^{144}Nd$ in Primary Minerals from Mafic and Ultramafic Rocks: Experimental Procedure and Implications for the Isotopic Characteristics of the Archean Mantle Under the Abatibi Greenstone Belt, Canada; Geochimica et Cosmochimica Acta, Volume 50, p.2335-2348.

Naldrett, A.J., Hewins, R.H., Dressler, B.O., and Rao, B.V.
1984: The Contact Sublayer of the Sudbury Igneous Complex; p.253-274 *in* The Geology and Ore Deposits of the Sudbury Structure, edited by E.G. Pye, A.J. Naldrett, and P.E. Giblin, Ontario Geological Survey. Special Volume 1, 603p. Accompanied by Map 2491, scale 1:50 000, Map NL-16/17-AM Sudbury, scale 1:1 000 000, and 3 charts.

Naldrett, A.J., Rao, B.V., and Evensen, N.M.
1986: Contamination at Sudbury and its role in ore formation; Institute Mining Metallurgy, Extract from Metallogeny of basic and ultrabasic rocks, p.75-91.

Noble, S.N., Lightfoot, P.C., and Scharer, U.
In Prep.: A Method for Single-Filament Isotopic Analysis of Nd Using in situ Reduction

Pearce, J.A., and Norry, M.J.
1979: Petrogenetic Implications of Ti, Zr, Y, and Nb Variations in Volcanic Rocks; Contributions to Mineralogy and Petrology, Volume 69, p.33-47.

Rowell, W.F., and Edgar, A.D.
1986: Platinum-Group Element Mineralization in a Hydrothermal Cu-Ni Sulphide Occurrence, Rathbun Lake, Northeastern Ontario; Economic Geology, Volume 81, p.1272-1277.

Shirley, S.B., and Hanson, G.N.
1986: Mantle Heterogeneity and Crustal Recycling In Archean Granite-Greenstone Belts: Evidence from Nd Isotopes and Tace Elements in the Rainy Lake Area, Superior Province, Ontario, Canada; Geochimica et Cosmochimica Acta, Volume 50, p.2631-2651.

Simkin, T., and Smith, J.V.
1970: Minor element distribution in olivine; Journal of Geology, Volume 78, p.304-325.

Taylor, H.P. Jr.
1980: The Effects of Assimilation of Country Rocks by Magmas on $^{18}O/^{16}O$ and $^{87}Sr/^{86}Sr$ systematics in igneous rocks, Earth and Planetary Science Letters, Volume 47, p.243.

Wager, L.R., and Brown, G.M.
1968: Layered Igneous Rocks; Oliver and Boyd, Edinburgh and London, 588p.

Watson, E.B., and Harrison, T.M.
1983: Zircon saturation revisited: Temperature and composition effects in a variety of crustal magma types; Earth and Planetary Science Letters, Volume 64, p.295-304.

Watson, B.E., and Ryerson, F.J.
1986: Partitioning of zirconium between clinopyroxene and magmatic liquids of intermediate composition; Geochemica et Cosmochimica Acta, Volume 50, p.2523-2526.

Wilson, J.R., and Engell-Sorensen, O.
1986: Basal Reversals in Layered Intrusions are Evidence for Emplacement of Compositionally Stratified Magma; Nature, Volume 323, p.616-618.

Zindler, G.A.
1980: Geochemical Processes in the Earth's Mantle and the Nature of Crust-Mantle Interactions: Evidence from Studies of Neodymium and Strontium Isotope Ratios in Mantle-Derived Igneous Rocks and Lherzolite Nodules; PhD dissertation, Massachusetts Institute of Technology, Cambridge, Massachusetts.

Grant 233 The Dating of Ontario's Gold Deposits

Paul W. Layer, N. Dawn McMaster, and Derek York

Department of Physics, University of Toronto, Toronto

ABSTRACT

Previous U-Pb and ^{40}Ar/^{39}Ar dating has been able to precisely constrain the age of gold emplacement in the Timmins and Hemlo camps (Masliwec *et al.* 1986). The current research attempts to do this for the Red Lake area, where U-Pb and ^{40}Ar/^{39}Ar ages currently bracket the gold to a time window ~80 Ma wide. Extensive sampling of most major lithologic units in Red Lake has supplied samples that are pre-, post- and syn-gold emplacement. The work to date has focused on the surrounding granitic batholiths in an attempt to constrain the cooling history of the area.

INTRODUCTION

The purpose of the project is to apply the ^{40}Ar/^{39}Ar method of dating to minerals associated with some of Ontario's gold deposits (e.g. Timmins, Hemlo, and Red Lake camps) so that reliable estimates can be made of the time(s) of gold formation. At the onset of this project, these times were only imprecisely known. While U-Pb dating of zircons and sphenes is beginning to produce an accurate volcano-stratigraphic framework for the evolution of the gold-bearing greenstone belts, it remains extremely difficult to position the gold-forming events within this time matrix.

An approach of bracketing gold has been developed which uses U-Pb dating of pre-ore bodies to define a maximum age of the gold and ^{40}Ar/^{39}Ar dating of post- or syn-ore micas to define a minimum age (Masliwec *et al.* 1986). In the Timmins camp, this approach has shown clear signs of being extremely useful in the dating of gold deposits. A number of the producing deposits are in porphyries. The crystallization age of these has been determined by S. Marmont (Geologist, Ontario Geological Survey, Toronto) by U-Pb dating of zircons. The gold is, therefore, younger than the associated zircon age. The gold is, however, apparently associated with a green-mica alteration product and is considered to be syn- or pre-mica. The authors ^{40}Ar/^{39}Ar-dated the green mica to get a minimum age of gold formation. The green mica has been shown to be a very suitable mineral for ^{40}Ar/^{39}Ar work. It has enabled us to bracket the age of formation of the Dome Mine deposit at between 2633± 6 Ma from micas and 2670±2 Ma from the zircons. Similarly, the Hollinger Mine has been bracketed between 2617±8 Ma and 2688±3 Ma (Masliwec *et al.* 1986).

At Hemlo it was found that the post-ore fuchsite has experienced a more tranquil post-crystallization history than that of the Dome and Hollinger Mines. The Hemlo gold is seen to be older than 2671±5 Ma from the ^{40}Ar/^{39}Ar work (Masliwec *et al.* 1986). A pre-ore feldspar-porphyry dike associated with the Cedar Lake Pluton gave a U-Pb zircon age of 2681±3 Ma (F. Corfu, Geochronology Laboratory, Royal Ontario Museum, personal communication 1987). Thus, the Hemlo gold was formed between 2671±5 Ma and 2681±3 Ma making it the most precisely dated Archean gold deposit known.

In the Red Lake area, gold formation, hydrothermal alteration, and activity on deformation zones are all intimately related to batholith intrusion and its resulting metamorphism (Andrews *et al.* 1986). Currently, the authors are collaborating with A.J. Andrews (Geologist, Ontario Geological Survey, Toronto) and co-workers to try to outline the thermal history of the contact zone of the Trout Lake Batholith and to position the time of hydrothermal activity and gold formation within this history.

Hornblende and mica from the contact zone yield beautiful plateaus with ages of approximately 2675 Ma and 2665 Ma respectively. At this time, cooling was evidently rapid and the subsequent history was tranquil. However, micas from the nearby Cochenour, Campbell, and A.W. White Mines, have been seriously disturbed, perhaps reflecting late activity in the gold-associated deformation zones. Micas from the Campbell and Cochenour Mines show ^{40}Ar/^{39}Ar spectra which are identical, within experimental error, and show a high-temperature age of 2629±6 Ma. The highest temperature ^{40}Ar/^{39}Ar age derived from micas from the A.W. White Mine is 2634±4 Ma (Masliwec *et al.* 1986).

U-Pb dating of the plutons which surround the greenstone belt has been used to constrain the ages of gold formation. The Dome Stock in the centre of the greenstone belt is most certainly pre-gold as it is cut by ore-hosting shear zones and has a U-Pb zircon age of 2718±1 Ma (Corfu and Wallace 1986). Andrews *et al.* (1986) have used the zircon and sphene age of the Trout Lake Batholith (2699± 2 Ma) to constrain the lower age of formation.

The argon results from the mines then indicated a much younger minimum age for gold emplacement than the zircon age by ~70 Ma. The need for further investigation was indicated to attempt to better constrain the age of gold emplacement and to unravel the thermal history of the area (as a complex thermal history may have resulted in the down-shifting of argon ages). Thus, the Red Lake area has been the focus of a more intense investigation.

Two objectives of this year's work have been to extend the Red Lake study by, first, focusing on the surrounding batholiths to attempt to understand the thermal history of the area, and, by second, using the laser-fusion system to generate single-grain, ^{40}Ar/^{39}Ar-age spectra. The results so far obtained show that intriguing variations in thermal history can be seen. The laser-fusion system can generate single-mineral-grain age spectra more precisely and quickly than the more traditional ^{40}Ar/^{39}Ar dating of many milligrams of sample. Furthermore, the laser-fusion system has shown that large age differences can be seen between different-sized grains from the same hand sample.

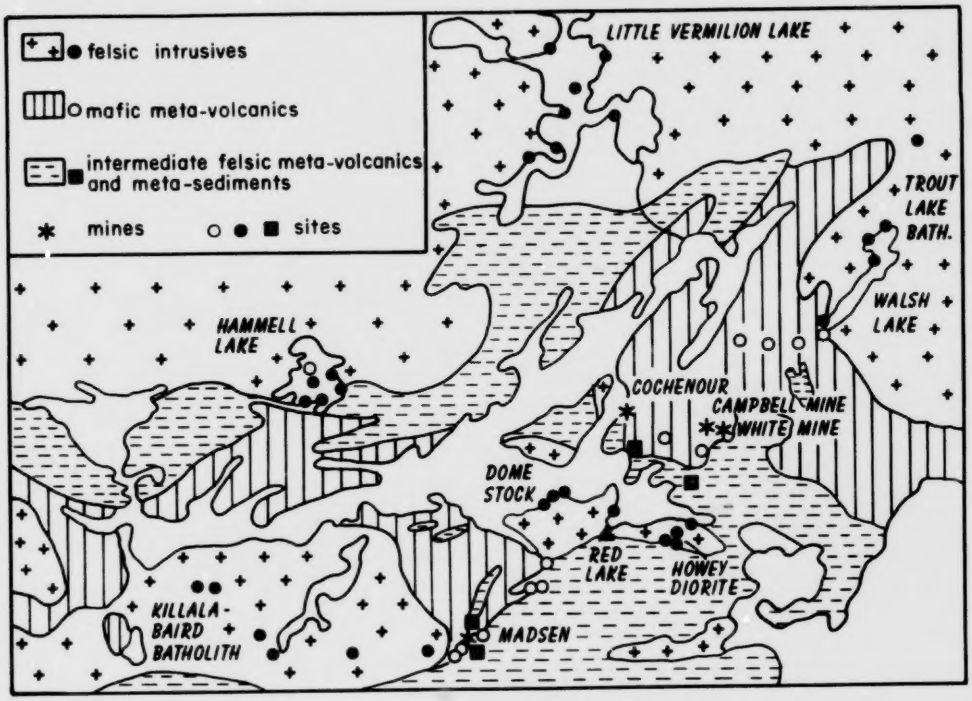

***Figure 233.1.** Generalized geological map of the Red Lake area showing surface sites of samples collected for $^{40}Ar/^{39}Ar$ dating and for paleomagnetic study. The mines where samples were collected are also shown.*

SAMPLING

Extensive sampling of rocks from the Red Lake area was done in October, 1986, with the assistance of M.J. Lavigne (Resident Geologist, Ministry of Northern Development and Mines, Red Lake). Figure 233.1 shows the extent of the surface sampling. Six plutonic bodies were sampled; the Trout Lake Batholith, the Dome Stock, the Vermilion Lake Batholith, the Hammell Lake Batholith, the Killala-Baird Batholith, and the Howie Diorite. In these bodies, six samples were collected at from four to seven sites. The samples were collected either as oriented hand samples or as oriented field-drilled cores, and are part of a reconnaissance paleomagnetic investigation of the plutonic rocks currently underway by V. Constanzo at the University of Toronto. Eighteen sites in surface exposures of the volcanic units were also sampled for geochronologic and paleomagnetic studies. In addition, samples were collected from the A.W. White and Campbell mines. Mine samples were chosen so as to pre- and postdate ore emplacement. The majority of the Red Lake mine samples were also oriented in the field for possible paleomagnetic work. As with the paleomagnetic survey, the main emphasis of the current investigation of the $^{40}Ar/^{39}Ar$ ages is on the batholiths which surround the greenstone belt.

EXPERIMENTAL METHODS

Stepwise $^{40}Ar/^{39}Ar$ heating of bulk samples of mineral grains was performed at the University of Toronto. Samples were heated in a Lindberg furnace and the fractions were measured with an MS10 mass spectrometer. Generally, 10 to 20 mg of sample were heated in the case of biotite and potassium feldspar, while 40 to 50 mg of sample were used in the case of hornblende.

In addition to this dating of bulk samples, the newly developed laser-fusion system is now being used to analyze single mica and hornblende grains from the Red Lake area. The laser-fusion system at the University of Toronto has been routinely used to step heat rocks and minerals (York *et al.* 1981; Bray *et al.* 1987; Layer *et al.* 1987). It consists of a Spectra-Physics 171-18 (18 watts) continuous argon-ion laser and a VG 1200S mass spectrometer with a Baur-Signer ion source and an electron multiplier. The ion source, operating at a 250 μA emission current, gives a sensitivity of 3 mA/Torr, and the electron multiplier has a gain of about 10^5. Typical background values for the extraction line were 7×10^{-14} ml STP for mass 36, 1×10^{-13} ml STP for mass 39, and 1.8×10^{-11} ml STP for mass 40.

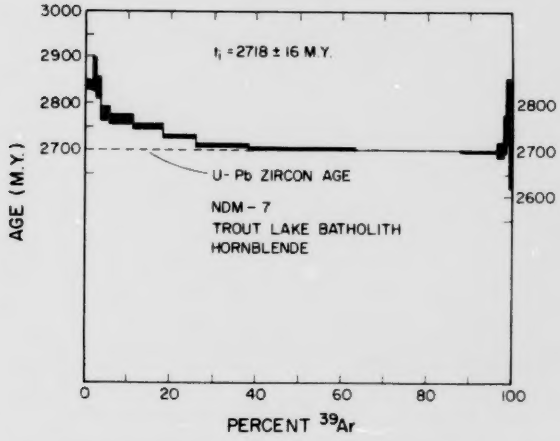

Figure 233.2. *Age spectrum of the Trout Lake Batholith hornblende. Dashed line represents the U-Pb age at the same site.*

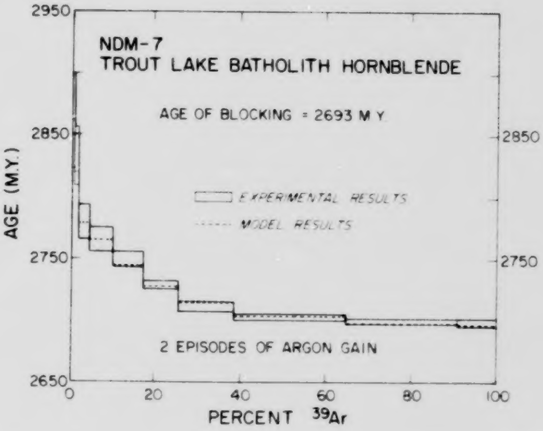

Figure 233.3. *The mathematically modeled segment of the hornblende spectrum from the Trout Lake Batholith (dashed) superimposed on experimental results (shown by their ±1σ error boxes). The model was of two episodes of gas gain and gave a blocking age of 2693 Ma. Note that all model results fit within the 1σ error boxes of the experimental results.*

An estimation of the temperature of each laser-heating step is made with a Barnes Engineering RM-2A infrared microscope. The microscope is calibrated for blackbody radiance, so a correction must be made by measuring the emissivity of each mineral grain (through the sapphire window) at low temperature (about 150°C) and assuming that this is constant at higher temperatures. Hornblendes typically have emissivities that are 90% that of blackbody and biotites have 70%, although there can be emissivity variations between grains from the same sample by as much as 20%. During laser heating, the infrared radiance of the samples is monitored and an apparent "temperature" is calculated from that after applying the emissivity correction. At 900°C the temperature resolution is about 3°C. This measurement of apparent temperature allows for selection of a prudent heating schedule which maximizes spectral resolution.

Samples are heated by the laser through a sapphire window with a beam size larger than the grain to ensure uniform heating. The gas fraction is purified with a liquid-nitrogen cold trap, degassed Ti sponge (at room temperature), and an SAES GP50W getter with ST101 zirconium-aluminium alloy operated at 400°C. Each step of a mineral-grain's, stepwise laser-heating experiment takes only 15 minutes and consists of the following: a) 30 second heating by the laser at a specific radiance ("temperature"); b) three minutes of gettering; c) inletting of the fraction into the mass spectrometer and waiting for equilibrium to be attained (60 seconds); and d) measuring the five argon isotopes (^{35}Ar, ^{37}Ar, ^{38}Ar, ^{39}Ar, and ^{40}Ar) by peak hopping (eight scans take about ten minutes).

Following data collection, the next heating step is done. The inlet-system background is monitored frequently (about every fourth step) and the background values are subtracted from the fractions that follow it. Using this procedure, a 20 to 25 step run can easily be completed in a working day.

RESULTS

TROUT LAKE BATHOLITH

U-Pb dating of the Trout Lake Batholith (Walsh Lake site) was performed by S. Noble in T. Krogh's laboratory at the Royal Ontario Museum. Zircon and sphene give an age of 2600±2 Ma (Andrews *et al.* 1986; S. Noble, PhD candidate, Department of Geology, University of Toronto, personal communication 1986). ^{40}Ar/^{39}Ar analyses were performed on hornblende, biotite, and potassium feldspar from the same site.

The hornblende-sample age spectrum (Figure 233.2), obtained by step heating a bulk sample 40 mg in size, shows excess argon in the initial and final fractions. Although the spectrum is complicated, it is rather orderly. As the effects of the excess argon diminish, the higher temperature fraction ages approach the U-Pb age. Mathematical modeling was performed on over 90% of the gas derived from the hornblende sample (fractions 2-11; Figure 233.3). The model, which was based on diffusion theory, consists of two pulses of gas gain, and yields a blocking age of 2693 Ma. As can be seen in Figure 233.3, all of the model ages fit within the 1σ error of the experimentally generated ages. This close similarity of the zircon, sphene, and hornblende ages implies that the Trout Lake Batholith apparently underwent very rapid initial cooling through the blocking temperatures of these minerals.

The age spectrum determined from a bulk sample of biotite from the Trout Lake Batholith shows a much younger age, plateauing at ~2600 Ma (Figure 233.4a). The grains in this grain-size separate were small (125 to 250 μm in diameter). A single grain from this size fraction was used in laser analysis. This grain was roughly 250 μm across and 24 fractions were extracted from it. A second grain, 1000 μm

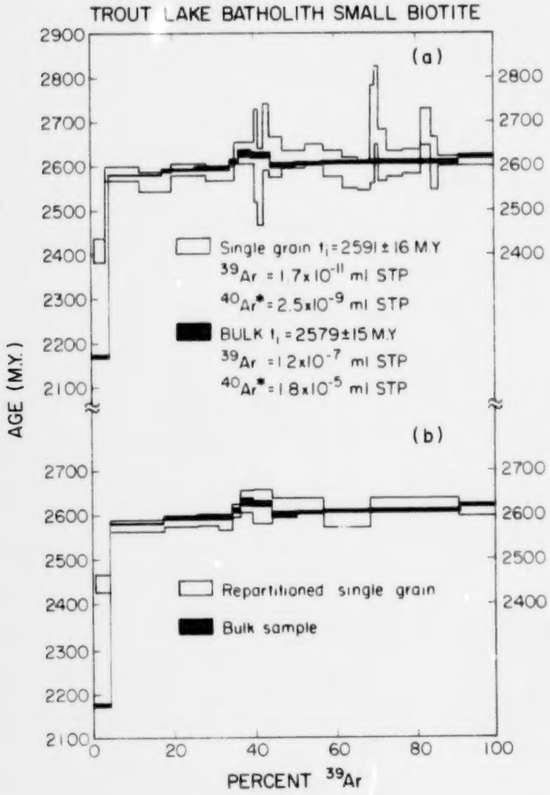

Figure 233.4. *(a) Bulk-sample spectrum (black) and single-grain spectrum (white) of 125 to 250 μm sized biotite grain from the Trout Lake Batholith. (b) Same as (a), however, the single-grain spectrum (white) has been repartitioned to the same percent ^{39}Ar steps as the bulk sample (black).*

in diameter, taken from the same hand sample was also analyzed to see if there was some relationship between grain size and plateau age. In Figure 233.4a, the authors show on the same graph, the age spectrum derived for this mineral, when analyzed in the traditional bulk way, and its age spectrum as generated by the laser.

As may be seen in Figure 233.4a, the bumpy feature of the bulk sample appears to be present in the single grain, although the far more detailed laser run may show significantly more spectral structure at higher temperatures. To make the comparison more realistic, the authors have repartitioned the gas release in the laser data so that the ^{39}Ar-step sizes are identical to those used in the bulk run. The result is shown in Figure 233.4b where a striking agreement may be seen between the laser spectrum and the conventionally derived bulk spectrum. This good agreement indicates consistency of both age and argon distribution among members of this grain-size separate.

The authors then step heated the much larger biotite flake whose mass was ~70 times the mass of the first biotite grain. In fact, it can be seen in Figure 233.5 that the age spectrum of the large grain (38 fractions) is systematically raised above the bulk (and the laser spectrum of the smaller grain) by ~70 Ma. The ages corresponding to the final 45 percent of the ^{39}Ar release from the large grain scatter about an integrated age (for this high-temperature segment) of ~2670 Ma, which approaches (within 1 percent) the concordant U-Pb age of 2600±2 Ma and the hornblende age of 2693 Ma derived from the modeling. Evidently, the larger biotite grains became closed for argon diffusion much earlier than the smaller ones in the cooling history of this body (Trout Lake Batholith), or, alternatively, they proved to be significantly more resistant to argon loss in any later events.

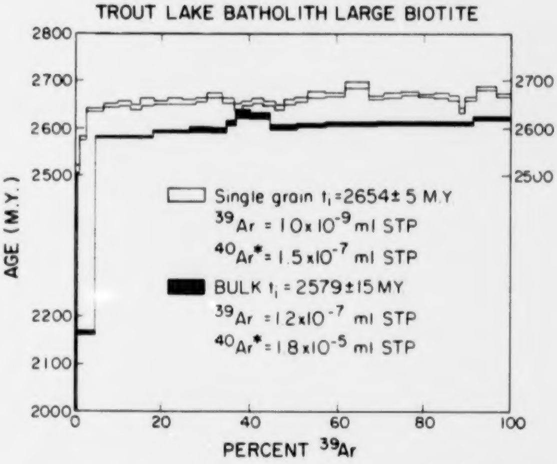

Figure 233.5. *Bulk-sample age spectrum (black) of 125 to 250 μm diameter biotite grain and the single grain age spectrum (white) for a large (~1000 μm diameter) biotite from the Trout Lake Batholith. Both size fractions are from the same hand sample.*

Evidently, the initial rapid cooling rate through the zircon, sphene, and hornblende blocking temperatures decreased somewhat since it took roughly 30 Ma for the large biotite to reach its blocking temperature, while another 70 Ma passed before the smallest biotite grains blocked.

HAMMELL LAKE BATHOLITH

U-Pb dating was performed by N.D McMaster (in T. Krogh's laboratory at the Royal Ontario Museum) on three zircon and two sphene fractions from the Hammell Lake Batholith. The resulting concordia plot, shown in Figure 233.6, yielded an age of 2717± 1.5 Ma, with both zircon and sphene giving effectively identical ages. ^{40}Ar/^{39}Ar analyses were performed on hornblende, biotite, and potassium-feldspar bulk samples from the same Hammell Lake site.

The hornblende age spectrum, shown in Figure 233.7, is reminiscent of the hornblende age spectrum for the Trout Lake Batholith; namely, with excess argon occurring at both ends of the spectrum. The

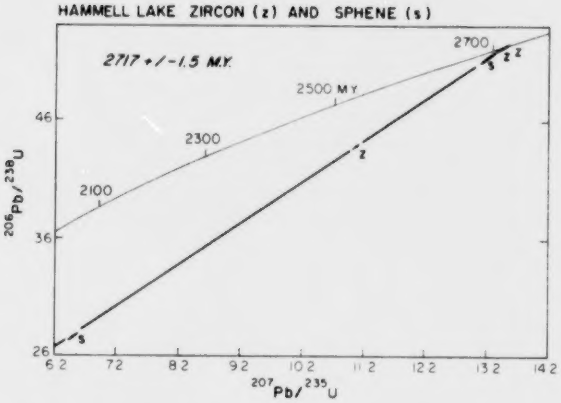

Figure 233.6. *U-Pb concordia diagram for three zircons and two sphenes from the Hammell Lake Batholith.*

Hammell Lake age spectrum, however, does show a small amount of argon loss in the first fractions. In this case, as the effects of the excess argon diminish, the high-temperature age fraction falls slightly lower than the U-Pb age of 2717 Ma.

Mathematical modeling of over 88% of the gas released (fractions 2-11; Figure 233.8) from the Hammell Lake hornblende gave a blocking age of 2702 Ma. This age is higher than that of the Trout Lake Batholith hornblende. This is perhaps not surprising since the Hammell Lake zircon and sphene ages are higher than those from the Trout Lake Batholith. The model used was that of a one-pulse gas gain (responsible for the excess argon) followed by a gas-loss event that produced the argon loss seen in the first fractions. The loss event was modeled at 2092 Ma, when about 0.6% of the total argon was lost. The gas-gaining event could have occurred any time between the time of formation of the hornblende, and the gas-loss event. In this case, all but one model age falls within 1σ error of the experimental results. As with the Trout Lake Batholith, the close similarity in age between the zircon, sphene, and hornblende, suggests rapid initial cooling of the Hammell Lake Batholith.

Biotite, from the same site as the other samples, gives a beautiful age spectrum (Figure 233.9). This near perfect plateau creeps up to give a high-temperature age of 2642± 5 Ma. The grain size of the fraction used in this bulk analysis (250 to 500 μm) was larger than that used with the Trout Lake Batholith. Laser analysis of one of the largest grains from this population shows a spectrum with a similar shape to the bulk spectrum (Figure 233.9); however, it has an integrated age 17 Ma older than the bulk-integrated age. The high-temperature age approaches 2680 Ma, much closer to the zircon, sphene, and hornblende ages. As with the Trout Lake Batholith, after the initial rapid cooling of zircon, sphene, and hornblende at roughly 2700 Ma, the cooling process slowed down and took about 60 Ma to pass through the blocking temperature of the bulk of the biotite.

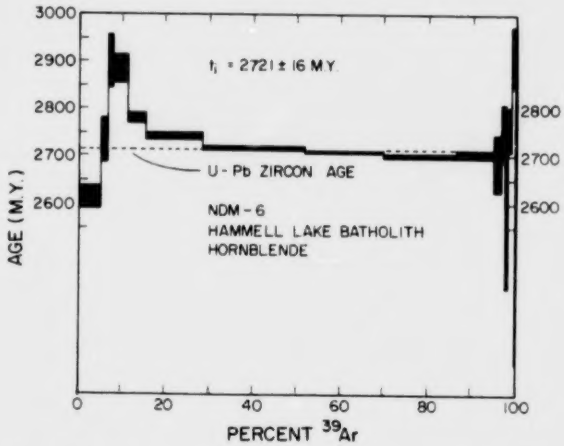

Figure 233.7. *Age spectrum of the Hammell Lake Batholith hornblende. Dashed line represents the U-Pb age at the same site.*

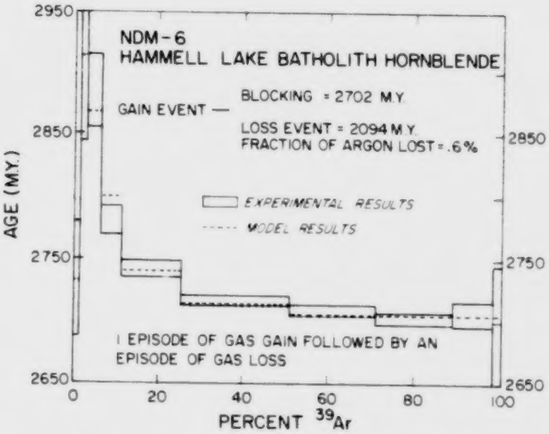

Figure 233.8. *The mathematically modeled segment of the hornblende spectrum from the Hammell Lake Batholith (dashed) superimposed on experimental results (shown by their ±σ error boxes). The model was of one episode of gas gain followed by an episode of gas loss and gave a blicking age of 2702 Ma. The loss event was modelled at 2092 Ma with a loss of only 0.6 percent of the total argon. All but one of the model results fit within the 1σ error boxes of the experimental results.*

KILLALA-BAIRD BATHOLITH

Six individual grains of biotite, 250 to 500 μ m in diameter, from a single hand sample were step heated with the laser-fusion system. The results are shown in Figure 233.10. Although the integrated ages are within 2% of each other and they plateau at ~2650 Ma, it can be seen that there are definite differences between the age spectra. As in the Trout Lake Batholith, the larger grains seem to record dif-

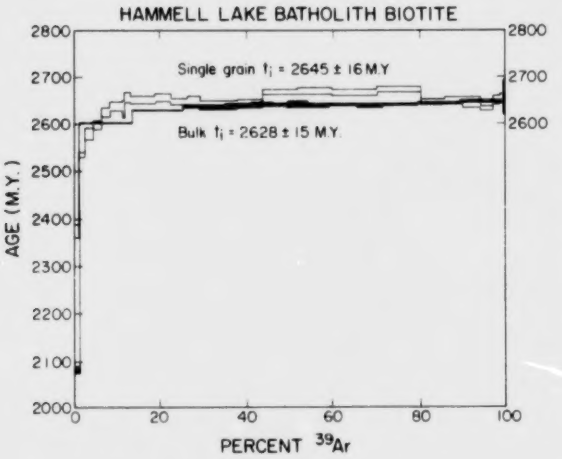

Figure 233.9. *Bulk sample age spectrum (black) of 250-500 μm diameter biotite grain, and the single grain age spectrum (white) of a 500 μm diameter biotite grain from the Hammell Lake Batholith. Both size fractions are from the same hand sample.*

ferent thermal histories than do the smaller grains. These grains apparently act as individual clocks recording their own perspective of the thermal history of the area. The plateau values seen in grains a, b, c, and e approach 2650 to 2660 Ma, again very close to the zircon age of 2704±2 Ma (Andrews *et al.* 1986).

The use of the laser as a microprobe for calcium and potassium also reveals vast differences in the ratio of these elements between grains, as can be seen in Figure 233.11. The difference is especially pronounced between samples b and c. While their total calcium-potassium ratios differ by a factor of 20, which is indicative of very different compositions, their integrated ages are identical within error and they have similar spectral shape.

DOME STOCK

The Dome Stock, in the centre of the Red Lake Greenstone Belt, has a zircon age of 2718±2 Ma (Andrews *et al.* 1986). Separates from the interior and sheared margin of the stock have been measured in laser step-heating experiments. The sample from the pluton's interior was taken from a fresh, blasted outcrop and no signs of alteration were seen. Fresh, unaltered biotite grains were extracted from the sample and measured 250 to 500 μm in diameter. Two grains were step heated and behaved consistently. Both showed some diffusional loss at low temperature, but reached plateaus of 2641±1 Ma and 2647±3 Ma for the last 60% of gas released.

In contrast, the sample from the sheared margin, (from the Flat Lake-Howey Bay Deformation Zone, in the Town of Red Lake), is highly altered and no biotite was identified. Small clumps of sericite and chlorite were measured by laser step heating. Two samples showed much more argon loss at low temperatures, and, in both cases, stable plateaus were not reached until a high temperature was achieved. Plateau ages of 2543±3 and 2632±3 Ma were obtained for only the last 40% of the age spectra. X-ray diffraction experiments currently underway by S. Marmont (Geologist, Ontario Geological Survey, Toronto) will hopefully identify the composition of these alteration-product minerals.

Although the results are only very preliminary, it is possible that the difference in ages between the interior and margin of the Dome Stock may reflect the alteration and shearing of the marginal zone; further work may allow the authors to date this deformation.

SUMMARY

^{40}Ar/^{39}Ar dating combined with U-Pb dating has provided valuable information on the cooling histories of the Trout Lake and Hammell Lake Batholiths. In both cases, after initial rapid cooling at ~2700 Ma through the blocking temperatures of zircon, sphene, and hornblende, as seen in the close similarity in the ages of the minerals, the cooling rate apparently decreased, and it took roughly 100 Ma, in the case of the Trout Lake Batholith, and 60 Ma, in the case of the Hammell Lake Batholith, to pass through the blocking temperature of the biotites.

The significant shift to higher ages seen in the spectra of the Trout Lake Batholith biotite, in going from a small (250 μm diameter) to a large (1000 μm diameter) grain (*see* Figures 233.4a and 233.5), suggests that similar variations may be found elsewhere. If this proves to be the case, single-grain dating will significantly enhance the information available for deducing the thermal history of an area.

The use of a laser makes automation of the whole ^{40}Ar/^{39}Ar method far simpler and more flexible in prospect than would ordinarily be the case. The authors expect to have such a fully automated system in use shortly. With such a system, the output will be dramatically increased. Projects such as the extensive Red Lake project, previously neglected because of their potential labor-intensity, will become feasible.

The authors, based on the results shown here, deduced that good-quality, single-grain age spectra can be obtained from biotite. Given sufficient potassium content and grain size, there would appear to be no lower limit to the age of single mineral grains that can be step heated. Laser analyses are currently underway on hornblendes and potassium-feldspar grains from both the Killala-Baird Batholith and the Dome Stock to compliment the biotite work that has been completed.

Information obtained thus far, in this Ontario Geological Survey supported project, has precisely constrained the age of gold at Timmins to be between 2633 Ma and 2670 Ma at the Dome Mine, and to be between 2617 Ma and 2688 Ma at the Hollinger Mine. An age range of 2671 Ma to 2681 Ma makes Hemlo the most precisely dated Archean gold deposit in Canada (and perhaps in the world). While the Red Lake gold emplacement is not as well constrained, the current study of the thermal history of this area should offer new insights to better constrain the age

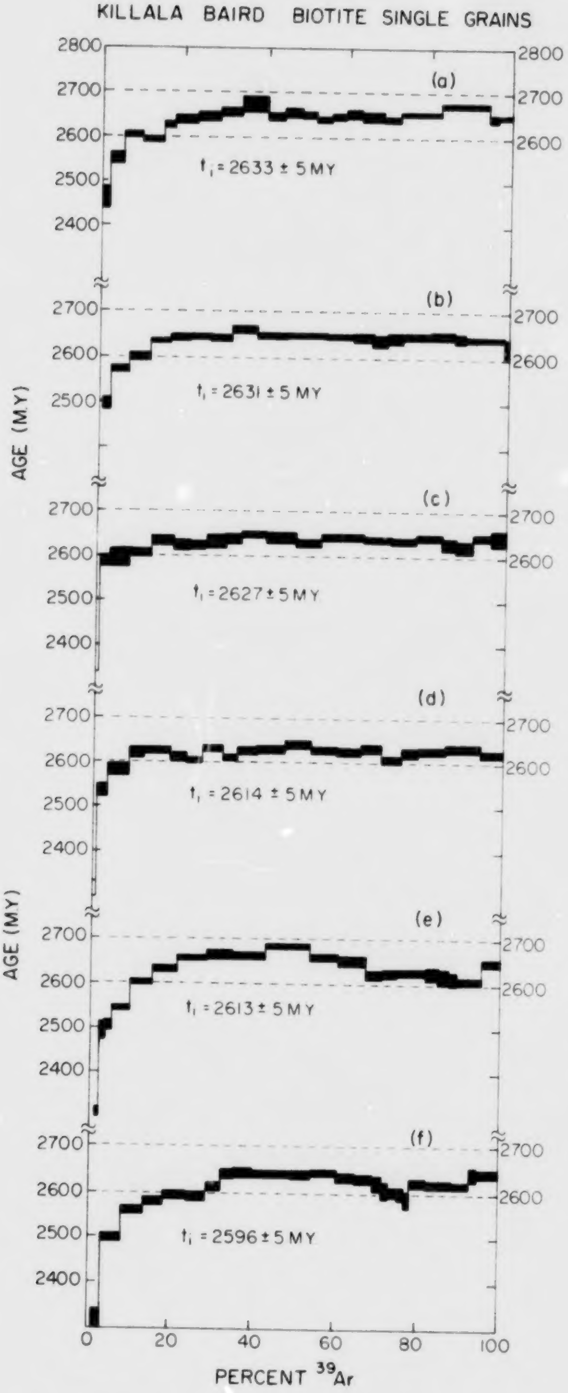

***Figure 233.10.** Laser generated age spectra for six biotite grains from the Killala-Baird Batholith. The dashed lines at 2600 Ma and 2700 Ma on each spectrum are for reference.*

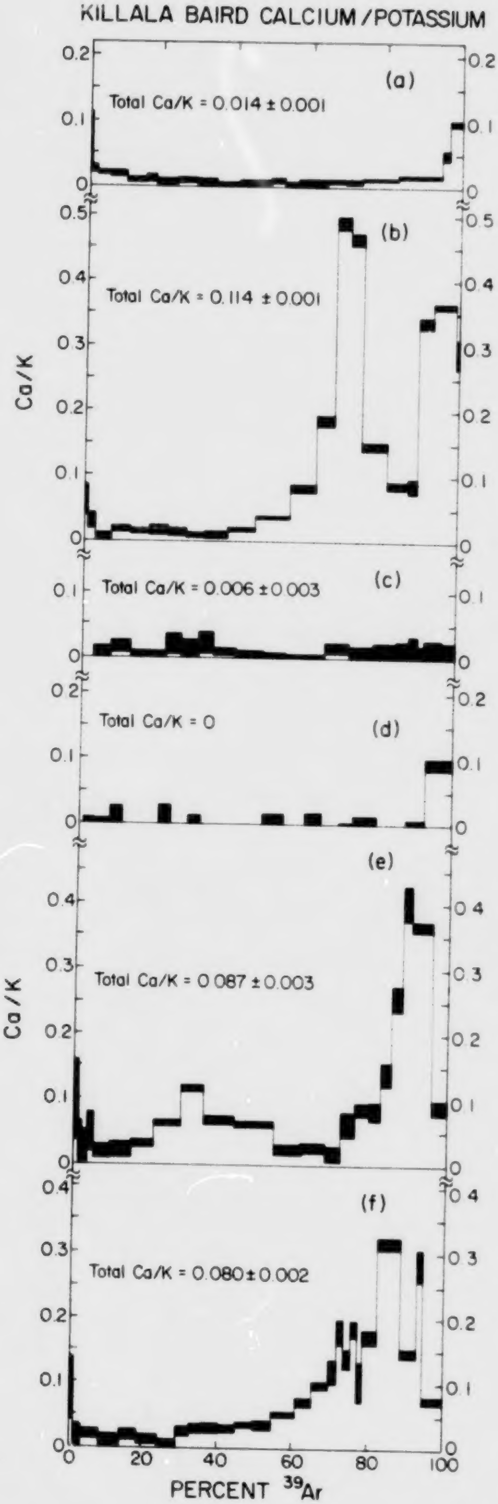

***Figure 233.11.** Calcium-potassium ratio spectra for the six biotite grains whose age spectra are shown in Figure 233.10.*

of gold emplacement in this economically important area.

ACKNOWLEDGMENTS

We are grateful to Dr. C.M. Hall (Research associate, University of Toronto, Toronto) and W.J. Kenyon (Technician, University of Toronto, Toronto) for assistance in the laboratory, and to Steve Noble (PhD candidate, Department of Geology, University of Toronto, Toronto) for providing samples of the Trout Lake Batholith. This research has been supported by grants to Derek York from the Ontario Geological Survey, the Natural Sciences and Engineering Research Council of Canada, and Texaco U.S.A.

REFERENCES

Andrews, A.J., Hugon, H., Durocher, M., Corfu, F., and Lavigne, M.J.
1986: The Anatomy of a Gold-bearing Greenstone Belt: Red Lake, Northwestern Ontario, Canada; p.3-22 *in* Proceedings of Gold '86, an International Symposium on the Geology of Gold: Toronto, 1986, Macdonald, A.J. ed., 517p.

Bray, C.J., Spooner, E.T.C., Hall, C.M., York, D., Bills, T.M., and Krueger, H.W.
1987: Laser probe ^{40}Ar/^{39}Ar and conventional K-Ar Dating of Illites Associated with the McClean Unconformity-related Uranium Deposits, North Saskatchewan, Canada; Canadian Journal of Earth Sciences, Volume 24, p.10-23.

Corfu, F., and Wallace, H.
1986: U-Pb Ages for Magmatism in the Red Lake Belt, Northwestern Ontario; Canadian Journal of Earth Sciences, Volume 23, p.27-42.

Layer, P.W., Hall, C.M., and York, D.
1987: The Derivation of ^{40}Ar/^{39}Ar Age Spectra of Single Grains of Hornblende and Biotite by Laser Step Heating, Geophysical Research Letters, in press.

Masliwec, A., McMaster, D., and York, D.
1986: The dating of Ontario's Gold Deposits; Grant 233, p.107-114 *in* Geoscience Research Grant Program, Summary of Research, 1985-1986, edited by V.G. Milne, Ontario Geological Survey, Miscellaneous Paper 130, 235p.

York, D., Hall, C.M., Yanase, Y., Hanes, J.A., and Kenyon, W.J.
1981: ^{40}Ar/^{39}Ar Dating of Terrestrial Minerals with a Continuous Laser, Geophysical Research Letters, Volume 8, p.1136-1138.

Grant 236 Au–Quartz Vein and Cu–Au–Ag–Mo–Anhydrite Mineralization, Hollinger–McIntyre Mines, Timmins, Ontario: $\delta^{13}C$ Values (McIntyre), Fluid Inclusion Gas Chemistry, Pressure (Depth) Estimation, and H_2O– CO_2 Phase Separation as a Precipitation and Dilation Mechanism

E.T.C. Spooner, C.J. Bray, P.C. Wood, D.R. Burrows, and N.J. Callan

Department of Geology, University of Toronto, Toronto

ABSTRACT

Carbon isotope analyses indicate that carbonate associated with Au-quartz vein mineralization in the McIntyre Mine is isotopically similar to that from the Hollinger Mine (-3.3±0.4‰ (1σ), n=8; compare to -3.0±1.5‰ (1σ), n=14)(σ=standard deviation, n= number of samples), and that carbonate in altered albitite dikes (-3.1‰, -2.8‰) is isotopically similar to that associated with the gold mineralization.

The following gases have been detected in primary and strain-related secondary inclusions in quartz and scheelite from the Hollinger and Renabie Mines using a zero blank, high temperature (~105°C) crushing system attached directly to the inlet system of a Hewlett Packard 5890 gas chromatograph, with a Porapak Q packed column at 50°C and a thermal conductivity detector: (N_2±CO±Ar±O_2±NO), NO, CH_4, CO_2, N_2O, C_2H_6, and H_2O (in order of retention time). CH_4/(CH_4+CO_2) molar ratios decrease upwards in the Hollinger Mine from 18.00±7.35% (n = 6; 1500- and 1800-foot levels) to 1.37±0.81% (n = 5; surface; 200- and 800-foot levels). This decrease is interpreted to be a result of progressive H_2O-CO_2 phase separation reflecting the high gas/liquid partition coefficient of CH_4 (Drummond and Ohmoto 1985). The fact that the ratios decrease to values similar to those found in the Renabie Mine (1.07±0.35%; n = 6) which, in contrast, consists of an oxidized Archean Au-quartz vein system (anhydrite; negative $\delta^{34}S$), is evidence for H_2O (liquid) oxidation by reduced gas (H_2, CH_4, H_2S) loss during H_2O-CO_2 phase separation; a possible mechanism for the generation of oxidized Archean Au-quartz and Cu-Au-Ag-Mo-anhydrite vein systems.

Samples from close proximity to graphitic material from surface show clear, relative CH_4 increases to CH_4/(CH_4+CO_2) ratios of 5.94-16.56% confirming carbon isotope exchange with CH_4 as a mechanism for producing isotopically less negative carbonate in association with graphitic interflow material (e.g. Fyon *et al.* 1983).

Very approximate pressure and depth estimates for the upper part of the Hollinger Mine, based on fluid inclusion properties, P-T (pressure/temperature) sections through the H_2O-NaCl-CO_2 immiscibility volume (Gehrig *et al.* 1979), and evidence for lithostatic fluid pressure are 500+200/-300 bars and 1.9+0.8/-1.1 km respectively.

H_2O-CO_2 phase separation, fluid inclusion evidence for which has been described from the Hollinger-McIntyre and Pamour #1 Deposits and several deposits in Western Australia (Groves *et al.* 1984; Walsh *et al.* 1984; Wood *et al.* 1984, 1986a; Ho *et al.* 1985) can, together with other factors, explain several features of Archean Au-quartz vein systems including:

1. coprecipitation of Au-Ag, pyrite, and other sulphide minerals
2. coprecipitation with carbonate (e.g. Arnórsson 1978)
3. mineralization over large vertical intervals of ~1000 m to as much as 3230 m (Kolar, India)
4. generation of oxidized Archean Au-quartz and Cu-Au-Ag-Mo-anhydrite systems by loss of reduced gas species (H_2, CH_4, H_2S)
5. hydraulic fracturing
6. volumetric inflation, including dilation of shear zones (e.g. the Renabie Mine) and expansion from relatively insignificant root zones (based significantly on the work of Drummond and Ohmoto 1985).

Significant quartz precipitation can only signify a temperature drop, for temperatures less than the solubility maximum (~385°C at 500 bars).

INTRODUCTION

This report is a continuation of two published previously (Spooner *et al.* 1985; Wood *et al.* 1986b) and three recent papers (Burrows and Spooner 1986; Burrows *et al.* 1986; Wood *et al.* 1986a) which discuss various aspects of the geological characteristics and geochemistry of the Hollinger-McIntyre Au system. The main objectives of this report are:

1. to present and discuss carbonate $\delta^{13}C$ values from Au mineralization in the McIntyre Mine to improve coverage of the Hollinger-McIntyre system as a whole, and to discuss the $\delta^{13}C$ values of carbonate from altered albitite dikes and carbonate associated with graphitic material
2. to present and discuss the results of gas chromatographic analysis (HP 5890) of fluid inclusion gases released by a hot (~105°C) crushing technique from quartz (~1.5 g) and scheelite (~2.5 g) from the Hollinger Mine
3. to discuss a method based on a H_2O-CO_2 phase separation for estimating the approximate pressure and depth of formation of the Hollinger-McIntyre system
4. to discuss H_2O-CO_2 phase separation, which is indicated from fluid inclusion observations

TABLE 236.1. δ^{13}C VALUES FOR CARBONATE ASSOCIATED WITH Au-QUARTZ VEIN MINERALIZATION, McINTYRE, CARBONATE FROM ALTERED ALBITITE DIKES, AND CARBONATE ASSOCIATED WITH GRAPHITIC MATERIAL.

Sample Number	Sample Description	δ^{13}C (%o; PDB)
Au-QUARTZ VEIN MINERALIZATION		
M28 - S510 (v)	Ankerite-quartz-chalcopyrite-Au vein from within albitite dike; 2800′ level.	- 3.2
M36 - S241 (v)	Ankeritic carbonate vein in mafic flow; 3600′ level.	- 3.7
M36 - S243 (v)	Ankeritic carbonate vein in mafic flow; 3600′ level.	- 3.1
M36 - S243 (w)	Altered wall-rock; as above.	- 3.3; - 3.4
M38 - S219 (v)	Ankeritic carbonate vein in mafic volcanics; 3800′ level.	- 4.0
M38 - S219 (w)	Altered wall-rock; as above.	- 3.3
M38 - S293 (v)	Ankeritic vein carbonate; 3800′ level	- 2.6
M38 - S294 (v)	Ankeritic vein carbonate; 3800′ level	- 3.0; - 2.7
$\bar{x} \pm \sigma$	8 McIntyre values	- 3.3 ± 0.4
$\bar{x} \pm \sigma$	14 Hollinger values	- 3.0 ± 1.5
$\bar{x} \pm \sigma$	22 Hollinger/McIntyre values	- 3.1 ± 1.2
ALTERED ALBITITE DIKES		
M23 - S265a	Altered albitite dike; 2300′ level	- 3.1
M38 - 194	Albitite dike; 3800′ level	- 2.8
CARBONATE ASSOCIATED WITH GRAPHITIC MATERIAL		
H12 - S159a (v)	Carbonate from vein hosted in graphitic interflow unit. 1200′ level, Hollinger	- 2.9; - 2.6
H12 - S159b (v)	Graphitic interflow unit; mixture of carbonate and graphitic material. 1200′ level, Hollinger — carbonate	- 1.1
	— graphitic material	- 23.4; - 23.5

δ^{13}C analyses were carried out at the Isotope Lab., Department of Earth Sciences, University of Waterloo, Waterloo, Ontario N2L 3G1 by standard techniques. The estimated routine uncertainty is ± 0.2 %o (1σ). All samples from McIntyre unless otherwise stated.

(Wood *et al.* 1986a), as a mineral precipitation (e.g. Au-Ag, pyrite, carbonate), fluid oxidation, hydraulic fracturing, and shear zone dilation mechanism in Archean Au-quartz vein/shear zone systems

CARBONATE δ^{13}C VALUES, McINTYRE MINE

CARBONATE ASSOCIATED WITH Au-QUARTZ VEIN MINERALIZATION

δ^{13}C values for eight samples from the 2800-, 3600-, and 3800-foot levels of the McIntyre Mine (Table 236.1) have been determined in order to broaden coverage of the Hollinger-McIntyre system as a whole, since data from the McIntyre Mine have previously been lacking. Compared to the Hollinger data (-4.8 to -0.1‰; Wood *et al.* 1986a), the range of 1.4‰ from -4.0 to -2.6‰ (Table 236.1) is distinctly less, because less negative values are lacking. However, the arithmetic means are very similar at -3.3±0.4 (1σ)‰ for the McIntyre Mine and -3.0±1.5‰ for the Hollinger Mine (Wood *et al.* 1986a). Hence, the weighted mean δ^{13}C value for the Hollinger-McIntyre system is -3.1±1.2‰ (n=22).

CARBONATE FROM ALTERED ALBITITE DIKES

The altered albitite dikes discussed by Wood *et al.* (1986b) are distinctive in having high, secondary carbonate contents reflected in high CO_2 contents of 10.7% (Sample M23-S265a) and 11.5% (Sample M38-194). Hence, the δ^{13}C values of this carbonate have been determined for comparison with the Au-quartz vein and altered wall rock values. The two values of -3.1‰ and -2.8‰ (Table 236.1) lie on, and within, 0.3‰ of the revised mean value for mineralization (*see* above). Hence, the sources of the altered albitite and Au-quartz vein related carbonate are, presumably, the same.

CARBONATE ASSOCIATED WITH GRAPHITIC MATERIAL

Fyon *et al.* (1983) have presented carbon isotope data which indicate that Au-quartz vein carbonate associated with graphitic material is less negative than other carbonate. For example, 30 determinations from the #55 and #68 open pits at the Hollinger Mine average -0.6±0.5‰. Wood *et al.* (1986a) have presented two determinations of -1.1‰ and -1.0‰ from the #55 pit which are consistent with these data. In addition, data for two graphite-related samples are given in Table 236.1. One from a vein (Sample H12-S159a) shows a normal ^{13}C value of -2.8‰. However, the other from an intimate carbonate-graphite mixture (Sample H12-S159b) shows a distinctively less negative ^{13}C value of -1.1‰, consistent with Fyon *et al.*'s (1983) observations.

Interaction with graphitic material may modify carbonate δ^{13}C values in two possible ways; through direct contamination with graphitic carbon and/or through isotope fractionation with produced CH_4. The former cannot be the case, because Superior Province interflow graphitic material is isotopically negative, typically being between -35‰ and -20‰ (Schoell and Wellmer 1981), whereas the graphite associated carbonate is less negative. This relationship has been specifically confirmed in the case of Sample H12-S159b by analysis of the associated graphitic material giving duplicate δ^{13}C values of -23.5‰ and -23.4‰ (Table 236.1), exactly in Schoell and Wellmer's (1981) range. On the other hand Δ^{13}C CO_2-CH_4 at 280°C, the estimated mineralization temperature for the Hollinger-McIntyre system (Wood *et al.* 1986a), is +26‰ (Friedman and O'Neil 1977), the CH_4 being isotopically lighter. Hence, carbon isotope exchange between CO_2 and produced CH_4 would produce significantly more negative CH_4, and consequently less negative CO_2, which is exactly the observed trend. Gas chromatographic analysis of fluid inclusions in quartz associated with graphitic material show this predicted increase in the $CH_4/(CH_4+CO_2)$ ratio (*see* below), and therefore confirm this mechanism. Hence, CH_4/CO_2 carbon isotope partition must have occurred, a process about which there is significant debate (e.g. Drummond and Ohmoto 1985).

FLUID INCLUSION GAS CHEMISTRY

The chemistry of gases in fluid inclusions can provide information on species present, fluid conditions (e.g. fO_2), and fluid sources. Preliminary data, particularly $CH_4/(CH_4+CO_2)$ molar ratios, have been obtained from material from the Hollinger Mine containing best primary inclusions, dominantly secondary inclusions, and from close to graphitic material.

METHOD AND ANALYTICAL CONDITIONS

Carefully selected quartz and scheelite samples were first crushed in a jaw crusher and percussion mortar, and ~1.5 to 5 mm fragments hand-picked for further work. These separates were then cleaned in 25% HNO_3 for at least 1 hour at ~40°C, and then washed 3 to 4 times in deionised water then acetone, and allowed to air dry. Approximately 1.5 g of quartz or ~2.5 g of scheelite were loaded into a stainless steel (#316) crusher connected directly to the inlet system of a Hewlett Packard 5890 gas chromatograph equipped with a high sensitivity thermal conductivity detector. The crusher is a modified version of the design described by Andrawes and Gibson (1979). The main differences are that a 1.9 cm diameter piston, instead of a 1 cm, is used to take a larger sample size, the upper chamber is detachable from the crushing chamber to improve cleaning, and a completely separate helium supply is connected to the upper chamber. The crushing chamber is heated by two cartridge heaters inserted in cylindrical holes located on either side and below the sample position. After the crusher has been loaded, helium carrier gas is passed through the crushing chamber for ~15 hours (i.e. overnight) and heated on a timer for ~5 hours at 105°C. Helium is passed through the upper chamber at a low flow rate of <1 cm^3/min over the same time period. This procedure ensures that there is no air retained in the crusher or in the upper chamber, and that all absorbed H_20 and other gases have been removed from the sample and crusher walls.

In preparation for an analysis, the exhaust valve on the upper chamber is closed, and the helium pressure increased to 20 pounds per square inch (psi). The helium carrier gas flow rate through the crusher to the gas chromatograph is adjusted to 19.4 (±0.1) cm^3/min and the reference flow set to 50.0 (± 0.4) cm^3/min. These flow rates are recommended by Hewlett Packard to give the best sensitivity using packed columns. The pressure in the crusher is ~30 psi so that any gas leakage is out of, rather than into, the crushing chamber. The sample is crushed at 105°C to ensure instant volatilization of H_2O, a high internal fluid inclusion pressure, and to prevent gas adsorption on freshly broken mineral surfaces (e.g. Barker and Torkelson 1975) and the crusher walls, but not to cause gas reactions which might take place at a higher temperature. The crusher is positioned within a stainless steel frame containing a hydraulic ram connected to a hydraulic piston cylinder. The sample is first given a weak crush, equivalent to approximately a quarter of a full stroke on the hydraulic piston, in order to disaggregate it and reduce its total volume in preparation for the main crushes. The crush strokes must be sharp and sudden so that fluid inclusion gases are released into the helium carrier gas stream in bursts equivalent to usual syringe injections. This procedure is very successful as the chromatograms, discussed below, show. The pressure gauge on the hydraulic ram for the first crush registers anywhere between 0 and 300 psi, usually 0 psi. After all the gases from the first weak crush have been analyzed, the sample is given a full crush to a pressure typically between 2000 and 3000 psi. Successive third, and sometimes fourth, crushes give a final pressure of ~7000 psi. After crushing, the sample is a fine powder containing a few small, uncrushed fragments. It is estimated that ~80 to 90% of the contained gases are released. A great advantage of this approach is that more than one gas analysis, typically two to four, is obtained on individual sample aliquots (*see* below). Using this method, the system has a zero blank for all gases at the current detection limits as determined by sequen-

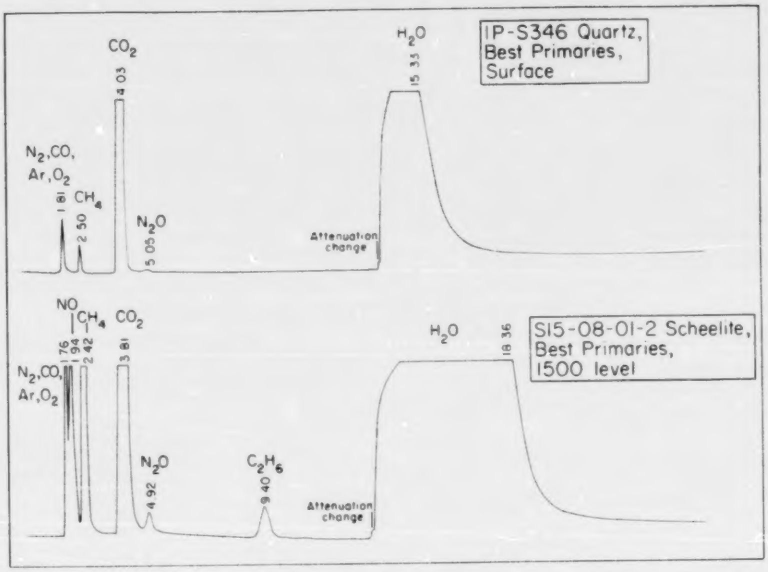

Figure 236.1. *Gas chromatograms of fluid inclusion gases released by crushing at ~105°C. Note the low CH_4 relative to CO_2 in the surface sample (1P-S346), the very minor N_2O, and no detectable NO or C_2H_6. In the sample from the 1500- foot level (S15-08-01-2), note the well-defined peaks for NO, N_2O, and C_2H_6. Numbers by peaks are retention times in decimal minutes.*
Sample weights: ~1.5 g (quartz) and ~2.5 g (scheelite) crushed, sieved to ~1.5 to 5 mm and cleaned. Gas chromatograph: Hewlett Packard 5890 with a 3392 integrator. Detector: TCD. Column: 6 foot by 1/8 inch Porapak Q at 50°C. Flow rates: 19.4±0.1 cm^3/min (He carrier) and 50.0±0.4 cm^3/min (reference).

tial crushing of Brazilian quartz preheated to 900°C for four hours. Preheating of Brazilian quartz was necessary to eliminate an H_2O peak caused, presumably, by the presence of fluid inclusions.

For the results reported here, the gases were analyzed using a 6 foot by 1/8 inch (1.83 m by 3.18 mm) column of acetone-washed Porapak Q kept at 50°C in order to reduce tailing of CO_2 by adsorption at ~25°C (very successful) and to elute H_2O in a reasonable length of time (~20 minutes). The thermal conductivity detector was kept at 120°C. The advantage of using Porapak Q is that the three key gases, CH_4, CO_2, and H_2O (*see* Figure 236.1) are cleanly separated. The principal disadvantage is that N_2, CO, Ar, and O_2 co-elute and overlap (?) NO (*see* Figure 236.1). The former gases will be separated and analyzed using a molecular sieve column in the future. Gas peaks are identified by comparison of observed retention times with retention times of gases in standard gas mixtures. Moles of gases released are determined from areas under peaks calculated by a Hewlett Packard 3392 integrator for standards and unknowns. The linear behaviour of the thermal conductivity detector has been checked for CH_4, CO_2, and H_2O and found to be very satisfactory. Successive crushes of an unknown, and standards, typically take ~5 to 6 hours to complete.

SAMPLES

Twenty samples from the Hollinger Mine and five samples from Au-quartz vein mineralization from the Renabie Mine area, 80 km northeast of Wawa, were chosen for analysis in the first instance (*see* Table 236.2). Eight of the Hollinger Mine samples were selected as they contain the best primary inclusions; three quartz from the surface, one quartz and one scheelite from the 15 level, and three scheelite from the 18 level. Four Hollinger Mine quartz samples were selected as they contain typical strain-related secondary inclusions from the 2, 8, 17, and 27 levels, and the final four Hollinger Mine quartz samples are from close proximity to graphitic material to look for chemical interaction effects.

Renabie Mine material is characterized by secondary inclusions reflecting the ubiquitous syn- and postmineralization strain (Callan and Spooner, this volume). Samples were chosen from the main zone on the 3265-foot level, the D extension part of the main zone on the 1400-foot level, the Nudulama zone on the 1400-foot level, a MoS_2 bearing shallow dipping quartz vein crosscutting the main vein structure on the 3105-foot level, and a glassy quartz-pyrite-anhydrite-MoS_2 vein near the main shaft on the 3105-foot level.

GASES DETECTED

The composite N_2+CO+Ar+O_2 peak (N_2+), and the CH_4, CO_2, and H_2O peaks were detected in all samples (for examples, see the chromatograms in Figure 236.1). The relative areas corresponding to relative abundances for the single component peaks are in the order $H_2O >> CO_2 > CH_4$. Detection of significant quantities of CH_4 confirms the possibility of producing less hydrogen isotopically negative H_2O by D/H

TABLE 236.2. FLUID INCLUSION GAS ANALYSIS RESULTS, HOLLINGER AND RENABIE DEPOSITS.

Sample No.	Sample description and location	Crush pressure (psi)	$CH_4/(CH_4+CO_2)$ (molar; %)	NO, N_2O and C_2H_6 detection
HOLLINGER - PRIMARIES				
1P - S346	Quartz; best primaries, constant ratio. #1 open pit.	0	1.58	minor N_2O
		2500	1.52	
		5500	1.52	
		Total	1.52	
33P - S342	Quartz; bets primaries, #33 open pit.	1800	0.82	very minor N_2O
		4800	0.79	
		Total	0.81	
400 - 2	Quartz; best primaries, constant ratio. #400 open pit	2000	0.30	minor N_2O
		4500	0.28	
		7000	0.36	
		Total	0.30	
S15-08-01-2	Scheelite; best primaries, variable ratio. 1500′ level	0	20.55	large NO, N_2O and C_2H_6
		1300	18.38	
		2800	10.70	
		5700	9.39	
		Total	14.73	
15-08-01-05	Quartz; best primaries. 1500′ level	700	6.12	very minor N_2O
		3400	6.29	
		6100	6.45	
		Total	6.28	
18-83-01-1	Scheelite; best primaries, constant ratio. 1800′ level	500	20.23	large NO, N_2O and C_2H_6
		900	14.38	
		3200	11.18	
		5000	9.78	
		Total	14.88	
18-83-01-2	Scheelite; best primaries, constant ratio. 1800′ level	0	28.78	large NO, N_2O and C_2H_6
		1700	24.49	
		~2650	16.89	
		2700	12.53	
		Total	23.99	
18-83-01-2 Duplicate	″ ″	300	26.59	n.d.
		3200	23.74	
		4800	15.93	
		Total	23.96	

exchange with CH_4, as discussed by Wood *et al.* (1986b). Very interestingly, three additional peaks have been detected, but only on samples with high CH_4 and N_2+. The first peak appears either as a high retention time shoulder on the N_2+ peak or, if present in large amounts, as a separate peak (Figure 236.1). It is provisionally identified as NO from published retention times and from an approximate correlation with the size of a peak identified as N_2O. The second peak appears on the high retention time side of CO_2 (Figure 236.1) and is identified as an N_2O peak from an exact correspondence with the retention time of standard N_2O. The third peak occurs midway between the CO_2 and H_2O peaks and is identified as a C_2H_6 peak from exact correspondence of unknown and standard retention times. As far as is known, these results, together with results from the Tanco granitic pegmatite from southeastern Manitoba, produced at the same time (Bray *et al.* in prep.), are the first to report detection of NO and N_2O from fluid inclusions in minerals (only N_2O from Tanco).

H_2, Ne, NH_3, and H_2S peaks were looked for but not detected.

RESULTS AND DUPLICATES

Results for $CH_4/(CH_4+CO_2)$ molar ratios and for detection of NO, N_2O, and C_2H_6 are given in Table 236.2. Molar ratios are given for different crush pressures together with means which are weighted according to the relative amounts of the gases released in each crush.

Four duplicates were run: two scheelite best primaries and one sample from near graphitic material from the Hollinger Mine, and the D extension sample (1400 level) from the Renabie Mine. The three Hollinger duplicate $CH_4/(CH_4+CO_2)$ molar ratios are in very good agreement relative to the total

TABLE 236.2. (cont'd.)

Sample No.	Sample description and location	Crush pressure (psi)	$CH_4/(CH_4+CO_2)$ (molar; %)	NO, N_2O and C_2H_6 detection
18-83-01-39	Scheelite; best primaries, constant ratio. 1800' level	600	28.86	minor NO, medium N_2O and large C_2H_6
		2000	21.11	
		3600	16.18	
		Total	23.24	
18-83-01-39 Duplicate	" "	300	26.39	medium NO and N_2O and large C_2H_6
		800	23.17	
		1400	19.06	
		4500	19.58	
		Total	22.25	
SECONDARIES				
2 - S321	Quartz; 200' level	0	2.13	minor N_2O
		1900	1.93	
		5000	2.05	
		Total	1.99	
8 - S309	Quartz; 800' level	0	4.40	very minor NO and minor N_2O
		1500	2.15	
		3800	2.24	
		6500	2.26	
		Total	2.24	
17 - S109	Quartz; 1700' level	0	28.69	very minor N_2O and C_2H_6
		1300	25.80	
		3500	25.89	
		6500	23.92	
		Total	25.36	
27 - S149	quartz; 2700' level	0	10.33	very minor N_2O
		1300	9.19	
		3600	9.10	
		6200	9.32	
		Total	9.21	
RELATED TO GRAPHITIC MATERIAL				
55P - S321	Quartz; #55 open pit	400	15.13	
		4500	14.82	
		6300	14.92	
		Total	14.93	
55P - S321 Duplicate	" "	100	14.77	very minor N_2O
		2100	14.66	
		5200	14.92	
		Total	14.77	

range: 23.99/23.96, 23.24/22.25 and 14.93/14.77, compared with 0.30-25.36. The Renabie duplicate shows more variability: 1.60/0.91 compared with a total range of 0.68-1.60

DISCUSSION OF RESULTS

$CH_4/(CH_4+CO_2)$ Molar Ratios from Different Crushes

Figure 236.2 shows data for different crushes of quartz and scheelite containing best primary inclusions, and quartz containing typical secondary inclusions. It can clearly be seen that the scheelite samples show a consistent decrease in the $CH_4/(CH_4+CO_2)$ ratios in successive crushes, whereas the quartz samples show very constant ratios. A qualitative explanation is that CH_4-rich inclusions, which are under a higher internal pressure than CO_2-rich inclusions (e.g. Figure 3.17 of Burruss 1981) break preferentially in scheelite because of its good cleavage, whereas quartz shows no preferential effects because it has to be fractured. Hence, it is essential to calculate results as weighted averages for scheelite.

Vertical Variation

$CH_4/(CH_4+CO_2)$ ratios for samples containing best primary inclusions from the Hollinger Mine show significant variability by a factor of 80 from a high value of 23.99% to a low of 0.30%. It can be seen clearly in Figure 236.3 that ratios from the deeper 15 and 18 levels are definitely higher (>6.28%) than ratios from surface samples (0.30 to 1.52%). This interesting

TABLE 236.2. (cont'd.)

Sample No.	Sample description and location	Crush pressure (psi)	$CH_4/(CH_4+CO_2)$ (molar; %)	NO, N_2O and C_2H_6 detection
55P - S323	Quartz; #55 open pit	500	16.64	very minor NO and minor N_2O
		3300	16.26	
		6400	17.05	
		Total	16.56	
55P - S330	Quartz; #55 open pit	0	11.04	very minor N_2O
		1600	5.76	
		4700	5.80	
		Total	5.94	
12 - S1596	Quartz; 1200' level	400	5.68	minor NO and N_2O
		2500	8.34	
		5300	10.61	
		Total	8.22	
RENABIE				
RN86 - 34	Quartz; D extension of main zone, 1400' level	1,000	1.38	-
		4000	2.08	
		Total	1.60	
RN86 - 34 Duplicate	" "	400	0.98	-
		2800	0.72	
		5500	1.36	
		Total	0.91	
RN86 - 88	Quartz; Nudulama zone, 1400' level	1700	1.11	-
		4400	1.37	
		Total	1.22	
RN86 - 5	Quartz; main zone 3265' level	1100	1.09	-
		3800	1.26	
		6400	1.65	
		Total	1.24	
RN86 -71	Quartz; quartz-MoS_2 shallow dipping vein cutting main vein at 3105' level	800	0.85	-
		3500	0.59	
		6300	0.84	
		Total	0.74	
RN86 - 62	Quartz; late quartz carbonate-MoS_2-anhydrite vein near shaft on 3105' level	1800	0.70	-
		4700	0.65	
		Total	0.68	

Analyst: C.J. Bray. For analytical methods see text. Crushes with insufficient gas released (e.g. first crushes) not recorded.

vertical trend, which confirms observations reported by Hanel *et al.* (1987) on general material, is also seen in the trace gases. Only minor amounts of N_2O are detected in the surface samples whereas the deep samples generally show relatively large amounts of NO, N_2O, and C_2H_6.

Data for quartz which contains secondary inclusions, from the Hollinger Mine, (Figure 236.3) are similar with two samples from between surface and the 15 level (2 and 8 levels) showing intermediate ratios of 1.99% and 2.24%, one a deep sample from the 17 level showing the highest ratio of 25.36%, and a very deep sample from the 27 level showing a value of 9.21% in the lower part of the higher range. Hence, it appears from these limited data (at present) that the secondary inclusions show similar gas signatures to the primary inclusions, an observation consistent with similar bulk compositions observed by Wood (1987) and an indistinguishable δD value (Wood *et al.* 1986b). The secondary inclusions are related to strain features. Hence, it appears that in the Hollinger Mine, the secondary inclusions may contain similar, or even the same, contents as the primary inclusions, and that strain has just rearranged the inclusion material approximately isochemically. This possibility is being tested rigourously. The combined data from primary and secondary inclusions suggest that there was a sharp decrease in $CH_4/(CH_4+CO_2)$ ratio in the upper, preserved ~460 m (~1500 feet) of the Hollinger-McIntyre system. The single sample from the 27 level lies within the 15/18 level range.

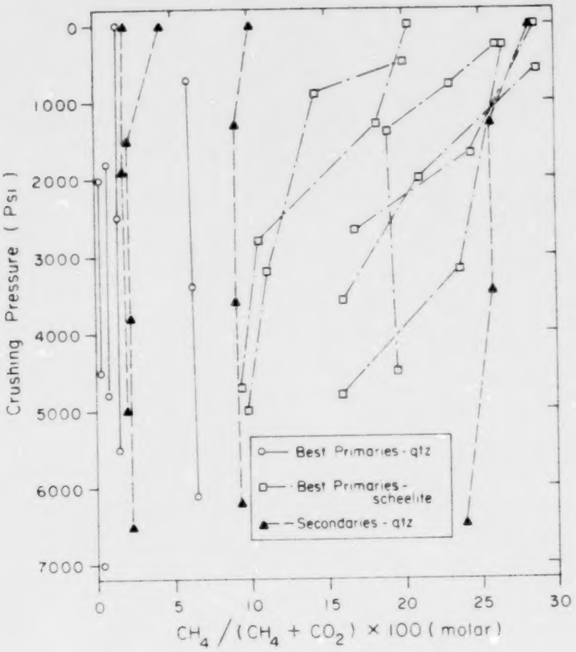

Figure 236.2. *$CH_4/(CH_4+CO_2)$ molar ratios for successive crushes of 14 samples at different crush pressures. Note that the ratios decrease consistently for scheelite, whereas they are relatively constant for quartz.*

Data from the 3265-, 3105-, and 1400-foot levels from the Renabie Mine and Nudulama Prospect show a very similar range of ratios (0.68 to 1.60%) to the surface Hollinger samples (0.30 to 1.52%). Two relatively late veins, both of which contain MoS_2, and one of which also contains coarse anhydrite, show the lowest values of 0.74 and 0.68%. Fine anhydrite is also present at the Renabie Mine in the main stage material (Callan and Spooner, this volume).

The decrease in $CH_4/(CH_4+CO_2)$ ratios in the upper ~460 m of Hollinger is interpreted to be a direct result of the H_2O-CO_2 phase separation deduced from optical and microthermometric observations (Wood *et al.* 1986a), since the gas/liquid partition coefficient for CH_4 is higher than that for CO_2 (e.g. Drummond and Ohmoto 1985). Progressive decreases in CH_4/CO_2 (x initial ratio) values calculated from Drummond and Ohmoto (1985) for isothermal closed and open systems at 350°C and 250°C are shown in Figure 236.4. It can be seen that gas fractionation is more effective at lower temperatures, at which partition coefficients are higher, and for open systems (Rayleigh fractionation). In the Hollinger Mine, CH_4/CO_2 ratios decrease to ~0.04 of their 18 level value ($CH_4/(CH_4+CO_2) \cong 20\%$). Hence, an interesting deduction can be made. For closed system conditions at a temperature of 250°C, which is ~30°C lower than the most frequently occurring temperature for Hollinger (Wood *et al.* 1986a), CH_4/CO_2 (x initial ratio) values are asymptotic at a value of ~0.25. At 280°C, the asymptotic value would be slightly higher, and definitely >0.04 (observed). Hence, Hollinger, although a lithostatically pressured system (Wood *et al.* 1986a), was not closed to gas/liquid separation by differential flow, corresponding to their viscosity and buoyancy differences (*see* section below). For perfect open system fractionation at 280°C, a CH_4/CO_2 (x initial ratio) value of ~0.04 is reached at ~8% phase separation; a reasonable value suggesting that gas partition in the upper levels of Hollinger may have approximated more closely to an open rather than to a closed system process.

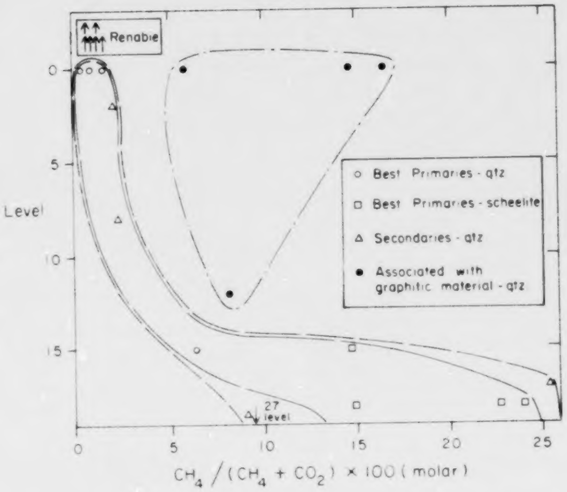

Figure 236.3. *$CH_4/(CH_4+CO_2)$ ratios for fluid inclusion gases released from quartz and scheelite from different levels from the Hollinger Mine, and for all depths from the Renabie Mine. Note that currently available data suggest similar trends of increasing CH_4 contents with depth for primary and strain related secondary inclusions from the Hollinger Mine, and that the Renabie CH_4 contents are similar to the CH_4 contents of the surface samples from the Hollinger Mine. Samples associated with graphitic material from the Hollinger Mine show clear evidence of relative CH_4 enrichment.*

These gas analyses show a gradational change in composition from high $CH_4/(CH_4+CO_2)$ molar ratios of 15 to 25% at depth in the Hollinger Mine (15 and 18 levels), where coexisting pyrite-pyrrhotite occur (Wood *et al.* 1986a), to low values at surface (0.3 to 1.52%) which are closely comparable to the values from the Renabie Mine (0.68 to 1.60%). Renabie is an oxidized Archean Au-quartz vein system containing anhydrite (Callan and Spooner, this volume) and negative $\delta^{34}S$ (sulphide) values. Hence, the gas analyses document a transition for reduced to oxidized fluids. In the last section of this report, H_2O-CO_2 phase separation is discussed as a possible mechanism for, amongst other things, producing oxidized from reduced Archean Au-quartz hydrothermal systems. These gas data provide supporting evidence.

Samples from Close to Graphitic Material

Four samples from close proximity to graphitic material were analyzed to look for interaction effects

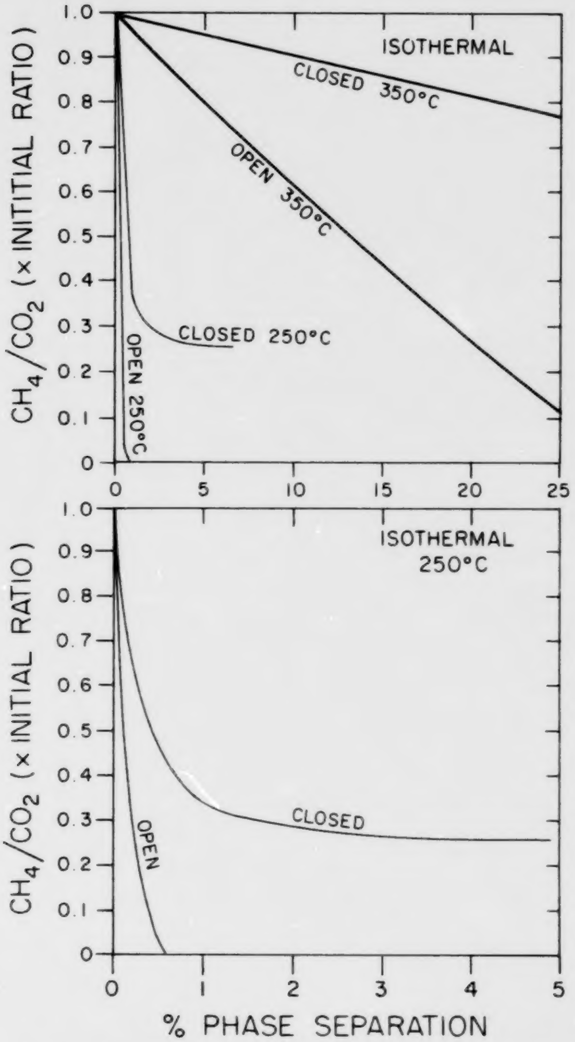

Figure 236.4. *CH_4/CO_2 (x initial ratio) values as a function of percent phase separation for isothermal, closed and open system conditions at 350°C and 250°C (calculated from Drummond and Ohmoto 1985).*

suspected from $\delta^{13}C$ data (*see* above). The three surface samples show very clear increases in CH_4 contents to $CH_4/(CH_4+CO_2)$ molar ratios in the range 5.94% to as high as 16.56%, relative to the surface primary inclusion bearing material (0.30 to 1.52%; Figure 236.3). One sample from close to graphitic material from the 12 level (8.22%) falls in the range of the surface graphite related samples, but is less distinct from nongraphite related samples because of their rise in CH_4 content at this level (Figure 236.3). There may be a possibility of distinguishing between high CH_4 fluids unrelated and related to graphitic material because the former have high NO, N_2O, and C_2H_6 values whereas, according to present data (*see* Table 236.2), the latter appear not to have.

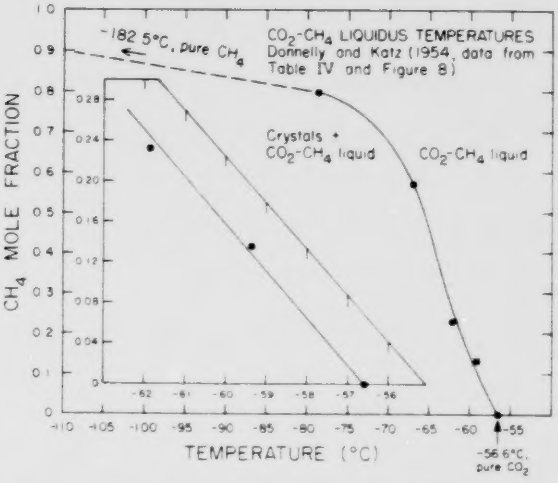

Figure 236.5. *Liquidus temperatures in the system CO_2-CH_4 from Donnelly and Katz (1954).*

The key point about these data is that the production of CH_4 by interaction with graphitic material, which was suggested to explain the less negative $\delta^{13}C$ values of carbonate associated with graphitic material (*see* above), has been found. Three of the analyzed samples actually come from one of the two open pits (#55) containing graphitic material which gives a $\delta^{13}C$ value of -0.6±0.5‰ (Fyon *et al.* 1983) in comparison with the general value of -3.1±1.2‰ (*see* above).

Comparison With CO_2 Melting Point Data

The measured fluid inclusion $CH_4/(CH_4+CO_2)$ molar ratios can be compared with CH_4 mole fractions deduced from measured CO_2 melting point depressions relative to pure CO_2, to check for consistency. Figure 236.5 gives liquidus temperatures in the system CO_2-CH_4 from Donnelly and Katz' (1954) original data, including an expansion of the -63°C to -55°C temperature range. The mean CO_2 melting point of -57.3°C (n=274) reported by Wood *et al.* (1986a) corresponds to 3.2 equivalent mole percent CH_4 relative to (CH_4+CO_2). Approximately 60% of the data reported by Wood *et al.* (1986a) is from levels shallower than the fifteenth for which the average measured mole percent CH_4 from primaries and secondaries is 1.37±0.81 (n=5), a value less than that given from microthermometry. However, as the gas chromatogram in Figure 236.1 shows, the N_2+ peak is actually larger than the CH_4 peak by a factor of 1.5. The gases contained in the N_2+ peak (N_2±CO±Ar±O_2) depress the freezing point of CO_2. Assuming that the effect is approximately molar, the combined mole percent of CH_4+N_2±CO±Ar±O_2 is very approximately 3.4 mole percent, a value in good agreement with that obtained microthermometrically. Hence, the measured gas chemistry and the estimates from measured CO_2 melting points appear to be consistent, providing that the effect of the additional (N_2±CO±Ar±O_2) gases is taken into account.

The lowest measured CO_2 melting point of -62.5°C (Wood *et al.* 1986a) corresponds to ~27 to

30 equivalent mole percent CH_4, in satisfactory agreement with a maximum measured value (to date) of 25.36 mole percent CH_4 (Sample 17-S109-quartz). As the gas chromatogram in Figure 236.1 shows, the N_2+ peak is not as significant relative to CH_4 at high CH_4 values. Hence, its relative contribution is not so large.

PRESSURE AND DEPTH ESTIMATION

It is obviously important to estimate the pressure and depth of formation of Archean Au-quartz vein systems, particularly because published estimates using the intersecting fluid inclusion isochore approach for Sigma (Robert and Kelly 1984), Pamour #1 (Walsh *et al.* 1984) and various Western Australian deposits (Ho *et al.* 1985) are erroneous. The reason why these estimates are in error is that evidence is provided for H_2O- and CO_2-rich fluids in contact in all three cases. Hence, trapping occurred on solvi in the simplified H_2O-NaCl-CO_2-CH_4 system. Since trapping took place on solvi, homogenization and trapping temperatures are equal, and it is logically not permitted to extrapolate to higher temperatures. Intersecting isochores (Roedder and Bodnar 1980) can only be used for pressure determination for H_2O- and CO_2-rich fluids which would have mixed had they come into contact, but which evidence suggests were simultaneously present but physically separated at the time of trapping; a fairly restrictive condition.

METHOD AND PRESSURE ESTIMATE

A method for pressure estimation is discussed here which was first developed by Macdonald (1983) for the Boss Mountain Mo Deposit, B.C. It relies on being able to estimate the bulk fluid composition before H_2O-CO_2 phase separation, and gives an estimate of the pressure at which phase separation initiated. The method is illustrated in Figure 236.6, which shows P-T sections through the immiscibility volume in the H_2O-NaCl-CO_2 system determined experimentally by Gehrig *et al.* (1979). The single phase fluid region is to the right of the curves, and the two phase region to the left. If the single phase fluid composition prior to unmixing can be estimated and the temperature of phase separation estimated from fluid inclusion homogenization temperatures, and if the fluid is in the compositional range worked on by Gehrig *et al.* (1979), then a pressure estimate can be determined from the vertical axis. The effect of CH_4 cannot be considered because no relevant data exist.

As can be seen, the P-T sections expand at lower pressures and roll over just before reaching the H_2O-NaCl critical curve. By comparing curves B and B′, which have the same bulk mole percent CO_2 (4.0 *m*), it can be seen how increasing [NaCl] from 0 to 1.9 *m* increases the immiscibility volume, and by comparing curves B, C, and D, which have similar [NaCl] values of 1.9, 1.8, and 1.7 *m*, respectively, it can be seen how increasing [CO_2] from 4.0 to 6.7 to 9.7 *m* also increases the immiscibility volume. Above 1000 bars, the method is not very good because the P-T sections are steep so that small uncertainties in temperature lead to large uncertainties in pressure.

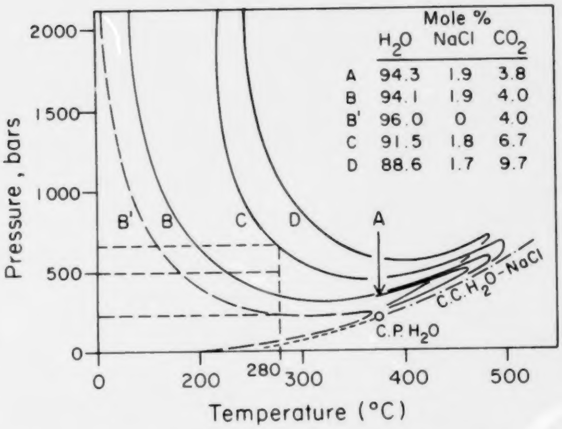

Figure 236.6. *P-T sections through the immiscibility volume in the system H_2O-NaCl-CO_2 from Gehrig et al. (1979). The single phase region is to the right of the curves.*

The very preliminary estimate for the Hollinger-McIntyre fluid composition prior to unmixing is ~93 mole percent H_2O, 6 equivalent mole percent CO_2 and only ~1 equivalent mole percent NaCl (Wood *et al.* 1986a). The very preliminary and probably inaccurate nature of this estimate must be emphasized because it is based on estimation of relative volumes of H_2O-NaCl and CO_2-rich phases in fluid inclusions. It can be improved from fluid inclusion microthermometric measurements (Parry 1986) and by fluid inclusion gas analysis. The estimated Hollinger-McIntyre fluid composition lies between that for curve B′, which contains both less NaCl and less CO_2, and curve C, which contains more NaCl and CO_2. Since the system temperature for Hollinger-McIntyre is quite well estimated at ~280°C at which intermittent phase separation occurred (Wood *et al.* 1986a), the upper and lower pressure constraints are ~700 bars and ~200 bars; values which are fairly robust to uncertainties in both composition and temperature (Figure 236.6). Interpolating first between curves B′ and B for [NaCl], and then between that point and a curve a little below C for lower [NaCl] gives a specific estimate of ~500 bars (Figure 236.6).

DEPTH ESTIMATE

Conversion of pressure estimates to depth estimates requires evidence for whether pressure was lithostatic or hydrostatic, or intermediate. In the case of Hollinger-McIntyre it is fairly clear from vein morphologies (Wood *et al.* 1986a, 1986b) that hydraulic fracturing took place and that openings which subsequently became mineral veins, were maintained open by high fluid pressures. Hence, pressure oscillated between σ_3+crack tip strength and σ_3+tensile strength (~70 bars) (σ=principal stress direction). Neglecting for the moment the differences between $\sigma1$, $\sigma2$, and $\sigma3$, because they are impossible to estimate, the relationship with the resolved vertical stress, and the difficulties involved in estimating real crack tip and tensile strengths, estimated P≅ lithostatic vertical stress. Hence, for a general density of overlying material (altered mafic flows and interflow sediments) of ~2.6 g cm^3, the pressure estimate of ~500+200/-300 bars is equivalent to a depth estimate of ~1.9+0.8/-1.1 km (i.e.~2 km).

DISCUSSION

An erosional layer of approximately 2 km above the upper ~300 m of the Hollinger Mine is not very thick, especially when it is considered that the McIntyre Mine has been mined downwards to a comparable depth of 2.4 km. However, it is not unreasonable for magma related systems such as Boss Mountain, B.C., which did not breach surface (Macdonald 1983). The Boss Mountain MoS_2 mineralization also formed under lithostatic pressure conditions at a lower pressure of ~330 bars (=~1.3 km below surface). A not particularly great depth of formation of ~2 to 4 km for the whole system is certainly consistent with the late timing of mineralization relative to deformation (Burrows and Spooner 1986; Wood *et al.* 1986a, 1986b) giving time for erosional removal of thickened material. If ~2 km of rock have been eroded from the Timmins area in ~2.65x10^9 years, a mean erosion rate of ~1 mm per 1000 years can be estimated.

CHEMICAL AND PHYSICAL CONSEQUENCES OF H_2O-CO_2 PHASE SEPARATION

Fluid inclusion evidence for H_2O-CO_2 phase separation has been documented for several Archean Au-quartz vein systems including the Hollinger-McIntyre (Wood *et al.* 1984, 1986a), Pamour #1 (Walsh *et al.* 1984), and Hunt, Morning Star, Mount Charlotte, Lake View, Paringa, Kanowna Main Reef, Red Hill, Water Tank Hill, and Lancefield Deposits (metasediments) in Western Australia (Groves *et al.* 1984; Ho *et al.* 1985). The evidence consists of primary inclusions with variable H_2O-CO_2 ratios which homogenize into the H_2O and CO_2-rich phases over the same temperature range (e.g. Wood *et al.* 1986a) or, in late vugs in some Western Australian deposits, of coexisting, separate, primary H_2O- and CO_2-rich inclusions with similar homogenization temperatures (Ho *et al.* 1985). In the Hollinger-McIntyre Mine, and the Hunt, Morning Star, Mount Charlotte, Kanowna Main Reef, and Red Hill Deposits in Western Australia, both Wood *et al.* (1986a) and Ho *et al.* (1985) have recognised that phase separation was intermittent and that, therefore, P/T conditions fluctuated either side of the immiscibility surface.

As discussed recently by, for example, Arnórsson (1978), Drummond and Ohmoto (1985), Reed and Spycher (1985) and Bowers (1986) phase separation (H_2O_l/H_2O_v; H_2O/CO_2) has inevitable, very strong effects on mineral solubilities, and also very important pressure effects. Hence, the objective of this section is to examine the chemical and physical consequences of H_2O-CO_2 phase separation in Archean Au systems, particularly because sulphidation reactions with Fe-rich host rocks, for which there is excellent evidence in many cases particularly involving metasomatised Fe-formations and Fe-rich tholeiites (e.g. Phillips and Groves 1984; Phillips *et al.* 1984; Macdonald 1984; Macdonald and Fyon 1986), do not appear to be a generally applicable gold precipitation mechanism because: a) many Archean Au systems do not occur in particularly Fe-rich host rocks; and b) in a significant number of Archean Au deposits, Au is contained within vein structures (e.g. Renabie, N. Pascalis) not in sulphidized wall rock. Even in the Hollinger-McIntyre System where it is estimated that 95% of the produced gold occurs in altered wall rock (Wood *et al.* 1986a), a gold precipitation mechanism other than, or in addition to, sulphidation must have been important because Au occurs in pyrite midzones (11.1 volume percent) indicating early Au saturation, whereas the bulk of the Au (80.5 volume percent) occurs in pyrite outer zones. Since the solution was Au saturated, or close to Au saturation, sulphidation reactions should have caused strong initial Au precipitation. By the time pyrite outer zones were deposited, a significant amount of the initially available Fe had been used up because there is analytical evidence for Fe addition, as well as S (Wood *et al.* 1986b).

H_2O-CO_2 phase separation provides the basis of a unified theory which has the potential to explain such features of Archean Au-quartz vein systems as very intimate Au-pyrite co-precipitation (e.g. Wood *et al.* 1986a) and the precipitation of other sulphides, carbonate precipitation, mineral (including Au) precipitation over vertical intervals of ~1000 to 3000 m, generation of oxidized Archean Au fluids by partition loss of reduced gas species (H_2, H_2S, CH_4) (e.g. Cu-Au-Ag-Mo-anhydrite orebody, McIntyre Mine; Burrows and Spooner 1986), hydraulic fracturing (e.g. Kerrich and Allison 1978; Phillips and Groves 1984; Wood *et al.* 1984), and volumetric inflation including dilation of ductile shear structures.

MODELING

This discussion of phase separation is based on Drummond and Ohmoto (1985) and, for carbonate precipitation, Arnórsson (1985). The principal features of Drummond and Ohmoto's (1985) calculations are as follows:

1. Fluid chemistry and mineral solubilities are calculated iteratively, with gas removal based on measured gas partition coefficients which increase essentially linearly with decrease in temperature, and which increase by ~0.1 to 0.2 log units per molal increase in [NaCl]. Gases define three groups; a high volatility group of nonpolar species including N_2, H_2, CH_4, and the rare gases with gas/liquid partition coefficients (molality ratios) of ~10^5 at 100°C, a medium volatility group of interactive species including $CO_2>H_2S>SO_2$ with partition coefficients of ~10^4 to 10^2, (100°C) and low volality NH_3 (~10 at 100°C).
2. The redox states of the solutions are calculated from:

   $$H_2S+2O_2=HSO_4^-+H^+ \qquad (1)$$

3. Results are given for adiabatic and isothermal cases, with the former being more effective because of the constraint of constant total enthalpy requiring temperature decrease. With aqueous phase boiling, drop in temperature is substantial because of a significant enthalpy of vapourization (e.g. 1% vapourization at 100°C leads to a ΔT of 8°C). However, enthalpies of exsolution of other dissolved components (e.g. CO_2) are small

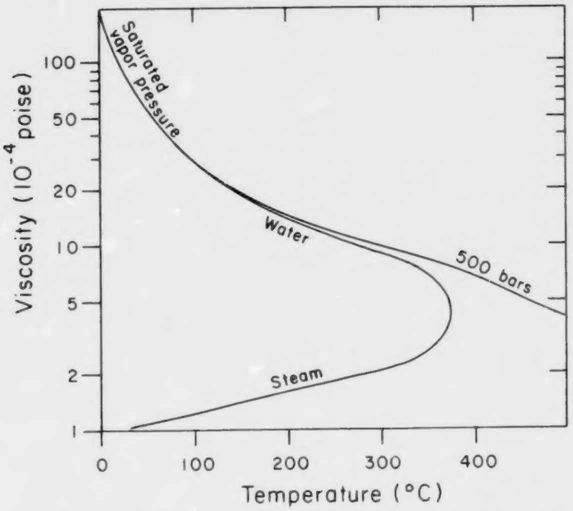

Figure 236.7. *Viscosities of water and steam along the two phase boundary and at 500 bars (modified from Ellis and Mahon 1977, Figure 4.5).*

(Drummond and Ohmoto 1985). Hence, isothermal calculations are more appropriate for H_2O-CO_2 phase separation.

4. Models are calculated by Drummond and Ohmoto (1985) for both closed (liquid and gas in constant total chemical equilibrium) and perfectly open (fractional/Rayleigh separation) alternatives, with the latter having markedly stronger chemical effects. Natural situations would appear to be intermediate because, on the one hand, liquid and vapour travel by essentially the same permeability paths, but at different speeds so that aliquots of vapour interact with fluid ahead in the flow path. On the other hand, it is easy to see how, in a lithostatically pressured system such as the evidence indicates Hollinger was (Wood *et al.* 1986a), selective vapour loss could have occurred from the system as a whole because of the viscosity contrast between vapour and liquid. For example, as the data in Figure 236.7 show, at 250°C H_2O_v, which is chemically more interactive than CO_2, has a viscosity ~6 times less than H_2O_l. In addition, in an active system it is unclear how well chemical reaction equilibrium would be maintained between liquid and an irreversibly forming, physically separate vapour phase. Measured CH_4/CO_2 ratios confirm that the Hollinger-McIntyre was not a perfectly closed system (*see* above).

EFFECTS ON fO_2 AND pH

Two of the principal effects of phase separation on fluid chemistry are on redox state through, for example, volatilisation of relatively reduced species such as H_2, CH_4, and H_2S, and on acid-base equilibria mainly through loss of CO_2.

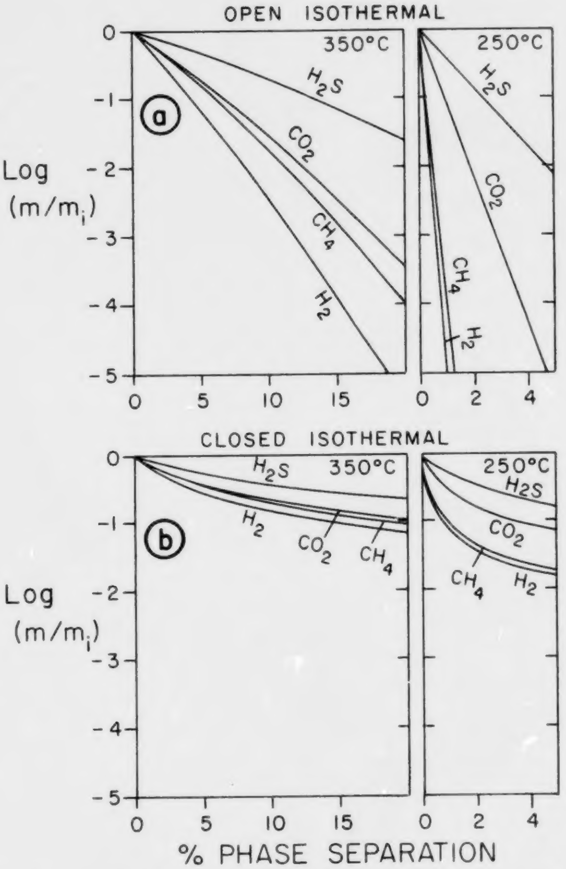

Figure 236.8. *Variation of the log of the ratio of the molality of a gas in the liquid (m) to its initial molality (m_i) with percent phase separation at 350°C and 250°C and for open and closed system conditions (modified from Drummond and Ohmoto 1985).*

Effect on fO_2

Figure 236.8 shows isothermal calculations of gas loss (log ratio of molality (*m*) to initial molality (m_i) in the liquid phase) with progressive phase separation for both open (Rayleigh) and closed (equilibrium) system cases (modified from Drummond and Ohmoto 1985, Figure 4, in which there is a small labeling error in the caption; from their Figure 3 it can be seen that the diagrams are for isothermal not isoenthalpic conditions). The temperatures of 250°C and 350°C are appropriate for the Hollinger-McIntyre Au-quartz vein system since fluid inclusion data indicate that mineralization at 277±48°C (1σ), and $\delta^{18}O$ values and mineral compositions indicate temperatures up to ~360°C (Wood *et al.* 1986a). The 3 *m* NaCl concentration is higher by a factor of three than that estimated for Hollinger-McIntyre (~1 *m*; Wood *et al.* 1986a). For a lower NaCl molality, the shapes of the curves would be the same, but the percent phase separation values slightly higher.

The principal features shown by the diagrams are: a) progressive gas loss in the order of their gas/liquid partition coefficients ($H_2>CH_4>CO_2>H_2S>SO_2$); b) more efficient gas loss under open system conditions, although significant changes occur for closed system conditions in the first four (250°C) to ten (350°C) percent phase separation; and c) more efficient gas loss at lower temperatures where partition coefficients are higher. Progressive loss of reduced species (H_2, CH_4, H_2S) can be seen leading, as Drummond and Ohmoto (1985, p.129) clearly state, to "...a relatively rapid oxidizing event...". For example, H_2 is reduced to 10^{-2} of its initial concentration in the first ~8% (350°C) and 0.5% (250°C) phase separation, and H_2S is reduced to 10^{-1} of its initial concentration in the first ~12% (350°C) and ~3% (250°C) phase separation, under open system conditions. The oxidation process would be more drawn out for closed system conditions.

Generation of Oxidized Archean Au Fluids

It can be seen clearly how H_2O-CO_2 phase separation can produce oxidized fluids from relatively reduced fluids such as those in the Hollinger-McIntyre system, which were in equilibrium with pyrite-pyrrhotite at depth (Wood *et al.* 1986a). Sulphate (anhydrite±barite)±hematite-bearing Archean Au-quartz vein systems with isotopically negative sulphur are not uncommon. Examples include the Cu-Au-Ag-Mo-anhydrite ore bodies in the McIntyre Mine (Burrows and Spooner 1986), paragenetic stage III of which is correlated with the main Au system, the Golden Mile, Kalgoorlie, Western Australia (Lambert *et al.* 1984; Cameron and Hattori 1985), the foliated tonalite/gneissose trondhjemite-hosted Renabie Deposit, near Wawa (Callan and Spooner, this volume), and the small Canadian Arrow Deposit in Hislop Township (Cherry 1983; Schwarcz and Rees 1985). Hence, progressive H_2O-CO_2 phase separation is suggested as a possible cause for the generation of oxidized Archean Au-quartz vein and related systems. This suggestion is supported by preliminary data (D.R. Burrows) which indicate CH_4 depleted liquid CO_2 in fluid inclusions, and slightly higher aqueous phase salinities (H_2O removal in CO_2), in the McIntyre Cu-Au ore body, and the fluid inclusion gas analytical data (*see* above) which indicate gradational generation of CH_4 depleted fluids at the top of the Hollinger-McIntyre system with similar CH_4/CO_2 ratios to the anhydrite bearing mineralization in the Renabie Mine.

Effect on pH

CO_2 loss, which is well illustrated in Figure 236.8, has the most important effect on pH causing a marked drop in $[H^+]$ through removal of the weak acid H_2CO_3:

$$H_2O+CO_2=H_2CO_3=H^++HCO_3^-=2H^++CO_3^{-2} \qquad (2)$$

Figure 236.9a shows that the higher the initial CO_2 content of the fluid, the larger the maximum potential pH increase. For Archean Au-quartz vein fluids, which may contain as much as 6 *m* CO_2 before phase separation (Wood *et al.* 1986a), the maximum pH change is large at ~3.5 log units (at 300°C). pH change is less immediate in closed compared with open systems, and at higher temperatures, at which gas/liquid partition coefficients are lower (Figure 236.9b).

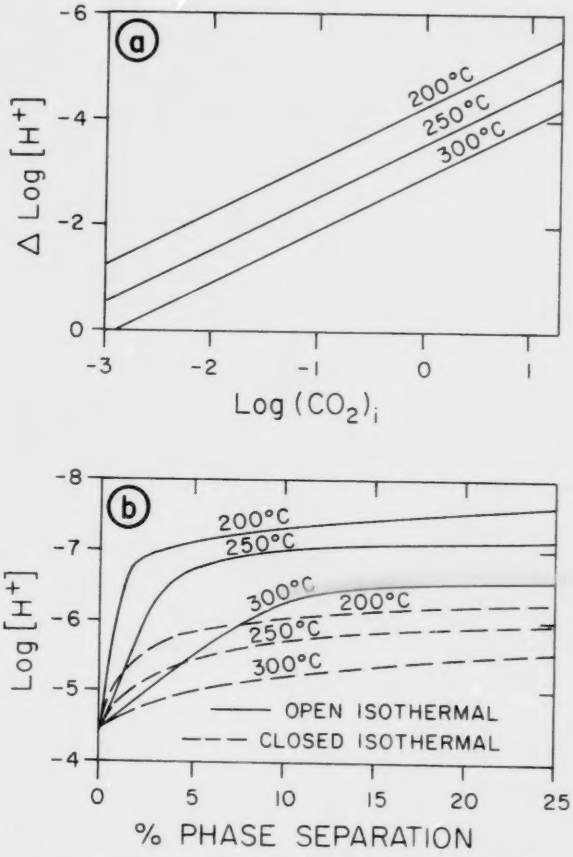

Figure 236.9. *(a) Variation of the maximum change in log $[H^+]$ with the log of the initial CO_2 molality at 200°C, 250°C, and 300°C for 1 m NaCl in the aqueous phase (modified from Drummond and Ohmoto 1985).*
(b) Log $[H^+]$ /percent phase separation paths for open and closed isothermal conditions with initial molalities of $H^+ = 10^{-4.5}$ m, $\Sigma Cl = 1.0$ m, $\Sigma Na = 0.9$ m, $\Sigma K = 0.1$ m, $\Sigma Ca = 0.003$ m, $\Sigma Mg = 0.001$ m, $\Sigma CO_2 = 0.3$ m, $\Sigma H_2S = 0.003$ m, and $\Sigma SO4 = 3x10^{-9}$ m (modified from Drummond and Ohmoto 1985).

Archean Au-Quartz Vein Mineralization Over Large Vertical Intervals

One of the characteristics of Archean Au-quartz vein/shear zone systems which differentiates them from Tertiary-Mesozoic epithermal precious metal mineralization in cordilleran and island arc settings is that they can be developed at relatively consistent grades over very large depth intervals in some of the deepest mines in the world. Examples include the Kolar Gold Field in southern India (3230 m), the Kirkland Lake area (e.g. the Wright-Hargreaves Deposit; 2490 m), the Hollinger-McIntyre Deposits (2400 m), the Sigma Deposit (1790 m), the Fairview Deposit in the Barberton area, South Africa (1500 m), the Renabie Deposit (1370 m), the the Golden Mile Deposit, Western Australia (1160 m), the Lamaque Deposit (1100 m), and also in Zimbabwe (~2000 m) and Ghana (~1000 m). Clearly, changes in chemical and/or physical variables were persistent and relatively constant over large depth ranges. Progressive H_2O-CO_2 phase separation in response to decreasing lithostatic pressure (approximately), together with temperature decrease, could provide an explanation since, as can be seen in this discussion of pH which is one of the most important factors which control mineral deposition (*see* below), the following factors cause extended chemical changes:

1. a high initial CO_2 content, such as has been found in Archean Au-quartz vein systems (e.g. ~6 *m*; Wood *et al.* 1986a)
2. closed, compared with open system behaviour
3. high initial temperatures of ~300 to 350°C such as have been found at the Hollinger-McIntyre Mine (Wood *et al.* 1986a)
4. relatively low salinities which have also been found (Ho *et al.* 1985; Wood *et al.* 1986a)

Drummond and Ohmoto (1985, p.144) actually state that "...the vertical extent of the deposit will be proportional to the amount of CO_2 exsolved during ascent...", and calculate a depth interval of in excess of 1000 m to exsolve 99% of the CO_2 in a solution containing "several molal" CO_2 at 350°C. The possibility of Archean Au-quartz mineralization extending significant vertical distances away from source regions, even after H_2O-CO_2 phase separation has started, may explain the apparent lack of intrusion/Au relationships in Western Australia which Ho *et al.* (1985), for example, have used as evidence against magmatic derivation.

PRECIPITATION OF GOLD, PYRITE, AND SILVER

Prediction of the overall effects of phase separation on mineral solubilities is far from obvious because of different opposing chemical effects in each case. For example, Au precipitation is promoted by loss of H_2S, but opposed by decreases in $[H^+]$ and $[H_2]$, whereas the effects on pyrite precipitation are the exact opposite. Silver precipitation as Ag^0, on the other hand, is not influenced by $[H_2S]$ directly, but is affected oppositely by $[H^+]$ and $[H_2]$ which, in the cases of Au and pyrite, operate in tandem. These conflicting factors indicate the necessity of quantitative modeling, and are discussed in greater detail below.

Gold

The solubility of Au in reduced S predominant, low $[Cl^-]$ near neutral fluids can be written (Seward 1973; 1984);

$$Au^0_{(s)} + 2H_2S = Au(HS)_2^- + H^+ + 1/2\ H_2 \qquad (3)$$

It can readily be seen how volatilisation of H_2S during phase separation, which is shown clearly in Figure 236.8, promotes the precipitation of Au because it removes $(HS)^-$, the ligand which carries Au in solution. Figure 236.10a shows that a decrease in $[\Sigma S]$ from 0.05 to 0.001 *m* leads to a two order of magnitude drop in Au solubility for fS_2 fixed by pyrite-pyrrhotite. On the other hand, decreases in $[H^+]$ and $[H_2]$, both of which also occur during phase separation, oppose the precipitation of Au. The effect of H^+ is clearly shown in Figure 236.10b; rises in pH in the high temperature, near neutral region (~5 to 6) lead to higher Au solubilities up to a pH of ~7 at 250°C.

A correct idea of the resultant effect can be seen from Seward (1984, Figure 5): an increase in pH by one order of magnitude leads to an increase in solubility by approximately the same amount, an effect which is outweighed by a decrease in $[\Sigma S]$ by a factor of ~50 (0.05 to 0.001 *m*) leading to solubility decrease of ~3 1/2 orders of magnitude. Nevertheless, the quantitative outcome depends on the relative changes in $[H_2S]$, $[H^+]$, and $[H_2]$ so that, at low temperature (~200°C), Au precipitation is delayed by a sharp initial rise in pH (Drummond and Ohmoto 1985).

Pyrite

The precipitation of pyrite can be written:

$$FeS_{2(s)} + H_2 + 2H^+ = Fe^{2+} + 2H_2S \qquad (4)$$

It can be seen that H_2, H^+, and H_2S occur on precisely the opposite sides of the equation as they do for Au, because S is combined in the solid phase, not as a liquid phase ligand. These conflicting effects are important to resolve because of the well known closeness of the Au-pyrite relationship in unstrained Archean Au-quartz vein systems (e.g. Wood *et al.* 1986a, in which ~0.1 μm inclusions of pyrite are shown within a 12 μm gold flake itself enclosed in pyrite).

The importance of $[H^+]$ on pyrite solubility can be seen from Figure 236.11a (modified from Crerar *et al.* 1978): a one order of magnitude increase in pH leads to a two order of magnitude decrease in Fe solubility at 350°C (~1000 to ~10 ppm Fe). A correct idea of the relative effects of $[H^+]$ and $[H_2S]$ can be seen from Figure 236.11b in which a one log unit decrease in $[\Sigma S]$ leads to approximately a one log unit rise in Fe solubility, whereas a one log unit increase in pH leads to a two log unit fall in Fe solubility.

Hence, a) although Au and pyrite solubilities are affected by diametrically opposite chemical effects during phase separation, they co-precipitate; and b), therefore, H_2O-CO_2 phase separation can explain the closeness of the Au-pyrite relationship in Archean Au-quartz vein systems.

Silver

The solubility of native Ag can be written:

$$Ag^0_{(s)} + H^+ = Ag^+ + 1/2\ H_2 \qquad (5)$$

H^+ and H_2 are now on opposite sides of the reaction compared with the Au and pyrite reactions. It is not immediately obvious what the outcome is during phase separation. However, from the strong effect of pH on metal solubilities, exemplified by pyrite, it might be expected that the pH effect would be more important and that Ag would precipitate. The quantitative models (*see* below) show that this is indeed the case.

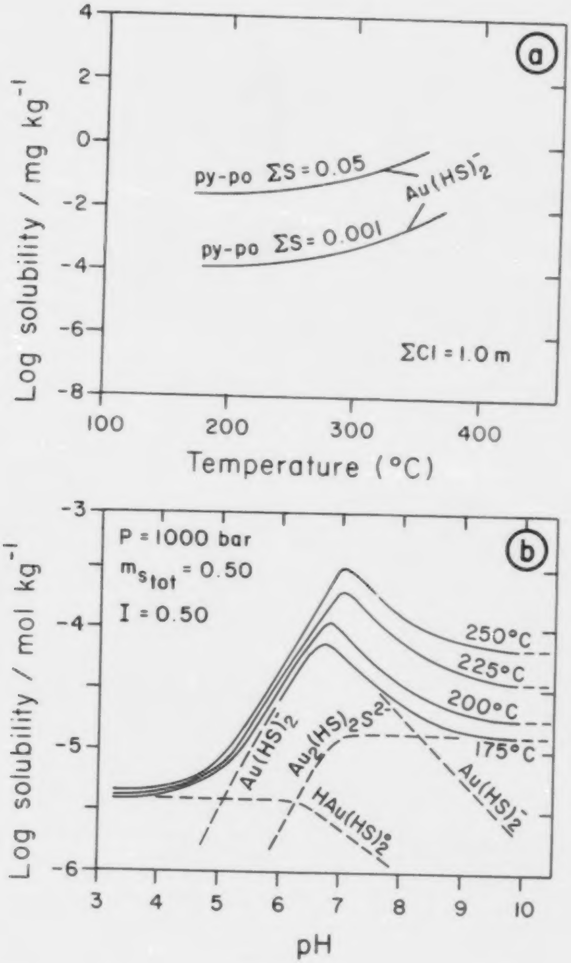

Figure 236.10. (a) Solubilities of Au as Au(HS)$_2^-$ as functions of temperature for fS_2 fixed by pyrite-pyrrhotite, for ΣS=0.001 and 0.05 m, and for ΣCl=1.0 m (modified from Seward 1984).
(b) Logarithm of the solubility of Au in sulphide solutions as a function of pH and temperature, with ionic strength (I)=0.50 and ΣS=0.50 m (modified from Seward 1973).

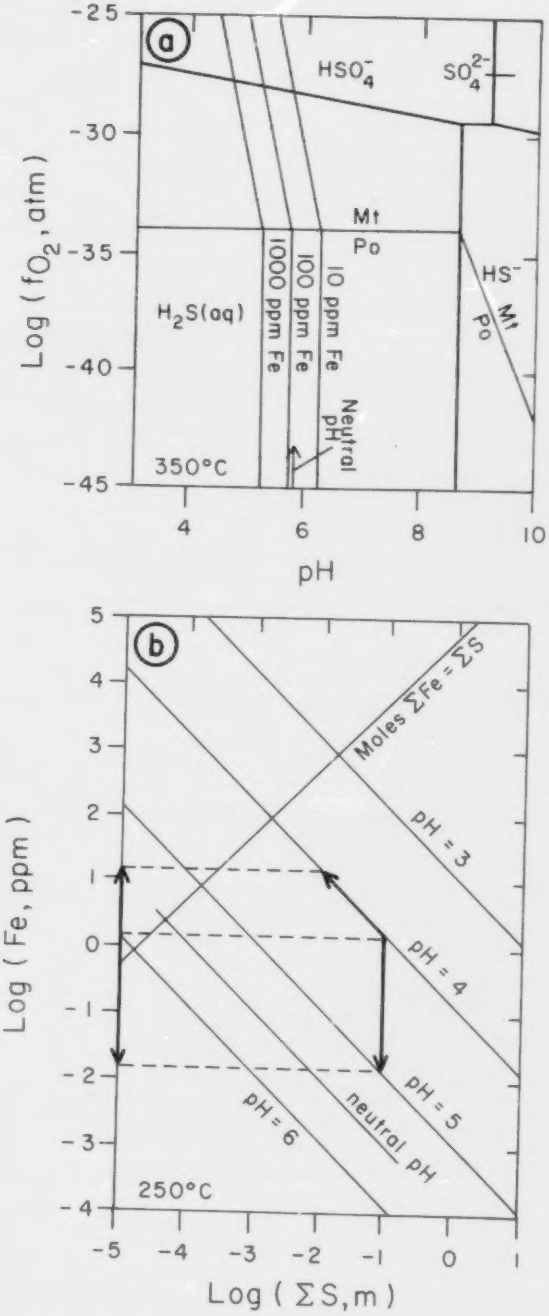

Figure 236.11. (a) Solubility of the assemblage pyrite+pyrrhotite+magnetite at 350°C and vapour saturated water pressure for total dissolved sulphur and NaCl concentrations of 10^{-3} and 2.0 m, respectively (modified from Crerar et al. 1978).
(b) Concentration of aqueous Fe^{2+} and FeCl$^+$ in 2.0 m NaCl solutions at 250°C and vapour saturated water pressure as a function of pH and total sulphur activity (modified from Crerar et al. 1978).

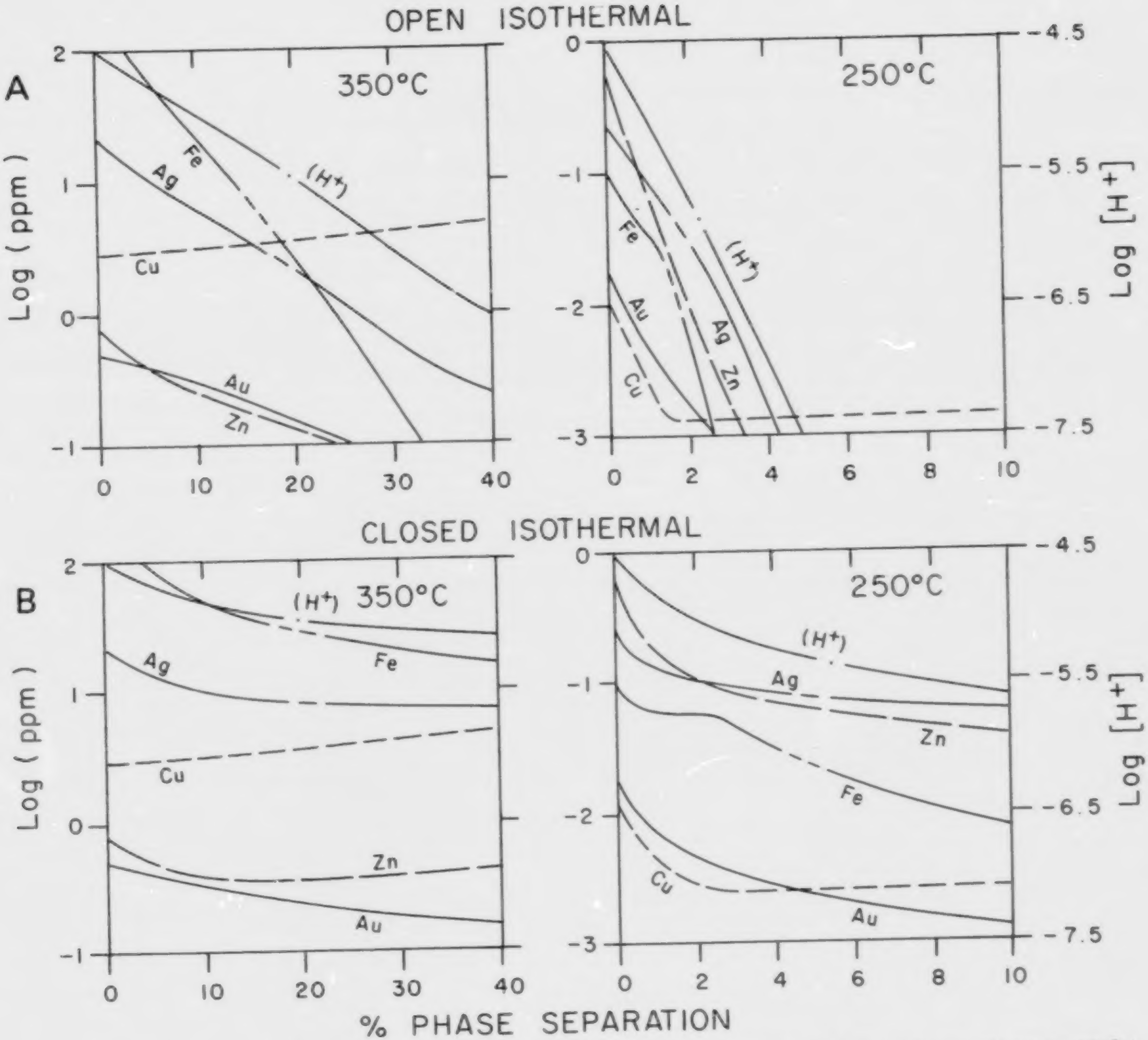

Figure 236.12. *Metal and proton concentration changes for isothermal phase separating systems at 350°C and 250°C and for open and closed system conditions. Initial molalities for the components are* $H^+ = 10^{-4.5}$ m, $\Sigma Cl = 1.0$ *m*, $\Sigma Na = 0.9$ m,, $\Sigma K = 0.1$ m, $\Sigma Ca = 0.003$ m, $\Sigma Mg = 0.001$ m, $\Sigma H_2S = 0.003$ m, $\Sigma CO_2 = 3.0$ m, *and* $\Sigma SO_4 = 3x10^{9}$ m *(modified from Drummond and Ohmoto 1985).*

MODELING ORE MINERAL PRECIPITATION

Figure 236.12, modified from Drummond and Ohmoto (1985), shows the results of modeling the effects of phase separation for isothermal open and closed systems at 350°C and 250°C, values which enclose the temperature estimates for the Hollinger-McIntype system (Wood *et al.* 1986a). $\Sigma CO_2 = 3.0$ *m*, a value close to the Hollinger-McIntyre estimate of ~6 *m*, $\Sigma Cl = 1.0$ *m*, the value estimated for Hollinger-McIntyre, $\Sigma H_2S = 0.003$ *m*, a value estimated to be reasonable based on current fS_2 and fO_2 estimates, and ΣSO_4 is very low at 3×10^{-9} *m* corresponding to a reduced S predominant fluid.

The following points can be noted from the diagrams:

1. The most important result is that, despite the different, conflicting chemical effects discussed above, Au, Ag, Fe, Zn, and Pb, which behaves very similarly to Zn, co-precipitate. The trends of decreasing solubility are similar to the trend of $[H^+]$ decrease. Hence, the quantitative models confirm that, in the case of Au, the H_2S loss effect wins, whereas for Ag, Fe, Zn, and Pb, the effect of $[H^+]$ drop wins. Occurrences of Au-Ag with sphalerite and galena are quite common (e.g. the Hollinger-McIntyre System for the former, Wood *et al.* 1986a; the Renabie Mine for the latter, Callan and Spooner, this volume). The only real exception is Cu at 350°C (and 300°C), but not at 250°C, because removal of Fe by Fe minerals prevents $CuFeS_2$ oversaturation. How-

ever, between 250°C and 300°C, chalcopyrite precipitates in both open and closed systems. It is also worth mentioning that, in most hydrothermal systems, fluid temperature will also be decreasing because of fluid expansion, some wall rock heat exchange, and internal fluid convection within vein structures. This effect, in addition to H_2O-CO_2 phase separation, may help explain why chalcopyrite is quite a common mineral in Archean Au-quartz vein systems.

2. There is a large contrast in behaviour between open and closed systems. In closed systems there are initial decreases in metal concentrations, followed by only slight decreases, essentially because the fluid chemistry becomes buffered by the solubilities of the gases present in the vapour phase in contact. In open systems, however, there are sharp, continuous drops in solubilities. Some intermediate behaviour is necessary to explain mineralization over large vertical intervals. In fact, in lithostatically pressured Archean Au systems, metal precipitation may be approximately proportional to relative gas loss.
3. In both open and closed systems, lower temperatures enhance mineral precipitation because of higher gas partition coefficients.
4. Although not shown here, the effect of higher $[CO_2]$, as in Archean Au-quartz vein fluids, is to markedly enhance the effectiveness of phase separation on causing mineral precipitation (compare to 3×10^{-2} *m*; Drummond and Ohmoto 1985).

GANGUE MINERAL PRECIPITATION

Carbonate

The precipitation of carbonates during gas loss (aqueous phase boiling) is well known from active geothermal systems (e.g. Arnórsson 1978). Hence, H_2O-CO_2 phase separation, together with reaction with divalent wall rock cations (Ca^{2+}, Mg^{2+}, Fe^{2+}, Mn^{2+}) can readily explain the coprecipitation of carbonate with Au-Ag, pyrite, and other sulphides in Archean Au-quartz vein systems (e.g. the paragenetic evolution diagram *in* Wood *et al.* 1986a). The reason why carbonate precipitates is that, although the total aqueous carbonate molality ($m\,CO_2 + m\,H_2CO_3 + m\,HCO_3^- + m\,CO_3^=$) decreases because of CO_2 loss, the concentration of CO_3 actually increases because the increase in pH displaces the following reaction to the right (Arnórsson 1978; Drummond and Ohmoto 1985; Reed and Spycher 1985):

$$H_2CO_3 = H^+ + HCO_3^- = 2H^+ + CO_3^{-2} \tag{6}$$

Carbonate then precipitates because its solubility product is exceeded:

$$\begin{aligned} &Ca(Fe^{II},Mg)(CO_3)_{2(s)} = \\ &Ca^{2+} + (Fe, Mg)^{2+} + 2CO_3^{-2} \end{aligned} \tag{7}$$

Albite

In the Hollinger-McIntyre System, albite occurs as fringes of tabular grains with carbonate projecting internally from vein walls. The abundance of albite decreases markedly from vein margins inwards. Anderson and Burnham (1983) have shown that a rise in pH increases the incongruent solubility of albite. Hence, this chemical aspect of H_2O-CO_2 phase separation cannot explain albite precipitation. Anderson and Burnham (1983) have also shown that low $[Cl^-]$ fluids favour transport of albite components because reduced ligand competition with available alkali permits the formation of alkali-alumina (e.g. $NaH_2AlO_3^0$) complexes in solution. Hence, Archean Au-quartz vein fluids are suitable for Al transport because of their relatively low salinities (e.g. Wood *et al.* 1986a).

A simple explanation for marginal albite precipitation, in addition to temperature decrease, is leaching of Na from wall rock, which has been documented from the Hollinger-McIntyre System (Wood *et al.* 1986b) and many other Archean Au-quartz vein systems (e.g. Roberts 1987). A highly speculative alternative is that Al forms a dawsonite ($NaAlCO_3(OH)_2$) like uncharged carbonate complex in solution which is stoichiometrically analogous to $NaH_2AlO_3^0$ ($NaAlO(OH)_2^0$). On phase separation, CO_2 would be lost from solution, the simplified reaction written below displaced to the left, and albite precipitated until the solution was depleted in Al:

$$\begin{aligned} &NaAlSi_3O_{8(s)} + CO_2\uparrow + 7H_2O = \\ &NaAlCO_3(OH)_2^0 + 3H_4SiO_4 \end{aligned} \tag{8}$$

Anhydrite

Anhydrite and minor barite are common gangue minerals in oxidized Archean Au-quartz vein systems (e.g. the McIntyre Mine Cu-Au-Ag-Mo-anhydrite; the Renabie Mine; and the Golden Mile Mine). Anhydrite can be present in very large amounts in, for example, stage I of the McIntyre mineralization (Burrows and Spooner 1986). Sulphates cannot be precipitated from cooling solutions because their solubilities increase with decreasing temperature. On the other hand, anhydrite precipitation can be readily explained by H_2O-CO_2 phase separation because of the solution oxidation effect associated with the loss of reduced species (H_2, CH_4, H_2S). If an approach to equilibrium is maintained between reduced and oxidized species, phase separating solutions from both reduced and oxidized S species predominance fields will move to fO_2 values slightly above the reduced S/oxidized S predominance field boundary, so that the slightly lower partition of SO_2 into the gas phase relative to H_2S is balanced. Starting from the reduced S species predominance field (e.g. pyrite-pyrrhotite in the Hollinger-McIntyre System; Wood *et al.* 1986a) anhydrite would be precipitated in amounts dependent on the degree of ΣS depletion before oxidation:

$$Ca^{2+} + H_2S + 4H_2O = CaSO_4 + 2H^+ + 4H_2\uparrow \tag{9}$$

Reaction (9) also shows that anhydrite precipitation is promoted by a decrease in $[H^+]$. It is worth noting that gas release from magmas can lead to magma oxidation, and release of later oxidized fluids, by analogous progressive loss of reduced gaseous species (H_2O, CH_4, H_2S).

Quartz

Although H_2O-CO_2 phase separation would, or could, cause the precipitation of carbonate, albite, and anhydrite, this is not the case with quartz, apart from the very minor amount induced by fractional H_2O loss into the predominantly CO_2 phase. No ligands are lost which would promote quartz precipitation because quartz dissolves as H_4SiO_4, and pH has no effect until values as high as 8 to 8.5 (100°C to 160°C) are reached (e.g. Henley 1983), where the formation of alkali-SiO_2 complexes such as NaH_3SiO_4 becomes important (Anderson and Burnham 1983). The only variable which can really cause quartz precipitation is temperature decrease; hence, the occurrence of quartz veins signifies a drop in fluid temperature. At P<~750 bars, quartz solubility, and probably that of other silicates, goes through a maximum decreasing at higher as well as lower temperatures (Figure 236.13). At 500 bars, the current preliminary estimate for the formation pressure of the Hollinger-McIntyre system (*see* section above), the temperature of maximum SiO_2 solubility is 385°C; hence, temperature conditions in the Hollinger-McIntyre system appear to have been consistently on the low temperature side of the maximum so that all fluid cooling would have been accompanied by quartz precipitation.

Hydrothermal behaviour at the Hollinger-McIntyre Mines is divisible into: a) an early hydraulic cracking and inflationary phase, with little vein filling and intense wall rock interaction at ~300°C to 360°C (Wood *et al.* 1986a); followed by b) a predominantly post-inflationary, fluid cooling and vein filling phase at ~330°C down to ~230°C (Wood *et al.* 1986a, for T estimates).

PRESSURE EFFECTS

H_2O-CO_2 phase separation has significant potential for generating high liquid/gas pressures because of volumetric expansion. For example, Drummond and Ohmoto (1985) note that most significant chemical changes in the liquid phase occur by the time the vapour has expanded to equal the volume of liquid; 10% phase separation at 350°C, and only 2% at 250°C. Such pressures generated in addition to the pressure produced by the fluid generation process itself (e.g. magmatic crystallization of dominantly anhydrous minerals) could explain the evidence for hydraulic fracturing (Kerrich and Allison 1978; Phillips and Groves 1984; Wood *et al.* 1984) and volumetric inflation (Wood *et al.* 1984) in Archean Au-quartz vein systems, including dilation of ductile shear structures (e.g. the Renabie Mine; Callan and Spooner, this volume). In particular, H_2O-CO_2 phase separation at a particular level might explain how Archean Au-quartz vein systems expand from relatively narrow and insignificant root zones characterized by thin, low grade veins and veinlets (e.g. the Hollinger-McIntyre System; Lamaque, D.R. Burrows and E.T.C. Spooner, personal observation; Nudulama and 'C' zones, the Renabie Mine area, N.J. Callan and E.T.C. Spooner, personal observation)

DISCUSSION

H_2O-CO_2 phase separation provides a unified theory which, in combination with other factors, has the potential to explain several features of Archean Au-quartz vein systems including:

1. intimate co-precipitation of Au-Ag, pyrite, and other sulphides

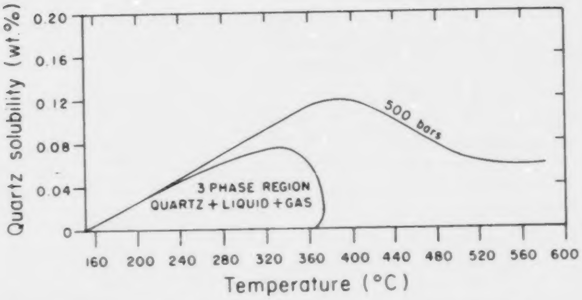

Figure 236.13. *Solubility of quartz as a function of temperature along the boundary of the three phase region and at 500 bars (modified from Kennedy 1950).*

2. co-precipitation with carbonate
3. mineralization over large vertical intervals of ~1000 m to as much as 3230 m
4. generation of oxidized Au systems containing anhydrite±hematite and sulphur isotopically depleted sulphides
5. hydraulic fracturing
6. volumetric inflation including dilation of ductile shear structures.

How widespread the evidence for CO_2 phase separation is in Archean Au-quartz vein systems can readily be determined from the characteristics of primary fluid inclusions (e.g. Ho *et al.* 1985; Wood *et al.* 1986).

A further point is that, should the consensus of thought ever consider Hemlo to be chemical-sedimentary in origin, as some controversial geological relationships (e.g. possible stratabound nature), high $\delta^{34}S$ barite (up to ~+12‰, compared with most stratiform Archean barite at ~+4‰), and apparently covariant barite $\delta^{34}S$ values, pyrite $\delta^{34}S$ values, and Au grades might possibly suggest (Cameron and Hattori 1985), then phase separation (H_2O-CO_2 and/or aqueous phase boiling) could explain two aspects of Hemlo. These aspects are the generation of an oxidized system, and the generation of a dense fluid which could produce a chemical-sedimentary horizon with a remarkably uniform Au grade (compare to Atlantis II deep, Red Sea). The former could be explained by the solution oxidation associated with the loss of reduced gas species which accompanies phase separation as discussed above, and could also explain the high sulphate $\delta^{34}S$ values and S isotopically depleted pyrite (down to -17.5‰). The second aspect could be explained by H_2O-CO_2 phase separation and/or high level aqueous phase boiling generating dense fluids, relative to Archean sea water which accumulated in topographic depressions, not necessarily above discharge points, and which formed mixed chemical-tuffacous sediments.

A final problem concerns the prevalent precipitation of Au and pyrite in metasomatised wall rock in the Hollinger-McIntyre Mines, since evidence discussed in the introduction to this section suggests that sulphidation reactions were insufficient. A possibility is that the hydraulically fractured host rocks were initially cold relative to the hydrothermal vein fluid. Fluid penetrating the wall rock cooled in intimate physical contact with it, whereas the vein fluid temperature remained relatively constant because of lack of heat exchange and internal convection. Hence, H_2O-CO_2 phase separation occurred particularly in the wall rock and caused the precipitation of Au, pyrite, and other sulphides. Evidence for the possibility of initially cold wall rock includes; a) the depth estimate of 2 km (*see* section above) giving an ambient temperature of ~100°C for a thermal gradient of ~50°C/km; and b) strain related secondary fluid inclusions giving homognization temperatures of <150°C (Wood 1987).

PRINCIPAL CONCLUSIONS

1. The mean of eight new carbonate $\delta^{13}C$ values from the 2800-, 3600-, and 3800-foot levels in the McIntyre Mine (-3.3±0.4‰) is indistinguishable from the Hollinger value of -3.0±1.5‰, whereas the spread is less (1.4‰ c.f. 4.7 ‰ total ranges). The weighted mean $\delta^{13}C$ value for the Hollinger-McIntyre system as a whole is -3.1±1.2‰ (n=22).
2. The carbon isotopic composition of carbonate in two altered albitite dikes is indistinguishable (-3.1‰, -2.8‰) from the Au associated carbonate, suggesting that the carbonates have the same origin.
3. The fluid inclusion gas analytical system, which uses a heated (~105°C) crusher modified from the design of Andrawes and Gibson (1979), has a zero blank for all gases at current detection limits, as determined by runs on heat-treated (900°C/4 hours) Brazilian quartz.
4. The following peaks have been detected using a Hewlett Packard 5890 gas chromatograph with a Porapak Q packed column at 50°C and a high sensitivity thermal conductivity detector: composite (N_2±CO±Ar±O_2±NO), and separate NO, CH_4, CO_2, N_2O, C_2H_6, and H_2O (in order of retention time). As far as is known, these results are the first to report NO and N_2O in gases from fluid inclusions in minerals.
5. Detection of significant quantities of CH_4 confirms the possibility of producing less hydrogen isotopically negative H_2O by D/H exchange with CH_4 (Wood *et al.* 1986b).
6. $CH_4/(CH_4+CO_2)$ molar ratios of quartz and scheelite samples containing best primary and strain related secondary inclusions show a similar upward decrease from 18.00±7.35% (1σ; n=6; 1500- and 1800-foot levels) to 1.37±0.81% (n=5; surface; 200- and 800-foot levels). The total range is large from 0.30% to 25.36%. This vertical decrease is interpreted to be a result of H_2O-CO_2 phase separation, since CH_4 has a high gas/liquid partition coefficient (Drummond and Ohmoto 1985).
7. The fluid inclusion gas chemistry and estimates of other gases present from measured CO_2 melting points appear to be qualitatively consistent providing that the effect of additional (N_2±CO±Ar±O_2) gases is taken into account.
8. $CH_4/(CH_4+CO_2)$ molar ratios from Au-quartz vein mineralization from the Renabie area, 80 km northeast of Wawa, are low (1.07±0.35%; n=6; all depths) and similar to the higher level and surface values from the Hollinger Mine. The Renabie is an oxidized Archean Au system (anhydrite; negative sulphide $\delta^{34}S$), whereas the Hollinger system is reduced (pyrite-pyrrhotite; $\delta^{34}S=+3.5\pm1.4$‰; Wood *et al.* 1986a). Hence, the gradational upward $CH_4/(CH_4+CO_2)$ decrease in the Hollinger system to values similar to those in the Renabie system documents H_2O (liquid) oxidation by reduced gas (H_2, CH_4, H_2S) loss during H_2O-CO_2 phase separation, a process suggested for the origin of oxidized Archean Au-quartz vein systems.
9. Samples from close proximity to graphitic interflow material from surface from the Hollinger Mine show clear increases in CH_4 contents to $CH_4/(CH_4+CO_2)$ ratios of 5.94 to 16.56%, relative to other surface material (0.30 to 1.52%). Hence, production of CH_4 by interaction with graphitic material, which could produce less carbon isotopically negative carbonate by exchange (Fyon *et al.* 1983) has been docmented.
10. A very approximate pressure estimate for the Hollinger-McIntyre Au mineralization, based on the estimated temperature of H_2O-CO_2 phase separation (~280°C; Wood *et al.* 1986a), the estimated fluid composition before unmixing (~93 mole percent CO_2, ~6 equivalent mole percent CO_2, ~1 equivalent mole percent NaCl) and P-T sections through the H_2O-NaCl-CO_2 immiscibility volume (Gehrig *et al.* 1979) is 500+200/-300 bars. Since evidence suggests that the Hollinger-McIntyre was a lithostatically pressured system (Wood *et al.* 1986a), this pressure estimate is equivalent to a depth estimate of ~1.9+0.8/-1.1 km.
11. H_2O-CO_2 phase separation, fluid inclusion evidence for which has been described from the Hollinger-McIntyre, and Pamour #1 Deposits, and several deposits in Western Australia (Groves *et al.* 1984; Walsh *et al.* 1984; Wood *et al.* 1984, 1986a; Ho *et al.* 1985), can, in combination with other factors, explain several features of Archean Au-quartz vein systems including: a) intimate co-precipitation of Au-Ag, pyrite, and other sulphides; b) co-precipitation with carbonate (e.g. Arnórsson 1978); c) mineralization over large vertical intervals of 1000 m to as much as 3230 m (Kolar, India); d) generation of oxidized Archean Au-quartz and Cu-Au-Ag-Mo-anhydrite systems by loss of reduced gas species (H_2, CH_4, H_2S); e) hydraulic fracturing; and f) volumetric inflation, including dilation of shear zones (e.g. the Renabie Mine, Callan and Spooner, this volume) and expansion of Archean Au systems from relatively insignificant root zones (based significantly on the work of Drummond and Ohmoto 1985).
12. Albite precipitated because of a combination of Na leaching from wall rocks and temperature decrease. An additional possibility is that it could precipitate from destabilization of a dawsonite-

like complex in solution ($NaAlCO_3(OH)_2^0$) stoichiometrically analogous to $NaH_2AlO_3^0$.

13. Significant quartz precipitation can only signify temperature drop, for temperatures less than the solubility maximum (~385°C at 500 bars).

ACKNOWLEDGMENTS

The authors are very grateful to Pamour Porcupine Mines Ltd. for permission to work in the Hollinger (Timmins) and McIntyre (Schumacher) Mines, and to Leysa Ligaya and Ann-Marie Matti (secretaries), and Subhash Shanbhag (draftsman) for their cheerful help. We also wish to thank Anne Thomas (graduate student, University of Toronto) for her invaluable help with the fluid inclusion gas analyses. The first two authors are particularly grateful to G. Norris, Chairman, Department of Geology, University of Toronto, for his support and encouragement. The fluid inclusion gas analytical work could not have been carried out without the initial help of a research grant from Exxon Minerals Company (Geologic Research Department), Houston, Texas which is acknowledged with very great appreciation; we particularly thank Dr. J.L. Walker, Dr. A.E. Bense and Mrs. J.P. Laurier. Finally, we acknowledge with gratitude the additional financial support of the Natural Sciences and Engineering Research Council of Canada in the form of an infrastructure grant (A0660) and an equipment grant (E5788) which was used to purchase the Hewlett Packard 5890 gas chromatograph.

REFERENCES

Anderson, G.M., and Burnham, C.W.
1983: Feldspar Solubility and the Transport of Aluminium Under Metamorphic Conditions; American Journal of Science, Volume 283-A, p.283-297.

Andrawes, F.F., and Gibson, E.K., Jr.
1979: Release and Analysis of Gases from Geological Samples; American Mineralogist, Volume 64, p.453-463.

Arnórsson, S.
1978: Precipitation of Calcite from Flashed Geothermal Waters in Iceland; Contributions to Mineralogy and Petrology, Volume 66, p.21-28.

Barker, C., and Torkelson, B.E.
1975: Gas Adsorption on Crushed Quartz and Basalt; Geochimica et Cosmochimica Acta, Volume 39, p.212-218.

Bowers, T.S.
1986: The Geochemical Consequences of H_2O-CO_2 Fluid Immiscibility on Ore Deposition; A Reaction Path Approach (Abstract); Geological Society of America Annual Meeting, Abstracts with Programs, Volume 18, p.548.

Bray, C.J., Thomas, A.V., and Spooner, E.T.C.
In Preparation: Fluid Inclusion Gas Geochemistry of the Beryl Fringe and Quartz Zone, Tanco Granitic Pegmatite, S.E. Manitoba (Abstract); Geological Society of America Annual Meeting, Abstracts with Programs, Volume 19.

Burrows, D.R., and Spooner, E.T.C.
1986: The McIntyre Cu-Au Deposit, Timmins, Ontario, Canada; p.23-39 *in* Proceedings of Gold'86, an International Symposium on the Geology of Gold, edited by A.J. Macdonald. Toronto, 517p.

Burrows, D.R., Wood, P.C., and Spooner, E.T.C.
1986: Carbon Isotope Evidence for a Magmatic Origin for Archean Gold-Quartz Vein Deposits; Nature, Volume 321, p.851-854.

Burruss, R.C.
1981: Analysis of Phase Equilibria in C-O-H-S Fluid Inclusions; p.39-74 *in* Short Course in Fluid Inclusions: Applications to Petrology, edited by L.S. Hollister, and M.L. Crawford, Mineralogical Association of Canada, 304p.

Cameron, E., and Hattori, K.
1985: The Hemlo Gold Deposit, Ontario: A Geochemical and Isotopic Study; Geochimica et Cosmochimica Acta, Volume 49, p.2041-2050.

Cherry, M.
1983: The Association of Gold and Felsic Intrusions—Examples from the Abitibi Belt; p.48-55 *in* The Geology of Gold in Ontario, edited by A.C. Colvine, Ontario Geological Survey, Miscellaneous Paper 110, 278p.

Crerar, D.A., Susak, N.J., Borcsik, M., and Schwartz, S.
1978: Solubility of the Buffer Assemblage Pyrite+Pyrrhotite+Magnetite in NaCl Solutions from 200 to 350°C; Geochimica et Cosmochimica Acta, Volume 42, p.1427-1437.

Donnelly, H.G., and Katz, D.L.
1954: Phase Equilibria in the Carbon Dioxide-Methane System; Industrial and Engineering Chemistry, Volume 46, p.511-517.

Drummond, S.E., and Ohmoto, H.
1985: Chemical Evolution and Mineral Deposition in Boiling Hydrothermal Systems; Economic Geology, Volume 80, p.126-147.

Ellis, A.J., and Mahon, W.A.J.
1977: Chemistry and Geothermal Systems; Academic Press, New York, 392p.

Friedman, I., and O'Neil, J.R.
1977: Compilation of Stable Isotope Fractionation Factors of Geochemical Interest; Article *in* Data of Geochemistry, edited by M. Fleischer, United States Geological Survey, Professional Paper 440-KK, 12p.

Fyon, J.A., Crocket, J.H., and Schwarcz, H.P.
1983: Ontario Geoscience Research Grant Program, Grant No.49—Application of Stable Isotope Studies to Gold Metallogeny in the Timmins-Porcupine Camp; Ontario Geological Survey, Open File Report 5464, 128p.

Gehrig, M., Lentz, H., and Franck, E.U.
1979: Thermodynamic Properties of Water-Carbon Dioxide-Sodium Chloride Mixtures at High Temperatures and Pressures; p.539-542 *in* 6th International Conference on High-Pressure Science and Technology, 1977, University of Colorado, Volume 1, Physical Properties and Materials Synthesis, edited by K.D. Timmerhaus and M.S. Barber, Plenum Press, New York.

Groves, D.I., Phillips, G.N., Ho, S.E., Henderson, C.A., Clark, M.E., and Woad, G.M.
1984: Controls on Distribution of Archean Hydrothermal Gold Deposits in Western Australia; p.689-712 *in* Gold '82—Proceedings of the International Symposium, Zimbabwe, edited by R.P. Foster, A.A. Balkema Publishers, Rotterdam, 753p.

Hanel, I.V., Kesler, S.E., Walsh, J.N., and Smith, T.J.
1987: Hydrothermal Fluids in Greenstone Gold Deposits of the Porcupine Camp, Superior Province, Ontario (Abstract); American Current Research on Fluid Inclusions, Program and Abstracts, p.40.

Henley, R.W.
1983: pH and Silica Scaling Control in Geothermal Field Development; Geothermics, Volume 12, p.307-321.

Ho, S.E., Groves, D.I., and Phillips, G.N.
1985: Fluid Inclusions as Indicators of the Nature and Source of Ore Fluids and Ore Depositional Conditions for Archean Gold Deposits of the Yilgarn Block, Western Australia; Transactions of the Geological Society of South Africa, Volume 88, p.149-158.

Kennedy, G.C.
1950: A Portion of the System SiO_2-H_2O; Economic Geology, Volume 45, p.629-653.

Kerrich, R., and Allison, L.
1978: Vein Geometry and Hydrostatics During Yellowknife Mineralization; Canadian Journal of Earth Sciences, Volume 15, p.1653-1660.

Lambert, I.B., Phillips, G.N., and Groves, D.I.
1984: Sulphur Isotope Compositions and Genesis of Archean Gold Mineralization, Australia and Zimbabwe; p.373-387 *in* Gold '82—Proceedings of the International Symposium, Zimbabwe, edited by R.P. Foster, A.A. Balkema Publishers, Rotterdam, 735p.

Macdonald, A.J.
1983: Boss Mountain Molybdenum Deposit: Fluid Geochemistry and Hydrodynamic Considerations; Ph.D. thesis, University of Toronto, 407p.
1984: Gold Mineralization in Ontario, 1: The Role of Banded Iron Formation; p.412-430 *in* Chibougamou-Stratigraphy and Mineralization, edited by J. Guha and E.H. Chown, Canadian Institute of Mining and Metallurgy, Special Volume 34.

Macdonald, A.J., and Fyon, J.A.
1986: Banded Iron: Gold Mineralization in a Number of Ontario Camps is Found in Banded Iron Formation; The Northern Miner Magazine, Volume 1, Number 9, p.33-35.

Parry, W.T.
1986: Estimation of XCO_2, P, and Fluid Inclusion Volume from Fluid Inclusion Measurements in the System $NaCl$-CO_2-H_2O; Economic Geology, Volume 81, p.1009-1013.

Phillips, G.N., and Groves, D.R.
1984: Fluid Access and Fluid-Wallrock Interaction in the Genesis of the Archean Gold-Quartz Vein Deposit at Hunt Mine, Kambalda, Western Australia; p.389-416 *in* Gold '82—Proceedings of the International Symposium, Zimbabwe, edited by R.P. Foster, A.A. Balkema Publishers, Rotterdam, 735p.

Phillips, G.N., Groves, D.I., and Martyn, J.E.
1984: An Epigenetic Origin for Archean Banded Iron-Formation-hosted Gold Deposits; Economic Geology, Volume 79, p.162-171.

Reed, M.H., and Spycher, N.F.
1985: Boiling, Cooling, and Oxidation in Epithermal Systems: A Numerical Modelling Approach; Reviews in Economic Geology, Volume 2, Geology and Geochemistry of Epithermal Systems, p.249-272.

Robert, F., and Kelly, W.C.
1984: Gold Mineralizing Fluid at the Sigma Mine, Abitibi Region, Quebec: A Fluid Inclusion Investigation; Geological Society of America Annual Meeting, Abstracts with Programs, Volume 16, p.636.

Roberts, R.G.
1987: Ore Deposit Models #11. Archean Lode Gold Deposits; Geoscience Canada, Volume 14, p.37-52.

Roedder, E., and Bodnar, R.J.
1980: Geologic Pressure Determinations from Fluid Inclusion Studies; Annual Review of Earth and Planetary Sciences, Volume 8, p.263-301.

Schoell, M., and Wellmer, F.W.
1981: Anomalous ^{13}C Depletion in Early Precambrian Graphites from Superior Province, Canada; Nature, Volume 290, p.696-699.

Schwarcz, H.P., and Rees, C.E.
1985: Sulphur Isotope Studies of Archean Gold Deposits; Grant 202, p.151-156 *in* Geoscience Research Grant Program, Summary of Research, 1984-1985, edited by V.G. Milne, Ontario Geological Survey, Miscellaneous Paper 127, 246p.

Seward, T.M.
1973: Thio Complexes of Gold and the Transport of Gold in Hydrothermal Solutions; Geochimica et Cosmochimica Acta, Volume 37, p.379-399
1984: The Transport and Deposition of Gold in Hydrothermal Systems; p.165-181 *in* Gold '82—Proceedings of the International Symposium, Zimbabwe, edited by R.P. Foster, A.A. Balkema Publishers, Rotterdam, 735p.

Spooner, E.T.C., Wood, P.C., Burrows, D.R., Thomas, A.V., and Noble, S.R.
1985: Geological, Fluid Inclusion, and Isotopic (Carbon and Sulphur) Studies of Au-Quartz-Carbonate-Pyrite-Scheelite Vein Mineralization and Intrusion-hosted Cu-(Au-Mo) Mineralization in the Hollinger-McIntyre System, Timmins, Ontario; Grant 236, p.229-246 *in* Geoscience Research Grant Program, Summary of Research 1984-1985, edited by V.G. Milne, Ontario Geological Survey, Miscellaneous Paper 127, 246p.

Walsh, J.F., Cloke, P.L., and Kesler, S.E.
1984: Fluid (CO_2-H_2O) Immiscibility and fO_2 as Factors in Gold Deposition: Pamour No.1 Mine, Timmins, Ontario (Abstract); Geological Society of America Annual Meeting, Abstracts with Programs, Volume 16, p.686.

Wood, P.C.
1987: The Hollinger-McIntyre Gold-Quartz Vein System, Timmins, Ontario: Geologic Characteristics, Fluid Properties and Light Stable Isotope Geochemistry; M.Sc. thesis, University of Toronto.

Wood, P.C., Burrows, D.R., Thomas, A.V., and Spooner, E.T.C.
1986a: The Hollinger-McIntyre Au-Quartz Vein System: Geologic Characteristics, Gold Occurrence, Fluid Properties and Light Stable Isotope Geochemistry; p.56-80 *in* Proceedings of Gold '86, an International Symposium on the Geology of Gold, edited by A.J. Macdonald, Toronto, 517p.

Wood, P.C., Burrows, D.R., and Spooner, E.T.C.
1986b: Au-Quartz Vein and Intrusion-hosted Cu-Au-Ag-Mo Mineralization, Hollinger-McIntyre Mines, Timmins, Ontario: Geological Characteristics, Structural Examination, Igneous and Hydrothermal Alteration Geochemistry, and Light Stable Isotope (Hydrogen and Oxygen) Geochemistry; Grant 236, p.115-137 *in* Geoscience Research Grant Program, Summary of Research, 1985-1986, edited by V.G. Milne, Ontario Geological Survey, Miscellaneous Paper 130, 235p.

Wood, P.C., Thomas, A.V., Burrows, D.R., Macdonald, A.J., Noble, S.R., and Spooner, E.T.C.
1984: CO_2-bearing Low-Moderate Salinity Fluids in Archean Gold-Quartz-Carbonate-(W-Mo) Vein Deposits and Magmatically Derived Mo, W, Ta and Sn Mineralization (Abstract); Geological Society of America Annual Meeting, Abstracts with Programs, Volume 16, p.700.

Grant 249 Geochemical Studies of Formation Waters From Paleozoic Strata, Southwestern Ontario

P. Dollar[1], S.K. Frape[1], R.H. McNutt[2], P. Fritz[1], and R.W. Macqueen[3].

[1]Department of Earth Sciences, University of Waterloo, Waterloo

[2]Department of Geology, McMaster University, Hamilton

[3]Institute of Sedimentary and Petroleum Geology, Geological Survey of Canada, Calgary

ABSTRACT

The groundwater of southwestern Ontario has been analyzed for: major, minor, and trace element geochemistry; stable isotope content; tritium; and strontium isotopic content. The results of these analyses indicate that most sedimentary formations contain very concentrated brines (>300 grams per litre (g/L) Total Dissolved Solids (TDS)), which have distinctive geochemical and isotopic signatures for individual units. Some samples that have been collected, however, appear to be mixtures of brines from various formations and/or mixtures of formation brines with more dilute groundwaters such as glacial meltwaters or recent meteoric waters. The mixing of various water masses would indicate that both paleo-migration and recent migration of groundwater has taken place. This, in turn, has a number of implications on the formation of economic deposits in the area, and on active and proposed waste disposal schemes.

INTRODUCTION

The chemical composition of formation waters within the Paleozoic strata of southwestern Ontario and Michigan are important for a variety of reasons. Water composition controls mineral scaling and corrosion of oilfield production equipment. Formation water salinities affect the calibration of electric logs which are used to determine petrophysical parameters, production zones, and hydrocarbon reserves. Casing leaks from fluid-bearing horizons, other than the producing zone, may be identified if there is sufficient variability between the chemical constituents of the two zones.

Formation waters are commonly associated with oil and gas accumulations and metallic mineral deposits in sedimentary basins. Examination of the inorganic chemical constituents that characterize these waters may reflect the origin and migrationary pathways of these fluids. Knowledge of the composition and variability of formation waters may also be used to evaluate the importance of rock-water interaction in their evolutionary history. This information is extremely useful when developing: (i) hydrocarbon generation models for evaluating source rocks and trapping mechanisms; and (ii) waste disposal strategies.

STRATIGRAPHIC AND STRUCTURAL CONTROLS

In order to appreciate possible hydrogeological fluid migration aspects of the study, it is necessary to be fully acquainted with the important stratigraphic and structural features which might influence fluid movement in the area.

Southwestern Ontario and Michigan are underlain by an essentially undisturbed Phanerozoic sedimentary succession which rests unconformably on Precambrian basement rocks, and is overlain by Pleistocene glacial deposits. The area of study extends from Oxford County, Ontario, in the east to Missaukee County, Michigan (USA), in the west. In the eastern part of the study area, Phanerozoic is represented by 875 m of strata that is Upper Cambrian to Upper Silurian in age. The sedimentary units generally thicken towards the depocentre of the Michigan Basin where a much more complete stratigraphic record occurs (Figure 249.1). In the central part of the basin, the Phanerozoic sequence ranges in age from Lower Cambrian to Upper Jurassic, and is greater than 5 km in total thickness. The present study characterizes inorganic chemical constituents in formation waters from nine hydrocarbon-bearing horizons and two salt mines located in southwestern Ontario and Michigan (Table 249.1).

The Algonquin and Findlay Arches, broad Precambrian highs separated by the Chatham Sag, trend northwest-southeast, dividing the Ontario Peninsula into two parts (Figure 249.2). These two structurally positive features were probably introduced during late Precambrian time, but were intermittently reactivated during the Paleozoic to form a broad platform between a more rapidly subsiding Michigan Basin on the west and the Appalachian Basin to the southeast (Sanford *et al.* 1985). The current regional dip of the Paleozoic rocks to the northwest of the arches is 6 to 9 m/km into the Michigan Basin; and to the southeast of the arches, the dip is 6 m/km into the Appalachian Basin (Winder and Sanford 1972). Paleozoic strata in the Chatham Sag are for the most part horizontal.

Sanford *et al.* (1985) have proposed a relatively active tectonic history for southwestern Ontario. Tectonically associated fault block readjustment has provided the structural control for the origin and development of southwestern Ontario's hydrocarbon traps. The implications of such tectonic movements on the hydrodynamic/fluid migration history are being examined.

SAMPLE COLLECTION AND ANALYSIS

The waters studied are oilfield brines from southwestern Ontario (Figure 249.3). Samples were initially collected in large polyethylene bottles from producing oil and gas wells and dry holes (no oil or natural gas encountered). Prior to geochemical analyses, samples were filtered through a hand-held Millipore filter system using 0.45 μm filters. A 500 mL aliquot for cation analyses was acidified to a pH of <2 using concentrated HCl. Analyses for cations were performed by atomic absorption spectrophotometry using standard analytical procedures. A second 500 mL aliquot was filtered and left unacidified to be used for

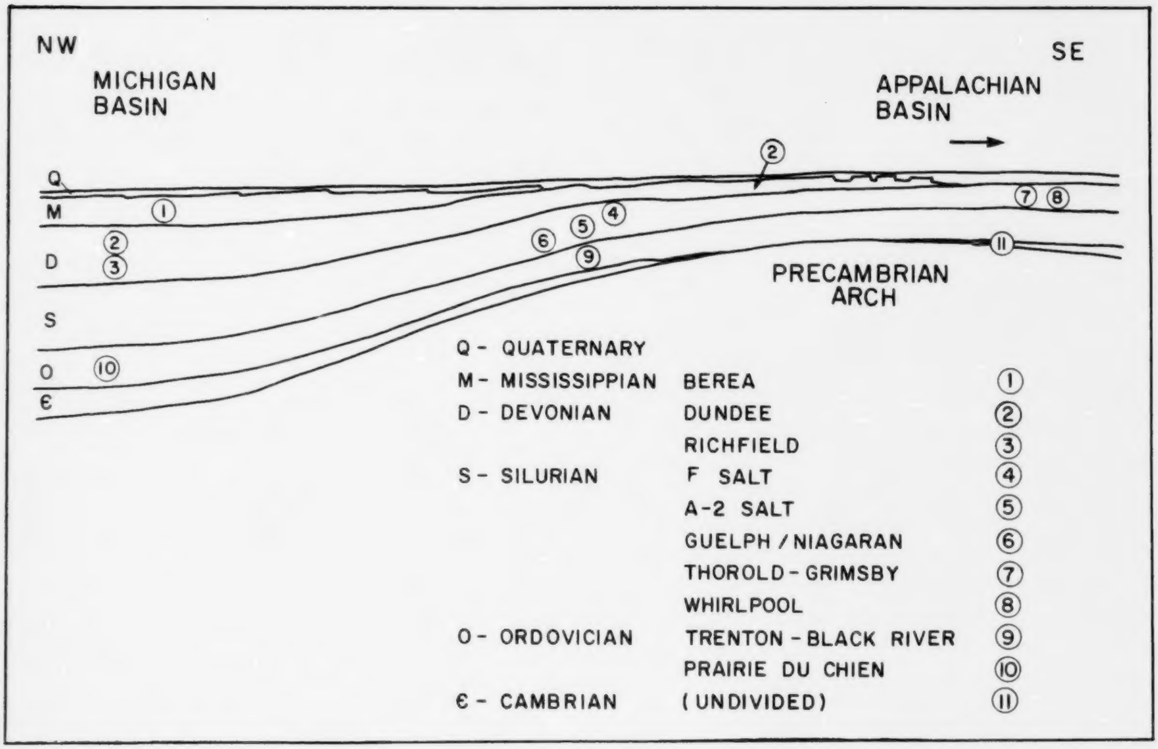

Figure 249.1. *Schematic representation of the Paleozoic strata on the western flank of the Michigan Basin.*

Table 249.1 Dominant reservoir lithologies for stratigraphic units sampled in southwestern Ontario and Michigan.

PERIOD	PRODUCING INTERVAL	LOCATION	LITHOLOGY
Mississippian	Berea	Mich	Sandstone
Devonian	Dundee	Ont/Mich	Carbonate
	Richfield	Mich	Carbonate
Silurian	F Unit	Ont	Salt
	A-2 Unit	Ont	Salt
	Guelph/Niagaran	Ont/Mich	Carbonate
	Thorold/Grimsby	Ont	Sandstone
	Whirlpool	Ont	Sandstone
Ordovician	Trenton- Black River	Ont/Mich	Carbonate
	Prairie du Chien	Mich	Sandstone
Cambrian	(Undivided)	Ont	Sandstone

analyses of SO_4^{2-}, Cl^-, and Br^- by a Dionex Auto Ion System 12 analyzer. All samples were treated using standard procedures, although certain special procedures as outlined by Dionex were used for Br^- analyses.

At all sites a 125 mL filtered sample was taken to be used for analyses of ^{18}O, deuterium, and tritium. Deuterium and ^{18}O analyses were done using conventional preparation techniques and mass spectrometry. However, because of the high salinities of the brines, it was necessary to correct the ^{18}O data according to the method proposed by Sofer and Gat (1972). Deuterium analyses were done on water vapour distilled from the brines. Distillations were performed at elevated temperatures to prevent formation of hydrated salts. Results are reported with respect to

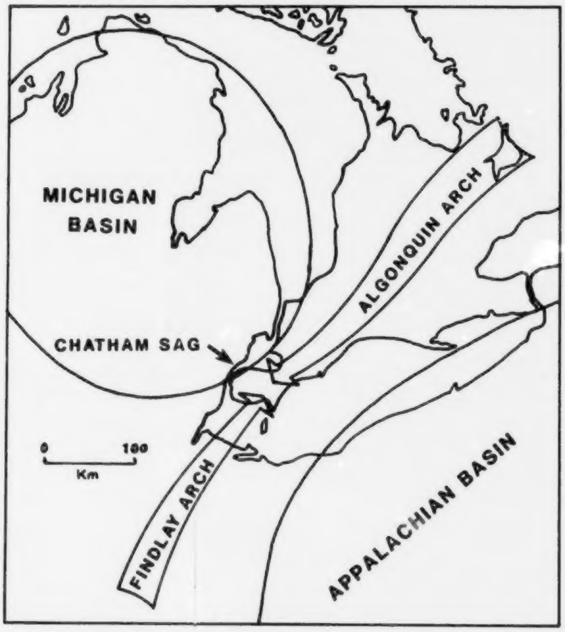

Figure 249.2. *Regional tectonic structures influencing the Paleozoic strata of eastern Michigan and southwestern Ontario.*

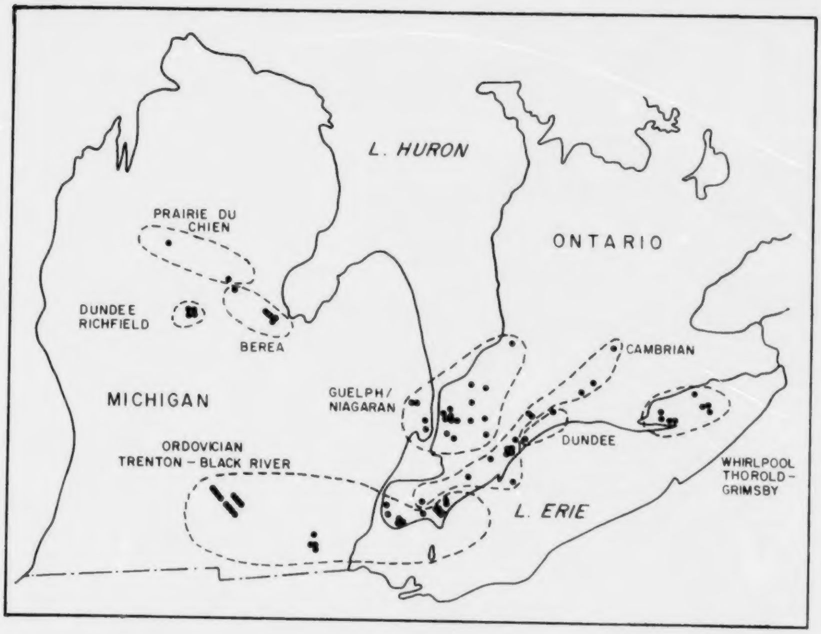

***Figure 249.3.** Location of groundwater samples, southwestern Ontario and Michigan.*

Table 249.2 Chemistry of typical formation waters from southwestern Ontario and Michigan.

Element mg/l	Berea	Dundee (Ont)	Dundee (Mich)	Richfield	F Salt	A–2 Salt	Guelph/ Niagaran	Thorold/ Grimsby	Whirlpool	Trenton/ Black River	Prairie du Chien	Cambrian
Ca	38600	635	40300	64900	47600	4530	52500	41050	48050	24325	87500	50560
Na	54800	3690	70600	23400	33500	93770	47300	25100	31725	42515	26700	45870
Mg	7810	630	6990	7960	16400	2900	9240	4930	4480	5170	8700	8600
K	740	85	3370	8320	5700	2660	3370	710	795	2660	18400	1480
Sr	1490	30	1120	2060	1620	190	840	403	467	545	2850	1285
Li	2.4	8.2	16.7	16.9	NA	1.8	10.8	15.1	17.5	9.7	8.2	3.4
Cl	179940	9095	202650	173130	232000	198000	197170	119635	150990	132230	249700	196040
Br	1270	50	1315	1970	3215	620	1925	805	1060	680	1930	1570
SO4	<15	795	166	205	108	434	173	382	376	375	63	166
TDS	300820	15030	312540	281985	340145	303110	312725	193100	238100	208750	394900	303650

the Vienna-SMOW standard. Accuracy is ±0.15‰ for ^{18}O, and ±2.0‰ for deuterium.

Strontium isotopic analyses were measured on a VG 354,5-collector mass spectrometer, following separation of Sr by standard ion-exchange techniques. Elution was carried out using 2.5 M HCl. Within-run precision of a single analysis is ±0.003‰. Repeated runs of Eimer & Amend and NBS 987 standards give 0.70802 and 0.71024 respectively.

All analyses of inorganic chemical constituents and hydrogen and oxygen stable isotopes were performed at the University of Waterloo. Analyses of strontium isotopes were done at McMaster University, Hamilton, Ontario.

RESULTS AND INTERPRETATION

MAJOR ELEMENT CHEMISTRY

Almost all groundwaters sampled in the present study are brines according to the classification scheme proposed by Davis (1964), since most contain >100 000 ppm total dissolved solids. Representative chemistries of the most concentrated brines from each stratigraphic horizon are presented in Table 249.2. The principal ions contained in these waters are Ca^{2+}, Na^{+}, and Cl^{-} with total concentrations in excess of 300 g/L at many sites. The most concentrated waters encountered in the Michigan Basin are from the Prairie du Chien sandstone. These waters have Total Dissolved Solid (TDS) near 400 g/L and are dominated by Ca, K, and Cl ions.

Reconstruction of chemical evolutionary paths of many highly saline formation waters are often attempted using the methodology presented by Carpenter (1978). The chemical evolution is traced by comparing the chemical composition of the subsurface water with that of seawater with the same Br concentration level. Comparison based on the Br data reveals that the average values for each Michigan Basin formation are depleted in SO_4 and Mg, and enriched in Ca relative to seawater (Figure 249.4). Most samples plot near the Cl evaporation line and below the Na evaporation line, past halite saturation. The only exceptions are the dilute groundwaters from the Dundee Formation in Ontario and the NaCl-dominated waters encountered in the F Unit salt. The majority of samples analyzed are depleted in K relative to seawater, except for the Richfield brine that is

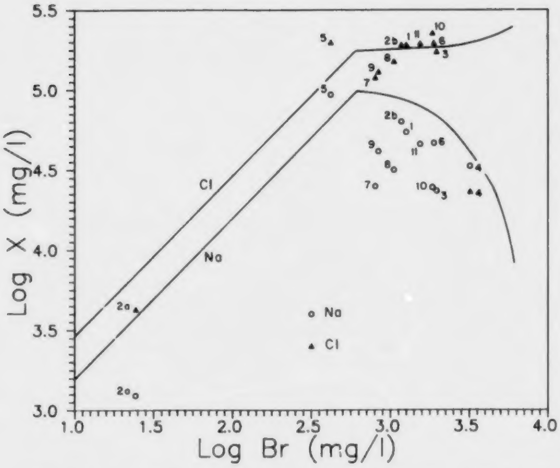

Figure 249.4a. *Composition of different chemical constituents of formation waters from the Michigan Basin with that of evaporating seawater at the same level of Br concentration. Na and Cl vs. Br. The solid line refers to the compositional change for evaporating seawater (after Carpenter 1978).*

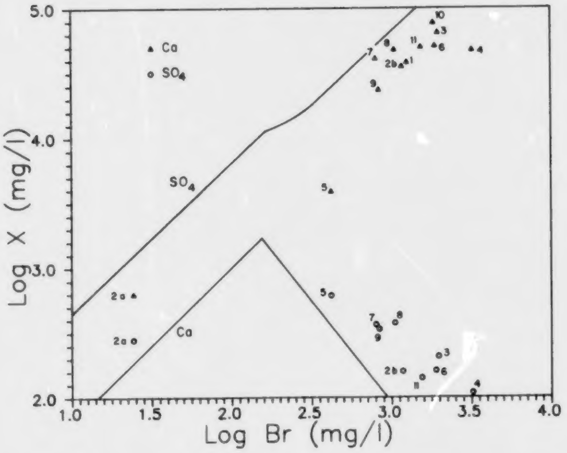

Figure 249.4b. *Composition of different chemical constituents of formation waters from the Michigan Basin with that of evaporating seawater at the same level of Br concentration. Ca and SO_4 vs. Br. The solid line refers to the compositional change for evaporating seawater (after Carpenter 1978).*

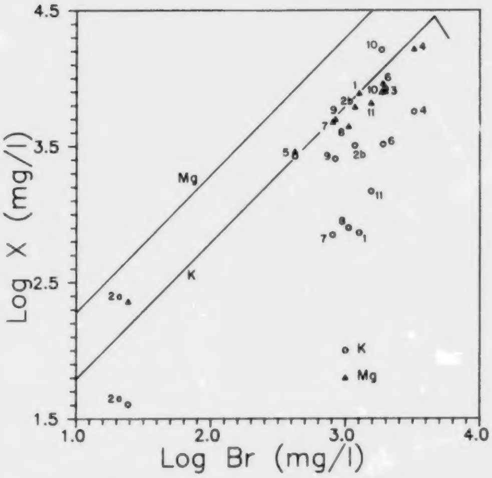

Figure 249.4c. *Composition of different chemical constituents of formation waters from the Michigan Basin with that of evaporating seawater at the same level of Br concentration. Na and Cl vs. Br. The solid line refers to K and Mg vs. Br. The solid line refers to the compositional change for evaporating seawater (after Carpenter 1978).*

Berea	1
Dundee (Ont)	2a
Dundee (Mich)	2b
Richfield	3
F Salt	4
A-2 Salt	5
Guelph/Niagaran	6
Thorold/Grimsby	7
Whirlpool	8
Trenton-Black River	9
Prairie du Chien	10
Cambrian	11

FIGURE 249.4. *LEGEND FOR a,b,c.*

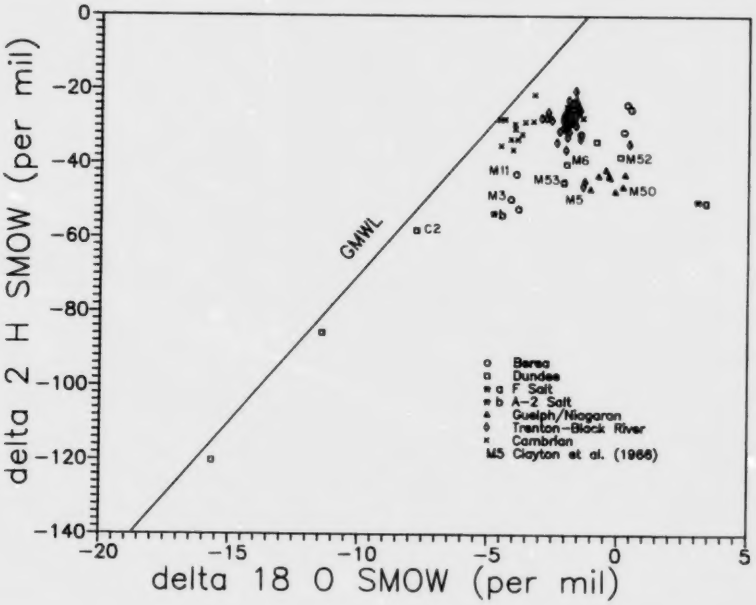

Figure 249.5a. *Stable isotopic composition (oxygen-18 and deuterium) for brines and saline waters from southwestern Ontario and Michigan. Data from Clayton et al. 1966 have been included for correlative purposes.*

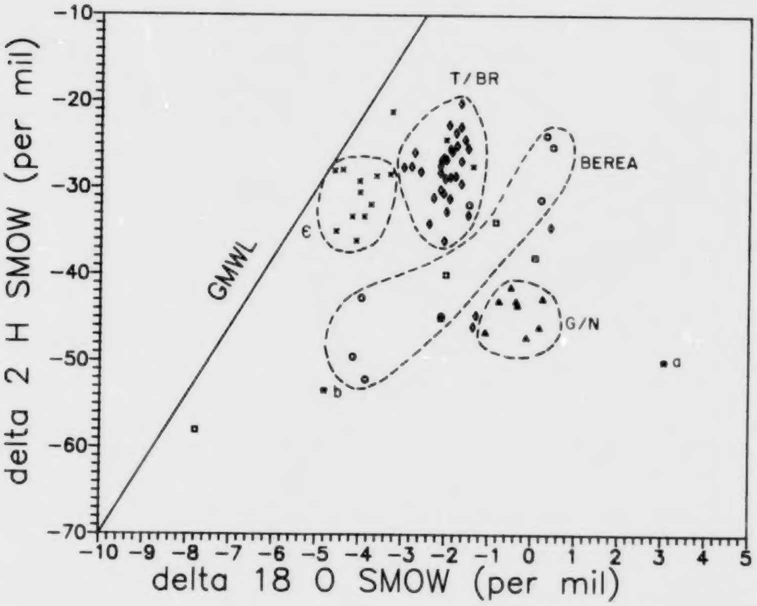

Figure 249.5b. *Stable isotopic composition (oxygen-18 and deuterium) for brines and saline waters from southwestern Ontario and Michigan. Distinct groupings by stratigraphic unit are shown to occur for many of the samples analyzed.*

similar to seawater, and the Prairie du Chien brine that is moderately enriched.

STABLE ISOTOPES (^{18}O and ^{2}H)

Oxygen and hydrogen stable isotopes are used in conjunction with geochemical compositional data to help better define the origin of water in oilfield brines of the area. Figure 249.5 shows the relationship between Oxygen-18 and Deuterium for the southern Ontario and Michigan brines and other selected groundwater data from areas adjacent to the study site. For correlative purposes, brines from the Michigan Basin (Clayton *et al.* 1966) are also included.

Brines from the present study plot below the global meteoric water line. The most concentrated brine samples from the different stratigraphic units have a narrow range of composition, with Cambrian and Ordovician waters positioned nearest the global meteoric water line. The lower salinity waters of the Silurian Salina and Guelph Formations and Mississippian Berea Formation depart significantly from the line. As an example, Berea samples with concentrations greater than 300 g/L TDS, plot in a very tight

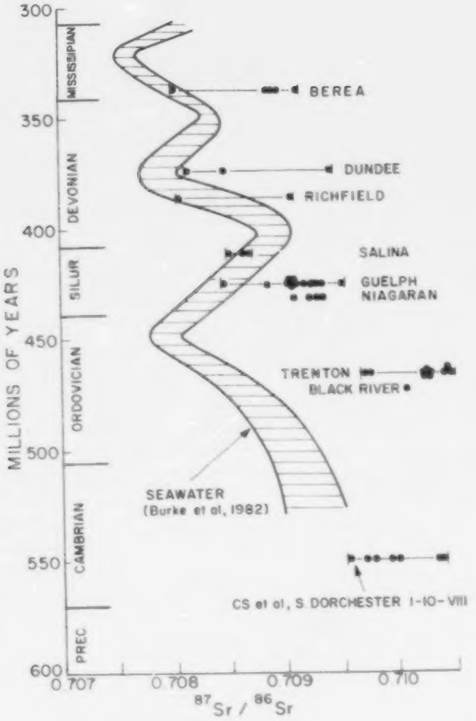

Figure 249.6. *$^{87}Sr/^{86}Sr$ ratios for brine samples from southwestern Ontario compared to seawater curve with time (after Burke et al. 1982).*

Table 249.3 Comparison of $^{87}Sr/^{86}Sr$ ratios for the whole rock, cement and brine for a typical Cambrian sample.

CS et al. S. Dorchester 1 – 10 – VIII 87Sr/86Sr Study	
1. Whole rock (1069 m)	= 0.73302
2. Calcite cement (1069 m) (leached with cold 0.5 HAc)	= 0.70964
3. Whole rock – leachate	= 0.73895
4. Brine (1063 – 1071 m)	= 0.70957

area at approximately 0.5‰ ^{18}O, and -30‰ ^{2}H. More dilute samples of Berea brines (<230 g/L) plot much closer to the meteoric waterline around an area centred on -4‰ ^{18}O and -50‰ ^{2}H. This trend, like that found for some other formations, is probably due to dilution with a component of fresh, more recent meteoric waters. Two low salinity samples from the Devonian age Dundee Formation are depleted in ^{18}O and ^{2}H, characteristic of waters recharged under cooler climatic conditions.

The brines show a large enrichment in ^{18}O, but a relatively small enrichment in deuterium. Hitchon and Friedman (1969) have attributed the ^{18}O enrichment of formation waters to the exchange of oxygen isotopes between water and carbonate minerals. Although exchange of deuterium takes place between waters and hydrogen compounds in sedimentary basins, the effect is minimized by the overwhelming mass of formation water relative to hydrogen compounds (most notably H_2S, Hitchon and Friedman 1969).

Several possible mechanisms could be used to account for the observed ^{18}O—^{2}H trend. The formation of clays and hydration of silicates has been shown to isotopically deplete the residual fluid in ^{18}O and enrich the fluid phase in ^{2}H (Fritz and Frape 1982). The end result of this process would be to move the isotopic composition of a fluid up and to the left on Figure 249.5. This is very interesting in light of the groupings and age distribution of the brines. In order to confirm this hypothesis, much more work will be required involving the identification and isotopic analyses of clay minerals in the various horizons.

Alternatively, the trends seen on Figure 249.5 could represent varying mixtures of two end members. As an example, a concentrated fossil Michigan Basin seawater, possibly similar in composition to a Canadian Shield brine.

In support of this view point, the work of Knauth and Beeunas (1986) is very interesting. They have discussed several ways to enrich ^{18}O. The most common sources of ^{18}O-enriched waters are connate brines, waters from gypsum dehydration, waters from salt, or mixtures. The major conclusion that these researchers have reached is that mixtures of meteoric waters and original formation or connate brines may be far more common in sedimentary basins than originally believed.

Work is presently underway to detail the influence of water-rock interaction versus mixing in each of the formations. However, whatever scenarios are developed for the ^{18}O—^{2}H distributions in the basins involved, they must agree in part or whole with other isotopic and geochemical trends.

STRONTIUM ISOTOPES ($^{87}Sr/^{86}Sr$ RATIOS)

Strontium isotopic results are shown in Figure 249.6 as a function of the age of the host rock that contains the brine. Also shown is the curve of Burke *et al.* (1982), describing the change in the $^{87}Sr/^{86}Sr$ composition of seawater over Paleozoic time. Because Sr has a long residence time in the ocean, its concentration and isotopic composition is uniform throughout the world's oceans at any given time (Veizer and Compston 1974). Therefore, there is the potential for Sr to be used as a geochronological tool for marine sediments and/or as an indicator of the changes in chemistry that occur during diagenesis. It is the latter that is of interest to us in this study.

The Sr seawater curve shows a large variation over the time interval under study, varying from a high of approximately 0.7095 in the Cambrian to a low of less than 0.7076 in the Middle Mississippian, with a series of cyclical oscillations in the interim. If the brines measured in this study are the same age as their host rock, then they all have $^{87}Sr/^{86}Sr$ values greater than that of seawater for the time period in question, with the exception of the Silurian Salina waters and one sample from each of the Guelph, Richfield, and Berea Formations. Such elevated ratios imply that there has been water-rock interaction *in situ*. If the water is not the same age as its present host, then the interpretation is more difficult. For example, if the Guelph brines were really Cambrian in age and subsequently migrated up-section, then what appears to be water-rock interaction in Guelph time may not be the case at all, i.e., there was only fluid migration with no water-rock interaction. No interaction seems a highly unlikely scenario based on our extensive experience studying the brines in rocks on the Precambrian Shield (Fritz and Frape 1982; Frape *et al.* 1984; McNutt *et al.* 1984).

The Ordovician samples are not as ambiguous; their ratios are higher than that of seawater for all of Phanerozoic time (Burke *et al.* 1982), so some water-rock interaction is indicated. (Seawater values for the Precambrian are poorly known overall, but must be lower in value. Veizer *et al.* (1982) propose that the $^{87}Sr/^{86}Sr$ ratio of Archean time was 0.7012 to 0.7025). The same may be said for the Cambrian samples, but not with the same conviction due to the limited number of samples, and the tendency of those we do have to break into two groups (Figure 249.6). One of the samples, CS *et al.*, Dorchester 1-10-VIII, possibly lies on the extrapolated seawater curve.

Of the samples studied to date, only the brines found in the Salina Formation have the same ratios as the seawater curve for that time. Therefore, it is possible that this brine has remained in its present host rock since Silurian time with essentially no water-rock interaction.

The drill hole CS *et al.*, South Dorchester 1-10-VIII was studied in detail to determine if the brine's $^{87}Sr/^{86}Sr$ value relates to the host rock. Both the core samples and the brine are from the Cambrian Mount Simon Formation at a depth of 1062 to 1071 m, immediately overlying the Precambrian basement. The rock is fine- to medium-grained arkose containing a suite of diagenetic minerals including dolomite, quartz, and feldspar overgrowths, clay minerals and calcite. A detailed Scanning Electron Microscope (SEM) and cathode luminoscopic study is now underway. Preliminary examination shows that the calcite cement is the last diagenetic phase to form, replacing earlier primary and secondary phases and infilling pore spaces. One sample was leached by a dilute solution of acetic acid to remove the calcite, but not dissolve the other minerals. The results are given in Table 249.3 for the sample from 1069 m. The whole-rock value of 0.7330 reflects the presence of feldspar with its high Rb/Sr ratio and probable Precambrian age. The leachate, representing the dissolved calcite, has a $^{87}Sr/^{86}Sr$ value identical to the brine, i.e., 0.7096 (compare lines 2 and 4, Table 249.3). The whole-rock minus leachate fraction (line 3, Table 249.3) increases in value, as expected, if only the low $^{87}Sr/^{86}Sr$ phase calcite dissolves.

The Sr isotopic composition of the brine in drillhole 1-10-VIII is slightly elevated with respect to the seawater curve for Cambrian time and reflects minor water-rock interaction. Whether this occurred *in situ* or not, cannot be confirmed until more studies are done. Isotopic equilibrium between calcite and brine imply that the former precipitated from the later. Therefore, the minimum residence time for the brine in its present host rock is the age of the calcite, an unknown at present. Future work on the application of Sr isotopes in sedimentary basins has to involve the separation and analysis of all the diagenetic phases. The separation will be painstaking, but the results will be rewarding in the further understanding of the origin and migration of oilfield brines.

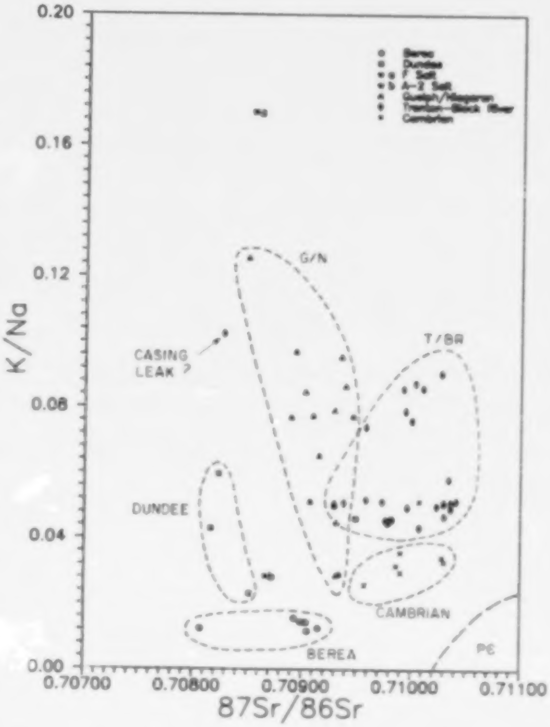

Figure 249.7. *A K/Na versus $^{87}Sr/^{86}Sr$ plot for brines and saline waters from the Paleozoic strata of southwestern Ontario and Michigan. Data from the Canadian Shield are added for comparison.*

DISCUSSION

Preliminary results and interpretation would suggest that three major groundwater types occur in the sedimentary rocks of southwestern Ontario. These would consist of: a) a distinctive formation brine which has similar geochemical and isotopic compositions throughout a particular formation; b) meteoric groundwaters which are generally found at shallower depths across the area; and c) a glacial meltwater which usually occurs in Devonian age sedimentary rocks. Several of the samples obtained to date appear to be mixtures of these various end members, or in some cases, mixtures of formation brines from strata of different ages.

Figure 249.7 is a plot of K/Na versus $^{87}Sr/^{86}Sr$ for selected water samples from several producing horizons. The K/Na ratio puts a relatively conservative cation Na against a very reactive cation, K. Potassium is easily weathered from many detrital silicate minerals and is a major component of several secondary clay minerals. Therefore, the use of this ratio may help to distinguish degrees of water-rock interaction, as well as distinguishing mineralogical composition (e.g. carbonates versus clastics).

Distinct groupings for each stratigraphic interval are shown in Figure 249.7. The Precambrian brines from the Sudbury area have the lowest K/Na ratio and the highest $^{87}\text{Sr}/^{86}\text{Sr}$ values. Brines from the Mississippian and Cambrian sandstones most closely resemble the Precambrian brines. Samples collected from carbonate reservoir rocks generally have higher K/Na ratios than their clastic counterparts. Other samples, such as some brines from Guelph-aged strata, plot near or among the Cambrian and Ordovician brines and would appear to be mixtures of the formation water end members. In several cases, some of these samples have strontium isotopic and/or stable isotopic compositions which would support this statement. Casing leaks from horizons other than the producing interval may also be detected using ratio plots. For instance, the Michigan Trenton-Black River sample that plots to the right of the Guelph/Niagaran Grouping is probably the result of such a leak. The most likely scenario is that this sample has been contaminated with a Niagaran brine resulting in the reduction of the $^{87}\text{Sr}/^{86}\text{Sr}$ isotopic value, and an increase in the K/Na ratio. This particular sample also plots in close proximity to the Guelph/Niagaran field on the oxygen versus deuterium diagram, providing further evidence. To date, no Niagaran wells have been sampled in this particular area, but future sampling should unequivocally provide more detailed information to prove this point.

Many additional ratio plots can be constructed with very similar results. In all cases they show strong individual groupings of Precambrian, Cambrian, and Ordovician brines with Precambrian fluids usually resembling Cambrian fluids more closely than Ordovician fluids. Based on very preliminary results, the apparent lack of overlap between brines from these variously aged rocks would argue against large-scale present-day migration and mixing between these units.

CONCLUSIONS

Several conclusions can be drawn on the basis of the work to date:

1. Very concentrated brines (>300 g/L TDS) exist in most Paleozoic strata of southwestern Ontario and Michigan. These brines are usually Ca-Na-Cl in composition; although some variability of Ca/Na does occur. Deep basin brines from the Prairie du Chien sandstones are Ca, K, and Cl solutions.
2. Devonian-aged strata in southwestern Ontario usually contain much more dilute saline waters (TDS <30 g/L), whose stable isotopic signature (^{18}O and ^{2}H) would suggest they were recharged under a cooler climate, probably the last period of deglaciation.
3. The most concentrated brines and waters from each unit have similar isotopic and geochemical characteristics which are distinct from the concentrated brines of other units.
4. Although Cambrian and Mississippian brines come closest isotopically and geochemically to known Precambrian brines at Sudbury, Ontario, very large geochemical differences exist. All Paleozoic brines have several orders of magnitude more Mg than any Canadian Shield brine, and the stable isotope composition of the various Paleozoic brines plots, as most sedimentary brines, to the right of the global meteoric water line.
5. Many samples taken in this study appear to be mixtures of different formation fluids, recent meteoric waters, and dilute subglacial meltwaters. Such mixtures would indicate both past and present migration of fluids within the area.

Considerably more detailed sampling and supporting diagenetic work is presently underway in order to evaluate the extent and timing of fluid migration and mixing.

ACKNOWLEDGMENTS

The authors wish to thank R.A. Trevail of the Petroleum Resources Laboratory, London, for his continued interest in the project and his help in obtaining samples. We would especially like to thank all the individual and corporate petroleum producers in southwestern Ontario and Michigan for allowing us access to samples. The analytical support of R. Kellerman, geochemistry and the isotope laboratory at the University of Waterloo, have been of great assistance. The technical support of I. McAndrew, D. Jones and C. Jager at McMaster University is greatly appreciated.

REFERENCES

Burke, W.H., Denison, R.E., Heatherington, E.A., Koepnick, R.B., Nelson, H.F., and Otto, J.B.
1982: Variation of Seawater $^{87}\text{Sr}/^{86}\text{Sr}$ Throughout Phanerozoic Time; Geology, Volume 10, p.516-519.

Carpenter, A.B.
1978: Origin and Chemical Evaluation of Brines in Sedimentary Basins; Oklahoma Geological Survey, Circular 79, p.6077.

Clayton, R.N., Friedman, I., Graf, D.L., Mayeda, T.K., Meents, W.F., and Shimp, N.F.
1966: The Origin of Saline Formation Waters. 1. Isotopic composition; Journal of Geophysical Research, Volume 71, p.3869-3882.

Davis, S.N.
1964: The Chemistry of Saline Waters by R.A. Dreiger-Discussion; Ground Water, Volume 2, Number 1, p.51.

Frape, S.K., and Fritz, P.
1982: The Chemistry and Isotopic Composition of Saline Groundwaters from the Sudbury Basin, Ontario; Canadian Journal of Earth Sciences, Volume 19, p.645-661.

Frape, S.K., Fritz, P., and McNutt, R.H.
1984: The Role of Water-Rock Interaction in the Chemical Evolution of Groundwaters from the Canadian Shield; Geochimica et Cosmochimica Acta, Volume 48, p.1617-1627.

Fritz, P., and Frape, S.K.
1982: Saline Groundwaters in the Canadian Shield-a First Overview; Chemical Geology, Volume 36, p.179-190.

Hitchon, B., and Friedman, I.
1969: Geochemistry and Origin of Formation Waters in the Western Canada Sedimentary Basin-I. Stable Isotopes of Hydrogen and Oxygen; Geochimica et Cosmochimica Acta, Volume 33, p.1321-1349.

Knauth, L.P., and Beeunas, M.A.
1986: Isotope Geochemistry of Fluid Inclusions in Permian Halite with Implications for the Isotopic History of Ocean Water and the Origin of Saline Formation Waters; Geochimica et Cosmochimica Acta, Volume 50, p.419-433.

McNutt, R.H., Frape, S.K., and Fritz, P.
1984: Strontium Isotope Composition of Some Brines from the Precambrian Shield of Canada; Isotope Geoscience, Volume 2, p.205-215.

Sanford, B.V., Thomson, F.J., and McFall, G.H.
1985: Plate Tectonics-A Possible Controlling Mechanism in the Development of Hydrocarbon Traps in Southwestern Ontario; Bulletin of Canadian Petroleum Geologists, Volume 33, Number 1, p.52-71.

Sofer, Z., and Gat, J.R.
1972: Activities and Concentrations of ^{18}O in Concentrated Aqueous Salt Solutions-Analytical and Geophysical Implications; Earth and Planetary Science Letters, Volume 15, p.232-238.

Veizer, J., Compston, W., Hoefs, J., and Nielsen, H.
1982: Mantle Buffering of the Early Oceans; Naturwissenschaften, Volume 69, p.173-180.

Veizer, J., and Compston, W.
1974: $^{87}Sr/^{86}Sr$ Composition of Seawater During the Phanerozoic; Geochimica et Cosmochimica Acta, Volume 38, p.1461-1484.

Winder, C.G., and Sanford, B.V.
1972: Stratigraphy and Paleontology of Paleozoic Rocks of Southern Ontario. Excursion A45-C45; Guidebook, 24th Session, International Geological Congress, Montreal, Quebec.

Grant 262 Geology, Geochemistry, and Economic Significance of Carbonaceous Host Rocks in Gold Deposits of the Timmins Area

Graham C. Wilson and John C. Rucklidge

IsoTrace Laboratory, University of Toronto

ABSTRACT

The results of this study of carbonaceous gold ores and host rocks in the Abitibi Belt, with emphasis on the Owl Creek Mine, illustrate the relationship of epigenetic gold mineralization to the mechanical and chemical properties of the local strata. Minor element and carbon isotope analyses are used to document the concentration of carbon in metasediments resulting from intensive pressure solution adjacent to zones of deformation, a process originally inferred by field and petrographic observations. Variation in reduced carbon content and $\delta^{13}C$ values near ore zones reflects the process of ductile shear by which the carbon is effectively mobilized, and by which the setting for late gold mineralization is prepared. These processes may be indicated on a regional scale by hydrocarbon contents in potential host rocks. Arsenic is an effective indicator element for gold in both sedimentary and volcanic units. A proportion of the gold is concentrated in quartz vein selvages as a result of local reduction against carbonaceous matter, but much is trapped within sulphide minerals, particularly in a porous habit of erratically arsenical pyrite which developed subsequent to growth of metamorphic pyrite porphyroblasts.

INTRODUCTION

A comparison of well-documented quartz-vein gold deposits indicates the prevalence of structural control, and that a very wide range of lithologies may serve as host rocks in different regions at different times. This paper describes specific chemical characteristics of deformed metasedimentary rocks and adjacent carbonatized metavolcanic rocks in the Timmins area; such features are to be expected in other parts of the Abitibi Belt and wherever faults and shear zones crosscut similar packages of strata with strong internal contrasts in competence and bulk chemistry.

SAMPLING LOCATIONS

The Owl Creek and Hoyle Pond Mines are situated in the poorly-exposed succession of metasedimentary and metavolcanic rocks underlying southern Hoyle Township. The two deposits lie between the Kidd Creek Mine metallurgical plant in the east and the new (Canamax Resources Incorporated) Bell Creek Mine to the west (Knoll 1986; Harron *et al.* 1987). Regional structural control on gold deposits in this area, as in other parts of the greenstone belt, is a consequence of major deformation zones (e.g. Shegelski 1986). The field data, geochemistry, and petrography derived from the two Kidd mines form the basis for this interpretation of carbonaceous ores, backed up by observations based on on-site visits and/or specimens from mines and showings, including the Hollinger, MacIntyre, and Kenilworth Properties (Porcupine Camp) and the Macassa, Lake Shore, Omega, and Kerr Addison Properties (Kirkland Lake-Larder Lake-Virginiatown trend).

The most productive site for this study has been the open pit at the Owl Creek Mine, and the most detailed work has involved successive working faces on Bench 3 and Bench 4. A suite of seven samples collected from Bench 3 in 1984 is referred to at length in the present paper. Photo 262.1 illustrates the general form of the north-dipping dominant vein structure in the pit.

MINERALOGY AND PETROGRAPHY

A mineralogical resume of the Owl Creek and Hoyle Pond deposits (Wilson and Rucklidge 1986) alluded to a volumetric dominance of pyrite in the opaque phases, and to the importance of sodic white micas, iron-rich chlorites, carbonates, and reduced carbon in vein selvages and mineralized wall rock. A few extensions and clarifications of the earlier work will be given in this paper.

The silicate mineralogy of productive veins is always quartz-dominated, although the proportion of carbonates varies and some late barren veinlets may be essentially pure calcite. Tourmaline and albite are locally abundant, more so at the Hoyle Pond Mine than at the Owl Creek Mine. Recent experimental work (Woodland and Walther 1987) indicates that the assemblage quartz-albite-paragonite, observed in Hoyle Pond vein selvages, is consistent with the transport of aluminum in high-salinity solutions. At the time of writing, no fluid inclusion data is available to cast direct light on this matter. However, primary fluid inclusions are quite abundant in the vein quartz, albeit subordinate in number to trails of small secondary fluid inclusions which define planes of weakness in the quartz. When sufficiently developed, these planes may also contain very fine grained reduced carbon (Photo 262.2).

The reduced carbon in the rocks is extremely fine grained, poorly reflecting, opaque material. Recent progress on carbon in Phanerozoic strata (Okuyama-Kusunose and Itaya 1987) indicates that organic debris is altered, via transitional forms, into well-ordered graphite, by contact or regional metamorphism. The Archean age, the fine grain size, and low reflectivity of carbon in the Timmins samples are consistent with the low degree of ordering expected in greenschist facies rocks.

A spectacular high-grade addition to our documented occurrences of visible gold at quartz-carbon contacts is provided by Royal Ontario Museum sample M13714, from the old Vipond Mine in Timmins (Photo 262.3). Coarse native gold occurs at the margin of a milky quartz vein in contact with the black host rock, in fractures penetrating into the vein from the contact, and adjacent to small inclusions of

Photo 262.1. Northeastern corner of the Owl Creek 3 Bench in Spring, 1985. The prominent structure dipping to the north (left) is the main "quartz dike" of the ore zone. This structure is a quartz-veined shear zone with inclusions of carbonaceous wall rock. To the north are carbonatized, pyritic, tholeiitic metavolcanics; to the south are argillitic metasedimentary rocks. Economic gold values occur in association with sulphide mineralization in both types of wall rock, and also within the selvages of the quartz veining.

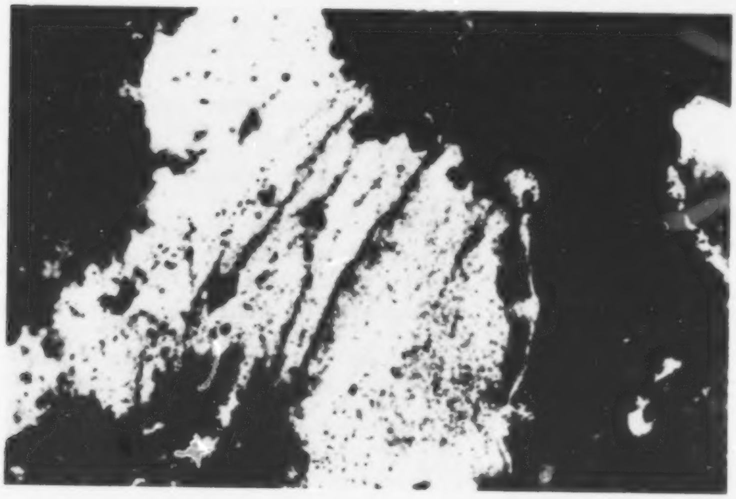

Photo 262.2. Within a doubly-polished thin section, dense clumps of fine-grained carbon are seen along well-developed grain boundaries in vein quartz. Trails of fine carbon cut across the quartz, following incipient grain boundaries, or other planes of weakness. View in cross-polarized light; long axis of photograph is 1.2 mm.

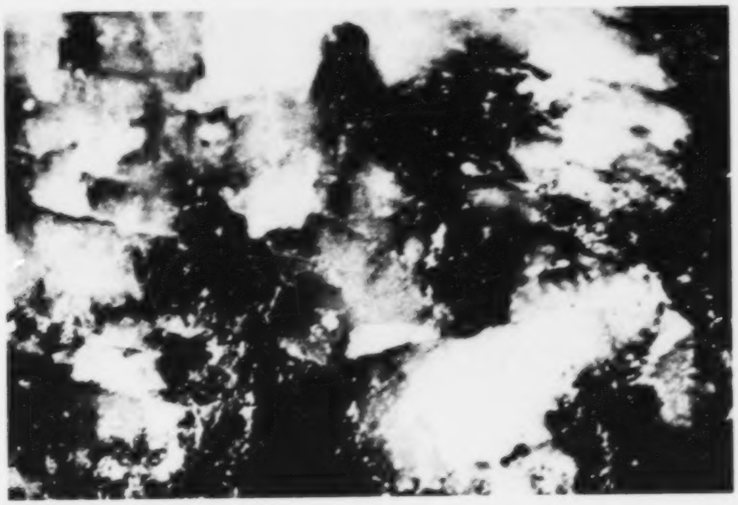

Photo 262.3. Spectacular native gold in sample from the Vipond Mine, Timmins. Area in photo is approximately 5.0 by 2.5 cm. See text for description.

carbonaceous matter which appear to have been spalled into the vein. A brief description of the old mine (Ferguson *et al.* 1968) suggests that the local geology is quite similar to that of the Hollinger Mine to the north and northwest. The Central vein system "is along a carbonaceous argillite which is up to 20 feet thick", and "Gold occurs around the margins of fine-grained pyrite, where there are breaks in the quartz, and near, or on, the contacts of inclusions of country rock with the vein material" (Ferguson *et al.* 1968, p.117-118).

A brief review of carbonaceous gold deposits (Wilson and Rucklidge, in press) indicates that in some major examples, such as Pueblo Viejo, Dominican Republic, and Carlin, Nevada, paragenetic considerations appear to exclude carbonaceous matter from playing a major role in gold precipitation. Also, in the smaller graphite-bearing deposit of the Red Pine Mine in Montana, the bulk of the gold was introduced in a sulphide association which predates the bulk of the graphite (Kinley 1987).

The microstructural features documented in the Timmins deposits (Wilson and Rucklidge 1986, in press) have parallels elsewhere. Thus, phyllosilicate laminae in quartz veins within the Meguma domain in Nova Scotia (e.g. *see* Mawer 1986) seem akin to carbon/mica foliae and stylolites at the Hoyle Pond Mine. Henderson *et al.* (1986) have described fabrics in the Goldenville Formation indicating that cleavage formation is the result of a 50% pressure solution removal of material from these rocks. Abundant and often multistage pressure shadows in the Timmins metasedimentary rocks attest to a complex history; to a degree they must exhibit clues to the tectonic evolution of the rock fabric (*see* White and Wilson 1978) and the chemical evolution of the mobile components. Individual shadows may consist of fibrous quartz alone, of blocky quartz and/or carbonate, and may have plate-like overgrowths of chlorite or white mica (traces of chalcopyrite may also occur). Pressure shadows occasionally approach rock-forming proportions, and may even reach centimetre dimensions in extreme cases (Photo 262.4).

Sulphide mineral assemblages are always pyrite-dominated. An important clarification concerns the relative timing of the pyrite forms found at the Owl Creek Mine. The paragenesis (Figure 262.1) as defined by Wilson and Rucklidge (in press) encompasses the following sequence:

1. early nodular pyrite, thought to be syngenetic/diagenetic in origin, which is affected by later deformation, and entrained by the secondary foliation. The nodules have not been studied in detail, and sulphur isotopic data on Fe-sulphides in the Superior province metasediments (e.g. *see* Strauss 1986) has not yielded an unequivocal answer to the question of pyrite genesis. Stratabound concentrations of pyrite occur in some sediments at the Owl Creek Mine (Photo 262.5a), but these rocks show signs of strong tectonic modification. An example is Owl Creek sample 725, a grey banded argillite with prominent pyrite bands, a relatively high carbonate content, strong pressure shadow development (notably, on coarse carbonate as well as on the usual pyrite nuclei), and, for reference, a low (background) gold content
2. porphyroblastic pyrite, both coarse and euhedral, crosscutting both original sedimentary bedding planes and later foliations (Photo 262.5b), and often enclosing irregular masses of the foliated matrix
3. porous, frequently arsenical, gold-related pyrite, including concentrations of small euhedra and overgrowths of later, sponge-like habit

Arsenic in the carbonaceous ores has been detected most commonly in arsenical pyrite. The arsenic content in the pyrite reaches a maximum near 2.0 weight percent. Much higher values have been reported elsewhere, e.g. 10 weight percent as a maximum for Idaho pyrites (Lewis and Shieh 1986). The bulk rock arsenic values are sometimes bolstered by the occurrence of arsenopyrite. In quartz-veined volcanic "grey zone" sample 709 from the Hoyle Pond Mine, minor amounts of arsenopyrite occur with volumetrically dominant, coarser pyrite. The exact na-

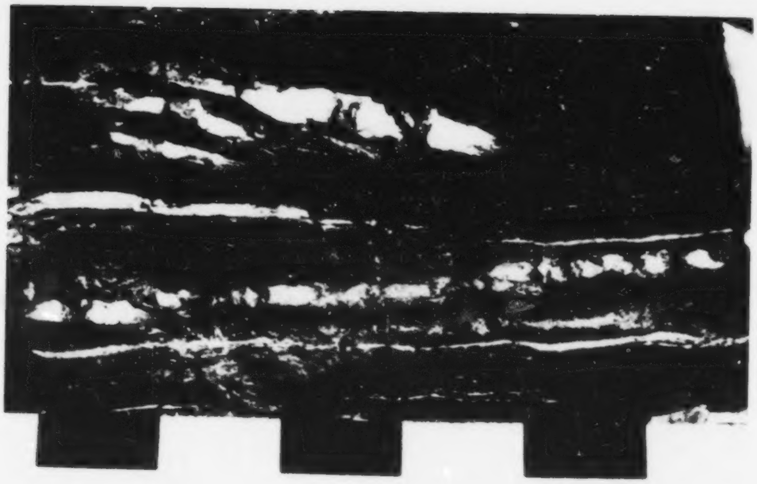

Photo 262.4. A spectacular example of a pressure shadow developed in argillite at the Owl Creek Mine, with centimetre-scale quartz "wings" on either side of a coarse pyrite nucleus. Usually less than 1 mm wide, the shadows abut pyrite (rarely carbonate), and generally consist of stocky quartz fibres.

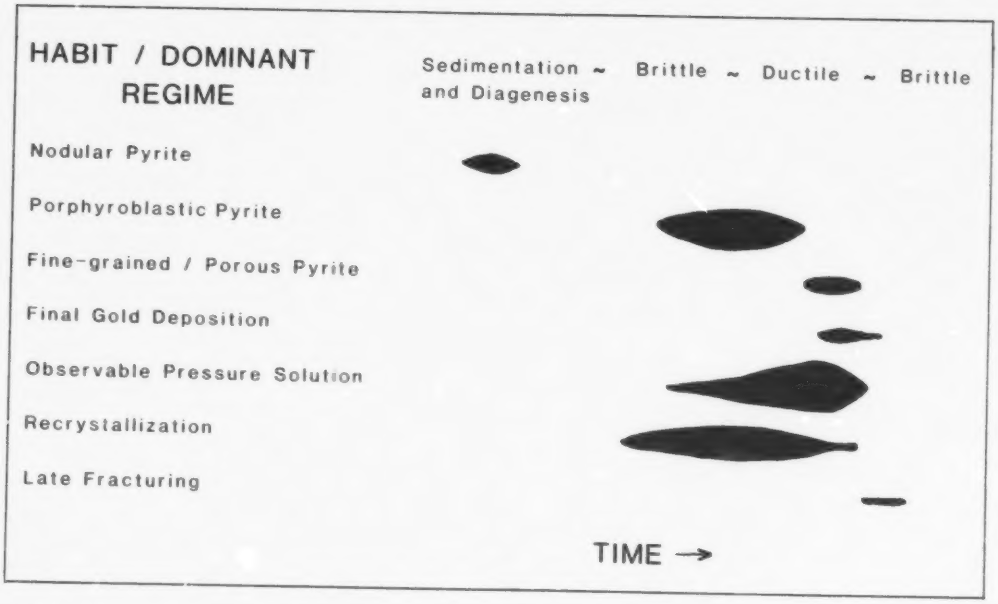

Figure 262.1. Inferred paragenetic relationships of major phases at the Owl Creek Mine (from Wilson and Rucklidge, in press). Note the relative timings inferred for the three distinctive habits of pyrite in the deposit.

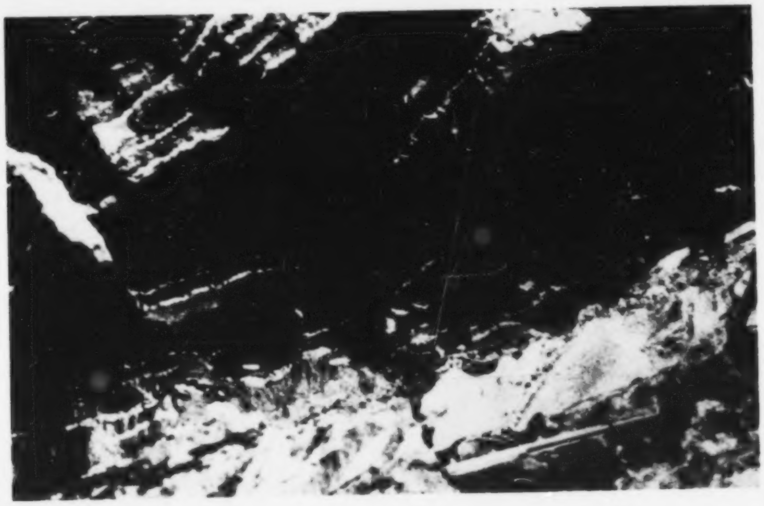

Photo 262.5a. *This, and the accompanying photograph, depict metasedimentary rocks south of the ore zone on the Owl Creek 3 Bench. Prominent pyrite banding occurs in a very fine grained argillite showing strong pressure solution, with removal of carbonate, concentration of silica fibres around the pyrite, and concentration of relatively inert carbon.*

ture of these sulphides is not fully resolved; both arsenical sulphides may show the porous form in auriferous samples, and the arsenopyrite gives low totals on electron microprobe analysis, although the energy spectra indicate that Fe, As, and S account for all the peaks that are visible, apart from sporadic trace amounts of Si and Cu, presumably related to tiny inclusions in the host sulphide. The compositional variation of these sulphides can provide important constraints on the nature of the mineralizing fluids, and it is suspected that this peculiar form may also be a significant clue to the conditions of crystallization. According to Rytuba (1986), arsenical pyrite was formed at Carlin by the adsorption of native arsenic onto pre-existing pyrite. Amorphous sulphides rich in As, Sb, Au, Ag, Hg, and Tl have been documented from hot springs in New Zealand (Weissberg 1969). Even if such precipitates could have formed in the veins, one might expect recrystallization to generate aggregates of fine crystals, such as the fine-grained euhedral arsenopyrite, coarser berthierite ($FeSb_2S_4$), and associated Sb phases present in the "Card Lake" Occurrence in Sewell Township, west of Timmins, an assemblage unusual for the Archean and for the Abitibi Belt. This last site, the subject of a number of exploration projects in the past (Assessment Files, Mining Recorder's Office, Ministry of Northern Development and Mines, Timmins), is noted as a mineralogical curiosity by Sabina (1974).

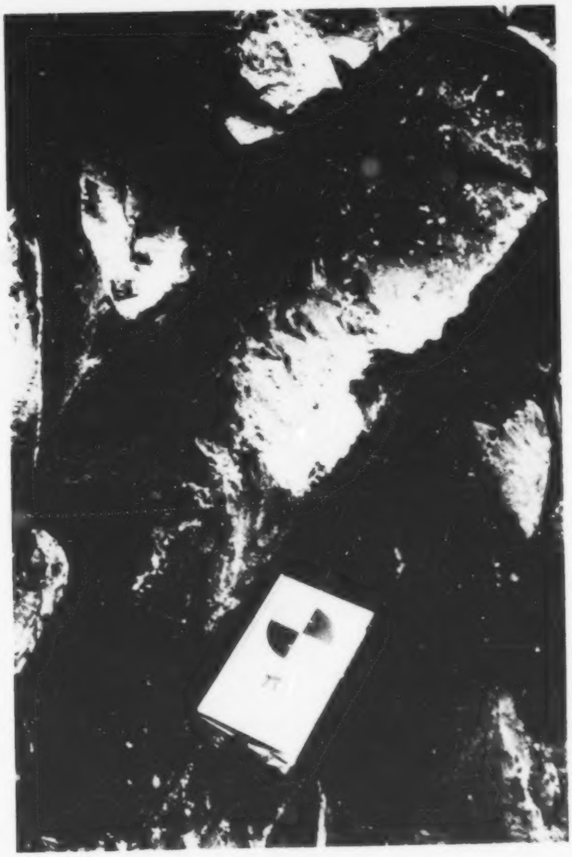

Photo 262.5b. *A few metres south of 262.6a, porphyroblastic pyrite grows in metasedimentary rocks, retaining its primary sedimentary layering.*

STABLE ISOTOPES, CARBON, CARBONATES AND HYDROCARBONS

A combination of geochemical techniques were applied to representative samples. The reduced carbon and carbonate contents of the samples, as reported here, were determined by X-Ray Assay Laboratories Limited, Don Mills. A summary of the methodology is included as it is pertinent to the following discussions. Carbon isotope measurements were made by the Environmental Isotope Research Laboratory, University of Waterloo, on both reduced and oxidized (carbonate) fractions of selected samples. These and other data are given in Table 262.1. With the exception of sample 414, each reduced carbon sample was measured twice, and the values quoted are averages (the average and extreme differences within each pair of measurements were 0.26‰ and 0.03 to 0.67‰ respectively). Carbonate samples were measured once (except for sample 421, which has the mean of two analyses).

Hand samples were crushed for major and minor element analysis, and small aliquots of the remnants were prepared for stable isotope measurements. Carbonate content as CO_2 was first determined by coulometry following hydrolysis of small (approximately 0.1 g) aliquots. So-called organic carbon was then measured by heating the same aliquots in the presence of an oxidizing agent, and repeat coulometry on the CO_2 evolved. The data reported here refer to "CO_2" (carbonate) and "C" (reduced) carbon in weight percent, and are all coulometric measurements. The authors prefer the nongenetic phrase "reduced carbon" in general, although the evidence seems good that this carbon is biogenic, incorporated into the sediment at time of deposition. As a check, "total carbon" was determined on separate 0.1 g aliquots with a LECO (induction furnace) total carbon analyzer. As this is a high-temperature process, any difference between the total carbon value and the sum C+(0.2729xCO_2) should be a refractory form of carbon, either "graphitic", (the analytical term employed) or, more exotically, carbon trapped within some other phase. Of two samples analyzed in 1984, and eleven samples in 1987, only the Nevadan sample 445 displayed a total carbon value significantly (0.69 weight percent) less than the total as calculated from the coupled measurements at lower temperature. Mean and extreme values for excess high-T carbon are 0.53 (0.13 to 0.83) and 2.45 (1.08 to 5.74) weight percent for 3 metavolcanic rock samples and 10 metasedimentary rock samples respectively. In five out of 13 samples, this residue may account for the balance of the absolute total carbon in the rock. The precise nature of the "extra carbon" is not critical to the observations which follow, so, in conclusion, some possible explanations are noted:

1. The "organic carbon" analyses have been found to be reproducible, and the excesses in the high-T measurements occur in some of the low-carbonate samples. A problem in calibration might be involved, but the offsets appear to be random.
2. Inhomogeneity between aliquots might be involved, but the incidence of high-T excesses (12/13 samples) seems too great for this to be likely.
3. A relatively ordered "graphite" may be present, accounting for the excesses. This is the authors' preferred explanation for the data. However, the excesses show no spatial relationship to the ore zone at the Owl Creek Mine. If true graphite occurs, it is very fine grained and intractable to conventional microscopy. Alternative techniques, possibly transmission electron microscopy, could provide useful information on the crystallinity of carbon in the Abitibi Belt metasedimentary rocks, and on possible modifications that it may undergo within shear zones.

Reduced carbon contents of the metavolcanic samples are quite low, (0.10 to 0.25 (mean 0.17) weight percent). In comparison, six, black, clearly carbon-rich metasediment samples average 8.3 weight percent C, while the remaining four metasediment samples (shades of grey in hand specimen, lacking copious amounts of loose, powdery or shiny "graphite") averaged only 0.31 weight percent (0.35 for three Owl Creek samples). It is worth noting that in the case of the metamorphosed argillites, a cutoff level of 1.0 weight percent reduced carbon separates the Owl Creek and Hollinger ore zone material from all the other samples.

The gold and carbon values correlate very well in the case of the Owl Creek sedimentary suite. It should be remembered, however, that while the gross carbon concentration may be engendered by the removal of more soluble phases in an episode of ductile shear, it is not the carbon concentration, *per se*, that is responsible for the gold enrichment. The enrichment in carbon (averaging 24 times by weight for the four "black" versus the three "grey" Owl Creek metasedimentary rock samples) is in part due to the removal of carbonate and silica by intense pressure solution, and in part to (arguable) the migration of extremely fine carbon along small-scale planes of weakness. Despite the association of carbon with quartz veining, no convincing evidence is found that a significant portion of the carbon can have moved in the fluid phase, and been deposited on the vein margins. It seems, from Table 262.1, that the background level of gold in unmineralized metasediments is probably below 10 ppb, and that a (order-of-magnitude) thousand-fold enrichment in gold cannot be generated on a mine scale by involvement of the host rocks alone. This finding accords with an average gold content for black shales of 14.7 ppb (Korobeynikov 1986). The carbon was concentrated during the same tectonic regime that prepared the rocks for later gold deposition. A proportion of the gold plates onto carbonaceous surfaces in quartz-veined argillite, but much of it is sulphide-hosted.

Carbon isotope ratios of Archean carbonaceous metasediments vary widely, $\delta^{13}C$ (‰ variation from PDB standard) of the organic material ranging from -47 to -15‰ (Strauss 1986; Schoell and Wellmer 1981). The data in Table 262.1 range from -34.3 to -19.4‰. Strauss's (1986) samples contained 0.1 to 15 percent total organic carbon, and one sample from the Owl Creek Mine was isotopically light (-31.5‰). The seven metasediment samples from the Owl Creek Mine (0.3 to 17.1 weight percent reduced carbon) range from -31.2 to -26.7‰, with a tendency for the lightest $\delta^{13}C$ values to occur in the most C-rich (and Au-rich) samples. Roughly speaking, the higher the ratio of carbonate to reduced carbon in the rock, the heavier (less negative $\delta^{13}C$) the latter's isotopic signature, suggesting a degree of equilibration between the two. This generalization can be extended to two altered tholeiites (samples 421 and 696B, Table 262.1), having $\delta^{13}C$=-23.4 and -19.4‰ respectively.

TABLE 262.1. C, CO_2, C ISOTOPE, AU AND AS VALUES FOR SELECTED SAMPLES.

Sample	Location	Field Notes	C %	CO_2 %	$\delta^{13}C$	(%o)	Au ppb	As ppm
					Carbon	Carbonate		
421	OC 3 Bench, Ore Zone	MVolc, scattered fgr py	0.25	18.5	-23.4	- 4.3	4600	370
417B	OC 3 Bench, Ore Zone	MSed, very C-rich, 2% py streaks	8.65	0.05	-29.9	-12.3	2100	940
416	OC 3 Bench, Ore Zone	MSed, C-rich	5.80	<0.01	-27.0		1400	170
415	OC 3 Bench, Ore Zone	MSed, very C-rich, 2% py nodules	17.1	<0.01	-31.2		14000	16000
414	OC 3 Bench, Ore Zone	MSed, C-rich	1.80	<0.01	-26.8		950	460
418A	OC 3 Bench, S. of Ore Zone	MSed, crenulated, with 2% porph. py	0.35	2.23	-26.9	-10.7	<10	170
419	OC 3 Bench, S. of Ore Zone	MSed, strongly cleaved, little py	0.40	0.01	-27.3		240	210
725	OC 4 Bench. S. of Ore Zone	MSed, crenulated, 5% py in bands	0.30	5.28	-26.7	-14.0	10	100
696B	HP By 11 vein, 3-11 drive	MVolc, 'grey zone', traces of py	0.15	4.78	-19.4		10	11
709	HP By 16 vein, 2-11 sublevel	MVolc, 'grey zone', traces of py	0.10	9.23			980	370
366B	Holl 121007 stope	MSed, C-rich, crenulated, 4% py bands	1.40	1.11			930	280
732	Kenil grab sample	MSed, near porphyry/py contact	0.20	0.44	-34.3		300	1500
445	JC fault zone	MSed, C-rich, no obvious sulphides	0.70	20.7			40	65

Of the 13 samples, 10 are metasediments, 3 are metavolcanics. Sampling sites are the Owl Creek, Hoyle Pond, Hollinger and Kenilworth (Naybob) Mines in the Timmins camp, and Jerritt Canyon Mine (Marlborough Canyon pit) in Nevada. All samples collected *in situ*, with the exception of mine dump grab-sample 732. This specimen is the only one which is heterogeneous in hand specimen (see Photo 262.2, Wilson and Rucklidge 1986); only foliated argillite was included in the assay material.

Six of the 13 samples appear extremely graphitic (black/sooty/shiny) in outcrop and hand specimen; two are exceedingly C-rich, while the others range from 0.7 to 5.8 wt.% 'organic carbon'. Detection limits for Au and As by IMAA; 10 ppb and 2 ppm respectively.

Note that samples 421-419 form a southward series across the ore zone at Owl Creek. The term 'ore zone' in this table refers to the prominent vein structure shown in Figure 262.1. Gold values are not restricted to this structure, but is is the focus of the minerlaization.

The three sedimentary carbonate fractions studied have $\delta^{13}C$ ranging from -14.0 to -10.7‰, while a single tholeiitic sample returned a value of -4.3‰. The latter value for carbonate alteration in the auriferous (4600 ppb Au) tholeiite is close to the mean value of -3.1±1.3‰ (n=289) for carbonate associated with 15 Au-mineralized sites in the Timmins area (Burrows *et al.* 1986). The preservation of distinct carbonate and carbon $\delta^{13}C$ values implies a fairly low formation temperature for the veining, as in the case of the Mother Lode in California, where wall rock ferroan dolomite has $\delta^{13}C$ no lighter than -4.9‰, while "graphitic" carbon in veins and wall rocks is -23 to -25‰ (Taylor 1986).

The occurrence of the lightest carbon (most negative $\delta^{13}C$) in the C-rich, intensely veined and deformed rocks is reminiscent of observations by Eichmann and Schidlowski (1975). They found that stringers of visible carbon in the Transvaal Dolomite of South Africa were ^{13}C-depleted ($\delta^{13}C$ = -37.1 to -41.2‰) relative to disseminated carbon (this "normal" carbon varied from -26.5 to -36.7‰). These authors attributed the isotopically light nature of the millimetre-thick carbonaceous layers to preferential transport of the lighter isotope from its earlier site in the carbonate matrix. In the case of the Owl Creek Mine, even rocks farthest from the ore zone have quite low carbonate contents relative to the African example, and the degree of concentration toward the ore zone is more intense. The survival of the lightest carbon adjacent to shear zone-hosted carbonatization is also notable.

Hydrocarbon contents of five whole-rock samples were measured by Mercury Hydrocarbons of Limerick, Ireland. The extraction process selects a 5 g aliquot from a much larger sample, and by coarse crushing, sieving, and heating, liberates a proportion of the hydrocarbon gases in the rock for analysis in a computerized gas chromatography system. Although only a fraction of the total gas, which is located on surfaces and microfractures, may be extracted, the data appear quite suitable for comparative studies (J. Carter, Mercury Hydrocarbons Limited, personal communication, 1987). The technique is intended less for close-spaced direct indication of gold potential, than for kilometre-scale regional surveys. Four of the selected samples were also analyzed by other techniques. The fifth is a background sample from the well known "Shovel Outcrop" composed of turbidite metasedimentary rocks exposed northwest of Porcupine Lake, some 8 km south-southwest from Owl Creek. Table 262.2 displays the data for key hydrocarbons in the samples. The samples are CH_4-dominated, and show ethene/ethane ratios averaging 5.3. The abundant methane is in accord with the wider survey of Gerdenich *et al.* (1986), who demonstrated that decrepitated fluid inclusions from Archean Au deposits are methane-rich. Their samples, also analyzed by gas chromatography, characterized metasediment- and volcanic-hosted vein Au deposits with ethene/ethane ratios averaging 0.007 and 1.4 respectively. Neither study has nearly enough samples (seven in Gerdenich *et al.* 1986, five in the present study) to properly investigate this topic. For present purposes, however, it is interesting to note that certain light and heavy hydrocarbons are substantially enriched in the Owl Creek open pit samples relative to the other samples, confirming that the method of hydrocarbon gas analysis has some promise for gold prospection in Archean terrains.

TRACE AND MINOR ELEMENTS (GOLD AND ARSENIC REVISITED)

A range of trace elements were measured in these samples. The assays for gold and arsenic (Table 262.1) are particularly revealing. The importance of arsenic as an indicator element for gold is demonstrated by the data in Table 262.1; a threshold value is hard to estimate from the data due to the preponderance of strongly gold-anomalous samples. Apart from local arsenopyrite-bearing material, pyrite must be the main repository of the element; according to a survey by Boyle and Jonasson (1973), pyrite in mineral deposits may carry 5 to 5600 ppm As, and in unmineralized rocks the smaller range of 100 to 1600 ppm. Since pyrite is ubiquitous in the ores, albeit present in variable amounts, arsenic appears to work for both metasedimentary and metavolcanic rocks, in distinction to the reduced carbon contents, which remain quite low in the altered lavas due to their relative competence and overall susceptibility to brittle as opposed to ductile deformation events.

Other data on the suite, concerning major, minor, and trace elements, including rare earth elements (REE), will be presented at a later date. The REE yield gently-sloping plots, essentially flat for the metavolcanic rocks, and moderately light rare earth element (LREE)-enriched for the metasedimentary rocks, as commonly found in Archean tholeiites and wackes respectively.

CONCLUSIONS

The data presented in this paper confirm the earlier contention (Springer 1985; Wilson and Rucklidge 1986) that carbonaceous host rocks exert a combined chemical and structural influence on external fluids introduced during intrusive or tectonic events. Carbon/carbonate ratios, carbon isotope data, and hydrocarbon contents of bulk rock samples all yield indications of the deformation zone localizing ore at the Owl Creek Mine. It is believed that similar processes have operated in the other sites examined, although the degree of carbon concentration is usually on a lesser scale. The isotopic and other data from this study are in accord with the tectonic concentration of sedimentary Archean carbon into deformation zones which are localized within narrow areas of high competency contrast, and which serve as foci for external (magmatic) fluids transporting Au, As, and other elements.

As the major variation in carbon contents is restricted to the metasedimentary rocks, whereas the variation in arsenic is not, arsenic remains the best pathfinder for gold on a grab-sample scale, barring gold itself.

In summary, extremely carbonaceous rocks signal tectonic disturbance near the ore zone, and although the gold-carbon correlation may be to a degree fortuitous in our limited set of data, abundant shiny "graphite" in outcrop or drillcore should alert

TABLE 262.2. CONTENT OF SELECTED HYDROCARBONS IN TIMMINS ROCKS.

Sample	Location	Field Notes	C %	Methane	Ethene	Ethane	Propene	Butene	n-butane
414	OC 3 Bench. Ore Zone	MSed. C-rich	1.80	896.5	26.3	11.1	53.7	50.6	13.0
418A	OC 3 Bench, S. of Ore Zone	MSed, crenulated	0.35	836.9	33.1	6.3	106.6	61.4	52.9
419	OC 3 Bench, S. of Ore Zone	MSed, strongly cleaved	0.40	744.4	37.8	2.8	17.5	4.3	31.6
695	'Shovel outcrop'	MSed, silty layer in turbidite		368.4	5.7	1.6	4.4	0.0	1.3
732	Kenil, grab sample	MSed, near porphyry/py contact	0.20	315.5	5.8	2.9	13.9	4.5	2.0

Whole-rock values for hydrocarbons is ppb by weight. Of 12 hydrocarbons analyzed, 2 were not detected in any sample and 7 were detected in all samples. This selection presents species considered most useful for delineation of the Owl Creek mineralization. See text for discussion.

Care was taken to ensure that the samples were free of natural (lichens, moss, etc.) and artificial (saw-blade oil) surface contaminants. From the fact that the samples from outcrops and dumps (695,732) have relatively low hydrocarbon values, and because the two samples with sawn surfaces (419,732) show no enrichments, we conclude that no significant contamination is involved.

the exploration geologist to favourable zones in the metasedimentary component of greenstone belts.

The final results of this study of reduced carbon and metal deposits, including an extensive review and supporting data, will be submitted for publication. Initially, it will be published as an Open File Report of the Ontario Geological Survey.

ACKNOWLEDGMENTS

Chemical data on crushed samples were provided by X-Ray Assay Laboratories, Don Mills, and confirmed in outline by neutron activation work at the Slowpoke Reactor Facility, University of Toronto. Stable isotope data on bulk samples were produced by the Environmental Isotope Laboratory, University of Waterloo. Hydrocarbon gas analysis was carried out at Mercury Hydrocarbons Limited, for Thermasearch Limited of Limerick, Ireland. Photos 262.3 and 262.4 are reproduced in this paper courtesy of the Royal Ontario Museum. Financial assistance for this work was provided by the Ontario Geoscience Research Fund, Grant 262, recipient J.C. Rucklidge.

REFERENCES

Boyle, R.W., and Jonasson, I.R.
1973: The Geochemistry of Arsenic and its Use as an Indicator Element in Geochemical Prospecting; Journal of Geochemical Exploration, Volume 2, p.251- 296.

Burrows, D.R., Wood, P.C., and Spooner, E.T.C.
1986: Carbon Isotope Evidence for a Magmatic Origin for Archaean Gold- Quartz Vein Ore Deposits; Nature, Volume 321, p.851- 854.

Eichmann, R., and Schidlowski, M.
1975: Isotopic Fractionation between Coexisting Organic Carbon- Carbonate Pairs in Precambrian Sediments; Geochimica et Cosmochimica Acta, Volume 39, p.585- 595.

Ferguson, S.A., Buffam, B.S.W., Carter, O.F., Griffis, A.T., Holmes, T.C., Hurst, M.E., Jones, W.A., Lane, H.C., and Longley, C.S.
1968: Geology and Ore Deposits of Tisdale Township; Ontario Department of Mines, Geological Report 58, 177p. Accompanied by Map 2075, scale 1:12 000 or 1 inch to 1000 feet.

Gerdenich, M.J., Hanel, I.V., and Kesler, S.E.
1986: Alkene/Alkane Hydrocarbon Gas Ratios in Fluid Inclusions from Archean and Tertiary Gold Deposits; Geological Society of America, Abstracts with Programs, Volume 18, Number 6, p.611.

Harron, G.A., Middleton, R.S., Durham, R.B., and Philipp, A.
1987: Geochemical and Geophysical Gold Exploration in the Timmins Area, Ontario: A Case History; Canadian Institute of Mining and Metallurgy Bulletin, Volume 80, Number 898, p.52- 57.

Henderson, J.R., Wright, T.O., and Henderson, M.N.
1986: A History of Cleavage and Folding: An Example from the Goldenville Formation, Nova Scotia; Bulletin of the Geological Society of America, Volume 97, p.1354- 1366.

Kinley, T.M.
1987: The Occurrence and Timing of Gold Mineralization at the Red Pine Mine, Western Tobacco Root Mountains, Southwestern Montana; M.Sc. Thesis, Montana State University, 129p.

Knoll, K.
1986: Bell Creek; Northern Miner Magazine, Volume 1, Number 10, p.33.

Korobeynikov, A.F.
1986: Gold Distributions in Black Shale Associations; Geochemistry International, Volume 23, Number 5, p.114- 124.

Lewis, R.D., and Shieh, Y.N.
1986: Stable Isotopic, Mineralogical and Wall Rock Investigation of the Yellow Pine Au, W, Ag, Sb, Hg District, Valley County, Idaho; Geological Society of America, Abstracts with Programs, Volume 18, Number 6, p.672.

Mawer, C.K.
1986: The Bedding-concordant Gold-Quartz Veins of the Meguma Group, Nova Scotia; p.135-148 *in* Turbidite-Hosted Gold Deposits, edited by J.D. Keppie, R.W. Boyle, and S.J. Haynes, Geological Association of Canada, Special Publication 32, 186p.

Okuyama-Kusunose, Y., and Itaya, T.
1987: Metamorphism of Carbonaceous Material in the Tono Contact Aureole, Kitakami Mountains, Japan; Journal of Metamorphic Geology, Volume 5, p.121- 139.

Rytuba, J.J.
1986: Arsenic Minerals as Indicators of Conditions of Gold Deposition in Carlin-type Gold Deposits; Journal of Geochemical Exploration, Volume 25, p.237- 238.

Sabina, A.P.
1974: Cobalt-Belleterre-Timmins, Ontario and Quebec; p.154-155 *in* Rocks and Minerals for the Collector, Geological Survey of Canada, Paper 73- 13, 199p.

Schoell, M., and Wellmer, F.-W.
1981: Anomalous ^{13}C Depletion in Early Precambrian Graphites from Superior Province, Canada; Nature, Volume 290, p.696- 699.

Shegelski, R.J.
1986: Geology and Origin of Gold Deposits in the Porcupine Gold Camp, Timmins, Ontario; p.136-139 *in* Gold '86 Poster Volume, Toronto.

Springer, J.S.
1985: Carbon in Archean Rocks of the Abitibi Belt (Ontario-Quebec) and its Relation to Gold Distribution; Canadian Journal of Earth Sciences, Volume 22, p.1945- 1951.

Strauss, H.
1986: Carbon and Sulphur Isotopes in Precambrian Sediments from the Canadian Shield; Geochimica et Cosmochimica Acta, Volume 50, p.2653- 2662.

Taylor, B.E.
1986: Origins and Isotopic Compositions of Mother Lode Hydrothermal Fluids and Gold Deposits with Comparison to Archean Analogues; p.149-150 *in* Gold '86 Poster Volume, Toronto.

Weissberg, B.G.

1969: Gold-Silver Ore-grade Precipitates from New Zealand Thermal Waters; Economic Geology, Volume 64, p.95- 108.

White, S.H., and Wilson, C.J.L.

1978: Microstructure of Some Quartz Pressure Fringes; Neues Jahrbuch für Mineralogie, Abhandlungen, Volume 134, Number 1, p.33- 51.

Wilson, G.C., and Rucklidge, J.C.

1986: Lithological Features and Economic Significance of Reduced Carbonaceous Rocks in Gold Deposits; Grant 262, p.177- 189 *in* Geoscience Research Grant Program, Summary of Research, 1985-1986, edited by V.G. Milne, Ontario Geological Survey, Miscellaneous Paper 130, 235p.

In Press: Mineralogy and Microstructures of Carbonaceous Gold Ores; Mineralogy and Petrology.

Woodland, A.B., and Walther, J.V.

1987: Experimental Determination of the Solubility of the Assemblage Paragonite, Albite, and Quartz in Supercritical H_2O; Geochimica et Cosmochimica Acta, Volume 51, p.365- 372.

Grant 265 Bacteria as Nucleation Sites for Mineral Authigenesis

F.G. Ferris[1], **W.S Fyfe**[1], **and T.J. Beveridge**[2]

[1]Department of Geology, University of Western Ontario, London

[2]Department of Microbiology, University of Guelph

ABSTRACT

The ability of bacterial cells to serve as nucleation sites for authigenic mineral formation has been investigated. Sediment samples, obtained from several different locations in Ontario, were examined by electron microscopy and energy dispersive X-ray spectroscopy. Individual bacterial cells and their remains were prominent in thin-sectioned plastic-embedded specimens as templates for authigenic mineral formation. The mineralization was usually observed on the walls of the bacteria, or was deposited around encapsulated cells growing in biofilms. In addition, laboratory simulations showed that the development of bacteria-associated mineralization facilitates the structural preservation (fossilization) of micro-organisms.

INTRODUCTION

A number of studies have shown that substantial quantities of dissolved metallic ions can be complexed by bacteria and their products (for a recent review *see* Beveridge and Fyfe 1985). This fixation of metallic ions arises through electrostatic interactions with anionic carboxyl or phosphoryl groups within the constituent polymers of the bacteria (Beveridge and Murray 1980; Ferris and Beveridge 1986). The molecular components in the walls and external sheaths of bacteria are particularly reactive, so metals tend to accumulate at the surfaces of the cells (Ferris and Beveridge 1985). The results of our present field work and laboratory investigations further indicate that these cellular structures not only tenaciously bind metallic ions, but also serve as templates for the formation of distinct authigenic mineral phases during early sedimentary diagenesis.

ANALYTICAL METHODOLOGY

SAMPLING PROCEDURES

Surficial sediment samples were collected in seepage areas near mine tailing impoundments at Onaping (northwest of Sudbury), Burchell Lake (west of Thunder Bay), and Rossport (on the northern shore of Lake Superior). Microbial biofilms were also scraped from submerged leaves at Rossport and rocks in the Irvin River near Salem, a small village north of Guelph. Immediately after the samples were collected, specimens were placed into 5 ml metal-free plastic tubes containing 1 ml of 1% (v/v) aqueous glutaraldehyde, a fixative for electron microscopy. When the samples were returned to the laboratory, they were prepared for electron microscopy by dehydration through an ethanol-propylene oxide series, and embedding in an epoxy resin (Epon 812). Thin-sections (150 nm in thickness) were then cut using a Reichert Ultra-cut E ultramicrotome and mounted on Formvar-carbon coated copper grids.

EXPERIMENTAL GEOLOGICAL AGING OF BACTERIA

Mid-exponential growth phase cultures of *Bacillus subtilis* were grown as previously outlined, and harvested by centrifugation (Beveridge and Murray 1980). After the bacteria were washed with pH 7.0 HEPES buffer, half of the cells were resuspended in a fresh 10 mM $FeCl_3$ solution at a concentration of 1.0 mg dry weight per millilitre; the remaining cells were used as controls (i.e. no sorbed iron). The suspensions were allowed to incubate at room temperature for 10 minutes, then the cells were pelleted by centrifugation and washed three times with deionized distilled water (DDW). The bacteria were then aged at 70°C in either DDW or an aqueous 300 ppm silica solution, for periods up to 150 days. Specimens were prepared for electron microscopy, as described above, at 15 day intervals.

ELECTRON MICROSCOPY

Thin-sectioned specimens were examined in either a Philips EM 300 or a Philips EM 400T electron microscope, at 60 KeV or 100 KeV respectively. The EM 400T was fitted with a STEM unit, goniometer stage, and an EDAX energy dispersive X-ray spectrometer. Both instruments were operated with a liquid nitrogen cooled anticontamination device in place at all times. Energy dispersive X-ray spectroscopy was conducted using electron beam spot sizes of 200 nm or less, and spectra were obtained by collecting counts for 100 seconds (live-time).

RESULTS AND DISCUSSION

BACTERIAL SUPPORTED IRON MINERALIZATION

A significant portion of the organic matter in acidic sediments that arise near mine tailing impoundments is derived from acidophilic bacteria which, unlike higher organisms, thrive under conditions of low pH (Brock 1974). In thin-sectioned samples of these sediments, bacterial cells were found in successive stages of mineralization by iron. The most common form of mineralization associated with the bacteria was amorphous ferrihydrite (Photo 265.1). However, cellular accumulations of various oxy-hydroxides (e.g. goethite) and oxides (e.g. hematite) were observed (Photo 265.2). Similar iron precipitates also develop on the external surfaces of iron-loaded bacteria in the laboratory (Photo 265.3).

At least a two-step depositional process is expected to be involved with bacterial-supported iron mineralization (Beveridge and Fyfe 1985). Metal binding studies conducted with isolated bacterial walls suggest that an initial stoichometric interaction between dissolved cations and the anionic bacterial polymers first saturates negatively charged sites. Then the hydrolysis of the bound iron forms distinct nucleii for subsequent mineralization at the bacterial

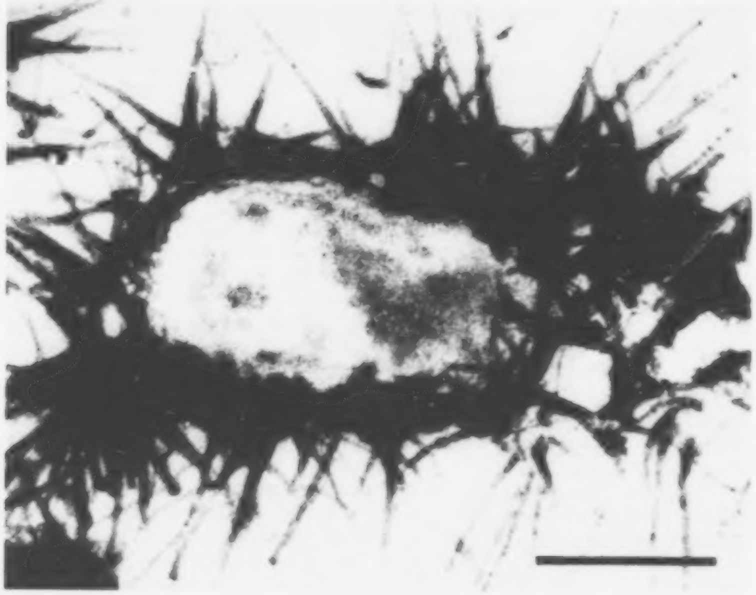

Photo 265.1. *Thin-section transmission electron micrograph showing a ferrihydrite encrusted bacterium in a sediment sample from a mine tailing impoundment seepage area near Onaping (bar=500 nm).*

cell surface. This not only provides an explanation for the present data, but also accounts for the presence of biogenic carbon in natural goethites (Yapp and Poths 1986), and the genesis of oolitic iron ores by bacteria (Champetier *et al.* 1987).

MINERALIZATION OF BACTERIAL BIOFILMS

The direct examination of bacteria as they grow in natural environments has demonstrated that microbial cells are typically surrounded by extensive accumulations of slime or capsular material (Costerton *et al.* 1985). As these encapsulated micro-organisms grow and divide, daughter cells are trapped within a common hydrated matrix, forming microcolonies of morphologically identical cells. This type of growth pattern is illustrated in Photo 265.4. The extracellular polymers that mediate microcolony formation also facilitate irreversible adhesion, so that most microcolonies develop directly on surfaces. Eventually, adjacent microcolonies coalesce to form adherent biofilms which often contain a consortium of different bacterial species. Members of these mixed microbial populations are immediately juxtapositioned, and this facilitates their physiological cooperation. Nutrient substrate transfer, and even hydrogen translocation, are possible, leading to the establishment of microenvironmental conditions that differ substantially from the external aqueous milieu (Costerton *et al.* 1985).

The chemical structures of many extracellular polymers from various aquatic micro-organisms are understood in considerable detail. Most are comprised of acidic muco-polysaccharides or polypeptides that can be expected to act as ion-exchange resins which will interact with charged molecules or ions (Costerton *et al.* 1985). Depending on the dissociation characteristics of the exopolysaccharide, the adsorbed molecules and ions may be available to the encapsulated bacteria at concentrations significantly higher than those available to planktonic micro-organisms. The uptake and retention of inorganic ions within these polyanionic matrices also favors the nucleation and epitaxial growth of authigenic mineral phases (Photos 265.5 and 265.6). This type of diagenetic process, coupled with an entrainment of small clastic particles, must, therefore, contribute to the mineralization of bacterial biofilms.

SILICIFICATION OF BACTERIA

Recently, individual bacterial cells in a geothermal sediment preserved in successive stages by iron-silica crystallites was described by Ferris *et al.* (1986). Similar results have been obtained in the laboratory by aging control (i.e. no sorbed metal) and iron-loaded cells of *B. subtilis* in aqueous 300 ppm silica solutions. In experimental runs using control bacteria, the cells were completely degraded by their own lytic enzymes after 15 days of aging. However, silica crystallites rapidly developed on the remaining cellular debris (Photo 265.7). This confirmed other experimental evidence which shows that organic matter from bacteria will act as a template for silica deposition (Birnbaum and Wiremann 1985). The initial association between the bacterial remnants and silica was probably established by the hydrogen bonding of mono- or polysilicic acid to available hydroxyl groups (Leo and Barghoorn 1976). A subsequent hydrolysis and polymerization of the bound silicic acid accounts for the formation of the silica crystallites (Iler 1980). The close distributional relationship that frequently exists between early diagenetic chert and sedimentary organic matter may be explained by this type of depositional process (Knoll 1985).

Although the precipitation of silica was slower with the iron-loaded cells, it eventually reached a stage comparable to the control situation (compare Photos 265.7 and 265.8). This difference suggests that cellular degradation actually enhances silica cry-

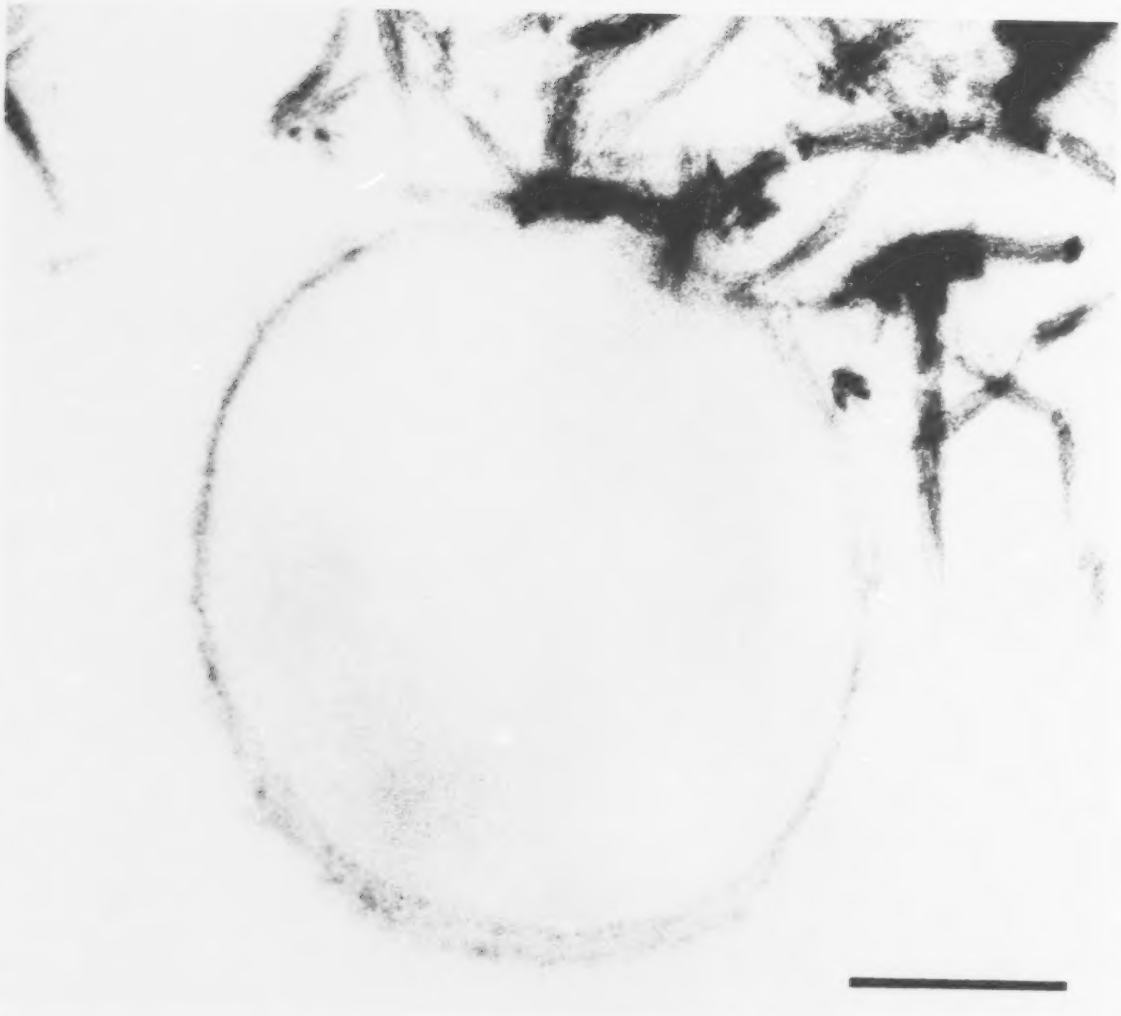

Photo 265.2. A thin-section profile of hematite microcrystals on the surface of a bacterium in a sediment sample from Burchell Lake (bar=200 nm).

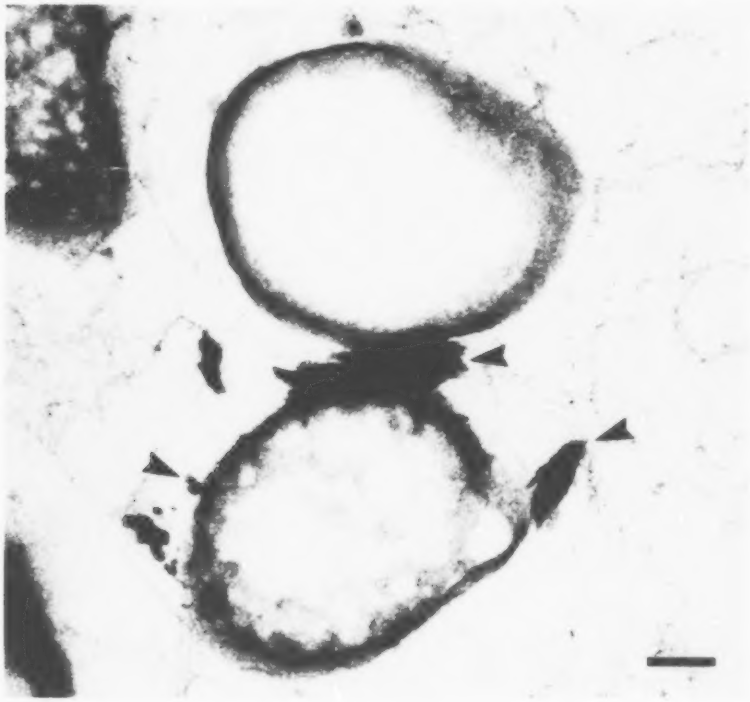

Photo 265.3. Iron-oxyhydroxide crystalloids (arrows) formed in the laboratory on the surface of an iron-loaded Bacillus subtilis cell (bar=200 nm).

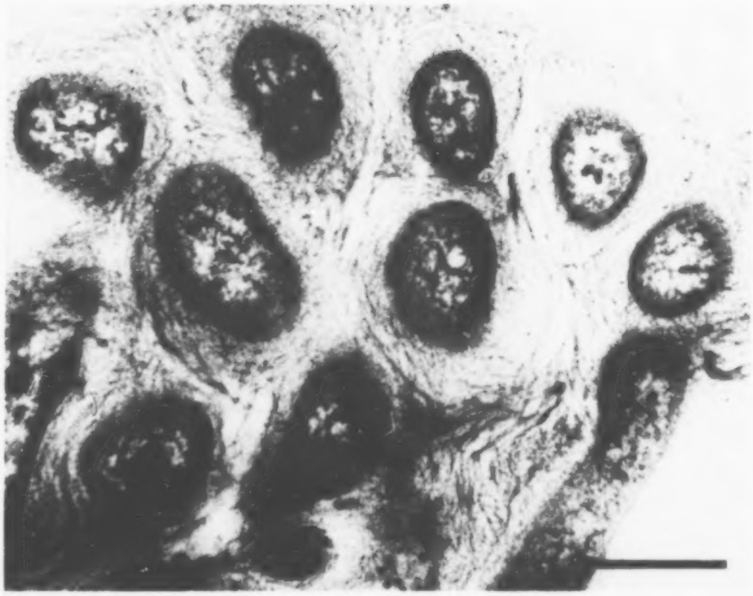

Photo 265.4. A transmission electron micrograph of a bacterial microcolony in an epilithic microbial biofilm from the Irvin River near Salem (bar=500 nm).

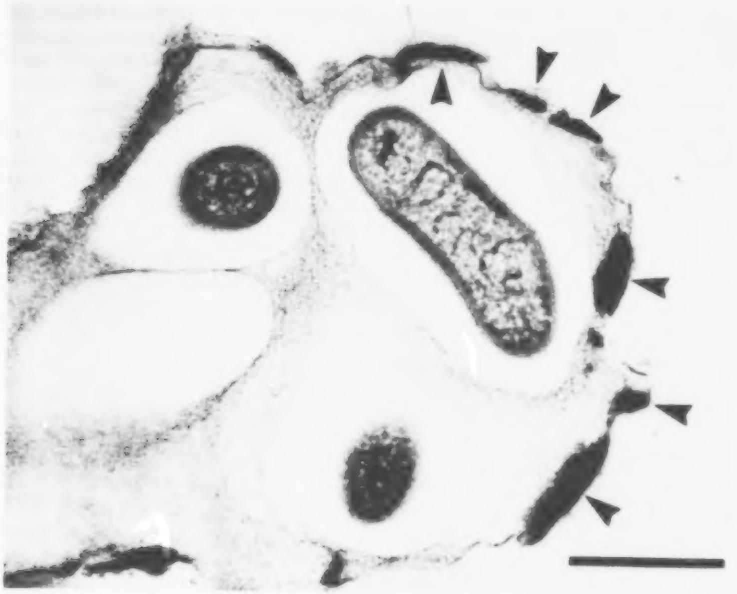

Photo 265.5. *Clay-type mineralization (arrows) associated with a bacterial microcolony in an epilithic microbial biofilm from the Irvin River near Salem (bar=500 nm).*

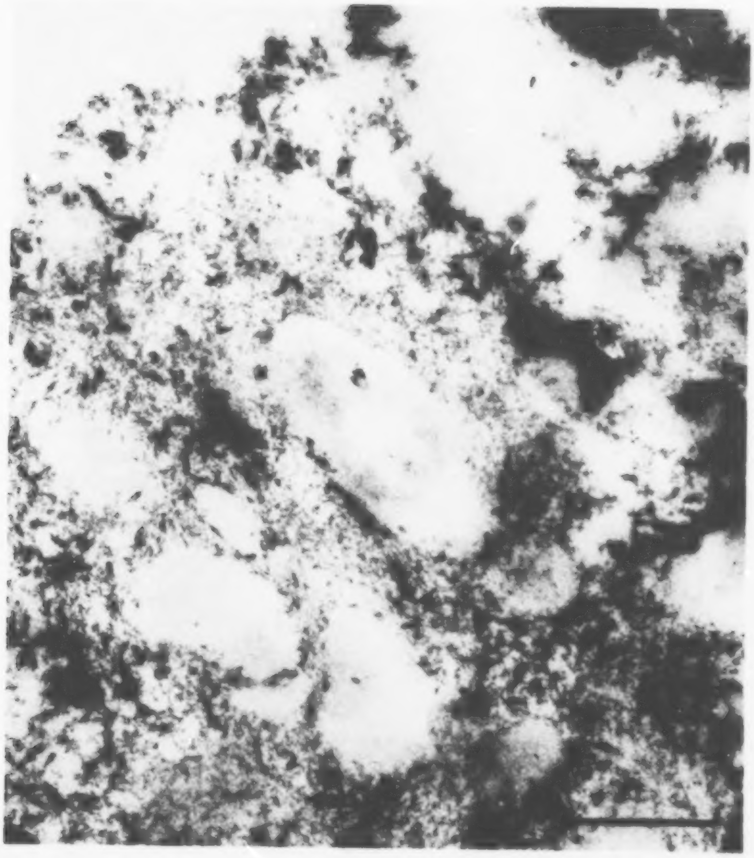

Photo 265.6. *Iron-oxyhydroxide mineralization associated with a microbial biofilm on a submerged leaf in a mine tailing seepage area near Rossport (bar=500 nm).*

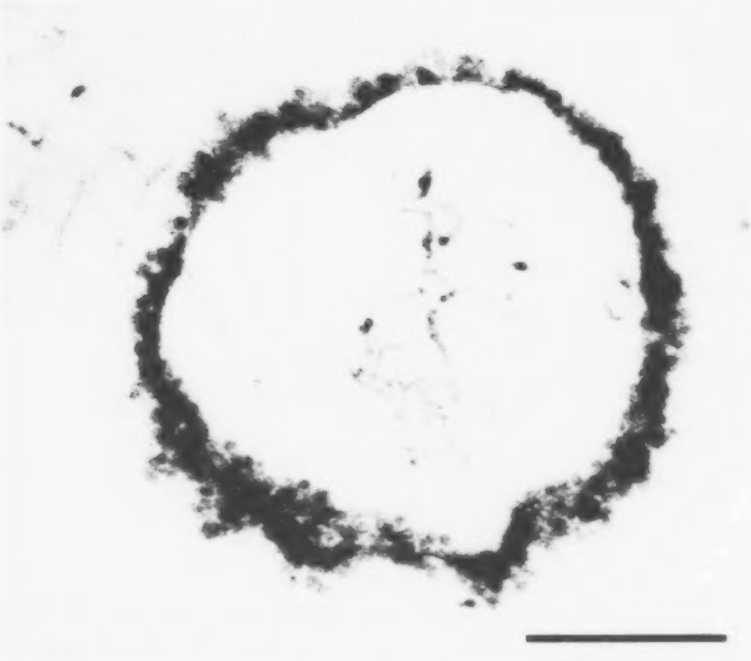

Photo 265.7. *Silicified cellular debris from control (no sorbed iron) Bacillus subtilis cells aged for 30 days at 70°C in an aqueous 300 ppm silica solution (bar=200 nm).*

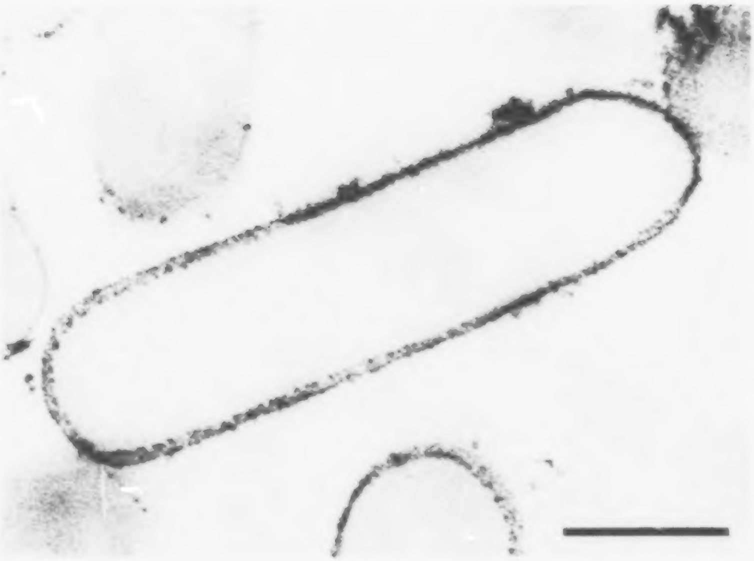

Photo 265.8. *An iron-loaded Bacillus subtilis cell aged in the presence of silica for 90 days. The cell wall has been completely mineralized by iron-silica crystallites and the rod-shape morphology of the bacterium has been preserved (bar=500 nm).*

stallite formation. However, the extent to which the bacteria were degraded by their own lytic enzymes determined whether intact structures conforming to the original morphology of the cells were preserved by silicification. In this context, the structural preservation of the iron-loaded *B. subtilis* cells was ensured by the inhibitory effect of the metal on the constituent lytic enzymes of the bacteria. Similar conditions must apply to our recent observation of bacteria perserved *in situ* by iron-silica crystallites (Ferris *et al.* 1986). The scavenging of iron from the environment by the bacteria probably prevented the rapid post-mortem degradation of the cells and this facilitated the silicification (fossilization) of intact cellular structures.

REFERENCES

Beveridge, T.J., and Fyfe, W.S.
1985: Metal Fixation by Bacterial Walls; Canadian Journal of Earth Sciences, Volume 22, p.1883-1898.

Beveridge, T.J., and Murray, R.G.E.
1980: Sites of Metal Deposition in the Cell Wall of *Bacillus subtilis*; Journal of Bacteriology, Volume 141, p.876-887.

Birnbaum, S.J., and Wireman, J.W.
1985: Sulfate-Reducing Bacteria and Silica Solubility: A Possible Mechanism for Evaporate Diagenesis and Silica Precipitation in Banded Iron Formation; Canadian Journal of Earth Sciences, Volume 22, p.1904-1909.

Brock, T.D.
1974: Biology of Microorganisms, Second Edition; Prentice Hall, Englewood Cliffs, New Jersey, 852p.

Champetier, Y., Hamdadou, E., and Hamdadou, M.
1987: Examples of Biogenic Support of Mineralization in Two Oolitic Iron Ores—Lorraine (France) and Gara Djebilet (Algeria); Sedimentary Geology, Volume 51, p.249-255.

Costerton, J.W., Marrie, T.J., and Cheng, K.-J.
1985: Phenomena of Bacteria Adhesion; p.3-43 *in* Bacterial Adhesion, edited by D.C. Savage and M. Fletcher, Plenum Press, New York, 864p.

Ferris, F.G., and Beveridge, T.J.
1985: Functions of Bacterial Cell Surface Structures; BioScience, Volume 35, p.172-177.
1986: Physicochemical Roles of Soluble Metal Cations in the Outer Membrane of *Escherichia coli*; Canadian Journal of Microbiology, Volume 32, p.594-601.

Ferris, F.G., Beveridge, T.J., and Fyfe, W.S.
1986: Iron-Silica Crystallite Nucleation by Bacteria in a Geothermal Sediment; Nature, Volume 320, p.609-611.

Iler, R.K.
1980: Isolation and Characterization of Particle Nucleii During the Polymerization of Silicic Acid to Colloidal Silica; Journal of Colloid and Interface Science, Volume 75, p.138-148.

Knoll, A.H.
1985: Exceptional Preservation of Photosynthetic Organisms in Silicified Carbonates and Silicified Peats; Philisophical Transactions of the Royal Society London, Volume B311, p.111-122.

Leo, R.F., and Barghoorn, E.S.
1976: Silicification of Wood; Botanical Museum Leaflets Harvard University, Volume 25, p.1-46.

Yapp, C.J., and Poths, H.
1986: Carbon in Natural Goethites; Geochimica et Cosmochimica Acta, Volume 50, p.1213-1220.

Grant 266 Anomalous Carbonate Till, Hemlo and Geraldton Area, Ontario: Origin and Applications

Stephen R. Hicock

Department of Geology, University of Western Ontario, London

ABSTRACT

Calcareous Shield tills were examined to determine how they were transported and deposited, and how they could affect gold exploration, aggregate quality, and acid rain susceptibility.

Two highly calcareous tills, deposited by lodgment and subglacial melt-out, are underlain by a local weakly calcareous till, and are overlain by a weakly calcareous supraglacial melt-out till. The entire till sequence can be explained by a single rapid glacial advance over uplands involving simultaneous stoss side upshearing of local rocks and lee side downward transport of distal debris, followed by stagnation. Rapid flow involved ice streaming and/or surging within the Superior glacial lobe and may also explain other carbonate drift belts on the Shield.

Supraglacial till comprises coarse local Precambrian materials and is richest in metals. Carbonate tills comprise finer, dominantly distal materials, with less metals. The supraglacial and local gritty sand tills are most likely to contain well-defined ore dispersal trains that may be traced upglacier to their source (probably within 30 km). The carbonate tills are too far traveled to contain distinct and traceable trains; however, they should make excellent buffers against acid precipitation, and dam cores for acidic mine tailings ponds. Little chert occurs in the tills and aggregate quality should be generally high.

INTRODUCTION

The normal recommendation in drift prospecting programs is to sample lodgment till, as opposed to other genetic types, because it is dominated by local clasts and should reflect nearby sources of till materials (Goldthwait 1971; Shilts 1975, 1984). However, the first phase of this project (Hemlo area) clearly demonstrated that lodgment tills in calcareous drift are a hindrance to mineral exploration because they contain abundant distally derived materials that cannot be easily traced upglacier to their source (Hicock 1986, in press). This conclusion was also reached by Geddes and Kristjansson (1986) and Karrow and Geddes (1987). In order to test this hypothesis and assess the regional implications of calcareous drift on gold exploration, the Geraldton area was also investigated during the second phase of the project. As with the Hemlo area, till genesis has important implications for the usefulness of drift prospecting, between Geraldton and Beardmore, in locating other gold sources.

This project was initiated in order to assess: a) the influence of carbonate till on mineral exploration on the Canadian Shield using drift prospecting; b) its response to acid precipitation; and c) to determine till genesis and propose a depositional model for the calcareous drift. These objectives are accomplished in the Geraldton area by analyzing the till character and stratigraphy in order to interpret its mode of formation, occurrence, and provenance.

Field work for phase 2, during three weeks in July, 1986, concentrated on 11 sites (Figure 266.1; mainly roadcuts) which were re-exposed with shovels then studied in detail for stratigraphic and structural relationships of sediment units. In the laboratory, granulometric analyses were performed by the hydrometer-sieve method of the American Society for Testing and Materials (1972), using 0.002 and 0.063 mm at the clay-silt and silt-sand boundaries, respectively. Carbonate analyses were done after the method of Dreimanis (1962) and geochemical analyses were completed by Barringer Magenta Limited of Toronto, using atomic absorption techniques on total digests of the -0.002 mm fraction of till matrices.

Till criteria and terminology used in this paper follow the system of the International Quaternary Association's Commission on Lithology and Genesis of Glacial Deposits as summarized by Dreimanis (1982).

PHYSICAL SETTING AND PREVIOUS WORK

The Geraldton area abounds with glacially aligned lakes and occupies a broad drumlinized trough with up to 100 m relief that is flanked by distinct uplands to the west, south, and east, as well as a subtle upland north of Geraldton (Figure 266.1). The area is underlain by a structurally-complex sequence of Precambrian lithologies including: metavolcanic (mainly greenstone), metasedimentary (including iron formation), and granitoid plutonic and gneissic rocks (Pye *et al.* 1966; Stott 1984a, 1984b). Diabase dikes have intruded other lithologies and minor patches of ultramafic rocks (mainly peridotite) occur on the bedrock surface.

Recent Quaternary studies north of Lake Superior have concentrated on surficial mapping and glacial lake studies (Farrand 1962; Zoltai 1965a, 1965b, 1967; Boissonneau 1966); Zoltai and Boissonneau recognized the carbonate-rich till, as did Sado (1975). Coker and Shilts (1979) generally described the till in a lake geochemistry study, and Fortescue and Geddes (1983), Geddes (1984), Kristjansson (1984, 1986), Geddes and Bajc (1985a, 1985b), Geddes *et al.* (1985), Woods (1985), Geddes and Kristjansson (1986), Geddes (1986), White (1986), Hicock (1986, in press), and Kristjansson *et al.* (in press) have described it in more detailed mapping and case studies. Gartner (1979, 1980a, 1980b) and Cooper (1983) provided engineering and terrain studies of the Geraldton area, and Karrow and Geddes (1987) summarized the implications of carbonate drift on radiocarbon dating, fossil shell preservation, acid precipitation buffering, and drift prospecting on the Canadian Shield.

TILL STRATIGRAPHY AND GENESIS

Four tills are recognized in the Geraldton area; two are highly calcareous and are sandwiched between tills with low carbonate content. The oldest is a locally-derived gritty, silty sand till observed by Krist-

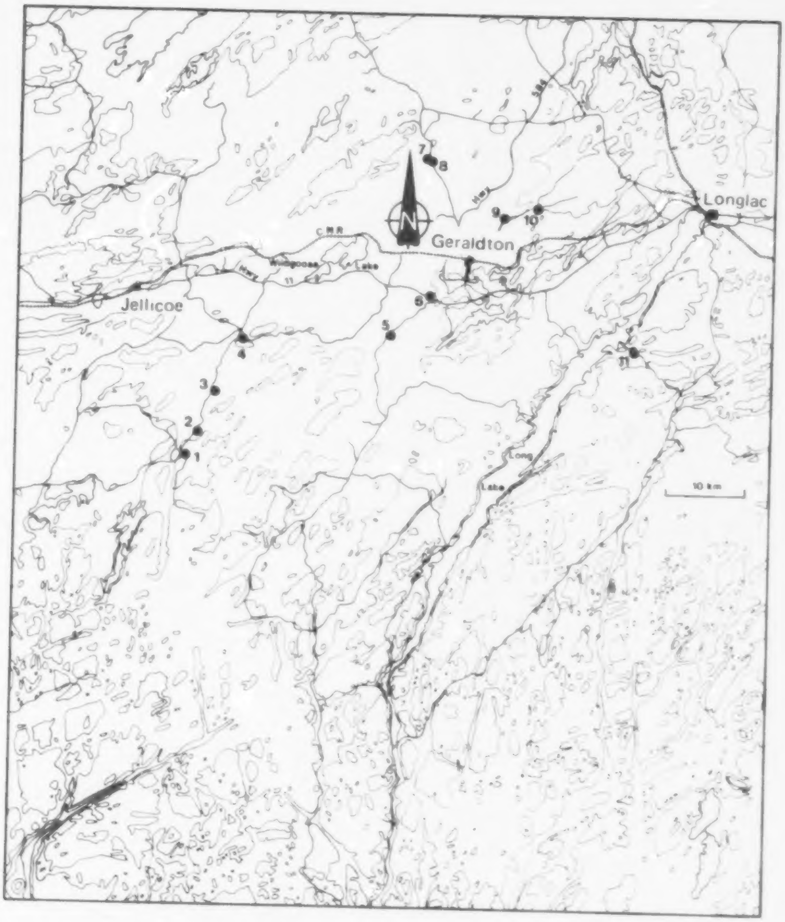

Figure 266.1. *Topographic map of the study area with site localities. Contour interval is 60 m.*

jansson (1984, 1986); it was not encountered in the sections studied by the author.

LODGMENT TILL

The overlying unit occurs in seven sections and comprises a dark grey, compacted, calcareous diamicton. It is fissile, stony, and contains striated, faceted, and bullet-nosed stones, as well as clasts of sand at site 11. Till matrix (-2.00 mm) comprises about 35% sand, 55% silt, 10% clay and 30 to 40% total carbonates (calcite and dolomite; Table 266.1). At sites 6 and 10, its upper portion was remobilized to produce a noncompacted massive diamicton.

Stones are generally subrounded to subangular and dominated by Paleozoic lithologies, indicating distal glacial transport. Parallel and transverse alignment of stones in the till, extension fractures, and shear planes within the unit, as well as displaced bedrock blocks in contact with the till, are consistently oriented with striae on the top surfaces of stones.

These characteristics indicate that this compact diamicton was deposited subglacially by lodgment (Dreimanis 1976, 1982; Shaw 1985).

MELT-OUT TILL

The compact calcareous till is overlain by a light grey, noncompacted, coarser-textured diamicton. This calcareous till was observed at five sites and commonly appeared to be massive, although at some sites it contains interlayered and lenticular silt, sand, gravel, and diamictic strata. Bedding is in places truncated by dropstones or draped over them. Striated and faceted stones, as well as clasts of sorted sediment and compact till are abundant. Till matrices contain 60 to 70% sand, 20 to 30% silt, under 5% clay, and 25 to 35% carbonate (Table 266.1). Stones are generally subrounded, and distal clasts dominate the pebble assemblages. Alignment of stones is commonly parallel to striae on the top surfaces of stones within the till. At some sites, the unit extends to the ground surface where it has been heavily oxidized and leached of carbonate by soil development (Table 266.1, sites 2 and 10).

These data indicate that this unit was deposited subglacially, mainly by melt-out (Dreimanis 1976, 1982; Shaw 1982, 1983, 1985), but with subglacial stream and subglacial debris flow having formed some of the gravelly and diamictic strata.

TABLE 266.1. GERALDTON TILL MATRIX AND PEBBLE DATA.

Till Unit	Site on Fig. 266.1	Matrix Grain Size (-2.0mm fraction) %sand	%silt	%clay	Matrix Carbonate (-0.063mm fraction) %carb	cal/dol	Pebble data (1-10cm fraction) roundness	Distal/Prec
Supraglacial	3	62	37	1	11	0.2	sa-sr	0.5
meltout	2 oxidized	61	37	02	0	0	sr-sa	1.0
	2	62	36	02	22	0.2	sr-sa	0.9
	7 upper	70	28	02	24	0.3	sr-sa	0.9
	7 lower	65	33	02	27	0.5	sa-sr	1.3
	9	74	23	03	33	0.7	sr-sa	1.4
	10 oxidized	63	34	03	0	0	sa-sr	1.6
	10	59	38	03	32	0.5	sr-sa	5.7
lodgment	1	45	48	07	26	0.5	sa-sr	1.2
	4 upper	42	50	08	44	0.9	sr-sa	2.6
	4 lower	38	55	07	31	0.7	sr-sa	3.8
	5	34	59	07	37	0.9	sr-sa	4.6
	6 clasts	23	68	09	39	0.7	sr-sa	4.3
	in meltout	30	53	17	33	0.9	sr-sa	-
	6 remobilized	35	59	06	35	0.6	sr-sa	5.3
	6	31	53	16	32	1.4	sr-sa	1.9
	8	43	48	09	26	0.7	sr-sa	6.1
	10 remobilized	32	62	06	35	0.6	sr-sa	4.9
	11	43	48	09	35	0.9	sr-sa	-
	11	36	56	08	32	0.9	sr-sa	1.2

cal=calcite, dol=dolomite, carb=total calcite and dolomite, Distal=Paleozoic+Proterozoic (wacke) lithologies; prec=Archean lithologies, sa=subangular, sr=subrounded

SUPRAGLACIAL DRIFT (TILL AND BOULDER MANTLES)

At site 3, a noncompacted, weakly calcareous, coarse-textured diamicton (Table 266.1), dominated by subangular Precambrian clasts (many of them rotten), comprises the section, which contains a large angular block of highly calcareous till. The section occurs in a mound mantled by large subangular granitoid boulders. Other boulder-mantled mounds occur near the site and Precambrian blocks commonly mantle the ground surface at other sites. Stone alignment at site 3 is bimodal and unrelated to ice movement.

This material was most likely deposited by supraglacial melt-out, commonly as kames and Precambrian boulder mantles. Younger glaciofluvial and glaciolacustrine sediments were studied by Kristjansson *et al.* (in press).

GLACIER MOVEMENT AND CLASTIC DISPERSAL

An accurate knowledge of glacier movement directions in the Geraldton area is essential for developing a strategy for mineral exploration by drift prospecting, as well as constructing a depositional model for the tills and determining their source areas. Zoltai (1967), Sado (1975), and Kristjansson *et al.* (in press) determined that general ice advance was toward the southwest.

LODGMENT TILL

All fabric orientations (pebble long axes) in the lodgment till display both parallel and transverse clast alignment indicating that glacier advance was toward the southwest, which agrees with the dips of extension fractures, shear planes, and displaced bedrock, as well as striae on stones within the till. Distal lithologies dominate the stones (*see* Table 266.1) but local rocks have been incorporated, including serpentinized peridotite originating just southward of Geraldton.

MELT-OUT TILL

Fabric orientations in the melt-out till suggest that glacial advance was generally to the southwest, which is supported by striae on stones in the unit. Distal clasts are commonly the most abundant, but stones of local to intermediate provenance (including peridotite) were also upsheared into the ice when it was actively advancing prior to melt-out deposition.

TABLE 266.2. GEOCHEMICAL ANALYSES OF GERALDTON TILL SAMPLES (-0.002 mm fraction).

Site	Till Facies	Cu ppm	Ni ppm	B ppm	Mn ppm	Zn ppm	Mo ppm	As ppm	Sb ppm	W ppm	Te ppm	Au ppb
1	lodgment	90	65	22	460	120	<1	11.0	0.2	6	<0.2	5
2	meltout	190	145	35	790	195	<1	7.5	0.2	20	<0.2	29
2	meltout oxidized	200	500	31	760	140	<1	20.0	0.3	12	0.2	4
3	supraglacial	600	375	38	1250	200	<1	23.5	0.5	350	0.2	145
4	lodgment	100	60	39	560	145	<1	6.0	0.2	16	<0.2	1
4	lodgment	60	55	35	480	110	<1	5.0	0.2	4	<0.2	15
5	lodgment	60	40	28	460	115	<1	5.0	0.2	6	<0.2	34
6	lodgment clast in meltout	55	40	43	520	100	<1	4.5	0.2	12	<0.2	17
6	lodgment clast in meltout	47	40	31	490	90	<1	4.0	<0.2	<4	<0.2	10
6	lodgment remobilized	55	45	36	540	105	<1	4.5	0.2	4	<0.2	12
6	lodgment	45	35	36	475	95	<1	4.0	0.2	8	<0.2	2
7	meltout	125	50	36	780	195	<1	5.5	0.2	8	<0.2	16
7	meltout	85	30	31	640	140	<1	3.5	0.2	100	<0.2	5
8	lodgment	80	60	40	530	150	<1	4.5	<0.2	16	<0.2	2
9	meltout	130	60	40	640	160	<1	7.5	0.2	4	<0.2	13
10	meltout	70	55	33	610	135	<1	7.0	0.2	4	<0.2	37
10	meltout oxidized	80	75	9	300	100	<1	11.0	0.2	6	<0.2	1
10	lodgment remobilized	90	45	37	520	135	<1	5.5	0.2	4	<0.2	4
11	lodgment	90	65	28	530	120	<1	26.5	0.3	4	<0.2	11
11	lodgment	60	55	28	570	105	<1	16.5	0.2	4	<0.2	<1

SUPRAGLACIAL DRIFT

The bimodal fabric in supraglacial till at site 3 is unrelated to ice movement, but the drift is clearly dominated by angular local clasts, including peridotite derived from the northeast.

SUMMARY

The glaciotectonic and fabric data agree with the ice movement data of Zoltai (1967), Sado (1975), and Kristjansson *et al.* (in press) and clearly indicate southwestward advance. Paleozoic, peridotite, and dark wacke clasts confirm this since they originated from bedrock sources to the northeast. The Paleozoic pebbles were derived from the James Bay Lowland, at least 120 km distant, and the wackes from the eastern side of Hudson Bay (Shilts 1980, 1982, 1984). Pebble assemblages indicate that ice advanced southwestward across lithological contacts rather than parallel to them.

GEOCHEMICAL GLACIAL DISPERSAL

Atomic absorption analyses of the -0.002 mm fraction in till matrices for eight metals and three semimetals are presented in Table 266.2. This size fraction was chosen because it most accurately reflects preweathering proportions of metals in the till matrix (Shilts 1975, 1984).

The supraglacial melt-out till is clearly richest in metals, especially gold, whereas the highly calcareous tills contain lesser amounts. Melt-out till is generally richer in metals than the lodgment facies, but has lesser matrix carbonate. The relationship between metal content and matrix carbonate is demonstrated in Figure 266.2 for four representative metals; in general, as matrix carbonate increases, metal content decreases. This trend reflects relative dilution of metals of local to intermediate provenance by distal carbonate matrix during glacial transport and deposition. Supraglacial till has low carbonate matrix and better reflects the local bedrock geochemistry.

MODE OF GLACIAL TRANSPORT AND TILL DEPOSITION

The entire till sequence in the Geraldton area can be explained by one glacial advance over uplands to the northeast (Figure 266.1). The carbonate-rich tills probably resulted from rapid ice stream erosion of carbonate bedrock in the James Bay Lowland and subsequent deposition in the lee sides of uplands where englacial debris was transported downward to the basal zone as the glacier experienced enhanced extending flow, followed by stagnation. The depositional model for phase I of this project (Hemlo) also applies here and was presented by Hicock (1986; in press). Extending flow was probably also part of the

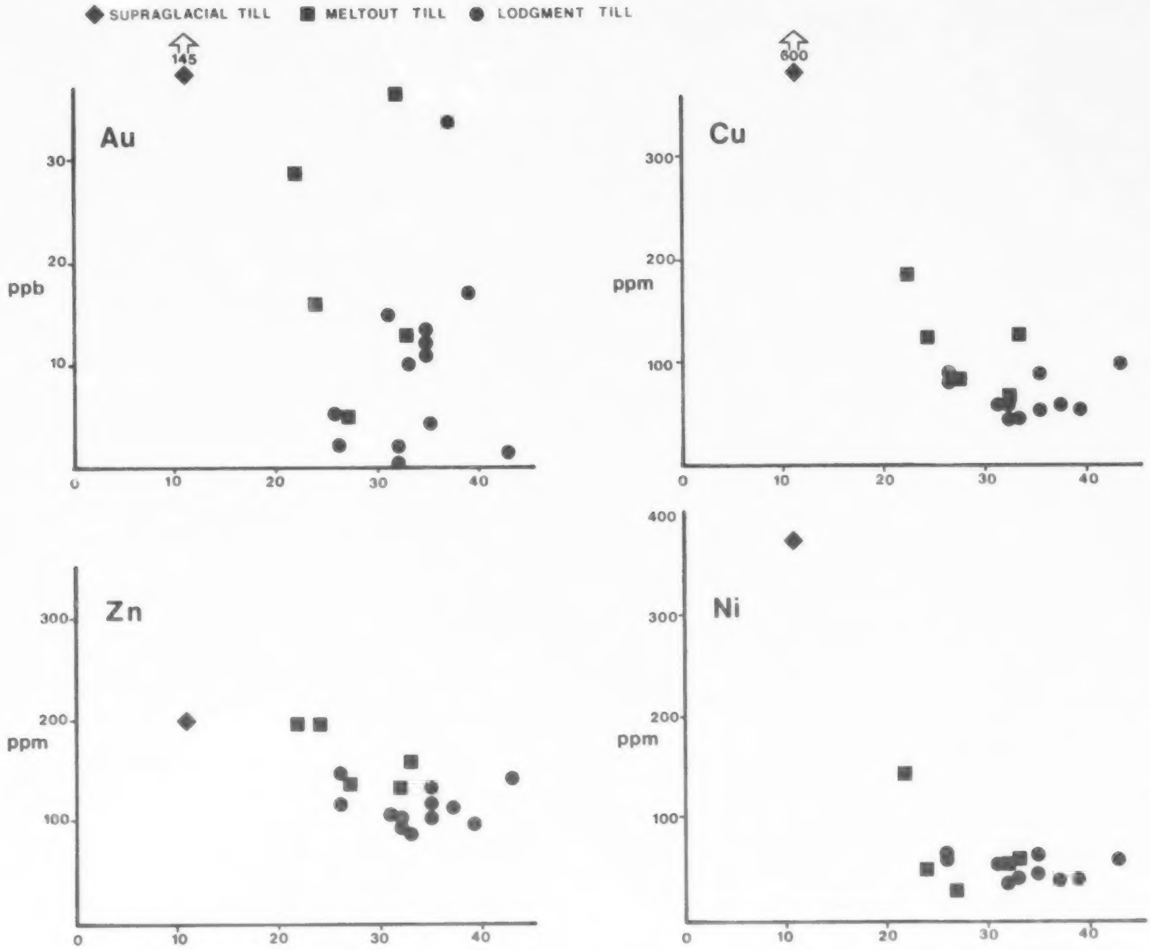

Figure 266.2. Geochemical comparison of representative metals in Geraldton Till matrices (-0.002 mm fraction), excluding leached samples from sites 2 and 10, with percent matrix carbonate (-0.063 mm fraction).

rapid glacial movement (surging and/or ice streaming) in prominent lobes along the southern margin of the Late Wisconsinan Laurentide Ice Sheet (Wright 1973; Boulton and Jones 1979; Boulton *et al.* 1985; Clayton *et al.* 1985; Beget 1986; Hicock *et al.* in press), in this case the Superior lobe. In this way, large quantities of Paleozoic carbonate debris were rapidly transported great distances over the Canadian Shield and deposited on it as belts of thick carbonate till (c.f. Karrow and Geddes 1987; Hicock *et al.* in press).

In the Geraldton area, glacier ice streaming from the northeast (probably out of the James Bay Lowland via the Albany-Drowning corridor and Nakina) met the stoss side of the granitoid upland belt north of Geraldton. Local compressive flow was induced and diverted around the uplands (as well as inducing upshearing of glacial debris), eroding the local bedrock and depositing Kristjansson's (1984, 1986) local gritty sand till. The englacial zone overrode the retarded basal ice and continued the stoss-side upshearing of local debris to or near the glacier surface. It then spilled over the bedrock step and into a structural trough southwest of Wildgoose Lake while its debris was transported downward with extending flow. This resulted in lodgment of englacial debris on top of the gritty sand till, in the lee side of the upland.

After the glacier reached its maximum extent, it probably stagnated in the Geraldton area where much glacial debris was deposited by subglacial melt-out. A late rejuvenation of the glacier occurred during general downwasting which carved drumlins into the carbonate tills and probably correlates with the deposition of an upper lodgment till in the Hemlo area (Hicock 1986, in press).

Finally, upland stoss-side debris that was upsheared to or near the glacier surface was passively lowered onto the underlying calcareous melt-out and lodgment tills by supraglacial melt-out, in some places as kames. This is supported by the various late glacial ice retreat and disintegration features in the area (Zoltai 1967; Sado 1975; Kristjansson 1986; Kristjansson *et al.* in press).

ECONOMIC AND ENVIRONMENTAL ASPECTS

As with the first phase of the project (Hicock 1986, in press), these results and interpretations indicate that an understanding of till genesis, stratigraphy, and ice movements are important for mineral exploration strategies and environmental considerations. Some recommendations are presented below for the Geraldton area.

DRIFT PROSPECTING

The supraglacial melt-out till and the local gritty sand till, in which significant gold was also found (F. Kristjansson, Geologist, Engineering and Terrain Geology Section, Ontario Geological Survey, Toronto, personal communication, 1987), are best to sample in overburden drilling programs. They comprise material that has been transported for relatively short distances (mainly derived from uplands less than 30 km upglacier; Figure 266.1) and are, therefore, most likely to contain well-defined dispersal fans of ore anomalies which may be traced back to their source (c.f. Shilts 1976, 1984). This is exemplified by the relatively high gold value in the supraglacial till, which occurs within an area of gold exploration.

The calcareous tills, however, are a hindrance to drift prospecting (Kristjansson 1986) because they contain mainly distally-derived material (much of it from at least 120 km away) which mask dispersed ore of local to intermediate provenance. Any disperal fans within the calcareous tills will probably be too diffuse to recognize (with ore values near background this far downglacier from distal ore sources) or to successfully trace the anomalies back to their source.

AGGREGATE QUALITY

As in the Hemlo area (Hicock 1986), chert is a minor component in the drift studied around Geraldton and should cause no problems with gravel use. Rotted clasts of granitoid and metasediments were found in several sections. At site 3, the supraglacial till was dominated by completely decomposed purple metasedimentary clasts and the unit will present a problem for aggregate use if this is found to be a trend in it.

ACID RAIN

The calcareous tills should be excellent buffers. They are as calcareous as those overlying carbonate bedrock in southern Ontario where till matrix carbonate would attain a maximum.

Map unit 3 of Kristjansson *et al.* (in press) is the least susceptible to acid rain. Thus, a map of acid rain susceptibility could be constructed based on the matrix carbonate of the various sediment units in the area, such as that attempted by Woods (1985, p.45) for the Hemlo area.

Lakes within areas of calcareous glacial drift are more alkaline than those without and also serve as buffers (Woods 1985, p.45; Coker and Shilts 1979).

TAILINGS DAM CORES

The calcareous lodgment till would probably make good low-permeability cores with high capacity for buffering acidic mine tailings, as it does in the Hemlo area (Hicock 1986).

ACKNOWLEDGMENTS

F.J. (Rik) Kristjansson (Engineering and Terrain Geology Section, Ontario Geological Survey, Toronto) provided invaluable logistical and scientific support throughout the course of this study. E.V. Sado (Engineering and Terrain Geology Section, Ontario Geological Survey, Toronto) suggested the project and was generous with advice and support. J.-A. Potter and E.A. Gray (Department of Geology, University of Western Ontario, London) were field assistants. D. Slater (Ministry of Natural Resources Fire Station, Geraldton) generously permitted our use of base facilities. S.L. Brown (Department of Geology, University of Western Ontario, London) performed laboratory analyses and assisted in drafting the diagrams. Research was funded by the Ontario Geoscience Research Grant Program.

REFERENCES

American Society for Testing and Materials
1972: Standard Method for Particle-size Analysis of Soils; p.112-122 *in* Annual Book of Standards D422-63, Philadelphia, Pennsylvania.

Beget, J.E.
1986: Modeling the Influence of Till Rheology on the Flow and Profile of the Lake Michigan Lobe, Southern Laurentide Ice Sheet, U.S.A.; Journal of Glaciology, Volume 32, p.235-241.

Boissonneau, A.N.
1966: Glacial History of Northeastern Ontario: 1. The Cochrane-Hearst Area; Canadian Journal of Earth Sciences, Volume 3, p.559-578.

Boulton, G.S., and Jones, A.S.
1979: Stability of Temperate Ice Caps and Ice Sheets Resting on Beds of Deformable Sediment; Journal of Glaciology, Volume 24, p.29-43.

Boulton, G.S., Smith, G.D., Jones, A.S., and Newsome, J.
1985: Glacial Geology and Glaciology of the Last Mid-latitude Ice Sheets; Journal of the Geological Society of London, Volume 142, p.447-474.

Clayton, L., Teller, J.T., and Attig, J.W.
1985: Surging of the Southwestern Part of the Laurentide Ice Sheet; Boreas, Volume 14, p.235-241.

Coker, W.B., and Shilts, W.W.
1979: Lacustrine Geochemistry Around the North Shore of Lake Superior: Implications for Evaluation of the Effects of Acid Precipitation; Geological Survey of Canada, Paper 79-1C, p.1-15.

Cooper, A.J.
1983: Nakina Area, District of Thunder Bay and Cochrane; Ontario Geological Survey, Northern Ontario Engineering Geology Terrain Study 19. Accompanied by Maps 5125 and 5126, scale 1:100 000.

Dreimanis, A.
1962: Quantitative Gasometric Determination of Calcite and Dolomite by Using Chittick Apparatus; Journal of Sedimentary Petrology, Volume 32, p.520-529.
1976: Tills: Their Origin and Properties; p.11-49 *in* Glacial Till, edited by R.F. Legget, Royal Society of Canada, Special Publication 12.
1982: Genetic Classification of Tills and Criteria for Their Differentiation; p.12-31 *in* International Quaternary Association, Commission on Genesis and Lithology of Quaternary Deposits, Report of Activities 1977-1982, edited by C. Schluchter, Honggerberg, Zurich, Switzerland.

Farrand, W.R.
1962: Postglacial Uplift in North America; American Journal of Science, Volume 260, p.181.

Fortescue, J.A.C., and Geddes, R.S.
1983: A Small Scale Geochemistry/Quaternary Geology Study in the Hemlo Camp, District of Thunder Bay; p.159-160 *in* Summary of Field Work, 1983, by the Ontario Geological Survey, edited by John Wood, Owen L. White, R.B. Barlow, and A.C. Colvine, Ontario Geological Survey, Miscellaneous Paper 116, 313p.

Gartner, J.F.
1979: Jellicoe Area, District of Thunder Bay; Ontario Geological Survey, Northern Ontario Engineering Geology Terrain Study 27. Accompanied by Map 5077, scale 1:100 000.
1980a: White River Area, District of Thunder Bay; Ontario Geological Survey, Northern Ontario Engineering Geology Terrain Study 61 and Maps 5094 and 5998.
1980b: Longlac Area, District of Thunder Bay; Ontario Geological Survey, Northern Ontario Engineering Geology Terrain Study 28. Accompanied by Maps 5078 and 5081, scale 1:100 000.

Geddes, R.S.
1984: Quaternary Geology of the Hemlo Area; p.97-99 *in* Summary of Field Work, 1984, Ontario Geological Survey, edited by John Wood, Owen L. White, R.B. Barlow, and A.C. Colvine, Ontario Geological Survey, Miscellaneous Paper 119, 309p.
1986: Till Genesis and Glacial Dispersion, Page Williams A Zone, Hemlo; p.182-186 *in* Summary of Field Work and Other Activities, 1986, by the Ontario Geological Survey, edited by P.C. Thurston, Owen L. White, R.B. Barlow, M.E. Cherry, and A.C. Colvine, Ontario Geological Survey, Miscellaneous Paper 132, 435p. Accompanied by 1 chart.

Geddes, R.S., and Bajc, A.F.
1985a: Quaternary Geology of the White Lake (Hemlo) Area, District of Thunder Bay; Ontario Geological Survey, Map P.2849, Geological Series-Preliminary Map, scale 1:50 000.
1985b: Quaternary Geology of the Cedar Lake (Hemlo) Area, District of Thunder Bay; Ontario Geological Survey, Map P.2850, Geological Series-Preliminary Map, scale 1:50 000.

Geddes, R.S., Bajc, A.F., and Kristjansson, F.J.
1985: Quaternary Geology of the Hemlo Region, District of Thunder Bay; p.151-154 *in* Summary of Field Work and Other Activities, 1985, Ontario Geological Survey, edited by John Wood, Owen L. White, R.B. Barlow, and A.C. Colvine, Ontario Geological Survey, Miscellaneous Paper 126, 351p.

Geddes, R.S., and Kristjansson, F.J.
1986: Quaternary Geology of the Hemlo Area: Constraints on Mineral Exploration; Canadian Journal of Geology of CIM, Volume 1, p.5-8.

Goldthwait, R.P.
1971: Introduction to Till, Today; p.3-26 *in* Till: A Symposium, edited by R.P. Goldthwait, Ohio State University Press, Columbus, Ohio.

Hicock, Stephen R.
1986: Carbonate Till on the Canadian Shield: Economic and Environmental Implications in the Hemlo Area, Ontario; Grant 266, p.210-217 *in* Geoscience Research Grant Program, Summary of Research, 1985-1986, edited by V.G. Milne, Ontario Geological Survey, Miscellaneous Paper 130, 235p.
In Press: Genesis of Carbonate Till in the Lee Sides of Precambrian Shield Uplands, Hemlo Area, Ontario; Canadian Journal of Earth Sciences.

Hicock, S.R., Kristjansson, F.J., and Thorleifson, L.H.
In Press: Ice Streaming on Deformable Carbonate Till of the Canadian Shield; Nature.

Karrow, P.F., and Geddes, R.S.
1987: Drift Carbonate on the Canadian Shield; Canadian Journal of Earth Sciences, Volume 24, p.365-369.

Kristjansson, F.J.
1984: Till Sampling and Gold Exploration, Beardmore-Geraldton Area; p.97-98 *in* Report of Activities 1983, Regional and Resident Geologists, edited by C.R. Kustra, Ontario Geological Survey, Miscellaneous Paper 117, 275p.
1986: Quaternary Geology of the Beardmore-Geraldton Area, District of Thunder Bay; p.172-175 *in* Summary of Field Work and Other Activities, 1986, by the Ontario Geological Survey, edited by P.C. Thurston, Owen L. White, R.B. Barlow, M.E. Cherry, and A.C. Colvine, Ontario Geological Survey, Miscellaneous Paper 132, 435p. Accompanied by 1 chart.

Kristjansson, F.J., White, T.N., and Gaudino, S.P.
In Press: Quaternary Geology, Wildgoose Lake Area; Geological Series-Preliminary Map, Ontario Geological Survey.

Pye, E.G., Harris, F.R., Fenwick, K.G., and Baillie, J.
1966: Tashota-Geraldton Sheet, Thunder Bay and Cochrane Districts; Ontario Department of Mines, Map 2102, scale 1:253 440 or 1 inch to 4 miles.

Sado, E.V.

1975: Quaternary Geology of the Wildgoose Lake Area, District of Thunder Bay; p.128-129 *in* Summary of Field Work, 1975, by the Geological Branch, edited by V.G. Milne, D.F. Hewitt, K.D. Card, and J.A. Robertson, Ontario Division of Mines, Miscellaneous Paper 63, 158p.

Shaw, J.

1982: Melt-out Till in the Edmonton Area, Alberta, Canada; Canadian Journal of Earth Sciences, Volume 19, p.1548-1569.

1983: Forms Associated with Boulders in Melt-out Till; p.3-12 *in* Tills and Related Deposits, edited by E.B. Evenson, C. Schluchter, and J. Rabassa, A.A. Balkema, Rotterdam, Netherlands.

1985: Subglacial and Ice Marginal Environments; p.7-84 *in* Glacial Sedimentary Environments, edited by G.M. Ashley, J. Shaw, and N.D. Smith, Society of Economic Mineralogists and Paleontologists, Short Course 16.

Shilts, W.W.

1975: Principles of Geochemical Exploration for Sulphide Deposits Using Shallow Samples of Glacial Drift; Canadian Institute of Mining and Metallurgy Bulletin, May, 1985, p.73-80.

1976: Glacial Till and Mineral Exploration; p.205-224 *in* Glacial Till, edited by R.F. Legget, Royal Society of Canada, Special Publication 12.

1980: Flow Patterns in the Central North American Ice Sheet; Nature, Volume 286, p.213-218.

1982: Quaternary Evolution of the Hudson/James Bay Region; Naturaliste Canadienne, Volume 109, p.309-332.

1984: Till Geochemistry in Finland and Canada; Journal of Geochemical Exploration, Volume 21, p.95-117.

Stott, G.M.

1984a: Geraldton Sheet, Thunder Bay and Cochrane Districts; Ontario Geological Survey, Map P.241 (Rev.), Compilation Series-Preliminary Map, scale 1:126 720 or 1 inch to 2 miles.

1984b: Lake Nipigon Sheet, Thunder Bay District; Ontario Geological Survey, Map P.257 (Rev), Compilation Series-Preliminary Map, scale 1:126 720 or 1 inch to 2 miles.

White, T.N.

1986: Genesis and Depositional Model of the Pleistocene Till Sequence in the White River Area of Ontario; B.Sc. Thesis, University of Western Ontario, London.

Woods, E.A.

1985: The Relationship Between the Surficial Geology and Lake Water Alkalinity in the Hemlo-Manitouwadge Area, Ontario; B.Sc. Thesis, University of Western Ontario, London.

Wright, H.E., Jr.

1973: Tunnel Valleys, Glacial Surges, and Subglacial Hydrology of the Superior Lobe, Minnesota; p.251-276 *in* The Wisconsinan Stage, edited by R.F. Black, R.P. Goldthwait, and H.B. Willman, Geological Society of America Memoir 136.

Zoltai, S.C.

1965a: Glacial Features of the Quetico-Nipigon Area, Ontario; Canadian Journal of Earth Sciences, Volume 2, p.247-269.

1965b: Surficial Geology of the Thunder Bay Map Area; Ontario Department of Lands and Forests, Map S265, scale 1:506 880 or 1 inch to 8 miles.

1967: Glacial Features of the North-Central Lake Superior Region, Ontario; Canadian Journal of Earth Sciences, Volume 4, p.515-528.

Grant 275 Deformation of the Sudbury Structure and its Footwall

W.S. Shanks and W.M. Schwerdtner

Department of Geology, University of Toronto

ABSTRACT

The southern segment of the granophyre ring of the Sudbury Igneous Complex contains prominent C-S fabrics produced by northwest-directed ductile shear. This intense deformation probably occurred in the same regional stress field that generated the reverse faults and thrusts found south of the Sudbury Structure. Ongoing structural analysis will test the hypothesis that the tectonic deformation of the Sudbury Structure was caused entirely by reverse ductile shear and associated faulting. Another objective of the structural analysis is to make a proper estimate of the original diameter ratio of the unstrained Sudbury Structure. Laboratory research is directed toward a better use of available strain gauges, such as concretions in the Chelmsford Formation and various types of fragments in the Onaping Formation. A detailed structural map is being made that will cover the deformed portion of the Sudbury Structure, to be published upon completion of this project.

INTRODUCTION

The Sudbury Structure holds the largest known Ni-Cu deposits on earth, but its origin and tectonic history are still a matter of heated debate. No detailed structural study has been made of the Sudbury Igneous Complex, and the deformation of the wall rocks is not well understood. Therefore, the authors started a long-range project to remedy this situation and thereby assist in the search for new Ni-Cu deposits.

This paper summarizes the progress after 3.5 months of field work and subsequent laboratory study. It focuses on the ductile deformation of parts of the Sudbury Structure and contains no information on the wall rocks. All of the field data were obtained above ground. Research has greatly benefited from earlier structural work, notably that of Brocoum and Dalziel (1974), Card and Hutchinson (1972), Clendenden (1986), Dressler (1984a, 1984b), Morris (1984), Muir and Peredery (1984), Rousell (1972, 1975, 1984), and Stevenson (1972, 1984).

RESEARCH GOALS

A field-based structural analysis is being conducted to; a) produce a detailed structural map of the deformed portion of the Sudbury Structure, b) attempt to estimate the original ratio of principal horizontal diameters of the Sudbury Structure, and c) reconstruct the kinematics of tectonic deformation of the original Sudbury Structure. This entails a critical assessment of natural strain gauges used by previous workers and the discovery of suitable kinematic indicators.

DETAILED STRUCTURAL MAPPING

Field mapping in 1986 covered the western core of the Sudbury Structure (Figure 275.1) and the southwestern portion of the Sudbury Igneous Complex. A detailed survey was made of the fold system in the Chelmsford Formation (Rousell 1972, 1984) and a number of important relationships were established.

Folds are of different orders (Ramsay 1967, p.355) and do not adhere to a simple *en echelon* pattern as implied by Rousell (1972, 1984). The upright folds belong to a pervasive system of sinuous and bifurcating structures that seems to extend across the entire core of the Sudbury Structure (Shanks 1987, Figure 10). Individual folds of the wave trains are markedly noncylindrical and doubly plunging (Figure 275.1). The dominant trend of the hinge-plane traces is 050° to 070°, but the lack of northwest-trending linear zones of hinge-line depressions and culminations is difficult to explain with Rousell's (1984, p.84) hypothesis of horizontal cross folding under northeast-southwest compression. More probably, the curvature of fold hinges and the associated change in fold amplitude is largely caused by the termination and bifurcation of folds as typically found in buckle systems (Photo 275.1). Buckle folding in bedding seems to have occurred throughout the Chelmsford Formation, which involves an alternating sequence of strong wacke beds (1 to 5 m thick) and weak siltstone beds (<2 m thick).

The southwestern part of the Igneous Complex contains highly strained granophyre rocks and noritic to gabbroic phases that show little macroscopic evidence of pervasive deformation. However, there are enough narrow mylonite zones in the noritic and gabbroic rocks to demonstrate that the entire Igneous Complex was subjected to regional deformation. Field work in 1987 was specifically directed toward the problem of the deformational responses of the "norite".

Schistosity (flattened mineral aggregates) in the granophyre dips consistently to the southeast (Figure 275.2), and is subperpendicular to the lithological contacts in the southwestern part of the Sudbury Structure (Morris 1984). Convincing evidence was found that schistosity was produced in a broad zone of pervasive ductile shear, which includes at least the upper part of the Onaping Formation.

Within the southwestern Sudbury Structure, and possibly elsewhere as well, the Onaping Formation was deformed in a ductile manner that resulted in prolate fragments. The fragments define pronounced, steeply plunging linear fabrics that cannot be readily explained by ductile simple shear, and pose an important structural problem.

NATURAL STRAIN GAUGES

All major rock units in the Sudbury Structure contain at least one potential strain gauge (Rousell 1984, Clendenden 1986), but most of these common gauges cannot be used at present (Shanks 1987). The Chelmsford Formation is rich in football-size concretions (Brocoum and Dalziel 1974), but their original shape and time of formation are uncertain (Photo 275.2; Shanks 1987, Appendix A).

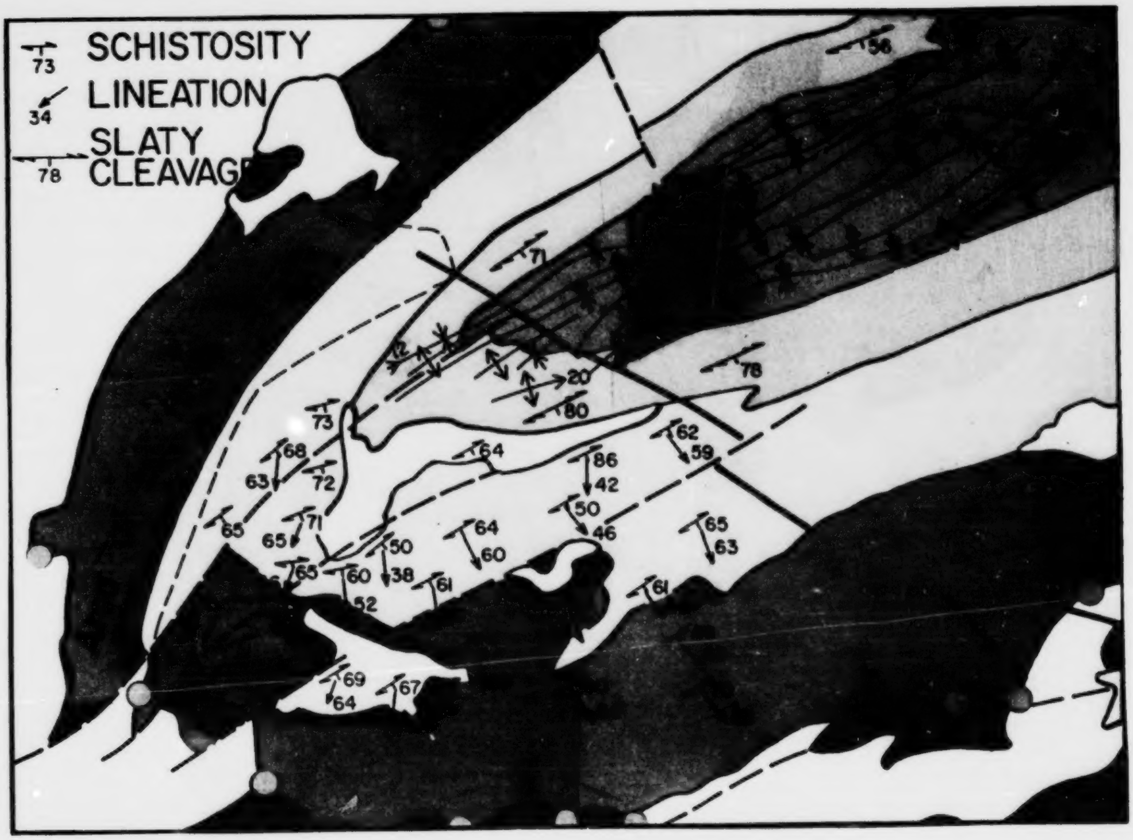

Figure 275.1. *Horizontal traces of fold hinge surfaces (opposing arrows) within the core of the Sudbury Structure (simplified from Shanks 1987, Figure 10). Small solid circles indicate mines.*

The Onwatin Formation seems to lack macroscopic strain gauges, but its slaty cleavage should provide a minimum value of the total-strain ratios (Ramsay 1967, p.180) as well as the principal-strain directions. Small-scale folds are locally present in the Onwatin Formation, and could yield valuable information about the progressive strain.

The Onaping Formation is practically undeformed in the northern part of the Sudbury Structure, where the shapes and original fabrics of inclusions (fragments, shards, and so on) can be ascertained. Most types of inclusions are apt to be stronger than the rock matrix, and cannot be easily used as gauges of total rock strain. Shanks (1987, p.12) started to investigate this problem and found that most types of inclusions have no original preferred orientation. Moreover, at least one common variety of ductile inclusions is strained as much as the rock. This is revealed by identical results of strain analysis based on; a) the shape and orientation of deformed inclusions (Robin 1977), and, b) the relative displacement between centres of neighbouring inclusions (Fry 1979, Crespi 1986).

Coarse varieties of strained granophyre contain excellent mineral-aggregate fabrics (mafic clots, and so on), which are being used as gauges of total rock strain. No conventional strain gauges seem to occur in fine-grained granophyre and norite.

ESTIMATE OF ORIGINAL RATIO OF PRINCIPAL HORIZONTAL DIAMETERS

Several workers have estimated the length of the original northwest-southeast diameter of the entire Sudbury Structure, or at least the core of its map pattern (for example, Brocoum and Dalziel 1974, Rousell 1984, Morris 1984, Clendenden 1986). However, only the diameter ratio is needed in assessing whether the original Sudbury Structure was subcircular in plan view and could have been caused by meteorite impact (Naldrett 1984). Most previous workers assumed that the present horizontal diameter is the same material line as the original diameter, but this assumption is untenable because of the strong northwest-southeast gradient in total strain across the Sudbury Structure (c.f. Schwerdtner 1977). These workers also assumed that all rocks were present as well as being undeformed at the onset of the tectonism that distorted the original Sudbury Structure. In view of such restrictive assumptions, the original ratio of principal horizontal diameters must be regarded as being still unknown. The chance that the present attempt will be successful at estimating this ratio will

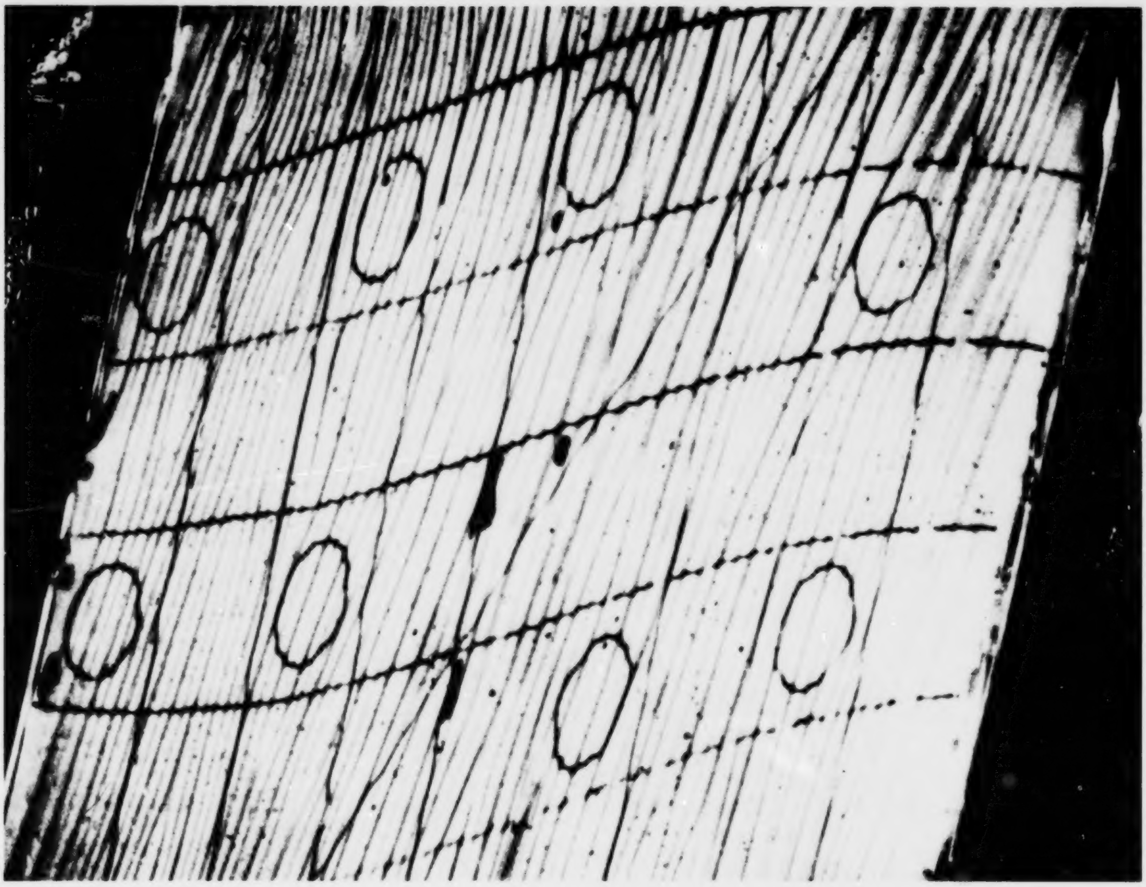

Photo 275.1. *Transparent model of a system of upright buckle folds in plan view (15 by 15 cm), formed by noncoaxial horizontal compression. Load was applied by clockwise rotation of dark levers and glass plates fixed at top and bottom of the model. Undeformed strong member = 1 mm thick rubber sheet with a square grid of black lines, a single black diagonal and large marker circles. Weak matrix = gelatine with a few black air bubbles. Diffuse dark lines subparallel to black diagonal are hanges of buckle folds. Note common bifurcation and termination of buckle folds and wavy (corrugated) appearance of the black grid lines after buckle folding.*

depend largely on the reliability of the potential gauges of total strain.

Two principal methods are available for estimating the original horizontal dimensions of large geological bodies. Method 1 utilizes markers of the paleohorizontal plane, and Method 2 utilizes the geometric surface which coincides with the present erosion surface (Schwerdtner 1985, Figure 1). Owing to the absence of depositional layering within most outcrops of the Onaping Formation and the Igneous Complex, only Method 2 can be used for the entire erosional remnant of the Sudbury Structure. This method relies on the compatibility between small finite elements within a large geological structure (Cobbold and Percevault 1983) and has recently been employed in estimating the original width of an Archean greenstone belt (Schultz-Ela 1987).

Method 1 can only be applied to the core of the Sudbury Structure (Chelmsford Formation), where bedding attitudes are available. These bedding attitudes permit the delineation of outcrop patterns of folds (Figure 275.1; Shanks 1987, Figure 10) and the projection of folded surfaces to depth (Ragan 1985, Chapter 12) and the construction of a northwest-southeast vertical section.

The projection methods assume that the fold style is perfectly parallel, a first-order approximation in most natural buckle systems (Suppe 1985). Unfortunately, the folds in the central Sudbury Structure are rarely seen in profile, but they tend to be open (e.g. in road cuts near the town of Chelmsford). All open folds may be regarded as quasi-parallel, as shown in Ramsay's (1967, p.366) t'/α, and T'/α, plots. This means that vertical sections can be constructed across fold trains within the Chelmsford Formation and used to restore the minimal northwest-southeast length of undeformed bedding planes across parts of the central Sudbury Structure. This

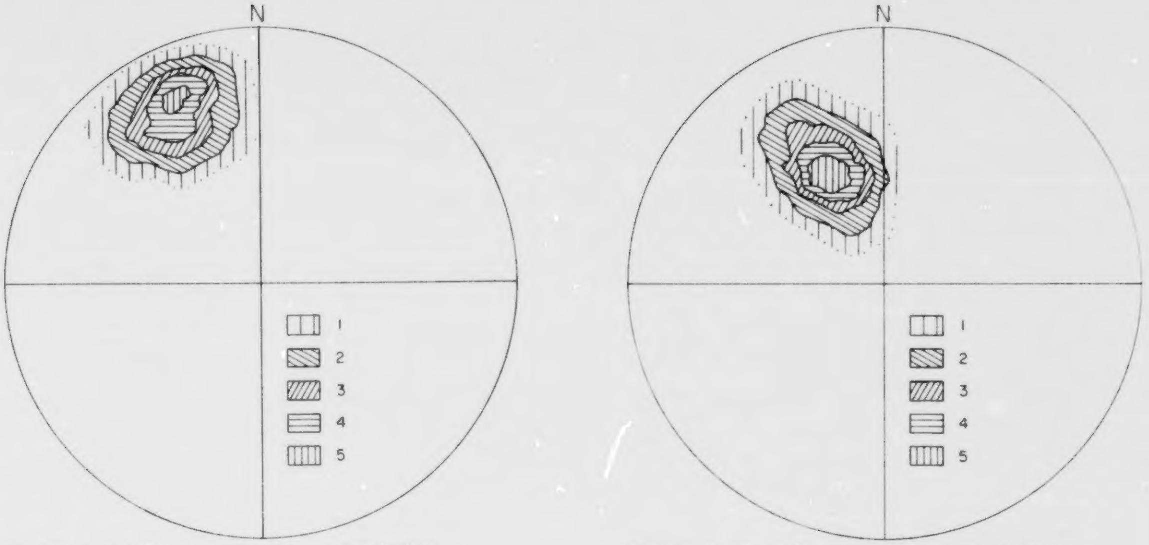

Contoured plot of S-planes in lower hemisphere stereographic projection

Contoured plot of C-planes in lower hemisphere stereographic projection

Figure 275.2. *Machine-contoured stereoplots (lower hemisphere) using the Gaussian weighting function (after Robin and Jowett 1986),*
(a) 43 poles to schistosity planes (S),
(b) 47 poles to C-planes, 1-5 are fields of increasing density. Contours are at $0.43+\sigma$, $0.43+4\sigma$, $0.43+8\sigma$, and $0.43+28\sigma$ in Figure 275.2a, as opposed to $0.47+2\sigma$, $0.47+4\sigma$, $0.47+8\sigma$ and $0.47+36\sigma$ in Figure 275.2b (σ = standard deviation).

can be accomplished by measuring the northwest-southeast arc length of individual bedding surfaces, within a train of folds, from their outcrop traces on one flank of the central Sudbury Structure to those on the other flank. The original lengths thus obtained are divided by the present northwest-southeast horizontal distances between the respective outcrop traces to estimate the reciprocal value of northwest-southeast overall strain.

This estimate can be improved by considering also the uniform thickening of beds associated with buckling, which is accomplished by means of reliable strain data. The northeast-southwest overall strain is probably small, but can also be estimated on the basis of strain data. In case of no northeast-southwest change in overall length, the reciprocal value of northwest-southeast overall strain corresponds to the length ratio of a pair of undeformed line segments located on the principal horizontal diameters of the oval map pattern. If this length ratio is close to the diameter ratio of the central map pattern (Chelmsford Formation), then the Sudbury Structure was probably subcircular at the onset of regional deformation.

KINEMATIC INDICATORS IN THE SOUTHERN IGNEOUS COMPLEX

Apart from its prominent schistosity (S-fabric), the deformed granophyre also exhibits discrete planar discontinuities that have tentatively been interpreted as C-planes (Figure 275.2b and Berthe *et al.* 1979). However, these discontinuities may also be shear bands (Coward 1984, Figure 19) or Riedel shears; field work was carried out in 1987 to test this possibility. Shanks (1987) regarded the features in question as C-planes of a simple-shear zone, and estimated the extreme-strain ratio from the angle between the centres of the maxima for C- and S-poles (Figure 275.2). He found that this principal axial ratio is 7.53 and the corresponding unit shear =2.38. These values would be incorrect if the discontinuities turn out the shear bands, or if the deformation is not purely by ductile simple shear.

Because the centre of the maximum for S-poles is less inclined than that for the supposed C-poles, the sense of shear corresponds to that of northwest-directed thrusts. If the discontinuities turn out to be shear bands instead of C-planes, then the shear zone boundaries dip more steeply to the southeast than is suggested by Figure 275.2b, but the sense of shear would not be affected. This indicates clearly that the southern segment of the granophyre ring, if not the entire southern Igneous Complex, was subjected to progressive ductile shearing with the displacement sense of thrusts or reverse faults. The lowermost Onaping Formation had a similar fate, but no kinematic indicators were found in the other stratigraphic members whose path of deformation may have been comparable to that of the granophyre.

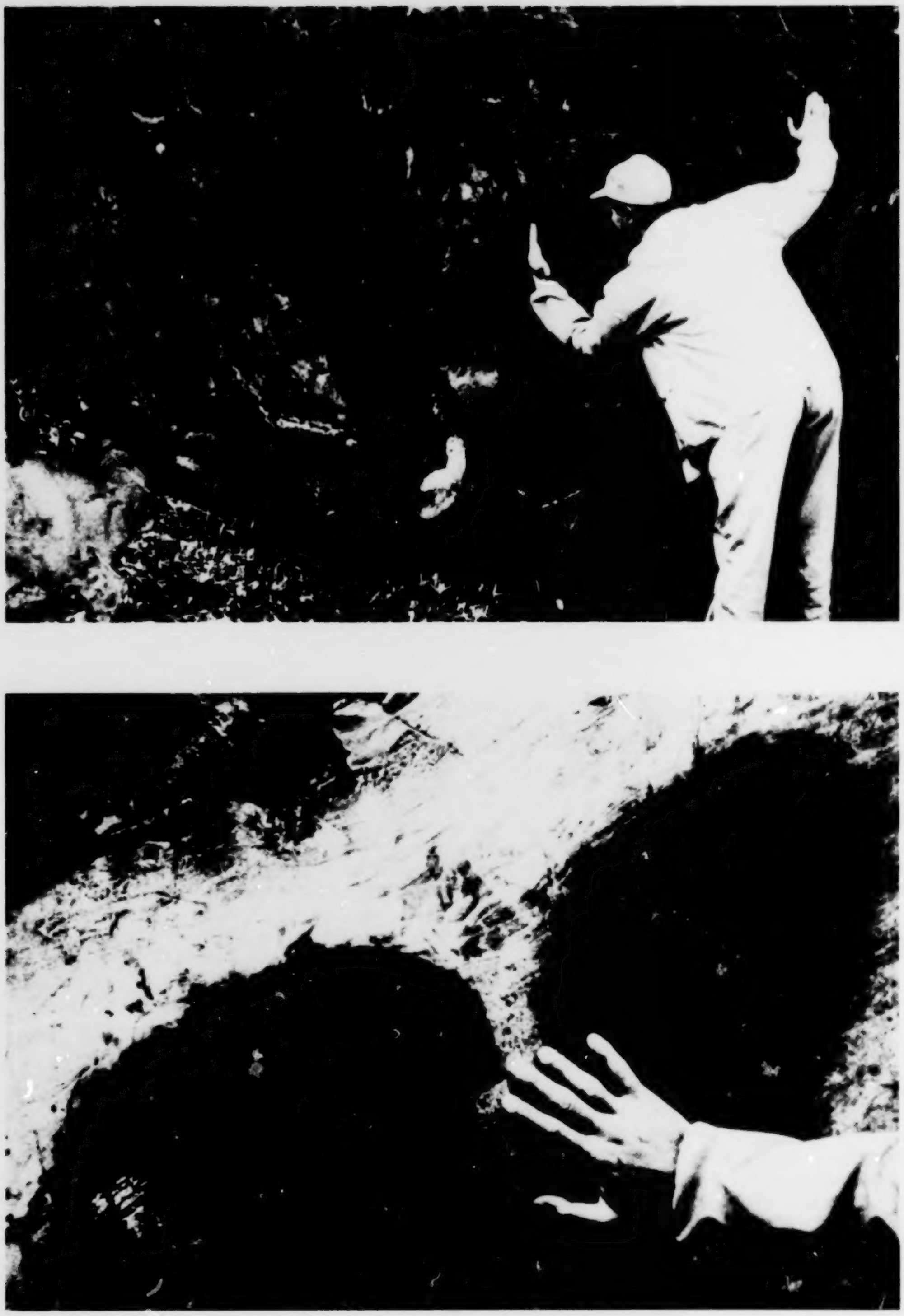

Photo 275.2. *Small road cut near Chelmsford in which the orientation of deformed concretions varies between wacke (a) and siltstone (b) beds. This suggests that the undeformed concretions in siltstone were markedly elongated parallel to bedding.*

CONCLUSIONS

The beds of the Chelmsford Formation (exposed core of the Sudbury Structure) comprise a northeast-trending system of buckle folds which has been mapped in detail and will be used, together with various other strain gauges, to estimate the original diameter ratio of the undeformed Sudbury Basin. The fold pattern can be explained fully by northwest-southeast compression, possibly associated with the northwest-directed ductile shear of the southern granophyre segment and reverse faulting south of the Sudbury Structure.

ACKNOWLEDGMENTS

The authors would like to thank Burkhard O. Dressler (Geologist, Precambrian Geology Section, Ontario Geological Survey, Toronto), for guidance in the field and P.-Y.F. Robin (Professor, Department of Geology, University of Toronto) for helpful advice in matters of strain analysis.

REFERENCES

Berthé, D., Choukroune, P., and Jegouzo, P.
1979: Orthogneiss, Mylonite and Non-coaxial Deformation of Granites; Journal of Structural Geology, Volume 1, p.31-42.

Brocoum, S.J., and Dalziel, W.D.
1974: The Sudbury Basin, the Southern Province, the Grenville Front, and the Penokean Orogeny; Geological Society of America Bulletin, Volume 85, p.1571-1580.

Card, K.D., and Hutchinson, R.W.
1972: The Sudbury Structure: Its Regional Geological Setting; p.67-78 *in* New Developments in Sudbury Geology, edited by J.V. Guy-Bray, Geological Association of Canada, Special Paper 10.

Clendenden, W.S.
1986: Finite Strain Study of the Sudbury Basin; Unpublished M.Sc. Thesis, Department of Geological Sciences, University of Colorado, Boulder, Colorado.

Cobbold, P.R., and Percevault, M-N.
1983: Spatial Integration of Strains Using Finite Elements; Journal of Structural Geology, Volume 5, p.299-305.

Coward, M.P.
1984: Major Shear Zones in the Precambrian Crust; Examples from NW Scotland and Southern Africa and Their Significance; p.207-236 *in* Precambrian Tectonics Illustrated, edited by A. Kröner and R. Greiling, E. Schweizerbartsche Verlagsbuchhandlung (Nägele und Obermiller), Stuttgart.

Crespi, J.M.
1986: Some Guidelines for the Practical Application of Fry's Method of Strain Analysis; Journal of Structural Geology, Volume 8, p.799-808.

Dressler, B.O.
1984a: General Geology of the Sudbury Area; p.57-82 *in* The Geology and Ore Deposits of the Sudbury Structure, edited by E.G. Pye, A.J. Naldrett, and P.E. Giblin, Ontario Geological Survey, Special Volume 1, 603p. Accompanied by Map 2491, scale 1:50 000, Map NL-16/17, scale 1:1 000 000, and 3 charts.
1984b: The Effects of the Sudbury Event and the Intrusion of the Sudbury Igneous Complex on the Footwall of the Sudbury Structure; p.97-136 *in* The Geology and Ore Deposits of the Sudbury Structure, edited by E.G. Pye, A.J. Naldrett, and P.E. Giblin; Ontario Geological Survey, Special Volume 1, 603p. Accompanied by Map 2491, scale 1:50 000, Map NL-16/17, scale 1:1 000 000, and 3 charts.

Fry, N.
1979: Random Point Distribution and Strain Measurement in Rocks; Tectonophysics, Volume 60, p.89-105.

Morris, W.A.
1984: Paleomagnetic Constraints on the Magmatic, Tectonic, and Metamorphic History of the Sudbury Basin Region; p.411-427 *in* The Geology and Ore Deposits of the Sudbury Structure, edited by E.G. Pye, A.J. Naldrett, and P.E. Giblin; Ontario Geological Survey, Special Volume 1, 603p. Accompanied by Map 2491, scale 1:50 000, Map NL-16/17, scale 1:1 000 000, and 3 charts.

Muir, T.L., and Peredery, W.V.
1984: The Onaping Formation; p.139-210 *in* The Geology and Ore Deposits of the Sudbury Structure, edited by E.G. Pye, A.J. Naldrett, and P.E. Giblin, Ontario Geological Survey, Special Volume 1, 603p. Accompanied by Map 2491, scale 1:50 000, Map NL-16/17, scale 1:1 000 000, and 3 charts.

Naldrett, A.J.
1984: Summary, Discussion, and Synthesis; p.533-569 *in* The Geology and Ore Deposits of the Sudbury Structure, edited by E.G. Pye, A.J. Naldrett, and P.E. Giblin, Ontario Geological Survey, Special Volume 1, 603p. Accompanied by Map 2491, scale 1:50 000, Map NL-16/17, scale 1:1 000 000, and 3 charts.

Ragan, D.M.
1985: Structural Geology: An Introduction to Geometrical Techniques; 3rd Edition, Wiley and Sons, New York, N.Y.

Ramsay, J.G.
1967: Folding and Fracturing of Rocks; McGraw-Hill Book Company, New York, N.Y.

Robin, P.-Y.,F.
1977: Determination of Geologic Strain Using Randomly Oriented Strain Markers of any Shape; Tectonophysics, Volume 42, p.T7-T16.

Robin, P.-Y.,F., and Jowett, E.C.
1986: Computerized Density Contouring and Statistical Evaluation of Orientation Data Using Counting Circles and Continuous Weighting Functions; Tectonophysics, Volume 121, p.207-223.

Rouseli, D.H.
1972: The Chelmsford Formation of the Sudbury Basin —a Precambrian Turbidite; p.79-91 *in* New Developments in Sudbury Geology, edited by J.V. Guy-Bray, Geological Association of Canada, Special Paper 10.
1975: The Origin of Foliation and Lineation in the Onaping Formation and the Deformation of the Sudbury Basin; Canadian Journal of Earth Sciences, Volume 12, p.1379-1395.
1984: Structural Geology of the Sudbury Basin; p.83-75 *in* The Geology and Ore Deposits of the Sudbury Structure, edited by E.G. Pye; A.J. Naldrett and P.E. Giblin, Ontario Geological Survey, Special Volume 1, 603p. Accompanied by Map 2491, scale 1:50 000, Map NL-16/17, scale 1:1 000 000, and 3 charts.

Schwerdtner, W.M.
1977: Geometric Interpretation of Regional Strain Analyses; Tectonophysics, Volume 39, p.515-531.
1985: Preliminary Estimates of the Amount of Continuous Horizontal Shortening Across an Archean Greenstone Belt; Canadian Journal of Earth Sciences, Volume 22, p.506-513.

Schultz-Ela, D.D.
1987: Strain Modification Along the Northern Boundary of the Vermilion District, Minnesota; p.243 *in* Abstracts with Programs 1987, 21st Annual Meeting of the North-Central Section of the Geological Society of America.

Shanks, W.S.
1987: Deformation of the Sudbury Structure, a Ph.D. Topic Proposal; Unpublished manuscript, Department of Geology, University of Toronto, Toronto.

Stevenson, J.S.
1972: The Onaping Ash-Flow Sheet, Sudbury, Ontario; p.41-48 *in* New Developments in Sudbury Geology, edited by J.V. Guy-Bray, Geological Association of Canada, Special Paper 10.
1984: Sudbury Problems and Suggestions for Further Research; p.523-531 *in* The Geology and Ore Deposits of the Sudbury Structure, edited by E.G. Pye, A.J. Naldrett and P.E. Giblin, Ontario Geological Survey, Special Volume 1, 603p. Accompanied by Map 2491, scale 1:50 000, Map NL-16/17, scale 1:1 000 000, and 3 charts.

Suppe, J.
1985: Principles of Structural Geology; Prentice-Hall, Englewood Cliffs, New Jersey.

Grant 276 Platinum Group Element Abundances in Mafic and Ultramafic Rocks: Preliminary Geochemical Studies at the Lac des Iles Complex, District of Thunder Bay

G.E. Brügmann and A.J. Naldrett

Department of Geology, University of Toronto

ABSTRACT

The Lac des Iles Complex consists of several mafic and ultramafic intrusions which contain economically interesting platinum group element- (PGE-) bearing Ni-Cu sulphide mineralization. The different plutonic centres have been studied using geochemical and isotopic methods to constrain their petrogenesis. Platinum group element abundances are used to develop concepts explaining the origin of the sulphide mineralization.

Sm-Nd isotope analysis of whole rock and mineral separate samples from the southern ultramafic centre lie on a $^{143}Nd/^{144}Nd$ versus $^{147}Sm/^{144}Nd$ isochron with an age of 2736±28 Ma and an initial $^{143}Nd/^{144}Nd$ of 0.509150±30 ($E_{Nd}=+1.2$). This age is interpreted to be the time of intrusion of the ultramafic complex. The southern ultramafic centre consists of a wehrlite core which is surrounded by websterite and gabbronorite cumulates. Major and trace element variations reflect the zoning of the complex, in that MgO, Cr, and Ni contents decrease, and Al_2O_3, Na_2O, TiO_2, Zr, Y, and rare earth element (REE) contents increase from the core to the margin.

Based on petrographic and geochemical studies, the northern ultramafic centre can be subdivided into at least four cyclic units which ideally consist of dunite to wehrlite cumulate at the base, followed by clinopyroxenite and websterite, locally grading into gabbronorite. This indicates similar crystallization sequences in both ultramafic centres: olivine, olivine+clinopyroxene, clinopyroxene, clinopyroxene+orthopyroxene, and clinopyroxene+orthopyroxene+plagioclase.

The gabbroic complex has been subdivided into eastern and western intrusive phases which consist mainly of gabbro and norite to gabbronorite cumulates, respectively. Latter phases host PGE-bearing mineralization and appear to intrude the gabbroic cumulates. Compared to the western gabbro, the eastern gabbro is depleted in MgO, Cr, and Ni, which implies different parental magma compositions. REE and Nd isotope ratios in noritic to gabbronoritic intrusions of the western gabbro suggest that they are formed from chemically distinguished parental magmas.

Both ultramafic and gabbroic intrusions of the Lac des Iles Complex contain PGE-bearing Ni-Cu sulphide mineralization. However, differences in chalcophile element patterns suggest different ore formation processes. The mineralization of the gabbroic part is characterized by rather constant and very low Ir, but high and variable Au, Pd, and Pt abundances. The association with pegmatitic gabbro and the high Pd/Ir ratios in the order of 10 000 imply a late stage magmatic origin. Sulphide saturation was probably caused by the mixing of gabbronoritic magma with silica and volatile-rich components. Sulphides in the ultramafic part display chalcophile element patterns typical of deposits associated with mafic and ultramafic volcanic rocks. They are depleted in Ir, Os, Ni, and Co relative to Au, Pd, and Pt. Pd/Ir ratios vary between 10 and 30. Mineralization occurs in cumulates of websteritic to gabbronoritic compositions at the base of harzburgitic to lherzolitic rocks. This might represent a zone of mixing of fractionated residual liquid with fresh pulses of more primitive magma which caused sulphide liquation.

INTRODUCTION

This research project is primarily concerned with the problem of understanding the behaviour of platinum group elements (PGE) during formation and fractional crystallization of mantle magmas and the origin of PGE mineralization. The study area is located on the Lac des Iles Complex, approximately 80 km northwest of Thunder Bay (Figure 276.1). During the first year of the project, the main emphasis was given to the major and trace element characteristics of the different rock suites and to the noble metal distribution. This work is the basis of future detailed studies of noble metal variations in whole rocks and mineral separates in order to describe the precious metal distribution more quantitatively.

GEOLOGICAL BACKGROUND

The Lac des Iles Complex lies within the Wabigoon Subprovince and has recently been mapped by Sutcliffe (1986). The Complex consists of several mafic intrusions which intrude gneissic tonalites of Archean age. The mafic intrusions display a circular configuration, the centre of which is composed of hornblende tonalite and biotite granodiorite rocks which were emplaced shortly after or contemporaneously to the mafic plutons. The Lac des Iles Complex is the largest of the mafic bodies and has been mapped by Pye (1968) and Sutcliffe and Sweeny (1985, 1986). These authors distinguished an ultramafic part located around the Lac des Iles and a gabbroic part to the south of it (Figure 276.1). Absolute ages are not known and age relationships between the different intrusive phases are not well constrained.

Macdonald (1985) and Sweeny and Sutcliffe (1986) mapped part of the gabbroic intrusion in detail. Previous studies concentrated on several occurrences of PGE-bearing sulphide mineralization, especially the Roby Zone (Dunning 1979; Watkinson and Dunning 1979; Talkington and Watkinson 1984). Based on mineralogical and chemical differences, Dunning (1979) distinguished between two intrusive

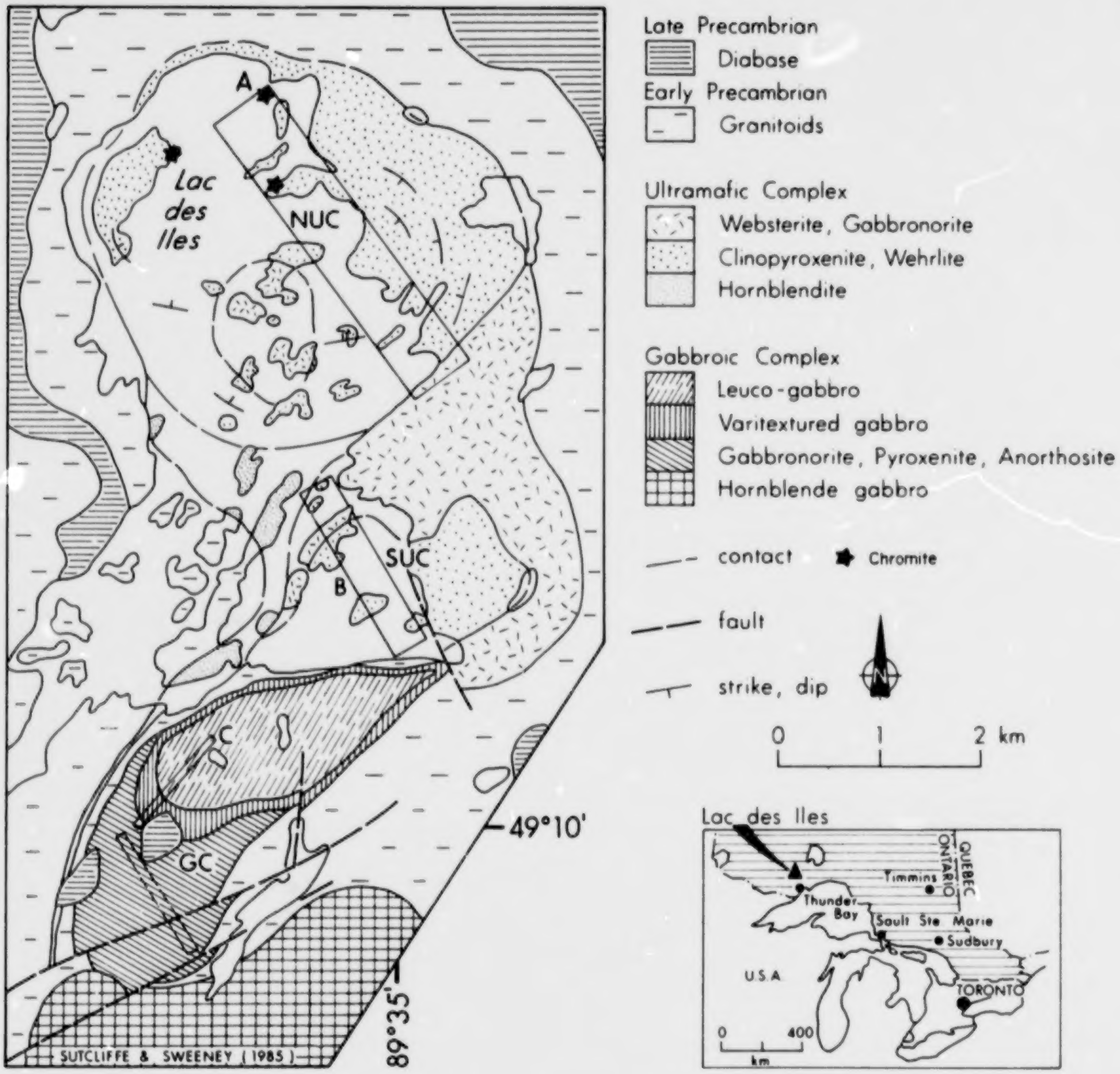

Figure 276.1. Location and geology of the Lac des Iles Complex (modified after Sutcliffe and Sweeny (1985)) and location of sample traverses. A,B,C. NUC: Northern Ultramafic Complex; SUC: Southern Ultramafic Complex; GC: Gabbroic Complex.

phases, a gabbroic eastern gabbro (plagioclase-clinopyroxene cumulates), and a noritic to gabbronoritic western gabbro (orthopyroxene-clinopyroxene±plagioclase cumulates). Primary mineralogy is rarely preserved; alteration to saussurite and uralite is dominant. The interface between the eastern and western gabbro is very complex and heterogeneous on a centimetre and metre scale. The interface consists of melanocratic to leucocratic and coarse-grained to pegmatitic gabbro and gabbro breccia, and is intruded by dikes consisting of websterite to gabbronorite and tonalite. This zone is interpreted to be the result of the magmas which gave rise to the eastern and western gabbro mixing together (Sweeny and Sutcliffe 1986). This zone hosts the major PGE mineralization of the Roby Zone. The economically most important ore metals are Pd, Pt, and Au. Based on their abundances and the lithological association of the mineralization, Macdonald *et al.* (1987) distinguished three categories of mineralization:

1. low grade mineralization (less than 1000 ppb PGE+Au) occurring in pegmatoidal gabbro, leucocratic gabbro, and gabbro breccia
2. mineralization with up to 15 ppm PGE+Au associated with an intrusive websteritic-gabbronoritic dike
3. high grade mineralization (up to 35 ppm PGE+Au) in gabbro pegmatite dikes

Macdonald *et al.* (1987) suggested that mineralization resulted from the mixing of gabbro and tonalite and that the degree of noble metal enrichment in pegmatite gabbro reflects increasing fractionation of a late stage magmatic phase.

The ultramafic centres at Lac des Iles also contain PGE-bearing sulphide mineralization, but so far they are of minor economical interest. The southern ultramafic complex consists of a wehrlite core, surrounded by websterite, which grades into gabbronorite (Figure 276.1). The northern ultramafic complex is built up of several cycles of dunite, wehrlite, clinopyroxenite, websterite, and gabbronorite. Due to lack of outcrop, single units can often only be traced for tens or even fewer than tens of metres, and the generally massive structure of the rocks also complicates the interpretation of geometrical relationships between different units and of the whole complex. These rocks represent meso- to adcumulates, and suggest a crystallization sequence of olivine, olivine-clinopyroxene, clinopyroxene, clinopyroxene-orthopyroxene, and finally clinopyroxene-orthopyroxene-plagioclase (Sutcliffe and Sweeny 1985). Olivine is generally completely altered to serpentine and magnetite; occasionally, fresh olivine cores can be observed in thin sections of wehrlites and clinopyroxenites. Pyroxenes and plagioclase are fresh to moderately altered.

SAMPLES AND ANALYTICAL TECHNIQUES

SAMPLES

Field work in 1986 concentrated on rock sampling and examining detailed geological relationships in the gabbroic and ultramafic complexes. Rock samples were collected along sections which represent the lithological sequence in the different intrusions. Locations of traverses are indicated in Figure 276.1. Lithological sequences and sample points are shown in the geological profiles of Figures 276.2, 276.3, and 276.9.

ANALYTICAL METHODS

Major element chemistry of the rock samples has been determined by conventional X-ray fluorescence analysis (XRF) on glass pellets. Trace element determinations such as Ni, Cr, V, Zr, Y, Rb, and Sr were performed by XRF using powder pellets. REE and Sc have been determined by instrumental neutron activation analysis (INAA). The noble metals Au, Pd, Pt, Ir, and Os were analyzed by means of radiochemical neutron activation analysis as described by Brügmann (1985) and Brügmann *et al.* (in press). Samples have been irradiated at the Slowpoke reactor, University of Toronto, for 16 hours in a thermal neutron flux of $2 \cdot 10^{11}$ ns^{-1}cm^{-2}, or at the reactor of the McMaster University, Hamilton, for 72 hours in a flux of $3 \cdot 10^{13}$ ns^{-1}cm^{-2}. Furthermore, preliminary Sm-Nd isotopic data have been obtained for whole rocks and mineral separates. They have been determined at the Max-Planck-Institut für Chemie, Mainz, F.R.G. The accuracy of the XRF analyses are estimated to be better than 5%, except trace elements analyses of Rb, Zr, and Y, in the concentration range of 2 to 10 ppm, for which the accuracy is between 10 and 30%. The accuracy of REE analyses are generally better than 30%, Sc determination is better than 5%. Data quality of the noble metal analyses depends on thermal neutron flux; however, precision for Au and Ir is better than 10%, for Pd, it is better than 20%, and for Pt and Os, it is better than 30%. Accuracy is similar to previous estimates of Brügmann *et al.* (in press), within 10% for all elements.

RESULTS AND DISCUSSION

The results of major and trace element determinations are summarized in Table 276.1. Major and trace element variations along the sample traverses of the gabbroic and ultramafic intrusions are shown in Figures 276.2, 276.3, and 276.9. Rocks are named after the classification of Streckeisen (1979), based on their normative mineralogy.

GEOCHEMISTRY OF THE ULTRAMAFIC INTRUSIONS

Figures 276.2 and 276.3 show lithological profiles and major and trace element variations along the sampling sections in the northern and southern ultramafic intrusions. The following description of the lithological sequences is based on observations in thin sections and calculations of the normative mineralogy.

The southern centre is built up of a wehrlite core which gradually grades into olivine-clinopyroxenite. This is surrounded by websterite grading into gabbronorite. This implies a crystallization sequence of: olivine-clinopyroxene, clinopyroxene-orthopyroxene, clinopyroxene-orthopyroxene-plagioclase. Major and trace element variations nicely reflect this change from ultramafic to mafic compositions (Figure 276.2). Thus, MgO, Ni, and Cr contents systematically decrease from the core to the margin of the intrusion, whereas Al and Sr contents increase, indicating the crystallization of plagioclase. At the same time, concentrations of the incompatible elements Na, Ti, Y, Zr, and REE increase, as well as element ratios like Zr/Ti and Zr/Y. This probably reflects the increasing amount of interstitial liquid and the change from adcumulate to mesocumulate/orthocumulate textures.

Based on lithological repetitions and chemical variations, the northern ultramafic centre can be subdivided into at least four cycles which are interpreted as either individual intrusions or several inputs of new primitive magma batches into the magma chamber (Figure 276.3). Due to lack of outcrop, the relative position of the central part of the profile in Figure 276.3 is not well defined; it may either represent another cycle (or even several cycles) or the extension of cycle 1 to 3, to give the intrusion a circular shape. Ideally, a cycle consists of a dunite base grading into wehrlite and clinopyroxenite. This is overlain by websterite, which locally grades into gabbronorite. This lithological sequence is very similar to that of the southern ultramafic centre indicating a similar crystallization order.

The northern part of the northern ultramafic complex (cycle 4 of the profile in Figure 276.3) appears to be a separate intrusion. It consists of a websterite core surrounded by clinopyroxenite and olivine clinopyroxenite. Within the olivine clinopyroxenite, a thin,

TABLE 276.1. MAJOR AND TRACE ELEMENT DATA FOR SAMPLES FROM THE LAC DES ILES COMPLEX. MAJOR ELEMENTS ARE RECALCULATED TO 100% ANHYDROUS; FeO*=total FeO.

	LDI-01	LDI-02	LDI-03	LDI-04	LDI-05	LDI-06	LDI-07	LDI-08	LDI-09	LDI-10
SiO_2	51.98	52.29	51.07	50.96	51.32	51.03	50.91	50.53	52.24	50.54
TiO_2	0.20	0.14	0.09	0.18	0.13	0.27	0.30	0.19	0.14	0.19
Al_2O_3	14.33	8.47	18.62	17.33	21.10	14.46	13.40	25.08	17.14	24.6
FeO*	10.92	10.72	6.73	6.40	6.47	9.17	9.74	4.94	8.54	5.18
MnO	0.21	0.22	0.12	0.13	0.11	0.16	0.19	0.07	0.16	0.08
MgO	12.34	20.66	10.82	10.06	6.12	9.37	10.11	4.37	8.45	4.54
CaO	8.09	6.66	10.50	12.89	11.58	13.65	13.50	11.56	10.67	2.75
Na_2O	1.46	0.64	1.63	1.66	2.84	1.76	1.61	2.93	2.43	0.26
K_2O	0.45	0.19	0.41	0.37	0.31	0.11	0.23	0.32	0.22	0.26
P_2O_5	0.02	0.01	0.01	0.02	0.02	0.02	0.01	0.03	0.01	0.02
Cr	425	627	205	137	64	38	40	121	100	97
Ni	339	1049	499	321	123	81	89	131	68	117
Co	67	86	46	45	48	67	65	33	37	28
V	163	147	89	170	120	305	331	106	125	113
Rb	17	4	13	11	7	0	3	8	4	5
Sr	182	43	192	185	293	170	172	357	138	309
Zr	9	4	5	11	6	9	9	14	3	10
Y	3	0	2	5	2	4	5	2	5	3
Sc	34	41	24	44	35	74	68	16	31	16

	LDI-11	LDI-12	LDI-13	LDI-14	LDI-15	LDI-16	LDI-17	LDI-18	LDI-19	LDI-20
SiO_2	51.98	49.00	48.37	49.16	50.88	50.65	45.71	49.22	50.95	50.55
TiO_2	0.15	0.16	0.18	0.21	0.26	0.34	0.13	0.31	0.22	0.25
Al_2O_3	1.72	1.69	2.26	6.09	2.78	13.65	1.73	5.26	15.64	11.74
FeO*	6.56	9.60	12.04	11.30	13.59	6.70	13.10	11.10	6.76	9.17
MnO	0.18	0.18	0.22	0.21	0.27	0.14	0.24	0.22	0.15	0.2
MgO	20.92	26.41	28.08	21.86	25.23	12.54	30.92	19.58	10.39	14.93
CaO	18.17	12.66	8.57	10.56	6.70	14.66	8.02	13.68	13.69	11.94
Na_2O	0.29	0.25	0.22	0.51	0.24	1.12	0.19	0.51	1.61	1
K_2O	0.02	0.03	0.04	0.08	0.03	0.18	0.02	0.10	0.57	0.2
P_2O_5	0.01	0.01	0.02	0.02	0.02	0.02	0.02	0.02	0.02	0.02
Cr	3783	3564	4415	2660	3644	375	4032	1907	987	1068
Ni	454	803	986	763	784	262	1001	566	314	258
Co	60	0	0	77	0	0	0	0	51	62
V	136	136	154	177	188	188	128	206	170	170
Rb	0	0	0	0	0	0	0	0	8	2
Sr	32	20	20	116	22	390	17	96	319	292
Zr	3	5	6	8	9	16	5	15	10	11
Y	4	5	6	6	6	9	4	8	5	6
Sc	69	0	0	43	0	0	0	0	45	55

TABLE 276.1. cont'd.

	LDI-21	LDI-22	LDI-23	LDI-24	LDI-25	LDI-26	LDI-27	LDI-28	LDI-29	LDI-30
SiO_2	49.68	42.73	46.81	53.46	51.23	53.08	52.74	51.59	53.62	51.85
TiO_2	0.21	0.08	0.17	0.25	0.22	0.27	0.27	0.16	0.14	0.1
Al_2O_3	8.71	1.09	1.79	2.99	2.33	3.17	2.63	11.60	1.64	1.2
FeO*	9.17	12.29	11.97	6.09	9.24	5.95	6.38	7.71	5.36	5.68
MnO	0.19	0.19	0.16	0.14	0.20	0.16	0.16	0.20	0.17	0.17
MgO	18.66	43.32	33.07	20.71	25.67	20.30	19.75	16.09	20.31	23.36
CaO	12.47	0.20	5.85	16.01	10.88	16.76	17.68	10.65	18.46	17.39
Na_2O	0.65	0.06	0.15	0.31	0.20	0.28	0.35	0.63	0.27	0.23
K_2O	0.24	0.01	0.02	0.03	0.02	0.02	0.03	1.36	0.02	0.01
P_2O_5	0.02	0.02	0.01	0.01	0.01	0.01	0.01	0.01	0.01	0.01
Cr	1562	8662	5387	3393	3968	3285	2820	771	3409	2608
Ni	801	1403	1219	439	621	445	394	251	337	302
Co	0	109	83	0	66	0	50	52	46	0
V	158	76	131	226	175	221	214	151	129	113
Rb	3	0	0	0	0	24	0	24	0	0
Sr	172	2	16	26	18	24	28	179	29	25
Zr	10	2	6	10	6	8	10	6	4	4
Y	6	0	5	9	6	9	9	3	4	4
Sc	0	11	31	0	54	0	80	47	55	0
	LDI-31	**LDI-32**	**LDI-33**	**LDI-34**	**LDI-35**	**LDI-36**	**LDI-37**	**LDI-38**	**LDI-39**	**LDI-40**
SiO_2	52.51	52.02	52.34	51.53	45.86	40.63	52.81	53.91	52.78	52.38
TiO_2	0.17	0.23	0.24	0.19	0.07	0.15	0.16	0.15	0.19	0.17
Al_2O_3	1.92	2.53	2.86	9.52	0.53	2.06	2.00	1.64	2.05	1.64
FeO*	5.56	9.27	9.67	8.09	7.95	14.52	5.63	10.05	4.15	5.64
MnO	0.15	0.21	0.23	0.19	0.19	0.27	0.15	0.27	0.13	0.16
MgO	19.31	19.99	20.38	16.09	45.15	40.88	18.83	25.73	20.17	19.85
CaO	20.03	15.50	13.99	13.46	0.11	1.35	19.96	8.04	20.17	19.85
Na_2O	0.32	0.22	0.25	0.72	0.09	0.11	0.39	0.19	0.34	0.28
K_2O	0.02	0.01	0.02	0.20	0.02	0.01	0.06	0.01	0.01	0.01
P_2O_5	0.01	0.01	0.01	0.01	0.02	0.02	0.01	0.01	0.01	0.01
Cr	3170	1631	1270	909	3540	22834	2854	3124	4680	2230
Ni	474	461	326	259	1803	2004	323	418	391	334
Co	0	68	0	58	0	0	0	0	0	0
V	93	239	241	190	43	106	122	131	130	133
Rb	0	0	0	2	0	0	0	0	0	0
Sr	40	16	22	227	3	4	39	13	36	31
Zr	8	6	7	7	0	2	8	3	7	7
Y	5	7	7	6	2	0	6	3	7	5
Sc	0	81	0	60	0	0	0	0	0	0

TABLE 276.1. cont'd.

	LDI-41	LDI-42	LDI-43	LDI-44	LDI-45	LDI-46	LDI-47	LDI-49	LDI-54	LDI-55
SiO_2	52.64	53.52	52.68	53.03	53.89	53.76	53.32	43.75	51.16	52.01
TiO_2	0.22	0.11	0.16	0.17	0.13	0.16	0.17	0.07	0.11	0.29
Al_2O_3	2.35	1.28	2.05	1.69	1.54	2.08	2.45	0.59	19.19	8.5
FeO*	9.20	4.99	6.43	6.79	9.70	10.52	6.29	12.17	5.39	16.37
MnO	0.23	0.16	0.17	0.19	0.26	0.25	0.15	0.19	0.12	0.29
MgO	21.76	20.13	21.86	19.37	25.08	28.09	20.28	42.57	10.52	15.16
CaO	13.34	19.52	16.35	18.45	9.20	4.98	16.88	0.46	11.14	6.67
Na_2O	0.24	0.26	0.27	0.27	0.18	0.14	0.37	0.15	2.04	0.52
K_2O	0.01	0.02	0.02	0.03	0.01	0.01	0.07	0.02	0.31	0.17
P_2O_5	0.01	0.01	0.01	0.01	0.01	0.01	0.02	0.02	0.01	0.02
Cr	3010	2590	11070	1820	1350	10860	3120	1	1	292
Ni	415	330	546	320	592	692	369	0	0	2082
Co	0	0	0	0	0	0	0	0	0	112
V	201	127	149	187	144	143	146	0	0	0
Rb	0	0	0	0	0	9	0	0	10	4
Sr	19	23	25	27	12	8	35	3	205	42
Zr	6	3	5	6	3	0	13	0	10	14
Y	6	4	5	6	3	2	6	0	4	5
Sc	0	0	0	0	0	0	0	0	0	48

	LDI-57	LDI-58	LDI-59	LDI-60	LDI-61	LDI-62	LDI-63	LDI-64	LDI-65
SiO_2	51.58	57.01	52.38	52.03	50.96	52.48	53.65	53.35	52.11
TiO_2	0.16	0.11	0.12	0.08	0.10	0.12	0.15	0.12	0.16
Al_2O_3	17.13	18.55	18.49	20.48	24.65	16.73	17.31	23.22	17.06
FeO*	9.35	7.34	6.42	6.02	3.84	7.09	7.3	4.42	7.59
MnO	0.14	0.13	0.13	0.12	0.07	0.15	0.15	0.08	0.14
MgO	11.42	6.05	8.77	9.04	5.88	10.60	8.39	4.95	8.82
CaO	8.57	6.07	11.09	9.79	11.44	9.33	10.38	8.15	11.72
Na_2O	1.47	4.35	2.35	2.15	2.39	2.31	2.45	4.20	2.12
K_2O	0.16	0.34	0.23	0.27	0.64	1.17	0.19	1.48	0.26
P_2O_5	0.02	0.02	0.02	0.01	0.02	0.02	0.02	0.02	0.02
Rb	4	7	4	6	18	32	3	38	6
Sr	207	480	243	265	306	209	294	414	239
Zr	6	11	10	6	10	9	11	8	10
Y	3	2	3	2	3	4	4	3	4
Sc	0	0	0	0	0	0	0	0	48

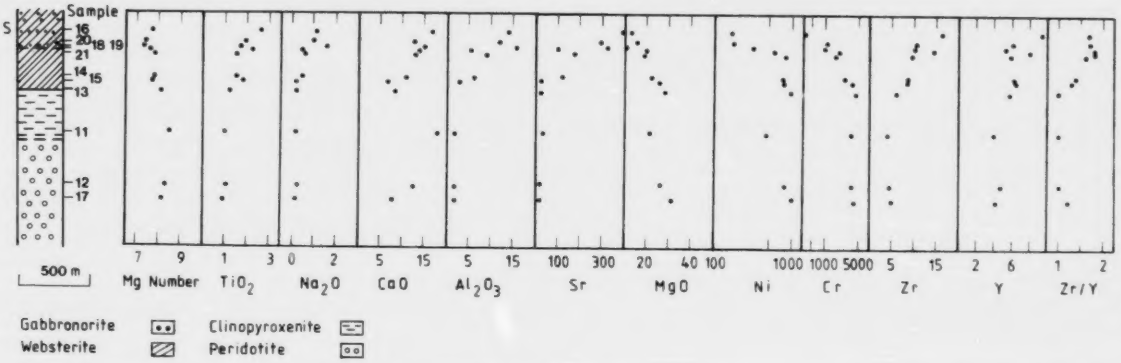

Figure 276.2. *Geological profile and major and trace element variations along sample traverse B of the southern ultramafic intrusion of the Lac des Iles Complex.*

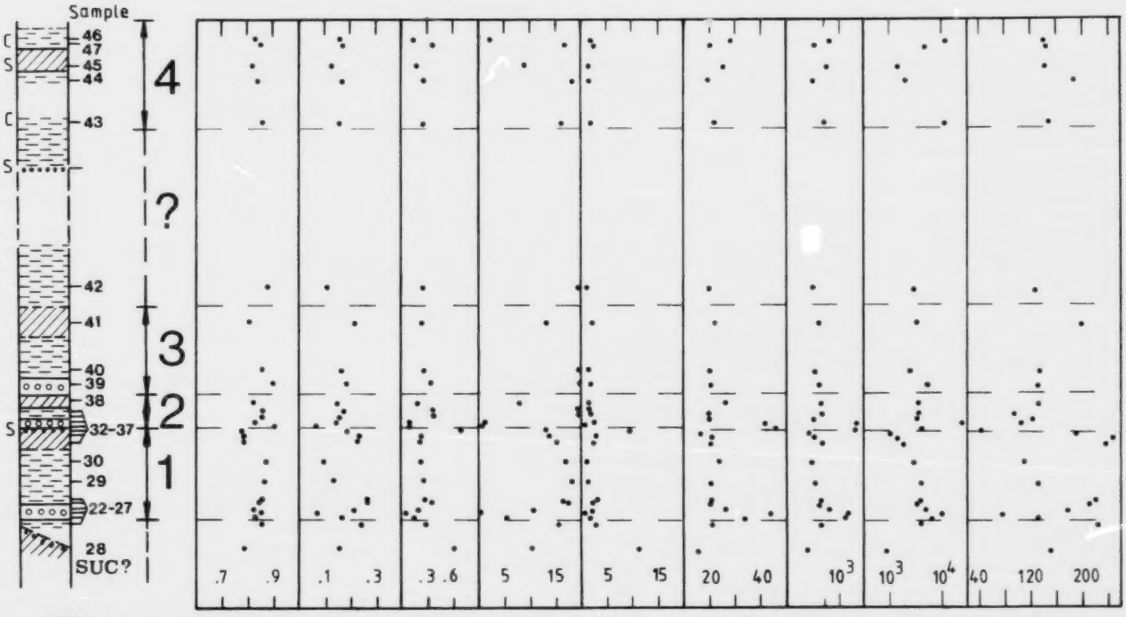

Figure 276.3. *Geological profile and major and trace element variations along sample traverse A of the northern ultramafic intrusion of the Lac des Iles Complex. Symbols as in Figure 276.2.*

less than 1 cm thick chromitite seam has been discovered (sample LDI-43). In this part of the intrusion, previous field parties also discovered thin chromitite seams in olivine clinopyroxenites (Sutcliffe and Sweeny 1986; Linhardt and Sutcliffe 1986). The outcrops of the chromitite seams are indicated in Figure 276.1, and they may define the shape of this separate intrusion.

A few samples from the bases of cycle 1 and 2 have harzburgitic to lherzolitic compositions (samples LDI-22, 23, 35). Thin section examination of these samples revealed that olivine crystals were replaced by orthopyroxene. This implies that olivine was not in equilibrium with its host liquid. However, orthopyroxene is probably not an early liquidus phase of the magma forming the main masses of the two cycles because websterite cumulates appear later in the lithological sequence. Interestingly, lherzolitic and harzburgitic samples overlie gabbronorite, which contains PGE-bearing sulphide mineralization. An interpretation of these observation is discussed below (*see* section on Noble Metal Distribution in the Ultramafic Centres).

Most samples of the northern ultramafic complex have adcumulate textures locally grading to mesocumulates. The very low concentration of in-

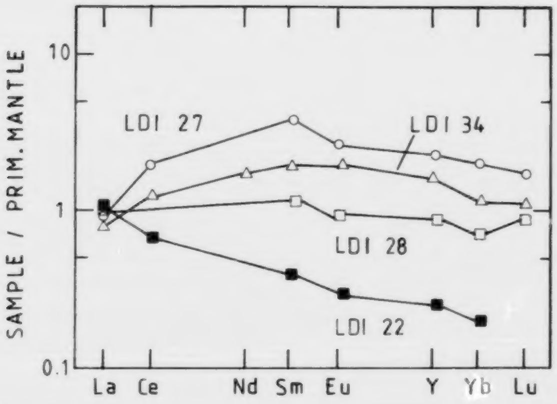

Figure 276.4. REE patterns in samples of the ultramafic part of the Lac des Iles Complex. See Table 276.2 for normalizing values for primitive mantle.

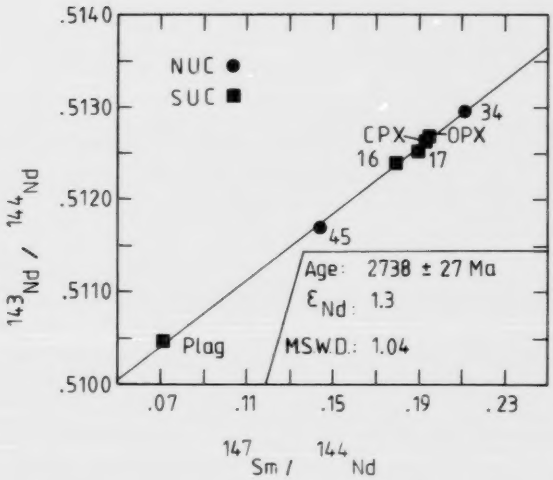

Figure 276.5. Sm-Nd-Isochron diagram of mineral separate and whole rock analyses of samples from ultramafic intrusions of the Lac des Iles Complex; Age calculation is based on data for samples of the southern ultramafic complex.

compatible elements such as Zr, Ti, Y, and REE also indicates that these cumulates contain minor amounts of interstitial liquid. REE data are summarized in Table 276.2. The shape of REE patterns are controlled by the main cumulate mineral phase. Gabbronorite, websterite, wehrlite, and clinopyroxenites display convex patterns and intermediate REE form a pronounced maximum (Figure 276.4). This pattern is typical of clinopyroxene and suggests that clinopyroxene is the main REE carrier. Dunites are light-REE enriched relative to intermediate and heavy REE. Due to the very low REE partition coefficients between olivine and silicate magma, these REE abundances probably reflect the composition of interstitial liquid. This might also represent the REE pattern of the parental magma.

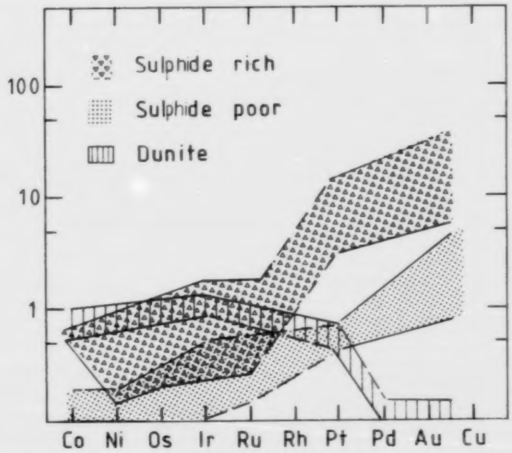

Figure 276.6. Chalcophile element patterns of selected samples from the southern and northern ultramafic centres of the Lac des Iles Complex. See Table 276.4 for normalizing values for primitive mantle. Ni 2110 ppm, Cu 28 ppm.

Sm-Nd-ISOTOPE SYSTEMATICS OF THE ULTRAMAFIC CENTRES

Results of Sm-Nd-isotope analyses are reported in Table 276.3. Samples include whole rocks from different ultramafic and mafic intrusions and mineral separates of sample LDI-16 from the southern ultramafic centre. Figure 276.5 shows an isochron diagram for the ultramafic centres. Whole rock and mineral separate samples from the southern ultramafic complex give an age of 2736±28 Ma. This agrees very well with ages reported from other mafic intrusions of the Wabigoon Province (Morrison *et al.* 1985; Shirley *et al.* 1986) and is interpreted as the time of the intrusion of the southern ultramafic magma. The sample of cycle 1 of the northern ultramafic centre also plots along this isochron, indicating a similar age. However, sample LDI-45 of cycle 4 plots significantly below the regression line. Thus, the parental magma forming this part of the northern ultramafic complex had different Nd isotope characteristics than the southern and the base of the northern ultramafic centres. This supports the previous suggestion that cycle 4 represents a separate intrusive phase. E_{Nd}(T) values for the southern centre and cycle 1 of the northern centre are about 1 to 1.4 and indicate that the source of the parental magmas was time-averaged depleted in light REE relative to CHUR for the Archean mantle. However, if we look at all Nd isotope data, E_{Nd}(T) values vary significantly between 0 and 2. Based on an extended database, including granitoidal samples, Brügmann *et al.* (in preparation) conclude that these variations are likely due to to assimilation of older continental crust. The alternative explanation is that the mantle source of the parental

TABLE 276.2. REE CONTENTS OF MAFIC AND ULTRAMAFIC ROCKS FROM THE LAC DES ILES COMPLEX.

	La	Ce	Nd	Sm	Eu	Yb	Lu
LDI-01	1.05	1.9	1.2	0.28	0.19	0.32	0.04
LDI-02	0.36			0.18	0.05	0.41	0.06
LDI-03	0.74		0.89	0.2	0.11	0.24	0.05
LDI-04	0.8	2.2		0.32	0.12	0.34	0.06
LDI-05	0.9	2.1		0.27	0.14	0.28	0.03
LDI-06	0.75	1.9	1.5	0.47	0.16	0.59	0.07
LDI-07	0.6			0.47	0.16	0.55	0.09
LDI-08	2	4.2	1.9	0.31	0.34	0.18	0.02
LDI-09	0.21			0.16	0.11	0.38	0.05
LDI-10	1.27			0.3	0.25	0.17	0.04
LDI-11	1			0.7	0.16	0.4	0.07
LDI-14	0.5	2.7		0.7	0.19	0.5	0.07
LDI-19	0.7	2.9		0.74	0.2	0.62	0.1
LDI-20	1.1	3		1.02	0.23	0.55	0.11
LDI-22	0.59	1.1		0.15	0.04	0.07	
LDI-23	0.44			0.64	0.11	0.41	0.07
LDI-25	0.3	1.9		0.76	0.17	0.5	0.06
LDI-27	0.57	3.1		1.48	0.39	0.85	0.12
LDI-28	0.62			0.46	0.14	0.3	0.06
LDI-29	0.66	2.6	2	0.75	0.17	0.32	0.05
LDI-32	0.4	1.54	2.8	1.05	0.22	0.6	0.1
LDI-34	0.53	2.1	2.2	0.77	0.3	0.49	0.08
LDI-55	1.19		1.89	0.52	0.19	0.63	0.11
LDI-65	0.98			0.38	0.19	0.48	0.07
Prim. Mantle	0.64	1.66	1.23	0.4	0.15	0.42	0.07

liquids forming the various Lac des Iles intrusions was heterogeneous on a very small scale.

NOBLE METAL DISTRIBUTION IN THE ULTRAMAFIC CENTRES

Occurrences of PGE-bearing Ni-Cu sulphides in the ultramafic complex have previously been reported by Sutcliffe (1986) and Linhardt and Sutcliffe (1986). So far, no high grade mineralization comparable to that of the Roby Zone in the gabbroic part of the Lac des Iles Complex has been found. Sulphide mineralization mainly occurs in rocks of websteritic to gabbronoritic composition. Samples studied here contain less than 1% sulphide and the main sulphide minerals are chalcopyrite, pyrrhotite, and pentlandite.

Table 276.4 summarizes PGE concentrations determined in this study. In addition to previous studies, it also provides data for Ir and Os. PGE contents in samples of the ultramafic centres vary by up to two orders of magnitude. Pd/Ir ratios are typical for mafic rocks, ranging from 10 to 30. Samples of the gabbroic part have much higher Pd/Ir ratios (>1000) as well as higher Pt/Ir and Au/Ir ratios. These differences are mainly caused by lower Ir, but higher Pd, Pt, and Au abundances in samples from the gabbroic part and should imply different parental magma compositions, and/or different processes of sulphide liquation and segregation. Figure 276.6 shows chalcophile element patterns of selected samples. Elements are ordered according to increasing incompatibility in silicate liquids and concentrations are normalized to a model primitive mantle composition, represented by spinel lherzolites. Compared to the common practice of chondrite normalization, this method allows direct comparison of highly chalcophile elements (PGE and Au) with less chalcophile elements (Ni, Co, Cu) in mafic and ultramafic rocks. Figure 276.6 shows two different types of PGE patterns. Samples of websterite and gabbronorite composition are similar in that they are enriched in Au, Pd, and Pt relative to Co, Ni, and Ir. Such patterns are typical for sulphide-poor and sulphide-bearing mafic and ultramafic volcanic rocks and are probably caused by fractionation during fractional crystallization and mantle melting. Thus, Co, Ni, and Ir are compatible to mafic minerals such as olivine, and their concentration in magmas decrease with fractional crystallization of such mineral. On the other hand, Au, Pd, Pt, and Cu generally are incompatible to silicate minerals and therefore become enriched during fractionation of silicate melts (Naldrett and Barnes 1986; Brügmann *et al.* in press). Dunite and wehrlite samples display a complementary pattern. They are depleted in Au, Pd, and Pt relative to Ir, Os, Ni, and Co. This is in agreement with our hypothesis, as elements such as Ni, Co and probably Ir (Brügmann *et al.* in press), partition into olivine, whereas Au, Pd and Pt are incompatible. The low abundances of latter metals suggest that there is only a low amount of interstitial liquid left in the cumulates. The patterns also indicate that these dunites and wehrlites contain insignificant amounts of sulphide because magmatic Ni-Cu sulphides are enriched in Au and Pd relative to Ir, Os, Ni, and Co.

In the ultramafic centres, PGE-bearing sulphide mineralization almost exclusively occurs in websterite and gabbronorite and is overlain by peridotites. As already pointed out, these peridotites contain olivine, which is not in equilibrium with its environment, be-

TABLE 276.3. Nd ISOTOPIC DATA FOR SAMPLES FROM THE LAC DES ILES COMPLEX.

Sample		Sm ppm	Nd ppm	^{147}Sm/ ^{144}Nd	^{143}Nd/ ^{144}Nd	2-sigma Error	ENd(T) 2738 Ma
LDI-06	GA.NO	0.472	1.506	0.189649	0.512509	16	-.03
LDI-03	GA.NO	0.197	0.892	0.133566	0.511595	12	1.90
LDI-55	GA.NO	0.516	1.89	0.164619	0.512073	10	0.28
LDI-17	WEHRL	0.565	1.82	0.18816	0.512553	16	1.36
LDI-16	GA.NO	1.37	4.62	0.179624	0.512400	15	1.38
OPX-16	OPX-MI	0.402	1.25	0.194892	0.512676	16	1.39
CPX-16	CPX-MI	3.32	10.35	0.193920	0.512633	18	0.89
PLAG-16	PLAG-M	0.287	2.41	0.071816	0.510446	17	1.23
LDI-34	GA.NO	0.77	2.205	0.211213	0.512955	30	1.08
LDI45	CPX	0.31	1.3	0.143865	0.511705	18	0.41

Abbreviations: GA.NO: Gabbronorite
WEHRL: Wehrlite
OPX-MI: orthopyroxene mineral separate
CPX-MI: clinopyroxene mineral separate
PLAG-Mi: plagioclase mineral separate
CPX: clinopyroxenite.

TABLE 276.4. NOBLE METAL CONTENTS (PPB) IN MAFIC AND ULTRAMAFIC ROCKS OF THE LAC DES ILES COMPLEX.

	Au	Pd	Pt	Ir	Os
LDI- 2	168	2090	620	0.2	
LDI- 4	12.1	110	<50	0.1	
LDI-19	8.7	44	<50	1.9	
LDI-21	16.2	102	40	3.0	
LDI-22	0.1	<3	<30	4.5	
LDI-26	1.0	3	<30	1.0	
LDI-27	8.0	35	40	4.0	
LDI-30	3.0	6	<30	0.8	
LDI-32	13.7	25	45	5.2	
LDI-34	24	80	109	7.0	
LDI-35	0.15		6	3.8	4.1
LDI-36	0.13		4	3.7	3.2
LDi-37	5.4		30	2.5	2.3
LDI-38	6.9		42	1.5	0.9
LDI-39	0.8		4	0.4	0.7
LDI-41	2.6		26	2.0	2.5
LDI-45	13.9	40	64	3.0	
Prim.Mantle	1.0	4	8	3.6	3.3

cause it is replaced by orthopyroxene. One explanation could be that during the intrusion of a new magma pulse into the magma chamber, the new magma mixed partly with the remaining, more fractionated liquid. Olivine, which crystallized in the rather primitive magma, settled to the bottom of the magma chamber into a hybrid magma of more evolved composition. There, it reacted with the melt to form orthopyroxene. Mixing of a mafic magma with a fractionated, silica-rich liquid may also cause sulphide liquation. As pointed out by Irvine (1975) and Naldrett and Macdonald (1980), adding silica to a magma can result in a reduction of the solubility of sulphide liquid. Therefore, it is suggested that sulphide mineralization in websteritic to gabbronoritic rocks of the ultramafic complexes was formed by the mixing of a new input of fresh, more primitive magma with fractioned liquid near the bottom of the magma chamber. Naldrett and Campbell (1979) showed that the PGE content of a sulphide liquid depends on the silicate/sulphide liquid mass ratio, the R-factor. The relatively low PGE concentrations in the sulphide mineralization of the ultramafic part of the Lac des Iles Complex suggest a low R-factor, i.e. sulphide liquid equilibrated with a rather low amount of silicate magma. The mixing of magmas near the bottom of the magma chamber might very well be a local phenomenon. Thus, the low PGE content in sulphide mineralization of the ultramafic centres is consistent with the model.

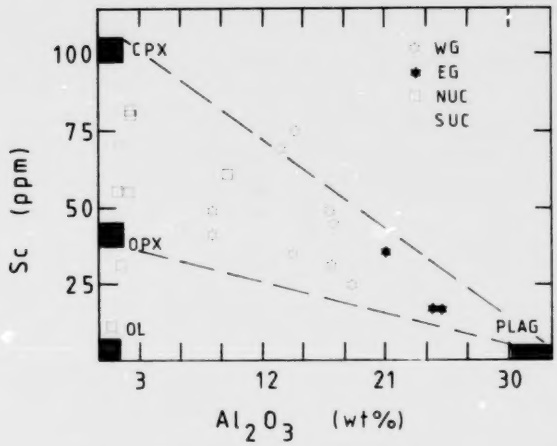

Figure 276.7. *Al_2O_3 versus Sc variation in mafic and ultramafic rocks from the Lac des Iles Complex. Mineral compostion determined by microprobe analyses and neutron activation analyses of mineral separates. EG - eastern gabbro, WG - western gabbro.*

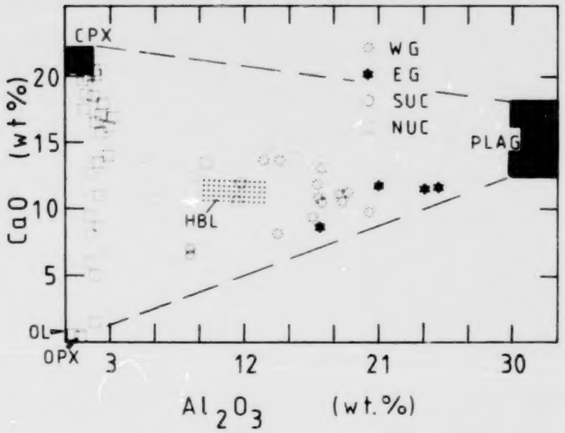

Figure 276.8. *Al_2O_3 versus CaO variation in mafic and ultramafic rocks form the Lac des Iles Complex. Mineral composition determined by microprobe analyses.*

GEOCHEMISTRY OF THE GABBROIC INTRUSION

Most of the samples of the gabbroic part of the Lac des Iles Complex are pervasively altered to uralite and sausserite. Therefore, identification of the primary mineralogy using thin sections and chemical mineral analysis is often impossible. Similarily, calculation of the normative mineral content heavily depends on the assumption that this alteration was isochemical and that redistribution of elements was insignificant. Samples of the eastern gabbro display inconsistencies between normative mineralogies and field descriptions, which could indicate that certain major elements were mobile during alteration. Thus, previous workers describe eastern gabbro rocks as plagioclase-clinopyroxene cumulates, whereas normative mineralogy calculations indicate the presence of significant amounts of orthopyroxene (samples LDI-8, 10, 57). This could imply redistribution of especially SiO_2 and CaO, compounds which are known to be very susceptible to alteration. However, comparison with immobile compounds, such as Al_2O_3 and Sc (the normative calculation of orthopyroxene and clinopyroxene is also independent of these compounds), indicates that this is probably not the explanation. Thus, in Figure 276.7, samples of the eastern gabbro clearly plot in the ternary space of clinopyroxene, plagioclase, and orthopyroxene. The variation of CaO and Al_2O_3 is almost identical (Figure 276.8) as are variations including compounds such as MgO, FeO, Na_2O and Sr (not shown here). Estimates of the amount of plagioclase, orthopyroxene, and clinopyroxene, based on these compounds variations, are in good agreement with the normative calculations. This suggests that during the alteration of the gabbroic complex, major elements did not suffer severe redistribution and that eastern gabbro rocks also contain orthopyroxene. An alternative explanation is that magmatic hornblende was an important crystallizing mineral phase. Thus, in the variation diagram of CaO and Al_2O_3 (Figure 276.8) eastern gabbroic rocks plot close to a mixing line between plagioclase and hornblende. However, so far in the eastern gabbro, magmatic hornblende has not been unambiguously identified. It is a common crystallizing phase in most of the mafic intrusions of the Lac des Iles area (Sutcliffe 1986), and primary hornblende has been observed even in gabbronoritic rocks of the western gabbro and the ultramafic complexes. It is interesting that leucogabbros of the southwestern part of the gabbroic intrusion (samples LDI-60 to 64), which have been described as plagioclase-clinopyroxene cumulates, display similar chemical characteristics as rocks from the eastern gabbro. Intensive microprobe analysis have to be performed to elucidate this problem, which is of major importance for the interpretation of the petrogenesis of the gabbroic complex.

Previous workers subdivided the gabbroic intrusion into an eastern and western gabbro (Dunning 1979; Watkinson and Dunning 1979; Sweeny and Sutcliffe 1986) and interpreted them as separate, not comagmatic, phases. This is based on:

1. mineralogical differences: the eastern gabbro has no orthopyroxene, is oxide-rich (magnetite), and sulphide poor; the western gabbro contains orthopyroxene as a cumulus phase, and is the source of sulphur and the ore metals which give rise to the mineralization in the Roby Zone
2. chemical differences: the eastern gabbro is more fractionated having lower Mg-numbers (MgO/MgO+FeO) and higher Al_2O_3 and CaO contents than the western gabbro

This subdivision represents a simplification of the geology as it is now known. For example, the southwestern part of the western gabbro also contains leucogabbro, which is very similar to eastern gabbro rocks. It also contains magnetite-rich zones (Macdonald 1987; A.J. Macdonald, Geologist, Mineral Deposits Section, Ontario Geological Survey, personal

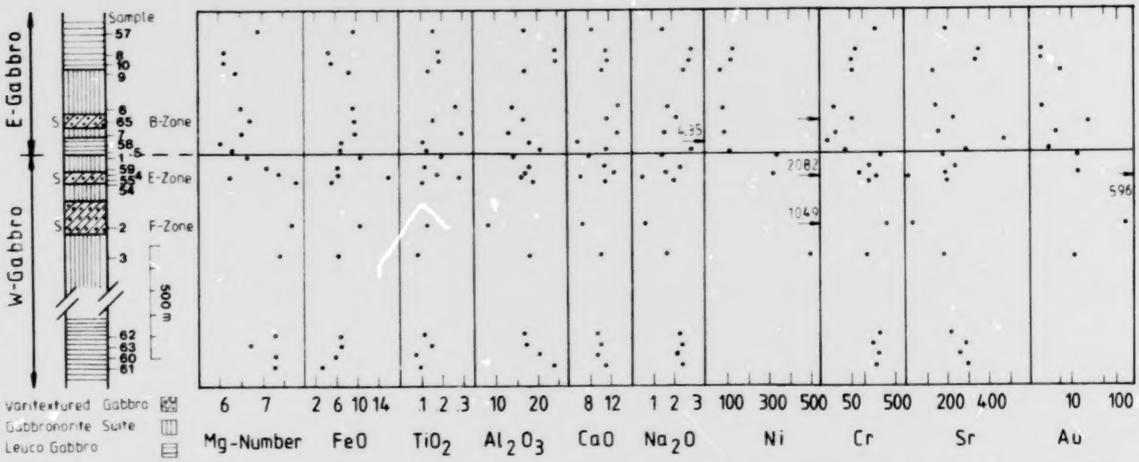

Figure 276.9. Geological profile and major and trace element variations along sample traverse C of the gabbroic intrusion of the Lac des Iles Complex.

communication, 1987). On the other hand, the eastern gabbro contains gabbronoritic rocks (samples LDI-6 7, 9). This zone appears to be intrusive into leucogabbro (Sweeny and Sutcliffe 1986) and also contains sulphide mineralization (B- and H-zone).

Figure 276.9 shows major and trace elements variations along a profile through the gabbroic complex. At the contact of the western to eastern gabbro, MgO/MgO+FeO (Mg#) clearly decreases from about 0.75 to less than 0.65 confirming observations of previous studies. Similarily, concentrations of Ni and Cr decrease (Figure 276.9). The variations of Al, Ca, Na, and Sr do not indicate significant differences between the two gabbroic phases. Incompatible trace elements such as the REE, Rb, and Zr do not show systematic trends either. Their abundances are probably controlled by the amount of interstitial liquid in the cumulates. Surprisingly, gabbronorites of the B- and H-zone in the eastern gabbro also have a lower Mg#, and lower Ni and Cr contents than most rocks of the western gabbro. A gabbronorite dike in the western gabbro (LDI-55) also has a lower Mg#, comparable to those of the eastern gabbro. However, the estimated Mg# of these gabbronorites could be too low as they contain cumulus magnetite (1 to 2%). This is also indicated by high concentrations of Ti, V, Co, and Sc (Figure 276.9 Table 276.1), elements which strongly partition into magnetite. Because the chilled sample LDI-9, which contains no visible magnetite, also has a low Mg#, the influence might be insignificant. The different Mg# and Ni and Cr concentrations of western and eastern gabbro and between gabbronoritic phases suggest that they originated from different parental magma.

REE patterns and preliminary Sm-Nd isotope data also indicate differences in the composition of the parental liquids of websteritic to gabbronoritic cumulates. These samples have variable REE patterns, ranging from flat to light REE enriched (Figure 276.10). Some of the differences in the shape of the REE pattern might be caused by fractionation of clinopyroxene or hornblende. However, gabbronorites with light-REE-enriched and flat REE patterns might have similar low E_{Nd} values of about O, whereas one norite with a light-REE-enriched pattern has a significantly higher E_{Nd} value of about 2 (Figure 267.10; Table 276.3). The variable E_{Nd} value suggests that, during uprise through older continental crust, the parental magma of gabbronorites was contaminated with a crustal component. An alternative interpretation is that the parental liquids of the gabbronoritic phases formed in mantle sources with different REE and isotopic compositions. Leucogabbros of the eastern gabbro are light-REE-enriched and show large positive Eu anomalies, as expected in plagioclase cumulates (Figure 276.10). Leucogabbros of the southwestern part of the western gabbro display similar REE patterns (A.J. Macdonald, geologist, Ontario Geological Survey, personal communication, 1987) and could suggest a common origin with gabbros of the eastern gabbro. The different Mg# in these gabbros do not necessarily imply different sources for the magma, because the Mg# of mafic minerals would

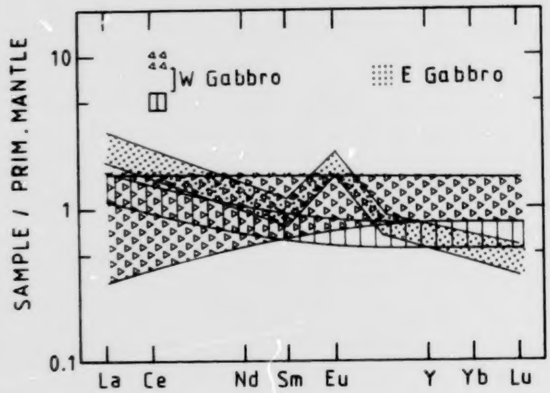

Figure 276.10. REE patterns in samples from the gabbroic part of the Lac des Iles Complex.

change concurrently with progressive fractionation of a silicate liquid. Therefore, Mg# of anorthositic cumulates cumulates would decrease during evolution of the parental melt.

The following tentative model for the genesis of the gabbroic complex, constrained by the geological and geochemical evidence summarized above, is proposed. It suggests the intrusion of a mafic magma, forming the leucogabbro cumulates of the eastern and western gabbro. Shortly after, several geochemically distinguished gabbronorite phases were emplaced. This intrusion sequence appears to be well constrained due to the occurrence of discordant websterite to gabbronorite dikes in leucogabbro. Furthermore, the relatively good preservation of the orthopyroxene-bearing rocks compared to the pervasive altered leucogabbros suggests that they were perhaps emplaced after the alteration of the leucogabbros. However, the occurrence of ductile deformation and mixing phenomena implies that leucogabbro cumulates were not completely solidified at the time of the websterite-gabbronorite intrusion. To explain the severe alteration of the leucogabbro, a volatile rich parental magma is suggested. If this is the case, hornblende was most probably a liquidus phase of the eastern gabbro magma, together with plagioclase and ±clinopyroxene, which would explain the major and trace element characteristics of the leucogabbros. Alternatively, intrusion of volatile-rich phases, such as granite and tonalite, could also explain the alteration.

NOBLE METAL GEOCHEMISTRY OF THE GABBROIC COMPLEX

The PGE deposit at the interface of the western and eastern gabbros (Roby Zone) is one of the most advanced prospects in North America. PGEs occur in sparsely disseminated sulphides (chalcopyrite, pyrrhotite, pentlandite, and pyrite) in pegmatoidal gabbro, pegmatite dikes, anorthositic lenses, websterite-gabbronorite dikes, and magmatic breccias (Macdonald *et al.* 1987). Dunning (1979) and Watkinson and Dunning (1979) describe braggite and vysotskite as the most abundant platinum group minerals (PGM). The high grade mineralized zones appear to be associated with the websteritic-gabbronoritic intrusions.

Figure 276.9 shows the distribution of the chalcophile elements Au and Ni along the profile through the western and eastern gabbros. Compared to the western gabbro, the eastern gabbro has significantly lower Au and Ni contents. One explanation could be that the eastern gabbro is depleted in chalcophile elements due to the segregation of an immiscible sulphide liquid. However, given a sulphide-silicate partition coefficient in the order of 10^4 to 10^5, the Au contents in the eastern gabbro are far to high to be in equilibrium with a sulphide liquid. Furthermore, besides low Ni and Co contents, the eastern gabbro also has low Cr concentrations, an element which usually does not partition into sulphide melts. Therefore, the low abundances of Ni, Co, and Cr in eastern gabbro samples likely reflect their lower content of mafic minerals compared to western gabbro rocks. As sulphide minerals have not been observed in thin sections and sulphur contents of the samples are very low (less than 100 ppm), Au variation in the eastern gabbro is probably controlled by the amount of interstitial liquid.

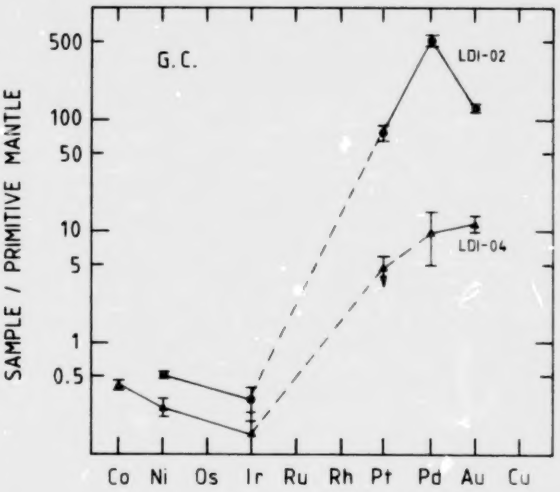

Figure 276.11. *Chalcophile element abundances in selected samples from the gabbroic part of the Lac des Iles Complex.*

Excluding the eastern gabbro implies that the websterite-gabbronorite suite of the western gabbro is the source of the PGEs. The most important mineralization indeed occurs in a discordant, Fe-rich gabbronorite dike (sample LDI-55), which contains about 2% sulphides. Chalcophile element patterns (Figure 276.11) indicate a coherent increase of all chalcophile elements. This probably reflects increasing amounts of sulphide in the samples. Assuming that the sulphide-silicate partition coefficients are similar for all precious metals, then similar concentration variations and constant Pd/Ir ratios are expected. However, whereas Pd, Pt, and Au contents vary by a factor of 50, Ir contents vary only by a factor of 5, which gives rise to variable Pd/Ir ratios. Furthermore, the samples have very high Pd/Ir ratios of more than 1600. Data of Naldrett *et al.* (1980) even indicate ratios in the order of 10 000. These ratios are significantly higher than those observed in magmatic sulphide deposits associated with mafic and ultramafic volcanic rocks (Pd/Ir<300; Naldrett 1981). Such high Pd/Ir ratios have been found only in hydrothermal sulphide deposits, like the Rathbun Lake mineralization in northwestern Ontario (Rowell and Edgar 1986). This implies that either the Lac des Iles mineralization is of hydrothermal origin or that postmagmatic hydrothermal solutions changed the primary noble metal distribution. The occurrence of pegmatitic phases hosting high grade PGE mineralization clearly indicates the importance of late magmatic processes. However, it appears that these pegmatites formed by crystallization of a mafic intercumulus liquid rather than by subsolidus replacement. Field observations show that after the intrusion of the mineralized gabbronoritic dike, pegmatoidal gabbro released fractionated pegmatitic dikes, which eventually crystallized as anorthositic, quartz-bearing veins (Macdonald 1987). During this fractionation, there appears to be a coherent concentration increase of Au, Pd, and Pt with light REE. This suggests that during crystallization of the late magmatic residual liquid, Au, Pd, and Pt behaved incompatibly and eventually formed the high grade ore in pegmatitic dikes. The coherent increase of incompatible elements such as REE in mineralization associated with pegmatite phases, suggests that during extensive fractional crystallization of a late stage, volatile-rich liquid, Au, Pd, and Pt became enriched in the liquid phase, whereas compatible elements, such as Ir, Ni and Co remained in residual minerals. The extreme fractionation eventually caused sulphide saturation and gave rise to the formation of Au, Pd, and Pt-rich, but Ir-, and probably also Os- and Ru-poor, mineralization.

There still remains the problem of what causes sulphide liquation in the gabbronoritic dike of the Roby Zone. The close association of this mineralization with pegmatitic gabbro could imply that mixing of more primitive mafic-ultramafic melts with patches of fractionated, volatile-rich liquids/fluids caused sulphide saturation. The volatile-rich component could be either residual, interstitial liquid of the early leucogabbro cumulates, or could be introduced with tonalite intrusions. The mineralized gabbronorite dike in the Roby Zone contains interstitial magmatic hornblende and has an exceptionally low E_{Nd} value (Table 276.2). This favours the idea that the mixing of mafic-ultramafic magma with crustal components triggered sulphide liquation.

CONCLUSIONS

The Lac des Iles Complex, District of Thunder Bay, consists of several mafic and ultramafic intrusions which contain economically interesting PGE-bearing Ni-Cu sulphide mineralization. The different plutonic centres have been studied using geochemical and isotopic methods to constrain their petrogenesis. Platinum group element abundances are used to develop concepts explaining the origin of the sulphide mineralization.

Previous workers distinguished between a gabbroic complex and an ultramafic complex; the latter can be further subdivided into a northern and southern intrusive body. Sm-Nd isotope analysis of whole rock and mineral separates samples from the southern ultramafic centre lie on a ^{143}Nd/^{144}Nd versus ^{147}Sm/^{144}Nd isochron with an age of 2736±28 Ma and an initial ^{143}Nd/^{144}Nd of 0.509150±30 ($E_{Nd}=+1.2$). This age is interpreted as the time of intrusion of the ultramafic complex. The positive E_{Nd} value indicates a time-averaged depletion in Sm/Nd relative to CHUR for the Archean mantle beneath this area. REE characteristics show that the mafic to ultramafic parental liquids are light-REE-enriched relative to intermediate and heavy REE. This implies that either the magmas assimilated incompatible element-rich continental crust during its uprise, or a "metasomatic" enrichment of the mantle source occurred shortly before magma genesis.

The southern ultramafic centre consists of a wehrlite core which is surrounded by websterite and gabbronorite. All samples represent cumulates with adcumulate to orthocumulate textures. Major and trace element variations reflect the zoning of the complex in that MgO, Cr, and Ni contents decrease, and Al_2O_3, Na_2O, TiO_2, Zr, Y, and REE contents increase from the core to the margin. Based on petrographic and geochemical studies, the northern ultramafic centre can be subdivided into at least four cyclic units which ideally consist of dunite to wehrlite cumulate at the base, followed by clinopyroxenite and websterite, which locally grades into gabbronorite. These cyclic units are interpreted to represent new inputs of fresh, primitive magma. Cycle 4 in the northern part of the ultramafic complex might be a separate intrusive body. The magmatic stratigraphy in both ultramafic centres suggests the following crystallization sequences: olivine, olivine+clinopyroxene, clinopyroxene, clinopyroxene+orthopyroxene, clinopyroxene+orthopyroxene+plagioclase.

The gabbroic complex has been subdivided into eastern and western intrusive phases, which consist of cumulates mainly of gabbroic and noritic to gabbronoritic composition, respectively. The latter phases host PGE-bearing mineralization and appear to intrude the gabbroic cumulates. Compared to the western gabbro, the eastern gabbro appears to be MgO, Cr, Ni, and Co depleted, implying different parental magma compositions. REE and Nd isotope ratios in noritic to gabbronoritic intrusions of the western gabbro also suggest that they formed from chemically distinguished parental magmas.

Both ultramafic and gabbroic intrusions of the Lac des Iles Complex contain PGE-bearing Ni-Cu sulphide mineralization. However, differences in chalcophile element patterns suggest different ore formation processes. The mineralization of the gabbroic part are characterized by rather constant and low Ir, but high and variable Au, Pd, and Pt abundances. The association with pegmatitic gabbro and the high Pd/Ir ratios in the order of 10 000 imply a late stage magmatic origin. A coherent increase of Au, Pd, and Pt concentrations with REE contents suggests that high Au, Pd, and Pt but low Ir, Ni, and Co contents of mineralization in pegmatite gabbro are caused by extensive fractional crystallization, which eventually lead to sulphide saturation. In the Roby Zone, a sulphide saturated, Fe-rich gabbronorite dike hosts the main PGE mineralization. Here, sulphide liquation might be caused by the mixing of gabbronorite with a volatile-rich component, which probably originated from granitic phases. Sulphides in the ultramafic part display chalcophile element patterns typical for deposits associated with mafic and ultramafic volcanic rocks. They are depleted in Ir, Os, Ni, and Co relative to Au, Pd, and Pt; and Pd/Ir ratios vary between 10 and 30. Mineralization occurs in cumulates of websteritic to gabbronoritic compositions at the base of harzburgitic to lherzolitic rocks. This might represent a zone of the mixing of fractionated residual liquid with fresh pulses of more primitive magma, which caused sulphide liquation.

Lithological units and geochemical features observed in the Archean Lac des Iles area are very similar to those found in Phanerozoic complexes in the North American Cordillera. These complexes also show compositional zonation where intrusions of ultramafic to mafic composition are separated by tonalite and granodiorite plutons (Kelemen and Ghiorso 1986). These complexes also contain abundant hornblende phases, similar to the Lac des Iles area (Sutcliffe 1986). Furthermore, gabbro pegmatites are common constituents of mafic intrusive rocks in such complexes (Beard and Day 1986). Chemical variations are also very similar. For example, trends in AFM diagrams are indistinguishable, following a calc-alkalic fractionation curve. Finally, the western Cordillera also hosts important precious metal mineralization. These observations suggest that the Lac des Iles Complex, and maybe the anomalously PGE-rich District of Thunder Bay may have been formed in a similar tectonic environment - a subject of further research.

ACKNOWLEDGMENTS

R.G.V. Hancock and M.J. Gorton, University of Toronto, and T. Reischmann, Max-Planck-Institut für Chemie, Mainz, Federal Republic of Germany, are thanked for assistance during XRF, INAA, RNAA, and Nd-isotope analysis. We are most grateful to R.A. Sutcliffe and A.J. Macdonald, Ontario Geological Survey, for many discussions during the course of this study and logistical support during field work.

REFERENCES

Beard, J.S., and Day, H.W.
1986: Origin of Gabbro Pegmatite in the Smartville Intrusive Complex, Northern Sierra Nevada, California; American Mineralogist, Volume 71, p.1085- 1099.

Brügmann, G.E.
1985: Geochemistry of Noble Metals and Lithophile Elements in Komatiite Flows from Alexo, Canada, and Gorgona, Colombia; Ph.D. Thesis, Johannes Gutenberg-Universität, Mainz, F.R.G., 261p. (in German).

Brügmann, G.E., Arndt, N.T., Hofmann, A.W., and Tobschall, H.J.
In Press: Noble Metal Abundances in Komatiite Suites from Alexo, Ontario, and Gorgona, Colombia; Geochimica et Cosmochimica Acta.

Brügmann, G.E., and Naldrett, A.J.
In preparation: Geochemistry and Sm-Nd Isotopic Characteristics of the Gabbroic Part of the Lac des Iles Complex, Northwestern Ontario, Canada.

Brügmann, G.E., Sutcliffe, R.H., and Naldrett, A.J.
In preparation: Crustal Evolution in the Lac des Iles Area, Northwestern Ontario, Canada: Evidence from Trace Element and Sm-Nd Isotope Characteristics of Mafic and Granitoid Intrusions.

Campbell, I.H., and Naldrett, A.J.
1979: The Influence of the Silicate: Sulphide Ratios on the Geochemistry of Magmatic Sulphides; Economic Geology, Volume 74, p.1503- 1506.

Dunning, G.R.
1979: The Geology and Platinum-Group Mineralization of the Roby Zone, Lac des Iles Complex, Northwestern Ontario; Unpublished M.Sc. Thesis, Carleton University, Ottawa, Ontario, 129p.

Irvine, T.N.
1975: The Crystallization Sequence in the Muskox Intrusion and Other Layered Intrusions - II. Origin of Chromite Layers and Similar Deposits of Other Magmatic Ores; Geochimica et Cosmochimica Acta, Volume 39, p.991- 1020.

Kelemen, P.B., and Ghiorso, M.S.
1986: Assimilation of Peridotite in Zoned Calc-alcaline Plutonic Complexes: Evidence from the Big Jim Complex, Washington Cascades; Contributions to Mineralogy and Petrology, Volume 94, p.12- 28.

Levinson, A.A. (Ed)
1981: Precious metals in the Northern Cordillera: Special Publication Association of Exploration Geochemists, Volume 10, 214p.

Linhardt, E., and Sutcliffe, R.H.
1986: Petrological and Economic Geological Studies on the Northern Lac des Iles Complex, District of Thunder Bay; p.80-81 *in* Summary of Field Work and Other Activities 1986, Ontario Geological Survey, edited by P.C. Thurston, Owen L. White, R.B. Barlow, M.E. Cherry, and A.C. Colvine, Ontario Geological Survey, Miscellaneous Paper 132, 435p.

Macdonald, A.J.
1985: The Lac des Iles Platinum-Group Metals Deposit, Thunder Bay District, Ontario; p.235-241 *in* Summary of Field Work and Other Activities 1985, Ontario Geological Survey, edited by John Wood, Owen L. White, R.B. Barlow, and A.C. Colvine, Ontario Geological Survey, Miscellaneous Paper 126, 361p.
1987: PGE Mineralization and the Relative Importance of Magmatic and Deuteric Processes: Lac des Iles Deposit, Ontario, Canada; Geo-Platinum 87 Symposium, Open University, Milton Keynes, U.K., 1987, Abstract.

Macdonald, A.J., Brügmann, G.E., and Naldrett, A.J.
1987: Coeval Felsic, Mafic and Ultramafic Magmas: Magma Mixing During Formation of PGE-rich Ni-Cu Sulphides at Lac des Iles, Ontario, Canada; 5th Magmatic Sulphide Conference, Harare 1987, IGCCP Project 161, Abstract.

Morrison, D.A., Davis, D.W., Wooden, J.L., Bogard, D.D., Maczuga, D.E., Phinney, W.C., and Ashwal, L.D.
1985: Age of the Mulcahy Lake Intrusion, and Implications for the Evolution of Greenstone-Granite Terrains; Earth and Planetary Science Letters, Volume 73, p.306- 316.

Naldrett, A.J.
1981: Platinum-Group Element Deposits; p.197-231 *in* Platinum-Group Elements: Mineralogy, Geology, Recovery, edited by L.J. Cabri, Canadian Institute of Mining and Metallurgy, Special Volume 23, 267p.

Naldrett, A.J., and Barnes, S-J.
1986: The Behaviour of Platinum-Group Elements during Fractional Crystallization and Partial Melting with Special Reference to the Composition of Magmatic Sulphide Ores; Fortschritte Mineralogie, Volume 64, p.113- 133.

Naldrett, A.J., Innes, D.G., and Sowa, J.
1980: Platinum-Group Element Concentrations in Some Magmatic Ores in Ontario; Ontario Geological Survey, Miscellaneous Paper 93, p.171- 178.

Naldrett, A.J., and Macdonald, A.J.
1980: Tectonic Settings of Some Ni-Cu Sulphide Ores: Their Importance in Genesis and Exploration; Geological Association of Canada, Special Volume, p.633- 657.

Pye, E.G.
1968: Geology of the Lac des Iles Area, District of Thunder Bay; Ontario Department of Mines, Geological Report 64, 47p. Accompanied by Maps 2135 and 2136, scale 1:31 680 or 1 inch to 1/2 mile.

Rowell, W.F., and Edgar, A.D.
1986: Platinum-Group Element Mineralization in a Hydrothermal Cu- Ni Sulphide Occurrence, Rathbun Lake, Northeastern Ontario; Economic Geology, Volume 81, p.1272- 1277.

Shirley, S.B., and Hanson, G.N.
1986: Mantle Heterogeneity and Crustal Recycling in Archean Granite- Greenstone Belts: Evidence from Nd Isotopes and Trace Elements in the Rainy Lake Area, Superior Province, Ontario, Canada; Geochimica et Cosmochimica Acta, Volume 50, p.2631- 2651.

Streckeisen, A.
1979: Classification and Nomenclature of Volcanic Rocks, Lamprophyres, Carbonatites, and Melilitic Rocks: Recommendations and Suggestions of the IUGS Subcommission on the Systematics of Igneous Rocks; Geology, Volume 7.

Sutcliffe, R.H.
1986: Regional Geology of the Lac des Iles Area, District of Thunder Bay; p.70-75 *in* Summary of Field Work and Other Activites 1986, Ontario Geological Survey, edited by P.C. Thurston, Owen L. White, R.B. Barlow, M.E. Cherry, and A.C. Colvine, Ontario Geological Survey, Miscellaneous Paper 132, 435p.

Sutcliffe, R.H., and Sweeny, J.M.
1985: Geology of the Lac des Iles Complex, District of Thunder Bay; p.47-53 *in* Summary of Field Work and Other Activities 1985, Ontario Geological Survey, edited by John Wood, Owen L. White, R.B. Barlow, and A.C. Colvine, Ontario Geological Survey, Miscellaneous Paper 126, 361p.
1986: Precambrian Geology of the Lac des Iles Complex, District of Thunder Bay; Ontario Geological Survey, Map P.3047, Geological Series-Preliminary Map, scale 1:15 840 or 1 inch to 1/4 mile. Geology 1985.
1986: Geology and Platinum Group Element Mineralization of the Roby Zone, Lac des Iles Complex; p.82- 84 *in* Summary of Field Work and Other Activities 1986, Ontario Geological Survey, edited by P.C. Thurston, Owen L. White, R.B. Barlow, M.E. Cherry, and A.C. Colvine, Ontario Geological Survey, Miscellaneous Paper 132, 435p.

Talkington, R.W., and Watkinson, D.H.
1984: Trends in the Distribution of the Precious Metals in the Lac des Iles Complex, Northwestern Ontario; Canadian Mineralogist, Volume 22, p.125- 136.

Watkinson, D.H., and Dunning, G.
1979: Geology and Platinum-Group Mineralization, Lac des Iles Complex, Northwestern Ontario; Canadian Mineralogist, Volume 17, p.453- 462.

Grant 280 Lead Isotope Study of Gold Mineralization in the Dome Mine Quartz–Fuchsite Vein

R.P. Moritz, J.H. Crocket, and A.P. Dickin

Department of Geology, McMaster University, Hamilton

ABSTRACT

The quartz-fuchsite vein environment in the Dome Mine, Timmins area, has been the subject of a lead isotope study. The vein is characterized by a consistent gold-galena association. Both metals are most certainly coeval and were deposited by the same hydrothermal fluid. The present study seeks to recognize possible sources of the lead, and perhaps, gold. Isotopic compositions were obtained for five galena samples from the quartz-fuchsite vein, two porphyry samples, and one slate composite. The isotopic signatures of the galenas are slightly too radiogenic to be derived directly from a mantle source. A multistage model is considered. In this model, the porphyries were derived at about 2685 Ma from a mantle reservoir with a μ_1 value of 7.73. On a $^{207}Pb/^{204}Pb$ versus $^{206}Pb/^{204}Pb$ diagram, the majority of the galena samples are colinear with the porphyries and the slates. This pattern may be interpreted as evidence of a genetic association between the quartz-fuchsite vein and the porphyries.

INTRODUCTION AND AIM OF THE STUDY

The highest grade ore vein in the Dome Mine, Timmins area, is a distinctive quartz vein characterized by narrow fuchsite-chlorite bands (Rogers 1982). The quartz-fuchsite vein (QFV) environment has been the subject of a project to evaluate the source of gold, the nature of the ore transporting fluids, and the mechanism of gold deposition in auriferous quartz lodes. An integrated study of the vein has involved underground mapping of the essential structural elements of the vein, a fluid inclusion investigation, lithogeochemistry of the host rocks, trace element geochemistry of the vein, and a sulphur and lead isotope study.

Galena is consistently associated with native gold in the QFV. This consistent association suggests that lead and gold were carried by the same hydrothermal fluid. Any information obtained from the lead isotopic composition of the galenas may be directly relevant to the gold. Thus, as part of the entire project, the lead isotopic study seeks to recognize possible sources of the lead, and perhaps, gold.

Four different sources of gold have been advocated for Archean deposits. Felsic intrusions are cited by Fyfe and Henley (1973), Burrows *et al.* (1986), Mason and Melnik (1986a, 1986b), Wood, Burrows, and Spooner (1986), and Wood, Burrows, Thomas and Spooner (1986). Alternatively, lateral secretion from local wall rocks has also been proposed as a source of the precious metal by Pyke (1976) and Boyle (1979). On the other hand, a larger and deeper crustal rock reservoir in which the ore fluids are produced by metamorphic outgassing at the greenschist-amphibolite facies boundary has been suggested by Fyfe and Henley (1973), Kerrich and Fryer (1979), Phillips and Groves (1983), and Phillips *et al.* (1986). Fyon *et al.* (1984), and Colvine *et al.* (1984) developed a fourth model, which links ore fluid generation and granulite development in the lower crust. Thus, in the present state of knowledge, lead isotopes should prove useful in constraining possible gold sources. In particular, the lead isotope signature may be evaluated in terms of local rock sources or deep lower crust and/or upper mantle sources.

GEOLOGICAL SETTING OF THE DOME MINE QUARTZ–FUCHSITE VEIN

The quartz vein under study is one of various types of gold mineralization recognized in the Dome Mine (Rogers 1982). It is situated in a steeply dipping zone of highly altered rocks, comprising the Dome Fault. This fault strikes southwest, and is thought to be a branch of the Destor-Porcupine Fault (Holmes 1968; Hodgson 1983) (*see* Figure 280.1). The zone of highly altered rocks lies between a slate unit to the north and metabasalts, namely the Southern Greenstones, to the south (Figures 280.1 and 280.2). It dies out to the northeast, whereas to the southwest it bends southward between the two major porphyries in the Dome Mine environment, namely the Preston and the Paymaster porphyries, and grades into ultramafic rocks (Figure 280.1). This zone consists of altered porphyry lenses and completely carbonatized rocks (Figure 280.2).

The carbonatized rocks are most probably altered komatiites, as evidenced by major and trace element geochemistry (relatively high MgO, Cr, Ni, and Ir contents), flat unfractionated rare earth element (REE) patterns, and textures resembling flow top breccias. Previous geochemical studies suggest the same protolith for these carbonatized rocks (Fryer *et al.* 1979; Roberts and Reading 1981). Their mineralogy is dominated by magnesite, dolomite, quartz, and chlorite, and variable amounts of fuchsite. They are often coarse grained and massive, lacking any important flattening as evidenced by the presence of flow top breccias. When schistosity is locally developed, it is parallel to the regional penetrative fabric (Roberts *et al.* 1978; Roberts 1981).

The felsic rock lenses are highly deformed, sericitized, and albitized quartz-feldspar porphyries. These felsic rocks appear to be petrographically similar to the Preston Porphyry (McAuley 1983). The mode of emplacement, either intrusive or extrusive, is still not resolved and remains controversial (Pyke 1982; McAuley 1983). According to McAuley (1983), these porphyries predate regional metamorphism.

THE QUARTZ–FUCHSITE VEIN

The QFV is subparallel to the northern contact between the slates and the carbonatized rocks (Figure 280.2). For most of its extension, the immediate wall rocks are the altered komatiites. However, the QFV can be found to mark the boundary between the carbonatized rocks and the slates.

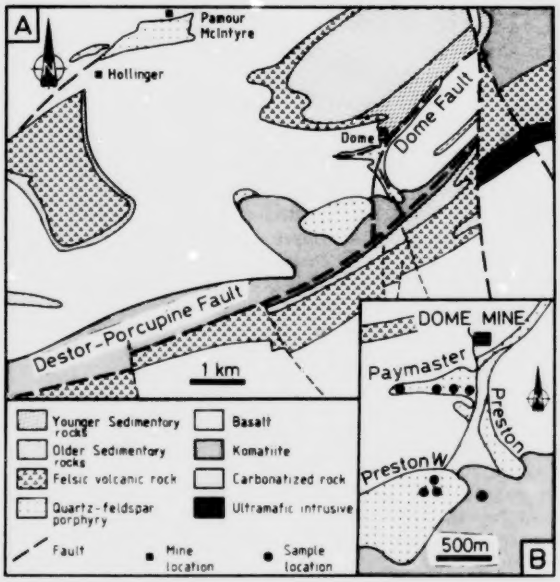

Figure 280.1. *Generalized geology of the Timmins area (after Davies 1977; Roberts 1981; Pyke 1982; Hodgson 1983).*
Sample locations of whole rocks at the surface, south of the Dome Mine.

The mineralization is entirely hosted within the 500 by 550 by 3.5 m average width quartz vein, which occurs between the 6th and 17th levels of the mine. The QFV strikes southwest and dips 75° to the southeast. It is discontinuous along strike, and it occurs as a chain of quartz lenses, bounded by faults or shears of variable orientations (Figure 280.2). Underground mapping indicates that quartz deposition occurred during several stages of opening along a fault. The QFV is composed of two main quartz types: one which is massive and barren, and consists almost entirely of quartz; and a second type which has bands of chlorite and fuchsite. The latter type constitutes the mineralized part of the vein (Photo 280.1).

Two high grade zones are present in the QFV. The larger is located in the western extremity of the vein, and the other in its eastern part. Both high grade zones are oriented parallel to the regional lineation (Roberts *et al.* 1978; Roberts 1981), and to the slickenslides present along the chlorite and fuchsite bands. The banding in the western ore zone is due mainly to fuchsite, whereas chlorite is predominant in the eastern ore zone banding.

The bands are subparallel to the walls of the vein. Their width is usually in the millimetre range. Thicker bands can be recognized as slivers or inclusions of carbonatized komatiite and slate wall rock. Thin section textural evidences indicate that fuchsite

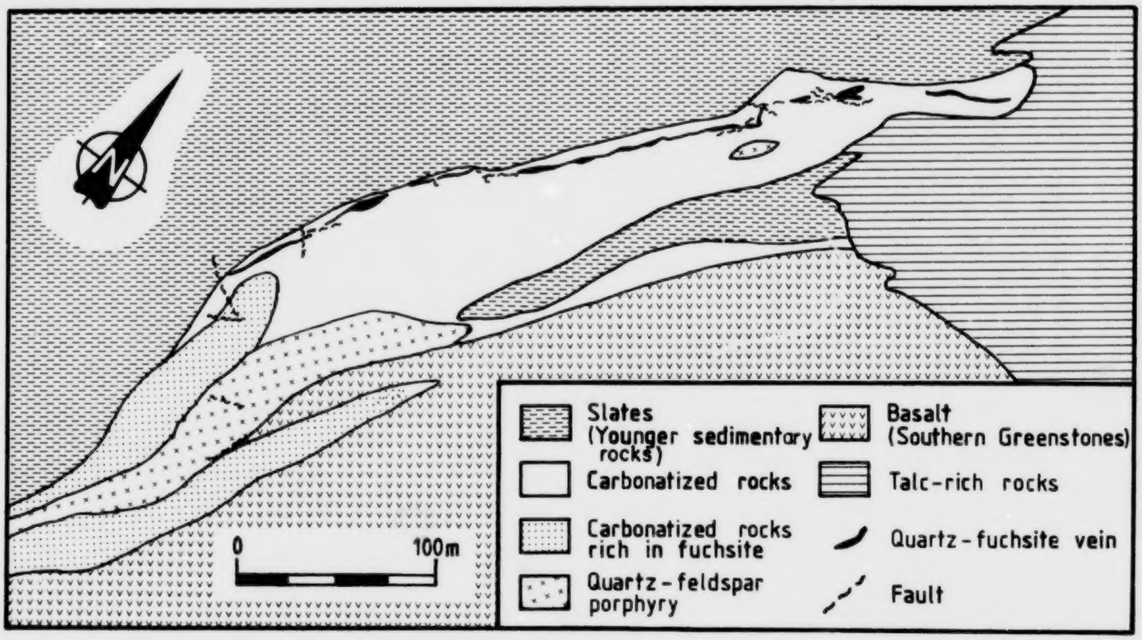
N
0
100m
Slates (Younger sedimentary rocks)
Carbonatized rocks
Carbonatized rocks rich in fuchsite
Quartz-feldspar porphyry
Basalt (Southern Greenstones)
Talc-rich rocks
Quartz-fuchsite vein
Fault

Figure 280.2. *Local geology of the Dome Mine quartz fuchsite vein on the 12th level (adapted from Dome Mine 12th level plan).*

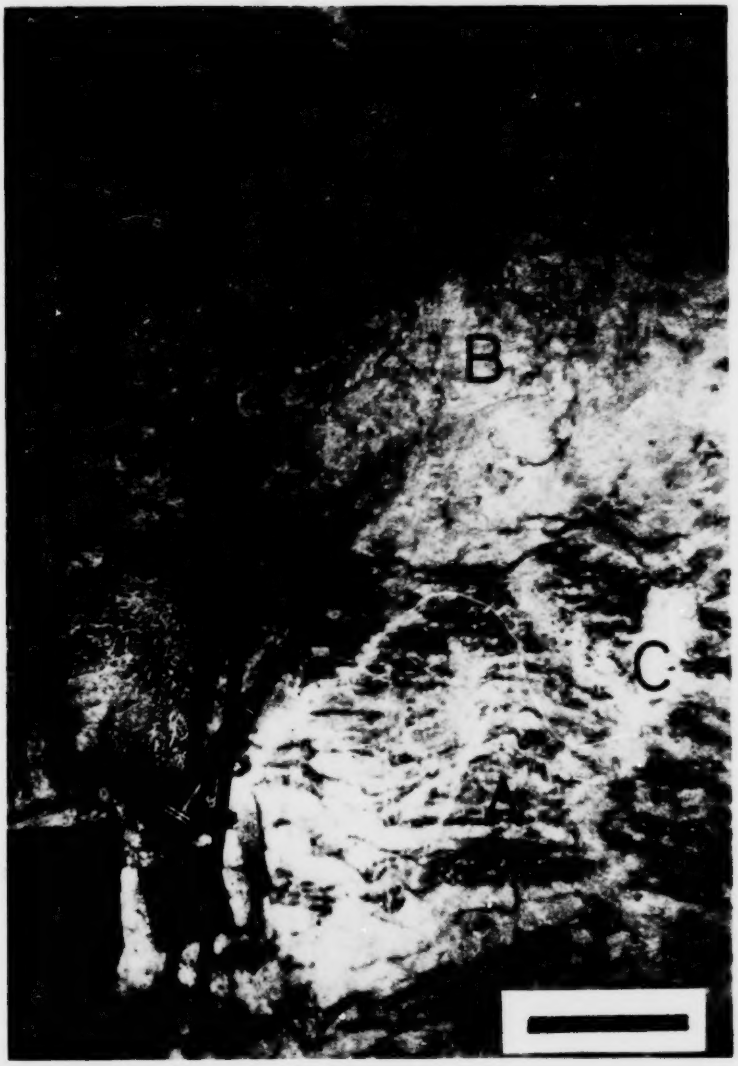

Photo 280.1. *Typical ore zone of the quartz-fuchsite vein. A: fuchsite and chlorite bands. Native gold and galena are located along and between these bands. Quartz between the bands has a cataclastic texture. B: Massive, unmineralized and coarse-grained quartz. C: Late stage discordant quartz vein. Scale bar corresponds to 20 cm.*

postdates chlorite and wall rock carbonates. The quartz between the fuchsite and chlorite bands has a cataclastic and recrystallized texture, whereas the quartz from barren zones is coarser grained and less deformed.

Native gold and galena are the main opaque minerals. These minerals occur both along the fuchsite and chlorite bands, and in the fractured quartz between the bands. Galena has only been observed in the upper part of the vein (between the levels 8 and 13), and is always intergrown or in association with native gold (Photo 280.2). However, gold is present in the lower levels of the vein (levels 15 to 17) without galena. Tellurides (altaïte, melonite, hessite, tetradymite) are present as well, and intergrown with gold and galena. Pyrite is poorly represented in the QFV environment. It is almost absent in the vein itself, and only present as a minor constituent of the wall rocks, unlike much Dome gold ore (Rogers 1982), and other major gold ores (Boyle 1979; Colvine *et al.* 1984). Late stage carbonates are also present.

Thus, the characteristics of the QFV, and in particular, the intimate gold-galena spatial association, are particularly relevant to the lead isotope systematics to recognize possible sources of gold in Archean auriferous deposits, since the structural and the local rock environment are well established. The gold-galena association is so consistent, that a strong inference that both metals are coeval and deposited by the same hydrothermal fluid can be assumed. This inferred similarity in age has also been documented by earlier studies in the Timmins area (Hurst 1935; Ferguson *et al.* 1968).

PREVIOUS GEOCHRONOLOGICAL STUDIES

Previous geochronological work in the Dome Mine (Masliwec *et al.* 1986) makes the QFV an even more attractive target for a lead isotope study. A cry-

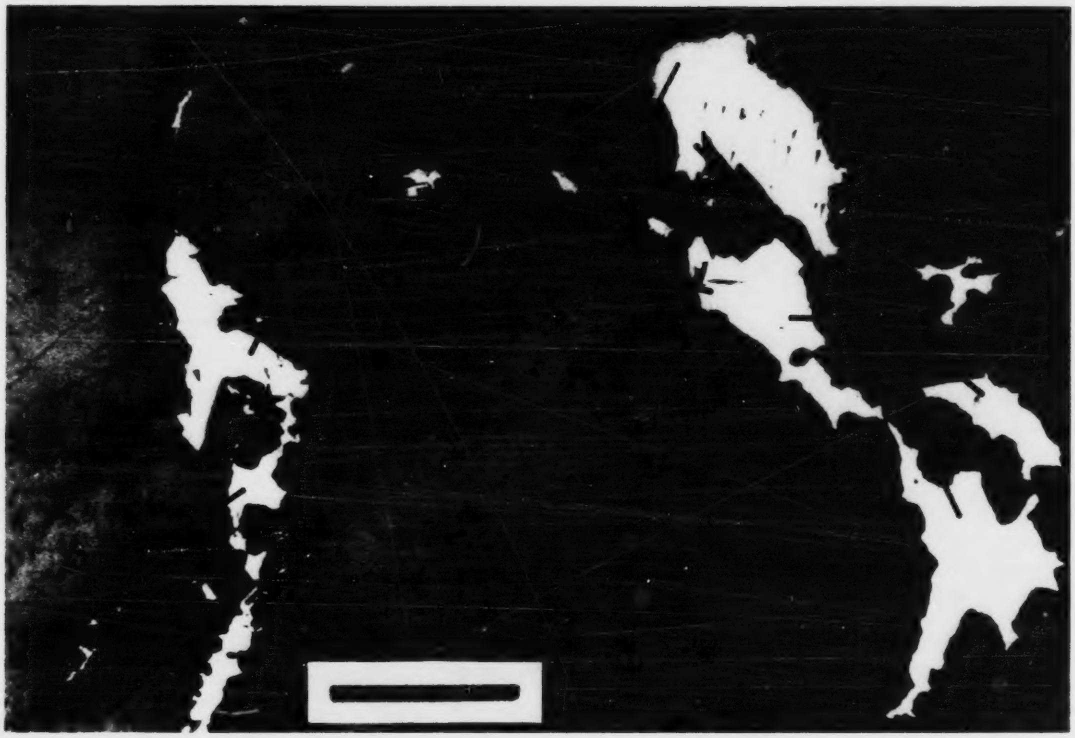

Photo 280.2. Typical gold-galena association in the quartz-fuchsite vein. Au=native gold; Gn=galena; Q=quartz. Scale bar corresponds to 0.2 mm.

stallization age of 2685±3 Ma was obtained by U-Pb dating of zircons for the Preston porphyry (S. Marmont *in* Masliwec *et al.* 1986). Moreover, Masliwec *et al.* (1986) obtained an $^{40}Ar/^{39}Ar$ age of 2633±6 Ma for the fuchsite associated with the gold mineralization. Thus, since the porphyries predate the gold mineralization, which in turn is considered to be pre- or syn-fuchsite, it is possible to bracket the formation of the gold mineralization between 2633±6 Ma and 2685±3 Ma. These two ages constrain lead isotope models used for the source rock investigation of lead and gold.

METHODOLOGY

SAMPLING

Eight galena samples were collected in the two high grade zones. All but one came from the banded zones of the QFV. They are typically in grain boundary contact with gold (Photo 280.2), or occur with gold in the same thin-section. Sample 8006 is the only sample analyzed, so far, where a grain boundary contact between both opaque minerals was not observed. The one sample which was not collected in the banded part of the vein comes from an oblique quartz vein, which is present in the wall rock, but in contact with QFV (#12003 in Figure 280.3).

Whole rock lead isotope compositions were determined on various rocks from the Dome Mine, particularly those in the Dome Fault environment. Slates, carbonatized rocks, and a porphyry lens were sampled along a drift on the 12th level, which cuts the QFV perpendicularly (Figure 280.3). Samples were taken at variable distances from the vein, in order to recognize possible changes in the lead isotope ratios across it. The Preston porphyry, the Preston West porphyry, and an ultramafic flow were sampled at the surface south of the Dome Mine (Figure 280.1b).

ANALYTICAL

The rock samples were crushed to pass 200 Mesh. A 200 mg split was digested in HF for four days, followed by a 12 hour dissolution in HNO_3, and finally another 12 hour digestion in HCl. The dry residue was dissolved in 1 M HBr. Pb was separated by anionic exchange in HBr columns, and collected with a 6 M HCl solution. The galenas were dissolved in 0.01 M HNO_3, and the Pb was purified by electrodeposition on a Pt-electrode. Isotopic ratios were measured on a VG 365 mass spectrometer.

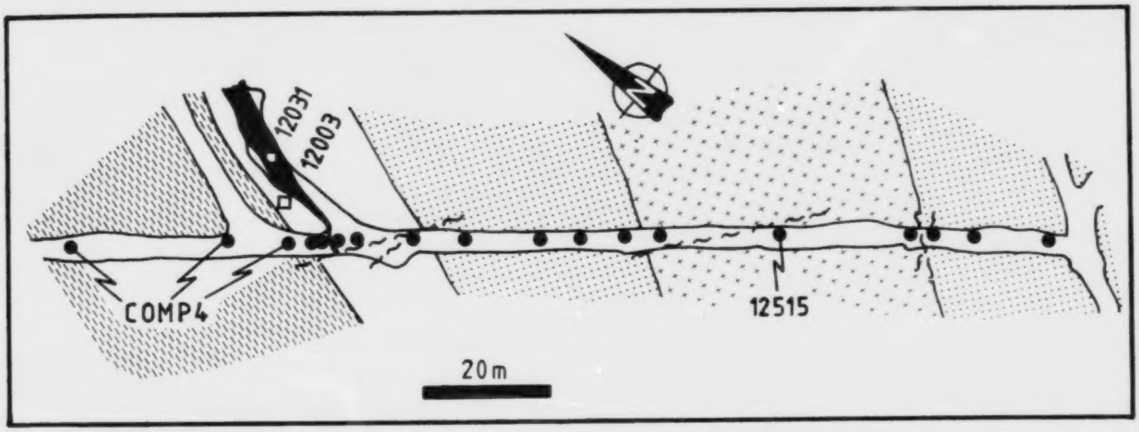

Figure 280.3. *Sample locations across the quartz-fuchsite vein on the 12th level. Dots=whole rock samples; squares=galena samples. Numbered samples are samples analyzed to date. For geology see the legend on Figure 280.2.*

THEORETICAL CONSIDERATIONS

The manipulation and interpretation of lead isotope data follows the procedure of Faure (1986) and Gulson (1986). The basic approach in a source rock investigation is to determine or infer the lead isotopic composition of the possible source rocks at their time of formation, and compare these compositions with that of the ore, also at its time of formation. Thus, two distinct situations can be expected for the galenas of the QFV:

1. Lead derived directly from a mantle source, without any contamination from older radiogenic crust, would show isotopic compositions characteristic of a uranium-poor reservoir. In such a case, we would find on conventional $^{207}Pb/^{204}Pb$ and $^{208}Pb/^{204}Pb$ versus $^{206}Pb/^{204}Pb$ diagrams, that the lead isotope ratios of the galenas would cluster tightly on a single-stage growth curve with a typical mantle $^{238}U/^{204}Pb$ ratio (μ; between 7.5 and 8.0). Such a scenario could be envisaged for lead deposited from a fluid interacting with mafic-ultramafic volcanic rocks, or from a fluid generated by metamorphic outgassing of such a rock pile. Lateral secretion from the local carbonatized komatiites could result in a similar pattern, but with more scatter. However, given the low lead content of unaltered komatiites, it is doubtful that these wall rocks contributed much of the lead now present in the galenas of the QFV.
2. Lead generated by upper crustal felsic rocks would be more radiogenic than lead typical of the first case. In conventional lead-lead diagrams, the isotope ratios would cluster off a mantle growth curve indicating a multistage evolution for the galena-leads. In the very special case, where the Dome Mine porphyries; that is, the Preston and the Paymaster porphyries, were the source of the lead, one might find that the lead isotope ratios of the porphyries and of the galenas are colinear. The simplest case is where the mantle is the magma source, and crustal contamination is absent or negligible. In this case, the line defined by the isotope ratios of the galenas and the porphyries would intercept the mantle growth curve at the very same point where the 2685±3 Ma isochron (age of the Preston porphyry) intersects the mantle growth curve.

There will be some limitations in the degree of confidence with which one or the other of these scenarios can be applied to explain the lead isotope signature of the galenas. These limitations are the following:

1. The age difference between the porphyries and the vein fuchsite is apparently about 50 Ma. In order to generate much radiogenic lead in this short time span, the porphyries must be fairly rich in uranium and thorium.
2. If the ore fluid was derived from depth (the greenschist-amphibolite facies boundary and/or the lower crust-upper mantle environment), it may have been modified by reaction with the rock column during its ascent. Depending on the mix of felsic and mafic-ultramafic rocks, leads may have become more radiogenic than those characteristic of single stage mantle extraction.
3. Since the rocks under study are fairly old, it is expected that any initial colinearity of isotope ratios was destroyed by subsequent mobilization of uranium and thorium, which scattered the ratios off the line. Any metamorphic or alteration event postdating the formation of the galenas and of the host rocks might have altered the original isotope ratios. Thus, scatter of the data can be foreseen. A confident choice of one or the other model will be subject to the extent of the spread of the data.

These two simplistic hypothetical models bracket a broad range of more complicated lead isotope patterns. Mixing of leads from different sources is conceivable; for instance, lead leached out from a variety of wall rocks including the porphyries. The gold deposit model linking ore fluid generation with the granulitization of the lower crust would generate

TABLE 280.1. LEAD ISOTOPE RATIOS OF THE GALENA SAMPLES FROM THE DOME MINE QUARTZ-FUCHSITE VEIN.

Sample Number	$\frac{^{206}Pb}{^{204}Pb}$	$\frac{^{207}Pb}{^{204}Pb}$	$\frac{^{208}Pb}{^{204}Pb}$
8006	13.619	14.606	33.322
8010	13.407	14.462	33.027
12003	13.388	14.465	33.062
12031	13.462	14.462	33.050
13010	13.494	14.483	33.105

TABLE 280.2. LEAD ISOTOPE RATIOS OF PORPHYRIES AND SLATES FROM THE ENVIRONMENT OF THE DOME MINE QUARTZ-FUCHSITE VEIN. All samples were collected on 12 level.

Sample Number	Rock Type and Name of Lithology	$\frac{^{206}Pb}{^{204}Pb}$	$\frac{^{207}Pb}{^{204}Pb}$	$\frac{^{208}Pb}{^{204}Pb}$
12302	Preston porphyry	18.799	15.480	37.770
12515	Porphyry lens from the zone of highly altered rocks	18.002	15.338	36.188
COMP4	Composite sample of slates from the Younger sediments	18.149	15.353	38.445

TABLE 280.3. MODEL μ_1 AND MODEL AGES CALCULATED FROM THE ISOTOPIC COMPOSITION OF THE GALENAS FROM THE DOME MINE QUARTZ-FUCHSITE VEIN.

Sample Number	Single-Stage Model		Two-Stage Model age (Stacey and Kramers 1975)	Superior Province Model age (Thorpe 1982)
	μ_1	Age		
8006	7.72	2.472	2.567	2.566
8010	7.54	2.534	2.553	2.597
12003	7.57	2.555	2.587	2.620
12031	7.48	2.483	2.478	2.538
13010	7.51	2.473	2.480	2.532

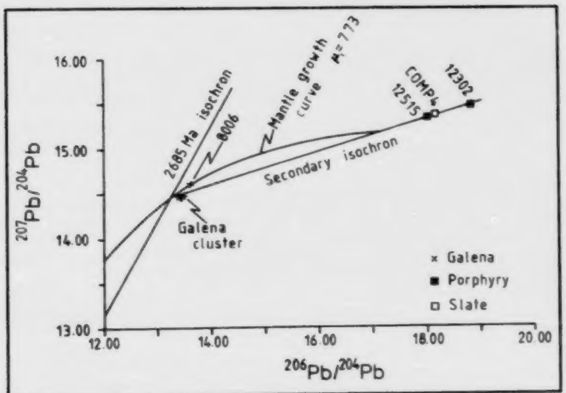

Figure 280.4. Lead isotope data from galenas of the quartz-fuchsite vein, and porphyries and slates from the Dome Mine. Also plotted are the isochron corresponding to the age of the Preston porphyry (2685 Ma), the secondary isochron defined by the age of the Preston porphyry and the lead isotope ratios of the porphyry and slate samples, and the sample growth curve with a μ_1 value of 7.73. (See text for discussion, and appendix IV for the calculation of the isochrons and the mantle growth curve).

a complex lead isotope pattern, since the lead now present in the galenas would have resided in at least three systems with different $^{238}U/^{204}Pb$ ratios, that is, mantle, lower crust, and upper crust.

PRELIMINARY RESULTS AND DISCUSSION

Isotopic ratios were obtained for five galena samples (Table 280.1), two porphyry samples, and one composite slate sample (Table 280.2). The current data must be taken with caution, since analysis of other samples and of replicates is on-going. In order to simplify the reading of the report, all model calculations are given in Appendices II to IV. Appendix I lists the constants and symbols used in the lead-lead age and model calculations.

The galena samples have similar isotope ratios. In a $^{207}Pb/^{204}Pb$ versus $^{206}Pb/^{204}Pb$ diagram they form a tight cluster (Figure 280.4). One sample, #8006, has an isotopic composition differing significantly from the other four (Table 280.1, Figure 280.4). Ages have been calculated according to three different lead isotope models: the Single-Stage Model (Faure 1986), Stacey's and Kramers' (1975) Two-Stage model, and the local lead evolution model developed for the Superior Province by Thorpe (1982). Calculated ages are given in Table 280.3, and their determination is given in Appendices II and III. The Single- and the Two-Stage models yield very similar ages for most of the galenas. Ages obtained with Thorpe's (1982) model are slightly lower than the 2633±6 Ma date given for the fuchsite by Masliwec *et al.* (1986). Thus, the ages calculated with the three different models lie outside the age bracket given by the $^{40}Ar/^{39}Ar$ fuchsite age and the zircon U-Pb for the Preston porphyry, that is, 2633± 6 Ma to 2685± Ma. This discrepancy can be explained if the galenas contain some radiogenic lead, and thus yield younger ages than the other geochronological methods. Possible reasons explaining such a divergence are:

1. The galenas were contaminated with radiogenic lead during a metamorphic or an alteration event postdating their crystallization.
2. During their crystallization, the galenas incorporated lead generated by a radiogenic source, that is, high level crustal rocks.

The first hypothesis might explain the isotopic ratios of sample 8006. However, more spread in the ratios from the other samples would be expected, if postcrystallization radiogenic lead contamination was the unique explanation for the isotopic composition of all samples. The second hypothesis is favoured because it explains more rigorously the consistent isotopic composition of most of the galena samples. Given the age constraints of the fuchsite and the Preston porphyry ages, the lead isotope signature of the galenas cannot be interpreted in a Single- or a Two-Stage lead evolution model. Moreover, with a Single-Stage model, the lead isotope ratios yield μ_1 values ($^{238}U/^{204}Pb$ ratios) of approximately 7.5, which are acceptable for an Archean mantle in general (Table 280.3; *see* equation for the calculation of μ in Appendix II); however, such a μ_1 value is a lower estimate for the Superior Province mantle in the Archean (for instance, Dupré and Arndt 1987, Shirey and Carlson 1987). Thus, the slightly radiogenic composition of the galenas requires consideration of a multi-stage lead evolution model.

The zircon U-Pb age for the Preston porphyry, that is, 2685±3 Ma, permits us to calculate the slope of the secondary isochron along which the lead isotope ratios of the porphyries should lie, if contamination can be ruled out. This slope has a value of 0.1835 (*see* Appendix IV). It matches perfectly the distribution of the two porphyry samples and the composite slate sample (Figure 280.4). It is not surprising to find a colinear relationship for the slates and the porphyries, since the former are most probably derived from the felsic rocks (Kerrich and Fryer 1979). If, as a first approach, it is assumed that the porphyries were derived from a mantle reservoir unaffected by older radiogenic crust, then it is possible to model a mantle growth curve with a μ_1 value of 7.73 (*see* Appendix IV). This latter value agrees better with independently calculated μ_1 values for the Archean mantle (for example, Dupré and Arndt 1987, Shirey and Carlson 1987), than the μ_1 value obtained from the isotopic composition of the galenas in a Single-Stage model. In such a case, where the porphyries were derived at about 2685 Ma from a mantle with a μ_1 value of 7.73, the main galena cluster lies along the secondary isochron defined for the felsic rocks (Figure 280.4). Such a pattern may be interpreted as evidence of a genetic affiliation between the QFV and the porphyries of the Dome Mine environment. Moreover, the location of the galena cluster close to the mantle growth curve is in agreement with a short time span to generate the radiogenic component in the galena lead.

Alternatively, the linear array formed by the galena cluster and the rock leads analyzed to date might be fortuitous; that is, the porphyries and the gold mineralization are of the same age, but not from the same source. However, given the close spatial association of gold mineralization and porphyries in the Timmins area, the latter interpretation seems less credible than the model linking emplacement of felsic intrusions and generation of gold mineralization.

The isotopic composition of sample #8006, with lead ratios differing from the other samples, is not well understood at present. Its composition might be the result of a postmineralization event (that is, metamorphism, alteration); or, on the other hand, the main galena cluster and this "anomalous" sample may lie on a mixing line (*see* Figure 280.4).

CONCLUSIONS AND FUTURE OBJECTIVES

The preliminary results permit drawing some very interesting conclusions, and indicates further lines of modeling and research:

CONCLUSIONS

1 The slightly radiogenic isotopic signatures of the galenas cannot be explained with a Single-Stage model, with Stacey's and Kramers' (1975) Two-Stage model, or with Thorpe's (1982) local lead evolution Superior Province model. Thus, the lead of the galenas was not derived directly from a mantle source.

2. As a first approach, the lead isotopic composition of the porphyries and the slates in the Dome Mine environment can be interpreted with a multistage model. In this model, the porphyries were derived at about 2685 Ma from a mantle reservoir with a model μ_1 value of 7.73. Such a figure agrees with μ_1 values obtained from other independent studies (for example, Dupré and Arndt 1987, Shirey and Carlson 1987). If such a multistage model proves to be correct, then it may be inferred that no significantly older crust was present under the Superior Province.

3. The majority of the lead compositions from the galenas cluster close to the secondary isochron defined by the porphyries. This pattern may indicate a possible genetic affiliation between the quartz-fuchsite vein and the local porphyries. Thus, it supports the gold deposit model linking emplacement of the porphyries and generation of gold mineralization.

4. At present, as evidenced by one "anomalous" galena sample (#8006), whose isotopic signature differs from the other galena samples, mixing of lead from different sources cannot be ruled out.

FUTURE OBJECTIVES

Three other galena samples have still to be analyzed. Their isotopic compositions may indicate if mixing of lead from various sources took place. The analyses of other porphyry samples are expected to confirm their present distribution along a secondary isochron. Replicate analyses will be carried out in order to assess the precision of the isotopic ratios, and thus of the calculated model ages and μ values. In this way, we may estimate the degree of confidence which can be given to the scenarios used to explain the isotopic signatures of the galenas. An improvement of the quality of the analytical procedures is ongoing, and may allow the obtaining of precise lead isotope ratios for low lead concentration rocks, that are the altered komatiites.

ACKNOWLEDGMENTS

The authors would like to thank the management of Dome Mines Limited for access to the quartz-fuchsite vein; Dean S. Rogers (Chief Geologist, Dome Mine) for arranging the field work and for helpful guidance and discussions. Field work was supported by an NSERC grant to J.H. Crocket.

REFERENCES

Boyle, R.W.
1979: The Geochemistry of Gold and its Deposits; Geological Survey of Canada, Bulletin 280, 584p.

Burrows, D.R., Wood, P.C., and Spooner, E.T.C.
1986: Carbon Isotope Evidence for a Magmatic Origin for Archean Gold-Quartz Vein Ore Deposits; Nature, Volume 321, p.851-854.

Colvine, A.C., Andrews, A.J., Cherry, M.E., Durocher, M.E., Fyon, A.J., Lavigne, M.J., Jr., Macdonald, A.J., Soussan Marmont, Poulsen, K.H., Springer, J.S., and Troop, D.G.
1984: An Integrated Model for the Origin of Archean Lode Gold Deposits; Ontario Geological Survey, Open File Report 5524, 98p.

Davies, J.F.
1977: Structural Interpretation of the Timmins Mining Area, Ontario; Canadian Journal of Earth Sciences, Volume 14, p.1046-1053.

Dupré,B. and Arndt, N.T.
1987: Pb Isotopes in Archean Komatiites, Basalts and Sulfides; Terra Cognita, Volume 7, p.272.

Faure, G.
1986: Principles of Isotope Geology; Second Edition, John Wiley and Sons, 589p.

Ferguson, S.A., Buffam, B.S.W., Carter, O.F., Griffis, A.T., Holmes, T.C., Hurst, M.E., Jones, W.A., Lane, H.C., and Longley, C.S.
1968: Geology and Ore Deposits of Tisdale Township, District of Cochrane; Ontario Department of Mines, Geological Report 58, 177p. Accompanied by Map 2075, scale 1:12 000 or 1 inch to 1000 feet.

Fryer, B.J., Kerrich, R., Hutchinson, R.W., Peirce, M.G., and Rogers, D.S.
1979: Archean Precious-Metal Hydrothermal Systems, Dome Mine, Abitibi Greenstone Belt: 1. Patterns of Alteration and Metal Distribution; Canadian Journal of Earth Sciences, Volume 16, p.421-439.

Fyfe, W.S., and Henley, R.W.
1973: Some Thoughts on Chemical Transport Processes, with Particular Reference to Gold; Mineral Science Engineering, Volume 5, p.295-303.

Fyon, J.A., Schwarcz, H.P., and Crocket, J.H.
1984: Carbonatization and Gold Mineralization in the Timmins Area, Abitibi Greenstone Belt: Genetic Links with Archean Mantle CO_2-Degassing and Lower Crustal Granulitization; p.431 *in* Abstracts with Program, Geological Association of Canada/ Mineralogical Association of Canada, Volume 9.

Gulson, B.L.
1986: Lead Isotopes in Mineral Exploration; Developments in Economic Geology, Elsevier, Volume 23, 245p.

Hodgson, C.J.
1983: The Structure and Geological Development of the Porcupine Camp—A Re-evaluation; p.211-225 *in* The Geology of Gold in Ontario, edited by A.C. Colvine, Ontario Geological Survey, Miscellaneous Paper 110, 278p.

Holmes, T.C.
1968: Dome Mines Limited; p.82-98 *in* Geology and Ore Deposits of Tisdale Township, by S.A. Ferguson and Associated Geologists, Ontario Department of Mines, Geological Report 58, 177p.

Hurst, M.E.
1935: Vein Formation at Porcupine Ontario; Economic Geology, Volume 30, p.103-127.

Kerrich, R., and Fryer, B.J.
1979: Archean Precious-Metal Hydrothermal Systems, Dome Mine, Abitibi Greenstone Belt: II. REE and Oxygen Isotopes Relations; Canadian Journal of Earth Sciences, Volume 16, p.440-458.

Masliwec, A., McMaster, D., and York, D.
1986: The Dating of Ontario's Gold Deposits; Grant 233, p.107-114 *in* Geoscience Research Grant Program, Summary of Research, 1985-1986, edited by V.G. Milne, Ontario Geological Survey, Miscellaneous Paper 130, 235p.

Mason, R., and Melnik, N.
1986a: The McIntyre-Hollinger Investigation, Timmins, Ontario: a Gold Dominated Porphyry Copper System; p.577-583 *in* Current Research, Part B, Geological Survey of Canada, Paper 86-1B.
1986b: The Anatomy of an Archean Gold System—The McIntyre-Hollinger Complex at Timmins, Ontario, Canada; p.40-55 *in* Proceedings, Gold '86, an International Symposium on the Geology of Gold, Toronto, edited by A.J. Macdonald.

McAuley, J.B.
1983: A Petrographic and Geochemical Study of the Preston, Preston West and Paymaster Porphyries, Timmins, Ontario; Unpublished M.Sc. Thesis, Laurentian University, 118p.

Phillips, G.N., and Groves, D.I.
1983: The Nature of Archean Gold-Bearing Fluids as Deduced from Gold Deposits of Western Australia; Journal of the Geological Society of Australia, Volume 30, p.25-39.

Phillips, G.N., Groves, D.I., Ho, S.E., and Neall, F.B.
1986: A Metamorphic-Replacement Model for Genesis of Archaean Gold Deposits; p.125-132 *in* International Conference on the Metallogeny of the Precambrian, Prague, 1986.

Pyke, D.R.

1976: On the Relationship of Gold Mineralization and Ultramafic Volcanic Rocks in the Timmins Area, Northeastern Ontario; Canadian Institute of Mining Bulletin, Volume 69, p.79-87.

1982: Geology of the Timmins Area, District of Cochrane; Ontario Geological Survey, Report 219, 141p. Accompanied by Map 2455, scale 1:50 000.

Roberts, R.G.

1981: The Volcanic-Tectonic Setting of Gold Deposits in the Timmins Area, Ontario; p.16-28 *in* Genesis of Archean, Volcanic-Hosted Gold Deposits, Symposium Held at the University of Waterloo, March 7, 1980, edited by E.G. Pye and R.G. Roberts, Ontario Geological Survey, Miscellaneous Paper 97, 175p.

Roberts, R.G., and Reading, D.J.

1981: Volcanic-Tectonic Setting of Gold Deposits in the Timmins District—Carbonate-Bearing Rocks at Dome Mine; p.222-228 *in* Geoscience Research Grant Program, Summary of Research 1980-1981, edited by E.G. Pye, Ontario Geological Survey, Miscellaneous Papers 98, 340p.

Roberts, R.G., Carnevali, J., and Harris, J.D.

1978: The Volcanic-Tectonic Setting of Gold-Quartz Vein Systems in the Timmins District, Ontario; p.187-190 *in* Current Research, Part B, Geological Survey of Canada, Paper 78-1B.

Rogers, D.S.

1982: The Geology and Ore Deposits of the #8 Shaft Area, Dome Mine; Canadian Institute of Mining, Special Volume 24, p.161-168.

Shirey, S.B., and Carlson, R.W.

1987: Pb and Nd Isotope Evolution of the Archean Crust and Mantle; Terra Cognita, Volume 7, p.272.

Stacey, J.S., and Kramers, J.D.

1975: Approximation of Terrestrial Lead Isotope Evolution by a Two-Stage Model; Earth and Planetary Science Letters, Volume 26, p.207-221.

Thorpe, R.I.

1982: Lead Isotope Evidence Regarding Archean and Proterozoic Metallogeny in Canada; Revista Brasileira de Geociências, Volume 12, p.510-521.

Wood, P.C., Burrows, D.R., and Spooner, E.T.C.

1986: Au-Quartz Vein and Intrusion-Hosted Cu-Au-Ag-Mo Mineralization, Hollinger McIntyre Mines, Timmins, Ontario: Geological Characteristics, Structural Examination, Igneous and Hydrothermal Alteration Geochemistry, and Light Stable Isotope (Hydrogen and Oxygen) Geochemistry; Grant 236, p.115-137 *in* Geoscience Research Grant Program, Summary of Research, 1985-1986, edited by V.G. Milne, Ontario Geological Survey, Miscellaneous Paper 130, 235p.

Wood, P.C., Burrows, D.R., Thomas, A.V., and Spooner, E.T.C.

1986: The Hollinger-McIntyre Au-Quartz Vein System, Timmins, Ontario, Canada: Geologic Characteristics, Fluid Properties and Light Stable Isotope Geochemistry; p.56-80 *in* Proceedings of Gold '86, an International Symposium on the Geology of Gold: Toronto, edited by A.J. Macdonald.

APPENDIX I

CONSTANTS AND SYMBOLS USED IN THE Pb-Pb AGE AND MODEL CALCULATIONS

Symbol	Meaning	Value
λ_1	Decay constant for ^{238}U	1.55125×10^{-10}/year
λ_2	Decay constant for ^{235}U	9.8485×10^{-10}/year
k	Present $^{238}U/^{235}U$ ratio	137.88
a_0	Primeval $^{206}Pb/^{204}Pb$ ratio	9.307
b_0	Primeval $^{207}Pb/^{204}Pb$ ratio	10.294
μ	Present $^{238}U/^{204}Pb$ ratio	variable
T	Age of the Earth in the Single-Stage model	4.55×10^9 years
T'	Date of geochemical differentiation in Stacey's and Kramers' model (1975)	
T*	Date of source age in Thorpe's model (1982)	4.06×10^9 years
m	Slope of a secondary isochron	
i	Intercept of a secondary isochron and the $^{207}Pb/^{204}Pb$ axis	

APPENDIX II

SINGLE-STAGE MODEL CALCULATIONS

This model assumes that radiogenic Pb was produced by decay of U and Th in the source region and that the resulting Pb (primeval plus radiogenic) is then separated from its parents and incorporated into ore deposits as a Pb-rich mineral, in the present case galena. The isotopic composition of such Pb remains constant with time.

If t years ago, Pb was withdrawn without isotopic fractionation from a U-bearing system of age T, then the $^{206}Pb/^{204}Pb$ and $^{207}Pb/^{204}Pb$ ratios of such Pb is:

Equation (II.1)

$$^{206}Pb/^{204}Pb = a_0 + \mu\,(e^{\lambda_1 T} - e^{\lambda_1 t})$$

Equation (II.2)

$$^{207}Pb/^{204}Pb = b_0 + (\mu/k)\,(e^{\lambda_2 T} - e^{\lambda_2 t})$$

Equations II.1 and II.2 can be combined to calculate the time t at which Pb was extracted, which in the present case is the age of the QFV-galenas:

Equation (II.3)

$$M = \frac{(^{207}Pb/^{204}Pb) - b_0}{(^{206}Pb/^{204}Pb) - a_0} = \frac{1}{k}\,\frac{(e^{\lambda_2 T} - e^{\lambda_2 t})}{(e^{\lambda_1 T} - e^{\lambda_1 t})}$$

Three unknowns are present in equation II.3; the two isotope ratios and t. The lead ratios are obtained by isotopic analysis of the galena samples. Thus, equation II.3 can be solved for t (age of the galenas) using Table 19.2 in Faure (1986, p.315). After t is obtained, μ can then be calculated using either equation II.1 or equation II.2.

APPENDIX III

TWO–STAGE MODEL OF LEAD EVOLUTION (STACEY AND KRAMERS 1975)

In this model the evolution of Pb started with primordial isotope ratios 4.57×10^9 years ago. At a more recent date $T'=3.7\times10^9$ years, the U/Pb ratio of the reservoir was changed by geochemical differentiation and then remained constant to the present. The initial $^{206}Pb/^{204}Pb$ and $^{207}Pb/^{204}Pb$ ratios of this new system are 11.152 instead of 9.307 (a_0) and 12.998 instead of 10.294 (b_0) respectively. Thus, equation II.3 is as:

Equation (III.1)

$$M = \frac{(^{207}Pb/^{204}Pb) - 12.998}{(^{206}Pb/^{204}Pb) - 11.152} = \frac{1}{k}\,\frac{(e^{\lambda_2 T'} - e^{\lambda_2 t})}{(e^{\lambda_1 T'} - e^{\lambda_1 t})}$$

This equation can be solved for t (age of galenas) using Table 19.4 in Faure (1986, p.322).

SUPERIOR MODEL AGE CALCULATION (THORPE 1982)

On the basis of lead minerals associated with Superior Province syngenetic and synvolcanic deposits, Thorpe (1982) determined a source age of 4.06×10^9 years (T^*), with initial $^{206}Pb/^{204}Pb$ and $^{207}Pb/^{204}Pb$ ratios which are respectively 10.242 and 11.9556. Thus, equation II.3 can be rewritten as follows:

Equation (III.2)

$$M = \frac{(^{207}Pb/^{204}Pb) - 11.9556}{(^{206}Pb/^{204}Pb) - 10.242} = \frac{1}{k}\,\frac{(e^{\lambda_2 T^*} - e^{\lambda_2 t})}{(e^{\lambda_1 T^*} - e^{\lambda_1 t})}$$

t can then be derived from this equation and tables similar to those given by Faure (1986, Tables 19.2 and 19.4).

APPENDIX IV

CALCULATION OF THE 2.685×10^9 YEARS ISOCHRON

Single-Stage leads that were removed from source regions with different μ values at the same time t must lie on the same isochron. Such an isochron can be calculated using equations II.1 and II.2. In these equations, if t is kept constant, at 2.685×10^9 years, then μ remains the sole variable. Different μ values yield $^{207}Pb/^{204}Pb$ ratios as a function of $^{206}Pb/^{204}Pb$ ratios, which plot on the same line or isochron.

CALCULATION OF THE SECONDARY ISOCHRON FITTING THE DISTRIBUTION OF THE LEAD ISOTOPE RATIOS OF THE PORPHYRIES AND THE SLATES

If a sample of Pb passed through two U-bearing systems characterized by different $^{238}U/^{204}Pb$ ratios (μ_1 and μ_2), then the $^{206}Pb/^{204}$ and $^{207}Pb/^{204}Pb$ ratios of that sample are:

Equation (IV.1)

$$(^{206}Pb/^{204}Pb) = a_0 + \mu_1(e^{\lambda_1 T} - e^{\lambda_1 t_1}) + \mu_2(e^{\lambda_1 t_1} - e^{\lambda_1 t_2})$$

Equation (IV.2)

$$(^{207}Pb/^{204}Pb) = b_0 + (\mu_1/k)\,(e^{\lambda_2 T} - e^{\lambda_2 t_1}) + (\mu_2/k)\,(e^{\lambda_2 t_1} - e^{\lambda_2 t_2})$$

where t_1 is the time when Pb was removed from system 1 and transferred to system 2, and t_2 is the time when Pb was removed from system 2 after which its isotopic composition remained constant. $t_2=0$, since Pb evolution continues up to the present, when the isotopic composition is determined. Moreover, we simplify the Single-Stage component of equations IV.1 and IV.2 with A and B respectively. Thus, we obtain:

Equation (IV.3)

$$(^{206}Pb/^{204}Pb) = A + \mu_2(e^{\lambda_1 t_1} - 1)$$

Equation (IV.4)

$$(^{207}Pb/^{204}Pb) = B + (\mu_2/k)\;\;(e^{\lambda_2 t_1} - 1)$$

Both equations can be combined to eliminate μ_2:

Equation (IV.5)

$$m = \frac{(^{207}Pb/^{204}Pb) - B}{(^{206}Pb/^{204}Pb) - A} = \frac{1}{k}\,\frac{(e^{\lambda_2 t_1} - 1)}{(e^{\lambda_1 t_1} - 1)}$$

This is the equation of a family of straight lines passing through a point with A and B as coordinates, and whose slopes are given by:

Equation (IV.6)

$$m = \frac{1}{k}\,\frac{(e^{\lambda_2 t_1} - 1)}{(e^{\lambda_1 t_1} - 1)}$$

In other words, a two-stage Pb lies on a secondary isochron that passes through a point on the growth curve of system 1 and whose slope depends only on the interval of time t_1-t_2 during which the lead resided in system 2. In the present case, $t_1-t_2=2.685\times10^9$ years. This latter value and equation IV.6 were used to calculate the slope of the secondary isochron fitting the distribution of the lead isotopic composition from the porphyries and the slates. This slope has a value of 0.183526.

CALCULATION OF THE μ_1 VALUE OF THE SOURCE RESERVOIR OF THE PORPHYRIES

The $^{206}Pb/^{204}Pb$ and $^{207}Pb/^{204}Pb$ ratios of the porphyry and slate samples lying along the secondary isochron are related to each other by an equation in the form of:

Equation (IV.7)

$$(^{207}\mathrm{Pb}/^{204}\mathrm{Pb}) = i + m\,(^{206}\mathrm{Pb}/^{204}\mathrm{Pb})$$

The lead isotope ratios of the porphyry and slate samples and the slope m can be used to determine i. The average value obtained for i is 12.029. Thus, i represents the intercept between the secondary isochron and the ^{207}Pb/^{204}Pb axis.

Since the 2.685x10^{9} years isochron, the secondary isochron with a slope m=0.183526 and the growth curve of the porphyry source reservoir must have a common intercept, we can use equations II.1, II.2, and IV.7 to determine the μ_1 value of this reservoir. Equations II.2 and IV.7 can be combined in the form of:

Equation (IV.8)

$$i + m\,(^{206}\mathrm{Pb}/^{204}\mathrm{Pb}) = b_0 +$$

$$(\mu/k)\ (e^{\lambda_2 T} - e^{\lambda_2 t})$$

Equations II.1 and IV.8 in turn can be combined as follows:

Equation (IV.9)

$$i + m\,[a_0 + \mu\,(e^{\lambda_1 T} - e^{\lambda_1 t})] = b_0 +$$

$$(\mu/k)\ (e^{\lambda_2 T} - 3^{\lambda_2 t})$$

Finally, the growth curve is determined using equations II.1 and II.2 and μ_1 obtained in equation IV.9. μ is kept as a constant in both equations II.1 and II.2, and different values for t yield ^{207}Pb/^{204}Pb ratios as a function of ^{206}Pb/^{204}Pb ratios, which when plotted allow us to trace the growth curve with the given μ_1 value.

Grant 284 Paleomagnetism and Rock Magnetism of the Mulcahy Lake Gabbro and the Lac des Iles Complex

H.C. Palmer

Department of Geophysics, University of Western Ontario, London

ABSTRACT

Anisotropy of magnetic susceptibility data from sites within the Mulcahy Lake Gabbro faithfully mimic megascopic foliation and modal layering. At a number of localities within the Mulcahy Lake Gabbro, a magnetic lineation can be defined that at one locality at least, parallels the lineation recorded by the major phase, orthopyroxene. If the magnetic lineations reflect magmatic flow, currents were to or from the north and northeast assuming a "U" or bowl-shaped initial configuration of the body. Remanence data from the Mulcahy Lake Gabbro also confirm the original shape and attitude of the body, inasmuch as Archean-like remanence directions can only be obtained when the layering and foliation are restored to predeformation attitudes.

The ultramafic part of the Lac des Iles Complex is megascopically massive to only weakly foliated and, as a consequence, magnetic fabrics are more poorly defined. A complicating factor in the ultramafic part of the Lac des Iles Complex is its variably serpentinized nature. As a consequence of serpentinization, two generations of magnetite are present in some localities. Second generation magnetite obscures the primary magnetic fabrics. Magnetic fabrics in the gabbroic parts of the Complex complement field-measured megascopic foliations. The original remanence in the Complex has largely been overprinted by nearby Proterozoic diabase. As a consequence, any pre-Logan Sill internal deformation within the Complex remains undetected.

INTRODUCTION

This research project is primarily concerned with defining layering, understanding its mode of formation, and defining its subsequent deformation in each of two mafic bodies exposed in the Wabigoon Subprovince of the Superior Province. These bodies are the Mulcahy Lake Gabbro and the Lac des Iles Complex.

The Mulcahy Lake Gabbro (Figure 284.1) is a 6 km thick layered intrusion of tholeiitic bulk composition (Morrison *et al.* 1986). The Mulcahy Lake Gabbro exhibits several types of layering including planar laminations of feldspar and pyroxenes, rhythmic modal layering of minerals (phase ratio layering), and cryptic layering defined by systematic compositional variation (Sutcliffe and Smith 1985).

The Lac des Iles Complex (Figure 284.2) consists of an ultramafic intrusion centred on Lac des Iles, and a gabbroic intrusion south of the lake (Sutcliffe and Sweeny 1986). Within the ultramafic part of the complex, igneous lamination and layering are only locally visible. The gabbroic intrusion is divisible into a leucogabbro enveloped by gabbronorite. The gabbroic intrusion is divisible into a leucogabbro to the east and a gabbronorite to the west, with subsidiary mixed-magma, pyroxenite and anorthosite phases. The leuco-gabbrro is weakly layered due to the development of magnetite-rich layers, pyroxene-rich layers, and locally has an igneous lamination (Sutcliffe and Sweeny 1986). Most of the sulphide mineralization of economic importance occurs near the eastern gabbro-western gabbro interface.

The primary techniques used in this study are the measurement of anisotropy of magnetic susceptibility (AMS) and the natural remanent magnetization (NRM).

The anisotropy of magnetic susceptibility in minerals, the dependence of susceptibility on the direction along which it is measured in a sample, arises from either fundamental anisotropy in the crystal structure or from nonsphericity in the shape of mineral particles (Collinson 1983). Since magnetite is the dominant magnetic phase in these Archean rocks, any magnetic anisotropy measured will be a reflection of the preferred alignment of nonspherical magnetite particles. Cumulus magnetite of elongated or platy shape can be aligned by magmatic flow and intercumulus magnetite grains may have their shapes controlled by the alignment of nonequant major cumulate phases. Thus, magnetic anisotropy has come to be used as a profitable tool for the detection of rock fabrics which might not otherwise be apparent.

The NRM, in contrast to the AMS, exists independently of a presently applied magnetic field. The NRM is the rock's permanent magnetization. It is a vector resultant of several magnetizations which a rock has acquired during its history. Some of these magnetic components may be geologically recent; isothermal remanence may be acquired by lightning strikes at the outcrop or by viscous decay and viscous buildup over years in geologically recent magnetic fields. Geologically useful components of the NRM are those acquired during initial cooling and those acquired as a result of postsolidus chemical reactions in which a new ferrimagnetic phase is grown in the ambient earth's magnetic field. These geologically useful remanences are called thermoremanent magnetization (TRM) and chemical remanent magnetization (CRM) respectively. In igneous rocks, the TRM is the desired component and its isolation may provide evidence for differential rotation of parts of an intrusive body or for rotation of the igneous body as a whole. The isolation of the TRM component from the total NRM in a rock is based on the belief that at least some of the TRM resides in ferrimagnetic grains with the highest blocking temperatures and remanent coercivities. Its isolation in old, coarse-grained rocks necessitates exhaustive and time-consuming thermal and alternating field demagnetization experiments.

The objectives of this study are to define the orientation of magnetic rock fabrics and to correlate these with rock fabrics as viewed in outcrop. Where megascopic fabrics are not visible, the AMS data are

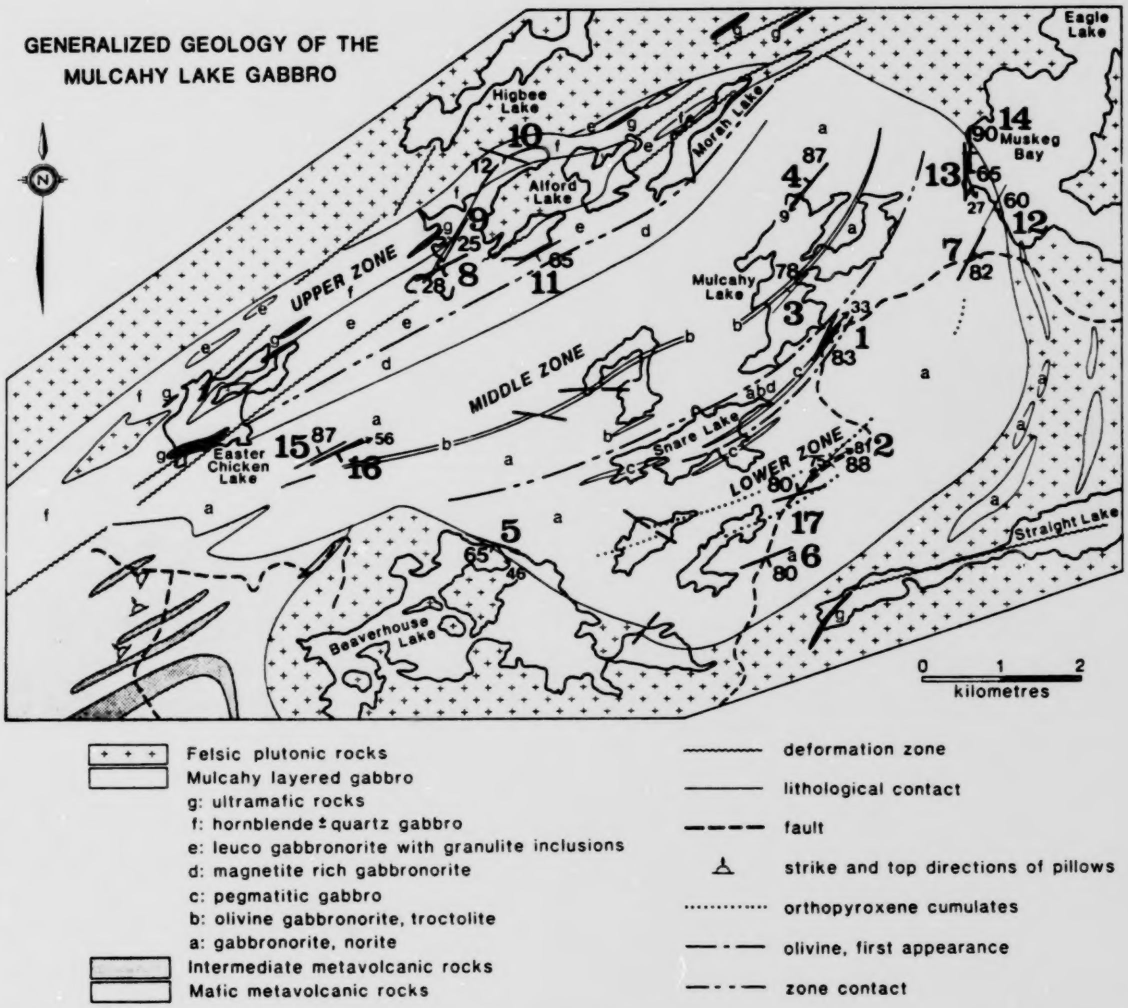

Figure 284.1. *Geological map of the Mulcahy Lake Gabbro with AMS data which is portrayed in Figure 284.3 represented with strike and dip symbols. For those sites where K-max is determined with an $\alpha_{95}<10^\circ$, a magnetic lineation is considered to be defined and this is represented by a plunge symbol. The weight of the symbol is controlled by the precision with which K-min is determined:*
Heavy weight = Mean K-min having $\alpha_{95}<5^\circ$
Medium weight = Mean K-min having $\alpha_{95}<10^\circ$
Light weight = Mean K-min having $\alpha_{95}>10^\circ$

used to extend the spatial range of fabric information. The remanence data may be used to test the hypothesis that the Mulcahy Lake Gabbro represents a tilted U-shaped sheet (Morrison *et al.* 1986) and may enable the determination of the original attitude of the members of the Lac des Iles Complex.

FIELD AND LABORATORY PROCEDURES

An average of five field-drilled cores (samples) were taken at 17 sites within the Mulcahy Lake Gabbro and at 34 sites within the Lac des Iles Complex. Because many of the rocks in these bodies are sufficiently magnetic to affect magnetic compass readings, all azimuthal components of orientation for the samples were obtained by sun compass.

From each oriented sample, typically two paleomagnetic specimens were prepared. The anisotropy of magnetic susceptibility of each specimen was measured using a Sapphire Instruments SI-2 instrument coupled to a Zenith 150 personal computer. The determination of the principal axes of the susceptibility ellipsoid for each specimen was made by two repeat measurements using a six position orientation pattern. The natural remanence (NRM) of all specimens was measured using a Schonstedt DSM-1 spinner magnetometer. At least three independently oriented specimens from each collecting site in the

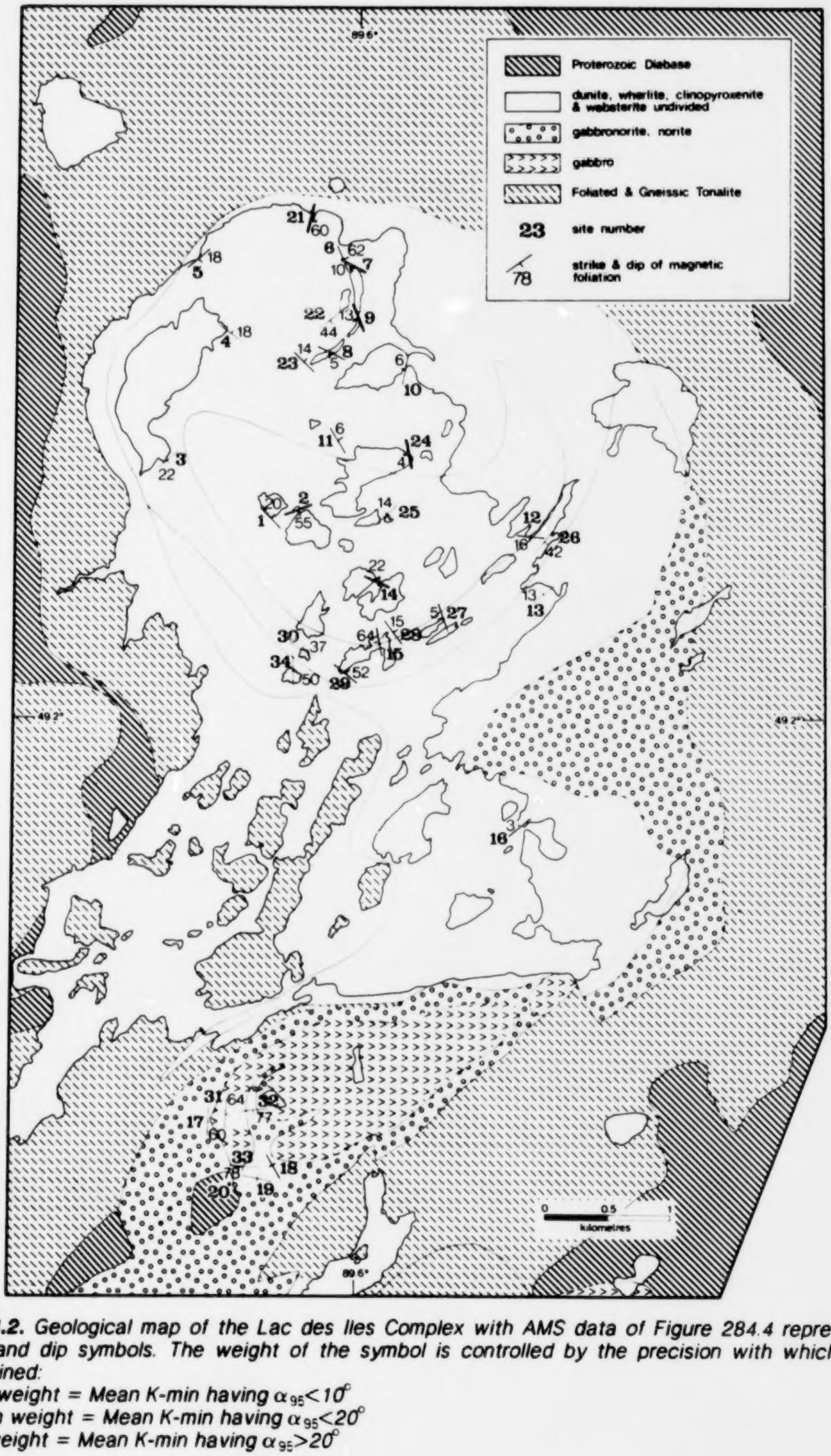

Figure 284.2. *Geological map of the Lac des Iles Complex with AMS data of Figure 284.4 represented by strike and dip symbols. The weight of the symbol is controlled by the precision with which K-min is determined:*
Heavy weight = Mean K-min having $\alpha_{95} < 10^{\circ}$
Medium weight = Mean K-min having $\alpha_{95} < 20^{\circ}$
Light weight = Mean K-min having $\alpha_{95} > 20^{\circ}$

Mulcahy Lake Gabbro and at least two from each site in the Lac des Iles Complex were subjected to alternating field (AF) demagnetization. Only a few specimens have been examined by thermal demagnetization. For the demagnetization experiments, Schonstedt GSD-5 and TSD-1 instruments were employed. Characteristic directions, and any other components manifested by linear segments on orthogonal demagnetization diagrams (Zijderveld 1967), were estimated using the Principal Component Analysis computer program of Kirschvink (1980) as modified by Halls (1986).

MAGNETIC ANISOTROPY RESULTS

The magnetic anisotropy of a rock can be visualized as a triaxial ellipsoid with semiaxes proportional to K_1, K_2, and K_3. Depending on the relative values of these quantities, the geometry of the figure can range from a prolate ellipsoid, through a sphere, to an oblate ellipsoid. A number of numerical measures, depending on K_1, K_2, and K_3, of anisotropy magnitude, degree of lineation, and foliation and of shape have been proposed and these are summarized by Tarling (1983, Table 6.3).

A complementary way of analyzing AMS data is to plot the directions of maximum, intermediate, and minimum susceptibility axes on stereo or equal area net diagrams for each specimen and assess the groupings of these directions on a site-by-site basis (Figures 284.3 and 284.4). In interpreting the alignment of susceptibility axes, it must be remembered that susceptibility axes lack polarity. As a consequence, most directions are plotted on the lower hemisphere; upper hemisphere directions have been chosen for some axes in order to produce more homogeneous within-site groupings. A magnetic foliation plane can be mapped as the plane normal to the mean of the minimum susceptibility axes for each site. Since the K_1, K_2, and K_3 axes are constrained to be orthogonal, the magnetic foliation plane contains the mean maximum and mean intermediate axes. The AMS directional results, plotted on equal area net projections, are shown in Figure 284.3 for Mulcahy Lake Gabbro sites and in Figure 284.4 for Lac des Iles sites.

With respect to the AMS directional data from the Mulcahy Lake Gabbro, a number of features are apparent (Figure 284.3):

1. Groupings of minimum, intermediate, and maximum axes are generally good; the data from sites 3, 9, 12, and 15 are exceptions.
2. The magnetic foliation planes have steep attitudes; sites 8, 9, and 10, all at high stratigraphic levels, are exceptions.
3. Maximum axes are well grouped at sites 1, 2, 4, 5, 13, 16, and 17, implying that magnetic lineations are developed at these locations.

The attitudes of the magnetic foliation planes have been plotted in Figure 284.1 as conventional strike and dip symbols. In addition, at the seven sites where the maximum susceptibility axes are well grouped ($\alpha_{95}<10^\circ$), plunge symbols have been added to the strike and dip symbol. An inspection of Figure 284.1 shows that the magnetic attitudes are in excellent agreement with the trend of layering and foliation in the lower and middle zones. In general, foliation is not well developed in upper zone rocks but, where present, dips are steep (Sutcliffe and Smith 1985). Although foliation was not observed in the field at upper zone sites 8, 9, and 10, magnetic foliation planes have shallow attitudes at these localities. The reason for the lack of agreement between field-measured foliations and magnetic foliations in the upper zone is not understood.

The magnetic lineations recorded from the lower and middle zone rocks may have petrological significance in terms of paleoflow patterns. Morrison *et al.* (1986) reported conventional fabric results from an orthopyroxene cumulate at their locality 3. These authors found that orthopyroxene *c* axes lie within the plane of layering with a 70° plunge to the southwest. Their study locality is near sites 2 and 17 of the present study where plunges of 81° and 75° have been measured. These results suggest that magnetic lineations, reflecting the preferred alignment of magnetite, are indirect estimators of the linear fabric of the major minerals in these rocks. If this alignment is an indicator of paleoflow pattern, its original orientation may be of some petrological interest. The major problem with this type of analysis is to decipher the original attitudes of the layers containing the lineations. Blackburn (1978) established, from observations along a cross section through the central part of the gabbro, that the layers face to the northwest. He further speculated that the body was emplaced as a sheet and subsequently tilted into its present vertical position. The subsequent mapping of Sutcliffe and Smith (1985) and the petrological work of Morrison *et al.* (1986) indicated that the structure is akin to a tilted bowl. If this analogy is correct, six of the seven well-determined lineations are from sites parallel to the base of the bowl; restoration of these lineations to their pretilt attitude is straightforward and these restored lineations are recorded in Table 284.1. These azimuths are not random but are north and northeasterly in trend. Whether paleoflow, implied by these trends, was toward the north and northeast or from the north and northeast, is indeterminate. The well determined lineation recorded at site 13 (Figure 284.3b), located on the eastern bulbous end of the intrusion (Figure 284.1), presents more ambiguity in restoration. Resuming the bowl analogy, it would be located on the steep sides of the bowl. However, at the present time, the foliation dips outward rather than inward. The rocks at this location may have undergone two components of rotation; one, an oversteeping of initial dip about a north-south axis and two, the tilting to the northwest which affected the body as a whole. Undoing these inferred rotations sequentially produces a lineation with a bearing of 273° and a plunge of 50°. It should be understood that had the rotations been done in the opposite order, a different result would have been obtained as finite rotations are not commutative. However, the order chosen produced the more consistent pattern with the remanence data at site 12 which is also at the eastern, oversteepened end of the intrusion (*see* Figure 284.5). The geological history was probably one of simultaneous deformations and the correct approach to restoration would be a sequence of in-

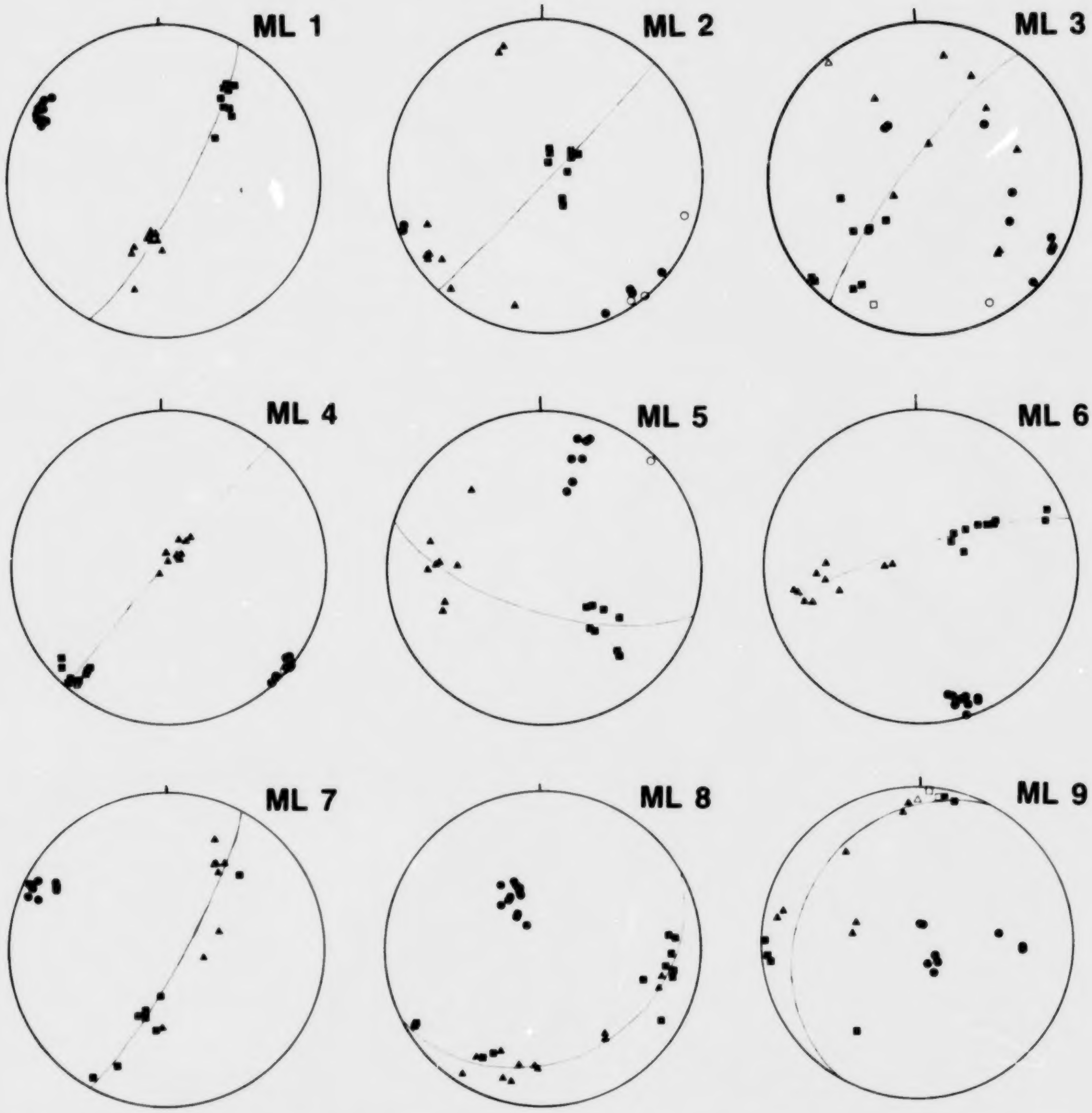

Figure 284.3a. *Equal area projections showing maximum (squares), intermediate (triangles), and minimum (dots) susceptibility axes in oriented specimens from Mulcahy Lake Gabbro sites. The minimum can be regarded as the pole to the magnetic foliation plane which contains the mean intermediate and mean maximum susceptibility axes.*

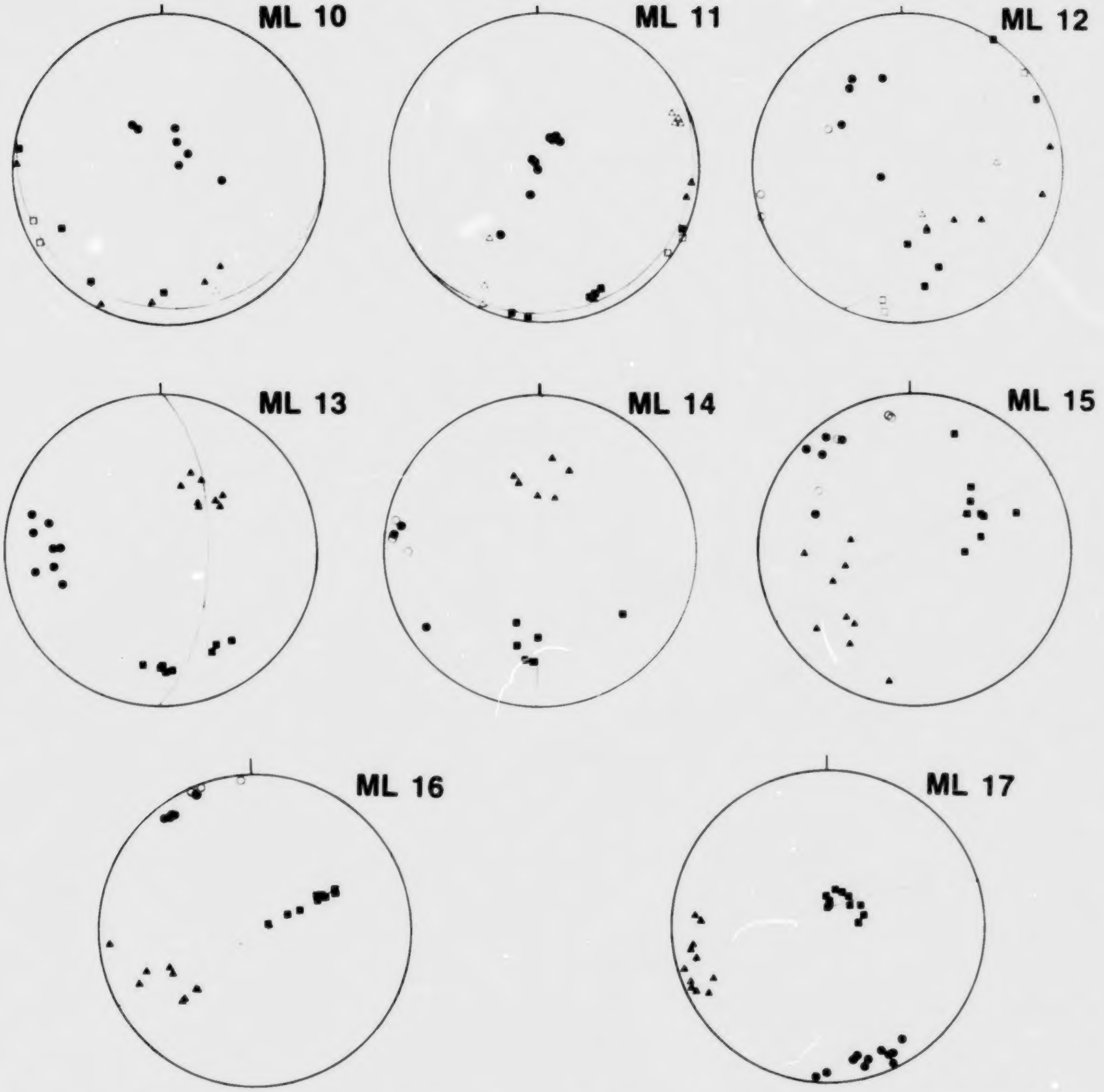

Figure 284.3b. *Equal area projections showing maximum (squares), intermediate (triangles), and minimum (dots) susceptibility axes in oriented specimens from Mulcahy Lake Gabbro sites. The minimum can be regarded as the pole to the magnetic foliation plane which contains the mean intermediate and mean maximum susceptibility axes.*

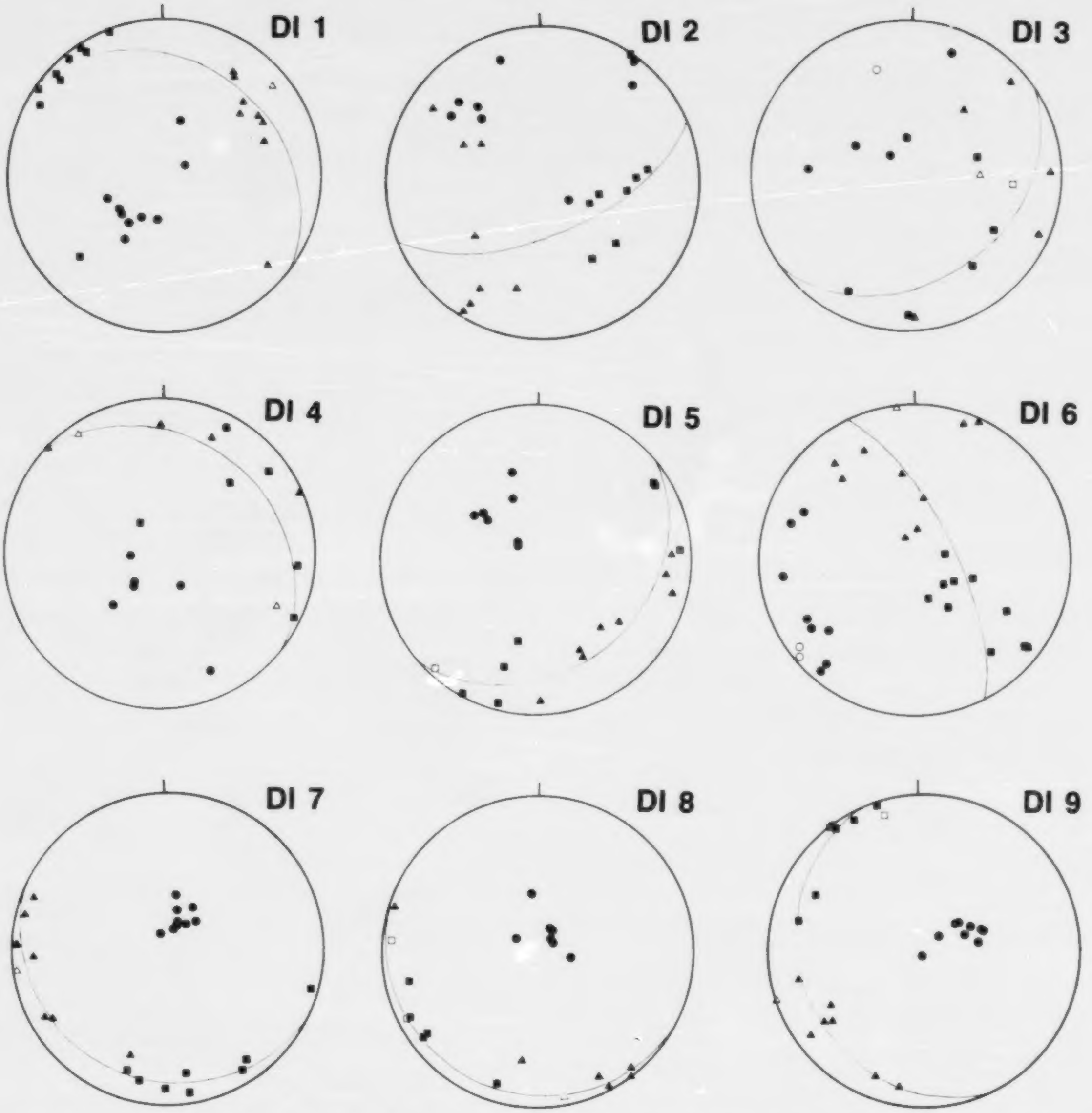

Figure 284.4a. *Equal area projections showing maximum (squares), intermediate (triangles), and minimum (dots) susceptibility axes in oriented specimens from Lac des Iles Complex sites. The minimum can be regarded as the pole to the magnetic foliation plane which contains the mean intermediate and mean maximum susceptibility axes.*

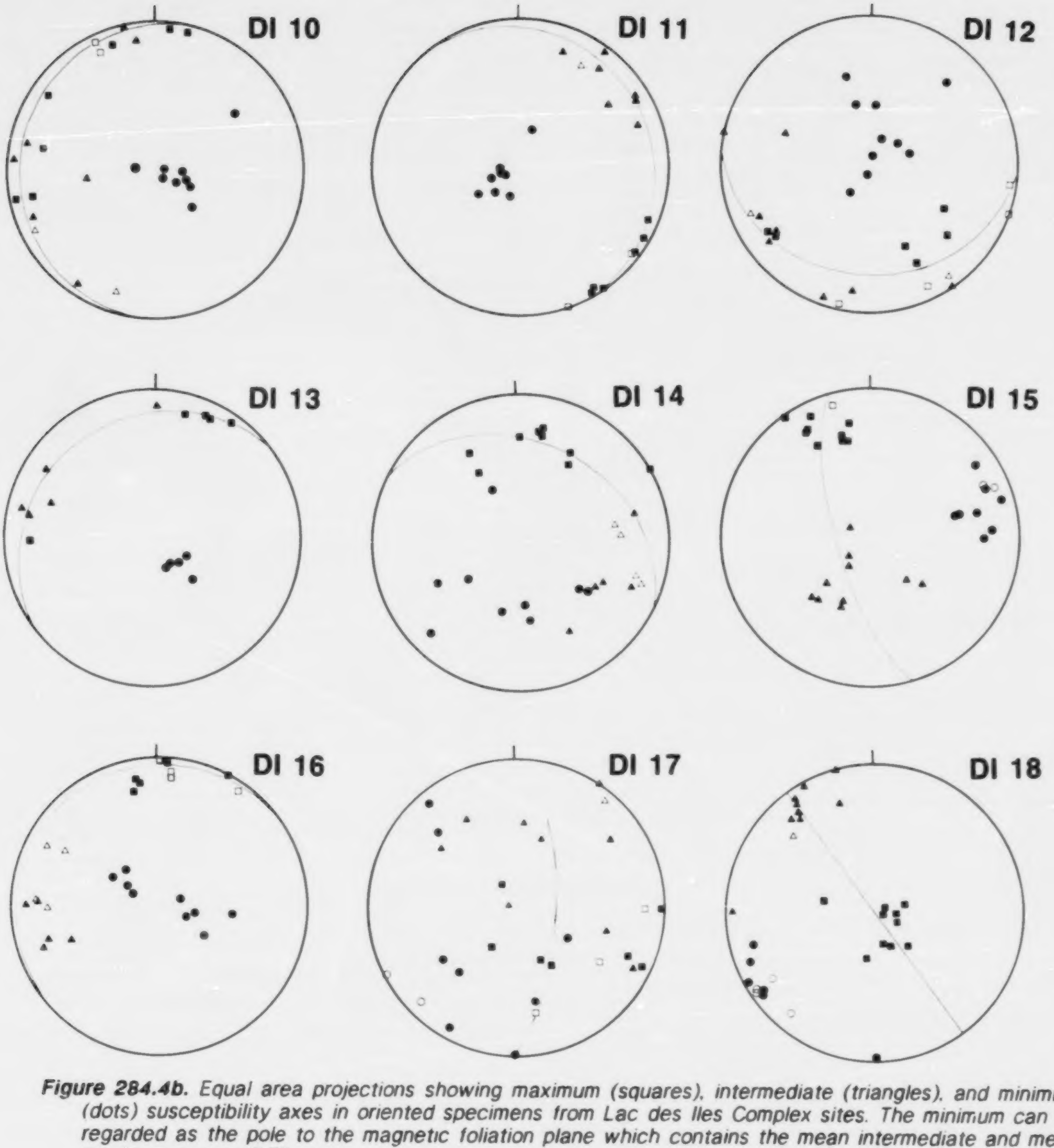

Figure 284.4b. *Equal area projections showing maximum (squares), intermediate (triangles), and minimum (dots) susceptibility axes in oriented specimens from Lac des Iles Complex sites. The minimum can be regarded as the pole to the magnetic foliation plane which contains the mean intermediate and mean maximum susceptibility axes.*

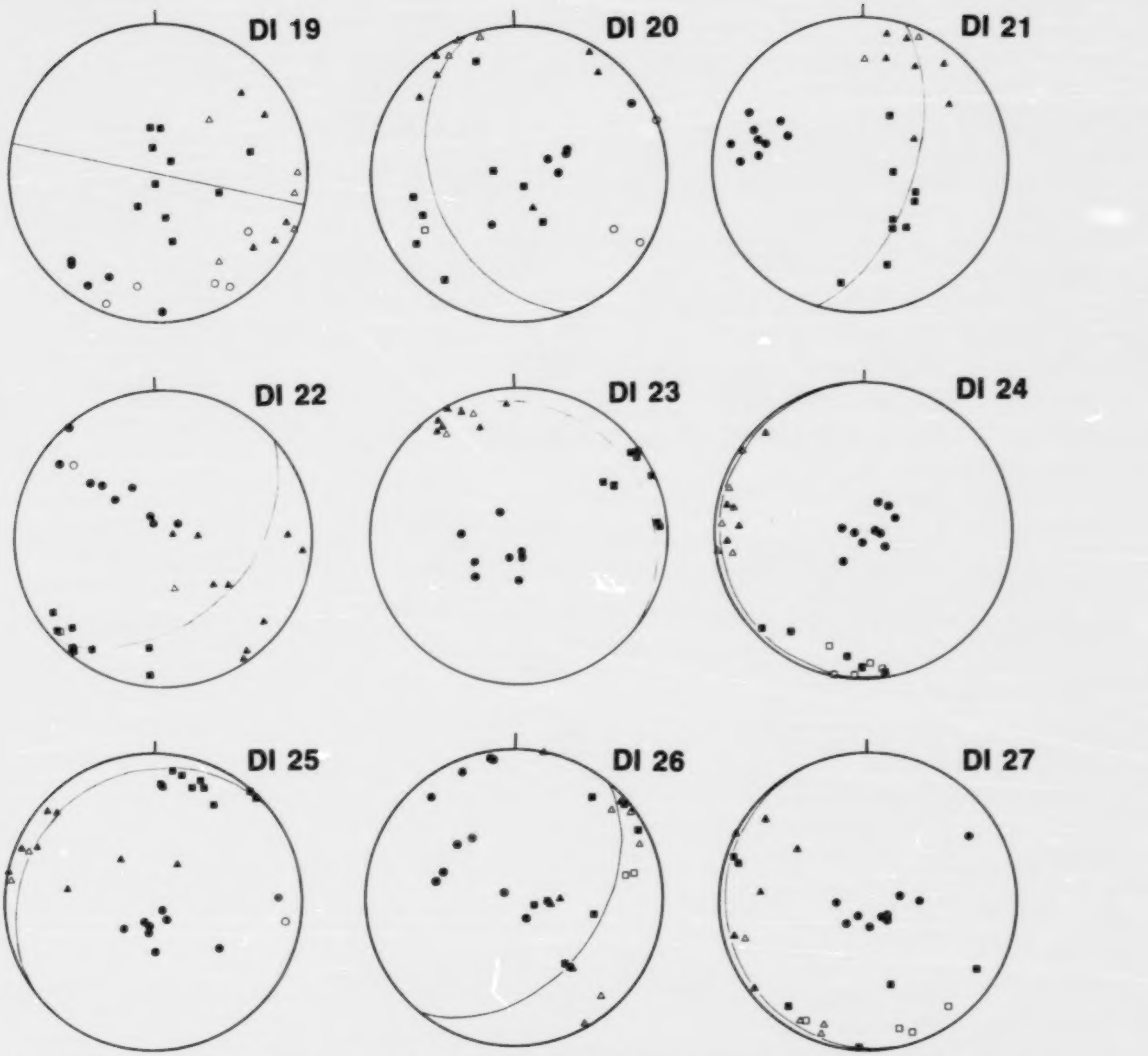

Figure 284.4c. *Equal area projections showing maximum (squares), intermediate (triangles), and minimum (dots) susceptibility axes in oriented specimens from Lac des Iles Complex sites. The minimum can be regarded as the pole to the magnetic foliation plane which contains the mean intermediate and mean maximum susceptibility axes.*

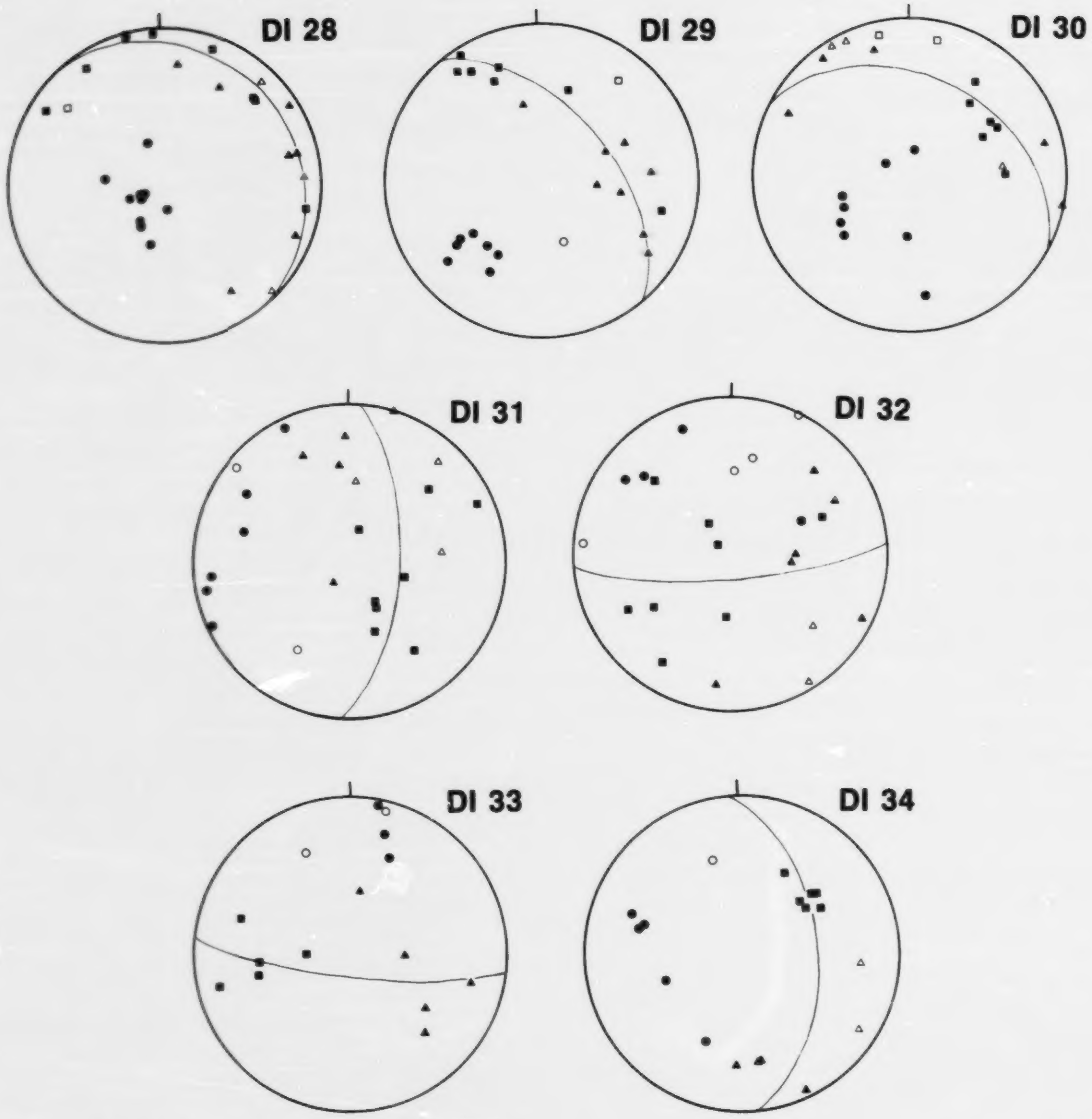

Figure 284.4d. Equal area projections showing maximum (squares), intermediate (triangles), and minimum (dots) susceptibility axes in oriented specimens from Lac des Iles Complex sites. The minimum can be regarded as the pole to the magnetic foliation plane which contains the mean intermediate and mean maximum susceptibility axes.

TABLE 284.1. RESTORATION OF MAGNETIC LINEATIONS IN THE MULCAHY GABBRO.

Site	Directions of K_{max}	Foliation/Layering Attitude	Facing Direction & Value of Dip	Restored Lineation Direction
ML-1	039° + 34°	030°/83°SE	300° + 97°	356°
ML-2	060° +81°	045°/88°SE	315° + 92°	324°
ML-4	223° +08°	042°/87°NW	312° + 87°	232° = 053°
ML-5	136° + 46°	110°/65°S	020° + 115°	058°
ML-16	066° + 56°	063°/88°SE	333° + 92°	007°
ML-17	032° + 75°	073°/80°NW	343° + 80°	356°
ML-13	166° + 27°	001/65°E	271° + 30° & 326° + 80°	273° + 50°

finitesimal rotations. Inasmuch as the amount of oversteepening is a guess, the infinitesimal rotation approach was not attempted.

An inspection of the AMS directional data from sites in the Lac des Iles Complex (Figure 284.4a,b,c,d) reveals that magnetic anisotropy is not as well developed as in the Mulcahy Lake Gabbro (Figure 284.3a,b). A second feature is that at the majority of Lac des Iles sites, the magnetic fabric is subhorizontal. The majority of the steeply inclined magnetic foliations (sites 17, 18, 19, 31, 32, and 33) are confined to the gabbros (Figure 284.2). Within the gabbros, the magnetic fabrics are in good agreement with the attitude of megascopic foliation. Within the ultramafic portion of the Lac des Iles Complex form lines are shown which divide regions dominated by clinopyroxenite, websterite, and dunite and wherlite. Magnetic fabrics, summarized as conventional strike and dip symbols in Figure 284.2. bear no systematic relationship to these petrological boundaries. The most probable complicating factor is that within the Lac des Iles Complex, serpentine is variably developed. The production of serpentine from olivine and orthopyroxene results in magnetite as an additional product of the reaction It is possible therefore, that at least some of the derived fabrics are resultants of primary and secondary magnetite fabrics.

REMANENT MAGNETIZATION

MULCAHY LAKE GABBRO

The selection criteria adopted for choosing geologically meaningful remanence directions from among the samples measured were:

1. the demagnetization data, when plotted on an orthogonal demagnetization diagram, produced a linear array which converged to the origin
2. the linear array was defined with a mean angular deviation (MAD) angle (Kirschvink 1980) less than 10°. Most accepted characteristic directions were, in fact, defined with MAD angles less than 5°
3. the characteristic directions selected had to have within-site consistency. The mean direction for a site had to be defined with a precision parameter (Fisher 1953) greater than 25.

Sites which satisfied the above selection criteria are shown in Figure 284.5a. An additional two sites (2 and 10) had samples which satisfied criteria 1 and 2 but whose site-means were defined with lower precision ($k>10<25$). These also are shown in Figure 284.5a. Thus only nine of the 17 sampling sites produced geologically meaningful information. The remaining eight sites contain a large number of samples with high intensities of NRM and the characteristic directions, although defined with high precision, lack within-site directional consistency. Most or all of these sites have had their remanence affected by the magnetic fields of lightning strikes.

A noteworthy feature of the results is that two polarities of remanence have been recovered. Reverse polarities are from sites in the lower two thirds of the intrusive whereas the normal polarity sites are in the upper third of the body. This stratigraphic separation of polarities suggests that a reversal of the earth's field took place during initial cooling. A confirmation that the remanence is primary is provided by the fold test where the site-mean characteristic directions are referenced to the paleohorizontal (Figure 284.5b). The overall precision of the mean, without regard to polarity, is defined with a k of 18 before unfolding and with a k of 26 when restored to the estimated paleohorizontal. The restoration of the directions to the paleohorizontal was done in the conventional manner, i.e. by rotation about the line of strike by the value of dip. An alternative restoration is shown (Figure 284.5b) for site 12. This site is located at the eastern margin (Figure 284.1) where initial dips may have been present. A compound rotation, using the same rotations as were used for the AMS data at site 13 (*see* Table 284.1) was performed. The more complex rotation improves the overall grouping of the remanence data and as a consequence, gives indirect support for the tilted bowl analogy used in the restoration of the fabric data at site 13. A third piece of evidence that the remanence data portrayed in Figure 284.5 is primary is that the remanence directions, when referenced to the present subvertical attitude of the layers, yield a pole position quite unlike any Superior Province Archean one (Dunlop 1985). All known Superior Province Archean magnetizations have moderate to shallow inclinations. Shallow inclinations can only be obtained in the Mulcahy Lake Gabbro when

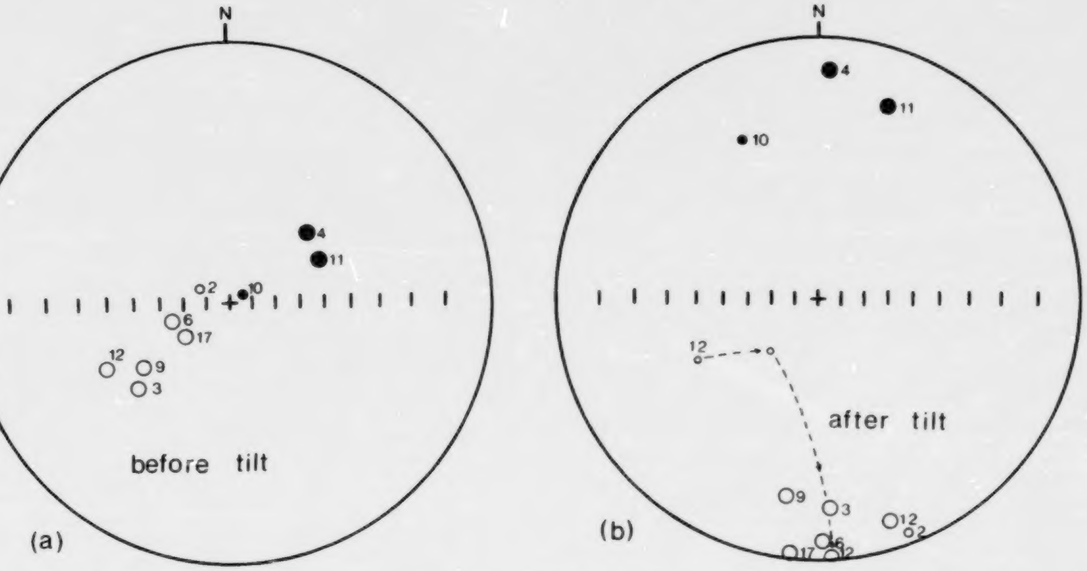

Figure 284.5. *The mean remanence direction from each of seven sites in the Mulcahy Lake Gabbro where the precision of the mean is defined with k>25 (large symbols). In sites 2 and 10, the precision of the mean is defined with k>10 and these are represented with small symbols. Solid symbols are on the lower hemisphere whereas open symbols are on the upper hemisphere. In (a) the directions are shown without a structural correction (before tilt) whereas in (b) the directions are shown after rotation about the line of strike by the value of dip (after tilt). All layers are assumed to face north or northwest. For site 12, an alternative method of restoration, involving two rotations, is shown.*

the remanence directions are referenced to the paleohorizontal (Table 284.2).

LAC DES ILES COMPLEX

The remanence in samples from the Lac des Iles Complex was analyzed in the same manner as was used for the Mulcahy Lake Gabbro. The majority of samples demagnetized to date have had their remanence reset to that possessed by the Logan Sills. The most direct evidence for this is provided by the results from site 20 (Figure 284.2) where the outlier of Proterozoic diabase was sampled in addition to nearby Archean gabbro. Both diabase and gabbro share a common characteristic direction which is identical to that recorded from the Logan Sills in the type area around Lake Nipigon and Thunder Bay (Palmer 1970; Robertson and Fahrig 1971). Many of the Archean gabbro and ultramafic samples, collected at sites far removed from the present outcrop limits of Proterozoic diabase, also share the Logan Sill remanence direction. Others progressively move toward it with demagnetization. Whether a meaningful lower coercivity component can be extracted from these latter samples by the method of converging remagnetization circles (Halls 1976, 1978) will have to await the completion of the demagnetization experiments. An inspection of Figure 284.2 shows that Proterozoic diabase (Logan Sills) crops out both to the east and west of the exposures of the Lac des Iles Complex. Since the Logan Sills occur as subhorizontal sheets, it seems probable that all current exposures of the Complex were once a few tens of metres below the lower contact of these sheets.

CONCLUSIONS AND FUTURE PLANS

Magnetic foliations, as reflected by low field anisotropy measurements, are in good agreement with field-measured megascopic foliations in the Mulcahy Lake Gabbro. Magnetic lineations, recovered from some localities within the Mulcahy Lake Gabbro, probably reflect magmatic flow directions. The present structure of the body is "U" or bowl shaped with the layers parallel to the base of the "U" facing northwest. Restoration of the lineations, recorded from layers in the base of the "U", to their original attitudes implies flow having north and northeasterly directions. At one locality on the eastern, oversteepened limb of the body, a steep, down-dip lineation is inferred. Pairs of oriented polished thin sections have been made from selected samples in which the magnetic anisotropy has been measured. These thin sections will be examined, using quantitative imaging techniques, to confirm the above conclusions by direct observation of the shapes of the magnetite grains.

Natural remanent magnetization, of probable predeformation age, has been recovered from half of the sampled sites in the Mulcahy Lake Gabbro. The structural corrections, applied to these data, give support to the structural corrections applied to the AMS lineation data from which the above paleocurrents have been inferred.

TABLE 284.2. MULCAHY LAKE SITE-MEAN REMANENCE DIRECTIONS AND POLES.

				In Situ		Tilt Corrected		Pole Positions	
Site #	N	R	k	D	I	D	I	Long	Lat
ML 2	4	3.843	19.	292°	- 75°	159°	- 02°	113°E	38°N
ML 3	3	2.999	1588.	227°	- 39°	176°	- 13°	92°E	47°N
ML 4	5	4.942	70.	049°	+ 49°	000°	+08°	87°E	44°N
ML 6	4	3.984	182.	254°	- 63°	179°	- 05°	88°E	43°N
ML 9	4	3.884	26.	240°	- 42°	193°	- 19°	67°E	49°N
ML 10	4	3.698	10.	054°	+ 84°	333°	+ 21°	126°E	46°N
ML 11	3	2.941	34.	065°	+ 49°	019°	+ 14°	60°E	45°N
ML 12	3	2.928	28.	243°	- 34°	178°	- 01°(a)	90°E	41°N
ML 17	4	3.959	73.	227°	- 68°	183°	+ 00°	83°E	40°N
MEAN	9	8.552	18.	060°	+ 57°				
MEAN	9	8.689	26.			358°	+ 10°		
MEAN	9	8.734	30.					90°E	45°N

Notes:

N is the number of samples used in the analysis; R and k are the statistical parameters of Fisher (1953); D and I are declination and inclination in degrees. Long and Lat are the Longitude and Latitude of the vertical geomagnetic pole.
(a) Tilt correction for this site involved a compound rotation.

In the calculations of means, directions have been converted to normal polarity and all poles are converted to northern hemisphere poles.

Magnetic fabrics from the gabbroic portions of the Lac des Iles Complex are in good agreement with field-measured megascopic foliations. Magnetic fabrics from the ultramafic portion of the Complex are, however, dominantly shallow with erratic trends in strike and dip. The fabric picture may be improved when filtering of the data is performed. Such filtering will involve: a) measures of the degree of anisotropy, and b) the quantitative removal of the contribution to the total fabric by secondary magnetite produced as a consequence of the serpentine reaction. The remanence data from the Lac des Iles Complex have only been partially analyzed. Whether sufficient remanence data, uncontaminated by the effects of nearby Proterozoic sills, can be obtained to resolve the deformational history of the complex remains to be seen.

ACKNOWLEDGMENTS

An initial paleomagnetic and AMS study on the Mulcahy Lake Gabbro was made by S. Wrigley and formed her B.Sc. thesis at the University of Western Ontario. Her results have been incorporated in this study. Able assistance in the field and laboratory during the Summer of 1986 was provided by K. Nurse during tenure of a NSERC summer scholarship. Logistical help, scientific advice, and hospitality during the 1986 field season were provided by R. Sutcliffe and A. Smith (Geologists, Precambrian Geology Section, Ontario Geological Survey, Toronto). Many of the laboratory measurements and much of the computer programming used in the study were ably performed by D. Lacina of the University of Western Ontario, London.

REFERENCES

Blackburn, C.E.
1978: Populus Lake—Mulcahy Lake Area; p.36- 39 *in* Summary of Field Work, 1978, by the Ontario Geological Survey, edited by V.G. Milne, O.L. White, R.B. Barlow and J.A. Robertson, Ontario Geological Survey, Miscellaneous Paper 82, 235p.

Collinson, D.W.
1983: Methods in Rock Magnetism and Palaeomagnetism; Chapman and Hall, 503p.

Dunlop, D.J.
1985: Paleomagnetism of Archean Rocks from Northwestern Ontario: V. Poohbah Lake Alkaline Complex, Quetico Subprovince; Canadian Journal of Earth Sciences, Volume 22, p.27- 38.

Fisher, R.A.
1953: Dispersion on a Sphere; Proceedings of the Royal Society of London, Series A, Volume 217, p.295- 305.

Halls, H.C.
1973: A Least Squares Method to Find a Remanence Direction from Converging Remagnetization Circles; Geophysical Journal of the Royal Astronomical Society, Volume 45, p.297- 304.
1978: The Use of Converging Remagnetization Circles in Palaeomagnetism; Physics of the Earth and Planetary Interiors, Volume 16, p.1-11.

1986: Paleomagnetism, Structure, and Longitudinal Correlation of Middle Precambrian Dikes from Northwestern Ontario and Minnesota; Canadian Journal of Earth Sciences, Volume 23, p.142- 157.

Kirschvink, J.L.
1980: The Least-Squares Line and Plane and the Analysis of Palaeomagnetic Data; Geophysical Journal of the Royal Astronomical Society, Volume 62, p.699- 719.

Morrison, D.A., Maczuga, D.E., Phinney, W.C., and Ashwal, L.D.
1986: Stratigraphy and Petrology of the Mulcahy Lake Layered Gabbro: An Archean Intrusion in the Wabigoon Subprovince, Ontario; Journal of Petrology, Volume 27, Part 2, p.303- 341.

Palmer, H.C.
1970: Paleomagnetism and Correlation of Some Middle Keweenawan Rocks, Lake Superior; Canadian Journal of Earth Sciences, Volume 7, p.1410- 1436.

Robertson, W.A., and Fahrig, W.F.
1971: The Great Logan Paleomagnetic Loop—The Polar Wandering Path from Canadian Shield Rocks During the Neohelikian Era; Canadian Journal of Earth Sciences, Volume 8, p.1355- 1372.

Sutcliffe, R.H., and Smith, A.R.
1985: Precambrian Geology of the Mulcahy Gabbro, District of Kenora; Ontario Geological Survey, Map P.2826, Geological Series-Preliminary Map, scale 1:15 840 or 1 inch to 1/4 mile. Geology 1984.

Sutcliffe, R.H., and Sweeny, J.M.
1986: Precambrian Geology of the Lac des Iles Complex, District of Thunder Bay; Ontario Geological Survey, Map P.3047, Geological Series-Preliminary Map, scale 1:15 840 or 1 inch to 1/4 mile. Geology 1985.

Tarling, D.H.
1983: Palaeomagnetism—Principles and Applications in Geology, Geophysics and Archaeology; Chapman and Hall, 379p.

Zijderveld, J.D.A.
1967: A.C. Demagnetization of Rocks: Analysis of Results; p.245- 286 *in* Methods in Palaeomagnetism, edited by D.W. Collinson, K.M. Creer, and S.K. Runcorn, Elsevier, Amsterdam.

Grant 286 The Geochemistry, Origin, and Economic Potential of Platinum Group Element Bearing Rocks of the Lac des Iles Complex, Northwestern Ontario

J.M. Sweeny and A.D. Edgar

Department of Geology, University of Western Ontario, London

ABSTRACT

This paper presents the results of the first year of a study of the Platinum Group Element (PGE) mineralization in the area of the Roby Zone, Lac des Iles complex, northwestern Ontario. The mineralized zone consists of several varieties of gabbroic rocks which can be distinguished, on the basis of detailed mapping, petrography, and whole rock and mineral chemistry (principally pyroxenes), as the western and eastern gabbros and the hybrid zone. The degree of alteration and grain.size of the gabbroic rocks varies, ranging from those in which alteration of pyroxenes is 100% to those with almost pristine pyroxenes. Twenty-four samples (four each from the western and eastern gabbros, 12 from the hybrid zone, and four channel samples from within this zone) have been analyzed for all PGEs, Au, Cu, Ni, and S. These values have been related to degrees of alteration in the rocks and compared with other PGE deposits using Cu/(Cu+Ni) versus Pt/(Pt+Pd) and chondrite normalized average in 100% S versus PGE+Au plots. These comparisons suggest that the Lac des Iles Deposit may have been formed by more than one process. Future examination of the minerals containing the PGEs, and of silicate minerals, will be done to support the hypothesis.

INTRODUCTION

This summary presents the results for the first year of an investigation into Platinum Group Element (PGE) mineralization in the Lac des Iles Intrusion, northwestern Ontario. The primary objectives of this research are:

1. To map and distinguish the gabbroic phases present within the PGE mineralization zone based on their mineralogy, petrography, and mineral and whole rock chemistry.
2. To relate the PGE mineralization to the stratigraphy of the intrusion based on the first objective.
3. To determine the processes whereby PGE mineralization appears to be associated with pegmatitic gabbroic dikes, breccias, and pyroxenites.
4. To assess the role played by fluids to PGE mineralization as indicated by the altered mineral assemblages.
5. To relate whether PGM (platinum group minerals in surficial samples occur in the same minerals as those found by Talkington and Watkinson (1984) in drill core samples and to assess whether the classification used by these authors is viable in light of detailed surface sampling.

Previous work in this area is detailed in reports by Pye (1968), Dunning (1979), Watkinson and Dunning (1979), Sutcliffe and Sweeny (1985, 1986), Macdonald (1986), Sweeny and Sutcliffe (1986), and Sutcliffe (1986). The results of this study will be in collaboration with ongoing studies of this intrusion being undertaken by the Ontario Geological Survey.

REGIONAL GEOLOGY

The Lac des Iles Complex is the largest of a series of mafic to ultramafic intrusions which form a circular structure approximately 30 km in diameter (*see* Figure 286.1; Sutcliffe 1986). The complex is within the Wabigoon Subprovince lying approximately 15 km north of the Wabigoon and Quetico Subprovince boundary. Initial mapping by Pye (1968) delineated the extent of the complex and recent mapping by Sutcliffe and Sweeny (1986) was undertaken at a scale of 1:15 840.

The Lac des Iles Complex consists of an ultramafic intrusion centred on Lac des Iles and a gabbroic intrusion located south of the lake (Pye 1968; Dunning 1979). The complex is of Archean age and was emplaced into older granitoid rocks, which are predominantly composed of gneissic tonalites. Sutcliffe (1986) showed that the gneisses are located on the periphery of the circular structure and the central portion is occupied by two younger granitoid phases. These include a foliated biotite-hornblende tonalite pluton in the southern part of the core, and a foliated to massive pluton of granodioritic to granitic composition in the northern part (Figure 286.1). These younger granitoids locally intrude the complex.

The ultramafic and mafic rocks of the complex have not been significantly metamorphosed or deformed. Rocks throughout the region are intruded by diabase sheets and dikes of late Proterozoic age (Sutcliffe and Sweeny 1986).

The most significant mineralization found in the region to date occurs in the gabbroic rocks of the southern portion of the Lac des Iles Complex; however, occurrences of PGEs have been identified in the ultramafic portion of the complex (Sutcliffe and Sweeny 1985, 1986). Other sites of PGE mineralization are found in the Tib Gabbro and Demars Lake Intrusion (Sutcliffe 1986) shown in Figure 286.1.

LOCAL GEOLOGY

Dunning (1979) subdivided the gabbroic part of the complex into an "eastern" and a "western" gabbro, and interpreted them as separate intrusive phases. The recent mapping of the area has outlined a complex zone of magma mixing approximately 60 to 300 m wide within the western gabbro adjacent to the contact with the eastern gabbro (Figure 286.2; Sutcliffe and Sweeny 1985, 1986). The outcrop textures indicate a mechanical mixing of the two gabbroic phases and mineral and whole rock chemistry suggest a compositional range between the eastern and western gabbros. This has been termed the

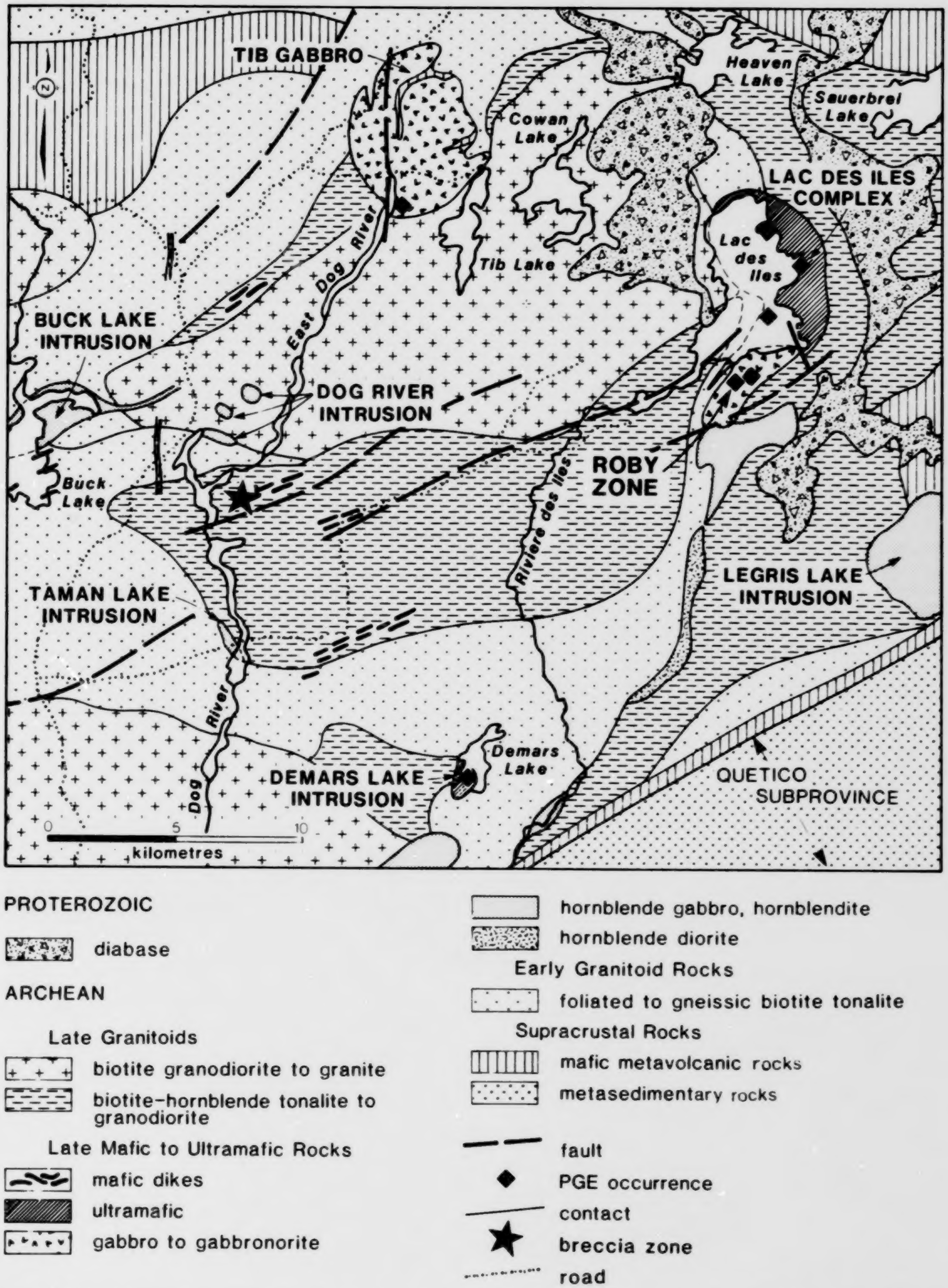

Figure 286.1. Regional geology of the Lac des Iles area showing known PGE occurrences (after Sutcliffe 1986).

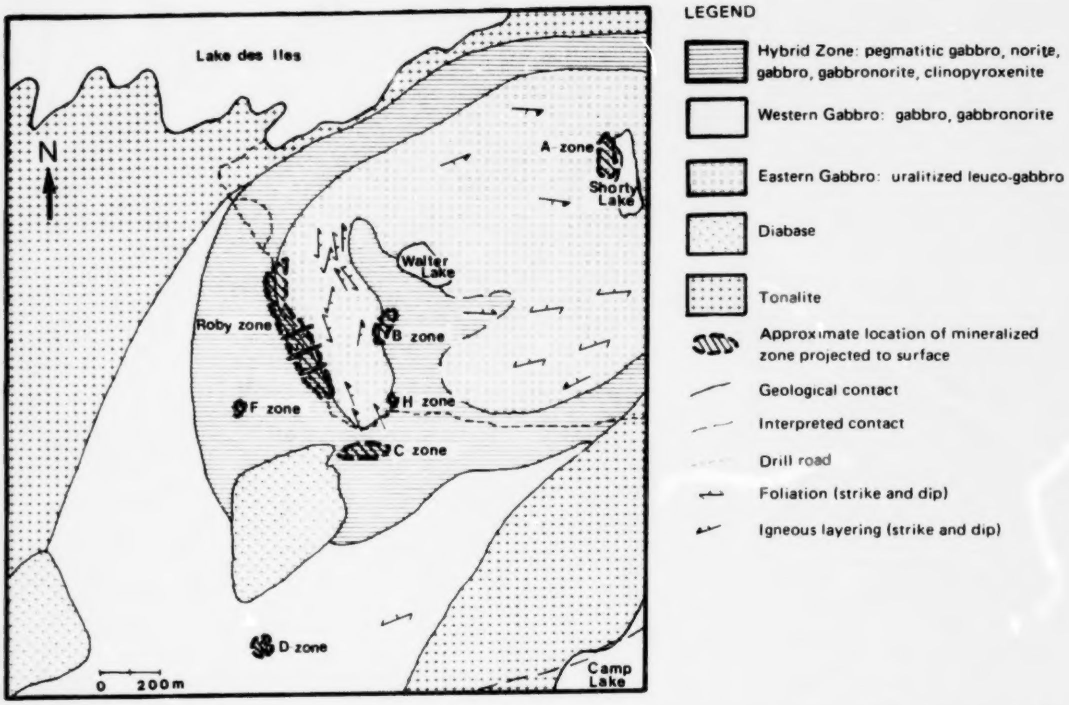
Lake des Iles
N
A zone
Shorty Lake
Walter Lake
Roby zone
B zone
F zone
H zone
C zone
D zone
Camp Lake
0 200m
LEGEND
Hybrid Zone: pegmatitic gabbro, norite, gabbro, gabbronorite, clinopyroxenite
Western Gabbro: gabbro, gabbronorite
Eastern Gabbro: uralitized leuco-gabbro
Diabase
Tonalite
Approximate location of mineralized zone projected to surface
Geological contact
Interpreted contact
Drill road
Foliation (strike and dip)
Igneous layering (strike and dip)

Figure 286.2. *Detailed geology of the Roby zone area showing its relationship to the eastern and western gabbros and the location of the hybrid zone (after Sutcliffe and Sweeny 1986; Sweeny and Sutcliffe 1986).*

"hybrid zone" in the present study. Figure 286.2 also shows the location of the mineralization zones "A" through "F" identified by Gunnex Limited in 1964, and the "Roby zone" outlined by Boston Bay Mines Limited and Texasgulf Incorporated in 1975 and 1976 (Sweeny and Sutcliffe 1986).

The rocks of the western gabbro consist of interlayered cumulate gabbros, gabbronorites, norites, and minor anorthosites. Both sulphide and PGE mineralization are associated with the mafic cumulate rocks as well as pegmatitic gabbroic phases and pyroxenites. Layering within the western gabbro is poorly defined, but does occur within gabbronorites and leucogabbros.

The eastern gabbro is composed mainly of gabbro to leucogabbro with uralitic alteration of clinopyroxene and is weakly layered due to the development of pyroxene-rich horizons (Sweeny and Sutcliffe 1986). These rocks locally show an igneous lamination which is also found in the western gabbro rocks.

The hybrid zone rocks are a combination of lithologies which include gabbros, gabbronorites, norites, pegmatitic gabbros, pyroxenites, and leucogabbros. These rock types appear to be representative of the phases present within the eastern and western gabbros. The main zone of PGE mineralization, the Roby zone, occurs within this heterogeneous hybrid zone.

PETROGRAPHY

Classification of the rocks is based on Streckeisen's (1976) system for mafic and ultramafic rocks. The eastern gabbro consists of medium-grained gabbro to leucogabbro with uralitic alteration of the clinopyroxenes. The western gabbro is generally fresher and consists predominantly of gabbronorite. The hybrid zone is heterogeneous, but is typified by units of coarse-grained to pegmatitic gabbro, norite, leucogabbro, gabbronorite, and pyroxenite (Sweeny and Sutcliffe 1986).

Modal analyses for some of the samples are presented in Table 286.1. These samples were selected because they contained a relatively fresh pyroxene and plagioclase. Many of the samples collected showed little or no primary pyroxene mineralogy and were assigned names based on their field relationships. In some cases the type of pyroxene can be determined from the habit and nature of the amphibole pseudomorphs. The following descriptions are based primarily on thin sections of fresh and altered rocks within the area shown in Figure 286.2. Plagioclase orthopyroxene cumulates appear to be more prevalent than clinopyroxene cumulate rocks.

GABBRO

These are cumulate rocks containing varying proportions of cumulus plagioclase, orthopyroxene, and intercumulus clinopyroxene. Grain size varies from medium to pegmatitic, with the largest grains occurring

TABLE 286.1. MODAL ANALYSES OF LAC DES ILES SAMPLES.

Sample #	Rock Name	Opx	Cpx	Plag	Amph	Chl	Bio	Epidote	Opaques
85-RHS-57	mela-gabbronorite	60	11	20	7	tr	-	-	2
85-RHS-750	norite (oxide rich)	20	-	53	2	-	1	-	25
85-RHS-753	norite	34	tr	58	3	2	-	1	2
85-RHS-775	gabbronorite	38	10	48	3	tr	-	-	1
86-LDI-002	mela-norite	70	tr	13	10	tr	0.5	-	6
86-LDI-010	norite	27	tr	63	7	1	tr	tr	1
86-LDI-019	gabbronorite	27	15	53	3	1	tr	-	1
86-LDI-031	gabbronorite	41	15	32	11	-	-	tr	tr
86-LDI-034	mela-norite	64	0.5	26	6	3	-	-	tr
86-LDI-043	gabbronorite	41	13	39	6	-	-	-	1
86-LDI-071	norite	50	4	37	3	2	0.5	-	3

in pegmatites in the hybrid zone. Altered pyroxenes, up to 15 cm in length, were found in some pegmatitic phases. Generally, the clinopyroxene is the first to alter to an assemblage of uralitic amphibole, chlorite, talc, and epidote. This is followed by alteration of orthopyroxene and lastly, plagioclase is altered to sericite, epidote, and chlorite.

Pegmatitic gabbro contains clots of sulphide mineralization up to 0.75 cm in size as well as disseminated sulphide mineralization along fractures and between grains. Minor crosscutting talc-magnetite veinlets and chlorite veins occur in most samples.

GABBRONORITE

These rocks generally contain fresh cumulus plagioclase and orthopyroxene and intercumulus clinopyroxene where both clinopyroxene and orthopyroxene content is greater than 10% of the rock. Gabbronorite is medium grained, but also occurs as a fine-grained phase in some samples. Alteration affects clinopyroxene first and only occurs as rims and along fractures in the orthopyroxene. Most orthopyroxene grains show bleb-type exsolution of clinopyroxene which then alter to amphibole.

In some samples, clinopyroxene occurs as large poikilitic grains enclosing orthopyroxene and plagioclase. Sulphide mineralization is intercumulus or occurs as blebs associated with alteration products such as amphibole, biotite, and chlorite.

NORITE

The plagioclase orthopyroxene cumulates occur throughout the hybrid zone and in areas of the eastern gabbro. They are generally fresh, medium grained, and may contain up to 60% orthopyroxene. Minor intercumulus clinopyroxene is present, but is usually altered to amphibole. Intercumulus magnetite was observed in samples near the B-zone (Figure 286.2). Alteration appears on the edges of orthopyroxene grains, or as veins of chlorite crosscutting the sample.

PYROXENITE

Pyroxenite occurs as distinct intrusive phases which crosscut both the eastern and western gabbro. These rocks contain no primary pyroxene, but minor (up to 10 percent) intercumulus plagioclase may be present. Fine-grained amphibole aggregates occur as pseudomorphs after medium- to coarse-grained cumulus clinopyroxene.

CHANNEL SAMPLES

A 1.3 m channel sample was taken across a pegmatitic gabbro dike which was intruding into norites and leucogabbros. The sample section consists of:

1. Twenty-seven cm of medium- to coarse-grained gabbronorite with cumulus orthopyroxene and plagioclase and intercumulus clinopyroxene. Alteration of pyroxenes is about 50%. Sulphide mineralization occurs as small clots around altered pyroxenes and as disseminated grains. This section contains <0.5% visible sulphide mineralization. Sample LDI-080 (Table 286.1) is representative of this section.
2. Eighteen cm of medium-grained norite containing approximately 50% cumulus orthopyroxene, 37% cumulus plagioclase, and 5% intercumulus clinopyroxene, as well as minor amphibole, chlorite, and biotite. This section is crosscut by small (0.25 mm) wide veinlets of talc-magnetite. Approximately 0.5% sulphide mineralization is present as clots associated with secondary amphibole and biotite. Sample LDI-081 (Table 286.1) was taken from this section.
3. Fifteen cm of pegmatitic gabbro with cumulus plagioclase and amphibole pseudomorphs after cumulus clinopyroxene and orthopyroxene. Sulphide mineralization occurs disseminated within pyroxene and as clots up to 2 mm in size interstitial to grains making up 1 to 2% of the section. Secondary chlorite and epidote are ubiquitous throughout the section. Sample LDI-082 (Table 286.1) is from this pegmatite.
4. Thirty-four cm of gabbronorite with amphibole pseudomorphs of cumulus orthopyroxene and intercumulus clinopyroxene. Chlorite and epidote alteration is present and minor quartz is associated with sulphide mineralization in highly altered areas of this section. Sulphide mineralization is present up to 1% interstitially to altered pyroxenes. Sample LDI-083 represents this section.
5. Thirty cm of intermixed leucogabbro, norite, and gabbro containing variably altered pyroxenes and

differing amounts of sulphide mineralization. This section is considered too heterogeneous to define separate units for analyses.

ANALYTICAL METHODS

Of the total 110 samples collected to date, 75 have been analyzed for whole rock chemistry at the Geoscience Laboratories, Ontario Geological Survey, Toronto. Major and trace element analyses were by X-ray fluorescence (X.R.F.) and Pt, Pd, and Au were determined by fire-assay (F.A.) and atomic absorption (A.A.).

Nuclear Activation Services Limited determined complete PGE+Au values by neutron activation (N.A.) for 20 of the 75 samples that were submitted for whole rock analyses. Another five separate samples were also analyzed for PGE, but whole rock chemistry was done at X-Ray Assay Limited in Don Mills. Sulphur, Cu, and Ni values have been determined by F.A. and A.A. at the Geoscience Laboratories, Ontario Geological Survey, Toronto.

A comparison of analyses for Pt, Pd, and Au between the F.A. and A.A. methods versus F.A. and N.A. methods show that for Pt, 16 out of 19 samples gave lower values by A.A. (up to 230 ppb less). For Pd, 10 analyses were higher by A.A. (up to 480 ppb) and eight analyses were lower by A.A. (up to 426 ppb). Gold determined by A.A. in 12 cases was higher by up to 430 ppb and lower in seven cases by up to 406 ppb. These differences likely represent the heterogeneous nature of the rock types where PGM's were unevenly distributed in samples.

Mineral chemistry was obtained using a MAC-400 electron microprobe at 15 kv and 250 μamperes on fresh orthopyroxene, clinopyroxene, and plagioclase grains. Analyses are given for 15 samples in which fresh pyroxenes were found. Plagioclase analyses were done on nine samples representing fresh norites, gabbronorites, and melanorites. Preliminary microprobe analyses have been performed on several amphiboles.

RESULTS

The results presented in this section are of a preliminary nature and the database is currently being expanded to include new samples or analyses.

PGE

Complete analyses for PGE's, Au, Cu, Ni, and S are presented in Table 286.2. Also included in this table is a rock name, based on modal analyses or visual estimation from thin sections and the percent alteration of pyroxenes. The table has been subdivided into four sections according to relative location within the eastern gabbro, western gabbro, or hybrid zone as well as results from the channel samples.

A plot of Cu/(Cu+Ni) versus Pt/(Pt+Pd) is shown in Figure 286.3. This also shows the positions of other PGE deposits for comparative purposes. The general field for Lac des Iles is shown.

Recalculating the PGE results to 100% sulphides (after Hoffman *et al.* 1979; Naldrett *et al.* 1980), and normalizing by chondrite values, allows plots to be constructed for PGE and Au. These plots are shown in Figures 286.4a, b, and c, along with profiles for other deposits. In the recalculation, values for samples which fell below detection limits were taken as one half of the detection limit value (Borthwick and Naldrett 1984).

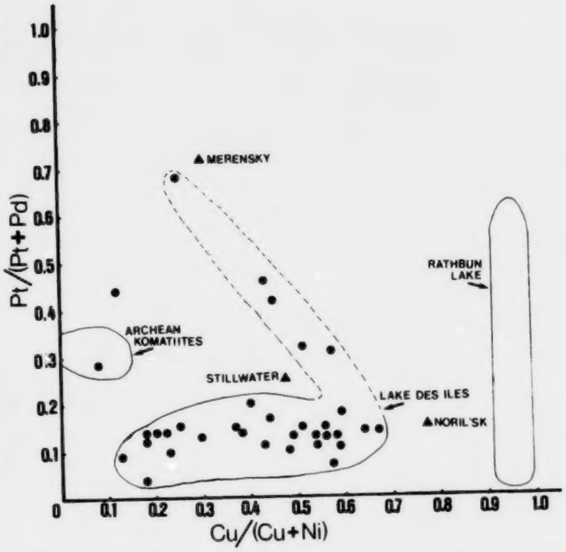

Figure 286.3. *Variation in Pt/(Pt+Pd) with Cu/(Cu+Ni) for Lac des Iles and other deposits.*

MINERAL CHEMISTRY

Electron microprobe data are presented in Tables 286.3, 286.4, and 286.5 showing sample number, rock type, representative major oxide values, and recalculated end members. The data in Table 286.3 are representative of cumulus orthopyroxene grains in which the cores and rims were probed. There was no significant core-rim variation encountered in the samples analyzed. Table 286.4 presents the data for core analyses of intercumulus clinopyroxene grains. The plagioclase analyses (Table 286.5) are for cumulus grain cores. Minor normal and reverse zoning was detected in several samples. The pyroxene data for the eastern and western gabbros have been plotted on the pyroxene quadrilateral (Figure 286.5) which also includes analyses of Dunning (1979) and Watkinson and Dunning (1979).

DISCUSSION

Based on these results, it is apparent that PGE concentrations occur in three different rock types:

1. altered pegmatitic gabbro with sulphide clots
2. altered intrinsic pyroxenite with low amounts of sulphide mineralization
3. fresh gabbronorite and norite with intercumulus sulphide mineralization

The hybrid zone contains the highest PGE values with the western gabbro containing the lowest PGE abundances (Table 286.2).

IGNEOUS STRATIGRAPHY

The complex nature of the relationship between gabbroic phases has been discussed by Sutcliffe and Sweeny (1985, 1986); Macdonald (1986); and Sweeny and Sutcliffe (1986) and this is substantiated by the mineral and whole rock data. The lack of good igneous layering, combined with poorly defined contacts between units, makes any interpretation of stratigraphy tenuous, especially when determining a top direction. The map presented in Figure 286.2 indicates that a unit of gabbronorite extends northeastward from the "C-zone" to the "B-zone". This unit truncates layering and foliation in the eastern gabbro and suggests that the western gabbro was emplaced after the eastern gabbro (Sweeny and Sutcliffe 1986). The gabbronorites of this unit are similar to western gabbro rocks but there is much more pegmatitic gabbro present as well as mixing textures.

Initially, the eastern and western gabbros were believed to be distinguishable based on their whole rock chemistry (Sutcliffe and Sweeny 1986; Sweeny and Sutcliffe 1986). This conclusion is supported by pyroxene analyses (Watkinson and Dunning 1979) which showed distinct compositional fields for each gabbro (Figure 286.5). However, the present study of pyroxene chemistry indicates that such a distribution does not exist and that the compositions of pyroxenes in the hybrid zone are comparable to those in the eastern and western gabbro (Figure 286.5). Plagioclase analyses also show no discernable trends between the two gabbroic phases, but they do exhibit a variation in average content between similar rock types (*see* Table 286.5).

PGE

The graph in Figure 286.3 shows that Lac des Iles rocks appear to follow two different trends. One trend with constant Pt/(Pt+Pd) and increasing Cu/(Cu+Ni) contains the majority of samples, while a second minor trend shows increasing Pt/(Pt+Pd) with decreasing Cu/(Cu+Ni). The former trend is compatible with that given by Naldrett *et al.* (1980) for the Lac des Iles area and the latter trend falls within that for tholeiitic-hosted PGE deposits.

The data for the channel sample in Table 286.2 indicate that the pegmatitic phase contains the highest PGE as well as the highest Cu, Ni, and Au compared to the rest of the section. Microprobe analyses of the amphibole and the identification of PGM's in this section will be completed soon.

Based on recalculation to normalized chondrites samples with low sulphur generally plot in the same range as do samples with higher sulphur contents (dashed line on Figure 286.4). The slopes of the lines between Pt and Au in the hybrid zone, as plotted in Figure 286.4b, differ from those in the eastern and western gabbros (Figures 286.4a and c). These slopes result from different sulphur values and hence may reflect different processes in the hybrid zone relative to those in the eastern and western gabbros.

One interesting trend observed is the opposite peaks for Ir and Ru between Naldrett's (1981) analyses and the present study (Figure 286.4b). The reason for this is unclear at the present time. The profile for the Lac des Iles Deposit is similar to that for Rathbun Lake, which has been interpreted as a hydrothermal deposit (Rowell and Edgar 1986).

Dunning (1979) and Watkinson and Dunning (1979) have given the rocks the following names, pyroxenites and amphibolites, due to the complete alteration of primary pyroxenes to amphiboles. The pyroxenes were interpreted as layers within the gabbroic phases, but recent mapping (Sweeny and Sutcliffe 1986; Macdonald 1986) indicated they are intrusive and are locally observed to crosscut both the eastern and western gabbros. Two samples of pyroxenite have been analyzed (Table 286.2, Figure 286.4c) and show relatively high values of PGEs with low amounts of S. As indicated in Figure 286.4c, the pyroxenite profiles show a similarity to the samples from the hybrid zone. These slightly later pyroxenites may have remobilized the Pt, Pd, and Au as they intruded into the crystallizing, PGE-rich western gabbro and hybrid zone.

FUTURE PLANS

Determination of PGM's within the ore zone using a JEOL 8600 model microprobe with EDS, WDS, and backscatter capabilities, combined with analyses of the secondary amphibole, will be carried out in an effort to characterize the fluids involved in the redistribution of PGEs. Analyses for F and Cl will be included in this work.

Further whole rock analyses will also include CO_2, Fe^{2+}, and Fe^{3+} determinations which will also be used to evaluate the composition of the fluids. These analyses may also help to distinguish the eastern and western gabbros from each other as well as their relationship to rocks of the hybrid zone. Further detailed mapping and selective sampling is being carried out in areas recently stripped by Boston Bay Mines Limited at the deposit site.

ACKNOWLEDGMENTS

The authors would like to thank R.H. Sutcliffe (Geologist, Ontario Geological Survey, Toronto) for discussions involving the geology of the area as well as the staff of Boston Bay Mines Limited for access to information and discussions on the geology of the deposit. Diane Forsyth is thanked for her assistance in preparing the manuscript.

REFERENCES

Borthwick, A.A., and Naldrett, A.J.
1984: Platinum-Group Elements in Layered Intrusions; Grant 106, p.13-35 *in* Geoscience Research Grant Program, Summary of Research 1983-1984, edited by V.G. Milne, Ontario Geological Survey, Miscellaneous Paper 121, 252p.

TABLE 286.2. PGE, Au, Cu, NI VALUES FROM ROCKS OF THE HYBRID ZONE, EASTERN AND WESTERN GABBROS AND CHANNEL SAMPLE.

Sample #	Rock	Pd	Pt	Os	Ir	Ru	Rh	Au	Cu	Ni	S	Mineralization
				(ppb^1)					(ppm^2)		(wt %)	
a. Hybrid Zone												
85-RHS-52	Gabbro*	2600	200	<3	0.3	<20	2	140	1260	950	0.42	-
85-RHS-57	Gabbronorite*	1800	310	<3	0.5	26	4	130	1740	1490	0.60	-
85-RHS-64	Gabbro*	750	180	<3	0.4	<19	2	80	870	1150	0.33	-
85-RHS-746	Gabbronorite	37	100	<3	0.7	<5	2	8	172	230	0.06	1%
85-RHS-747	Pegmatitic leucogabbro*	540	140	<3	0.3	<12	1	51	2340	1160	0.02	-
85-RHS-763	Leucogabbro*	510	130	<3	0.3	50	2	35	350	375	0.07	trace
85-RHS-772	Gabbro*	530	140	<3	0.3	<31	1	73	106	425	0.06	trace
85-RHS-773	Leucogabbro*	330	120	<3	0.2	<28	1	16	64	425	0.02	trace
85-RHS-775	Gabbronorite	1900	320	<3	0.2	28	2	280	1880	1970	0.54	1%
85-RHS-779	Leucogabbro*	280	100	<3	0.2	36	1	24	168	400	0.05	-
85-RHS-787	Gabbro	130	310	<7	0.9	120	11	19	96	285	0.13	2-3%
86-RHS-202	Pyroxenite dike*	3900	620	<3	<0.1	<7	<1	250	720	400	0.09	-

TABLE 286.2. (cont'd.)

Sample #	Rock	Pd	Pt	Os	Ir	Ru	Rh	Au	Cu	Ni	S	Mineralization
				(ppb[1])					(ppm[2])		(wt %)	
b. Eastern Gabbro												
85-RHS-743	Gabbro*	440	130	<3	0.3	<5	<3	410	184	126	0.02	trace
85-RHS-744	Pyroxenite dike*	350	93	<5	0.4	<16	<2	73	1100	810	0.08	trace
85-RHS-752	Gabbro*	28	69	4	0.2	46	1	7	38	167	0.02	-
85-RHS-786	Gabbro*	170	80	<4	0.3	<38	7	43	-	-	-	-
c. Western Gabbro												
85-RHS-65	Gabbronorite	29	<110	<3	0.6	<19	2	19	119	355	0.03	trace
85-RHS-67	Gabbronorite	450	420	17	1.2	<5	21	270	3450	3260	0.94	-
85-RHS-767	Leucogabbro*	<50	140	<6	1.2	<60	8	13	305	300	0.05	trace
85-RHS-769	Gabbronorite	440	130	<3	0.2	<5	<4	63	1750	2100	0.65	1%
d. Channel Sample												
86-LDI-80	Gabbronorite	1100	140	<3	0.4	20	2	77	600	510	0.14	<1%
86-LDI-81	Norite	1700	260	<3	0.4	<5	2	160	1200	950	0.24	0.5%
86-LDI-82	Pegmatite gabbro*	3700	460	3	0.5	29	4	200	1700	1200	0.73	2-3%
86-LDI-83	Norite	2100	320	4	0.5	<5	4	150	1400	1000	0.50	1-2%

1. Analyses of PGE and Au by neutron activation.
2. Analyses of Cu, Ni by fire assay.
* - The pyroxene in these samples has >95% alteration. Samples without this designation have <50% alteration of pyroxenes.
For values of PGE below the detection limit (as <) a value of one-half of the stated amount was used in the graphs according to the method of Borthwick and Naldrett (1984).

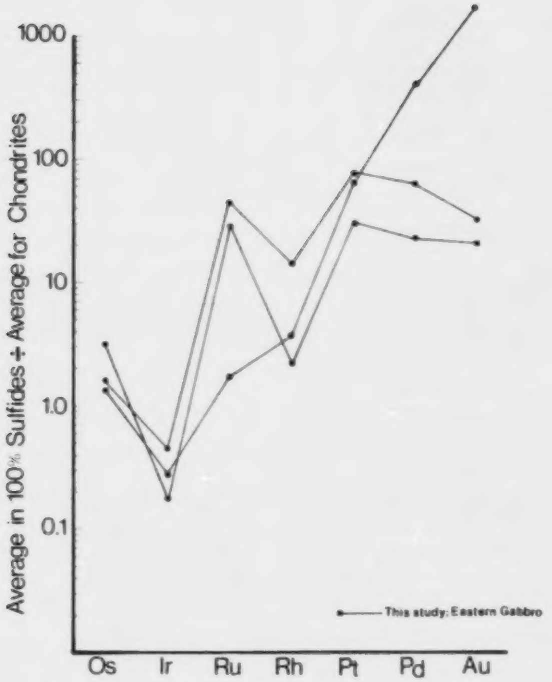

Figure 286.4a. *(Average in 100% sulphides)/(Average for chondrites) plotted against PGE and Au (after Naldrett 1980). Eastern gabbro.*

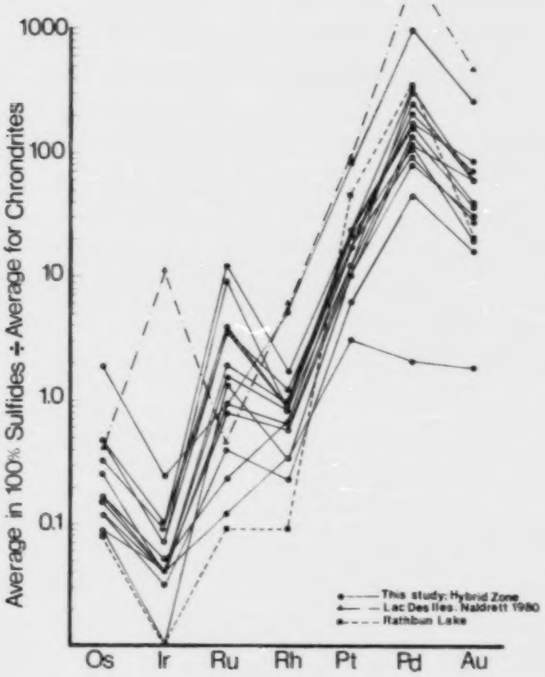

Figure 286.4b. *(Average in 100% sulphides)/(Average for chondrites) plotted against PGE and Au (after Naldrett 1980). Hybrid zone.*

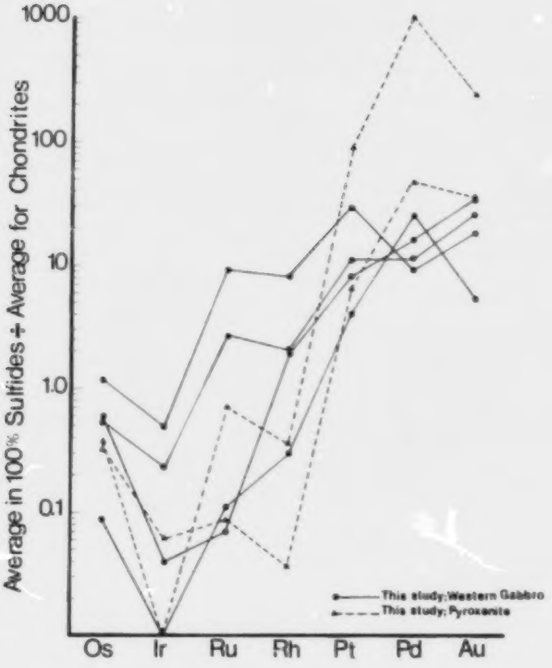

Figure 286.4c. *(Average in 100% sulphides)/(Average for chondrites) plotted against PGE and Au (after Naldrett 1980). Western gabbro.*

TABLE 286.3. REPRESENTATIVE ORTHOPYROXENE ANALYSES.

Sample # **Rock Type**	**85-RHS-57** **mela-gabbronorite**	**85-RHS-65** **gabbronorite**	**85-RHS-67** **gabbronorite**	**85-RHS-746** **gabbronorite**	**85-RHS-775** **gabbronorite**
SiO_2	53.06	53.60	54.18	52.89	54.75
TiO_2	0.19	0.10	0.10	0.78	0.14
Al_2O_3	2.11	1.47	1.89	1.80	1.81
Cr_2O_3	0.13	0.01	0.03	0.01	0.01
FeO	19.78	17.56	13.76	19.65	15.00
MnO	0.35	0.30	0.30	0.38	0.24
MgO	22.93	25.53	27.97	23.62	26.52
CaO	1.21	1.26	1.59	1.38	1.45
Na_2O	0.00	0.00	0.03	0.00	0.00
K_2O	0.00	0.02	0.01	0.00	0.00
Total	99.76	99.85	99.86	100.51	99.92
Fs	31.65	27.15	20.96	30.94	23.40
Wo	2.62	2.49	3.10	2.79	2.89
En	65.75	70.35	75.93	66.27	73.71

Sample # **Rock Type**	**86-LDI-033** **gabbronorite**	**86-LDI-041** **gabbronorite**	**86-LDI-043** **gabbronorite**	**86-LDI-060** **gabbronorite**
SiO_2	53.12	52.92	54.09	54.34
TiO_2	0.14	0.16	0.18	0.16
Al_2O_3	2.00	1.47	2.05	1.31
Cr_2O_3	0.14	0.07	0.15	0.00
FeO	17.56	21.17	17.23	15.37
MnO	0.29	0.41	0.32	0.18
MgO	24.76	22.54	24.79	27.18
CaO	1.45	1.35	1.42	1.44
Na_2O	0.00	0.01	0.00	0.01
K_2O	0.00	0.01	0.00	0.00
Total	99.46	99.95	100.23	99.99
Fs	27.52	33.14	26.89	22.62
Wo	2.92	2.75	2.91	2.84
En	69.56	64.11	70.19	74.53

Sample # **Rock Type**	**86-LDI-088A** **gabbronorite**	**86-LDI-010** **norite**	**86-LDI-011** **gabbronorite**	**86-LDI-019** **gabbronorite**	**86-LDI-031** **gabbronorite**
SiO_2	52.61	54.75	53.77	52.84	54.41
TiO_2	0.17	0.16	0.16	0.18	0.17
Al_2O_3	2.20	1.39	1.31	1.72	2.13
Cr_2O_3	0.14	0.00	0.09	0.00	0.15
FeO	19.30	16.67	17.47	20.56	16.29
MnO	0.36	0.18	0.33	0.28	0.35
MgO	23.33	27.05	24.56	22.83	24.89
CaO	1.60	1.25	1.66	1.96	2.05
Na_2O	0.00	0.01	0.00	0.01	0.00
K_2O	0.00	0.00	0.00	0.00	0.00
Total	99.71	101.46	99.35	100.38	100.44
Fs	29.26	23.48	27.33	31.36	25.61
Wo	3.32	2.46	3.36	3.99	4.00
En	67.42	74.06	69.31	64.65	70.38

TABLE 286.4. REPRESENTATIVE CLINOPYROXENE ANALYSES.

Sample # **Rock Type**	**85-RHS-57** **mela-gabbronorite**	**85-RHS-746** **gabbronorite**	**85-RHS-752** **gabbro**	**86-LDI-008A** **gabbronorite**
SiO_2	51.49	50.34	51.49	50.94
TiO_2	0.57	0.75	0.57	0.48
Al_2O_3	3.15	3.64	3.49	3.89
Cr_2O_3	0.21	0.00	0.01	0.17
FeO	9.25	8.09	7.94	8.44
MnO	0.20	0.18	0.15	0.48
Mg0	13.83	13.40	14.05	14.28
CaO	21.36	22.65	22.59	20.53
Na_2O	0.25	0.37	0.22	0.30
K_2O	0.00	0.00	0.04	0.00
Total	100.31	99.42	100.55	99.51
Fs	14.34	13.26	12.83	12.97
Wo	45.07	47.58	46.73	44.23
En	40.59	39.16	40.45	42.79
Sample # **Rock Type**	**86-LDI-011** **gabbronorite**	**86-LDI-019** **gabbronorite**	**86-LDI-031** **gabbronorite**	**86-LDI-043** **gabbronorite**
SiO_2	51.66	51.01	52.22	51.79
TiO_2	0.37	0.34	0.25	0.52
Al_2O_3	2.53	2.52	3.12	3.26
Cr_2O_3	0.08	0.00	0.18	0.19
FeO	8.52	9.75	9.34	7.91
MnO	0.23	0.16	0.27	0.23
Mg0	15.08	14.24	15.35	14.49
CaO	20.84	21.13	19.55	21.13
Na_2O	0.33	0.33	0.32	0.22
K_2O	0.00	0.00	0.00	0.01
Total	99.64	99.48	100.60	99.75
Fs	11.23	12.04	14.56	12.85
Wo	44.26	45.42	40.84	44.58
En	44.51	42.55	44.61	42.57

TABLE 286.5. REPRESENTATIVE PALGIOCLASE ANALYSES.

Sample # Rock Type	85-RHS-57 mela-gabbronorite	86-LDI-002 mela-norite	86-LDI-010 norite	86-LDI-011 gabbronorite	86-LDI-019 gabbronorite
SiO_2	50.42	53.44	48.84	51.79	51.21
Al_2O_3	32.01	29.71	32.53	30.50	31.73
Na_2O	3.66	5.16	3.41	4.43	3.73
CaO	14.13	11.84	14.96	13.08	13.89
K_2O	0.51	0.17	0.03	0.24	0.15
FeO	0.15	0.13	0.08	0.29	0.31
Total	100.88	100.45	99.85	100.33	101.02
AB	31.82	43.67	29.17	37.45	32.43
AN	67.88	55.41	70.68	61.25	66.71
OR	0.30	0.92	0.15	1.31	0.86

Sample # Rock Type	86-LDI-031 gabbronorite	86-LDI-033 gabbronorite	86-LDI-041 gabbronorite	86-LDI-043 gabbronorite
SiO_2	47.29	49.33	53.43	48.82
Al_2O_3	32.98	32.51	29.16	32.25
Na_2O	2.71	3.09	4.69	3.41
CaO	16.24	15.19	12.05	15.07
K_2O	0.07	0.01	0.21	0.06
FeO	0.23	0.13	0.28	0.08
Total	99.52	100.26	99.82	99.69
AB	23.09	26.90	40.83	28.97
AN	76.52	73.03	57.97	70.73
OR	0.39	0.07	1.20	0.31

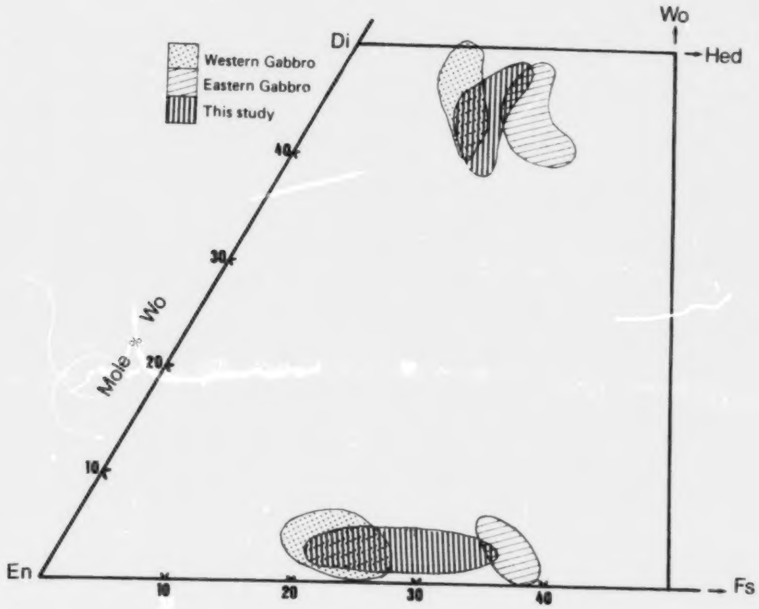

Figure 286.5. *Compositions of pyroxenes replotted in the system Wo-En-Fs.*

Dunning, G.R.
1979: The Geology and Platinum Group Mineralization of the Roby Zone, Lac des Iles Complex, N.W. Ontario; Unpublished M.Sc. Thesis, Carleton University, Ottawa, 129p.

Hoffman, E.L., Naldrett, A.J., Alcock, R.A., and Hancock, R.G.V.
1979: The Noble Metal Content of Ore in the Levack West and Little Stobie Mines, Ontario; Canadian Mineralogist, Volume 17, p.437- 452.

Macdonald, A.J.
1986: Interim Results of the 1986 Field Season, Lac des Iles; Unpublished Report, 57p.

Naldrett, A.J.
1981: Platinum Group Element Deposits; p.199- 231 *in* Canadian Institute of Mining and Metallurgy, Special Volume 23.

Naldrett, A.J., Innes, D.G., and Sowa, J.M.
1980: Platinum Group Element Concentrations in Some Magmatic Ores in Ontario; Grant 17, p.171- 178 *in* Geoscience Research Grant Program, Summary of Research, 1979-1980, edited by E.G. Pye, Ontario Geological Survey, Miscellaneous Paper 93, 262p.

Pye, E.G.
1968: Geology of Lac des Iles Area, District of Thunder Bay; Ontario Department of Mines, Geological Report 64. Accompanied by Maps 2135 and 2136, scale 1:31 680 or 1 inch to 1/2 mile.

Rowell, W.F., and Edgar, A.D.
1986: Platinum Group Element Mineralization in a Hydrothermal Cu-Ni Sulfide Occurrence, Rathbun Lake, Northwestern Ontario; Economic Geology, Volume 81, p.1272- 1277.

Streckeisen, A.
1976: To Each Plutonic Rock Its Proper Name; Earth Science Review, Volume 12, p.1-33.

Sutcliffe, R.H.
1986: Regional Geology of the Lac des Iles Area, District of Thunder Bay; p.70- 75 *in* Summary of Field Work and Other Activities, 1986, by the Ontario Geological Survey, edited by P.C. Thurston, Owen L. White, R.B. Barlow, M.E. Cherry, and A.C. Colvine, Ontario Geological Survey, Miscellaneous Paper 132, 435p.

Sutcliffe, R.H., and Sweeny, J.M.
1985: Geology of the Lac des Iles Complex, District of Thunder Bay; p.47- 53 *in* Summary of Field Work and Other Activities, 1985, by the Ontario Geological Survey, edited by John Wood, Owen L. White, R.B. Barlow, and A.C. Colvine, Ontario Geological Survey, Miscellaneous Paper 126, 351p.
1986: Precambrian Geology of the Lac des Iles Complex; Ontario Geological Survey, Map P.3047, Geological Series- Preliminary Map, scale 1:15 840 or 1 inch to 1/4 mile.

Sweeny, J.M., and Sutcliffe, R.H.
1986: Geology and Platinum Group Element Mineralization of the Roby Zone, Lac des Iles Complex; p.82- 84 *in* Summary of Field Work and Other Activities, 1986, by the Ontario Geological Survey, edited by P.C. Thurston, Owen L. White, R.B. Barlow, M.E. Cherry, and A.C. Colvine, Ontario Geological Survey, Miscellaneous Paper 132, 435p.

Talkington, R.W., and Watkinson, D.H.
1984: Trends in the Distribution of the Precious Metals in the Lac des Iles Complex, Northwestern Ontario; Canadian Mineralogist, Volume 22, p.125- 136.

Watkinson, D.H., and Dunning, G.R.
1979: Geology and Platinum Group Mineralization, Lac des Iles Complex, Northwestern Ontario; Canadian Mineralogist, Volume 17, p.453- 462.

Grant 288 Gneissose Trondhjemite/Tonalite Hosted Au-Quartz Vein Mineralization, Renabie Mine Area, Wawa: Geological Characteristics and Shear Zone Control

N.J. Callan and E.T.C. Spooner

Department of Geology, University of Toronto

ABSTRACT

Significant Au-quartz vein mineralization in the Renabie area (e.g. Renabie Mine: 5.5 million tonnes at ~6 g/tonne Au and ~2 g/tonne Ag) occurs outside the confines of a greenstone belt and is hosted in marginal trondhjemitic/tonalitic components of the Wawa Domal Gneiss Terrane. Au-quartz veins occupy variably oriented brittle/ductile shear zones which rotate and crosscut regional flattening fabric in the host intrusions.

Structural data obtained so far suggest reverse, south-side-up, sinistral shear displacements on west to west-northwest trending shears (e.g. Nudulama and C zone shears), and a reverse west-side-up, sinistral shear displacement on the northwest-trending Braminco #21 vein shear. Kinematics are currently less well constrained for the dominant west-northwest to northwest and west-southwest to southwest shears comprising the more complex Renabie vein system, although orientations appear to be consistent with a conjugate shear set.

Shear zone-hosted ore zones with prolate shapes show consistent plunges, often parallel to subparallel with ductile and brittle lineations in the shear zones. Plunges are also subparallel with major lithological contacts.

Initiation of shearing appears to have predated the introduction of mineralizing fluids, and though fabric and other strain features displayed by the mineralization indicate that shear deformation continued throughout of mineralization. Vein formation occurred predominantly by overpressured fluid injection parallel to shear fabric, which generated distinctive "crack-seal" type vein filling structures. The mineral suite associated with gold includes quartz, pyrite, galena, tellurides, molybdenite, carbonate, anhydrite, and minor tourmaline, and is typical of Archean Au-quartz vein deposits.

INTRODUCTION

Archean Au-quartz vein/shear zone mineralization in the Renabie area, located near Missanabie, ~80 km northeast of Wawa, is unusual because it is located outside the confines of a greenstone belt (Michipicoten) in intrusive gneissose trondhjemites and tonalites of the Wawa Domal Gneiss Terrane (tonalite-trondhjemite-granodiorite (TTG) material). The mineralization is clearly important for exploration because it is significant (e.g. Renabie Mine past-production and known reserves are 5.5 million tonnes at ~6 g/tonne Au and ~2 g/tonne Ag), has a satisfactory cash operating cost (~$US 240 per ounce because of large ~8 to 12 m stoping widths), and is in lithologies which have received relatively little exploration attention. If there is one Renabie deposit, then there could be more in the tonalitic/trondhjemitic rocks which surround and intrude Archean greenstone belts, an area of several thousand square kilometres in Ontario. The Renabie area Au mineralization is clearly also important for genetic reasons because of its location in intrusive rocks outside a greenstone belt. Questions are raised, such as: are high level greenstone belt processes really relevant to the formation of Archean Au-quartz vein fluids, or, on the other hand, is the Renabie area Au mineralization unrepresentative so that points of general genetic relevance cannot be drawn?

The Renabie Mine has been in production, with some interruptions, since 1941, after its discovery in 1939 by a poacher in the Chapleau Crown Game Preserve. Production to date has been ~4 million tonnes at ~6.6 g/tonne Au and ~2.1 g/tonne Ag. Production has been based on a shaft to the 3105-foot level, a decline from the 3105-foot level for trackless mining, and an internal shaft to 4500 feet. Current reserves defined by drilling down-plunge from a crosscut on the 3105-foot level are 1.5 million tonnes at ~6 g/tonne Au. Mill rate is being expanded to 700 tonnes/day by 1988 from 525 tonnes/day. The Renabie Mine is currently operated by Royex Gold Mining Corporation (International Corona Resources Limited) who share ownership equally with American Barrick Resources Corporation.

Similar mineralization to that at the Renabie Mine occurs in the Braminco #21 (Canreos Minerals (1980) Limited; Missibay Mining Limited) and the Nudulama (Anglo Dominion Gold Exploration Limited) vein structures. High SiO_2 (~77% SiO_2) flux ore containing ~4.8 to 6.6 g/tonne Au has been mined and trucked to the Kidd Creek Mines Limited smelter in Timmins recently. Exploration in the last few years has been quite active in the Renabie area and southwest to the Kremzar (Canamax) and Magino (Muscocho/McNellen) projects.

This report summarizes the results of field work carried out in 1985 and 1986. The objectives of this report are:

1. to describe the geological relationships, geometrical characteristics, and structural controls on the Au-quartz vein/shear zone mineralization
2. to discuss the field evidence for a relative time sequence of igneous intrusive, deformation, mineralization, and hydrothermal alteration processes in the Renabie area
3. to describe the characteristics of the mineralization based on field and hand specimen observations

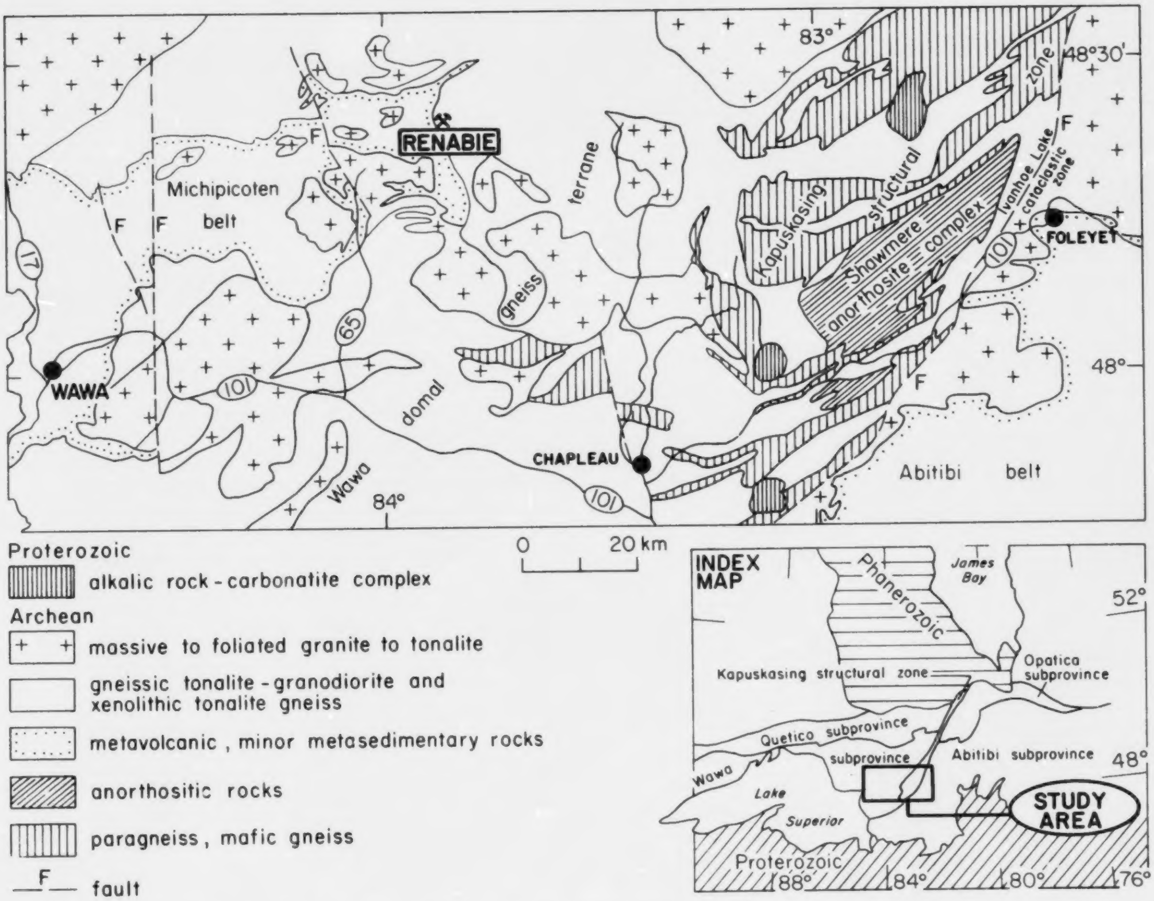
83°
48°30'
48°
84°
RENABIE
WAWA
CHAPLEAU
FOLEYET
Michipicoten belt
Wawa domal gneiss terrane
Kapuskasing structural zone
Shawmere anorthosite complex
Ivanhoe Lake cataclastic zone
Abitibi belt
F
17
65
101
0 20 km
Proterozoic
alkalic rock-carbonatite complex
Archean
massive to foliated granite to tonalite
gneissic tonalite-granodiorite and xenolithic tonalite gneiss
metavolcanic, minor metasedimentary rocks
anorthositic rocks
paragneiss, mafic gneiss
F fault
INDEX MAP
Phanerozoic
James Bay
52°
Kapuskasing structural zone
Opatica subprovince
Quetico subprovince
Wawa subprovince
Abitibi subprovince
48°
Lake Superior
STUDY AREA
Proterozoic
88°
84°
80°
76°

Figure 288.1. *Geology of the Wawa-Abitibi area showing location of the study area (modified from Percival 1986).*

REGIONAL GEOLOGICAL RELATIONSHIPS

The regional geological setting (Figure 288.1) is characterized by a 120 km easterly transition from predominantly greenschist facies metavolcanics of the Michipicoten greenstone belt to the west, through the generally amphibolite facies tonalite, trondhjemite, and granodiorite (TTG) gneisses of the Wawa Domal Gneiss Terrane (WDGT), to the southwest-trending units of granulite grade paragneiss, mafic gneiss, tonalite, and anorthosite comprising the Kapuskasing Structural Zone (Percival 1986). The eastern boundary of the Kapuskasing Structural Zone is marked by a sharp lithological, structural, and metamorphic discontinuity—the Ivanhoe Lake Cataclastic Zone (ILCZ). The section is interpreted to be an oblique Archean crustal cross section corresponding to ~25 vertical kilometres which was uplifted on a northwest-dipping reverse fault, represented at surface by the ILCZ.

Au-quartz vein mineralization in the Renabie area is located within the Missinabi Lake Batholith (MLB) which intrudes the eastern extremity of the Michipicoten greenstone belt. The MLB forms a discrete mafic tonalitic intrusive phase of the areally extensive WDGT and is thought to represent one of its oldest components (Percival 1981).

GEOLOGICAL RELATIONSHIPS IN THE RENABIE MINE AREA

The contact between the metavolcanics of the Michipicoten greenstone belt to the west and the intrusive phases of the MLB to the east in the Renabie Mine area is arcuate in shape, swinging from northwest to north-northwest in the south, to north-northeast to northeast approximately 1.7 km north of the Renabie Mine (*see* Figure 288.2). Interpolation between the position of the contact at surface and its exposure in the southern exploratory crosscut, 3105-foot level in the Renabie Mine, indicates an average dip of ~50° to the southwest. The dip of the contact on the 3105-foot level shows a steepening to ~70°.

The nature of the contact is variable. Excellent intrusive relationships are observed in a 5 to 10 m wide contact zone at surface ~500 m west of the Braminco #21 vein, where fine-grained granitic ma-

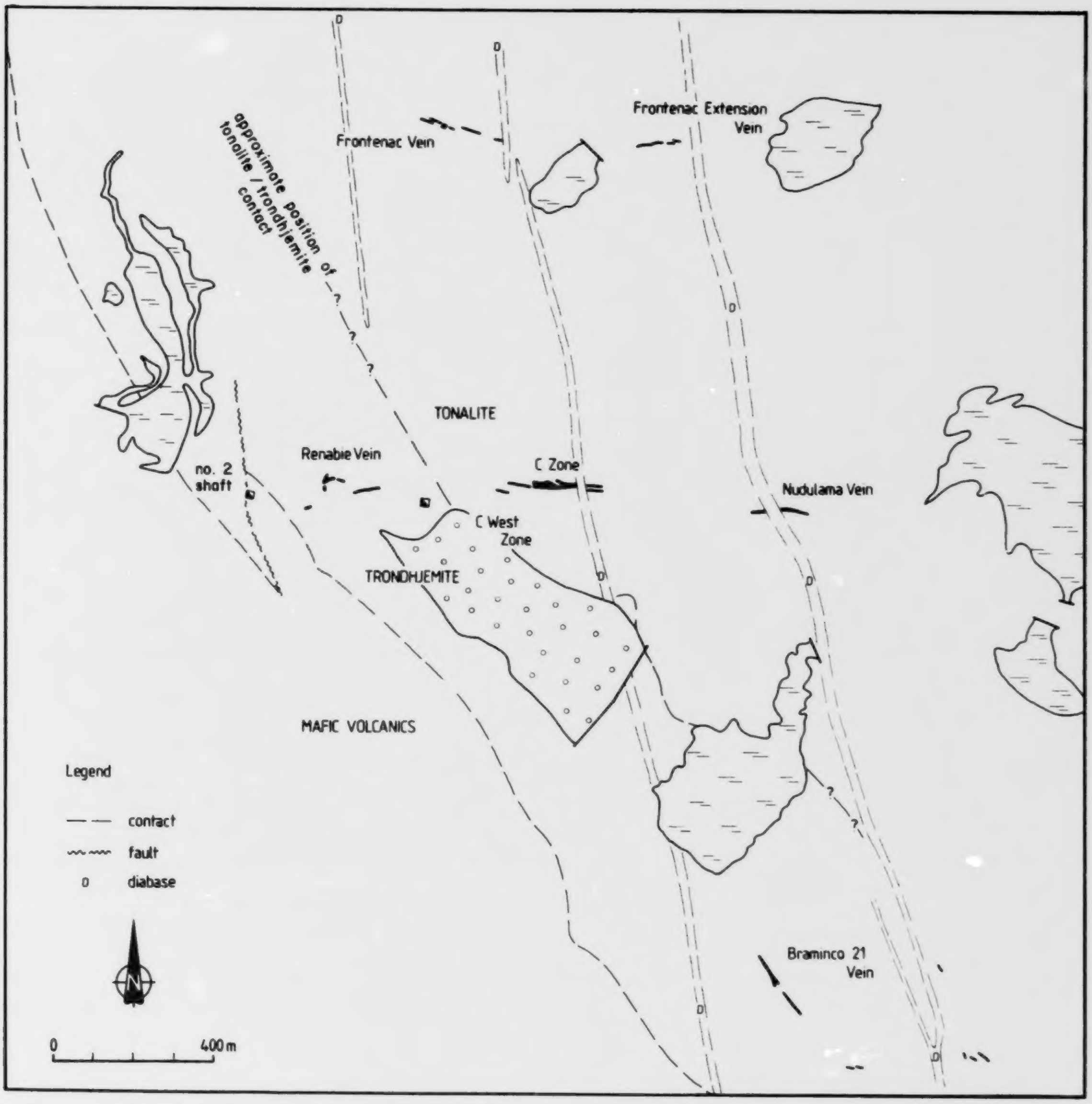

Figure 288.2. Simplified geology of the Renabie Mine area showing major lithological contacts and distribution of the major Au-quartz veins (modified from Ferguson 1968).

terial containing mafic volcanic xenoliths invades the adjacent mafic metavolcanics.

However, in the southern exploratory crosscut, 3105-foot level, in the Renabie Mine, the contact is marked by a 25-cm hybrid zone of highly foliated mafic metavolcanics and intrusive trondhjemite. The strain intensity in the trondhjemite decreases progressively over 40 m away from the contact as indicated by a marked coarsening of foliation and a decrease in the intensity of folding of aplitic/pegmatitic veins which have acted as passive strain markers.

The contact has been offset by north-northwest- to north-trending brittle faults as shown by the subvertical "shaft" fault at the Renabie #2 shaft which has an approximate vertical displacement of 180 m. This fault may be related to a subparallel set of faults showing a sinistral transcurrent component of movement which are observed to offset the Renabie orebody.

A penetrative foliation is developed in the mafic metavolcanics. Its orientation is generally concordant with that of the metavolcanic/intrusive contact. Foliation is also variably developed in the intrusions and is also concordant to subconcordant with the contact with the mafic metavolcanics.

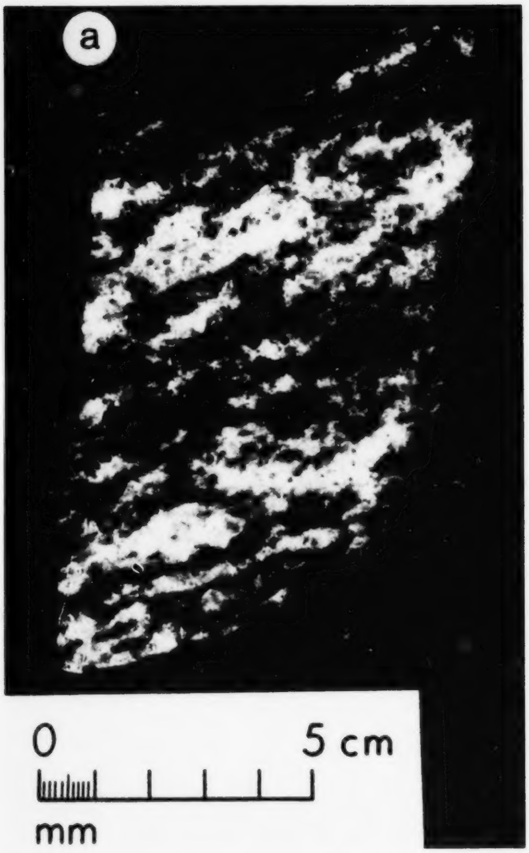

Photo 288.1a. *Well foliated trondhjemite from marginal zone, 3105-foot level, Renabie Mine.*

All lithologies are transected by northwest- to north-northwest-trending diabase dikes which also crosscut, and therefore postdate mineralization.

Lamprophyre dikes of variable orientation, consisting either of foliated fine-grained chloritic material, or a fine-grained unfoliated matrix rich in biotite platelets and lithic fragments, also crosscut mineralization. The former type are crosscut by the diabase dikes, but no crosscutting relationships were observed between the two varieties themselves or between the biotite/lithic fragment variety and the diabase.

INTRUSIVE LITHOLOGIES

Mineralization is hosted by two main intrusive lithologies, both of which contain aplitic/pegmatitic minor phases.

GNEISSOSE TRONDHJEMITE

The marginal lithology adjacent to the mafic metavolcanics forms a zone varying in width from ~200 m on the 3105-foot level, Renabie Mine to ~350 m at surface. It is characterized by a trondhjemitic normative bulk composition and a coarse 5 to 10 mm scale 'S' fabric defined by epidote- and biotite-rich foliae enclosing domains rich in quartz and greenish buff saussuritized plagioclase (Photo 288.1a). Rare hornblende needles are also present.

TONALITE

To the east of the gneissose trondhjemite, and of unknown easterly extent, is a finer grained, more melanocratic lithology with a tonalitic normative bulk composition. The tonalite exhibits a variably developed 'S' fabric concordant with that in the adjacent trondhjemite, and occasional centimetre-scale banding defined by grain size and/or compositional variation. Weakly foliated examples (Photo 288.1b) show distinctive apple green, subhedral, zoned plagioclase phenocrysts up to 0.5 cm in size; fine disseminated pyrite is also present. Locally developed in the Nudulama east pit is a distinctive textured variety showing biotite clots up to ~1.5 cm in size.

Locally contained in the tonalite are bands up to ~30 cm thick of a finer grained more mafic phase which commonly lacks plagioclase phenocrysts. These are best developed in the vicinity of the trondhjemite/tonalite contact and have an orientation concordant with both this contact and the regional foliation. The mafic bands are locally pyrite rich.

CONTACT RELATIONSHIPS AND RELATIVE TIMING

The 3105- and 1400-foot levels of the Renabie Mine provide key exposures of the gneissose trondhjemite/tonalite contact. On the 3105-foot level, the contact, oriented at 320° and dipping southwest, shows a sharp juxtaposition of weakly foliated, almost granular, plagioclase phenocrystic tonalite against coarsely foliated trondhjemite. The more complex contact on the 1400-foot level is represented by a 30 m wide zone of coarsely foliated trondhjemite and granular tonalite, interleaved on a centimetre to metre scale, once again with very sharp contacts between the two lithologies (Photo 288.1c).

Three observations, made on the 1400-, 2900-, and 3105-foot levels of the Renabie Mine, which support the interpretation of a slightly younger tonalitic intrusive phase, include:

1. the marked strain differential between closely juxtaposed granular tonalite and strongly foliated trondhjemite, particularly in the interleaved contact zones
2. gneissose trondhjemite/granular tonalite contacts which shallowly crosscut the 'S' fabric in the foliated trondhjemite
3. rare (?) xenoliths of gneissose trondhjemite within tonalite. The rarity of this feature renders it the least reliable criterion

REGIONAL FABRIC DEVELOPMENT WITHIN INTRUSIVE PHASES

As mentioned above, both intrusive lithologies exhibit a regional 'S' (flattening) fabric, striking ~340° northwest and dipping at 60 to 70° to the southwest. This orientation is concordant to subconcordant with the foliation in the adjacent mafic metavolcanics and with major lithological contacts. No regional lineation

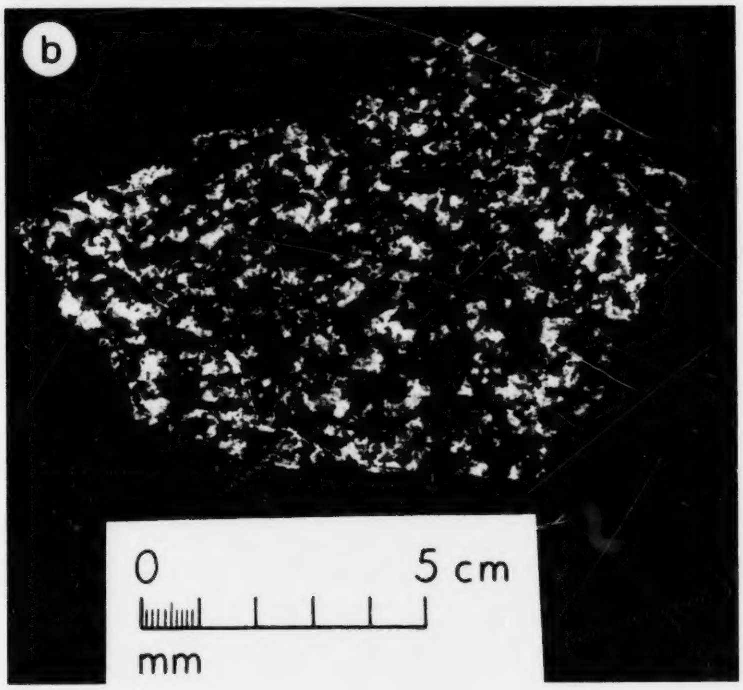

Photo 288.1b. *Almost granular tonalite from 3105-foot level, Renabie Mine. Note altered plagioclase phenocrysts.*

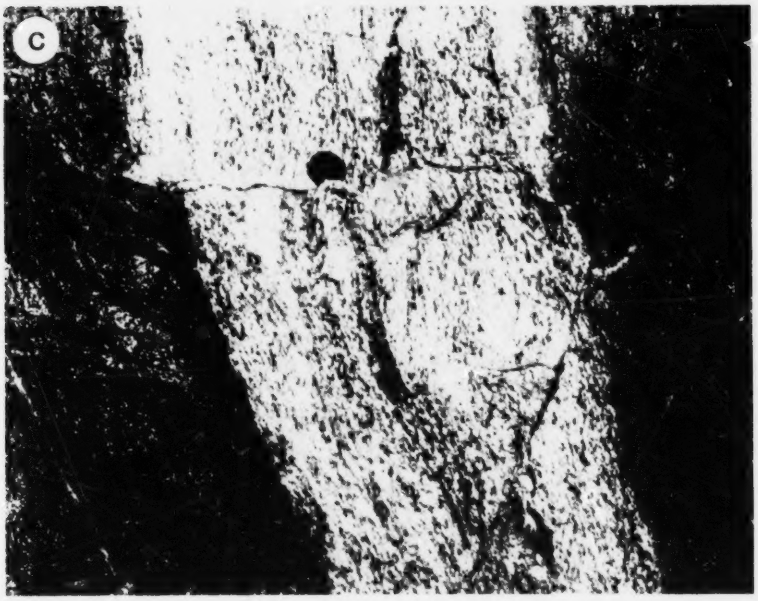

Photo 288.1c. *Interleaving of gneissose trondhjemite and tonalite from the complex. 40 m wide contact zone on the 1400-foot level, Renabie Mine. Note the sharp nature of the contacts.*

fabrics were identified, although Bruce (1944) reports west plunging linear elements at the metavolcanic/gneissose trondhjemite contact.

The parallelism of the interleaved trondhjemite/tonalite contact on the 1400-foot level of the Renabie Mine with the regional fabric suggests that this fabric may have controlled the emplacement of the younger tonalitic phase. Indeed, the weak foliation and occasional banding in the tonalite indicates that the stress field responsible for regional fabric development was, in fact, still active during tonalite emplacement.

MINOR INTRUSIVE PHASES

Gneissose trondhjemite commonly contains aplitic and pegmatitic dikes ranging in width from 5 to 40 cm, with rare composite dikes comprising aplitic margins with pegmatitic cores. The orientations of these dikes vary widely. That most of the regional fabric was superimposed on these earlier aplitic/pegmatitic dikes is indicated by:

1. the internal fabric within the dikes, which is concordant with the external host fabric
2. the development of serrated margins to the dikes, showing high angle orientations with respect to the host foliation. "Teeth" show concordancy with the external host foliation
3. isoclinal folding of aplitic/pegmatitic dikes which have acted as passive strain markers, particularly in close proximity to the highly strained trondhjemite/mafic metavolcanic contact. Internal and external foliations are axial planar

In addition to aplites and pegmatites, the tonalite also hosts microtonalite dikes ranging from 10 cm to 1 m in width. These are generally foliation subparallel, contrasting with the aplites and pegmatites which show highly variable orientations. The tonalite-hosted aplites and pegmatites typically exhibit less strain than those in the gneissose trondhjemite and appear to have been emplaced fairly late with respect to fabric development as indicated by:

1. good crosscutting relationships relative to host fabric and gneissose banding where the latter is developed
2. scalloping and slight strain intensification at dike margins but little internal fabric, suggesting that weak strain was imposed only at dike margins
3. displacement of dikes due to late movement along host fabric planes

Occasionally observed in the tonalite are millimetre- to centimetre-scale glassy quartz veinlets. These are generally discontinuous and may contain pyrite.

Emplacement of less strained later aplites/pegmatites, normally associated with the tonalite, in the gneissose (?) earlier trondhjemite, might be expected. From the criteria outlined above, they should be readily identifiable; however, they have not been observed.

Crosscutting relationships between aplites and pegmatites hosted in either lithology do not provide any consistent temporal relationships regarding emplacement of pegmatitic and aplitic phases.

Au–QUARTZ VEIN MINERALIZATION

DISTRIBUTION OF Au-QUARTZ VEINS

Five major vein/vein systems occur, the main Renabie vein system currently being mined, the Renabie C "west" zone (the western strike extension of the Renabie C zone, which is now inaccessible), the Nudulama vein, the Braminco #21 vein, and the smaller Frontenac extension vein. Their locations are shown in Figure 288.2.

The map shows two trends:

1. a dominant east-west trend exemplified by the Renabie vein-C zone-Nudulama association. The Frontenac and Frontenac extension veins show a similar relationship
2. a northwest trend shown by the Braminco #21 vein and its southern extension

In the case of the Renabie-C zone-Nudulama association it is possible that the vein systems are in some way structurally related. Surface drilling has failed to provide substantial evidence that they are contained within the same structure. They may be contained in shallow *en echelon* structures.

The similarity in style of mineralization observed at Braminco #21 with veins comprising the dominant east-west association suggests that the two trends were generated in the same mineralizing event, and therefore may be related structurally.

ORE ZONE/VEIN GEOMETRICAL CHARACTERISTICS

Ore zone/vein geometric range in complexity from the relatively simple forms, exhibited by the Renabie ore-body (depth>2475 feet), the Nudulama, C zone, and Braminco #21 veins, to complex three dimensional configurations typified by the Renabie orebody (depth<2475-foot level).

The Nudulama and C zones form elongate lenticular orebodies in plan view with dimensions of 156 by 20 m and 220 by 21 m, respectively. Strike varies from west to west-northwest with dips to the south of ~70° to 80°. The ore bodies exhibit a strong westerly plunge of 50°. In detail, they comprise a number of closely associated quartz bodies, varying in dimensions from centimetres to several metres and showing, qualitatively, prolate shapes with long axes plunging parallel to the west.

The plunge of the Renabie vein system is concordant with the other members of the east-west association (Figure 288.3). The remarkably continuous ore body has a consistent plunge of ~55° to ~260° southwest, paralleling the mafic metavolcanic/intrusive contact, though data from the 3265-foot level suggest that this plunge has shallowed to 30°; the dip of the contact is unknown at this level. Below the 2475-foot level, the orebody is dominated by a vertically persistent pipe, crudely elliptical in plan view, striking west-northwest and dipping at ~60° southwest. Dimensions on the 3105-foot level are 45 by 18 m, expanding to 160 by 27 m on the 3300-foot level (Figure 288.4). The main pipe is accompanied by subsidiary prolate pipe-like bodies which are vertically and laterally more discontinuous, often anastomosing with each other, or with the main pipe.

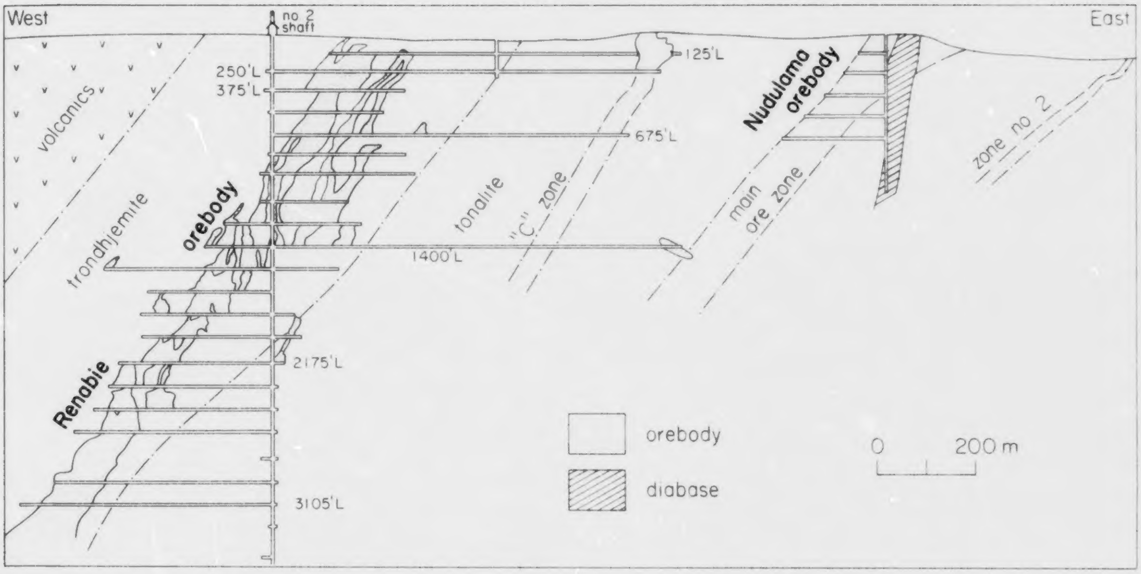

Figure 288.3. East-west vertical cross section through the Renabie C zone, Nudulama vein systems showing consistent ore body plunge parallel to subparallel with major lithological contacts.

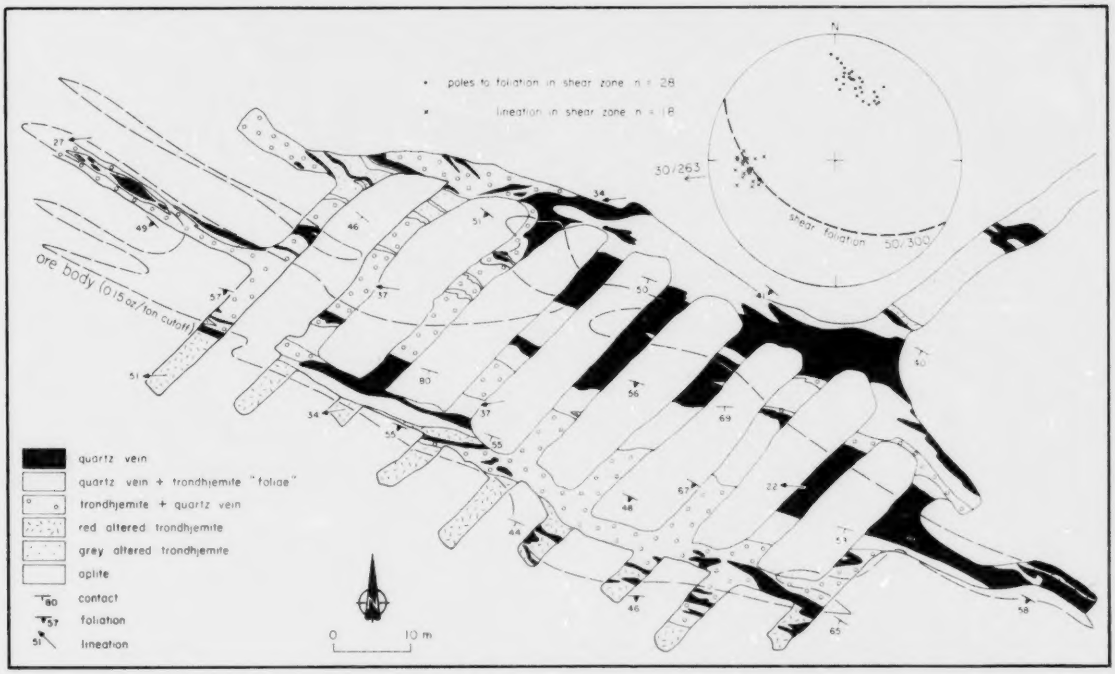
N
• poles to foliation in shear zone n = 28
▪ lineation in shear zone n = 18
30/263
shear foliation 50/300
Ore body (0.15 oz/ton cutoff)
27
49
46
51
57
37
50
34
41
40
80
56
69
22
67
48
44
46
65
58
55
53
quartz vein
quartz vein + trondhjemite "foliae"
trondhjemite + quartz vein
red altered trondhjemite
grey altered trondhjemite
aplite
80 contact
57 foliation
51 lineation
0
10 m

Figure 288.4. Geology, ore zone geometry, and structural elements of the main ore zone, 3265-foot level, Renabie Mine.

At higher levels, the Renabie orebody comprises a number of more distinct ore zones occupying three main orientations; northwest to west-northwest, north-northwest, and west to west-southwest. Zones are commonly elliptical in plan view and lack vertical continuity. Zones may change orientation along strike. On some levels (e.g. 925- and 1400-foot levels), certain zones, apparently once continuous, have been transected and offset sinistrally along late north-northwest brittle/ductile shears forming crude *en echelon* type geometries. This late brittle-ductile shearing event may also explain the 'S'-shaped geometry of the D orebody on the 125- and 250-foot levels. The geometry of the well exposed Frontenac extension vein would be analogous, showing sinistral displacement of the west-southwest trending vein by late north-northwest-trending brittle-ductile shearing.

The northwest striking Braminco #21 vein shows an inverted 'Y'-shaped geometry formed by its bifurcation to form the 6 m wide eastern vein and the 2 m wide western vein at the southern end of the ore zone. The hinge of the bifurcation plunges ~35° northwest. The zone dips to the west at ~55°, more shallowly than the regional foliation, and has a strike length of ~80 m.

Ore zone continuity may be disturbed by late crosscutting diabase and lamprophyre dikes.

SHEAR ZONE CONTROL ON MINERALIZATION

Shear zones are the dominant structural control on Au-quartz mineralization in the Renabie area. All the major orebodies are hosted within these structures. Shear zones, ranging in size from kilometre-scale deformation zones to metre-scale structures, and hosted in a variety of lithologies, have received much attention recently with respect to the localization of Archean Au mineralization, as well as more recent early Proterozoic (Aphebian) deposits. In many Archean (and Aphebian) granitoid-hosted Au deposits and showings, shear zones appear to be an important common feature (e.g. Poulsen and Franklin 1981; Wilkinson 1982; Poulsen 1983; Poulsen *et al.* 1986). The Renabie deposit appears to be unusual by virtue of its size and consistent Au grade.

Shear zones comprise narrow subparallel sided zones in which high strain concentrations, relative to the surrounding rocks, are localized (Ramsay 1980). They may be broadly classified into three types, ductile, brittle/ductile, and brittle, based on the relative importance of ductile and brittle processes. Each type is characterized by specific geometrical features (e.g. Hugon and Schwerdtner 1984; Poulsen 1986) though temporal evolution of the shear zone in response to changes in pressure, temperature, fluid or strain rate conditions may result in superimposition of features characteristic of different types of deformation.

Many of these features have been recognized in the Renabie area, although their interpretation has proved difficult owing to the orientation of the inferred XZ plane of the strain ellipsoid, the critical plane for observation of features in shear zones, especially for determination of displacement. This orientation is such that it is exposed neither in the horizontal plane (i.e. surface outcrop, backs of drifts), nor in the vertical plane (i.e. drift walls).

Shear Zone Geometries

The exposed shear zones comprising the approximately east- to west-trending Renabie C zone-Nudulama association typically show variation in strike within individual shears. Both the Nudulama and the C zone shears define shallow sigmoidal forms, particularly at surface. The strike at Nudulama (Figure 288.5) wanders from ~280° northwest in the east, through ~270° west, to ~283° northwest at the western extremity. The shear shows a variable dip to the south of ~76° to 80°. The C zone exhibits almost identical changes in strike, dipping to the south at 66° to 68°.

Possible explanations include:

1. inherent shear zone wandering (Poulsen 1986)
2. refraction of a more west-trending shear into a more west-northwest orientation due to anisotropy in the foliated host rocks
3. shear zone termination by tip curving (Ramsay 1980). The clockwise rotation would imply a dextral horizontal shear component, which is unlikely in the light of other kinematic indicators

The Renabie vein itself exhibits a more complex system of shears reflected in the ore body geometry discussed earlier. The geology from surface to the 375-foot level (Figure 288.6) is dominated by the B, D, and A zones which constitute an 'S'-shape, possibly reflecting sinistral north-northwest-trending brittle/ductile shearing of an originally west-northwest oriented shear zone, or flexure of a more west-southwest to southwest oriented zone by later sinistral shear in a process similar to sigmoidal tension gash formation. Both the west-northwest orientation of shear together with a more west-southwest to southwest orientation are conspicuous on the 125-, 250-, and 375-foot levels, often with persistent individual shears being correlateable from level to level (*see* Figure 288.6 D, E). Orientations are ~58°SW/305° and ~62°SE/249°. Both may host orebodies, although the former orientation generally hosts the more extensive zones, not only in the upper levels but also throughout the mine (e.g. the main zone below the 2475-foot level is oriented at ~60°SW/295°).

The Frontenac extension vein (Figure 288.7) may represent a close analogy to the structure observed in the Renabie B, D, and A zones at, and just below, surface. The slightly sinuous approximately east- to west-trending mineralized shear is sinistrally offset along a north-northwest-trending brittle/ductile shear with remobilized quartz forming lenses.

The Braminco #21 shear (Figure 288.8) is oriented at 55°SW/326°, dipping more shallowly than the regional foliation in the hosting gneissose trondhjemite, and trending more northwest than the regional fabric.

Shear Zone Boundaries

Boundaries vary from gradational (e.g. the Braminco #21 vein hanging wall contact, C "west" zone)—where shear fabric decreases in intensity, usually with a simultaneous decrease in alteration, and regional fabric becomes discernible again—to somewhat sharper contacts, often marked by more brittle fractures. The latter are well developed at Nudulama, with the fractures forming at the point where rotated regional fabric becomes asymptotic to the high strain part of the shear. The "brittle" type contacts may indicate late reactivation at the high strain boundary since fracture surfaces are commonly striated. Principal C-type fractures in the C "west" zone also represent later brittle-type fractures. Underground, boundaries exhibit similar variation (e.g. the main zone on the 3265-foot level shows a fairly sharp footwall contact but a more gradational hanging wall contact).

Regional Fabric Rotation

The surface exposures of the C "west" and Nudulama shears show rotation of the northwest- to north-northwest-trending regional fabric in the hosting tonalite, over a distance of 0.6 to 2.5 m, into parallelism with the west-northwest to west-trending shear plane (Photo 288.2a). This rotation implies a sinistral shear component in the horizontal plane although the lack of offset markers precludes a quantitative estimate of displacement. The Frontenac extension vein also exhibits a sinistral horizontal shear component as deduced from the rotation of the regional foliation. Foliation rotation may be observed both in the vertical and horizontal planes in the Braminco #21 pit. Regional foliation is observed to swing from a north-northwest trend into the northwest trend of the shear in the horizontal plane, while simultaneously shallowing in dip in the vertical plane as the foliation is deflected into the shear plane. This feature is more difficult to identify underground. A good example has been observed on the 1400-foot level where the north-northwest trending regional fabric is rotated sinistrally over 3.5 m into concordancy with the steep east-west shear hosting the D(E) orebody. Simultaneous steepening of foliation may not necessarily imply a normal shear component since horizontal shear alone may cause steepening of the regional foliation toward the shear. Foliation rotation is also observed at the hanging wall contact of the west-northwest-trending main ore zone on the 3335-foot level, Renabie Mine. This is discussed below.

Shear Zone Fabric

The shear zones are characterized by two predominant fabrics:

'C' Fabric A 'C' fabric, generally observed to be parallel to subparallel with shear zone boundaries, which is defined by a planar orientation of secondary sericite and some original biotite (in less altered zones) enclosing elongate quartzofeldspathic domains and Au-bearing quartz veins. In general, the orientation of shear foliation (S) relative to shear zone boundaries may be used to deduce shear sense (Ramsay 1980). This has proved problematical here owing to the markedly dominant C fabric, possibly a consequence of rotation of any pre-existing shear foliation into parallelism with shear boundaries as a result of large shear displacements.

Mineral Elongation A mineral elongation contained within the mylonitic fabric. This feature is best observed in the C "west" zone where elongate quartzofeldspathic rods, plunging 52°/267°, are enclosed in the sericitic/biotitic foliation (Photo 288.2 b,c). The elongation lineation in altered shear zone material in the main zone, 3265-foot level, Renabie Mine, again defined by elongate quartzofeldspathic domains, plunges at 30°/263°. This is coincident with an intersection lineation of the foliation on plunging quartz bodies enclosed within the foliation. The Frontenac extension vein also shows a mineral elongation best developed in the 0.3 m region, where regional foliation is rotated into the shear plane, and plunging 46°/263°.

Mineral elongations generated during ductile shear are important indicators of net shear direction. The examples described above would imply oblique net shear displacements.

Corresponding with these ductile lineations are more brittle lineations including slickensides on altered wall rock foliation surfaces (e.g. Nudulama) and rodding/striations on shear-hosted quartz lenticles (e.g. Frontenac Extension vein, B north zone; Photo 288.2d). Interestingly, the long axes of prolate Au-bearing quartz bodies also show, in a qualitative sense, a plunge concordant with both ductile and brittle lineations.

Slickensiding and weakly developed mineral elongation plunge 42°/282° at the Braminco #21 vein, approximately parallel with the plunge of the vein bifurcation hinge at its southern end.

Other Kinematic Indicators

Transected Dikes Passive strain markers in the form of aplitic/pegmatitic dikes hosted in the intrusions, and showing high angle orientation with respect to shear zones, are progressively rotated into the west to west-northwest shear at Nudulama (*see* Photo 288.2a), eventually evolving into well developed boudins as the deformed dike enters the high strain region of the shear. Deflection clearly indicates a sinistral horizontal component of shear. This is thought to be the origin of more isolated pegmatitic/aplitic boudins within the Nudulama and C "west" zone shears.

Shear Hosted Fold Structures Asymmetric folds are commonly developed in aplitic/pegmatitic dikes which have been caught up in the shear zones (Photo 288.2e). Quartz stringers also show fold development. Examples at Nudulama, the C "west" zone and B "north" zone, Renabie Mine generally show S-shaped asymmetry when viewed on the horizontal plane, suggesting a sinistral horizontal shear component. Folded quartz veins underground on the 3265-foot level, Renabie Mine, show Z asymmetry in a vertical plane suggesting normal displacement in this plane. Minor folding at Braminco, observed in both shear-hosted quartz veins and in the shear foliation itself, shows both S and Z type asymmetry when viewed approximately on the inferred XZ plane, although the latter appears to dominate. Interpretation of these asymmetrical folds requires caution for two reasons. Ideally, fold asymmetry should be viewed

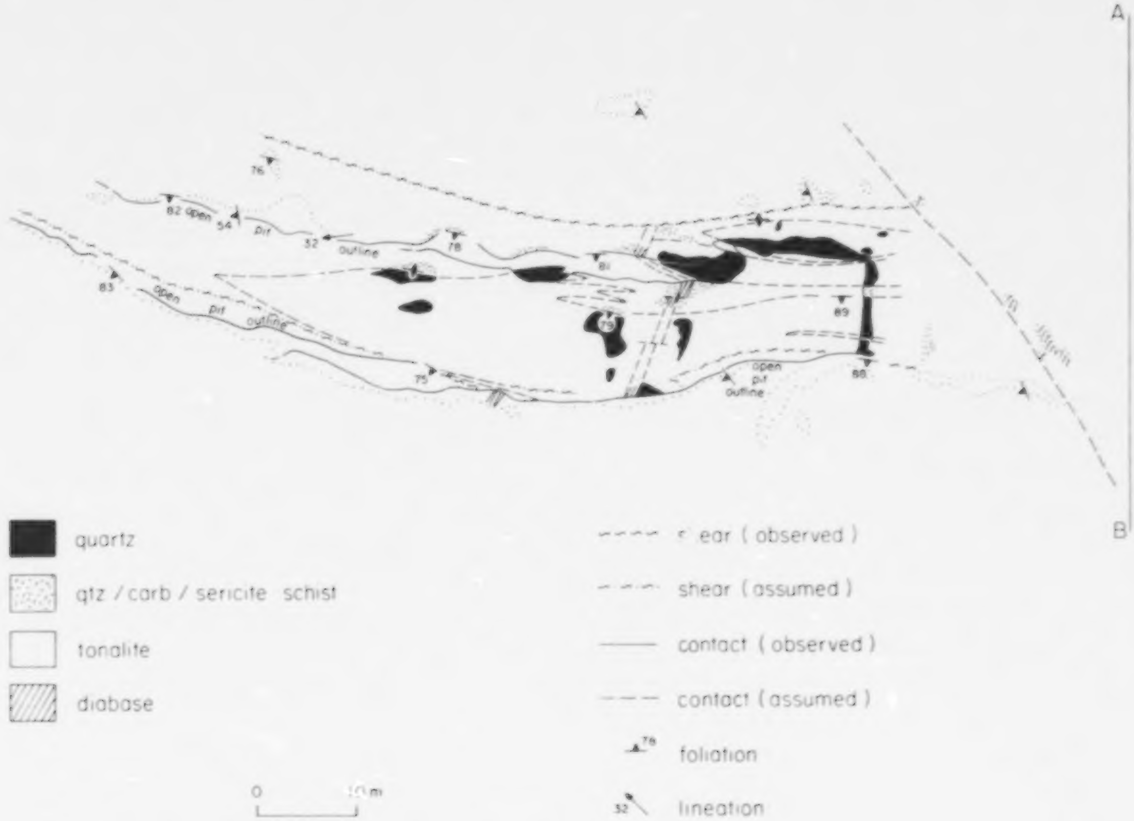

Figure 288.5. Geology and structural elements of the Nudulama vein.

on a plane parallel with the maximum extension direction, but perpendicular to foliation in the shear zone (i.e. the XZ plane of the strain ellipsoid). This plane is generally poorly exposed in the field. Under conditions of simple shear, passive rotation of both pre- and syn-shear linear structural elements (e.g. fold hinge axes) may result in progressive reorientation of these elements toward parallelism with the stretching lineation (Sanderson 1973; Skjernaa 1980; Bryant and Reed 1969).

In the case of preshear folds, this deformation would be superimposed on the earlier strain state, resulting in a total strain state which may be profoundly influenced by the preshear strain state. Hence, fold geometry may not necessarily be reflecting shear deformation alone.

Even syn-shear folds may undergo significant reorientation where fold hinge axes, which initially formed parallel to the intermediate strain axis (Y axis of the strain ellipsoid) and in optimum orientation for kinematic interpretation purposes, are progressively oriented towards parallelism with the stretching lineation. The coincidence of measured fold hinge orientations with that of stretching (mineral) lineation in the study area suggests that reorientation may have occurred under high shear strains. Preshear geometry of aplite/pegmatite veins could also be a significant factor in determining their present geometry.

Shear Bands An oriented sample taken from the northern margin of the C "west" zone shear, and cut in the XZ plane, shows a shear foliation on which weak planar surfaces are superimposed (see Photo 288.2b) which form an angle of ~30° with shear foliation. These may represent shear bands (White *et al.* 1980), alternatively referred to as an extensional crenulation cleavage (Platt and Vissers 1979) though they were not identified in a more highly strained sample as would be expected, perhaps suggesting correspondence to C type shears as opposed to C'. Their orientation would imply a reverse south-side-up component of shear.

KINEMATIC INTERPRETATION

Sense of movement is reasonably well constrained for the Braminco #21 shear. Regional foliation deflections in the hanging wall of the main shear and in parallel subsidiary shears provide good evidence for a sinistral horizontal shear component and a reverse, west-side-up vertical shear component. The interpretation is corroborated by west-northwest plunging mineral elongation and slickenside lineations.

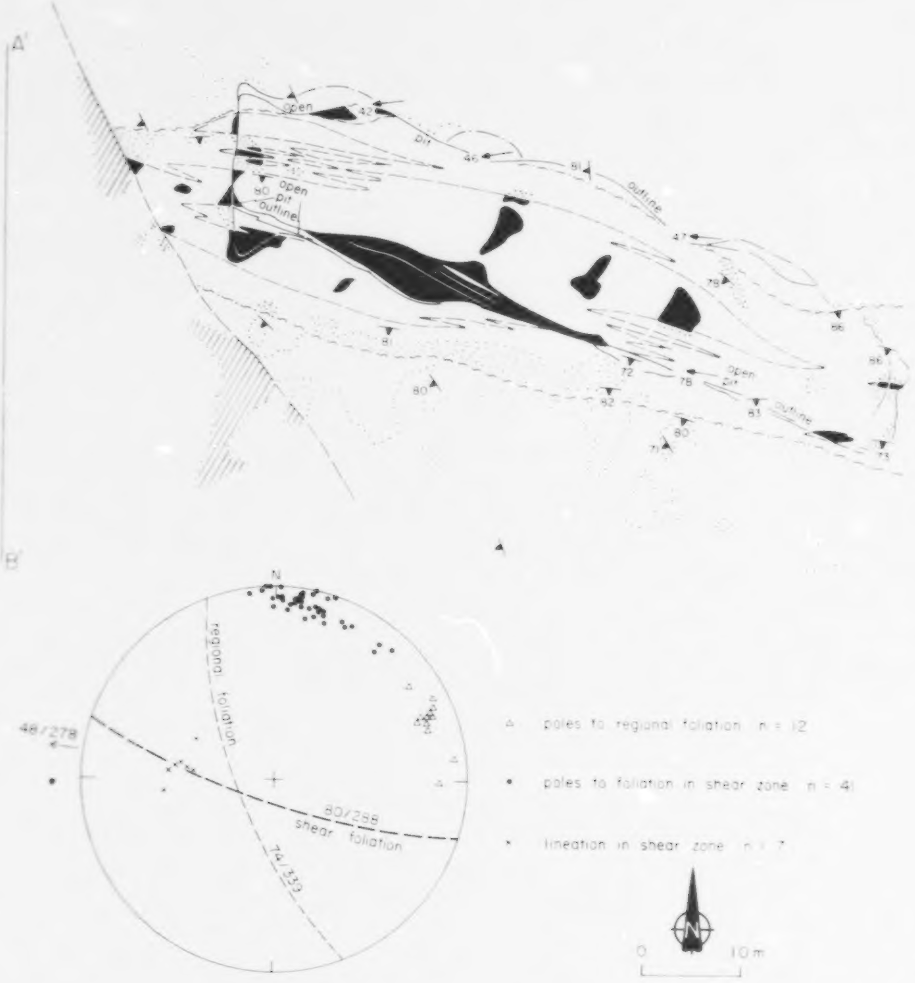

Observation of regional foliation deflection in a sinistral sense in the horizontal plane and steep west to west-southwest plunging lineations, including mineral elongations, at Nudulama and in the C "west" zone should, in theory, uniquely define shear directions for these shear zones. A sinistral, reverse, south-side-up sense of movement is indicated with the sinistral horizontal component being tentatively supported by fold asymmetry on the horizontal plane in the C "west" zone. Data on the vertical plane, however, are lacking due to poor exposure. Further work focusing on foliation within the shears and its relationship to shear zone walls may add a greater degree of certainty to this interpretation.

Similar features (i.e. regional foliation deflection in a sinistral horizontal sense and west plunging mineral lineations and quartz rodding) suggest a similar net shear displacement for the Frontenac Extension vein.

Interpretation of the Renabie vein system itself is problematical at present owing to poor constraints on net shear for the dominant shear zone orientations. Angular relations between shears in the more complex upper levels of the Renabie Mine (Figure 288.6 D) are suggestive of conjugate shear development. The two conjugate sets would be expected to show opposite shear displacements, commonly with an earlier set displaced by its later conjugate set. Though more work is needed to constrain shear displace-

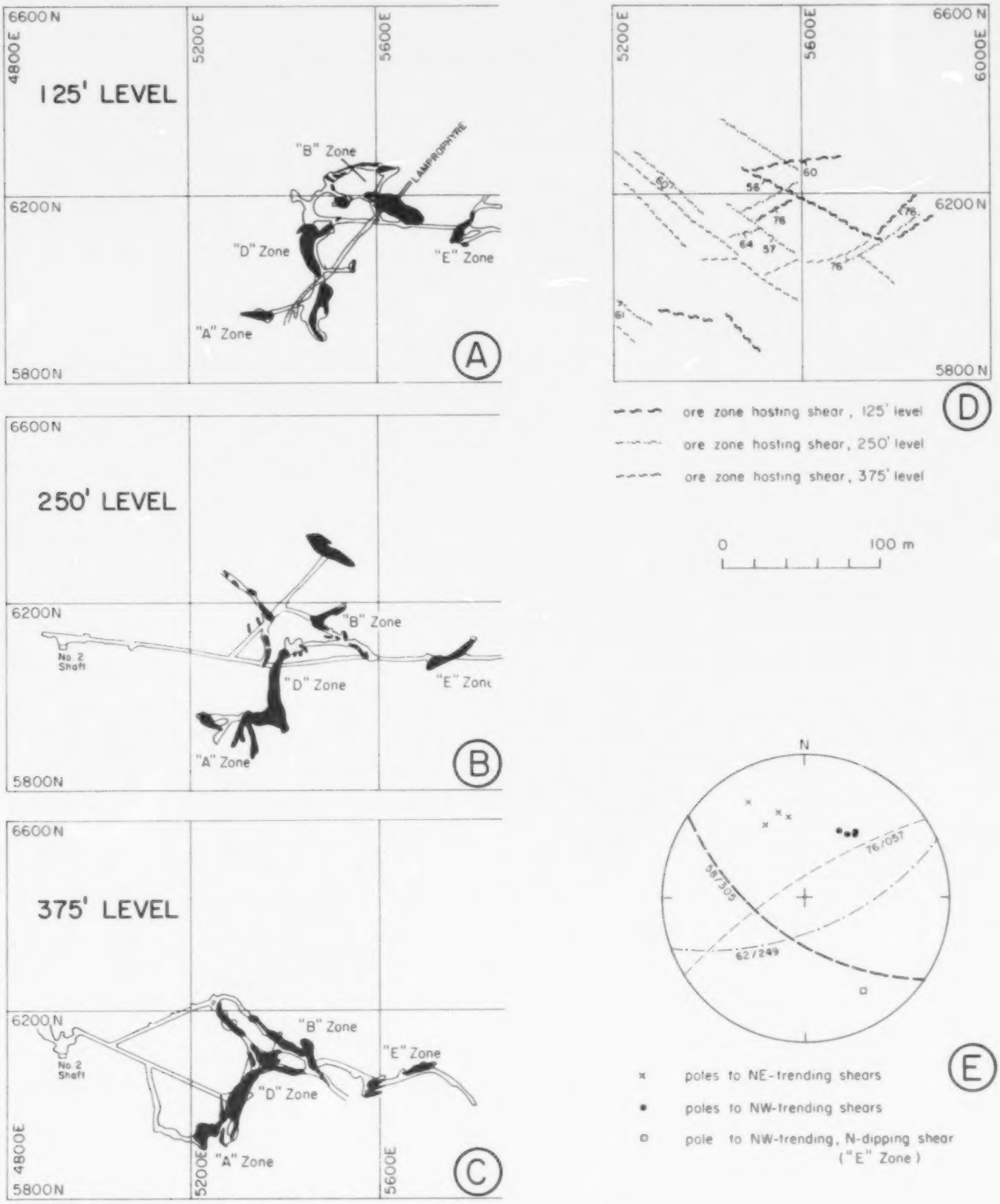

Figure 288.6. *A,B,C; ore zone geometries of the 125-, 250-, and 375-foot levels, Renabie Mine.*
D. Horizontal projection showing distribution of ore zone hosting shears on the 125-, 250-, and 375-foot levels. Dips are calculated where possible by extrapolation between levels. Note that the "D" zone structure has been omitted. Its possible origin is discussed in the text.
E. Stereographic projection (equal angle) showing the two dominant ore zone hosting shear orientations. A third orientation is shown by the "E" zone hosting shear.

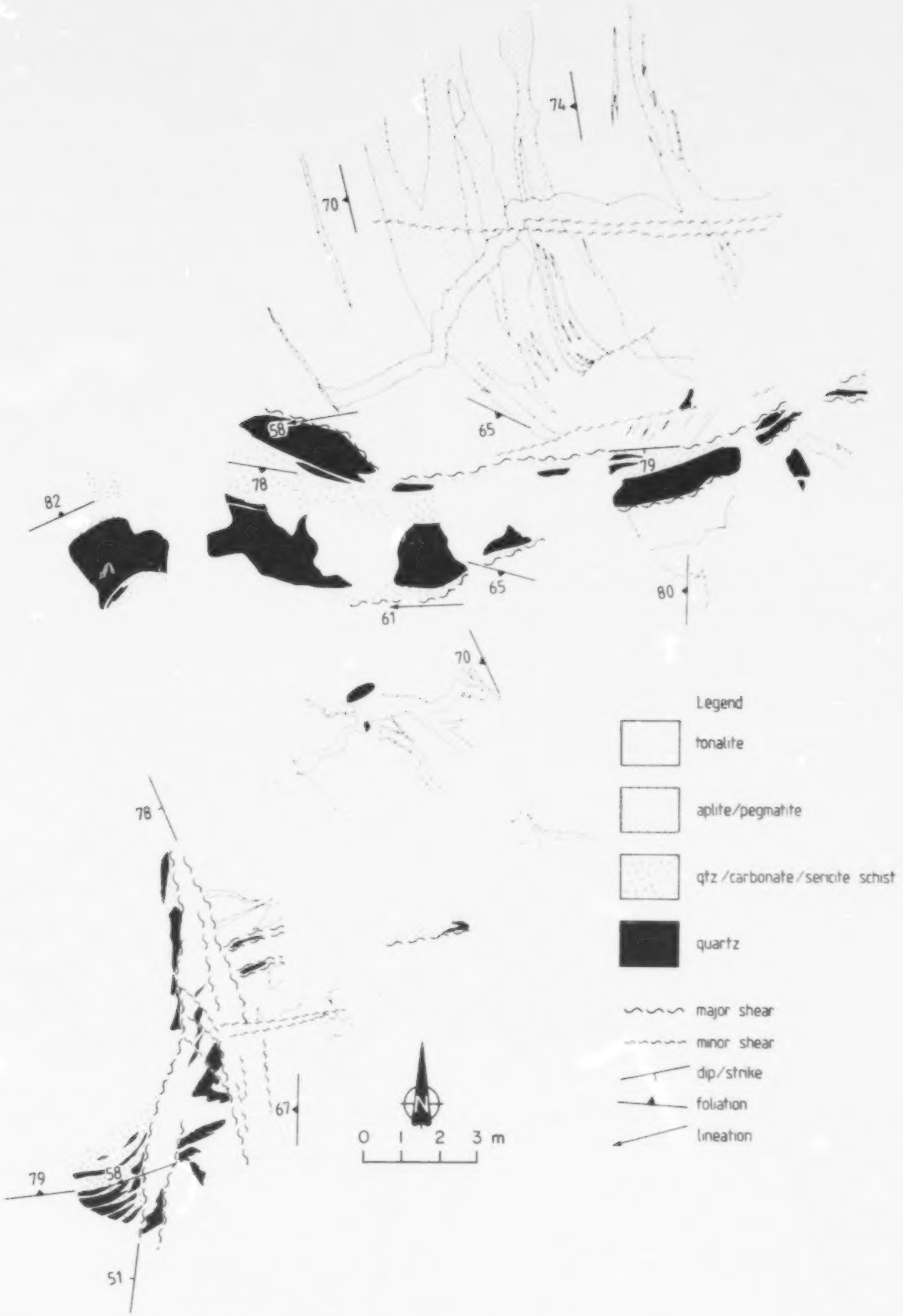

Figure 288.7. *Detailed geology of the Frontenac extension vein.*

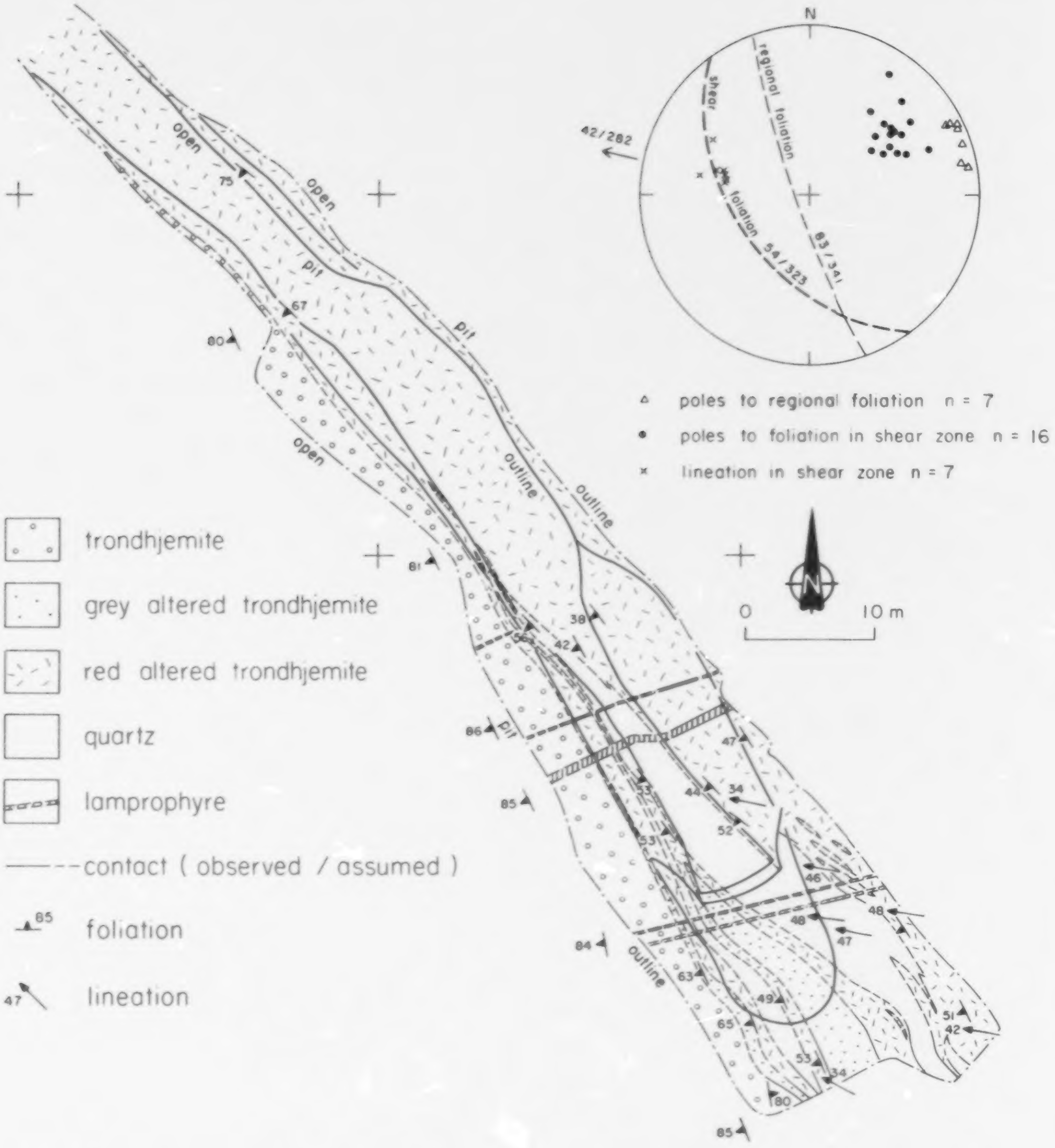

Figure 288.8. Geology and structural elements of the Braminco #21 vein.

ments, it is interesting to note that west-southwest- to southwest-trending shear-hosted orebodies often terminate rather abruptly against the better developed, more northwest-trending ore-hosting shears, and, on the 125- and 250-foot levels, appear to be displaced sinistrally in a horizontal sense.

Observations pertinent to the deduction of net shear displacement on the hosting shears in the Renabie vein system include:

1. west plunging lineations within the west-northwest-trending main zone shear on the 3265-foot level which indicate an oblique net shear displacement approximately parallel with the plunge of the orebody. This, together with its west-northwest orientation, suggests that the zone is developed in a shear structure closely analogous to the C zone and Nudulama shears. If net shear on such structures is consistent, it is possible that west-northwest shears generally ex-

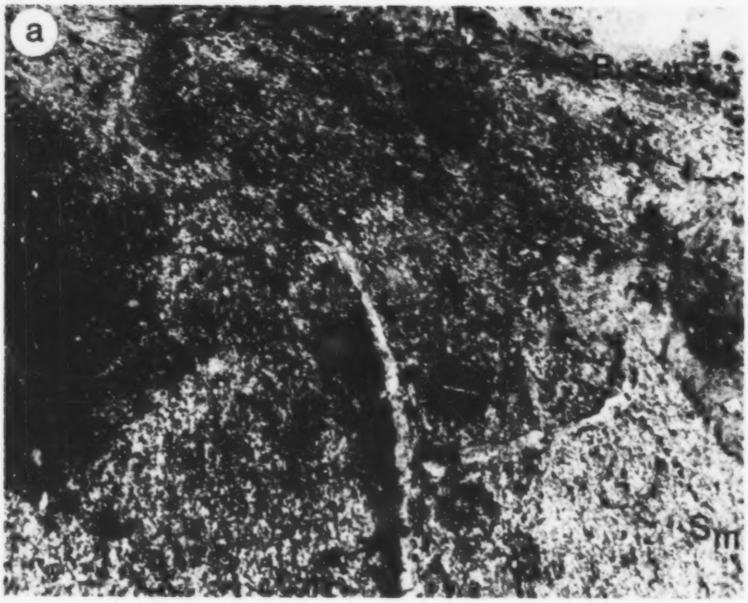

Photo 288.2a. *Rotation of regional foliation (S_m) and tonalite-hosted aplitic vein (A) into the hanging wall shear plane (SB), Nudulama west pit. A sinistral horizontal shear component is implied.*

hibit a reverse sinistral, south-side-up net shear displacement.

2. regional foliation trending 77°SW/352° swinging sinistrally in the horizontal sense, and progressively steepening in the vertical sense to 85°SW/274° into concordancy with foliation in the shear which hosts the northeast- to west-trending D (E) orebody on the 1400-foot level.
3. data from a slot on the 3335-foot level, which provides a rare section through the hanging wall contact of the main ore zone, show regional foliation trending 56°SW/328° being progressively rotated towards the shear to 74°SW/285°, defining a sinistral horizontal shear component. Minor folding observed in the shear fabric plunges 63°SE/162° and shows S-shaped asymmetry when viewed on the inferred XZ plane. This observation is consistent with a sinistral reverse, south-side-up oblique net shear displacement.
4. minor fold asymmetry within quartz veins in the main zone shear on the 3265-foot level indicates a normal shear component. The reliability of such indicators is in doubt as discussed earlier.

TIMING RELATIONSHIPS BETWEEN MINERALIZATION AND SHEAR ZONE DEFORMATION

Initiation of shear structures is interpreted to have predated mineralization since the strike extremities of the well mineralized shear zones, especially at Nudulama and, to a lesser extent, the C "west" zone show high strains typical of the shear zones but minimal observable hydrothermal alteration in outcrop. This characteristic is particularly evident at the western end of the Nudulama west pit where the shear zone is defined by a ~12 m zone of highly strained tonalite with well developed minor folds. Reduction in alteration intensity, but persistence of shear fabric, can actually be observed from the hanging wall, where the main quartz body lies, towards the footwall. A similar situation occurs at the western end of the C "west" zone. It is interesting to note that mineral lineations are commonly best developed in the less intensely quartz veined, narrower, strike extensions of shears. Where the shear has been strongly dilated by quartz vein emplacement the shear fabric is dominated by conspicuous flattening.

Most quartz emplacement occurred late during shear zone deformation but prior to the termination of shearing. Minor, probably earlier, veining shows high strain as strings, isoclinal folds, and boudins. Larger scale veins retain their integrity and show geometries which appear to be related to host shear kinematics (i.e. flattened, prolate forms plunging concordantly with subvertical plunging ductile lineations). Virtually all quartz shows rather granular textures indicative of some deformation, with associated ore and gangue minerals, especially pyrite and carbonate, showing fabrics and textures indicative of syndeformational precipitation.

Alteration associated with late syndeformational quartz deposition appears to promote enhancement of the deformation fabric, probably due to growth of initially strain free alteration minerals which may accommodate significant strain during shearing (e.g. sericite). This is termed reaction enhanced ductility (White and Knipe 1978; Beach 1980). Post-deformation alteration would tend to obliterate shear fabrics, whereas alteration minerals in the examples studied here typically form an integral part of the shear fabric, with the exception of unaltered regions within shears as noted above.

CHARACTERISTICS OF SHEAR ZONE HOSTED Au-QUARTZ VEINS

Shear zone-hosted quartz veins account for almost all the quartz veining observed in the area.

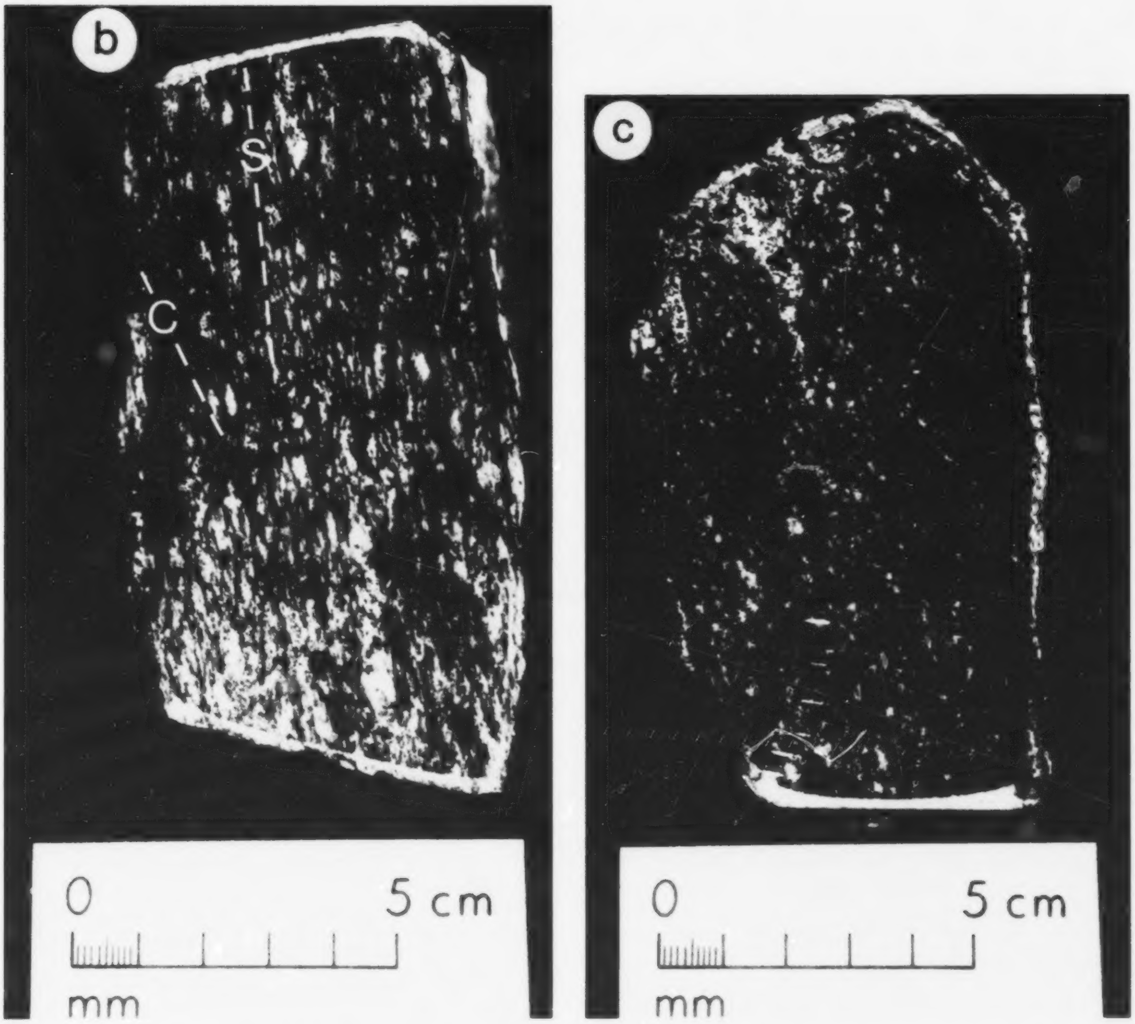

Photos 288.2b,c. *Strained tonalite from C "west" shear zone, cut in a plane parallel with the lineation and orthogonal to foliation (b) and perpendicular to lineation (c). The lineation is defined by the elongate quartzofeldspathic domains. Note weakly developed shear bands (C) in b.*

Volumetrically, quartz forms a major component of the shear zones; at Nudulama west pit, for example, the exposed face which represents almost the complete width of the shear (~12 m), comprises at least 75% quartz. Similarly the 3265-foot level, Renabie Mine, exhibits massive quartz veining up to 20 m in width.

Appearance

Quartz veins within shears show a range in width from centimetre scale stringers to metre scale veins and lenses. Veining is generally parallel to subparallel to shear foliation, and less commonly is observed to crosscut foliation in the form of spurs which splay off the foliation parallel veins (Photo 288.3a). These are indicative of hydraulic fracturing by overpressured mineralizing solutions, though generally, shear zones appear to have been dilated by pressurized fluid emplacement along the anisotropy represented by the sheared host rocks. The resulting "banded vein" comprises fabric parallel quartz veins on a centimetre scale separated from each other by millimetre to centimetre-scale wall rock foliae showing extensive sericitic and pyritic alteration (Photos 288.3b,c). These foliae appear to have been split away from the altered wall rock as a result of brittle failure at its margin during each vein emplacement event. The distinctive geometry is indicative of a "crack-seal" type of vein-filling mechanism (Ramsay 1980) and is well developed at Nudulama, the C "west" zone, Frontenac extension vein, the Braminco #21 vein hanging wall, and in the main zone between the 3105- and 3300-foot levels, Renabie Mine.

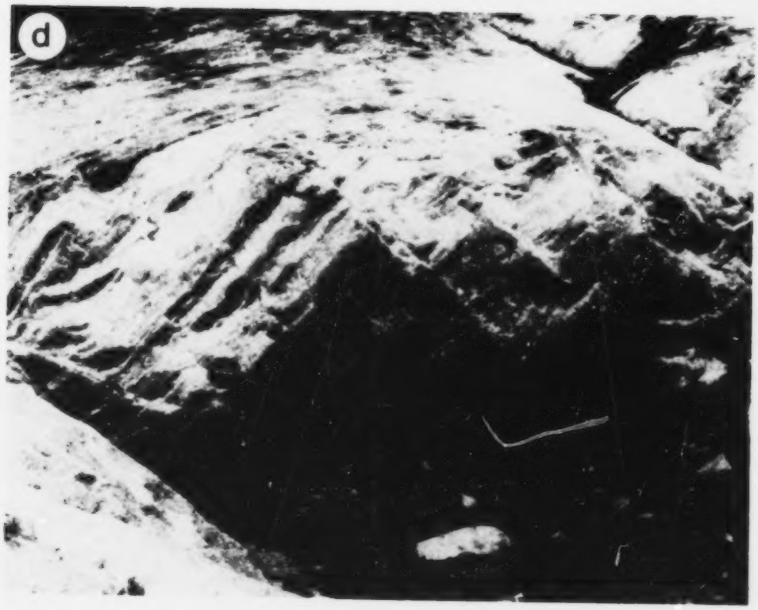

Photo 288.2d. *Westerly plunging striations on a westerly plunging quartz lens, B "north" zone, Renabie Mine.*

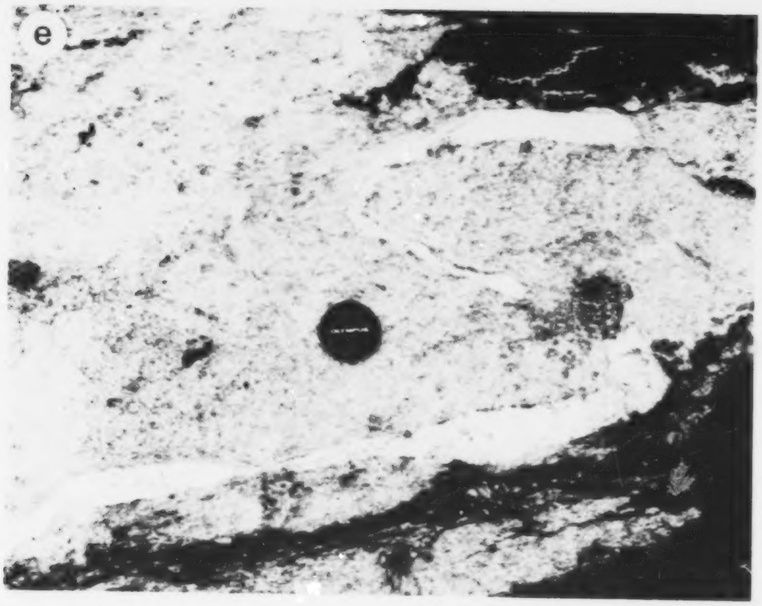

Photo 288.2e. *Asymmetrically folded aplitic/pegmatitic vein in C "west" shear zone, Renabie Mine. A sinistral horizontal component of shear is implied.*

Quartz veining may also be massive, with few altered wall rock inclusions. Massive "bull" quartz is well developed close to the footwall on the 3265-foot level, Renabie Mine (Photo 288.3d) and in the Nudulama E pit. The quartz is granular, pure white, contains no other mineral phases and typically contains poor Au values.

A significant part of the main zone on the 3300-, 3265-, and 3235-foot levels, Renabie Mine, comprises massive smoky grey-white quartz with green-grey sericitic streaks, bands, and veinlets, often with abundant, rather granular pyrite (Photo 288.3e). These define a fabric concordant with shear foliation. This massive quartz may reach widths of up to 20 m on the 3265-foot level.

In the main zone between the 3105- and 3300-foot levels at the Renabie Mine, the intensity of veining falls off gradually into the hanging wall. The latter shows a well developed shear fabric, extensive alteration in the form of silicification, sericitization, carbonate alteration, and pyritization, and a conspicuous red colouration, possibly related to carbonate alteration. Alteration progressively diminishes into the hanging wall, with simultaneous loss of the red col-

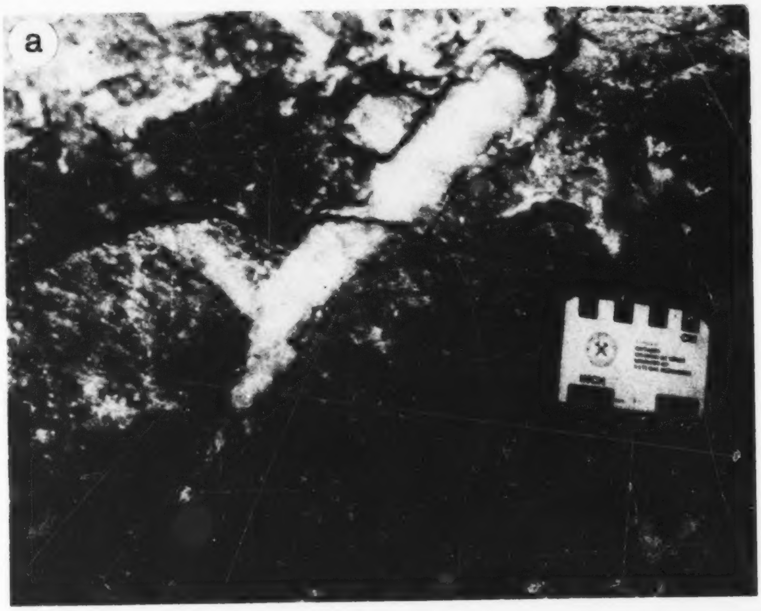

Photo 288.3a. *Quartz spur showing high angle crosscutting relationship to shear foliation, 3265-foot level, Renabie Mine.*

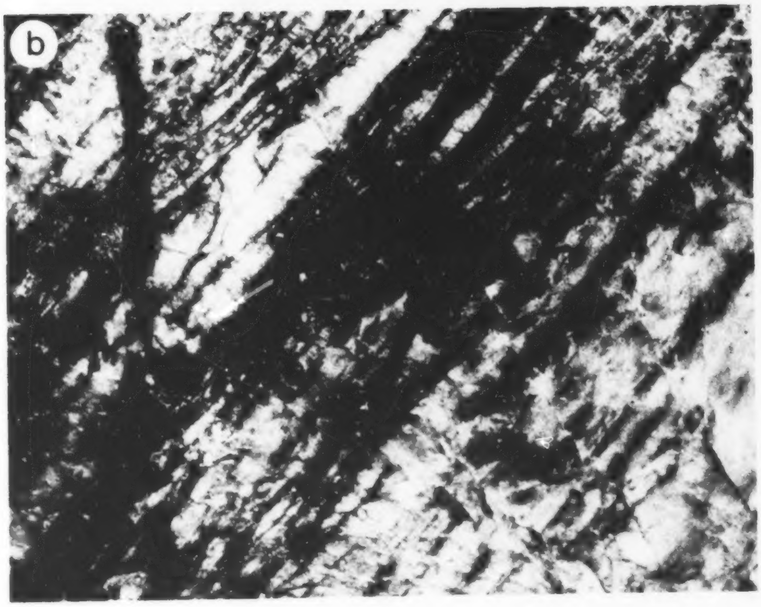

Photo 288.3b. *Banded quartz vein, 3265-foot level, Renabie Mine.*

ouration. Ore grade Au values persist into the red altered trondhjemite.

This zoned alteration is well developed around the shear-hosted quartz veins at Braminco.

Ore Mineralogy

Ore minerals comprise a small proportion of the vein material, rarely exceeding ~5% and commonly much less.

Pyrite Pyrite is the most abundant ore mineral; most other minerals occur only in trace amounts. It is commonly observed as anhedral or rarely euhedral to subhedral grains of variable size up to 0.8 cm across in trains or bands associated with sericite foliae and thin altered wall rock fragments (Photo 288.3f). Larger altered wall rock inclusions commonly show more disseminated fine-grained pyrite, and may exhibit banded selvages of pyrite at their contacts with enclosing quartz. Massive quartz veins may contain grains or clots of more solitary euhedral to subhedral pyrite up to ~1.5 cm in size, usually showing some fracture development. Smaller examples from a high

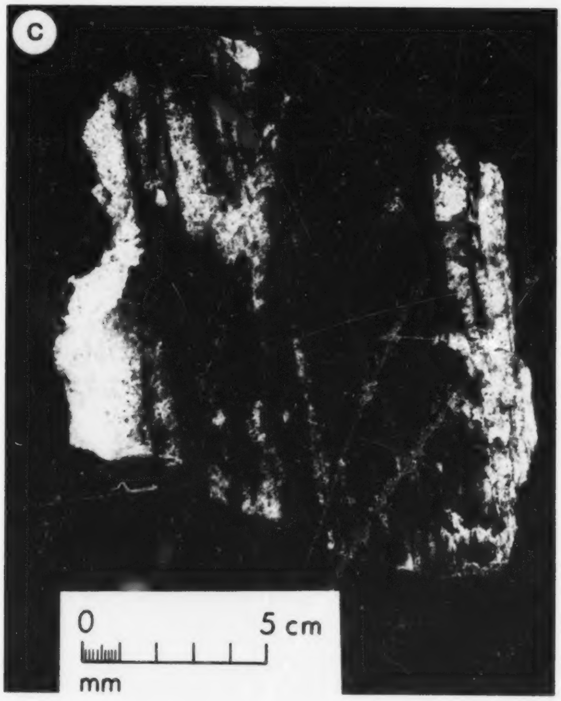

Photo 288.3c. *Sample from banded quartz vein, 3265-foot level, Renabie Mine, showing distinctive crack-seal type geometry, defined by fabric parallel quartz veins separated by altered, sheared wall rock foliae.*

grade shoot on the 3265-foot level, Renabie Mine, show development of euhedral but unusual, inequant grain shapes (e.g. tabular and prismatic pyrite), with flattening and elongation correlating in a qualitative sense with the foliation and lineation in the ore zone respectively.

More massive altered wall rock contains fine-grained disseminated pyrite, which, in highly strained, altered wall rock, may become markedly abundant to produce a pyritic schist with strained pyrite bands forming a strong foliation component (e.g. Nudulama E pit footwall).

Much of the textural evidence such as fracturing, granulation of larger grains to form trains and bands, and inequant euhedral habits suggests that deformation was still active during pyrite crystallization.

Chalcopyrite Chalcopyrite is typically associated with pyrite and exhibits an anhedral habit. It is considerably less abundant.

Galena Galena is observed fairly frequently and is commonly associated with higher Au grades. Fine-grained visible Au may often be present with galena. Galena rich shoots occur in the E vein at Braminco and on the 3265-foot level, Renabie main zone. It has also been identified on the 1400- and 250-foot levels. The mode of occurrence on the 3265-foot level is fairly typical (Photo 288.3g), with the galena forming discontinuous veinlets parallel with the fabric within the ore zone, as defined by altered wall rock foliae, sericite stringers, and pyritic strings. Galena veinlets may be isolated or focused on pyrite grains and clots. The "fabric" exhibited by the galena veinlets could be a result of syndeformational recrystallization, or emplacement into a late spaced fracture system, the development of which was controlled by the shear fabric anisotropy.

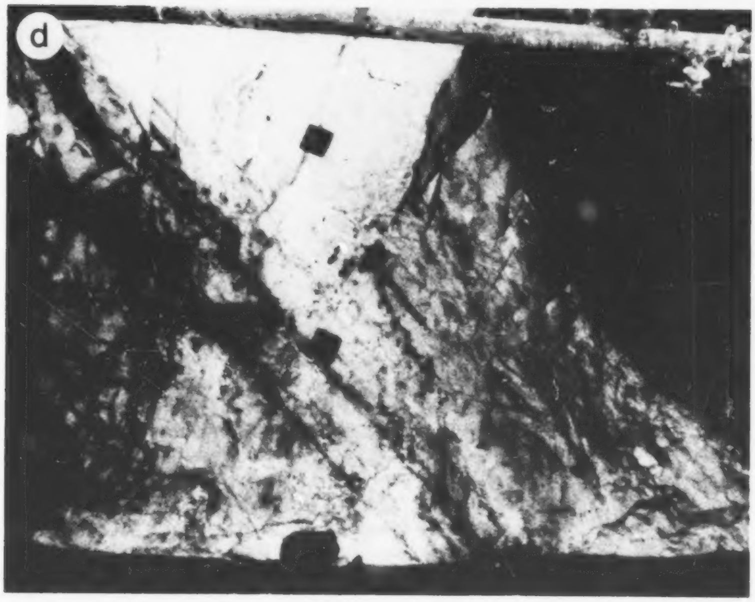

Photo 288.3d. *Massive, unmineralized "bull" quartz, footwall of main ore zone, 3265-foot level, Renabie Mine.*

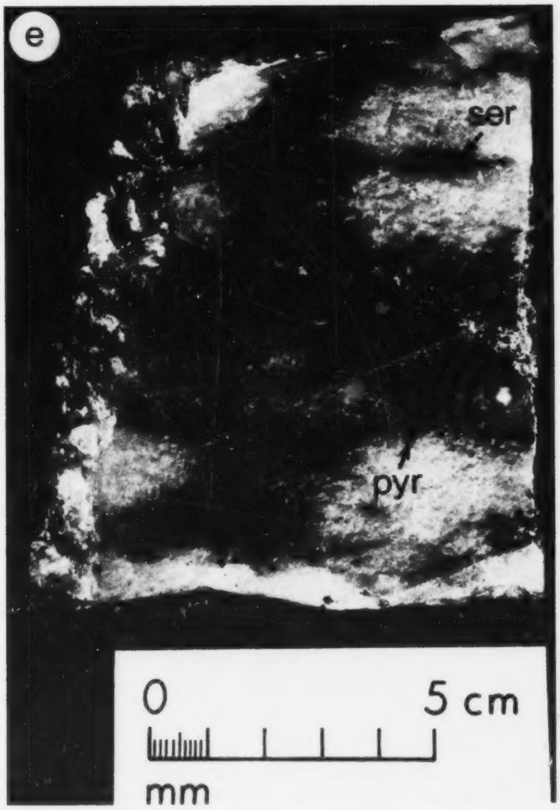

Photo 288.3e. *Typical massive mineralized quartz with foliation defined by green sericitic streaks with associated pyrite and chalcopyrite.*

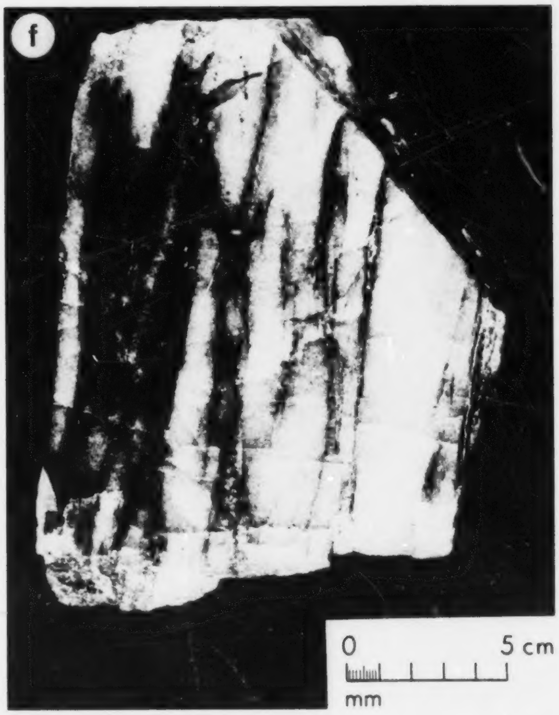

Photo 288.3f. *Banded vein material showing thin sericitic foliae and intensely altered, sheared wall rock foliae with extensive associated pyrite, Nudulama west pit.*

Tellurides In exceptional cases tellurides with associated visible Au may be identified in outcrop and hand specimen. Tellurides typically impart a dirty grey colour to the host quartz when present in sufficient quantities (e.g. high grade Au shoot, hanging wall of Nudulama E pit). Here altaite (PbTe) is identifiable due to its very high reflectivity and greenish white hue as opposed to the metallic grey of galena. Where visible, the tellurides show a fracture-fill habit similar to galena, or form more diffuse bands of dispersed, finer grains.

Molybdenite Molybdenite is conspicuous in the footwall of the main shear hosted vein at Nudulama, occurring within the sericitic and pyritic foliae which enclose lenticular quartz bodies. The molybdenite forms a metallic sheen on the foliation surfaces. These molybdenite "smears" also occur in the pyritic footwall schist of the Nudulama E pit.

Gold Visible Au is uncommon, though the strong galena/telluride Au association is a valuable guide to the location of fine visible Au (<1 mm). A telluride-rich shoot in the Nudulama E pit hanging wall has provided the best examples.

Gangue Minerals

Quartz Quartz is the dominant gangue mineral. It shows variable characteristics, ranging from a grey, vitreous and compact variety with a more blocky fracture, to a white, highly friable variety with a flaky, shard-like fracture. The fine grained, glassy, cellular, or bubble-like texture exhibited by much of the quartz indicates some degree of recrystallization associated with strain.

Carbonate Carbonate, generally granular with grains <2 mm in size, occurs as fabric-parallel elongate clots and stringers within more massive veins and as selvages associated with altered wall rock fragments and foliae. Wall rock is also pervasively carbonate metasomatized.

Sericite Sericite is a ubiquitous mineral forming variably continuous millimetre-scale foliae, as well as somewhat more dispersed patches within massive mineralized quartz. Sericite is commonly found along thin <1 mm spaced fractures parallel with shear foliation, and frequently encloses lenticular quartz bodies, often in association with other minerals. Wall rock fragments show extensive sericitic alteration as does the more massive wall rock where sericite, enclosing elongate quartzofeldspathic domains, forms the strong foliation present in the altered wall rock (e.g. 3265-foot level, Renabie Mine).

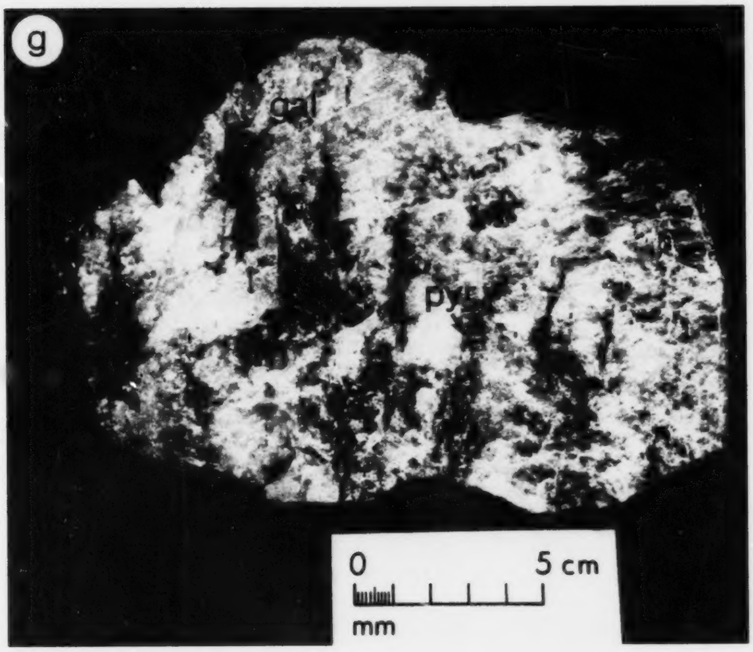

Photo 288.3g. *High grade ore sample from hanging wall ore shoot, 3265-foot level, Renabie Mine, showing foliation defined by galena bands/veinlets (arrowed), thin sericitic foliae and pyritic bands/ stringers.*

Photo 288.3h. *Late pyrite-anhydrite-MoS_2—bearing, tabular quartz veins cutting main shear-hosted mineralization, 3105-foot level, Renabie Mine.*

Anhydrite Anhydrite was only identified underground and is well developed in the main zone between the 3105- and 3300-foot levels. Here, it varies in colour from lilac to pale brown and occurs most frequently as marginal selvages and occasionally as more central clots associated with minor quartz veining in altered wall rock. The anhydrite may be intimately associated with sericite and pyrite. This habit is also observed on the 1400-foot level. Anhydrite may also occur in more massive quartz veins intergrown with granular carbonate and minor pyrite.

Tourmaline Tourmaline is uncommon in the vein systems in the Renabie area. The Braminco #21 vein shows rare tourmaline occurring as centimetre-scale clots forming selvages on sericitized wall rock foliae adjacent to the margins of the larger quartz veins. The tourmaline is fine grained in regions where quartz appears to be more recrystallized, or forms well developed acicular crystals in areas of less strained vitreous quartz. Fine grained, matt black tourmaline also occurs as fine selvages in millimetre-scale deformed quartz veining in altered wall rock. This latter habit was observed at one locality on the 3300-foot level, and on the 3375-foot level, Renabie Mine.

Fluorite Fluorite, occurring as a small centimetre-scale pod in highly altered wall rock, was identified on the 3300-foot level, Renabie Mine. This example was the only one observed.

Potassium Feldspar Rare pink potassium feldspar selvages are closely associated with tourmaline in the Braminco #21 vein.

CHARACTERISTICS OF QUARTZ-PYRITE-ANHYDRITE-MoS_2—BEARING VEINS

These veins constitute a very minor phase of the mineralization at the Renabie Mine, having been observed in three localities: on the 3105-foot level where they form subhorizontal tabular veins up to ~25 cm in width which crosscut the main shear-hosted mineralization (Photo 288.3h), in the "Barren Zone" (which forms the "tail" of the main zone on this level); in the shaft area, 3105-foot level, where veining is associated with an aplitic dike; and on the 1400-foot level where, again, subhorizontal tabular veining up to 10 cm in width transects a 1.5 m shear zone. The veins are characterized by more waxy, less strained quartz with subhedral pyrite up to ~1 cm across, lilac anhydrite selvages up to ~5 cm in width, and fine-grained (millimetre-scale) molybdenite flakes, generally occurring at vein margins. Au grade is unknown as yet.

PRINCIPAL CONCLUSIONS

1. Major Au-quartz vein mineralization in the Renabie area (5.5 million tonnes at ~6 g/tonne Au and ~2 g/tonne Ag) occurs in marginal trondhjemitic and tonalitic phases of the Wawa Domal Gneiss Terrane up to 1.7 km away from the adjacent Michipicoten greenstone belt.
2. Mineralization is hosted in brittle/ductile shear zones of variable orientation which observably crosscut and rotate the variably developed regional metamorphic flattening fabric and gneissic banding in the trondhjemites and tonalites.
3. Currently available structural data suggest a reverse, south-side-up, sinistral shear displacement for the west to west-northwest trending Nudulama, C zone, and Frontenac extension vein shears, and a reverse, west-side-up, sinistral shear displacement for the northwest-trending Braminco #21 vein shear.
4. Shear zones in the more complex Renabie vein system occupy a variety of orientations, often complicated by late crosscutting faults and dikes. West-southwest to southwest and west-northwest to northwest trending orientations are dominant, with the latter hosting the most extensive orebodies. Orientations are consistent with conjugate shear sets. Kinematics, however, are poorly constrained at present.
5. Prolate, shear-hosted ore zones show a consistent plunge, often parallel with ductile and brittle lineations in the hosting shears and subparallel with major lithological contacts in the area.
6. Initiation of shear zones predated the introduction of hydrothermal fluids.
7. Fabrics and other strain features exhibited by the mineralization indicate that mineralization and associated alteration occurred synchronously with shear deformation, possibly in the later stages.
8. "Crack-seal" type vein-filling structures are indicative of shear zone dilation by pressurized Au-bearing mineralizing fluids which used the anisotropy represented by shear zone fabric.
9. Associated minerals are typical of Archean Au-quartz vein/shear zone deposits and include quartz, pyrite, galena, tellurides, molybdenite, carbonate, anhydrite, and minor tourmaline.
10. Renabie-type deposits should be valid exploration targets since this type of deposit is unlikely to be unique in occurrence.
11. Since the Renabie area Au-quartz-vein/shear zone mineralization with a mineral/element association characteristic of Archean Au-quartz vein deposits occurs outside the confines of a greenstone belt, the possibility is raised that high level processes within greenstone belts may not have been important in the generation of Archean Au-quartz vein ore fluids. An alternative possibility is that processes within the underlying, intrusive TTG layer (tonalite-trondhjemite-granodiorite; Wawa Domal Gneiss Terrane) may have been those which were important. Hence, the Renabie area could be significant in the overall study of Archean Au-quartz vein/shear zone deposits.

Laboratory work in progress includes a detailed petrographic examination of host lithologies and mineralization, an examination of the major and trace element geochemistry of host intrusions and associated phases, and a fluid inclusion and light stable isotope study of the mineralization.

ACKNOWLEDGMENTS

The authors wish to thank Lyall Chapman and Chester Moore of Renabie Gold Mines Limited for permission to work at the Renabie Mine and, together with Ed Toivenen, for their generous assistance and cooperation underground. Thanks are also extended to Malcolm Slack of Canreos Minerals (1980) Limited and John McCombe of Missibay Mining Limited for permission to work at the Braminco Mine site. Special thanks to Steve Jenner (Geologist, Canreos Minerals (1980) Limited, Toronto) for his assistance and helpful discussion. Permission from O.A. Seiber of Anglo Dominion Gold Exploration Limited to work on the Nudulama Property is gratefully acknowledged. Thanks to Subhash Shanbhag and Brian O'Donovan (University of Toronto) for drafting and photographic assistance, respectively. Last but not least, thanks also to Dave Burrows (Graduate Student, University of Toronto) for stimulating discussion.

REFERENCES

Beach, A.

1980: Retrogressive Metamorphic Processes in Shear Zones with Special Reference to the Lewisian Complex; Journal of Structural Geology, Volume 2, p.257- 263.

Bruce, E.L.

1944: Geology of the Rennie-Leeson Area, District of Sudbury; Ontario Department of Mines, Annual Report for 1942, Volume 51, Part 8, p.1- 26.

Bryant, B., and Reed, J.C.

1969: Significance of Lineations and Minor Folds near Major Thrust Faults in the Southern Appalachians and the British and Norwegian Caledonides; Geological Magazine, Volume 106, p.412- 429.

Ferguson, S.A.

1968: Renabie Mines Limited, Nudulama Mines Limited and Adjoining Properties, Surface Geology, Parts of Rennie, Leeson and Brackin Townships, District of Sudbury; Ontario Department of Mines, Preliminary Geological Map P.492, scale 1:6000 or 1 inch to 500 feet.

Hugon, H., and Schwerdtner, W.M.

1984: Structural Signature and Tectonic History of Gold Bearing Rocks in Northwestern Ontario; Grant 149, p.164-176 *in* Geoscience Research Grant Program, Summary of Research 1983-1984, edited by V.G. Milne, Ontario Geological Survey, Miscellaneous Paper 121, 252p.

Percival, J.A.

1981: Stratigraphic, Structural and Metamorphic Relations between the Wawa and Abitibi Subprovinces and the Kapuskasing Structural Zone near Chapleau, Ontario; p.83- 90 *in* Current Research, Part A, Geological Survey of Canada, Paper 81- 1A.

1986: The Kapuskasing Uplift: Archean Greenstones and Granulites; *in* Geological Association of Canada, Canadian Geophysical Union, Joint Annual Meeting, Ottawa '86, Field Trip 16 Guidebook, 37p.

Platt, J.P., and Vissers, R.L.M.

1979: Extensional Structures in Anisotropic Rocks; Journal of Structural Geology, Volume 2, p.377- 410.

Poulsen, K.H.

1983: Structural Setting of Vein-Type Gold Mineralization in the Mine Centre-Fort Frances Area: Implications for the Wabigoon Subprovince; p.174- 180 *in* The Geology of Gold in Ontario, edited by A.C. Colvine, Ontario Geological Survey, Miscellaneous Paper 110, 278p.

Poulsen, K.H., Ames, D.E., and Galley, A.G.

1986: Gold Mineralization in the Star Lake Pluton, La Ronge Belt, Saskatchewan: A Preliminary Report; p.205- 212 *in* Current Research, Part A, Geological Survey of Canada, Paper 86- 1A.

Poulsen, K.H., and Franklin

1981: Copper and Gold Mineralization in an Archean Trondhjemitic Intrusion, Sturgeon Lake, Ontario; p.9- 14 *in* Current Research, Part A, Geological Survey of Canada, Paper 81- 1A.

Ramsay, J.G.

1980: The Crack-seal Mechanism of Rock Deformation; Nature, Volume 284, p.135- 139.

1980: Shear Zone Geometry: A Review; Journal of Structural Geology, Volume 2, p.83- 99.

Sanderson, D.J.

1973: The Development of Fold Axes Oblique to the Regional Trend; Tectonophysics, Volume 16, p.55- 70.

Skjernaa, L.

1980: Rotation and Passive Deformation of Randomly Oriented Planar and Linear Structures in Progressive Simple Shear; Journal of Structural Geology, Volume 2, p.101- 109.

White, S.H., Burrows, S.E., Carreras, J., Shaw, N.D., and Humphreys, F.J.

1980: On Mylonites in Ductile Shear Zones; Journal of Structural Geology, Volume 2, p.175- 187.

Wilkinson, S.J.

1982: Gold Deposits of the Atikokan Area; Ontario Geological Survey, Mineral Deposits Circular 24, 54p.

Grant 290 Improved Computer Interpretation of Gravity and Magnetic Data

R.C. Bailey[1] **and S.W. Reford**[2]

[1]Geology and Physics Departments, University of Toronto, Toronto

[2]Physics Department, University of Toronto, Toronto

ABSTRACT

Modern, automatic, computer-based gravity- and magnetic-modeling methods which do not require operator intervention or *a priori* specification of the topology of the model are almost always "extremal" methods. They do not generally produce geologically "reasonable" models. We propose an "extremal" method based on a "complexity" norm for density (or magnetization) models; namely, the mean value of the magnitude of the density (or magnetization) gradient. On the basis of analogous work done in unidimensional seismic-inversion problems, minimization of this norm, subject to fitting both the gravity (or magnetic field) measurements and the density (or magnetization) values obtained by direct sampling at the surface or underground, should lead to simple (reasonable) models. Numerical tests on synthetic data generated for simple, two-dimensional test structures (a tabular sill, a dipping thick dike of finite depth extent) indicate that this is the case.

INTRODUCTION

Potential field data, such as gravity or magnetic-field measurements, are used to infer the density or magnetization structure of the earth below the surface. A fundamental property of the solutions obtained for the structure is that they are not unique. It is normal for an infinite family of solutions to fit a given data set equally well. In the early days of potential-field interpretation, this was not a major obstacle to useful—if primitive—interpretation as the allowed models were normally restricted to a special group of structures. This led to questions such as "What is the spherical body of uniformly anomalous density which best fits the observations?." The real "anomalous body" was then presumed to be similar to the special model, at least in gross properties such as the total excess mass or depth to the centre of the mass. The advent of computers has made it possible to go much further than this. Computers make possible the easy generation of very complex models, many of whose features may be totally speculative in the sense of being allowed but not required by the data. This has made it mandatory for the question of non-uniqueness of solutions to be addressed. Despite the plethora of computerized inversion methods for modeling which are discussed in the literature, the most practical approach in mineral-exploration problems is still in many cases to judiciously "cut and try" models which are constructed to both fit *a priori* information and the data, and not be unnecessarily complicated otherwise. It is in obeying this last requirement, that of simplicity, that many current, automatic, computerized methods are deficient.

This paper first reviews the main ways in which computers are applied to the potential-field interpretation problem (using, for the sake of discussion, the gravity problem, in which the features of the methods are not obscured by the complexities of vector rather than scalar source parameters), and then describes a new method for automating the choice of "simple" models, and the results of applying this method to some synthetic data examples.

METHODS

Current computer methods of finding a density (or magnetization) model for the Earth that fits a given set of gravity (or magnetic) measurements are of two main types—manual and automatic. There are methods which combine some aspects of both, but this is a useful working classification.

By manual methods, we mean those in which the basic topological structure of the model (such as one or more polyhedral bodies of uniform density in a uniform host background) is chosen in advance and then modified as necessary by the interpreter. Manual methods, despite the possibility of bias by the interpreter, are still very useful for two reasons:

1. the simplicity of the models generated, typically with sharp density contrasts corresponding to lithologic changes, which are built into the type of model used
2. the ease with which *a priori* information can be incorporated in the model (such as known densities in certain locations as obtained by sampling)

By automated methods, we mean those in which the density as a function of position is free to vary arbitrarily. In practise, this means representing the Earth as a rectangular array of small cells, within each of which the density is uniform and has to be determined by the modeling algorithm. Automatic methods are almost all "extremal" methods. That is, of the very many density models which may produce an acceptable fit to the gravity data, the chosen one is that which "extremizes" some property.

CURRENT "EXTREMAL" METHODS

Models which minimize or maximize some quantity have various purposes, not necessarily that of finding a structure whose density distribution is the closest to the truth. Examples of current methods include the following:

Minimum Error of Fit

This is perhaps the worst method for purely automatic modeling. Since many models fit a given dataset acceptably, there is no reason to prefer that one whose fitting errors are the smallest. Indeed, the extreme complexity induced in the models by the attempts to squeeze the fitting error as small a value as possible normally renders such models useless without some additional smoothing or damping.

Least RMS Density Anomaly

This is the so-called "smallest" model yielded by the methods of Backus and Gilbert (1967, 1968). It tends to yield very smooth results, so that lithologic boundaries are blurred.

Minimum-Density Contrast

This is the "Ideal Body" approach pioneered by R. Parker (1974, 1975). An anomalous-density variation is found in which the total-density contrast from smallest to largest is as small as possible. This normally results in an anomalous body of uniform density in a unifrom host, but one whose boundaries can be exceedingly complex. The lower bound obtained for density contrast can be decisive in some interpretation problems (Chavez *et al.* 1987), but the density distribution obtained does not necessarily resemble the truth very closely.

Most Compact Bodies

This method is due to Last and Kubik (1983) and has been developed further by Guillen and Menischetti (1984). It produces simple bodies, which is an advantage. In the presence of noise in the data (which can be measurement error or a deviation from some modeling assumption such as that of two-dimensionality), it tends to a set of very small bodies (point masses in the limit) as far as possible. This can produce implausibly high-density contrasts unless the method is explicitly restrained.

Most Like A Preferred Shape

This method is due to Mottl and Mottlova (1972). Simple bodies again result, but the potential bias introduced by having to choose a "preferred shape" negates one of the advantages of automatic modeling.

THE SIMPLICITY NORM METHOD

The most useful solution for geological interpretation in practical exploration problems is in general the "simplest" or "most reasonable" structure that both fits the data and any *a priori* constraints (such as measured densities at the surface or down boreholes). The crucial problem is the quantitative definition of "simplest" and "most reasonable" as some sort of norm or unlikelihood function to be minimized; the computation of the model is then fairly straightforward. Although continuous density and magnetization variations certainly occur in nature, preferred modeling schemes are those which can generate sharp boundaries, corresponding to real discontinuous changes in lithology. By this we do not mean those schemes in which the boundaries (and thus a specific presumed structure) are put into the model *a priori* by the interpreter; we mean schemes in which smooth density variations are not favoured over sharp ones.

A suitable candidate for such a norm, as suggested by similar work on unidimensional modeling by Levy and Fullagar (1981) and Oldenburg *et al.* (1984) of seismic reflection data, is

$$\mathbf{S} = \int\!\!\int\!\!\int |\nabla\rho(x,y,z)| \; dx\, dy\, dz$$

where ρ is the density, and the volume integral is over the entire model volume.

Somewhat surprisingly (but, after the fact, less so), the straightforward, central-difference, discrete formulation of S, namely

$$S = \sum_i \sum_j \sqrt{\rho_x^2(i,j) + \rho_y^2(i,j)}$$

where the horizontal and vertical density gradients ρ_x and ρ_y are given by

$$\rho_x(i,j) = \frac{1}{2}\left[\rho(i+1,j) - \rho(i-1,j)\right]$$

and

$$\rho_y(i,j) = \frac{1}{2}\left[\rho(i,j+1) - \rho(i,j-1)\right],$$

works very badly. Like many discrete-operator equivalents to continuous operators, it generates parasitic oscillating solutions not possessed by the original continuous problem. In particular, the above formulation decouples the model cells into two independent sets corresponding to the black and white squares of a chessboard.

The best formulation of S seems to be simply the sum of the absolute values of the density differences across all cell boundaries in the model:

$$\mathbf{S} = \sum_i |\Delta\rho|_i$$

where the index i ranges over all intercell boundaries in the model, and $\Delta\rho$ is the change across the ith boundary. Density changes across the surface of the Earth are not included in this sum, since this marks an erosional rather than a lithologic boundary. Note that for a structure which is a single *uniform* anomalous body, the norm S is just the product of the density contrast and the body area (perimeter in two dimensions).

This should in fact measure something like what an interpreter would regard as "complexity", although there may be a considerable difference. However,

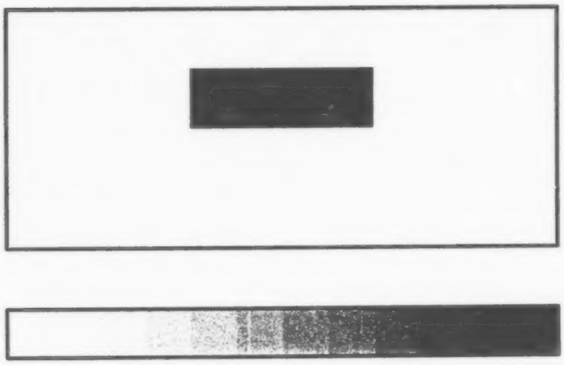

Figure 290.1. *A simple sill structure. The model density range is 0.0 to 1.0 g/cm³. The value of S is 8.0.*

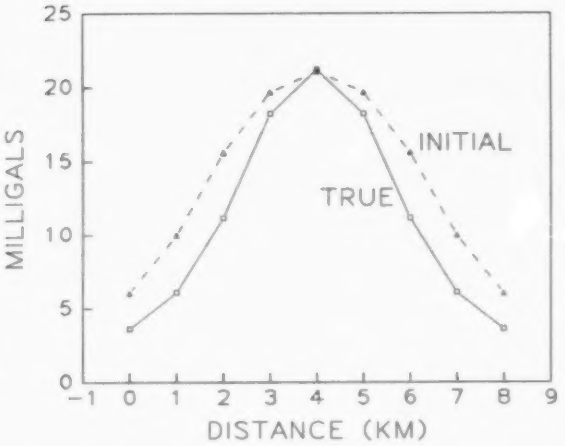

Figure 290.2. *The gravity anomaly (a) of the true structure shown in Figure 290.1 (squares and solid line), and, (b) the initial model in Figure 290.3 used to start the solution for the model of Figure 290.1 (triangles and dotted line).*

the minimization of S is in fact to be done while respecting any *a priori* density data from sampling. This use of such ancillary information greatly reduces the number of "simple" models which can fit the data. If a great deal of such information is included, the scope for differences between the simplicity judgement of this method and that of an interpreter is greatly reduced. Finally, it must be remembered that in cases where the Earth is actually complex in the "S" sense, the modeled result will be too simple.

COMPUTATIONAL METHODS

The program developed for test purposes operates by minimizing the simplicity norm described above, subject to the following constraints: a) that all $\rho(i)$ (the density of the i'th cell) be non-negative (inequality constraints); b) that $\rho(j)$ equal specified values in those cells j in which the density is known *a priori* (equality constraints); c) that the model fit the data adequately, i.e. that $m(k) < d(k) + e(k)$ and that $m(k) > d(k) - e(k)$ where $d(k)$ is the k'th measured datum, $m(k)$ is the value of that datum predicted by the model, and $e(k)$ is the size of maximum acceptable misfit to the k'th datum (inequality constraints); and, d) that $\rho(j) \leq \rho_M$ where ρ_M is the largest geologically reasonable density in the particular problem (inequality constraints).

At present, the simplicity norm algorithm uses a general-purpose, nonlinear optimization algorithm: a sequential augmented Lagrangian method described by Gill *et al* (1981), as implemented by the NAG Fortran library subroutine E04UAF. This is very convenient for test and developmental work as it is very general; unfortunately, it is also slow. It is an iterative procedure, and requires an initial guess at the solution. We have shown that the equations above, and the norm, can be rewritten in the form of a standard linear-programming problem, which can be solved much faster using the revised, simpler method.

UNCONSTRAINED OPTIMIZATION RESULTS

The information that enables manual interpretation to produce useful, simple models is normally in the form of density constraints defined by sampling at the surface or in boreholes or mines. Without such constraints (which are equivalent to *a priori* information about the geological structure), interpreted models may be meaningless. The method proposed here cannot circumvent the ambiguities enforced by the laws of potential-field theory, and will give equally meaningless results under similar circumstances. It is not intended to be applied without additional density information from sampling. Its virtue is that it readily allows the incorporation of such information.

Despite this fact that the method is intended to work in conjunction with density constraints obtained from sampling, it is instructive to examine the results obtained from data derived for some simple synthetic models without using such constraints. All the density models shown here are two-dimensional with infinite strike length, and are shown in section using grey-scale plots. The models each consist of a rectangular array of cells within which the density is constant. The top of each section represents the surface of the Earth, and there is no vertical exaggeration. The anomalous density outside the section shown is assumed to be zero. Beneath each such section is a grey-scale calibration bar, corresponding to a density range indicated in the caption. Gravity-measurement profiles, where shown, are across strike, and the data used consist of one measurement per model-grid interval, and occupy the same horizontal extent as the model sections shown. They are assumed to represent anomalous gravity after the removal of a regional trend or value. Finally, quoted values of S are comparable between models obtained for the

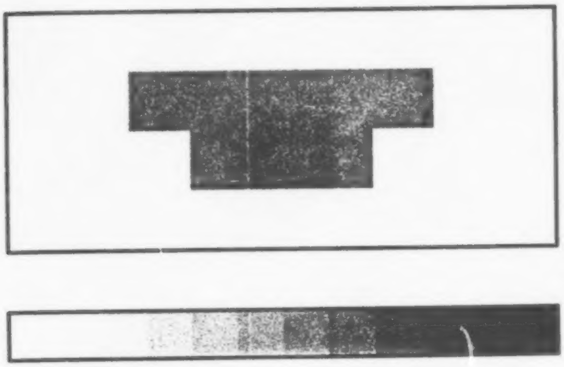

Figure 290.3. *The initial model used to start the solution for the model of Figure 290.1. The model density range is 0.0 to 0.5 g/cm^3. The density scale is -0.1 to +1.0 g/cm^3. The value of S is 7.0.*

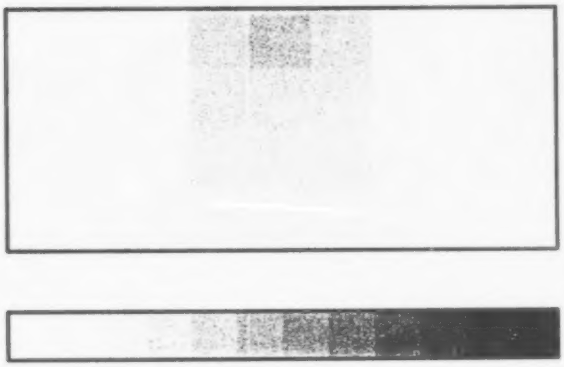

Figure 290.4. *The unconstrained solution for the data corresponding to the model of Figure 290.1. The model density range is -0.02 to 0.335 g/cm^3. The density scale is -0.1 to +1.0 g/cm^3. The value of S is 2.3.*

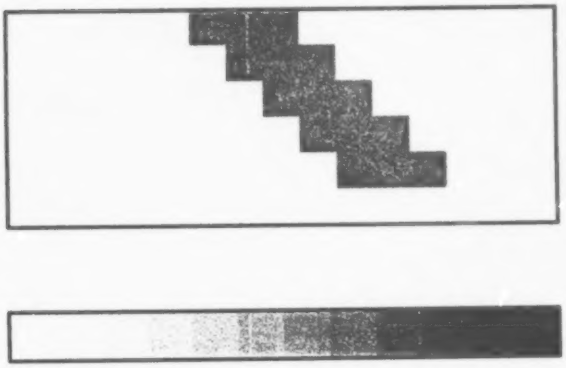

Figure 290.5. *The dipping-dike structure. The model density range 0.0 to 0.5 g/cm^3. The density scale is -0.1 to +1.0 g/cm^3. The value of S is 1.05.*

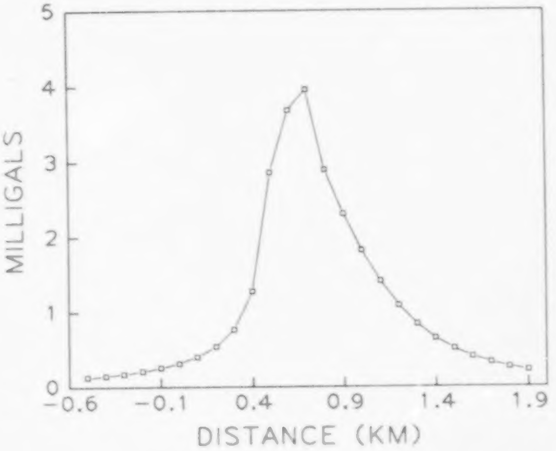

Figure 290.6. *The gravity anomaly for the dipping-dike structure shown in Figure 290.5.*

same dataset. The units used for S are gigagrams per square metre.

A very simple, sill-like model is shown in Figure 290.1. Synthetic gravity data (shown in Figure 290.2) were generated from this model. This is a rectangular prism 1 km thick, 3 km wide, and buried 1 km, with an anomalous density of 1.0 gm/cm^3. For test purposes, the model was made very simple, and comprises a 9 by 4 array of 1 km square cells.

The starting model used for the iterative solution is shown in Figure 290.3. Note that it has a lower S value than the true structure, but does not fit the data, as shown in Figure 290.2. The nine data points were assumed to have errors of 0.01 mgal, and any model fitting all points to within this margin is considered to be fitting adequately.

Figure 290.5 shows the model recovered by unconstrained minimization. Not surprisingly, it has a lower S value than the true structure shown in Figure 290.1. As one would expect, the highest densities are concentrated at the surface to reduce the value of the norm. There are two reasons for this: deeper sources would require higher densities to fit the data, thereby increasing the norm S; and, density contrasts across the surface are not penalized as noted above. There is little resemblance to the true structure shown in Figure 290.1.

Figure 290.6 shows the gravity response of another test structure, a dipping dike-like model whose density section is shown in Figure 290.5. The array of prisms, each prism being 100 m by 100 m, is 1500 m across and 600 m deep. The body itself is 300 m wide and 500 m in depth extent, outcrops at the surface, possesses an anomalous density of 0.5 gm/cm^3, and dips to the right at 45°. The data, taken at 100 m intervals, extend 500 m on either side of the prism array, giving a total of twenty-five data points. The true structure was used as the initial

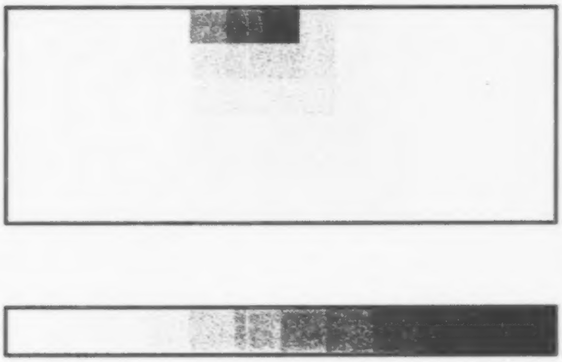

Figure 290.7. The unconstrained solution for the data corresponding to the dipping dike structure in Figure 290.5. The model density range is -0.05 to +0.69 g/cm^3. The density scale is -0.1 to +1.0 g/cm^3. The value of S is 0.48.

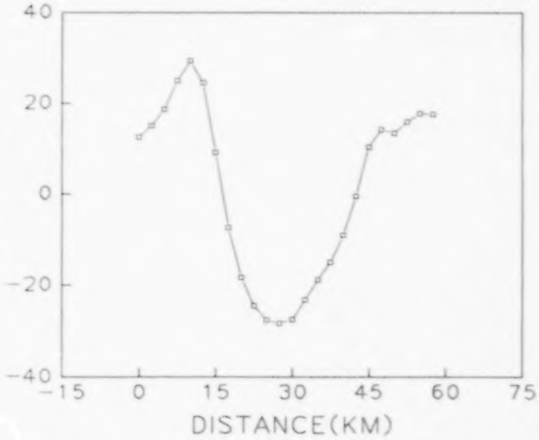

Figure 290.8. A gravity profile from Northern Ontario. See text for details.

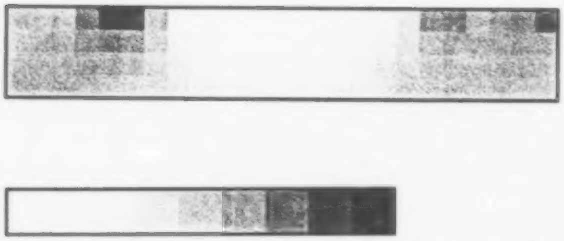

Figure 290.9. Unconstrained solution for the data of Figure 290.8. The anomalous density range is -0.16 to 0.23 g/cm^3. The density scale is -0.15 to +0.25 g/cm^3. The value of S is 1.6.

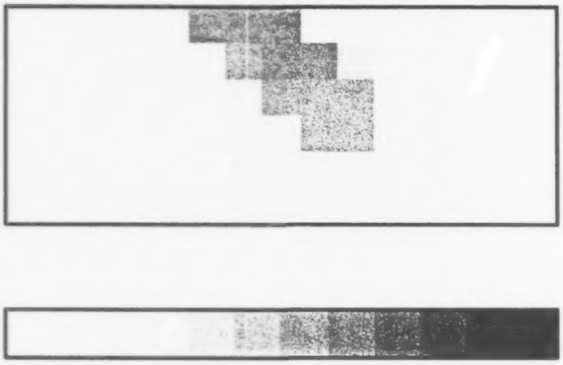

Figure 290.10. The solution for the dipping dike structure (Figure 290.5) with surface densities constrained. The model density range is -0.02 to 0.51 g/cc. The density scale is -0.1 to +1.0 g/cc. The value of S is 0.75.

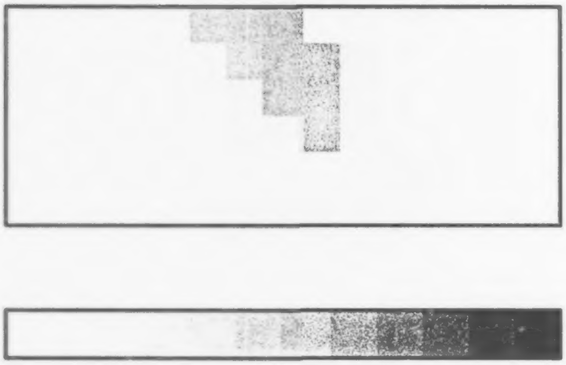

Figure 290.11. The solution for the dipping dike structure (Figure 290.5) with centre column densities constrained. The model density range is -0.05 to 0.50 g/cc. The density scale is -0.1 to +1.0 g/cc. The value of S is 0.74.

guess for the iterative procedure. With no constraints placed on the prism densities (Figure 290.7), there is again a concentration of high densities at the surface underneath the gravity-anomaly peak, and not much resemblance to the true structure.

Finally, a profile of real residual-gravity data, measured across a granodiorite batholith in northern Ontario, is shown in Figure 290.8. The batholith is bounded on either side by volcanic rocks (basalts, andesites, and tuffs). Some pockets of sedimentary rock overly the volcanics. A diabase also intrudes the volcanics to the left while a syenite stock underlies those to the right. The volcanics to the right are also cut by a major fault zone. The data have been coarsely sampled at a 2.5 km interval so that one would not expect much resolution of the complex geology on either side of the batholith. The main problem here is to determine the depth extent of the batholith.

The traverse is 57.5 km in length. The prisms in the model are 2.5 km square and extend the length of the profile and to a depth of 10 km. A starting model that showed no reflection of the geology, with all prism densities set to 0 gm/cm^3, was used, with no constraints imposed on the prism densities. The resultant model is given in Figure 290.9. The model has been separated into three distinct density units, although each unit is rather inhomogenous. There is a concentration of high-amplitude density values at the surface. At the centre of the batholith, the density grades from -0.16 gm/cm^3 in the top layer to -0.06 gm/cm^3 in the bottom layer. On the left, the anomalous density peaks at +0.23 gm/cm^{3}and on the far right, +0.15 gm/cm^3. Given a background density of 2.74 gm/cm^3, these anomalous density values at the surface seem to be slightly too large in amplitude for the mapped geology. On the basis of the previous synthetic-model results, this is exactly what one would expect when no surface-density constraints have been incorporated; the data are "explained" with structures which are not deep enough and are thus denser than they should be. The section in Figure 290.9 can be regarded as characteristic of unconstrained "simple" models; the apparent depths obtained must be regarded as underestimates.

CONSTRAINED OPTIMIZATION RESULTS

How do results differ if density constraints of the sort likely to be available from sampling are available? Re-examine first the sill-like model shown in Figure 290.1. If we assume that anomalous densities are all positive and in addition assume that surface sampling has established the correct surface-cell densities, so that they can be fixed at the correct values, the minimum S model obtained by the iterative algorithm is so close to the true model as to be indistinguishable from it on a grey-scale plot, and is therefore not shown. A similar result is obtained if we assume that anomalous densities are all positive and in addition assume that borehole sampling has established the correct cell densities in the central column, so that they can be fixed at the correct values.

For the dipping dike-like model whose density section is shown in Figure 290.5, and the same starting model as in the unconstrained case, fixing the surface densities, as might be possible with surface sampling, gives the interpreted result shown in Figure 290.10. Fixing the densities in the right-central column of the model in the top five cells, as might be possible with drillhole sampling, gives the interpreted result shown in Figure 290.11. Both of these are much closer to the true structure shown in Figure 290.5 than was the unconstrained result in Figure 290.7. Positivity constraints on the prism densities were not imposed as they had been in the previous example. It is worth noting that the method did not extend these models at depth more than necessary to fit the data and the constraints, as this would have increased the value of the norm.

CONCLUSIONS

The synthetic-model studies above have verified the suitability of the L1 density-gradient norm, in conjunction with density constraints obtained by surface- and drillhole-density sampling, for forcing density models obtained from gravity data to be "simple", although there is room for considerably more test work using real rather than synthetic data. Although the method is still experimental—and not particularly fast—it is expected that these problems can be solved by the application of linear-programming techniques.

REFERENCES

Backus, G., and Gilbert, F.

1967: Numerical formulation of a formalism for geophysical inverse problems; Geophysical Journal of the Royal Astronomical Society, Volume 13, p.247-276.

1968: The resolving power of gross Earth data; Geophysical Journal of the Royal Astronomical Society, Volume 16, p.169-205.

Chavez, R., Bailey, R.C., and Garland, G.D.

1987: Joint interpretation of gravity and magnetic data over axisymmetric bodies, with application to the Darnley Bay Anomaly, N.W.T., Canada; Geophysical Prospecting, Volume 35, p.374-392.

Guillen, A., and Menischetti, V.

1984: Gravity and magnetic inversion with minimization of a specific functional; Geophysics, Volume 49, p.1354-1360.

Gill, P.E., Murray, W., and Wright, M.H.

1981: Practical Optimization; Academic Press, 401p.

Last, B.J., and Kubik, K.

1983: Compact gravity inversion; Geophysics, Volume 48, p.713-721.

Levy, S., and Fullagar, P.K.

1981: Reconstruction of a sparse spike train from a portion of its spectrum and application to high resolution deconvolution; Geophysics, Volume 46, p.1235-1249.

Mottl, J., and Mottlova, L.

1972: Solution of the inverse gravimetric problem with the aid of integer linear programming; Geoexploration, Volume 1, p.53-62.

Oldenburg, D.W., Scheuer, S., and Levy, S.
1984: Recovery of the acoustic impedance from reflection seismograms; Geophysics, Volume 48, p.1235-1249.

Parker, R.L.
1974: Best bounds on density and depth from gravity data; Geophysics, Volume 42, p.315-334.
1975: The theory of ideal bodies for gravity interpretation; Geophysical Journal of the Royal Astronomical Society, Voiume 13, p.247-276.

Grant 291 Remote Sensing and Geobotany as an Aid to Mineral Exploration in Northern Terrains

A.E. Beswick, P.J. Beckett, G.M. Courtin, and G.O. Tapper

Centre in Mining and Mineral Exploration Research (CIMMER), Laurentian University, Sudbury

ABSTRACT

Field and laboratory studies aimed at developing geobotanical remote sensing as an exploration tool have been carried out over the past year. Field work involved the sampling of A and B horizons in soils and various vascular plants in the Gowganda area, including the detailed sampling in a 1 km^2 area adjacent to the abandoned Capital Mine site. More than 200 soil samples and over 550 vegetation samples (leaves, needles, twigs, trunk-wood cores, roots, and whole lichens and fungi) have been analysed for Mn, Co, Ni, Cu, Zn, As, and Pb. Despite the presence of silver-cobalt-nickel-arsenide mineralization at the Capital Mine site, no geochemical anomaly was found in either the soils or the vegetation relative to background values in the surrounding area. In general, higher metal levels were found in the A than in the B soil horizons. Plant-tissue metal levels are better correlated with the A than the B soil-horizon values, but overall, the correlations are weak, suggesting that plant–soil metal relations are complex.

Laboratory studies of metal uptake by plants, and their spectral responses in the visible to infrared range, indicate that a detectable spectral response occurs above 15 ppm Ni in white-birch leaves. A similar concentration of Cu in lichens causes chlorophyll breakdown and a marked spectral response.

INTRODUCTION

Research in the field of geobotany and its applications in mineral exploration has been an ongoing activity for several decades (*see* reviews by Cannon 1971; and Brooks 1972). It is important to recognize, however, that in the past geobotanical research has largely been concerned with the geochemical aspects of plant-soil relations. The ultimate objective of such studies has typically been to identify, in any given area (with thick overburden or poor outcrop) whether particular plants and different plant tissues (leaves, pine cones, bark, twigs, etc.) might be more sensitive indicators of bedrock metal anomalies than samples of the soils in which they grow. Traditional geobotanical studies, therefore, have tended to focus on an assessment of specific, increased metal concentrations in various plant tissues.

The advent and rapid development of remote sensing, however, requires a re-examination of geobotany as being a potentially powerful tool for mineral exploration. When geobotany is coupled with remote sensing, the changes in vegetation spectral reflectance being sought may not arise simply because of increased metal loading in foliar tissues, but rather, and perhaps more likely, because of physiological changes in the plants induced by metal toxicity.

The techniques of remote sensing, the use of airborne and space borne borne imaging systems, and the associated technologies of image processing and analysis, have been developing rapidly for more than a decade and have been used effectively in a variety of applications including agriculture, forest management, oceanography, meteorology, and mineral exploration (Gates 1970; Collins 1978; Rock 1982; Schwaller and Tkach 1985; Horler and Ahern 1986).

In terms of mineral-exploration applications, remote sensing using satellite-borne imaging systems have largely depended on imagery obtained through the multispectral-scanner (MSS) and the thematic-mapper (TM) remote-sensor programmes of the Landsat series of satellites, launched by the United States government starting with Landsat 1, in 1972, up to Landsat 5, launched in 1983.

Images from the remote-sensing systems carried by these satellites cover large areas of the earth's surface and can be obtained and processed relatively quickly and inexpensively. A single Landsat scene covers an area of approximately 185 km^2 with respective spatial resolutions of 80 m (MSS) or 30 m (TM) per picture element (pixel). The most successful geological applications of satellite remote sensing have been in areas where rocks and soils are exposed directly on surface; that is, in areas with little or no significant vegetation cover. In these areas, lithological and structural information on a regional scale can be obtained directly from the imagery, with little processing required. This is particularly the case where ground truth information is available, or has been assembled for small test-site areas within the larger scene (Kahle and Goetz 1983; Purdy *et al.* 1985).

More detailed information, such as mineralogical compositions of rocks, soils, and alteration zones, can be obtained from airborne sensors which have both higher spatial and spectral resolution (Ashley and Abrams 1980, Kahle and Goetz 1983). Once again, however, this information can only be obtained over areas with no significant vegetational cover.

In areas with extensive, dense, vegetational cover, such as most of the Canadian Shield, remotely-sensed lithological and geochemical information can only be obtained indirectly, regardless of whether the imagery is obtained from either airborne or satellite-borne systems. In order to obtain good-quality geological information from the imagery for these areas, it is essential; firstly, to identify, and hence distinguish, different plant species or communities using their remotely-sensed spectral characteristics; and secondly, to have a detailed understanding of the relationships between the vegetation cover and the rocks and soils upon which they grow.

Using currently available sensors, it is presently possible to distinguish between different plant species and communities utilizing their different spectral characteristics (Horler and Ahern 1986). It is also well known that certain plant species and communities have an affinity for soils with particular geochemical characteristics for which other species and communities have little or no tolerance (Kruckeberg 1954, 1969; Jenny 1980; Raines and Canney 1980). In terms of mineral exploration, for example, it has been established (Bazzaz *et al.* 1974; Chang and Collins 1980; Wickland 1982) that in areas with highly anomalous base-metal soil concentrations, such as occur in the proximity of massive-sulphide deposits, the local plant community is less healthy than similar communities growing in soils without such anomalous metal contents. This is a feature referred to as metal-induced vegetation stress (Horler *et al.* 1980). Such remote stresses are detectable through changes in the vegetation's spectral-reflectance characteristics as induced by metal uptake perhaps (Ward 1969). These spectral changes are commonly not visible to the naked eye. The most readily detectable spectral change due to either stress or early senescence is the so called shift of the "red edge" in the vegetation's spectral signature at wavelengths in the range 0.70 to 0.75 μm (Horler *et al.* 1983).

The extraction of geological information from appropriate imagery in areas with complete vegetation cover should be a relatively straightforward matter. Unfortunately, the problem is more complex than it first appears since the distribution and health of plant communities is also affected by a number of other factors, many of which are not geological in nature. Physical characteristics, such as the clay or moisture content of soils, can be a controlling factor in the distribution and health of plant communities (Kramer 1969; Ward 1969). Similarly, microclimatic variations in temperature, wind velocity, and drainage, which are influenced by local topography (Monteith 1973, Oke 1978), as well as the pathological effects due to insect or microbial infestations (Canney *et al.* 1979) can all have an influence on the nature of the vegetational characteristics.

At the present time, the relative importance of these various factors in confounding efforts to obtain geologically significant information from imagery for areas with extensive vegetational cover is not well understood. It is clear, therefore, that a considerable amount of detailed research needs to be done in well studied test-site areas before a full understanding is obtained of the geobotanical relationships and their spectral characteristics. Only when this understanding has been attained can geological and mineral-exploration-related interpretations be made with confidence. This research project is primarily concerned with developing such an understanding and a discussion of its objectives follows.

OBJECTIVES OF THE PROJECT

If geobotanical remote sensing is to become a viable tool in terms of utilizing plant spectral emission and reflectance characteristics for mineral exploration purposes, a number of fundamental questions, both botanical and geological in nature, have to be answered. A large number of different mineralized areas, such as those in the Superior Province of the Canadian Shield, are reasonably well understood geologically in terms of the nature of the mineralization, lithology, structure, overburden, bedrock, and soils geochemistry. The major requirement for effectively developing this new science, therefore, is to obtain a better understanding of the relationships between vegetation spectral characteristics, which can be sensed remotely, and the plant physiological responses, which are directly attributable to the presence of mineralization in the bedrock and associated overburden. It is also necessary to differentiate these effects from those attributable to nongeological environmental parameters.

In the context of this particular project, the overall objective is to develop the scientific basis of geobotanical remote-sensing techniques as a direct aid to mineral exploration in glacial and residual overburden in Northern Ontario. The primary objectives are here outlined:

1. understand the geochemical and biochemical processes involved in the release and uptake of various metals from bedrock and overburden into the various tissues of vascular (trees and shrubs) and nonvascular (lichen, mosses, and fungi) plants
2. determine the effects of metal-induced stress or enhanced growth on the chemical, structural, and spectral characteristics of vascular and nonvascular plants
3. determine the effects of ecological factors on plant spectral characteristics and to distinguish these from metal-induced effects
4. characterize spectral responses of a variety of plant species in areas with and without anomalous metal concentrations
5. determine the nature of temporal shifts in vegetation spectral responses in mineralized areas in order to optimize the use of seasonally acquired, remotely sensed data for mineral exploration in vegetated terrains

In order to meet these objectives, it was decided that a variety of closely integrated field and laboratory studies were necessary and that the field studies should be carried out in an area which met a variety of site-selection criteria judged appropriate to the objectives to be attained.

SITE DESCRIPTION

With the above objectives in mind, preliminary field studies, including bedrock, soil, and vegetation sampling, and an evaluation of the local topography, were carried out in the vicinity of several mineral deposits in the Gowganda silver-mining area, which is located some 150 km north of Sudbury. This reconnaissance survey covered the southern portion of Haultain township, the adjoining northern portion of Nicol township and the adjoining eastern portions of Van Hise and Milner townships (Figure 291.1.).

The geology of the area is described in Ontario Geological Survey Report 175 and accompanying Geological Maps 2348 and 2349 (McIlwaine 1978) from which the following brief summary has been made.

Within the area, basement rocks of Archean age consist of steeply dipping, mafic to intermediate metavolcanics and clastic metasediments. These rocks are unconformably overlain by fine to coarse-grained clastic metasediments of the Huronian Super-

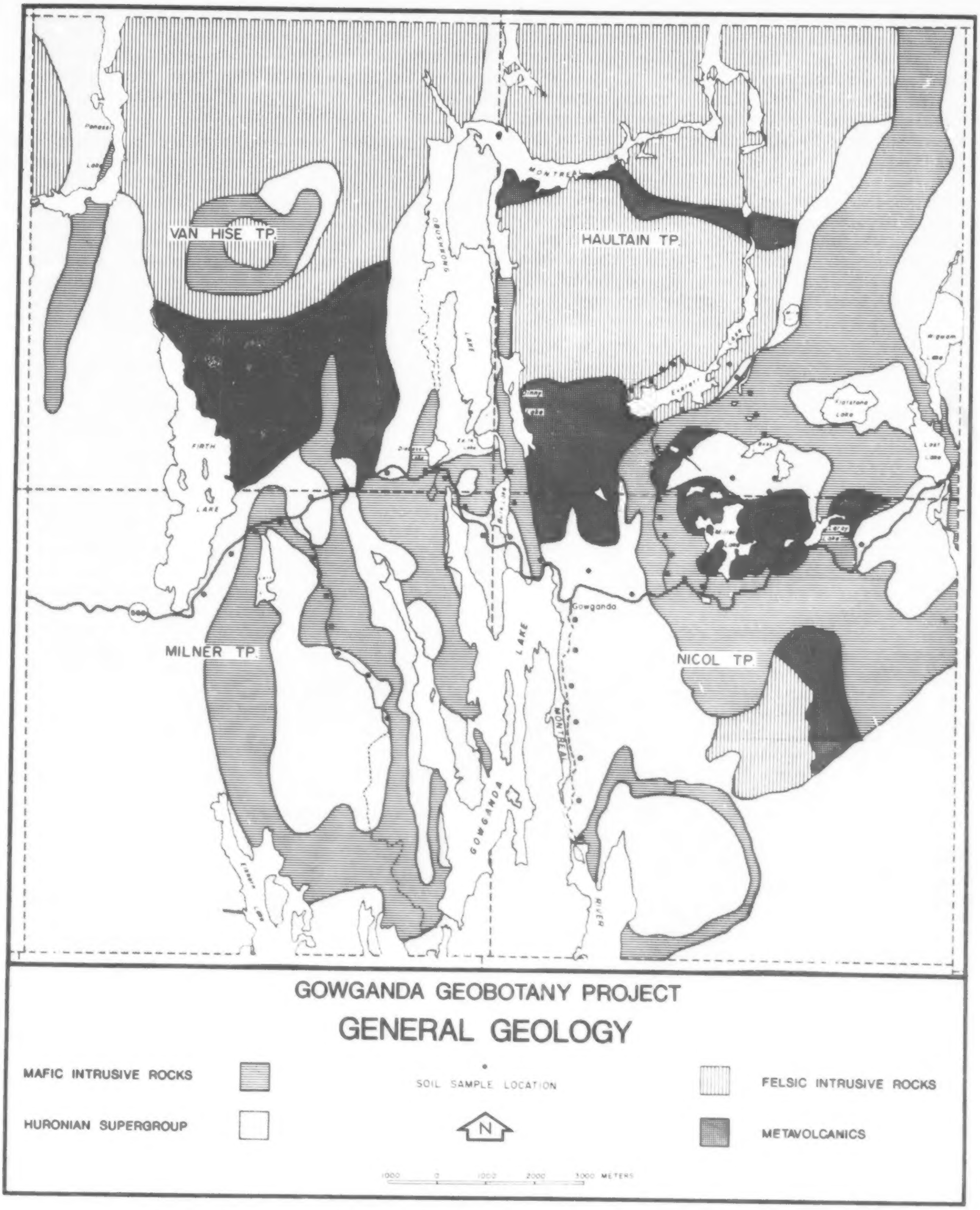

Figure 291.1. General geology of the Gowganda Geobotany Project.

group through which several mafic bodies of Nipissing Diabase have been intruded. Silver, occurring in association with cobalt-nickel-arsenide-bearing carbonate and quartz-carbonate veins, has been mined in the area since 1907. These deposits appear to be closely related to the distribution of Nipissing diabase intrusions, which commonly outcrop as low ridges throughout much of Haultain and Nicol townships. Much of the area is overlain by a thin, discontinuous cover of Pleistocene deposits comprised, for the most part, of sand and gravel whose composition appears to reflect that of the bedrock in the area. Eskers in the eastern portion of the study area have a southeastern trend, parallel to that of glacial striations in the area, indicating that the dominant direction of ice transport was from the northwest.

In terms of vegetational cover, the area lies near the northern fringe of the Boreal Forest-Northern Hardwoods ecotone. Three major plant communities dominate: almost pure stands of aspen poplar (*Populus tremuloides*); almost pure stands of black spruce (*Picea mariana*); and mixedwood stands of balsam fir (*Abies balsamea*), white spruce (*Picea glauca*), white birch (*Betula papyrifera*), and aspen poplar with speckled alder (*Alnus rugosa*) as the main understory shrub. The dominant soil-forming process is podzolization, and an entire soil-drainage catena may be found, ranging from well drained to saturated. Glei soils may be present in the wettest sites.

Following a reconnaissance survey of this area and an evaluation of preliminary analyses of soil and vegetation samples, a small area to the north of Kilpatrick Lake, having several soil samples with seemingly high arsenic (As) concentrations, was selected for further detailed soil and vegetation sampling. This site is located on a gentle, southwest-facing slope on the Agnico-Eagle Mines Limited property, some 4 km to the northeast of the Town of Gowganda, and covers an area of approximately 1 km^2 adjacent to the abandoned Capital Mine (Figure 291.2.). The southern half of the site is underlain by Archean mafic metavolcanics which are unconformably overlain by wackes of the Coleman Member of the Gowganda Formation in the northern half of the site. The latter rocks host the Capital Mine Deposit and, in addition, several cobalt-arsenide veins exposed by recent trenching performed near the abandoned mine shaft at the top of the slope.

With the exception of the area immediately adjacent to the mine shaft, which is covered with waste rock, the area (Figure 291.2.) has a dense and varied vegetational cover. The A and B soil horizons are well developed over most of the site. Field work to date, both on this site and in the surrounding area, is described below, followed by a description of related laboratory experiments.

FIELD WORK

In the field, vascular plants (trees and shrubs) and soils, occurring both proximal to the mineralization and in the surrounding nonmineralized area, provide the opportunity to determine whether or not preferential uptake of metals can be detected in one species relative to another and whether such uptake is most noticeable in a particular plant tissue such as the leaves or fruits. Both the mineral portion of the soil (B horizon) and the upper, organic layer (A horizon) were sampled to determine in which horizon the metals tend to be concentrated and whether plant-tissue metal contents are better correlated with those in one soil horizon versus the other.

Vascular-plant sampling involved collection of leaves, twigs, trunk wood, and roots of various tree species; the roots, shoots, and leaves of small woody plants; and the above-ground and below-ground portions of herbaceous plants. In the case of coniferous species, both first- and second-year needles and twigs were collected. Fruit samples were collected when present. The species and numbers of samples collected are shown in Tables 291.1 and 291.2. The locations of samples collected are shown in Figures 291.1 and 291.2. At the time of writing (May, 1987), all of the 90 A-horizon and 130 B-horizon soil samples collected, as well as 556 of the 1007 vascular-plant samples collected, have been analyzed for Cu, Ni, Co, Mn, Pb, Zn, and As by atomic-absorption techniques; the results are presented in a later section of this report.

Nonvascular-plant species such as fungi, lichens, and mosses are known accumulators of metals (Martin and Coughtrey 1982). Lichens and mosses have been used extensively to monitor airborne contaminants and may have potential use in separating the effects of long-range transport of aerial pollutants from the effects due to metals residing in the soils and parent rocks (Richardson et al 1980). The density of the tree canopy has prevented the development of an extensive ground cover of lichens in most of the area. However, because lichens are at least 95% fungal material, it is expected that mushrooms should possess most of the advantages that lichens now possess when used as geobotanical indicators. Therefore, fungi, such as mushrooms, were also collected on the site because they may provide a simple and inexpensive geobotanical tool. This idea was tested at the Kilpatrick Lake site where two types of mushroom study were undertaken.

The emphasis of the first study was to investigate the metal relationships between the mushrooms and the woody substrates on which they were growing. At least 3 g of mushroom material (bracket fungus) and 3 g of the corresponding wood substrate (fir, spruce, birch, or aspen) were collected in paper bags and dried in an oven at 45°C. The 225 samples were reduced to powder in a Wiley mill and, following acid digestion, analyzed for Cu, Ni, Zn, Mn, Co, and As using an atomic-absorption spectrophotometer. The major species were *Trichaptum abietinus* growing on balsam fir and *Gloeophyllum sepiarium* associated with spruce. Analytical results are presented in a later section.

The second mushroom study was undertaken to investigate the metal-enrichment factors existing between mushrooms and the organic-soil horizon on which they grow. In this study during the main mushroom season in early fall, 60 samples were collected together with the associated humus. The collected samples were dried and prepared as in the first study, except that sample grinding was performed by

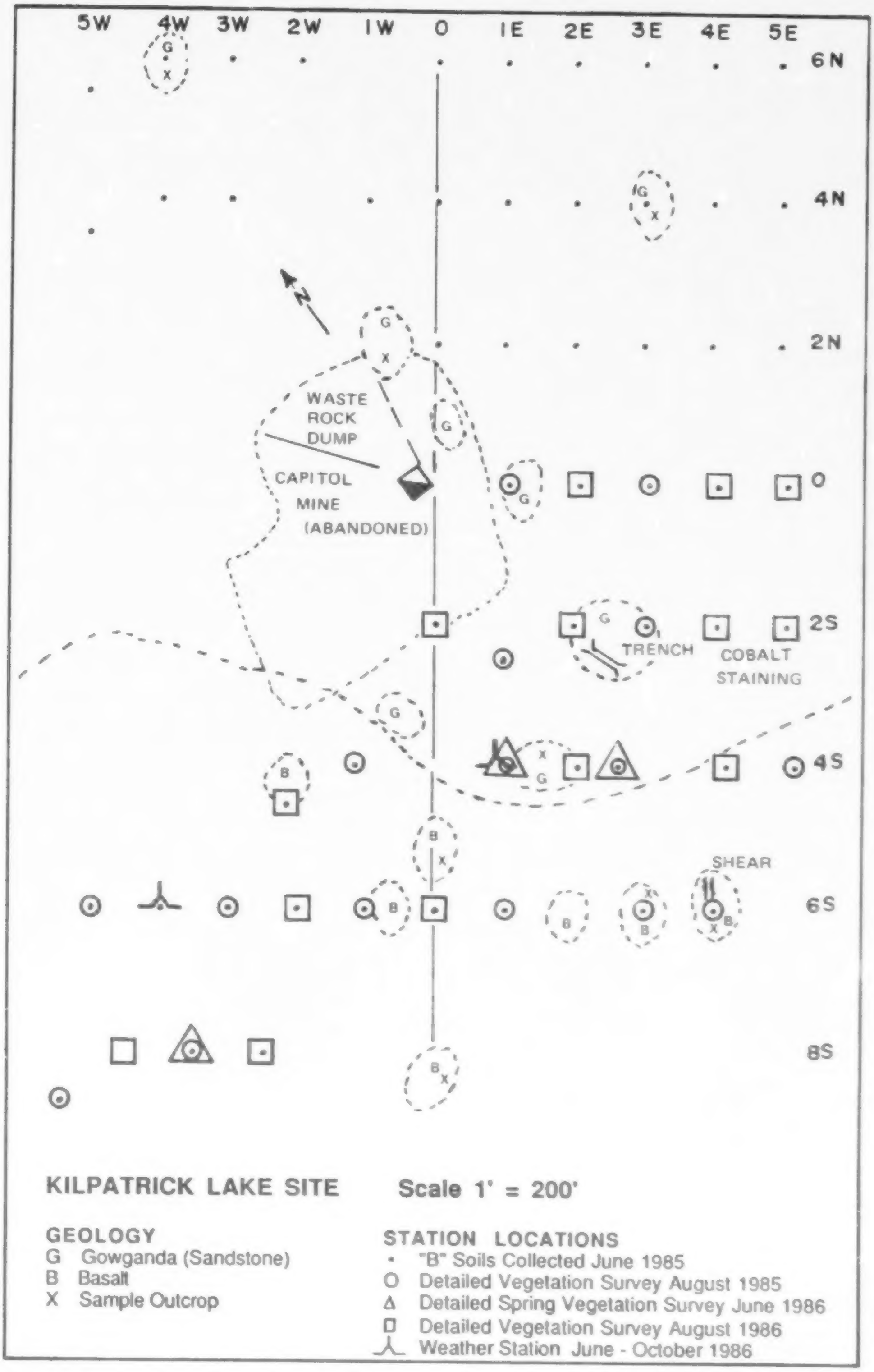

Figure 291.2. Diagram showing the geology and station locations of the Kilpatrick Lake Site.

TABLE 291.1. SAMPLE SIZE, SEPARATED BY TISSUE, FOR THE MAJOR ARBORESCENT AND HERBACEOUS SPECIES AT KILPATRICK LAKE SITE AND REGIONAL STATIONS: A TOTAL OF THIRTY-FOUR (34) SITES WERE SAMPLED,

SPECIES						
Trees & Shrubs	**Needles/Leaves**	**Twigs/Shoots**	**Fruit**	**Roots**	**Trunk**	**Totals**
Populus tremuloides (Trembling Aspen)	30	30	0	30	30	120
Alnus rugosa (Speckled Alder)	26	26	0	26	26	104
Prunus pennsylvanica (Pin Cherry)	12	12	0	12	12	48
Betula papyrifers (White Birch)	28	28	0	28	28	112
Abies balsamea (Balsam Fir)	53	53	0	37	37	180
Picea mariana (Black Spruce)	14	14	0	8	8	44
Picea glauca (White Spruce)	6	6	0	3	3	18
Ledum groenlandicum (Labrador Tea)	6	6	0	6	0	18
Diervilla lonicera (Bush Honeysuckle)	30	30	8	30	0	98
Kalmia angustifolia (Sheep Laurel)	4	4	0	4	0	12

HERBACEOUS	**Above Ground**	**Below Ground**	**Fruit**	**Total**
Vaccinium angustifolia (Late Lowbush Blueberry)	11	11	0	22
Vaccinium myrtilloides (Sour-top Blueberry)	28	28	1	57
Aralia nudicaulis (Wild Sarsaparilla)	29	29	0	58
Maianthemum canadense (Wild Lily of the Valley)	28	28	9	65
Trientalis borealis (Starflower)	10	missing (too delicate)	0	10
Clintonia borealis (Bluebead Lily)	19	19	3	41

TABLE 291.2. NUMBER OF SOILS SAMPLED, BY HORIZON, FOR THE KILPATRICK LAKE SITE AND SURROUNDING REGION.

		Kilpatrick Lake Site		**Regionals**	
Year	**Soil Horizon**	**June**	**August**	**June**	**August**
1985	A_0	-	16	40	-
1985	B_2	56	15	-	-
1986	A_0	16	13	-	5
1986	B_2	14	13	27	5

use of a pestle and mortar. The metal analyses are in progress.

Finally, two weather stations were established on the Kilpatrick Lake site to determine possible effects of microclimatic variations on metal uptake. Microclimatic variations could be a serious, confounding variable because of the potential to induce physiological stress. The two stations were established 400 m apart and at an elevational difference of 10 m. Masts 14 m high permitted data to be taken through the entire vegetational canopy (see Table 291.3 for details). Sensors mounted on the masts monitored windspeed and direction, the total incoming shortwave and photosynthetically active radiation, and constructed a temperature profile from measurements made beginning at the top of the canopy down to a soil depth of 0.5 m. The same masts were also used to support a profile of moss sample plates to monitor deposition of airborne metals.

LABORATORY WORK

Laboratory studies of the metal uptake to tree seedlings and tree-canopy foliage, when used in conjunction with handheld spectral radiometery, provide baseline data under controlled conditions. In this way confounding variables and possible synergisms are avoided thus providing an understanding of the basic mechanisms that are at work in the field situation.

Spectral-reflectance measurements of both white-birch canopy samples and caribou lichen were monitored in the laboratory under cumulative metal loading to determine the threshold levels of detectability and the pattern of spectral-reflectance shift when compared to a control. An artificial canopy was established in a polethylene basin with the help of florist's "oasis" and the leaves displayed more or less as if on the tree. The basin was filled with a 100 ppm solution of nickel occurring as nickel sulphate. Another basin, with its canopy, was filled with distilled water to act as a control. Both canopies were scanned daily for a five-day period with a Spectron portable radiometer (model CE 390 WB-P) calibrated against a barium-sulphate surface. Illumination was by means of a 600 W G.C.E. quartz halogen lamp. Leaf-metal content was determined on a Perkin-Elmer model 703 atomic-absorption spectrophotometer fol-

TABLE 291.3. MICROCLIMATE SENSOR TYPE AND DEPLOYMENT.

Parameter	Sensor Type & Model	Position
Wind speed	Met-One, model 013A	14.0 m (top of canopy)
Wind direction	Met-One, model 023A	14.0 m (top of canopy)
Shortwave incoming solar radiation	Matrix, Inc. Sol-a-Meter	14.0 m (top of canopy)
Photosynthetically active radiation	Lambda quantum sensor, model L1-190 SB	14.0 m (top of canopy)
Air temperatures	Shielded 20 SWG copper-constantan thermocouple	14.0 m (top of canopy) 12.0 m (mid canopy) 10.0 m (lower canopy) 7.5 m (below canopy) 5.0 m (mid trunk) 2.0 m (standard screen height) 0.5 m (shrub height) 0.2 m (herb height)
Soil temperature	20 SWB copper-constantan thermocouple	0.005 m (sub surface) 0.02 m (mineral soil) 0.05 m (mineral soil)

TABLE 291.4. VARIABILITY OF SEVEN (7) SOIL METALS IN B_2 SOIL HORIZONS COLLECTED AT KILPATRICK LAKE SITE (N = 57) AND REGIONAL SAMPLES (N = 68).

		Soil Metals						
Site	**Statistic**	**Cu**	**Ni**	**Co**	**Mn**	**Pb**	**Zn**	**As**
Kilpatrick Lake	Maximum	68	90	25	179	92	100	10
	Minimum	7	9	3	36	6	13	1
	$\bar{x}$	21.6	23.3	11.4	89.2	18.4	27.4	2.7
	$s\bar{x}$	12.0	12.0	4.6	28.7	10.9	15.0	1.8
	C.V.	55.6%	51.5%	40.4%	32.2%	59.2%	54.7%	66.7%
Regional	Maximum	518	103	27	549	143	268	10
	Minimum	7	9	4	40	10	13	0
	$\bar{x}$	32.8	27.6	11.0	131.9	23.6	49.4	3.2
	$s\bar{x}$	64.9	14.9	3.8	68.2	23.8	56.8	1.8
	C.V.	197.9%	54.0%	34.5%	51.7%	100.8%	115.0%	56.3%

$\bar{x}$ = mean; $s\bar{x}$ = standard deviation; C.V. = coefficient of variation

lowing ashing of the leaves and their subsequent dissolution in aqua regia.

Similar experiments to the one described above were also carried out on lichen samples. A lichen mat was placed in a shallow tray and immersed in a 100 ppm solution of copper, occurring as copper sulphate, for an hour, allowed to drain and then lightly sprayed to remove residual copper solution adhering to the lichen surface. Another mat was treated identically but received distilled water, rather than a copper solution, to act as a control. Spectral reflectance was measured daily for five days. Metal content was determined, as was done for the birch, and the results are presented in the following section.

Results

Data, resulting from the various field and laboratory work described above, are presented under the following appropriate subheadings.

Soils data

A comparison of B_2 soils, both at the mineralized Kilpatrick Lake site and in the surrounding nonmineralized area (Table 291.4), show that the soils from the nonmineralized areas had mean and maximum metal levels that were equally as high or higher than those at the mineralized Kilpatrick Lake site. Furthermore, metal contents in sets of four to six soil samples, collected within 1 m of each other at three different locations on the Kilpatrick site, all showed a high degree of variability (Table 291.5).

A comparison of metal contents in the A_0 and B_2 soil horizons shows that there is a greater concentration of metals in the organic layer (Table 291.6). This is true in all cases for Cu, Ni, Co, Mn, Pb, Zn, and As.

Metal Uptake to Vascular Plant Tissues

Analytical data obtained for seven metals occurring in various vascular-plant species are summarized in Table 291.7 as typical examples of the levels found. Complete analytical data are available from the authors on request.

In order to determine the relationships that exist between different species of vegetation and the different soil horizons for each of the seven metals, 756 correlations were examined statistically. Of these, 193 were characterized as significant ($p=<0.05$; where p represents the probability). Three species (balsam fir, white birch, and speckled alder) were involved in more than half of these significant correlations (Table 291.8). It was also observed that more metals showed a significant correlation between the vegetation and the A_0 soil horizon (32 significant correlations) than with the vegetation and the B_2 soil horizon (8 significant correlations). However, it should be noted that in several cases the very high degree of significance in correlation was the result of a series of low metal concentrations, both in the soil and in the vegetation, in conjunction with a single, high value. When such values were discarded as outliers, little more than half of the correlations remained significant. The omission of these high outlier values also resulted both in a lowering of the significance levels and a change in the slope of the regression line.

The following results highlight the details of the many correlations examined and are summarized in Table 291.8. As, Zn, and Co concentrations in balsam fir are positively correlated with soil concentrations, while Mn concentrations in first-year twigs are negatively correlated with the soil values. In white birch leaves, As, Zn, Pb, and Cu concentrations are positively correlated with those of their soils, whereas Ni and As concentrations in the trunk wood are negatively correlated with their soils. In the case of speckled alder, plant-part measurements of the concentrations of Zn, Cu, As, and Mn show positive correlations with their soils whereas Pb levels in twigs are negatively correlated in the same context.

These preliminary statistical examinations of the data indicate that the plant-soil metal levels are not strongly correlated. This suggests that the relations are complex and warrant more detailed examinations.

Metal uptake by nonvascular plants

The range of metal concentrations found in the two major mushroom species and their corresponding woody substrate are shown in Table 291.9. The substrate metal levels for both the fir and the spruce are similar to those found in the living trees (see vascular-plant results above). The metal levels in the mushrooms are generally higher than those of its substrate. Pearson correlation coefficients were determined to test the hypothesis that as metal levels increased in the substrate the metal levels would increase in the associated mushroom (see Table 291.9). In *Trichaptum*, significant positive relationships were found for Co ($p=<0.001$) and As ($p=<0.001$), two metals which are enriched in the deposits on the site. Ni and Pb just failed to meet the $p=0.05$ level and Cu showed no mushroom-substrate relationship.

The results shown in Table 291.9 seem to indicate that the mushrooms may show metal enrichment when compared to the woody substrate. For each metal, the enrichment factors (metal in mushroom/metal in substrate) were calculated and presented in Table 291.10. A ratio of 1 indicates no enrichment in the mushroom whereas factors greater than 1 indicate metal enrichment in the mushroom. In some cases (e.g. Cu, Ni, and Co) the median and the mean enrichment factor deviate from one another, with the case of the mean being greater than the median indicating a skewness in the frequency distribution of the data. A simple test of significance indicates that for all the elements, except for Mn in *Trichaptum*, there is significant metal-enrichment in the mushroom. The data also indicate that *Gloeophyllum* is a better accumulator of metals than is *Trichaptum* (Table 291.10). In both mushroom species, the Cu contents are greatly enriched as compared to that of their substrates; namely, up to 27 times in *Trichaptum* and between 4 and 34 times in *Gloeophyllum* (Table 291.10).

Although the mushrooms are accumulating metal relative to levels present in their substrates, apart from Co and As in *Trichaptum* there is no simple, direct relationship between the substrate's and mushroom's metal content. It may be that differential accumulation occurs, such that at low substrate concentration there is relatively higher metal enrichment in the mushroom. On the other hand at higher substrate metal levels, enrichment of metals in the mushrooms are much lower. This idea can be tested by looking at plots of the enrichment factor against the substrate metal level. Two examples are shown in Figures 291.3a and 291.3b for the mushroom *Trichaptum*. Copper shows very high mushroom uptake at low substrate metal levels, with the enrichment factor becoming smaller as substrate concentration increases. Conversely, cobalt uptake appears not to be related to the substrate's metal level. Hence, differential metal uptake may be an important factor that determines the lack of linear relationships between substrate and mushroom metal levels. One might also expect differential uptake to occur with the vascular plants, but this has yet to be determined.

Microclimate

An almost unbroken series of data, from mid-June to mid-September, 1986, was obtained from both weather stations. Measurements recorded include solar radiation, wind speed and direction, and a profile of the temperature as taken from the top of the tree canopy downward to a depth of 0.5 m within the soil. The data are currently in the process of being analyzed.

TABLE 291.5. VARIABILITY OF SIX (6) SOIL METALS AT KILPATRICK LAKE SITE IN THE A_0 AND B_2 SOIL HORIZON.

Site	Statistic	Soil Metal (ppm)											
		Cu		Ni		Co		Mn		Pb		Zn	
		A_0	B_2	A_0	B_2	A_0	B_2	A_0	B_2	A_0	B_2	A_0	B_2
K:L45 100E	$\bar{x}$	21.2	9.2	33.6	20.6	19.0	10.9	213.0	72.7	86.9	21.5	46.6	20.3
	$s\bar{x}$	2.5	2.4	12.0	6.5	7.6	3.1	95.0	27.0	9.2	3.8	13.4	4.8
	C.V.	11.8%	26.1%	35.7%	31.6%	40.3%	28.4%	44.6%	37.1%	10.6%	10.7%	28.8%	23.6%
		Cu		Ni		Co		Mn		Pb		Zn	
		A_0	B_2	A_0	B_2	A_0	B_2	A_0	B_2	A_0	B_2	A_0	B_2
K:L45 275E	$\bar{x}$	20.3	25.6	29.8	17.6	12.7	9.4	210.0	72.9	69.6	19.9	26.6	25.0
	$s\bar{x}$	6.7	8.5	9.1	2.6	3.8	1.6	177.0	16.7	21.2	1.4	6.7	3.2
	C.V.	33.1%	33.2%	30.4%	14.8%	30.1%	17.0%	84.3%	22.9%	30.4%	7.0%	25.6%	12.8%
		Cu		Ni		Co		Mn		Pb		Zn	
		A_0	B_2	A_0	B_2	A_0	B_2	A_0	B_2	A_0	B_2	A_0	B_2
K:L8s 300E	$\bar{x}$	36.1	41.4	34.7	42.5	16.9	38.8	1046.5	434.7	88.6	120.7	61.4	51.6
	$s\bar{x}$	9.8	29.0	11.13	25.2	7.5	13.1	697.3	451.7	14.2	83.9	12.8	26.4
	C.V.	27.1%	70.0%	32.07%	59.3%	44.4%	33.8%	66.6%	103.9%	16.0%	69.5%	20.8%	51.2%

$\bar{x}$ = mean; $s\bar{x}$ = standard deviation; C.V. = coefficient of variation

TABLE 291.6. VARIABILITY OF SEVEN (7) SOIL METALS IN A_0 AND B_2 HORIZONS FOR THE SAME PROFILE (N=16) KILPATRICK LAKE SITE.

Horizon	Statistic	Cu	Ni	Co	Mn	Pb	Zn	As
A_0	Maximum	52	245	103	860	55	330	5
	Minimum	10	13	2	71	19	14	1
	$\bar{x}$	24.0	40.0	14.2	241.4	39.0	54.1	2.1
	$s\bar{x}$	11.0	56.4	24.1	254.4	15.4	78.3	0.9
	C.V.	45.8%	141.0%	169.7%	105.4%	39.5%	144.7%	42.9%
		Cu	**Ni**	**Co**	**Mn**	**Pb**	**Zn**	**As**
B_2	Maximum	30	48	32	258	42	140	3
	Minimum	9	16	3	96	12	14	1
	$\bar{x}$	18.6	26.8	11.8	144.9	18.8	47.9	1.3
	$s\bar{x}$	7.02	9.3	5.9	41.2	7.6	35.1	0.6
	C.V.	38.7%	34.7%	50.0%	28.4%	40.4%	73.3%	46.1%

$\bar{x}$ = mean; $s\bar{x}$ = standard deviation; C.V. = coefficient of variation

Airborne-metal deposition.

The passive, airborne-metal-deposition monitors (moss plates), attached to the two weather-station masts, were sampled and replaced on a monthly basis. No chemical analyses are presently available owing to a backlog of samples for analysis.

Laboratory spectral-reflectance studies

Figure 291.4 shows a series of spectral scans for both control and nickel-treated white birch at the time of initiation and, respectively, at 24, 54, and 64 hours after the initiation of the experiment. The mean nickel level in the leaves (n=3) was 6.8 ppm at the beginning, and 27.1 ppm at the end of the experiment. The control (Figure 291.4a) shows a treatment effect in the far red and near infrared, where relative reflectance increased by about 20 percent after 54 hours. In the case of the nickel-treated birch (Figure 291.4b), the upward spectral-reflectance shift was much more marked (~30%), and the shoulder above the red edge, at about 0.79 μm, was much more abrupt. There was also an increase in visible-spectrum wavelengths with a maximum occurring in the green (~0.55 μm). After 64 hours, the introduction of freshly cut, leafy twigs, designed to mask the nickel-treated leaves (Figure 291.4b), showed a return to spectral values to within 5 percent of the reflectance values relative to those measured at the outset of the experiment.

Figure 291.5 illustrates the spectral-reflectance changes of copper-treated lichen. There appears to be little difference between the spectral response of the freshly copper-treated lichen from that of a control soaked in distilled water. With time, however, a gradual rise in the visible and a gradual decline in the infrared portion of the spectrum may be seen. At the same time the lichen became brown, which may account for the increased reflectance at visible wavelengths. The reduction in the infrared may be due to changes in wall structure brought about by the uptake of copper and perhaps a change in membrane permeability to water.

DISCUSSION AND CONCLUSIONS

The Kilpatrick Lake site was selected for study because at the outset it appeared to have many of the requirements necessary to meet the study objectives. The site is located on a productive mine property. At the upper edge of the sloping site, there is also an area of mineralization with silver-cobalt-arsenide veining clearly evident in shallow, open trenches. It was expected that the area downslope of the mineralization and in the same direction as movement of the Pleistocene ice sheet would yield a gradient of anomalous metal contents. Furthermore, it was expected that the intensity of the anomaly would decrease with increasing distance down ice, away from the veins and the mine property. Table 291.4 clearly indicates that this is not the case and that the regional background metal concentrations in the Gowganda-area soils are at least as high as at the site adjacent to the mineralization. Thus, although many aspects of the study have been conducted satisfactorily at the site, others have not. Nevertheless, the failure of certain aspects have been, by their very failure, extremely instructive.

The relationships that exist between the metal levels occurring in plants and the soils in which they are growing, as well as the laboratory work carried out to date, indicate several important points.

1. Each species acts independently with respect to metal uptake, with white birch, balsam fir, and speckled alder generally showing the best positive correlations with soil metal levels. Overall, however, plant-soil metal levels are not strongly correlated.
2. The organic soil (A_0) horizon tends to concentrate metals to a greater extent than the mineral soil (B_2) horizon. The reason is that the small amount of metals that are taken up by plants over time are eventually returned to the soil surface as organic material (leaves, twigs, etc) which, upon decay, adds its burden of metals to the organic horizon. Furthermore the primary constituent of the organic horizon is cellulose which is highly colloidal. As a result there is a strong

TABLE 291.7. RANGE IN SEVEN METAL VALUES (PPM) FOR SPECKLED ALDER, BALSAM FIR, AND WHITE BIRCH BY PLANT PART.

Plant Part	Cu	Ni	Co	Mn	Pb	Zn	As
Speckled Alder Leaves	6.4 - 15.9	4.5 - 24.0	2.0 - 39.0	66.0 - 4404.0	0.3 - 8.9	12.8 - 95.4	0.1 - 4.9
Speckled Alder Twigs	4.8 - 10.4	1.7 - 14.1	0.8 - 6.6	50.0 - 636.0	1.9 - 5.6	20.7 - 67.0	0.0 - 1.7
Speckled Alder Trunk	2.7 - 5.1	1.9 - 6.8	0.4 - 3.2	11.5 - 292.0	1.1 - 5.2	13.4 - 103.8	0.0 - 0.1
Speckled Alder Roots	4.6 - 15.3	3.1 - 18.6	1.6 - 8.8	34.0 - 236.0	4.1 - 17.8	13.7 - 91.0	0.4 - 6.4
Balsam Fir 1st Yr. Needles	2.9 - 8.7	4.0 - 13.2	0.6 - 4.8	213.0 - 867.0	0.5 - 7.5	22.9 - 130.0	0.1 - 2.0
Balsam Fir 2nd Yr. Needles	2.9 - 10.8	3.2 - 13.4	0.5 - 3.4	289.0 - 1787.0	0.9 - 3.7	38.4 - 771.0	0.1 - 2.0
Balsam Fir 1st Yr. Twigs	5.4 - 12.9	5.3 - 12.0	1.1 - 5.1	190.0 - 769.0	2.5 - 8.2	35.9 - 149.9	0.1 - 1.4
Balsam Fir 2nd Yr. Twigs	4.5 - 12.7	5.3 - 14.0	0.8 - 4.9	161.0 - 1378.0	2.1 - 14.9	35.0 - 623.0	0.2 - 2.2
Balsam Fir Trunk	1.7 - 4.0	0.2 - 2.9	0.1 - 1.4	29.0 - 176.8	0.4 - 9.2	12.5 - 62.0	0.0 - 0.3
Balsam Fir Roots	4.0 - 13.6	0.8 - 16.6	2.0 - 13.4	95.0 - 1134.0	5.0 - 15.4	31.8 - 255.5	0.6 - 4.7
White Birch Leaves	5.5 - 10.4	3.9 - 14.6	1.4 - 9.1	215.0 - 1552.0	1.3 - 5.0	61.0 - 555.0	0.1 - 0.9
White Birch Twigs	6.2 - 11.2	1.2 - 13.3	0.6 - 9.7	39.0 - 424.0	2.7 - 8.1	84.0 - 371.0	0.1 - 0.4
White Birch Trunk	1.2 - 2.6	1.0 - 4.0	0.4 - 1.5	28.4 - 150.5	1.1 - 9.9	24.1 - 154.2	0.0 - 0.3
White Birch Roots	6.6 - 20.5	3.0 - 17.4	1.7 - 7.9	51.0 - 437.0	6.3 - 30.2	47.0 - 180.0	0.7 - 4.0

TABLE 291.8. SIGNIFICANCE OF PLANT PART CORRELATIONS WITH "A" AND "B" SOIL HORIZONS FOR THE KILPATRICK LAKE SITE.

		SOIL METALS						
Species	**Plant Part**	**Cu**	**Ni**	**Co**	**Mn**	**Pb**	**Zn**	**As**
BALSAM FIR	1st yr. needles						ΔΔ ••	
	2nd yr. needles		••	ΔΔ				••
	1st yr. twigs			••	••(-)		••	••
	2nd yr. twigs							••
	trunks			ΔΔ				
	roots		•					•
WHITE BIRCH	leaves	•	••	••		••	ΔΔ ••	••
	twigs		••	••			••	
	trunks		Δ(-)					••(-)
	roots		••				••	••
SPECKLED ALDER	leaves			••			•	
	twigs		••	••		ΔΔ(-)	•	
	trunk	••						
	roots			••	Δ		ΔΔ ••	••

Legend:
• = significance ≤0.05 for "A" soils
•• = significance ≤0.01 for "A" soils
Δ = significance ≤0.05 for "B" soils
ΔΔ = significance ≤0.01 for "B" soils
(-) = negative correlation

affinity to bind ions by chelation and to minimize leaching downward and out of the soil profile. The organic horizon also tends to act like a sponge in retaining water. Therefore, it is within this zone that the bulk of plant feeder roots are found because it is here that the majority of nutrients and water are located.

3. Plant metal levels show stronger and more frequent positive correlations with metal levels occurring in the A_C soils than they do to those occurring in the B_2 soils. The main reasons for this are likely the same as those outlined under point 2 above.
4. It was not always the canopy-foliage portion of the trees and shrubs that showed the best correlations with soil metal concentrations. There are two possible reasons for this. Plants often have mechanisms that either bind absorbed metals in a way that prevents movement upward through the plant or that renders the metal nontoxic, or both (Rauser and Courvetto 1980). Alternately, where toxicity is not reduced, the physiological disruption suffered by the plant is not necessarily the result of high metal concentrations in the foliage. Copper, for instance, is well known to cause severe damage to fine feeder roots and can cause the plant to grow poorly or even to die (Salisbury and Ross 1985) without having unusually high Cu levels in its leaves. It is this sort of manifestation that is most likely to show up in remote-sensing imagery. At the Kilpatrick Lake site, this hypothesis could not be tested owing to failure of the MEIS electro-optical

TABLE 291.9. MINIMUM AND MAXIMUM METAL LEVELS (PPM) AND THE PEARSON CORRELATION COEFFICIENT (r) BETWEEN MUCHROOM AND SUBSTRATE.

a) in *Trichaptum abietinus* (n = 79)

Metal	Mushroom	Substrate	Pearson Correlation Coefficient (r)
Cu	2.5 - 30.7	0.6 - 8.9	0.091 ns
Zn	40.1 - 550.1	13.2 - 106.3	0.175 ns
Ni	1.4 - 13.1	1.0 - 9.7	0.198 ns
Co	0.3 - 9.2	0.4 - 4.8	0.427 *
Pb	2.8 - 25.6	0.6 - 28.2	0.196 ns
Mn	29.0 - 658.0	24.0 - 1197.0	0.163 ns
As	0.3 - 3.8	0.1 - 2.5	0.462 *

b) in *Gloeophyllum sepiarium* (n = 21)

Metal	Mushroom	Substrate	Pearson Correlation Coefficient (r)
Cu	15.2 - 62.8	1.7 - 10.3	0.145 ns
Zn	16.8 - 140.0	5.0 - 66.7	- 0.039 ns
Ni	2.3 - 39.7	1.0 - 12.0	0.091 ns
Co	0.6 - 17.8	0.3 - 14.0	- 0.037 ns
Pb	2.7 - 18.6	2.5 - 16.2	- 0.152 ns
Mn	58.0 - 297.0	20.0 - 193.0	0.346 ns
As	0.5 - 8.1	0.1 - 7.1	- 0.103 ns

ns, $p > 0.05$
***, $p \leq 0.05$**

remote sensor when the area was flown by the Canada Centre for Remote Sensing (CCRS).

5. Mushrooms appear to concentrate metals, particularly Cu, at significantly higher levels than are present in the humus or woody substrates on which they grow. These enrichments appear to be less pronounced as the metal levels in the substrate increase. Although mushrooms and other fungi are not likely to be seen by remote sensors, to the extent that lichens are also largely composed of fungal material, these results suggest that lichen carpets, if extensive and homogeneous enough, might be useful geobotanical remote-sensing indicators.
6. The laboratory study of the plant canopy's metal contents and spectral-reflectance responses indicates that the threshold level for detectability is around 15 ppm for nickel in white birch and that the amount of drought stress imposed on the leaves has a profound effect on the spectral reflectance (Courtin et al 1986). In the case of lichens, the same concentration of copper caused a breakdown of chlorophyll (Beckett and Courtin 1986). The resulting spectral shift is sufficiently marked to offer promise for aerial remote sensing where the forest canopy is sufficiently open to allow lichen mats to be viewed from above.

Two other aspects of these studies have yet to be evaluated:

1. The increasing amount of long-range transport of air pollutants from industrial activities must be considered as part of the burden of metal that is received by plant canopies. It is important to quantify this contribution if the amount that is being taken up through the plant is to be assessed correctly. Sampling of airborne metals by means of moss plates (Beckett 1984) is known to be very effective. Although the moss plates set out at Kilpatrick Lake have yet to be analyzed, it is not expected that the airborne-metal contributions will be great when compared with those from local sources.
2. The physiology of plants is strongly affected by the microclimate. Radiation is essential for photosynthesis, temperature affects the rate of all chemical reactions within the plant, wind affects water loss, and soil moisture affects water and nutrient uptake. Very preliminary analyses indicate little temperature variation, throughout the entire zone of growth, between the two weather stations at Kilpatrick Lake, in spite of the elevational difference that had been expected to cause cold air drainage. Radiation was discounted as a variable because of the short distance between sites. Soil moisture was not quantified but qualitative examination during soil sampling suggests there is a difference; indeed, the difference in soil temperature between the stations indicates that there may be a soil-moisture difference between sites. Soil moisture will be monitored regularly in the future to determine what

TABLE 291.10. ENRICHMENT OF SELECTED METALS IN TWO (2) MUSHROOM SPECIES.

a) in *Trichaptum abietinus* (n = 79)

Metal	Mushroom/Substrate Accumulation Ratio mean ± se	median	max	min
Copper	5.4 ± 0.5	4.0	27.0	1.0
Zinc	1.9 ± 0.1	1.7	9.2	1.0
Nickel	2.2 ± 0.2	1.7	8.2	0.4
Cobalt	1.3 ± 0.1	1.1	6.1	0.2
Lead	2.9 ± 0.5	1.5	29.5	0.3
Manganese	0.7 ± 0.1	0.6	2.8	0.1
Arsenic	3.2 ± 0.3	2.6	15.6	0.3

b) in *Gloeophyllum sepiarium* (n = 21)

Metal	Mushroom/Substrate Accumulation Ratio mean ± se	median	max	min
Copper	13.5 ± 1.9	10.0	33.8	4.2
Zinc	4.7 ± 0.8	4.5	17.2	0.4
Nickel	3.3 ± 0.6	1.9	9.0	0.5
Cobalt	6.4 ± 1.0	6.8	17.8	0.4
Lead	1.7 ± 0.2	1.7	4.3	0.4
Manganese	3.8 ± 0.4	3.9	7.9	0.9
Arsenic	2.8 ± 0.4	2.5	8.7	0.4

differences exist and whether or not the threshold level for drought stress is exceeded.

FUTURE WORK

The lack of any consistent geochemical anomaly in the soils of the Kilpatrick Lake site was unexpectedly disappointing, particularly in view of the mineralization exposed on the site. Unless some new and unforeseen relationships become apparent when the vegetation analyses are completed and further statistical evaluations have been undertaken, no further field work at the site appears warranted. If some new relationships are observed a small amount of additional sampling and analyses will be undertaken for purposes of confirmation. In any event, it is expected that an evaluation of all the Kilpatrick Lake sample data will be completed before the end of 1987. Further work related to the site will focus on an evaluation of recently acquired Landsat TM imagery for the area in terms of lithologic and land-cover mapping. The failure of the CCRS mission to obtain high-resolution, airborne MEIS imagery for the site makes it impossible to meet the original objective of evaluating this imagery for vegetational stress and it is not envisaged that plant spectral anomalies will be detectable in the TM data for this site.

This being the case, future research efforts will be focussed on a site in Kelvin Township, approximately 50 km west of the Town of Gowganda, where there is a small but distinct metal anomaly providing good geochemical data made available through the work of Closs and Sado (1982) at the Ontario Geological Survey, and where both MEIS and TM data are available on which preliminary work has been carried out by Singhroy *et al.* (1985) at the Ontario Centre for Remote Sensing. The Kelvin Township site offers a further advantage in that almost pure stands of a single tree species (jack pine, *Pinus banksiana*), with an understorey of lichens, are found growing both on and off the anomaly at different elevations, and probably under different soil-water regimes. As a result, this site, unlike the Kilpatrick Lake site, offers the potential to make comparisons of spectral reflectance with tree-canopy characteristics such as the following: metal level, canopy morphology, leaf colour, and leaf water content. It should be possible, therefore, to determine—at least for a single, common, northern species—whether or not a known metal anomaly with known soil metal levels can be detected by remote sensors via some change in the spectral-reflectance characteristics of the vegetation cover.

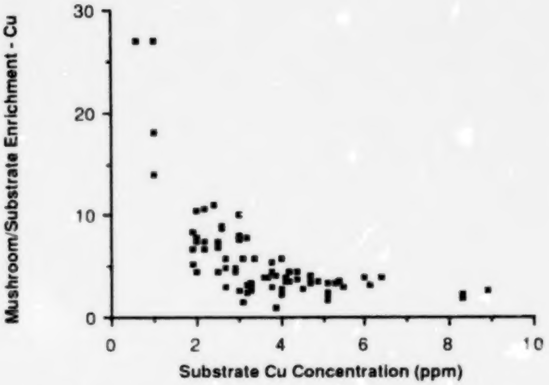

Figure 291.3a. *Relative uptake of copper in Mushroom (Trichaptum abietinus) compared to substrate copper concentration.*

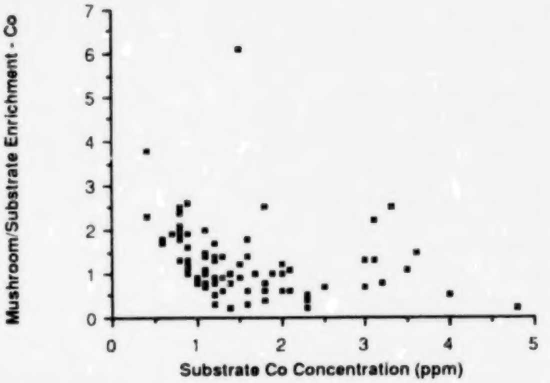

Figure 291.3b. *Relative uptake of cobalt in mushroom (Trichaptum abietinus) compared to substrate cobalt concentration.*

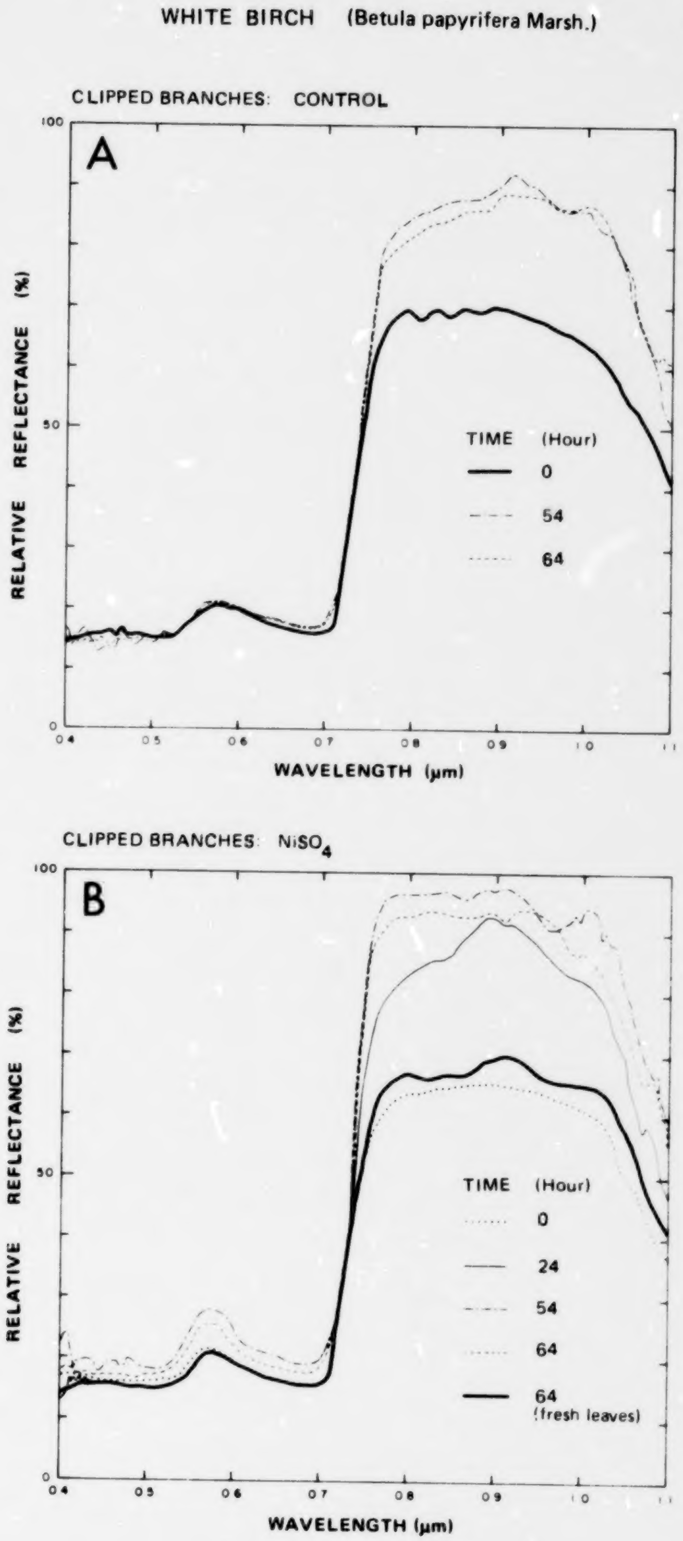

Figure 291.4. *(a) Spectral reflectance response of white birch (control). (b) Spectral reflectance response of white birch ($NiSO_4$).*

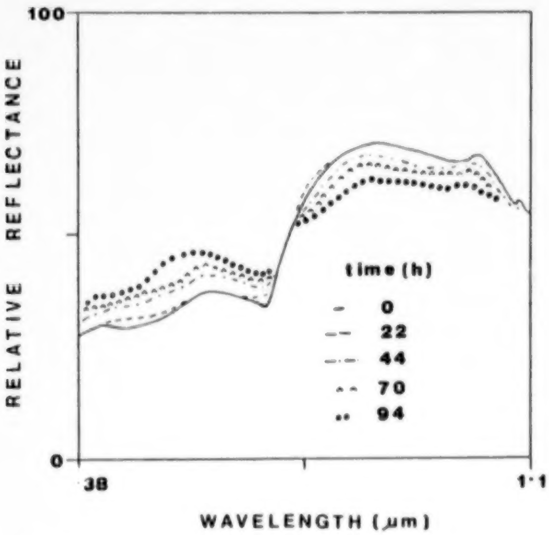

Figure 291.5a. *Spectral reflectance response of control lichen (Cladonia Rangiferina).*

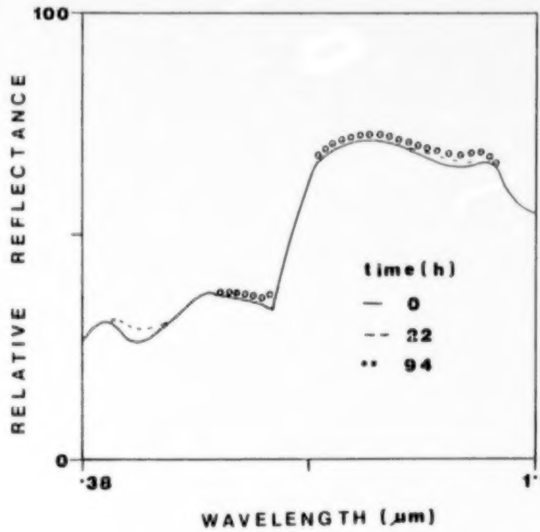

Figure 291.5b. *Spectral reflectance response of copper-treated lichen (Cladonia Rangiferina).*

With the benefit of the experience and background knowledge gained as a result of the Kilpatrick Lake study, future field work on the Kelvin Township site will emphasize vegetation sampling for metals analysis. No data of this type are currently available. In addition, further soil sampling will be undertaken over the anomaly to allow for a detailed examination of plant-soil metal relations in the area and to allow for a comparison with data already obtained from the Kilpatrick Lake site.

Airborne MEIS and Landsat TM imagery will be evaluated over the upcoming year for signs of vegetational stress using a PC-based, PCI/Imavision image-processing system, recently purchased by CIMMER from PCI Inc. of Toronto.

In addition to the above, laboratory studies of metal uptake by plants and their spectral responses will be continued. Saplings of both white birch and balsam fir, judged to be between three and five years old, have already been transplanted to 30 cm (12 inches) diameter peat pots for a controlled study of metal uptake with time. Six replicates of four metal levels plus two controls will be monitored on a monthly basis for metal concentration in the foliage. At the same time the canopies will be scanned with a portable spectral radiometer to determine threshold levels of detectability by remote sensors in these two, very common, northern tree species. Similar laboratory studies on nonvascular plants will also be continued in order to enhance data obtained to date.

REFERENCES

Ashley, R.P., and Abrams, M.J.
1980: Alteration Mapping Using Multispectral Images, Cuprite Mining District, Esmeralda County, Nevada; United States Geology Survey Open File Report, Number 80-367.

Bazzaz, F.A., Carlson, R.W., and Rolfe, G.L.
1974: The Effects of Heavy Metals on Plants. Part 1 Inhibition of Gas Exchange in Sunflower by Pb, Cd, Ni, and Ti; Environmental Pollution, Volume 7, p.241-246.

Beckett, P.J.
1984: Using Plants to Monitor Atmospheric Pollution. Laurentian University Review, Volume XVI, Number 2, p.49-66.

Beckett, P.J., and Courtin, G.M.
1986: Spectral-Reflectance From Lichens Treated with Copper; Proceedings of the Fifth Thematic Conference: "Remote Sensing for Exploration Geology," Reno, Nevada, 1986.

Brooks, R.R.
1972: Geobotany and Biogeochemistry in Mineral Exploration; Harper and Row, New York, 292p.

Canney, F.C., Cannon, H.L., Cathrall, J.B., and Robinson, K.
1979: Autumn Colours, Insects, Plant Disease and Prospecting; Economic Geology, Volume 74, p.1673-1676.

Cannon, H.L.
1971: The Use of Plant Indicators in Ground Water Surveys, Geologic Mapping, and Mineral Prospecting; Taxon, Volume 20, Number 2-3, p.227-256.

Chang, S., and Collins, W.E.
1980: Toxic Effect of Heavy Metals on Plants; Abstract, p.122-124 *in* Official Program, 6th Annual Decora Symposium and Exposition, Sioux Falls, South Dakota.

Closs, L.G., and Sado, E.V.
1982: Bedrock and Overburden Geochemistry Investigations in the Midlothian Lake and Natal Lake Areas, Districts of Sudbury and Timiskaming; Ontario Geological Survey Study 24, 68p. Accompanied by five charts.

Collins, W.
1978: Remote Sensing of Crop Type and Maturity; Photogrammetric Engineering and Remote Sensing, p.43-55.

Courtin, G.M., Beckett, P.J., and Tapper, G.O.
1986: Shift in Spectral Response of Nickel — Loaded and Control Shoots of White Birch (*Betula papyrifera Marsh.*); Proceedings of the Fifth Thematic Conference: "Remote Sensing for Exploration Geology," Reno, Nevada, 1986.

Gates, D.M.
1970: Physical and Physiological Properties of Plants; Remote Sensing Special Reference to Agriculture and Forestry, National Academy of Science, Washington, p.224-252.

Horler, D.N.H., Ostrowski, J.A., and Melling, D.R.
1986: Development of Geobotanical Remote Sensing Technology; Grant 112, p.130-145 *in* Exploration Technology Development Program of the Board of Industrial Leadership and Development, Summary of Research, 1985-1986, edited by V.G. Milne and R.B. Barlow, Ontario Geological Survey, Miscellaneous Paper 131, 145p.

Horler, D.N.H., Barber, J., and Barringer, A.R.
1980: Effects of Heavy Metals on the Absorbtance and Reflectance Spectra of Plants; International Journal of Remote Sensing 1, p.121-136.

Horler, D.N.H., Dockray, M., and Barber, J.
1983: The Red Edge of Plant Leaf Reflectance; International Journal of Remote Sensing 4, p.273-288.

Horler, D.N.H., and Ahern, F.J.
1986: Forest Information Content of Thematic Mapper Data; International Journal of Remote Sensing, Volume 7, p.405-428, 1986.

Jenny, Hans
1980: The Soil Resource, Origin and Behavior; Springer-Verlag, New York.

Kahle, A.B., and Goetz, A.F.H.
1983: Mineralogic Information From a New Airborne Thermal Infrared Multispectral Scanner; Science 222, p.24-27.

Kramer, P.J.
1969: Plant and Soil Water Relationships: A Modern Synthesis; McGraw-Hill Book Company, New York.

Kruckeberg, A.R.
1954: The Ecology of Serpentine Soils 111 Plant Species in Relation to Serpentine Soils; Ecology, Volume 35 Number 2, p. 265-274.

Kruckeberg, A.R.
1969: Soil Diversity and Distribution of Plants, with Examples From North America; Madrono 20, p.129-154.

Martin, M.H., and Coughtrey, P.J.
1982: Biological Monitoring of Heavy Metals Pollution — Land and Air; London, Applied Science, p.475.

Mcllwaine, W.H.
1978: Geology of the Gowganda Lake-Miller Lake Silver Area District of Timiskaming; Ontario Geological Survey Report 175, 161p. Accompanied by Maps 2348 and 2349, scale 1:31 680 or 1 inch to 1/2 mile.

Monteith, J.L.
1973: Principles of Environmental Physics; Edward Arnold, London.

Oke, T.R.
1978: Boundary Layer Climates; Methuen, New York.

Purdy, T.L., Bailey, G.B., and Dwyer, J.L.
1985: Use of Thematic Mapper Data for Alteration and Geological Mapping in South-Central Nevada; Proceedings of the International Symposium of Remote Sensing of Environment, 4th Thematic Conference, Remote Sensing for Exploration Geology, Volume II, Ann Arbor, Michigan.

Raines, G.L., and Canney, F.C.
1980: Vegetation and Geology: *in* Remote Sensing in Geology, B.S. Seigal and A.R. Gillespie editors, John Wiley and Sons Inc., New York, N.Y., p.365-380.

Rauser, W.E., and Courvetto, N.R.
1980: Metallothionein Occurs in Roots of Acrostis Tolerant to Excess Copper; Nature; Volume 287, p.563-564.

Richardson, D.H.S., Beckett, P.J., and Nieboer, E.
1980: Nickel in Lichens, Bryophytes, Fungi and Algae. IN: Nickel in the Environment (J.O. Nriagu, Edition), p.368-406.

Rock, B.N.
1982: Mapping of Deciduous Forest Cover Using Simulated Landsat-D Tm data, in proceedings of the International Geoscience and Remote Sensing Symposium, Munich, p.3.1-3.5.

Salisbury, F.B., and Ross, C.W.
1985: Plant Physiology 3rd Edition, Wadsworth Publishing Company, Belmont, California.

Schwaller, M.R., and Tkach, S.J.
1985: Premature Leaf Senescence: RemoteSensing Detection and Utility for Geobotanical Prospecting; Economic Geology, Vol. 80, p.250-255.

Singhroy, V.H., Sado, E.V., and Bruce, W.
1985: Spectral Geobotany in Glaciated Environments: Test Over a Mineralized Till Site in Northern Ontario Presented at the Fourth Thematic Conference: "Remote Sensing for Exploration Geology", San Francisco, California, April 1-4, 1985.

Ward, J.M.
1969: The Significance of Changes in Infrared Reflectance in Sugar Maple, Induced by Soil Conditions of Drought and Salinity. Proceedings of 6th International Symposium on Remote Sensing of Environment, University of Michigan, Ann Arbor, p.1205-1225.

Wickland, D.E.
1982: Patterns of Vegetation Response to Heavy Metal Stress. In Proceedings of International Symposium on Remote Sensing of Environment: Second Thematic Conference "Remote Sensing for Exploration Geology II". Fort Worth, Texas, p.126.

Grant 294 Quaternary Geology and Geochemical Exploration in the Matheson Area

M.B. McClenaghan[1], O.P. Lavin[1], I. Nichol[1], and J. Shaw[2]

[1]Department of Geological Sciences, Queen's University, Kingston

[2]Department of Geography, Queen's University, Kingston

ABSTRACT

The Matheson area is of great interest for gold exploration because it is underlain by bedrock and structures similar to those of the Timmins Gold Camp. Exploration in the area, however, is hampered by extensive and thick overburden which covers most of the bedrock. For this reason, overburden geochemistry has become an important exploration method in the area. Exploration is further complicated by the existence of tills related to multiple glacial events.

The current research is concerned with identifying criteria for recognizing individual till sheets present in the area and their characteristics with respect to routine overburden exploration programs, primarily on the basis of data obtained from Ontario Geological Survey (OGS) sonic drillholes. The first year of research has focused on the examination of the multielement till geochemistry and the identification of regional patterns in these data. Results of this work indicate that bedrock composition is a major control on till composition. Tills can be divided into two groups based on their chemical composition: mafic and felsic. Correlation with the stratigraphy reveals that the uppermost till (Matheson Till), and occasionally the upper part of the older till sheets, appear to consistently have a felsic composition. The older tills, and not commonly, the lowermost part of the Matheson Till, generally have a mafic composition. The composition of the mafic till probably reflects that of the local greenstone bedrock, and thus is a better sampling medium to use for exploration in the Matheson area.

INTRODUCTION

The objectives of the current research are to identify criteria by which the various till sheets present in the Matheson area may be recognized, and to determine the stratigraphic relationships of the different till sheets using the geochemical, physical, and sedimentological characteristics of the tills encountered in OGS sonic drillholes. Establishing the regional Quaternary stratigraphy will make overburden till sampling a more effective method in the search for gold deposits in the Matheson area.

Known gold deposits in the Timmins area are associated with metasedimentary, metavolcanic, and intrusive rocks broadly related to the Destor-Porcupine Fault zone. The Timmins deposits were discovered primarily as a result of surface prospecting and exploration in areas of abundant bedrock outcrop or shallow overburden. The geology and structural setting characteristic of the Timmins Gold Camp extends eastwards through the Matheson area and into Quebec as part of the Abitibi Greenstone Belt (MERQ-OGS 1983). Thus, gold mineralization associated with these rocks and the Destor-Porcupine and Pipestone Fault zones are major exploration targets. The potential for discovery of economic gold deposits in the Matheson area is further improved by the presence of the Aquarius, St. Andrew Goldfields, and Maude Lake Deposits, and the more recent Canamax and Barrick Resources discoveries further to the east. Exploration in most of the Matheson area, however, is hampered by extensive and thick drift cover. For this reason, overburden drilling and till sampling have become important exploration methods for evaluating the gold mineralization potential of the bedrock in the area.

The glacial overburden is composed of sediments from several glacial events related to different ice transport directions. For exploration purposes, it is essential to know which till sheet is being sampled, and its corresponding ice transport direction, in order to trace overburden anomalies to their bedrock source. The Quaternary stratigraphy and ice transport directions in the Matheson area, however, are poorly documented or understood. This is a result of:

1. the lack of natural exposures showing sediments older than the youngest till sheet
2. the rare preservation of older till(s) below the youngest till sheet
3. the nature of reverse circulation drilling, the most common overburden drilling technique used in exploration, which makes detailed identification of distinct stratigraphic units difficult or impossible

In 1983, the Ontario Geological Survey began a five-year, multidisciplinary geoscience project (BRIM) aimed at stimulating mineral exploration in a 40 township area centred on Matheson and extending eastward to the Quebec border (Figure 294.1). Reconnaissance scale overburden drilling and till sampling, one component of the BRIM project, is being carried out in order to document the regional Quaternary stratigraphy and provide a database of till geochemistry (Baker *et al.* 1985). The rotasonic or, more commonly, sonic drilling method was chosen for this component because sonic drilling yields relatively undisturbed core samples which provide more detailed stratigraphic information than reverse circulation drilling methods. This allows for a more accurate identification of the Quaternary stratigraphy. Also, sonic core samples are better suited to core library storage.

The stratigraphy most commonly encountered in the sonic drillholes is lacustrine clay underlain by till, which in turn is underlain by bedrock. Locally, however, what appears to be one, and possibly two, older tills have been encountered. In most cases, the multiple till units are separated by glaciolacustrine clay or sand. Field work in the area has confirmed that the uppermost till, commonly referred to as the Matheson Till (informal name), was deposited by the most recent glacial advance, which was towards 160° to 170° (Baker *et al.* 1980; Vagners 1984; Richard *et*

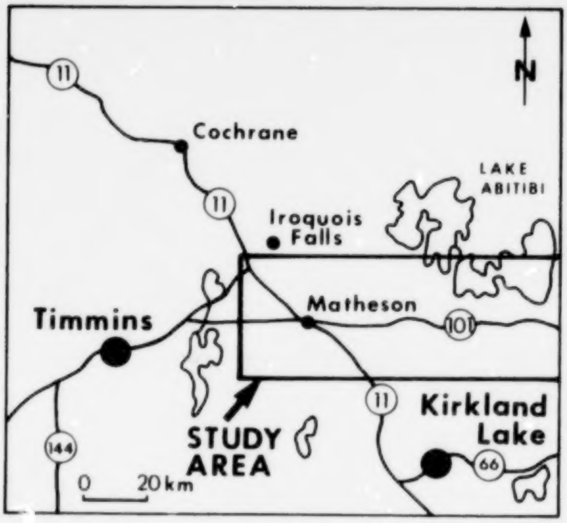

Figure 294.1. *Location of the study area in northeastern Ontario.*

al. 1980; Vagners 1984; Richard *et al.* 1985). An earlier ice advance crossed the area in a 240° direction (Steele *et al.* 1986).

Data from selected BRIM sonic drillholes, combined with existing knowledge of the general regional Quaternary stratigraphy available, are being investigated in order to provide a more detailed understanding of the Quaternary geology, and thus increase the effectiveness of overburden exploration programs in the area. The results presented in this paper focus on the preliminary delineation of till sheets on the basis of multi-element geochemical patterns in the BRIM till samples. A description of the methods employed, as well as the results obtained, are presented. These results represent the first year of the investigation.

Unsorted and unlithified sediment is referred to in this paper as till. Strictly speaking, till is a genetic term and is reserved for unsorted materials which are known to have been deposited directly from a glacier. Since materials encountered in drillholes can seldom be related directly to glacial processes, the term "diamicton", which is purely descriptive, would be more correct. However, the term "till" is retained here to be consistent with popular use of the term in exploration, and to avoid the introduction of another term which may add confusion to the discussion.

QUATERNARY STRATIGRAPHY

A general Quaternary stratigraphy for the Matheson area is known from previous overburden drilling and Quaternary mapping in the area. The uppermost and most abundant till is the "Matheson Till" (an informal name), deposited by the most recent glacial advance which was towards 160° to 170° (Baker *et al.* 1985). This till is overlain by the thick and extensive glaciolacustrine clay and silt deposits of Lakes Barlow and Ojibway. The existence of scattered occurrences of an older till below the Matheson Till is indicated from the BRIM sonic drilling, previous exploration overburden drilling, and the Quaternary stratigraphy exposed in an open pit at Maude Lake. The older till is often separated from the Matheson Till by glaciolacustrine sediments. However, in other places the presence of this till is suspected solely on the basis of distinctive "geochemical discontinuities". In a few sonic drillholes this till is separated from an underlying third till unit by glaciolacustrine sediments.

The Maude Lake pit is a man-made excavation dug through more than 15 m of overburden in order to expose the bedrock surface of a gold deposit. It is significant because it is the only stratigraphic section in the area exposing sediments older than the Matheson Till, and because it provides a unique opportunity for comparison with the stratigraphy of the sonic drillholes. The stratigraphy exposed in the pit walls, summarized from OGS (1986), consists of varved clay and silt grading downward into ice-proximal sandy varves. These in turn grade into a glaciolacustrine-fluvial sandy unit containing numerous debris flows. This sandy unit commonly lies on bedrock. The majority of the bedrock surface exposed on the pit floor has been striated by the most recent glacial advance (160°). A separate till unit below this sandy unit is exposed only in bedrock depressions. Rare crosscutting striations on the pit floor suggest an ice transport direction of 240° for this till. Measurements of pebble orientations completed as part of the current investigation confirm the ice transport direction of approximately 240° for this older till.

The regional stratigraphic framework discussed above has been identified from stratigraphic information recovered from overburden drilling in the area and the Maude Lake pit. Problems with interpretation of the limited stratigraphic information include:

1. Stratigraphic contacts identified on the basis of discontinuities in the stratigraphy and till geochemistry do not always correspond. In some cases, till geochemistry is similar above and below what appears to be a major stratigraphic contact. In other cases, significant "discontinuities" in the till geochemistry occur in what seems to be a single, continuous till unit.
2. Intervening sediments between tills may represent intervals between glacial events or intervals within a single glacial event. In some cases it is difficult or impossible to confidently determine the stratigraphic significance of these sediments.
3. There is a lack of absolute or relative age determinations for the Quaternary sediments in the Matheson area. Absolute age determinations aid in the establishment of timing of depositional events. Relative age determinations are useful in the correlation of drillholes.
4. Ice transport directions for the Matheson Till are well established; however, the knowledge of ice transport directions for tills below the Matheson Till is limited to crosscutting bedrock striations and the pebble fabric from the Maude Lake pit.

Data from BRIM sonic drillholes and the Maude Lake pit are being examined in detail in an attempt to address some of the problems identified above, and

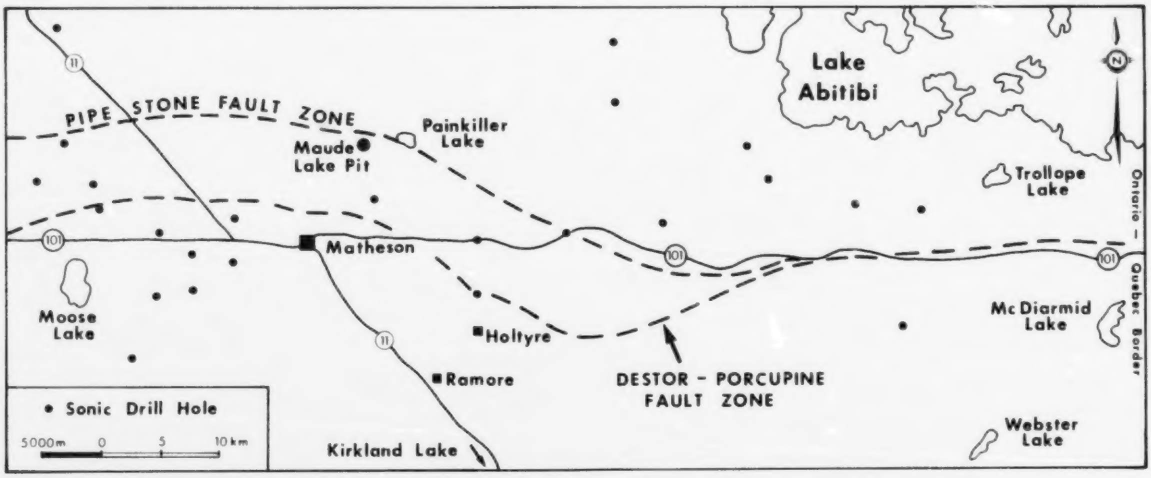

Figure 294.2. *Location of the 24 selected drillholes and the Maude Lake pit in the study area.*

thus provide a more useful stratigraphic framework for use in exploration.

DATA

Twenty-four BRIM sonic drillholes from the 1984 and 1985 drilling programs were selected for the investigation (Figure 294.2). Drillholes were selected on the basis of the following criteria:

1. wide and even geographic coverage of the study area
2. presence of vertically extensive sequences of glacial till
3. presence of possibly more than one till unit, based on stratigraphy and geochemistry

Wide geographic coverage is necessary for establishing a regional Quaternary stratigraphy, as local stratigraphy would be of only limited use in exploration in other parts of the BRIM area. The presence of vertically extensive sequences of till is important in order to maximize the number of till samples per hole. Holes containing multiple tills are required in order to establish the differences between till sheets.

Data provided by the Ontario Geological Survey (OGS) for this research project include: drill logs, multi-element geochemical data, mineralogical data and textural data for 277 till samples from the 24 drillholes, and five till samples from the Maude Lake pit. The drill logs are based on observations of the physical characteristics of the sediments made by personnel of the Ontario Geological Survey (OGS) (including M.B. McClenaghan), and contain such parameters as texture, sorting, stratification, clast content, colour, compaction, bed contacts, and bed thickness. The multi-element geochemical data includes analyses of three different fractions:

1. non-magnetic heavy minerals (H fraction), herein referred to as heavy mineral fraction
2. <0.063 mm fraction (G fraction), herein referred to as fine fraction
3. <1.7 mm fraction ground to <0.063 mm (T fraction), herein referred to as total fraction

The use of the non-magnetic heavy mineral fraction in gold exploration is well established. The <0.063 mm fraction, or fine fraction, was analyzed by OGS to evaluate the usefulness of the finer fraction of the till for gold exploration in the Matheson area (Steele *et al.* 1986). Analysis of the <1.7 mm fraction was carried out to assess the usefulness of a total till sample. The three fractions were analysed for a suite of trace elements. In addition, major oxides were determined for the total fraction samples. Details of elements determined, and analytical methods used by OGS, are provided in Table 294.1. The mineralogical data include identification of the major mineral components of a representative fraction of the non-magnetic heavy mineral concentrate. Textural data include grain size analyses of the <1.7 mm part of the till samples.

DATA EXAMINATION

Before examining these data in detail, the till samples from the 24 drillholes and the Maude Lake pit were classified as belonging to one of three possible till units on the basis of observed stratigraphy and, in some cases, obvious geochemical discontinuities: a) an uppermost till unit (Matheson Till); b) a "middle" till unit; or c) a "lower" till unit. Further, the till samples were rated on the basis of the degree of confidence placed on the till classification.

Focus of the research to date has been aimed at identifying stratigraphic units on the basis of the multi-element geochemical data. These geochemical data were first examined to evaluate the usefulness to the current research of each element analyzed in all three fractions. Elements were eliminated from a fraction in the initial BRIM data set if: a) not determined in both survey years (1984 and 1985); b) concentrations determined were at or below the lower detection limit for most of the samples; or c) analytical methods were not comparable between 1984 and

TABLE 294.1. ANALYTICAL METHODS FOR TRACE ELEMENTS AND MAJOR OXIDES (analytical methods summarized from Bloom 1987).

Fraction	Element	Analytical Method	Elements Included In Research
HEAVY	Au,As,Sb,Co,U,W	INAA	Au,As,Sb,Co,U,W
	Ag,Cu,Zn,Ni	DCP	Cu,Zn,Ni
	Sr,Ti,Zr	XRF-G	Ti,Zr
	Te	GFAA	
	Mo	INAA 1984,DCP 1985	
	Cr	INAA 1984,XRF-G 1985	
	Pb	DCP 1984,AA 1985	
FINE and TOTAL	As,Sb,Co,U,W	INAA	As,Co,U
	Ag,Cu,Pb,Zn,Ni	DCP	Cu,Zn,Ni
	Ti,Zr,Sr	XRF-G	Ti,Zr
	Au	FA-DCP	Au
	Te	GFAA 1984	
	Mo	INAA 1984,DCp 1985	
	Cr	INAA 1984,XRF-G 1985	
MAJOR OXIDES	SiO_2,Al_2O_3,MgO, CaO,Na_2O,K_2O, TiO_2,P_2O_5	XRF	SiO_2,Al_2O_3,MgO, CaO,Na_2O, K_2O, TiO_2,P_2O_5
	MnO		MnO
	Fe_2O_3	XRF 1985	
	CO_2	COUL 1984,COMB IR 1985	
	S	XRF 1984,COMB IR 1985	
	LOI	IGNITION 1985	

AA	Atomic absorption spectroscopy
COMB IR	Combustion in Leco induction furnace and measurement by infrared
COUL	Coulometry
DCP	Direct current plasma
FA-DCP	Fire assay preparation of a silver bead and direct current plasma spectroscopy finish
GFAA	Graphite furnace atomic absorption
INAA	Instrumental neutron activation
XRF	X-ray fluorescence spectroscopy: fused disk
XRF-G	X-ray fluorescence spectroscopy: pressed disk

1985. A list of the elements included in the research is provided in Table 294.1.

ELEMENT ASSOCIATIONS

Before attempting to discriminate individual till sheets on the basis of geochemical composition, the major controls of the geochemical composition must be considered. Element associations, as indicated from correlation coefficients, provide a means of recognizing the major control. Correlation coefficients for elements in each of the three fractions were computed and are summarized in Figure 294.3.

A group of strong, interrelated correlations are evident in both the fine and total till fractions (Figure 294.3a and 294.3b). Positive correlation coefficients of greater than 0.5 exist between Cu, Zn, Ni, Co, and Ti. These are negatively correlated with Zr in the fine fraction. These trace element associations are similar to element associations typically found in a series of volcanic rocks; that is, elements associated with minerals found in mafic volcanic rocks are positively correlated among themselves and negatively correlated with elements which commonly occur in felsic rocks. This feature is further demonstrated in Figure 294.3d, where correlations between the major oxides in the total fraction are shown. Silica is positively correlated with Na_2O and negatively correlated with MgO, CaO and TiO_2. The heavy mineral fraction displays much weaker element associations which are somewhat different from correlations in the fine and total fractions (Figure 294.3c). The positive inter-element associations between As, Sb, Ni, Cu, and Co are probably related to mafic heavy minerals and sulphide minerals. The slightly stronger correlation between U and Zr is most likely related to minerals associated with felsic rocks.

Based on correlations between elements, a major control over the chemical composition of the till appears to be the position of the source rocks within an igneous differentiation sequence. This implies that if the source areas of different till sheets or till units within a single till sheet have contrasting chemical compositions in this respect, these should be reflected by sharp contrasts in the chemical composition of the tills derived from the different bedrock sources. If the tills are derived from similar bedrock types, any chemical differences between till sheets will probably be much more difficult to identify.

a) Fine Fraction

	Au	As	Cu	Zn	Ni	Co	Ti	Zr
As	•							
Cu	•	○						
Zn	•	○	●					
Ni	•	○	●	⊙				
Co	•	○	●	⊙	●			
Ti	•	•	⊙	○	○	○		
Zr	- •	- •	- ●	- ⊙	- ⊙	- ⊙	- ○	
U	•	- •	- •	- •	- •	- •	- •	•

b) Total Fraction

	Au	As	Cu	Zn	Ni	Co	Ti	Zr
As	•							
Cu	○	○						
Zn	•	•	●					
Ni	•	○	●	●				
Co	•	•	●	●	●			
Ti	•	•	●	⊙	⊙	⊙		
Zr	- •	- •	- •	- •	- •	- •	- •	
U	•	•	- •	•	•	•	•	•

c) Heavy Mineral Fraction

	Au	As	Sb	Cu	Zn	Ni	Co	Ti	Zr	U
As	•									
Sb	•	○								
Cu	•	○	•							
Zn	- •	•	•	•						
Ni	•	○	○	⊙	•					
Co	•	- •	- •	○	•	○				
Ti	- •	- •	- •	•	•	- •	•			
Zr	- •	- •	- •	- •	•	- •	- •	•		
U	- •	•	•	- •	•	- •	- •	- •	⊙	
W	•	- •	- •	•	- •	•	○	•	- •	- •

d) Major Oxides

	SiO_2	Al_2O_3	MgO	CaO	Na_2O	K_2O	TiO_2	P_2O_5
Al_2O_3	- •							
MgO	- ●	•						
CaO	- ⊙	- •	○					
Na_2O	⊙	•	- ⊙	- ○				
K_2O	•	- ⊙	- •	•	- •			
TiO_2	- ○	⊙	○	•	- •	- ●		
P_2O_5	- •	- ○	•	○	- •	•	- •	
MnO	- ⊙	⊙	⊙	•	- •	- ⊙	●	- •

Legend

●	> 0.8
⊙	0.6 - 0.8
○	0.4 - 0.6
•	< 0.4
-	Negatively correlated

Figure 294.3. *Correlation coefficients for the heavy mineral, fine, and total trace element data, and for the total fraction major oxide data.*

GEOCHEMICAL DISCRIMINATION OF TILLS

Initial examination of the geochemical data for individual drillholes has identified sharp "geochemical discontinuities" corresponding to identified Quaternary stratigraphic contacts. An example of this feature is shown in Figure 294.4 where Cr values in drillhole 85-17 are plotted. Based on the observed stratigraphy, this hole is considered to have more than one till unit. Each till unit is separated by either clay and silt or sand. It can be seen that the highest Cr values for all fractions correspond to the "middle" till unit. The interpreted stratigraphic boundaries between individual till units delineated on the basis of the observed stratigraphy and corresponding Cr distribution pattern are shown in Figure 294.4.

Dramatic changes in till geochemistry where present, make identification of contacts between till units relatively easy, as demonstrated in Figure 294.4. However, dramatic changes, including those shown for Cr in drillhole 85-17, are not universally applicable across the BRIM area. In many cases, different elements are responsible for defining discontinuities in each hole.

SINGLE ELEMENT DISTRIBUTIONS

Single element abundances were plotted in order to determine if they significantly vary in the different till units definitely identified in the drillholes. A diagrammatic representation of summary statistical values for the single element distributions is provided in Figure 294.5. The trace element data for the fine and total fractions have quite similar mean and range of concentration values, with the fine fraction data generally being slightly higher. For this reason, only the fine till fraction data have been included in Figure 294.5. The "middle" and "lower" till units were grouped together due to the small number of samples in each category. Due to space limitations, only the elements that visually display good separation in mean concentration values and range of concentration values between the Matheson Till, "middle" till, and "lower" till for the fine and heavy mineral trace elements and total till major oxides, are shown in Figure 294.5. Gold is also shown for the fine and heavy mineral fractions because of its significance to exploration. The trace elements plotted in Figure 294.5 demonstrate that there is an obvious difference between mean and range of concentration values for the Matheson Till and the two lower tills. Both the "middle" and "lower" tills have quite similar mean and range of concentration values. In the heavy mineral fraction, Au values are higher and Ti and Zr values are lower for "middle" and "lower" tills when compared to the lower tills. Copper, nickel and gold values are all higher in the "middle" and "lower" tills for the fine till fraction. The major oxide data indicate that the "middle" and "lower" tills have lower SiO_2 values and higher TiO_2 and MgO values than the Matheson Till. The trace element data and major oxide data indicate that the "middle" and "lower" tills are quite similar geochemically and are enriched in elements associated with mafic rocks. The Matheson Till is enriched with elements associated with felsic rocks. Gold values are higher in the more mafic "middle" and "lower" tills.

Based on the patterns shown in Figure 294.5, a distinct chemical difference between the Matheson Till and the "middle" and "lower" tills is readily apparent. The Matheson Till contains significantly higher proportions of elements associated with felsic rocks, whereas the "middle" and "lower" tills contain higher proportions of elements associated with mafic rocks. Many elements show a similar discrimination between different till units, but no single element is obviously superior to the others. In addition, different elements appear to be the best discriminator for the different fractions. For these reasons, it was considered that a multi-variate statistical technique would be the best method of determining, quantitatively, the "best" combination of elements for discriminating between till sheets.

The multi-variate statistical technique "discriminant analysis" is well suited to this purpose. Discriminant analysis is designed to assist with problems of classification. It involves three steps which are carried out sequentially. First, "training groups" of samples are selected which are known to represent specific end members in the classification scheme. Discriminant analysis calculations are then performed on these training groups in order to arrive at a discriminant function, which consists of a constant and a coefficient for each of the variables in the analysis. The discriminant function can then be applied to those samples whose classification is uncertain in order to identify which group they belong to. In a simple two category classification, a sample is classified as belonging to one of the training groups if its discriminant score is positive and to the other group if it is negative. Details and examples of discriminant analysis are found in Klovan *et al.* (1967) and Davis (1973).

In this investigation, training groups include only those till samples from confidently identified stratigraphy. Initially, three training groups were identified from the known till samples; Matheson Till, "middle" till, and "lower" till. However, the "middle" and "lower" till samples were subsequently combined into one training group because of a limited number of samples in these two categories (14 and 18 respectively) and their geochemical similarity, as demonstrated in Figure 294.5. Of the original 282 till samples, 177 were included in the training groups.

Discriminant analysis was performed using the O'GAS program DISCRM (Lavin and Nichol 1981). The till trace element and major oxide data were treated as four separate data sets:

1. trace elements in the fine till fraction
2. trace elements in the total till fraction
3. trace elements in the heavy mineral till fraction
4. major oxides in the total till fraction

The DISCRM program performs the analysis in a step-wise manner; that is, variables are added to the discriminating function one at a time in order of decreasing discriminating power. Results of the four most important elements for each of the four data sets are shown in Table 294.2. As shown in the table, the first element entered into the equation results in approximately 90% of the training group samples being correctly classified into their respective groups.

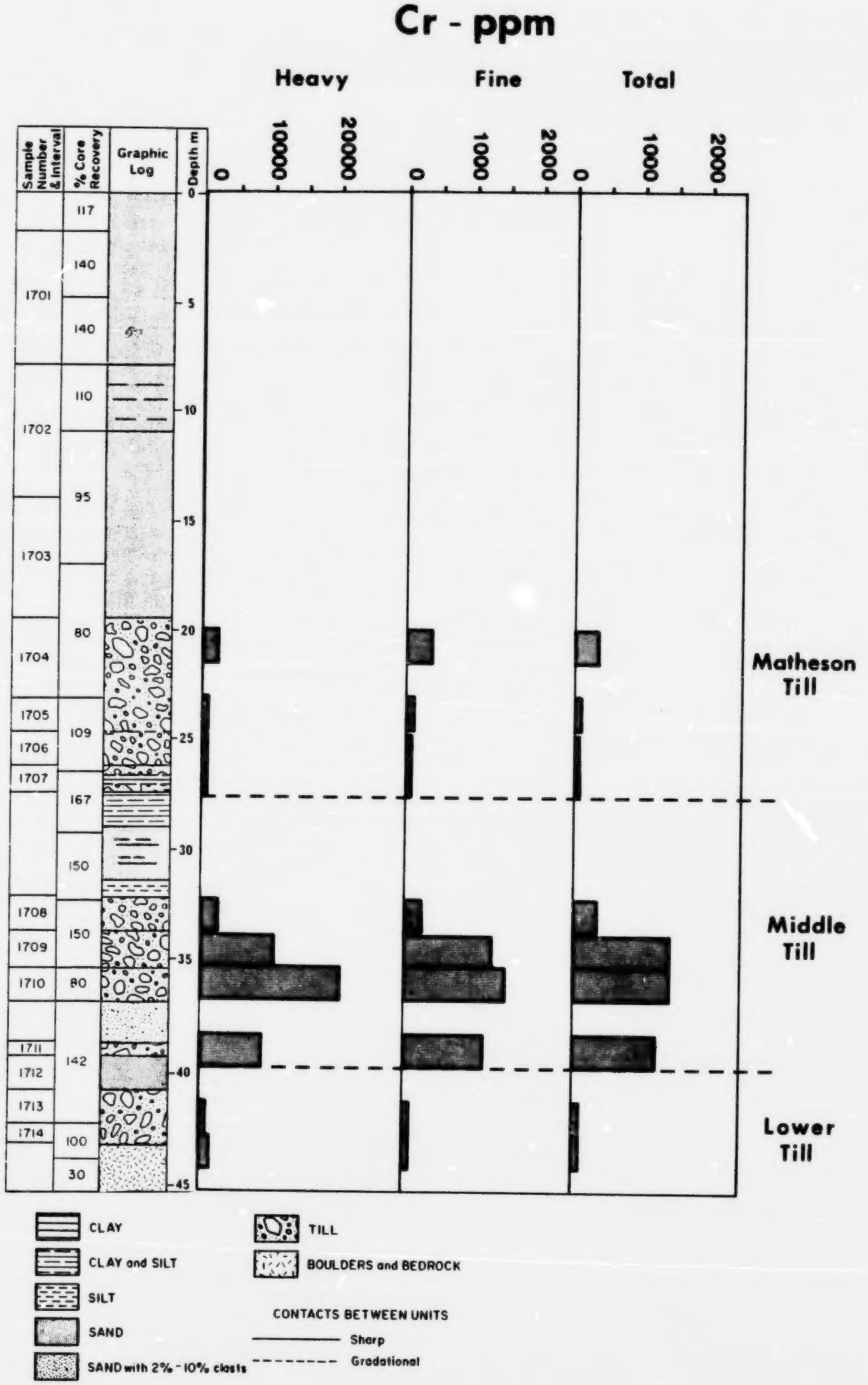

Figure 294.4. *Quaternary stratigraphy and corresponding Cr values (ppm) in the heavy mineral, fine and total till fractions for drillhole 85-17 (graphic log from OGS 1986).*

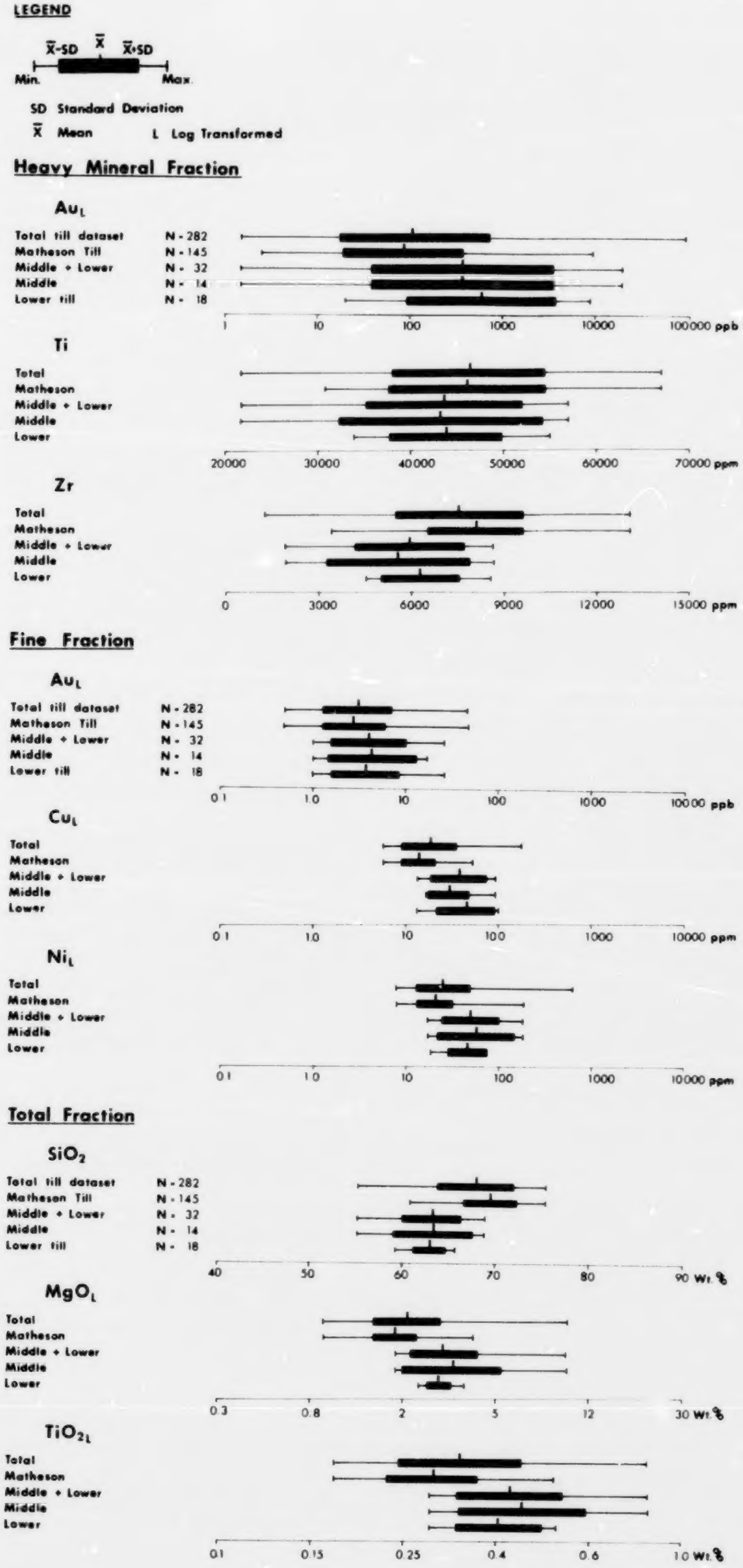

Figure 294.5. *Statistical summary of selected trace elements for the heavy and fine till fractions, and for selected major oxides for the total till fraction.*

TABLE 294.2. SUMMARY STATISTICS FOR DISCRIMINANT ANALYSIS OF HEAVY MINERAL, FINE AND TOTAL TRACE ELEMENTS AND MAJOR OXIDE DATA.

Fraction	Variables in Analysis	DISCRIMINANT ANALYSIS				
		Step	Variable Added	% Classified Correctly	F-Value**	Degrees of Freedom
Heavy	Au*,As*,Sb*, Cu*,Zn*,Ni*, Co*,W*,Ti, Zr,U	1	Ni	89.3	72	1,176
		2	Cr	89.3	51	2,175
		3	Co	89.8	41	3,174
		4	Au	91.0	34	4,173
Fine	Au*,As*,Cu*, Zn*,Ni*,Co*, Ti*,Zr,U	1	Cu	91.0	138	1,176
		2	Zn	90.5	76	2,175
		3	Zr	91.0	56	3,174
		4	Ti	91.6	44	4,173
Total	Au*,As*,Cu*, Zn*,Ni*,Co*, Ti*,Zr,U	1	Cu	91.0	210	1,176
		2	As	91.0	108	2,175
		3	Zr	91.6	74	3,174
		4	Ti	91.6	55	4,173
Major	SiO_2,MgO*, Na_2O,K_2O, TiO_2*,MnO*, P_2O_5,CaO, Al_2O_3	1	SiO_2	84.8	120	1,176
		2	MnO	91.5	92	2,175
		3	P_2O_5	92.6	77	3,174
		4	MgO	93.8	59	4,173

* indicates log transformed

** F-VALUE is a statistical measure of significance of the discrimination. Greater F-values generally indicate a statistically more significant discrimination. Actual significance can be read from standard statistical tables.

TABLE 294.3. DISCRIMINANT SCORE EQUATIONS AND CORRESPONDING THRESHOLDS FOR THE HEAVY MINERAL, FINE AND TOTAL TRACE ELEMENT AND MAJOR OXIDE DATA.

	Discriminant Function	Threshold Defined by Discriminant Analysis	% Classified Correctly
Heavy fraction	$DS = 17.30 - 10.10 (Ni_L)$	Ni = 54 ppm	89.3
Fine fraction	$DS = 17.26 - 11.60 (Cu_L)$	Cu = 31 ppm	91.0
Total fraction	$DS = 21.08 - 16.32 (Cu_L)$	Cu = 20 ppm	91.0
Major oxides	$DS = 56.77 - 0.58 (SiO_2) - 14.29 (MnO_L)$		91.5

DS Discriminant score

L indicates log transformed

Variables added subsequently add very little discrimination. This implies that the multi-element approach does not enhance discrimination significantly, making the simpler, single element approach preferable. Discriminant analysis has, however, drawn attention to which variable is the best discriminator on a regional scale and its optimum threshold value for a given fraction. The threshold is determined by evaluating the discriminant function where the discriminant score is equal to zero. The selected functions and threshold values for the four data sets are shown in Table 294.3. Note that in the case of the major oxides, the second variable (MnO) added sufficient discriminating power to warrant inclusion into the equation.

The sign of the coefficient for each element, as shown in Table 294.3, indicates whether values for that element are typically higher or lower in the Matheson Till. For the heavy mineral, fine, and total fraction trace elements, the coefficients for Cu and Ni are negative, indicating lower values in the Matheson Till group relative to the lower till groups. The reverse is true for SiO_2, which displays a positive coefficient, indicating greater values of SiO_2 in the Matheson Till. Thus, using the individual trace elements and the discriminant function for the major oxides, it is possible to classify all till samples, including those previously unclassified, into two groups: those with a more mafic composition, as indicated by lower SiO_2 and higher Cu, Ni, and MnO values, and those with a

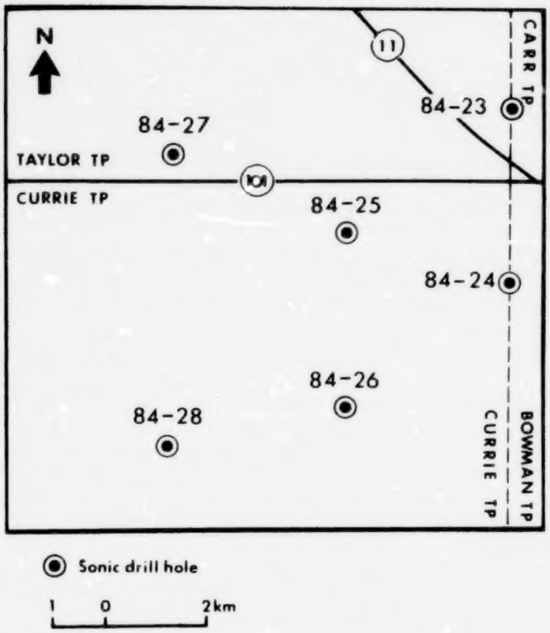

Figure 294.6. *Location of the six selected drillholes in the study area.*

more felsic composition, as indicated by a higher SiO_2 and lower Cu, Ni, and MnO values.

The critical trace elements for each fraction, as identified by discriminant analysis, and the discriminant score for the total till major oxides were plotted for each drillhole in order to evaluate the stratigraphic significance of the felsic-mafic classification. In particular, the stratigraphic position of misclassified training group samples and the classifications of previously unclassified samples were noted. Space limitations preclude the inclusion of all 96 profiles here; however, the results can be summarized as follows. In general, the groupings correspond with observed stratigraphic breaks. In 23 of the 24 drillholes, the Matheson Till exhibits a more felsic composition, and the "middle" and "lower" tills have more mafic compositions. Till samples from two holes thought to contain two or three separate tills on the basis of observed geochemical discontinuities in various elements were all classified as being felsic in composition, indicating that the entire sequence is geochemically similar to Matheson Till. This may indicate that the geochemical discontinuities are not significant on a regional scale. All four data sets produced similar patterns of groupings. The fine and total data groupings are almost identical. Detailed examination of the groupings indicates some relevant features:

1. In some holes with a significant vertical sequence of Matheson Till, the lowermost till sample, resting on bedrock, has a mafic composition. This lowermost sample, however, is commonly separated from the overlying till sequence by a sand or gravel unit.
2. The upper part of some middle and lower tills displays a more felsic composition than the lowermost parts.
3. For some till samples, the fine and total fraction Cu values indicate a mafic composition, while Ni values in the heavy mineral fraction indicate a felsic composition.

These exceptions are difficult to explain with the current information and require more detailed attention.

In summary, single trace element distributions and a two element discriminant function for the major oxides are efficient methods for the classification of till samples into felsic and mafic groupings. The results indicate that the Matheson Till has a more felsic composition than the older tills. The results must be interpreted in conjunction with stratigraphy in order to further define the relationships between the Matheson, "middle", and "lower" tills. Several "unexplained" or conflicting sample groupings require further examination.

GEOCHEMICAL CLASSIFICATION OF TILL UNITS OVER A RESTRICTED AREA

The discrepancies and misclassifications resulting from single element/discriminant score classification could be interpreted as representing systematic lateral or local variation in the geochemistry of the till sheets. Perhaps no single classification rule can be applied consistently over the entire area. Alternatively, the general classification rule holds over the entire area and local aberrations and oddities cause the classification function to break down at isolated locations. To test these possibilities, a subset of till samples from closely spaced drillholes was selected and subjected to an "unguided" multi-variate statistical clustering technique.

Six drillholes in relatively close proximity (represented by 64 till samples) were selected (Figure 294.6). The relatively close spacing of these drillholes allowed for detailed correlation between holes to be made on the basis of observed stratigraphy. These correlations were then compared to the classification by the cluster analysis. Both hierarchical cluster analysis and K-means cluster analysis were applied to the data set using the computer programs of SYSTAT (Wilkinson 1986).

Hierarchical cluster analysis is a multi-variate procedure for detecting natural groupings in a data set (Wilkinson 1986). Sample pairs are organized by the program according to their relative similarity, so that samples with the highest mutual similarity are grouped together (Davis 1973). Groups or clusters are associated with other groups until all the samples have been included in the classification scheme. The final result is a dendrogram; a graphic display of the hierarchical groupings of samples. Dendrograms for the major oxides and for the three fractions of trace element data were generated for each hole allowing identification of sample groupings which conflicted with the original stratigraphic interpretation. An example of a dendrogram for trace elements in the fine fraction for drillhole 84-28 is shown in Figure 294.7. Three separate till sheets separated by glaciolacustrine silt and clay have been identified in drillhole 84-28. The uppermost till (Matheson) extends from depths of 18 to 25 m, the "middle" till from 35.5 to 36.5 m, and the "lower" till from 39.5 to 60.5 m. Hierarchical cluster analysis has produced two large clusters of till samples based on the relative geochemical similarity of till samples from this drillhole. The upper cluster on the dendrogram consists of till samples from the Matheson and "middle" till units (samples 01 to 07). The lower cluster contains till samples from the lowermost till unit in the drillhole (samples 08 to 20). The clusters produced correspond, in general, with interpreted stratigraphy. The one sample representing the "middle" till sheet (07) has been grouped with the Matheson Till samples, indicating they have quite similar geochemistry when compared with the "lower" till samples.

K-means clustering is somewhat different from hierarchical clustering, in that it classifies samples into a specified number of groups. It is a splitting technique used to group samples such that between-group variation is as large as possible relative to within-group variation (Wilkinson 1986). In addition, and perhaps more importantly, it can be used to determine which elements are responsible for the clustering. K-means clustering was carried out using two groups.

The sample groupings based on cluster analysis for all till samples in the restricted area generally correspond to the observed stratigraphy, and are very similar to the results of discriminant analysis. Using hierarchical clustering techniques, all 64 till samples were clustered into two groups. The larger cluster of samples corresponds to Matheson Till and the smaller cluster corresponds to the "middle" and "lower" tills. K-means cluster analysis split the till samples into two groups almost identical to the two hierarchical clusters. K-means clustering also indicated that the elements responsible for the clustering are the same as those identified as significant in the discriminant analysis. The upper, or Matheson, till generally has a more felsic composition, while the two lower tills are generally more mafic in composition. The distribution of mafic and felsic tills for the six drillholes identified by cluster analysis is shown in Figure 294.8. Exceptions to the general trend are seen in the "lower" tills of drillholes 84-26 and 84-27, and the "middle" till of drillhole 84-28 (Figure 294.8). Cluster analysis indicates the composition of the "middle" till in drillhole 84-28 and the "lower" till in holes 84-26 and 84-27 are most similar to the Matheson Till. The till samples of drillhole 84-24 have exclusively a mafic composition. These same patterns were also identified by the single element discriminations discussed above.

Both hierarchical and K-means cluster analysis are useful in separating the till samples into two groups on the basis of felsic/mafic composition. These results correspond to and corroborate the discriminant analysis results, but do not significantly reduce the classification error noted, even when applied over a restricted area. This implies that the misclassified samples are simple aberrations to the general trend and should be recognized as such.

DISCUSSION

A combination of different statistical techniques applied to these data consistently indicate that geochemical composition of the till is dominated by variations which are similar to those found in a series of mafic to felsic volcanic rocks. When a till sample contains higher values of a mafic element such as Cu, Ni, Co, and so on, most other mafic elements are also higher in that sample. Conversely, till samples with higher concentrations of SiO_2, indicating a more felsic composition, generally have much lower values of mafic trace elements. This pattern is sufficiently consistent to allow reliable classification of samples as mafic or felsic based on values of a single indicative element.

The major variations in till composition appear to be strongly related to stratigraphic position. Till samples highest in the Quaternary stratigraphic section, and thus believed to be representative of the Matheson Till, are dominantly more felsic in composition. Samples that are closer to bedrock and normally separated from Matheson Till by interglacial sediments are dominantly more mafic in composition. Matheson Till has a relatively consistent felsic composition across the entire BRIM area, implying a consistent source area.

The BRIM area is underlain by primarily mafic to intermediate volcanic rocks and derived sedimentary rocks of the Abitibi Greenstone Belt (MERQ-OGS 1983). Thus, in the BRIM area, tills of local derivation are expected to have a strong mafic composition. However, the Matheson Till has a relatively consistent felsic composition. This may be related to a combination of the following:

1. The masking (protection) of the local mafic volcanic and sedimentary greenstone rocks by older tills and glaciolacustrine sediments, preventing extensive incorporation of the local mafic rocks into the Matheson Till.
2. A different ice transport direction, and thus different source rocks for the Matheson Till, as compared to the older tills.
3. The dynamics and thermal conditions of the ice sheet depositing the Matheson Till may have prevented incorporation of much local mafic bedrock over the BRIM area.

Problems remaining with these interpretations are:

1. A strongly mafic till sample occurs on bedrock at the base of some vertically continuous sections of otherwise felsic (Matheson) till.
2. The composition of the upper part of some "middle" and "lower" tills appears to be similar to the Matheson Till. The question arises as to whether this uppermost, felsic part represents a separate glacial event from the mafic, lower part, or merely a different facies from the same event.

The differences in geochemistry between stratigraphic units in the BRIM area are much easier to recognize than to explain. The complexities and lateral (and temporal) variation in a glacial system, particularly over such a wide area, make a simple explanation unlikely. Proving the validity of a particu-

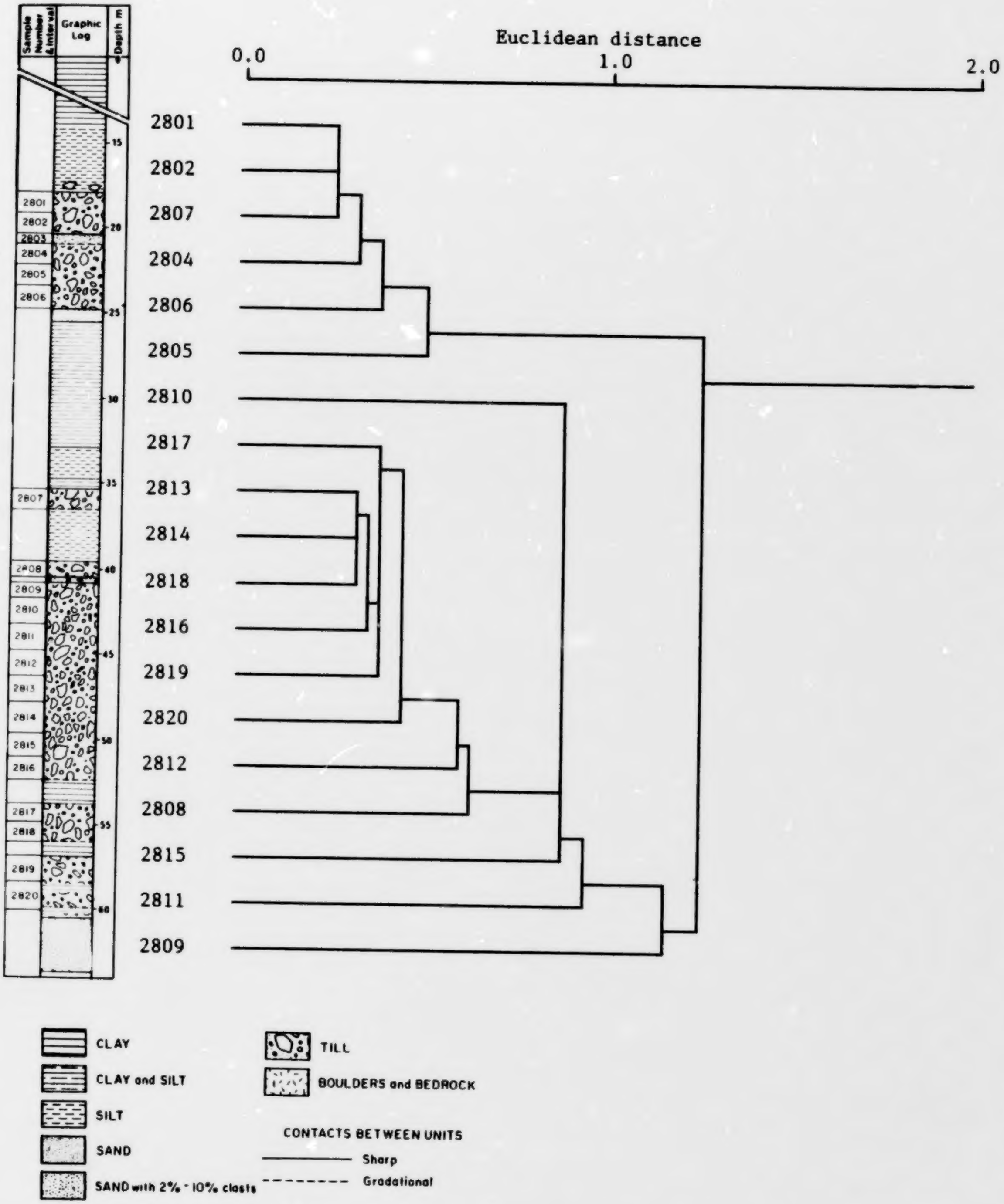

Figure 294.7. *Dendrogram and graphic log for the fine fraction trace element data of drillhole 84-28 (graphic log modified from OGS 1986).*

lar explanation for the geochemical differences will probably not be possible. Notwithstanding these uncertainties, a few (of many possible) simplistic explanations have been presented above. These models are not intended to be comprehensive answers to the questions raised by the geochemical

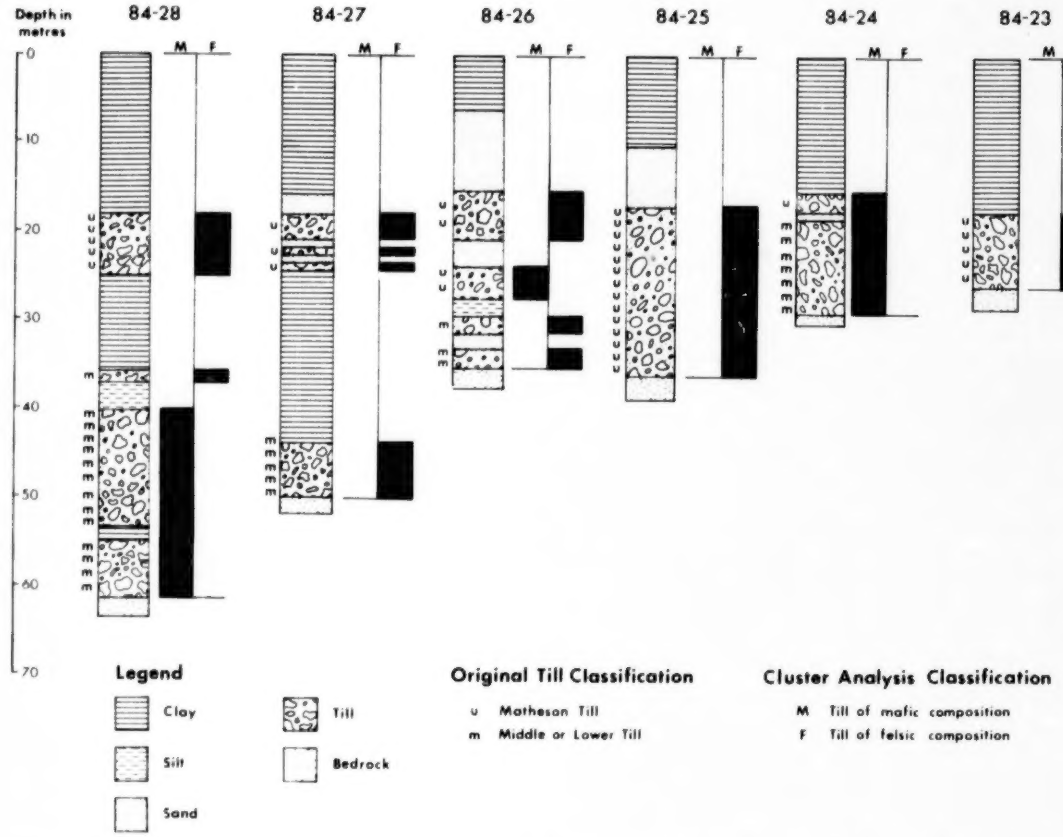

Figure 294.8. *Cluster analysis classification for the six selected drillholes (graphic logs modified from OGS 1986).*

differences between or within glacial stratigraphic units, but are a possible framework on which to base future work and to promote discussion. Future work is designed to shed light on the reasons for the empirical chemical differences in the stratigraphy, with a view to using chemical differences to assist in identifying till sheets in routine exploration programs.

CONCLUSIONS AND IMPLICATIONS FOR EXPLORATION

To date, the research carried out has focused on the examination of the multi-element till geochemistry on a regional scale. Multi-variate statistical techniques have helped to draw attention to regional patterns. Some preliminary conclusions can be drawn from this work:

1. Trace element data for the fine and total fractions are almost identical. This is not surprising since 40 to 60% of the <1.7 mm part of the till samples is composed of silt and clay. Continued inclusion of both fractions in the research may prove redundant, at which time one fraction may be eliminated.
2. The predominant control of the till geochemistry is major rock type variation in the source rocks.
3. Selected single elements, discriminant functions, and cluster analysis are equally effective techniques for dividing the tills into two major, geochemically distinct groups: those with a felsic geochemistry and those with a mafic geochemistry.
4. In general, the till geochemistry is related to stratigraphic position. The uppermost till in almost all drillholes is more felsic. "Middle" and "lower" tills are more mafic.
5. Differences between felsic and mafic till composition may be related to different bedrock source areas or relative position in the ice during transport.
6. Significant geochemical discontinuities usually occur at stratigraphic boundaries between till sheets, however, some geochemical discontinuities also occur within a till sheet.

The following points are of immediate importance for mineral exploration:

1. A regional approach to the interpretation of geochemical discontinuities is necessary in order to correctly interpret the Quaternary stratigraphy.
2. A simple determination of Cu in the fine-grained part of till samples should be helpful in determin-

ing till stratigraphy. The same appears apply for Ni concentrations in the heavy mineral fraction.

3. Gold values are significantly higher in the mafic till as compared to the felsic till.
4. The tills which have a mafic geochemistry are a better sampling medium because of their position at the base of the stratigraphic section and, more importantly, their local bedrock source. Gold mineralization is associated with mafic bedrock types in the Abitibi Greenstone Belt.

FUTURE WORK

Future work is intended to clarify the genetic reasons for the empirical chemical differences between tills identified thus far. A better understanding of the relationships between the stratigraphy and geochemistry of the Quaternary sediments will significantly improve overburden exploration techniques in the Matheson area. Future work is summarized below:

1. Examination of the >1.7 mm pebble-size fraction from till samples will be carried on in order to determine the proportions of various bedrock lithologies present. This fraction may give an indication of provenance of the individual till sheets. Special attention will be paid to proportions of felsic or mafic rock lithologies.
2. Investigation of the geochemical signatures of the individual till units will continue, including the examination of the relationships between multi-element geochemical data, mineralogical data, weight data, pebble counts, and sonic drillhole bedrock geochemical data.
3. Oriented drill core collected from selected locations during the 1987 OGS drill program will be examined to determine the presence and orientation of micro-fabrics in the hope of establishing paleo ice transport directions for the "middle" and "lower" till units in the Matheson area.
4. Microscopic and scanning electron microscopic (SEM) examination of sedimentological features of the tills will be performed in order to establish till facies not identified by the preliminary logging of the drill core. This will aid in the interpretation of the observed geochemical patterns.

ACKNOWLEDGMENTS

The authors would like to thank the Geophysics/Geochemistry section of the Ontario Geological Survey for making all data used in this research project readily available. C.L. Baker, L.B. Bloom, and K.G. Steele provided much helpful advice. J.M. Kuska and G.S. Cluett were of great assistance in the preparation of this paper.

REFERENCES

Baker, C.L., Seaman, A.A., and Steele, K.G.
1980: Quaternary Geology of the Ramore Area, Districts of Cochrane and Timiskaming; Ontario Geological Survey, Preliminary Map P.2381, Geological Series, scale 1:50 000. Geology 1979.

Baker, C.L., Steele, K.G., and McClenaghan, M.B.
1985: Reconnaissance Till Sampling Program, Matheson-Lake Abitibi Area, District of Cochrane; p.329-333 *in* Summary of Field Work and Other Activities 1985, Ontario Geological Survey, edited by John Wood, Owen L. White, R.B. Barlow, and A.C. Colvine, Ontario Geological Survey, Miscellaneous Paper 126, 351p.

Bloom, L.B.
1987: Analytical Methods, Quality Control Data and Previously Unpublished Geochemical Results: Reconnaissance Till Sampling Program, Matheson Area, Cochrane District; Ontario Geological Survey, Open File Report 5653, 149p.

Davis, J.C.
1973: Statistics and Data Analysis in Geology; John Wiley and Sons, 550p.

Klovan, J.E., and Billings, G.K.
1967: Classification of Geological Samples by Discriminant-Function Analysis; Bulletin of Canadian Petroleum Geology, Volume 15, Number 3, p.313-330.

Lavin, O.P., and Nichol, I.
1981: Q'GAS: A Minicomputer-based System to Aid in the Interpretation of Exploration-oriented Geochemical Data; Journal of Geochemical Exploration, Volume 15, p.521- 537.

MERQ-OGS
1983: Lithostratigraphic Map of the Abitibi Subprovince; Ontario Geological Survey/Ministère de l'Energie et des Ressources, Québec; 1:500 000; catalogued as "Map 2484" in Ontario and "DV 83- 16" in Québec.

Ontario Geological Survey
1986: Sonic Drillhole 84-23, Carr Township, District of Cochrane; Ontario Geological Survey, Geophysical/Geochemical Series Map 80779, scale 1:100 000. Geology 1984, 1985.

Ontario Geological Survey
1986: Sonic Drillhole 84-24, Bowman Township, District of Cochrane; Ontario Geological Survey, Geophysical/Geochemical Series Map 80759, scale 1:100 000. Geology 1984, 1985.

Ontario Geological Survey
1986: Sonic Drillhole 84-25, Currie Township, District of Cochrane; Ontario Geological Survey, Geophysical/Geochemical Series Map 80780, scale 1:100 000. Geology 1984, 1985.

Ontario Geological Survey
1986: Sonic Drillhole 84-26, Currie Township, District of Cochrane; Ontario Geological Survey, Geophysical/Geochemical Series Map 80781, scale 1:100 000. Geology 1984, 1985.

Ontario Geological Survey
1986: Sonic Drillhole 84-27, Carr Township, District of Cochrane; Ontario Geological Survey, Geophysical/Geochemical Series Map 80782, scale 1:100 000. Geology 1984, 1985.

Ontario Geological Survey
1986: Sonic Drillhole 84-28, Currie Township, District of Cochrane; Ontario Geological Survey, Geophysical/Geochemical Series Map 80760, scale 1:100 000. Geology 1984, 1985.

Richard, J.A., and McClenaghan, M.B.
1985: Quaternary Geology of the Porquis Junction Area, District of Cochrane; Ontario Geological Survey, Map P.2949, Geological Series-Preliminary Map, scale 1:50 000. Geology 1984.

Steele, K.G., Baker, C.L., and McClenaghan, M.B.
1986: Reconnaissance Till Sampling Program, Matheson-Lake Abitibi Area, District of Cochrane; p.398- 403 *in* Summary of Field Work and Other Activities 1986, Ontario Geological Survey, edited by P.C. Thurston, Owen L. White, R.B. Barlow, M.E. Cherry, and A.C. Colvine, Ontario Geological Survey, Miscellaneous Paper 132, 435p.

Vagners, U.J.
1984: Quaternary Geology of the Matheson Area, District of Cochrane; Ontario Geological Survey, Map P.2735, Geological Series-Preliminary Map, scale 1:50 000. Geology 1983.

Wilkinson, Leland
1986: SYSTAT: The System for Statistics; SYSTAT Incorporated, 528p.

Grant 298A The Geological Setting of Gold Deposits in the Porcupine Mining Camp

R. Mason and D.I. Brisbin

Department of Geological Sciences, Queens University, Kingston

ABSTRACT

Detailed mapping on the Tisdale volcanic sequences at Timmins has confirmed the justification for the traditional subdivision of the Tisdale Group into four formations, the Northern, Central, Vipond, and Gold Centre. In general, the four formations are distinctive and can be mapped as separate entities, but in detail, they show considerable variation along strike and are not internally consistent.

The "99 Flow", which separates the amygdaloidal flows of the Central Formation from the variolitic flows of the Vipond Formation, and the V10b flow top breccia which marks the top of the Vipond Formation (and the base of the Gold Centre Formation), are especially valuable as aids to stratigraphic correlation. The "99 Flow", mapped at the Paymaster and Dome Mines, appears to be equivalent to the massive V8c subunit which crops out elsewhere at Timmins.

The Gold Centre Formation is a monotonous sequence of uniform flows with zones of pillow breccia and poorly defined pillows. It crops out around the rim of the Porcupine Syncline and is not associated with any significant zones of alteration or mineralization apart from in the Dome area.

Early mafic dikes have been found cutting the Vipond sequence at the Paymaster Mine, and these dikes are themselves deformed by the late Archean regional cleavage and linear stretch fabric which affects the whole of the Timmins area.

Heterolithic breccia dikes on the Coniaurum Property have been shown to be composite, and other such dikes have been recognized at several localities in association with porphyry intrusions.

INTRODUCTION

Despite 75 years of mining and geological studies in the Porcupine Camp, the relationship of gold deposits to the geological environment in which they occur is still poorly understood. Recent underground and surface mapping, together with compilations of existing data on the McIntyre-Hollinger gold system at Timmins (Mason and Melnik 1968, Mason *et al.* 1986) have emphasized the need for a comprehensive study of the stratigraphy, structure, and metamorphism of the Porcupine Camp. Mason *et al.* (1986) have described the detailed stratigraphy at the McIntyre Mine, based on the earlier work by Griffis (1960), and their work forms the starting point for this study.

The current project involves field-based studies in the Porcupine Camp. Intensive mapping will be completed in Tisdale Township and the northern portion of Deloro Township (Figure 298A.1). The original proposal for this project was to map the whole of the Timmins Camp, including the mines to the east of the Burrows-Benedict Fault. Because of the current Ontario Geological Survey mapping program at Timmins, it has been decided to restrict this study to the area west of the fault and north of the Destor-Porcupine Fault, and to concentrate efforts toward more detailed investigation of mineralized areas around the Dome Mine and the old Aunor-Delnite Mines. Mapping is being carried out at a scale of 1 inch to 500 feet (1:6000) with more detailed mapping in selected areas. Mapping of a newly stripped area on the Delnite Property in northern Deloro Township was completed at a scale of 1 inch to 20 feet (1:240) (Brisbin *et al.* this volume). Compilation and underground mapping at Dome Mines was also begun in the 1986 field season.

During the 1986 field season, the bulk of surface mapping was completed in southwest Tisdale Township in an area extending east from the Hollinger Mine to Gold Centre, north to the Coniaurum Property and south toward the Paymaster Property. A preliminary objective of the study was to establish the style of vertical and lateral lithofacies changes within the mafic volcanic flows of the Tisdale Group. The distribution of strain and hydrothermal alteration, and possible relationships with porphyries and/or mineralization will be investigated during the 1987 field season.

LITHOLOGY AND STRATIGRAPHY

Since 1899, when W.A. Parks first surveyed the Timmins area and reported that the area had gold potential, and following the discovery of gold in 1909, numerous geologists from the Ontario Department of Mines, the Ontario Geological Survey, and the mining companies at Timmins have reported on the geology of the Timmins area. The early workers (Hore 1913; Whitman 1915; Robinson 1923; Burrows 1911, 1912, 1915, 1925) recognized the major formations and lithotypes, and subdivided the sequence at Timmins into the Keewatin and Timiskaming Series, which were in turn intruded by Algoman felsic porphyries and Matachewan basic dikes. The Keewatin sequence is chiefly composed of volcanic units, with minor interflow sedimentary units, and is separated from the dominantly sedimentary Timiskaming sequence by an unconformity (Burrows 1915, 1925).

Burrows (1925) first reported that the Keewatin sequence had been folded prior to erosion and deposition of the Timiskaming sedimentary sequence. Graton and McKinstry (1933) and Hurst (1936) were the first to make a clear separation of sedimentary units in the Keewatin sequence from those of the later Timiskaming sedimentary sequence.

Graton and McKinstry (1932, 1933) were the first to correlate the various mine sequences at Timmins. They subdivided the volcanic sequence into four units, using a massive "dacitic" flow which had been numbered the "99 flow" by mine geologists, and two variolitic pillowed basaltic flow units as consistent marker horizons through the area. The 99 flow owes its value as a marker unit as much to the fact that it

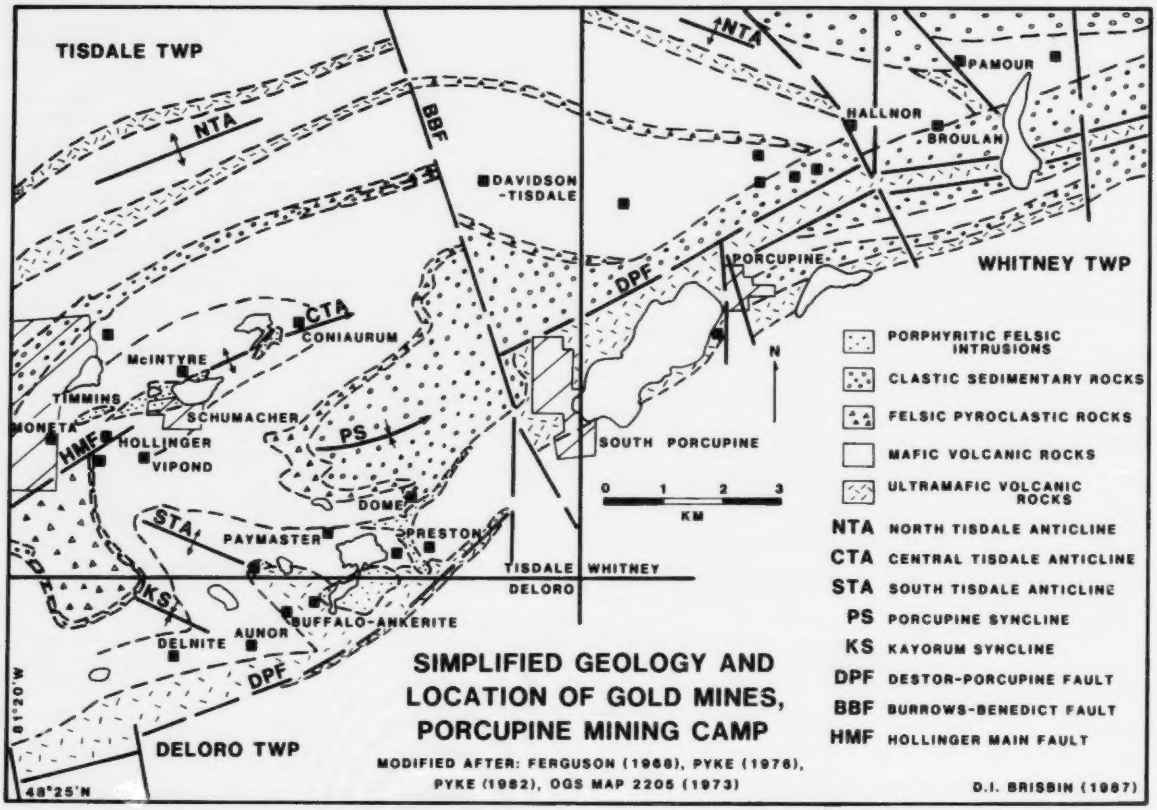

Figure 298A.1. Map showing simplified geology and location of gold mines in the Porcupine Mining Camp.

separates two distinctly different volcanic sequences above and below it, as it does to its own continuity.

Thus the 99 flow was interpreted as the basal unit of a sequence of pillowed, massive, and brecciated basaltic flows characterized by thick units of variolitic pillow basalts, named the "Vipond Series". Above the Vipond Series, a group of basaltic flows with well-defined flow top breccias was named the "Gold Centre Series". Below the 99 flow, a distinctive sequence of pillowed amygdaloidal basalts, massive units similar to the 99 flow, and brecciated flows was named the "Central Series". The Central Series was recognized as being important as it contains most of the productive gold veins at the Hollinger and McIntyre Mines. At the base of the sequence, and confined to the core of a major anticlinal structure to the north of the Pearl Lake porphyry and the main workings on Hollinger and McIntyre, the "Northern Series" consists of a sequence of massive and pillowed amygdaloidal basaltic flow units and related breccias.

The hydrothermal alteration associated with the mineralized zones in the Timmins camp has led to the description of some flows as "andesitic" and "dacitic" when in fact they are altered magnesian and iron-rich tholeiitic basalts (Pyke 1982). The massive leucoxene-bearing "dacites", which occur in all formations of the Tisdale Group, and are typified by the "99 flow", appear to be iron tholeiites (Pyke 1982).

Hurst (1935) and Langford (1941) separated the basal part of the Central Series, which consists of prominent and stratigraphically useful breccia units at the McIntyre Mine (the "95" and "55" flows), into the McIntyre Series, but this subdivision was abandoned by later workers. However, these units are so specific to the Central Tisdale Anticline, and to the McIntyre in particular, that it is not surprising that Hurst and Langford thought they should be separated. Graton and McKinstry (1933) recognized that the reliable marker horizons were restricted to the 99 flow and the variolitic flows in the Vipond Series. The 95C ("chickenfeed") unit (in the Central Series), was also used as a valuable and consistent marker horizon at the McIntyre and Hollinger Mines, together with the 55 flow unit above it.

Jones (1948) adopted the use of "Formation" in place of "Series", and Dunbar (1948) named the entire sequence the Tisdale Group. Using a variolitic flow (V8), a brecciated variolitic lava ("chickenfeed" V10b), and the massive 99 flow in the Vipond Series as key markers, Furse (1954) made the first detailed field-based subdivision of the Keewatin sequence for the Pearl Lake section of the Porcupine (Timmins) gold camp, and this is still in common use in the area (Ferguson 1968). Ferguson (1968) further separated a sequence of felsic pyroclastic rocks, which rest unconformably on formations of the Tisdale Group, as the "Krist Fragmental" Series.

Pyke (1975, 1981, 1982) redefined the stratigraphy in the Timmins area and subdivided the Tisdale Group into three formations; a Lower Volcanic Formation below the 99 flow unit, a Middle Volcanic Formation equivalent to the old Vipond and Gold Centre Series, and an Upper Volcanic Formation equivalent to the Krist fragmental sequence. Pyke's work was the first to introduce chemical classification of the volcanic rocks into the stratigraphic framework. The Lower Volcanic Formation includes a komatiitic sequence at the base and its upper limits are based on the recognition of the uppermost magnesian tholeiites in the sequence. The Middle Volcanic Formation is characterized by iron-rich tholeiitic units, and its base was taken as the first readily recognizable iron tholeiite in the lower part of the Tisdale Group (the 99 flow), although there are prominent iron tholeiite flows in the Central and Northern Series below the 99 flow. Thus, the boundary between the Lower and Upper Volcanic Formations occurs in the middle of the old mines sequence at the base of the Vipond Formation. However, the Northern and Central Formations (Series) have more in common with the Vipond and Gold Centre Series as defined by Graton and McKinstry (1933) than they do with the basal komatiitic sequence.

The stratigraphy at the McIntyre Mine (Robinson 1923; Hurst 1936; Langford 1941; Furse 1948) was established by careful mapping of the tops and bottoms of individual flow and interflow sedimentary units. Lithological and structural differences were noted, massive flows were distinguished from pillowed and brecciated flows, amygdaloidal pillowed flows were distinguished from variolitic pillowed flows, and the continuity of certain units was established. Brecciated flows at the base of the Central Formation (the "McIntyre Series" of Hurst (1936) and Langford (1941)) provide good marker units to the north of the Pearl Lake porphyry.

Following a major re-appraisal of the geology and the potential for further ore at the McIntyre Mine, Griffis (1962; and in Ferguson (1968)) established the most detailed subdivision of the stratigraphy of the Tisdale Group yet published. Mason *et al.* (1986) presented a modified version of Griffis' (1960) stratigraphy for the McIntyre Mine. Griffis (1962) reported on the convenience of adopting the use of the terms "uniform lava" and "structured lava" as a means of distinguishing massive flow units from those flows which exhibit pillows, flow textures, and other primary structures. Instead of the emphasis on flow contacts and related features as a means of establishing stratigraphy, major compilations were prepared at 1:100 scale using only "uniform" versus "structured" as a principal means of correlation.

Unfortunately, as the earlier geologists had discovered, massive units grade into structured units along strike and vice versa, so that correlations of massive or structured units from underground exposures and borehole information is generally inaccurate and quite misleading. The geological interpretation at the McIntyre Mine changed from a simple south-facing sequence of volcanic units disrupted by the Pearl Lake porphyry intrusion (1923 to 1954) to a complexly folded and abnormally thickened volcanic sequence; Ferguson's (1968) compilation of mine plans and his map of Tisdale Township reflect this.

In the present study, the Tisdale Group stratigraphy, summarized by Ferguson (1968), is retained as a framework for more detailed study of lithostratigraphic facies variations. Prior to this study no attempts to trace detailed stratigraphy away from the McIntyre Mine had been made. Surface mapping in the 1986 field season confirmed the continuity of the Gold Centre, Vipond, and upper Central Formations over much of Tisdale and northern Deloro Townships. Many individual flow units within each of the above formations do not display the same continuity. Facies variations within the volcanic flow units occur both vertically and laterally. In particular, the detailed stratigraphy established by Mason *et al.* (1986) at the McIntyre Mine, cannot be traced in its entirety even to the adjoining Coniaurum and Hollinger Properties.

As noted above, the lateral gradation of uniform flows into pillowed and/or brecciated flows precludes the correlation of flows based upon the distinction of uniform versus flow-structured. Instead, the emphasis has been placed on the use of flow contacts to map flow units. In addition, the deformation of primary pillow shapes during the development of regional flattening and stretch fabrics renders the use of pillow features as indicators of stratigraphic facings questionable. Flow tops, and the vertical gradation from uniform, to pillowed, to brecciated and/or hyaloclastite-textured units within individual flows are considered more reliable indications of facing.

Figures 298A.2 and 298A.3 illustrate the stratigraphy of the Tisdale Group as exposed in four separate areas of southern Tisdale Township. The Coniaurum, Gold Centre, and the Paymaster and Dome sections are representative of Tisdale Group stratigraphy on the north limb, the closure and the south limb of the Porcupine Syncline respectively. The Central, Vipond, and Gold Centre Formations are described below.

CENTRAL FORMATION

On the Coniaurum Property, a section from the top of the 55 flow to the top of the C15 is intermittently exposed (Figure 298A.2). The Central Formation consists of amygdaloidal pillowed flows (C13, C15) and pillow breccias (55, C15) with an intercalated uniform flow (C14). The C14 unit is typically fine grained, aphanitic, and nonamygdaloidal, and it contains local areas of poorly developed pillows. Pillowed units (C13, C15) are typified by pillows less than 100 by 50 cm in plan view. The pillows have narrow selvages, 1 to 3 mm wide and are typically densely amygdaloidal with amygdules ±1 mm in diameter. Inter-pillow areas may contain hyaloclastite, breccia fragments, or small pillows less than 15 cm across. Pillows may also be tightly packed without significant inter-pillow material. In addition to its presence between pillows, pillow breccia comprises the only exposure of the 55 flow and occurs as lateral facies equivalents to pillowed flows in the C15 at the top of

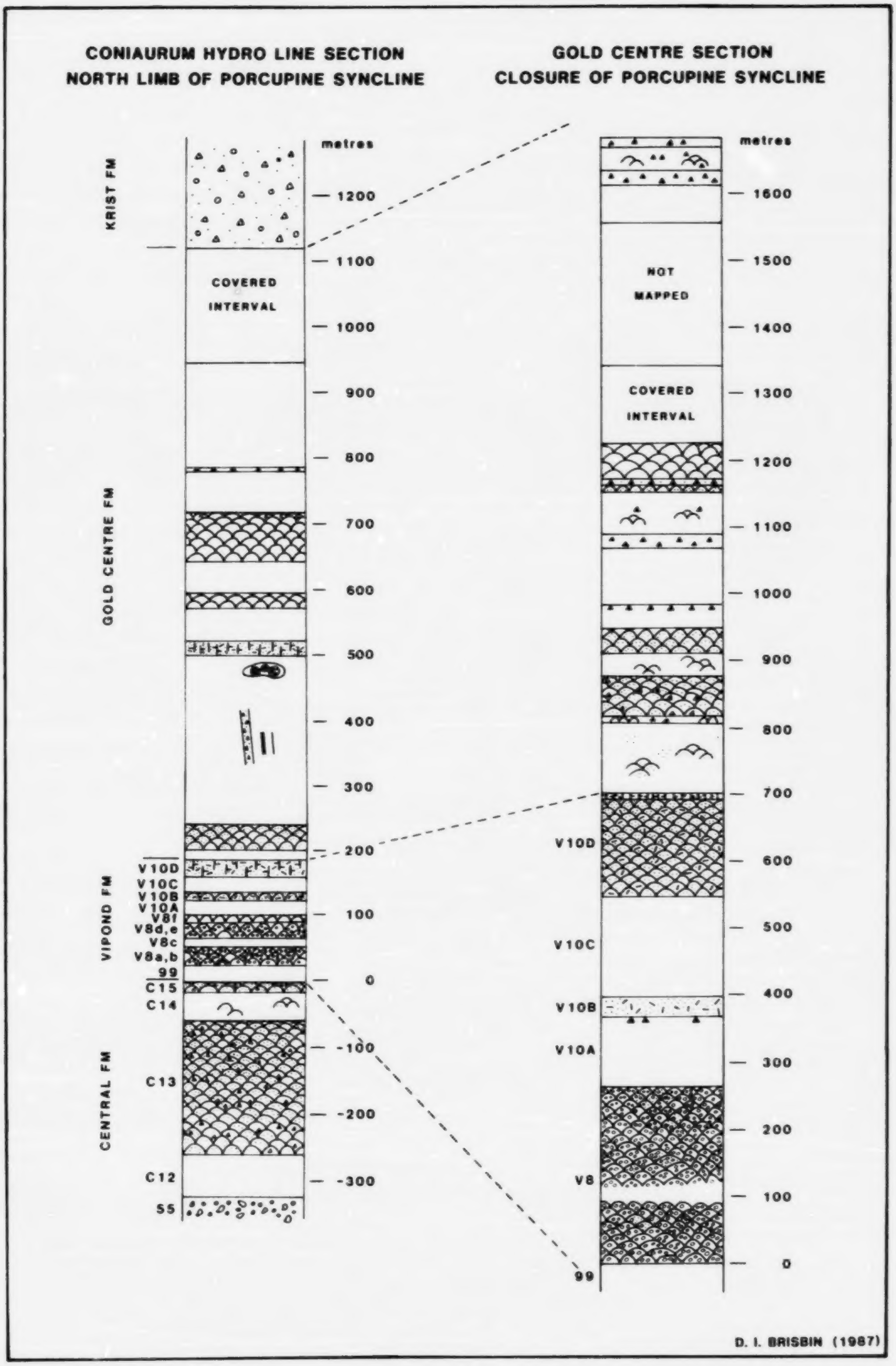

Figure 298A.2. Stratigraphic columns for the northern limb and closure of the Porcupine Syncline.

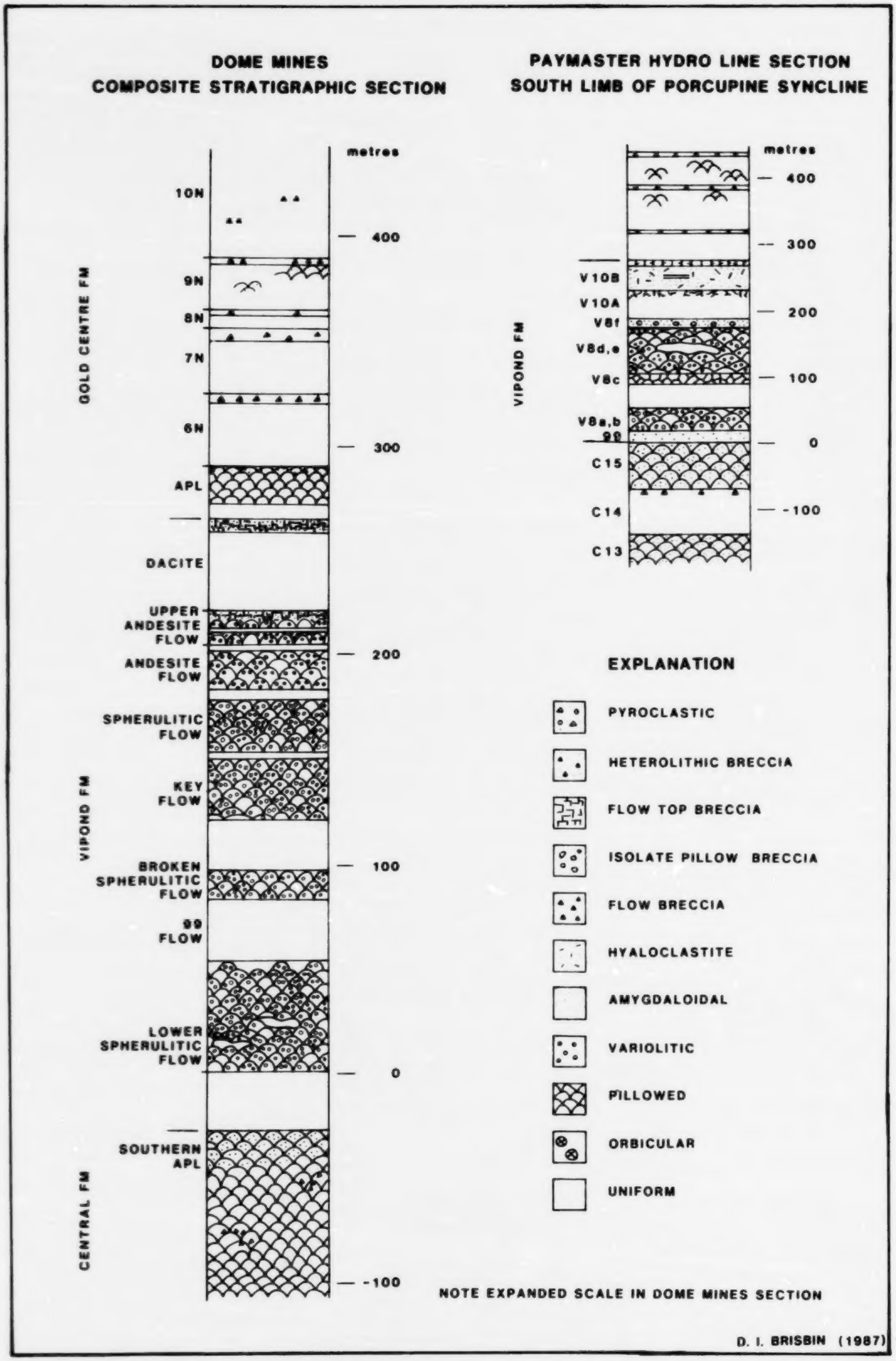

NOTE EXPANDED SCALE IN DOME MINES SECTION

D. I. BRISBIN (1987)

Figure 298A.3. Stratigraphic columns for the Dome Mine area and the southern limb of the Porcupine Syncline.

the Central Formation. Fragments in both cases are irregular in shape, commonly 1 to 10 cm across in plan view and often have selvages.

The thick sequence of pillow breccias between the 55 flow and the C13 amygdaloidal flow recognized by Mason *et al.* (1986) south of the Pearl Lake Porphyry on the McIntyre Property, does not appear to extend onto the Coniaurum Property. The C12 variolitic pillow lava present at the McIntyre Mine (Mason *et al.* 1986) has not been recognized on the Coniaurum Property, and may be only locally developed at the McIntyre Mine.

South of the Paymaster Porcupine shaft (*see* Figure 298A.1), the C13, C14 and C15 units are exposed. Here they are similar to exposures on the Coniaurum Property. Pillows are less than 150 by 50 cm in plan view and amygdules are sparsely to densely packed and are ±1 mm in diameter. Selvages on the pillows are less than 10 mm wide. The C14 unit is uniform, fine-grained, and locally has a poorly developed breccia along its upper contact. Tan coloured leucoxene crystals 0.3 mm in size are present in the C14 and C15 units.

VIPOND FORMATION

The Vipond Formation consists of a package of variolitic pillow lavas, pillow and hyaloclastite breccias, and uniform lavas which includes the "99 Flow" the V8 and V10 flow units. The base of the Vipond Formation is the "99 Flow" which, as exposed throughout most of the map area, is a uniform fine-grained flow with locally prominent leucoxene crystals. Although the 99 Flow averages 25 m thick at the McIntyre Mine (Griffis 1960) and up to 120 m thick on the Hollinger Property (Ferguson 1968), it thins to only 5 m near the Bishop shaft on the Coniaurum Property (Figure 298A.2).

In the Dome-Paymaster sections (Figure 298A.3), a uniform massive flow within the V8 has been taken as the "99 Flow" (Ferguson 1968), and by comparison with the sequence in the Central Tisdale anticline, this massive flow should be the V8c subunit of the V8 flow unit. At the Paymaster Mine, the C15 amygdaloidal pillow lava is overlain by a 20 m thick aphanitic unit which contains amygdules but which lacks well-formed pillows, and at Dome, the C15 unit is overlain by a uniform massive flow, in turn overlain by the "Lower Spherulitic Flow" (which would correspond to the V8b subunit elsewhere).

The authors would prefer to maintain the relative stratigraphic position of the "99 Flow" throughout the map area, as it separates the amygdaloidal flows of the Central Formation from the variolitic flows of the Vipond Formation.

Griffis (1960) subdivided the V8, as exposed at the McIntyre Mine, into six subunits labelled A to F from base to top. At the McIntyre Mine, the poorly pillowed, nonvariolitic V8a unit at the base of the V8 is distinguished from the well pillowed, variolitic V8b which forms such a striking marker unit. The V8a cannot be distinguished on the adjacent Coniaurum and Hollinger Properties (Spiedel 1987) nor does it appear to be present in the Vipond-Gold Centre and Paymaster-Dome areas.

The V8c is a uniform, fine-grained, massive subunit and is about 25 m thick. It has been mapped on the Coniaurum, Hollinger, and Vipond Properties, and on the Dome and Paymaster Properties to the southeast. An amygdaloidal, polygonite-structured zone up to 15 m thick, is present at the top of the V8c on the Paymaster Property (Figure 298A.3) and the top part of the V8c at the McIntyre Mine is characterized by polygonite structures.

Above the uniform V8c unit, another thick package of variolitic pillow lavas (V8d and V8e subunits) can be distinguished. Again, the separation by Griffis (1960) of V8d (20 to 60 m of variolitic pillow lava) from V8e (10 to 120 m of "giant" variolitic pillow lava), cannot be maintained away from the McIntyre Mine (Figures 298A.2 and 298A.3). Some thin, uniform lava intervals were mapped on the Coniaurum Property in the variolitic pillow lavas overlying the V8c, but their continuity along strike appears to be limited to a few tens of metres.

The uppermost subunit of the V8 flow unit, the V8f, is usually a poorly pillowed unit characterized by hyaloclastite breccias and it ranges in thickness from 0 to 30 m at McIntyre. The V8f can be traced intermittently on the Vipond and Hollinger Properties, south and southwest of the McIntyre Mine (Spiedel 1987). On the Coniaurum Property, the top of the V8 is nonvariolitic and is characterized by poorly developed pillows. A distinct subunit at the top of the V8 was not identified on the Vipond-Gold Centre section (Figure 298A.2). A unit similar to the V8f, up to 10 m thick, is locally present on the Paymaster property (Figure 298A.3).

At the Dome Property, the V8 flow unit consists of "Lower Spherulitic Flow, 99 Flow, Broken Spherulitic Flow, Key Flow" and "Spherulitic Flow" (from base to top). With the exception of the 99 Flow (which the authors would correlate as V8c) and, locally, the bases of the Key Flow and Spherulitic Flow, these subunits are dominated by variolitic, thick selvage pillow flows. Although the overall character of the V8 at Dome Mines is similar to that at the McIntyre Mine, in detail the subunits within the V8 cannot be correlated between these two sections.

Thus, the V8 flow unit is an internally complex and variable entity which nevertheless forms a consistent stratigraphic unit as a whole.

The V9 interflow sedimentary unit is not exposed in the map area, although it is well developed in the Hollinger and McIntyre Mines. It has not been recognized at Dome Mines.

Overlying the V9, (or the V8 where the V9 is absent), the V10 flow unit, forms the upper portion of the Vipond Formation. It is composed dominantly of hyaloclastite breccias with varying degrees of pillow preservation, and lesser amounts of variolitic pillow lava (identical in appearance to the same lithology within the V8) and uniform lava. Griffis (1960) subdivided the V10 into four subunits at the McIntyre Mine, (V10a-d from base to top). A uniform, very fine-grained lava (V10a), is present throughout the map area. There is local development of poorly defined pillows and breccia in the upper portion of the V10a.

Another uniform lava, the V10c, is similar in appearance to the V10a but it separates the V10b and V10c hyaloclastite breccia subunits and may be locally absent. Where the V10c is absent the V10b and V10d subunits cannot be separately distinguished.

Both the V10b and V10d are characterized by hyaloclastite breccia ("chickenfeed") within and interstitial to variolitic pillows. The broken varioles appear as white "porcellanic shards" (Griffis 1960), and these units are most striking in appearance when the groundmass is chloritic and dark green in colour. In some cases, pillows have been well preserved, in others they have been destroyed by the brecciation process.

Flow-top breccias have been used as stratigraphic guides by many previous workers at Timmins. So far, the authors have found that the most prominent, well developed, and consistent *in situ* flow top breccia occurs at the top of the Vipond Formation (V10d subunit). This flow top has been cracked and penetrated by seawater to a much greater depth (up to 5 m) than any other flow top so far encountered. The authors distinguish here between *in situ* brecciation of a flow top resulting from cooling and penetration of seawater, and a pillow-breccia rubble formed by auto-brecciation of a moving flow.

At the Dome Mine, two units within the upper Vipond sequence have strikingly "flow-textured" upper portions and uniform basal portions. They overlie the well-formed variolitic pillow flows of the V8 and underlie the uniform, pillowed and flow brecciated flows of the Gold Centre Formation. The lower of the two units known as the "Andesite Flow", has a uniform base correlated with the V10a unit. The upper portion of this flow is correlated with the V10b and it varies from a sequence with a uniform base and hyaloclastitic/variolitic top to one with up to three such transitions (Figure 298A.3). The "Dacite Flow" overlies the "Andesite Flow" and has a uniform basal portion which is correlated with the V10c. The upper hyaloclastitic portion of the Dacite Flow has a distinctive so-called "ropey flow top" and is correlated with the V10d. The ropey flow top has the same texture as the V10d flow top, which is so distinctive in surface exposures throughout southern Tisdale Township and is also used as a marker for underground mapping at the Dome Mine.

GOLD CENTRE FORMATION

The Gold Centre Formation consists of the uppermost portion of the mafic volcanic flows of the Tisdale Group exposed in the study area. It is exposed around the closure of the Porcupine Syncline (Figure 298A.1) and is overlain by the Krist Fragmental Formation and wackes and argillites of the Porcupine Group. Despite an apparent thickness of 800 m exposed in the Coniaurum and Gold Centre areas (Figure 298A.2) this unit has not been previously described in any detail. The Gold Centre Formation is significantly lacking in both hydrothermal alteration and mineralization, which may account for its geological neglect.

A section along the main powerline, southeast from the Bishop shaft on the Coniaurum Property, exposes 300 m of uniform lava which overlies the V10d subunit. This section is generally and characteristically uniform and medium grained, although it has a 40 m thick pillowed interval near its base, and a curious 10 m thick "orbicular" flow (megavarioles up to 15 cm in diameter with no signs of pillow development) near its top. The rock has a "grainy", possibly hyalo-tuffaceous texture, characterized by the slight positive weathering of white grains which are unevenly disseminated throughout a green chloritic groundmass, and disseminated tan coloured leucoxene crystals. The top of this thick uniform subunit is marked by a hyaloclastitic flow-top breccia similar to that at the top of the Vipond Formation (V10d) and mapped as such by Ferguson (1968). The uppermost 400 m of the Gold Centre Formation exposed along this section is characterized by uniform lavas intercalated with pillowed flows (with narrow selvages) and thin zones of flow breccia.

In the Gold Centre area to the south, pillowed flow and flow breccia units are more common within the Gold Centre Formation, comprising roughly 50 percent of the exposed section, and the gradation from a uniform base up through a pillowed interval to a flow top rubble (breccia) within a single flow is better exposed in this area. Within any flow, the uniform, pillowed, or breccia interval may be absent. In addition, each of the three textures may be locally developed in intervals dominated by a different texture (e.g. local development of pillows in the uniform basal portions of the flow). In particular, the pillowed and breccia textures are often intimately associated, with breccia fragments and hyaloclastite often filling interpillow areas in pillowed portions of flows.

At Dome Mines, the Gold Centre Formation is subdivided into the APL, 6N, 7N, 8N, 9N, and 10N flows. These flows are typically uniform-textured with mixed flow breccia and hyaloclastite tops (*see* Figure 298A.3). The flow breccias, which are characteristic of the upper portions of flow within the Gold Centre Formation are autobreccia rubbles developed by the brecciation of a cooled crust on a moving lava flow. Pillowed intervals appear to be of relatively minor importance in the Gold Centre Formation as exposed at Dome Mines, with the only significant development occurring in the upper portion of the "APL" near the base of the formation (*see* Figure 298A.3).

The lack of alteration and mineralization in the Gold Centre Formation supports Roberts' (1981) observation that the main centres of gold mineralization in this part of the Porcupine Camp are preferentially related to the central Tisdale Anticline and South Tisdale Anticline.

EARLY MAFIC DIKES

Pre-fabric mafic dikes were discovered in outcrops on the Paymaster Property in 1986 and these remain to be mapped in detail during the 1987 field season. As far as can be ascertained, these dikes are the first reported Archean mafic dikes at Timmins (assuming that the fabric is late Archean), and the authors presently assume that they were related to the Tisdale volcanism.

HETEROLITHIC BRECCIAS

Piroscho (1985) and Mason and Melnik (1986) have drawn attention to the development of heterolithic breccias at the Coniaurum and McIntyre Properties in association with porphyry intrusions. The north trending breccia dike which was discovered by Piroscho on the Coniaurum Property (Figure 298A.2) is in fact a composite dike with at least two generations of breccia in it. Heterolithic breccias have also been discovered in several localities on the Hollinger Property and at the Buffalo-Ankerite Property, and they are suspected at the Dome Mine.

ACKNOWLEDGMENTS

This research project is being funded by the Ontario Geological Survey through Ontario Geoscience Research Fund Grant 298.

The authors are grateful to Pamour Porcupine Mines Limited and Dome Mines Limited for access to their properties and geological records. In addition, the advice and assistance of the geological staff of both companies is gratefully acknowledged, with special acknowledgment to Dean Rogers, Chief Geologist, Dome Mine, for his experienced guidance and knowledge of the local geology.

The authors would also like to thank Karen Brisbin for her help with illustrations and Larke Zarichny for preparation of the manuscript.

SELECTED REFERENCES

Burrows, A.G.

1911: The Porcupine Gold Area; Ontario Bureau of Mines, Annual Report for 1911, Volume 20, Part 2, p.3- 33. Accompanied by Map 20e, scale 1:63 360 or 1 inch to 1 mile, and Map 20f, scale 1:126 720 or 1 inch to 2 miles.

1912: The Porcupine Gold Area, Second Report; Ontario Bureau of Mines, Annual Report for 1912, Volume 21, Part 1, p.205- 249. Accompanied by Maps 21a and 21c, scale 1:63 360 or 1 inch to 1 mile.

1915: The Porcupine Gold Area, Third Report; Ontario Bureau of Mines, Annual Report for 1915, Volume 23, Part 3, p.1-57. Accompanied by Map 24d, scale 1:24 000 or 1 inch to 200 feet, and Map 24e, scale 1:12 000 or 1 inch to 1000 feet.

1925: The Porcupine Gold Area; Ontario Bureau of Mines, Annual Report for 1924, Volume 33, Part 2, p.1-84. Accompanied by Map 33a, scale 1:24 000 or 1 inch to 2000 feet.

Dunbar, W.R.

1949: Structural Relations of the Porcupine Ore Deposits; p.422-456 *in* Structural Geology of Canadian Ore Deposits, Volume 1, Canadian Institute of Mining and Metallurgy, Montreal.

Ferguson, S.A.

1968: Geology and Ore Deposits of Tisdale Township, District of Cochrane; Ontario Department of Mines, Geological Report 58, 177p., Accompanied by Map 2075, scale 1:12 000 or 1 inch to 1000 feet.

Furse, G.D.

1948: McIntyre Mine; p.482-496 *in* Structural Geology of Canadian Ore Deposits, Volume 1, Canadian Institute of Mining and Metallurgy, Montreal.

1954: Geology of the Pearl Lake Section of the Porcupine Gold Area; Canadian Institute of Mining and Metallurgy Bulletin, Volume 47, p.197- 201.

Graton, L.C., and McKinstry, H.E.

1932: Geology of the Hollinger Mine: Selected Chapters of Final Report; Unpublished Report, Hollinger Mine.

1933: Outstanding Features of Hollinger Geology; Transactions of the Canadian Institute of Mining and Metallurgy, Volume 36, p.1- 20.

Griffis, A.T.

1960: Stratigraphy at McIntyre; Unpublished Report, McIntyre Mine.

1962: A Geological Study of the McIntyre Mine; Canadian Institute of Mining and Metallurgy Bulletin, Volume 55, Number 598, p.76- 83.

Hore, R.E.

1913: On the Origin of the Porcupine Gold Deposits; Canadian Mining Journal, Volume 34, p.548- 551.

Hurst, M.E.

1935: Vein Formation at Porcupine, Ontario; Economic Geology, Volume 30, p.102- 127.

1936: Recent Studies in the Porcupine Area; Transactions of the Canadian Institute of Mining and Metallurgy, Volume 39, p.448- 458.

Jones, W.A.

1984: Hollinger Mine; p.464-481 *in* Structural Geology of Canadian Ore Deposits, Volume 1, Canadian Institute of Mining and Metallurgy, Montreal.

Langford, G.B.

1941: Geology of the McIntyre Mine, American Institute of Mining and Metallurgical Engineering Transactions, Volume 144, p.151- 169.

Mason, R., and Melnik, N.

1986: The McIntyre-Hollinger Investigation, Timmins, Ontario, Part 2: A Gold Dominated Porphyry Copper System; *in* Current Research, Part B, Geological Survey of Canada Paper 86- 1B.

Mason, R., Melnik, N., Edmunds, C.F., Hall, D.J., Jones, R., and Mountain, B.

1986: The McIntyre-Hollinger Investigation, Timmins, Ontario, Part 1: Stratigraphy, Lithology and Structure; *in* Current Research, Part B, Geological Survey of Canada Paper 86- 1B.

Piroscho, D.W.

1985: Relationship of Hydrothermal Alteration to Structure and Stratigraphy at the Coniaurum and Davidson Tisdale Gold Deposits, Tisdale Twp., Northeastern Ontario; Unpublished M.Sc. Thesis, Queen's University, 102p.

Pyke, D.R.

1976: On the Relationship of Gold Mineralization and Ultramafic Volcanic Rocks in the Timmins Area; Ontario Division of Mines, Miscellaneous Paper 62, 23p.

1978: Regional Geology of the Timmins-Matachewan Area, Districts of Cochrane and Timiskaming; p.73- 77 *in* Summary of Fieldwork, 1978, edited by V.G. Milne, O.L. White, R.B. Barlow, and J.A. Robertson, Ontario Geological Survey, Miscellaneous Paper 82.

1982: Geology of the Timmins Area, District of Cochrane; Ontario Geological Survey, Report 219, 141p. Accompanied by Map 2455, scale 1:50 000.

Roberts, R.G.

1981: The Volcanic-Tectonic Setting of Gold Deposits in the Timmins Area, Ontario; p.16- 28 *in* Genesis of Archean Volcanic Hosted Gold Deposits, edited by E.G. Pye, and R.G. Roberts, Ontario Geological Survey, Miscellaneous Paper 97.

Robinson, H.S.

1923: Geology of the Pearl Lake Area, Porcupine District, Ontario; Economic Geology, Volume 18, p.753- 771.

Speidel, F.

1987: Stratigraphy and Structure of the Vipond Formation at the Hollinger-Vipond Properties, Timmins, Ontario: A Re-evaluation; Unpublished M.Sc. Project Report, Queens University, Kingston, 72p.

Whitman, A.R.

1915: The Rocks of the Porcupine District; Transactions of the Canadian Institute of Mining and Metallurgy, Volume 18, p.256- 276.

Grant 298B Geology of the North Zone of the Delnite Mine at Timmins, Ontario

D.I. Brisbin, F. Speidel and R. Mason

Department of Geological Sciences, Queens University, Kingston.

ABSTRACT

Newly exposed outcrops of the northern ore zone at the Delnite Mine show four separate mineralized quartz-carbonate vein systems in an altered basaltic unit within a sequence of Lower Tisdale mafic and ultramafic volcanic rocks. The basaltic unit strikes west, dips about 60°N, and is flanked by highly altered and sheared talc-chlorite-ankerite schists. Two small lenses of quartz porphyry intrude the basaltic unit. All lithological units are carbonatized and the mineralized basaltic unit is sericitized and pyritized, especially adjacent to mineralized vein structures.

The mineralized structures and hydrothermal alteration are cut by planar fabrics related to late cleavage, linear stretch fabric, and shear zone development. The cleavages are defined by recrystallized sericite and chlorite, and the veins are folded, boudinaged, and recrystallized. Shear zones parallel or subparallel to strike reflect local zones of more intense cleavage development. West-northwest-trending shear zones displace lithological contacts and mineralized structures with a consistent right lateral sense of movement.

INTRODUCTION

The Delnite Mine is located in northwestern Deloro Township (Figure 298B.1). Production by Delnite Mines Limited from 1937 to 1964 amounted to 920 404 ounces of gold and 73 423 ounces of silver from 3 847 364 tons of ore (Ferguson *et al.* 1971, p.61-62). In 1964, the property was sold to Aunor Gold Mines Limited. Delnite shafts numbers 2 and 3 were used by Aunor to access the downplunge extension of the Aunor orebody. Production statistics from the Delnite Property (Aunor Gold Mines Limited in the 1960s and Pamour Porcupine Mines Limited in the 1970s) are not published.

During the Summer of 1986, Pamour Porcupine Mines Limited stripped an oval-shaped area roughly 135 m long by 80 m wide on the North Zone (Figure 298B.2) of the Delnite Property, approximately 225 m south of No. 2 shaft. Test-hole drilling of the stripped area with an airtract drill was in progress at the end of the field season. If drill results are favourable, a small open pit will be developed on the North Zone. The stripping afforded the opportunity to examine a well exposed vein system at a past-producing mine in a portion of the Porcupine Camp where surface exposure is scarce. The geology of the mine was described briefly by Taylor (1948) and the property included in a preliminary map by Ferguson (1959) and a compilation map by Pyke (1982). The authors mapped the stripped area at a scale of 1 inch to 20 feet (1:240) as part of the work under Ontario Geoscience Research Fund Grant 298 (Mason and Brisbin, this volume). In addition, available outcrops on the Aunor and Delnite Properties were mapped at a scale of 1 inch to 500 feet (1:6000).

OUTLINE OF GEOLOGY

The map area (Figure 298B.2) is situated on the southern flank of the Kayorum Syncline, approximately 750 m north of the "Destor-Porcupine Fault". The Aunor and Delnite Properties are underlain by an intercalcated sequence of mafic and ultramafic flows, which strike 080° and dip 60°N. Taylor (1948) described this sequence at the Delnite Mine as greenstones, tuffs, carbonatized andesites, and talc-chlorite schists, all of Keewatin age.

Ferguson (1959) and Pyke (1982) assign the mafic-ultramafic sequence to the lower portion of the Tisdale Group. Ferguson's (1959) preliminary map indicates the mafic flows to be typically amygdaloidal and pillowed. Recent mapping by the authors on the Delnite, and adjacent Aunor, Properties confirms Ferguson's descriptions. The amygdaloidal, pillowed flows are typified by narrow (<5 mm) selvages and amygdules averaging 1 mm in diameter. Thus, they are lithologically identical to, and in a similar stratigraphic position to, the Mg-tholeiitic flows of the Central Formation (lower Tisdale Group) exposed in Tisdale Township to the north.

Ultramafic lithologies are poorly exposed in the map area, except in the stripped area on the Delnite Property. Where observed, they occur as uniform, medium-grained, highly carbonatized units, or as moderately to strongly schistose talc-chlorite-carbonate schists. No primary textures were observed. One unit noted by Ferguson (1959) crops out just east of the Delnite No. 2 shaft, and near Skynner Lake west of the study area. This unit weathers brown with a distinctive grainy and locally fragmental appearance. Cunnison and Mullen (1986) describe the outcrops near Skynner Lake as being basaltic komatiites. The relative abundance of ultramafic lithologies in the lower part of the Tisdale Group in the Aunor-Delnite area contrasts with the lack of these lithologies in the Central Formation on the Hollinger, McIntyre, and Coniaurum Properties of southwestern Tisdale Township (Mason and Brisbin, this volume).

Taylor (1948) identified two generations of felsic sills, namely quartz porphyries and "old intrusives", but the basis used to differentiate the two sets of intrusions was not described. Quartz porphyries are only exposed in the stripped area of the Delnite Property.

A pervasive west-trending schistosity is weakly to strongly developed in all lithologies and dips about 60°N. Pillows and varioles of the V8, well exposed on a hydro line just north of the Aunor access road (Figure 298B.2) show a stretch lineation plunging gently to the west, which conforms to the western plunge of the ore bodies at Aunor and Delnite. The narrow pillow selvages and small amygdules characteristic of pillowed mafic flows in the study area are obscured in more strongly schistose intervals.

The gold-bearing veins at the Aunor and Delnite Properties are hosted in carbonatized mafic flows

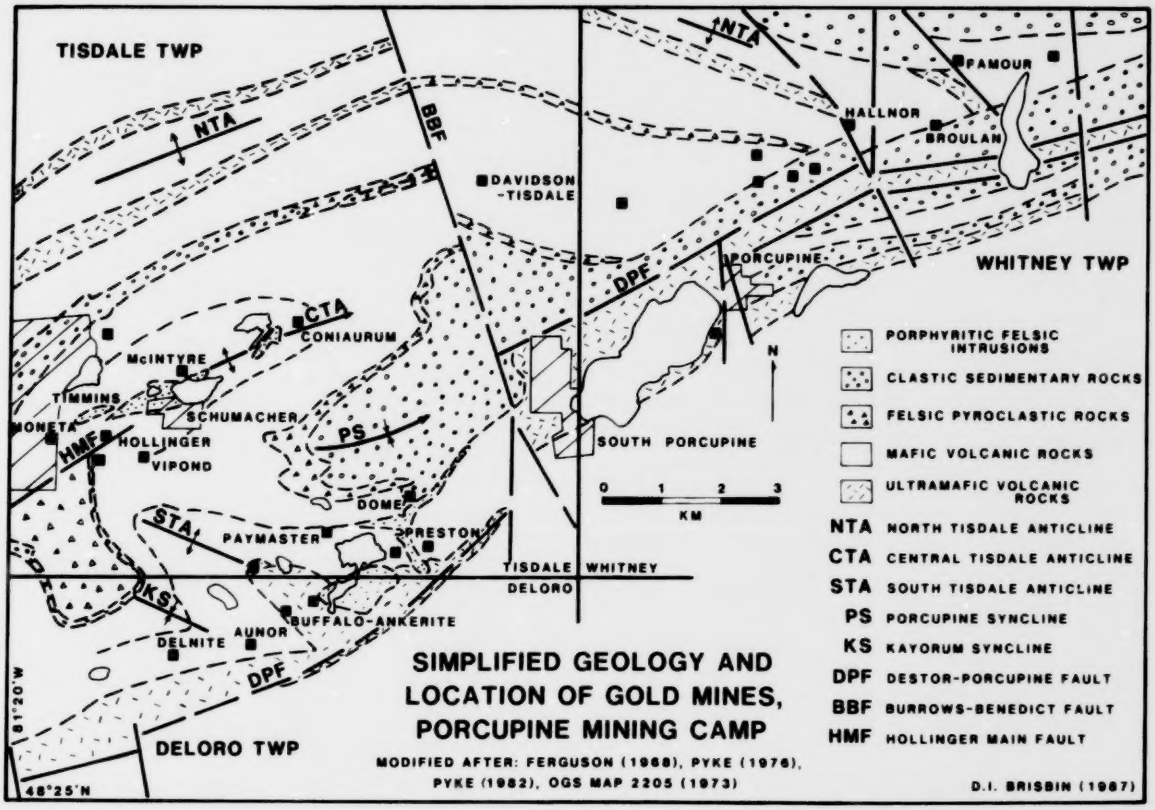

Figure 298B.1. *Map showing the position of the Delnite Mine in the Porcupine Mining Camp.*

(Taylor 1948; Buffman 1948). On the Delnite Property, two zones of quartz-carbonate-ankerite veins were mined, hosted in two mafic flow units described as "highly carbonated andesites" by Taylor (1948). The northernmost of the above two flow units also hosts the Aunor orebody. Buffman (1948) described the ore host at Aunor as "pillowed, fine-grained andesite" with "irregular bands of medium, even-grained, carbonated andesite". Lesser amounts of ore are hosted by quartz porphyries at Aunor and Delnite, and diorite at Aunor (Buffman 1948; Taylor 1948). The "andesites" are in fact highly altered iron tholeiites.

GEOLOGY OF THE NORTHERN ZONE, DELNITE MINE

Lithology

Seven lithological units are exposed in the area stripped on the north ore zone at Delnite. From north to south, they are: north basalt, "carbonate rock", talc-chlorite-ankerite schist, "carbonate rock", central basalt, porphyry, and talc-chlorite-ankerite schist (*see* Figure 298B.3). These units are described below.

Only one exposure of the "north basalt unit" is present in the map area, and it crops out on the northern side of the stripped area on which the old Delnite Property mine vault is located. It is a massive to very weakly schistose unit which is medium grey in colour, aphanitic, moderately carbonatized, and weakly chloritic. Trace amounts of fine-grained, disseminated pyrite are present. Over most of the outcrop, the flow appears massive but, locally, thin curvilinear fractures are present and may be remnant pillow selvages. There is no veining associated with this unit and only weak alteration with trace amounts of pyrite.

There are two intervals of massive "carbonate rock" exposed in the northern half of the stripped area, separated by the central talc-chlorite-ankerite schists. In addition there is a lense of "carbonate rock" on the southern side of the central basalt unit. In general, "carbonate rock" is only weakly strained, is highly carbonatized, and contains only localized and minor fine-grained pyrite. It is buff to grey in colour and massive to weakly schistose (with intensity of schistosity increasing adjacent to contacts with the talc-chlorite-ankerite schist). "Carbonate rock" can be differentiated from carbonatized basalt by its coarser grain size and thicker ±2 cm brown weathering rind. Locally, a spotted texture occurs due to the presence of disseminated black anhedral tourmaline(?) crystals. A similar texture was observed in the southern "schist" where fine black tourmaline needles were positively identified. In addition to carbonate, lesser amounts of fuchsite, sericite, and chlorite are locally present in variable amounts.

The carbonate rock is host to abundant creamy white quartz-carbonate veins which are variable in

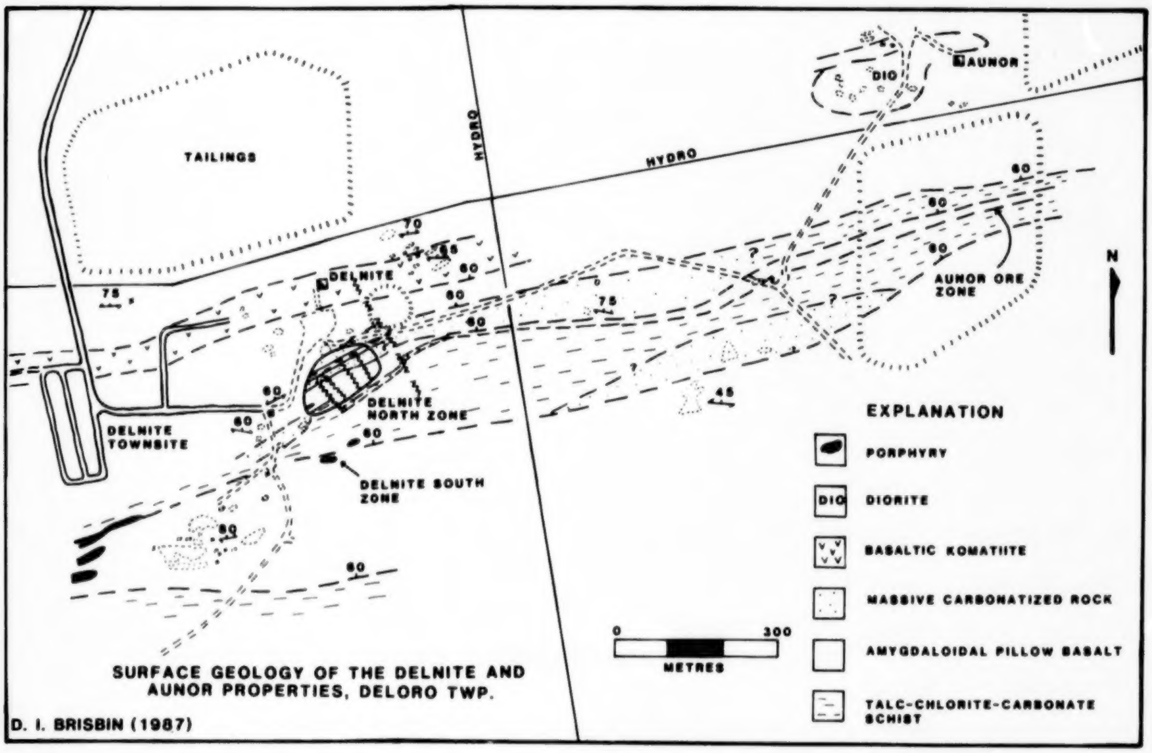

Figure 298B.2. *Map showing the surface geology of the Delnite and Aunor Properties.*

orientation and are barren of sulphide mineralization. They are commonly less than 5 cm thick and usually comprise 10 to 25% of the rock (locally up to 45%). These veins appear to be unrelated to veining in the central basalt, with which pyrite, gold, and chalcopyrite mineralization is associated (*see* below). The carbonate rock is similar in many respects to the "carbonate rock" on the Dome Mines Property and may represent carbonatized ultramafic rock. J. Houle (Geologist, Pamour Porcupine Mines Limited, personal communication, 1986) has reported spinifex textures in these rocks underground at Delnite.

Two zones of talc-chlorite-ankerite schist are exposed in the extreme south, and between the two "carbonate rock" units. These "schists" are moderate to high strain zones, generally with no sulphide mineralization, and they may contain up to 25% creamy-white quartz-carbonate veins (<2 cm thick). These minor veins, which have been extensively deformed, are devoid of any sulphide content. The central schist unit shows changes in the attitude of schistosity across its width which conform to the expected geometry of fabrics in a shear zone. The schist is blue-grey in colour with iron-rich patches characterized by rusty weathering, and they are composed of chlorite, ankerite, and talc with localized quartz-carbonate veins. The southern schist unit is poorly exposed over a 3 m width in a trench on the southern side of the stripped area. It is green in colour and locally contains up to 5% acicular crystals of black tourmaline and up to 0.5% disseminated pyrite grains (<3 mm in size).

The "central basalt" unit is host to all mineralized zones where veining is associated with wall rock pyritization and alteration. The abundance of veining, intensity of alteration, and concentration of pyrite are variable but interrelated. Preliminary sampling by W. Fink (Geologist, Pamour Porcupine Mines Limited, personal communication, 1986) indicated that only zones of veining with coincident pyritization of wall rocks contain significant gold values. Fabric is generally weakly developed, except in discrete shear zones, where schistosity is moderately to strongly developed. The mineralized basalt unit as a whole is greenish grey in colour, aphanitic and moderately carbonatized, weakly chloritized, and sericitized. Pyrite content is generally less than 5%.

Four systems of veining occur within the central basalt and the basalt adjacent to vein structures is strongly carbonatized, weakly to strongly silicified, and weakly to moderately sericitized (± fuchsite). Pyrite generally comprises 1 to 5% of the rock (average of 2 to 3%) but is locally concentrated up to 10 to 20% in wall rock adjacent to veins. The mineralized zones are generally only weakly schisted but may locally become moderately schistose.

Small (up to 20 cm in diameter) pillows with narrow selvages, and poorly defined pillow breccia texture, were observed near the western end of the pit. A breccia texture is also present in the host

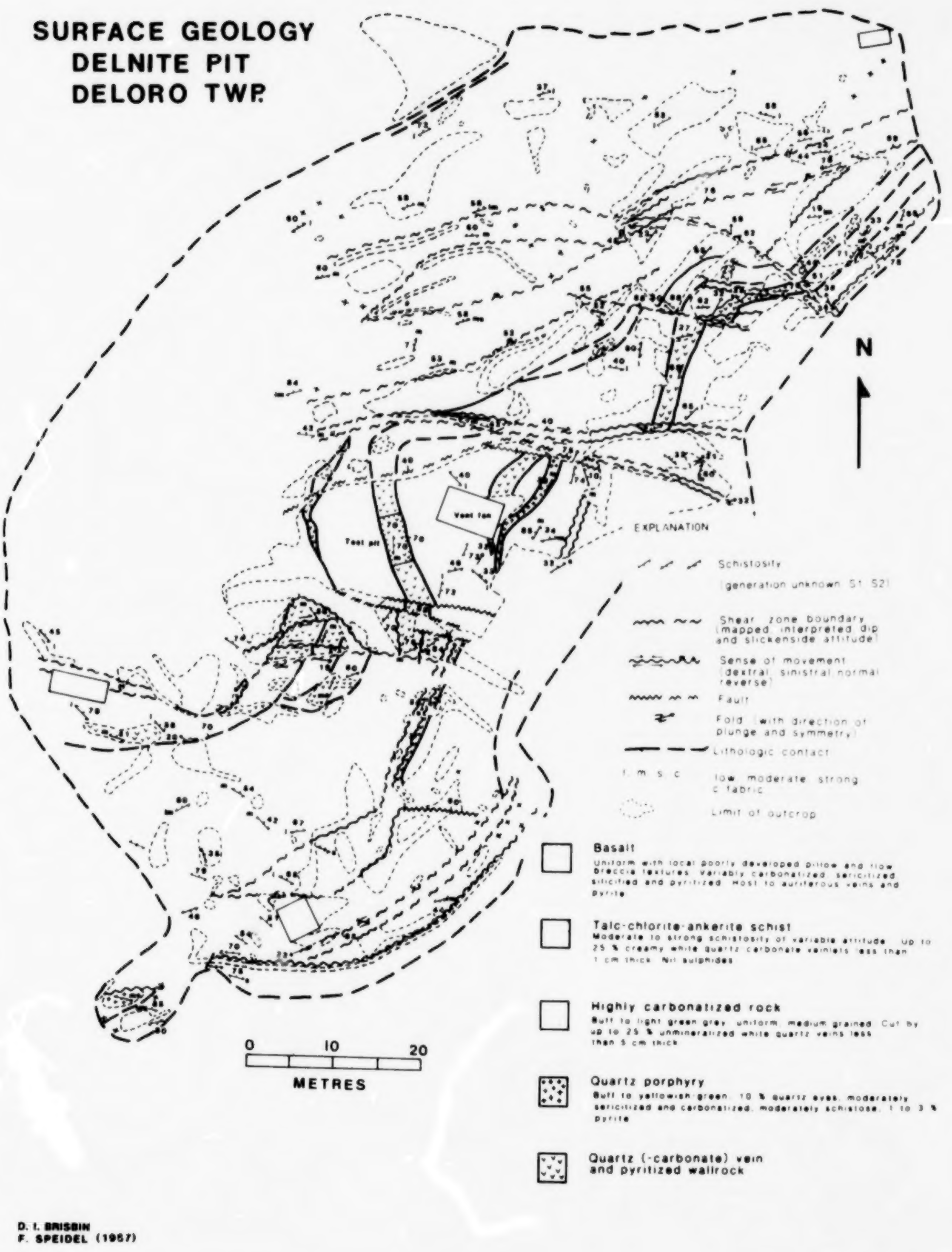
SURFACE GEOLOGY
DELNITE PIT
DELORO TWP.
N
Test pit
Test pit
EXPLANATION
Schistosity
(generation unknown S1 S2)
Shear zone boundary (mapped interpreted dip and slickenside attitude)
Sense of movement (dextral sinistral normal reverse)
Fault
Fold (with direction of plunge and symmetry)
Lithologic contact
l m s c
low moderate strong c fabric
Limit of outcrop
Basalt
Uniform with local poorly developed pillow and flow breccia textures. Variably carbonatized, sericitized, silicified and pyritized. Host to auriferous veins and pyrite
Talc-chlorite-ankerite schist
Moderate to strong schistosity of variable attitude. Up to 25 % creamy white quartz carbonate veinlets less than 1 cm thick. Nil sulphides
Highly carbonatized rock
Buff to light green grey, uniform, medium grained. Cut by up to 25 % unmineralized white quartz veins less than 5 cm thick
Quartz porphyry
Buff to yellowish-green. 10 % quartz eyes, moderately sericitized and carbonatized, moderately schistose, 1 to 3 % pyrite
Quartz (-carbonate) vein and pyritized wallrock
0
10
20
METRES
D. I. BRISBIN
F. SPEIDEL (1987)

Figure 298B.3. *Map of the geology of the Denite pit.*

basalts of the test pit vein where exposed on the northern face of the vent raise outcrop.

Two slivers of "porphyry" are present in the map area and these are located on the northeast of the vent fan and in the extreme southwestern corner of the pit. The porphyry is typically yellowish-green to buff, moderately sericitized and carbonatized, with about 10% of 1 to 2 mm sized quartz eyes. The outcrop beside the vent fan is highly fractured and cut by numerous thin (<0.5 cm) white to grey quartz-carbonate veins. Fine-grained pyrite is concentrated (1 to 3%) along fractures.

Structure

Lithological contacts (S_0) are not well exposed in the study area but appear to strike west-southwest and dip steeply to the north. Examination of underground plans and sections confirms these apparent relationships. Schistosity (S_1) is developed subparallel to lithological contacts, and average 270/60°N. Variability in attitude of S_1 is due to the development of a crenulation cleavage (S_2) and disruption of lithological contacts, schistosity, and mineralized zones by crosscutting faults and shear zones. Both the schistosity and crenulation cleavage are defined by alignment of the alteration minerals sericite and chlorite. Spatial and temporal relationships between crenulation cleavages and shear zones are not clear but the shear zones appear to represent zones of more intensely developed schistosity, and the schistosity is crenulated. Discrete shear zones occur as strike-parallel features in moderately to strongly schistose talc-chlorite-ankerite schists. The walls of these shear zones strike 250° to 270° and dip 50° to 70°N. Another strike-parallel shear zone occurs along the northern margin of the "ankerite vein" in the southern portion of the map area. Four crosscutting shear zones strike west-northwest and dip steeply east-northeast. They show a consistent right-hand offset, displacing both lithological contacts and mineralized structures. The dragfolding and right-hand offset of the "test pit" vein along a west-northwest striking shear zone is clearly shown in Figure 298B.3. Boudinaged blocks of quartz and altered/pyritized wall rock were observed within the shear zone between the two offset limbs of the vein.

Veining and Mineralization

The four zones of quartz-carbonate veining and associated mineralization in the central basalt include, from north to south:

1. a discontinuous zone of stockwork veining which is present along the central basalt/"carbonate rock" contact. This zone is best developed in the western end of the pit where it is 4 to 9 m wide. To the east of the most westerly shear zone, the zone is narrow and discontinuous
2. the "test pit" vein zone which is present from the eastern end of the pit to near the western end, where it appears to terminate against the vein described above. It is offset along strike by four right-handed shear zones but can be followed via a distinctive 20 to 45 cm thick blue quartz vein. Immediately adjacent to the blue quartz vein is a zone of highly altered basalt, 1 to 1.5 m wide, which is composed of carbonate, sericite, fuchsite, quartz, and 3% pyrite. Northwest of the above zone is a 60 cm wide unit of highly silicified and quartz-veined rock with lesser fuchsite, sericite, carbonate, and 3% fine-grained pyrite
3. a white quartz-carbonate vein, 3 to 3.5 m wide, which outcrops over a strike length of 4.5 m, immediately east of the vent fan (Figure 298.3). The vein breaks up into veinlets to the northeast where it appears to terminate against a northwest-striking shear zone. Basalts on the hanging wall (north) side contain about 15 to 25% irregular white quartz-carbonate veinlets up to 2 cm thick and 3% pyrite cubes up to 3 mm in size. Footwall basalts only contain 0.5% pyrite and about 5% quartz-carbonate veinlets.
4. a zone of stockwork quartz-carbonate veining, 6 to 12 m wide, which cuts massive, moderately carbonatized basalts northeast of the raise collared in the southwestern part of the pit (Figure 298B.3) This zone, known as the "ankerite vein" at the Delnite Property, crops out from the raise to a northwest-striking shear zone northeast of the raise. The basalts contain to 3% pyrite and trace chalcopyrite over a width of 30 to 60 cm adjacent to a shear zone on the northern side of the vein zone, and gold values are confined to this zone. Basalts to the south of the "ankerite vein" do not contain significant sulphide or gold mineralization (W. Fink, personal communication, 1986) although they contain numerous veins. To the east, across the northwest striking shear zone mentioned above, the continuity of the "ankerite vein" is uncertain.

The quartz-carbonate veining, alteration, and mineralization have been superimposed on both volcanic lithologies and quartz porphyries and thus they postdate these lithologies. Zones of coincident veining, alteration, and mineralization (including gold) are confined to a central altered basalt unit and two lenses of porphyry hosted within it. This unit is more competent relative to adjacent talc-chlorite-ankerite schists and massive carbonatized rocks, and thus would have been more susceptible to fracturing. Both schistosity and a locally developed crenulation cleavage are defined by alignment of alteration minerals in wall rock basalt. In addition, four west-northwest striking, east-northeast dipping shear zones crosscut and offset lithological contacts and veins. Thus the formation of all of the planar fabrics here appears to postdate hydrothermal alteration and mineralization.

REFERENCES

Buffam, B.S.W.
1948: Aunor Mine; p.507-515 *in* Structural Geology of Canadian Ore Deposits, Volume 1, Canadian Institute of Mining and Metallurgy, Montreal.

Cunnison, K.M., and Mullen, D.V.
1986: Strongly Carbonated Basaltic Komatiite at the Top of the Lower Formation of the Tisdale Group, 1.6 kilometers west of the Delnite Mine Shaft; p.7- 13 *in* Exceptional Exposures of Archean Subaerial and Shallow Subaqueous Volcanic Rocks and Associated Ore Deposits, Field Trip 5 Guidebook, GAC-MAC-CGU Joint Annual Meeting, 1986, Ottawa.

Ferguson, S.A.
1959: Deloro Township, Northwest Quarter; Ontario Department of Mines, Preliminary Geological Map P.11, scale 1:6000 or 1 inch to 500 feet.

Ferguson, S.A., Groen, H.A., and Haynes, R.
1971: Gold Deposits of Ontario Part 1, Districts of Algoma, Cochrane, Kenora, Rainy River and Thunder Bay; Ontario Division of Mines, Mineral Resources Circular 13, 315p.

Pyke, D.R.
1982: Geology of the Timmins Area, District of Cochrane; Ontario Geological Survey, Report 219, 141p. Accompanied by Map 2455, scale 1:50 000.

Taylor, R.B.
1948: Delnite Mine; p.504-507 *in* Structural Geology of Canadian Ore Deposits, Volume 1, Canadian Institute of Mining and Metallurgy, Montreal.

Grant 300 The Genesis of Silver Vein Deposits in the Thunder Bay Area, Northwestern Ontario

S.A. Kissin and E.A. Jennings

Department of Geology, Lakehead University, Thunder Bay

ABSTRACT

Silver vein deposits in the Thunder Bay area occur in two northeasterly trending zones, known as the Island Belt and the Mainland Belt. Deposits within these belts form a spectrum of deposits ranging from barren quartz-calcite veins with minor base metals, to silver and base-metal sulphide±barite, to five-element (Ag-Ni-Co-As-Bi) veins. A survey of fluid inclusions and sulphur isotopes was made from representative deposits. Fluid inclusion homogenization temperatures indicate that the veins formed over wide ranges of temperatures ranging from maxima of 350° to 450°C to minima less than 100°C. Temperatures did not, however, differentiate the deposits. Salinities vary widely from 2 to 30 equivalent weight percent NaCl, and boiling occurred sporadically. Sulphur isotopic studies of sulphide minerals and barite revealed a range of compositions and suggest that equilibrium within deposits was not generally obtained. Source sulphur was likely distinctly lighter than sedimentary sulphide minerals of the Rove shale, a hypothesized source of sulphur. The results indicate that the deposits could not be the result of mobilization of solutions due to heating by Keweenawan hypabyssal intrusions, but that a more general source within the Proterozoic basin must be called upon.

INTRODUCTION

The silver vein deposits in the Thunder Bay area of northwestern Ontario are a diverse group, varying in both composition of the ores and geographic location. The first mine north of Lake Superior was the Prince Mine in 1846, originally developed for its copper (Ingall 1888). The discovery of the Silver Islet Mine, in operation from 1869 to 1884, and briefly from 1921 to 1922, led to the development of large-scale mining activities on the mainland, where mines were continuously in operation from 1882 to 1911 (Sergiades 1968). Total production from the camp is estimated at 4 701 000 ounces Ag (Sergiades 1968), dwarfed by much greater production from the Cobalt-Gowganda camp (500 000 000 ounces Ag; Owsiacki 1984), but in its day, the Thunder Bay silver camp was a major producer of silver of international significance.

Since the close of continuous mining operations in 1911, there have been recurrent attempts to renew activities, mostly in existing mines. Except for a small amount of silver production during partial dewatering of the Silver Islet Mine in 1921-1922, none of these attempts has, until recently, resulted in either new discoveries or additional production from older properties. However, in 1981, QC Explorations Limited dredged material from the Silver Islet workings. Reevaluation of silver grades in stockpiled ore has led to a significant improvement in grade estimates, resulting in recent silver production from the camp (G.C. Patterson, Resident Geologist, Ontario Ministry of Northern Development and Mines, Thunder Bay, personal communication, 1984).

GEOLOGICAL BACKGROUND

GENERAL FEATURES

The silver vein deposits are described in numerous publications and reports from the period of active mining; however, few of these provide much in the way of technical data. The literature of this early period is contained in a comprehensive bibliography compiled by Tanton (1931), whose work marks the beginning of the application of modern science to the problem of the origin of the deposits.

The deposits were first subdivided into five groups based on their geographic position by Ingall (1888). Four groups—the Coast Group, Port Arthur Group, Rabbit Mountain Group, and Silver Mountain—yielded significant silver from their various mines (Bowen 1911), while the Whitefish Lake Group consisted only of minor prospects. The linear arrangement of deposits within the Coast Group on the one hand and the remaining groups on the other was appreciated by Bowen (1911), who designated them the "grey argillite belt" and the "black slate belt", respectively. The designations are neither clear nor accurate, as the sedimentary host rocks are the Aphebian Rove Formation shales in most cases, and the belts were renamed the Island Belt and the Mainland Belt, respectively, by Oja (1967). The Island Belt deposits occur in an arcuate zone of offshore islands and adjacent mainland areas in Lake Superior, extending from near the U.S. Border at the mouth of the Pigeon River northeasterly to the end of the Sibley Peninsula. The Mainland Belt, occurring mostly in clusters comprising the four groups of Ingall (1888), lie in a parallel zone 30 km to the west extending from Whitefish Lake to Silver Harbour at Thunder Bay. The Dorion lead-zinc-barite veins, lying northeast of the northern end of the Mainland Belt, have been included in discussions of the silver veins by some workers (for example, Tanton 1931; Stanton and Russell 1959), but have been convincingly differentiated from them by Franklin and Mitchell (1977). These deposits are hosted entirely within the Sibley Group sedimentary rocks or within Archean basement inferred to have been covered by them, and show no spatial relationship with igneous intrusions. Most significantly, they do not carry more than traces of silver.

The Thunder Bay silver veins, as delineated above, are mostly hosted in Rove Formation shales, locally intruded by Keweenawan diabase sills (the Logan sills), diabase dikes (the Pigeon River dikes), and gabbro dikes (the Pine River-Mount Mollie gabbro; Geul 1970, 1973). Veins may occur predominantly within dikes (for example at Silver Islet), in the Island Belt, but seldom maintain width nor tenor within diabase sills in the Mainland Belt (Ingall 1888; Tanton 1931). Only the Port Arthur Group deposits are hosted in the underlying Gunflint Formation, and extend as deeply as the Archean basement, while the 3A Mine vein is hosted entirely in the Archean basement. Two showings in the northerly end of the Island Belt, Edward Island and Porphyry Island, are hosted entirely in the Keweenawan Osler volcanic rocks.

More recent work has come from Guillet (1963), who reported on barite occurrences in the Island Belt, Geul (1970, 1973), whose descriptions of townships include portions of the Island Belt, and Franklin (1970), who completed a study on metallogenesis in the Thunder Bay area concentrating on deposits in the Mainland Belt. More recently, Franklin *et al.* (1986) have provided some data on fluid inclusion and lead isotope studies, as well as a modern overview of the region.

THE PROBLEM OF THE "FIVE-ELEMENT VEINS"

There is a spectrum of silver vein deposits in the Thunder Bay area, culminating in the fully developed suite of Ni-Co-arsenide minerals found at Silver Islet. The Silver Islet ores are of the five-element type (Halls and Stumpfl 1972), one of the most enigmatic of all deposit types, which has defied genetic categorization on a world-wide basis.

The Thunder Bay veins likewise suffer the lack of an accepted genetic mechanism. Certain aspects of the geological setting, however, serve to make the Thunder Bay veins more amenable to study. These include the following:

1. Igneous activity since the Archean is limited to Keweenawan hypabyssal intrusions.
2. The timing of ore deposition is well constrained to the Keweenawan by geological relationships.
3. Structural control of ore deposition is strong, with most Mainland Belt veins occupying northeasterly trending fault structures, while Island Belt veins occupy northwesterly trending fractures that cut diabase and gabbro dikes.
4. The sedimentary host rocks in the area are limited to the Gunflint and Rove Formations, both Aphebian units distinctly earlier than igneous. Most of the deposits of the area are actually within Rove Formation shales, and only a few of the deep vein systems penetrate as deeply as the underlying Gunflint Formation. Only two of the productive veins penetrate the Archean basement, and, in fact, most are remote from it.
5. All of the Proterozoic rocks of the area are unmetamorphosed and undeformed except for jointing and tensional faulting. The units are essentially flat-lying with regional dips generally less than 5°.

These factors limit possible sources of the vein-forming fluids. Fractionation of a fluid from a granitic source is precluded, and the small size and clear lack of hydrothermal activity eliminate the hypabyssal mafic intrusions. The clear spatial association with these intrusions, and shallow depth of the vein systems militate against derivation from a mafic source at depth.

The previously proposed hypothesis that seems most applicable to the Thunder Bay veins is the theory of distillation of vein components from metal-rich source rocks by heated solutions (Franklin 1970; Boyle and Dass 1971). The heat source would presumably be the Keweenawan sills and dikes, based on the close association of ores and the intrusions. Smyk (1984) further showed the existence of two types of deposits in the Island Belt, an Ag-Co-Ni-Bi-As type (for example, Spar Island, Silver Islet) and a base metal sulphide-barite type with variable silver content (for example, Pie Island, Prince Mine). In a comparison of the Island Belt with the Mainland Belt, he found that the latter are mineralogically simple for the most part and lack barite in most cases.

The temporal and spatial association of the deposits suggests that they were formed by the same mechanism. In attempting to account for the spectrum of mineral assemblages observed, however, differing temperatures of deposition might be considered as a possible source. The five-element type veins are associated with gabbro dikes, a distinctly deeper and hotter source than the shallow and thin diabase sills associated with simpler vein mineralogies. Theoretical support for temperature-dependence appears in the work of Susak and Crerar (1985) who demonstrated a strong temperature-dependence for complex formation in various metals.

This hypothesis was then tested by a detailed survey of fluid inclusion homogenization temperatures, as well as freezing studies. Sulphur isotopic data were also obtained in order to attempt to assess temperatures and sources of sulphur in the ores. Sphalerite compositions were also determined in order to calculate conditions of sulphur fugacity.

METHODOLOGY

Fluid inclusion studies were conducted using a Chaixmeca heating freezing stage (range from 150° to 600°C), which was calibrated for the temperature range spanned in this study. Due to uncertainties regarding its magnitude, and clear evidence of hydrostatic conditions in some inclusions as seen by boiling, homogenization temperatures were not corrected for pressure.

Sulphur isotopic analyses were done by standard techniques by Geochron Laboratories Division, Kreuger Enterprises Incorporated, Cambridge, Massachusetts.

Microprobe analyses of sphalerite were conducted on an ETEC microprobe with an energy-dispersive analytical package at the University of Toronto. A beam current of 105 nA and potential of 20 kV were employed. Data were reduced by the computer program PESTRIP, a University of Toronto version of Statham's (1976) procedure. Synthetic sphalerite standards containing 5 and 25 mole percent FeS, natural chalcopyrite, and synthetic Ag_2S, MnS, and CdS were used for calibration.

RESULTS

The silver veins of the Thunder Bay area have long been known to occur in geographic groupings (Figure 300.1a), which are useful in considering the characteristics. The deposits occur mainly in two linear zones (Figure 300.1b), known as the Mainland Belt

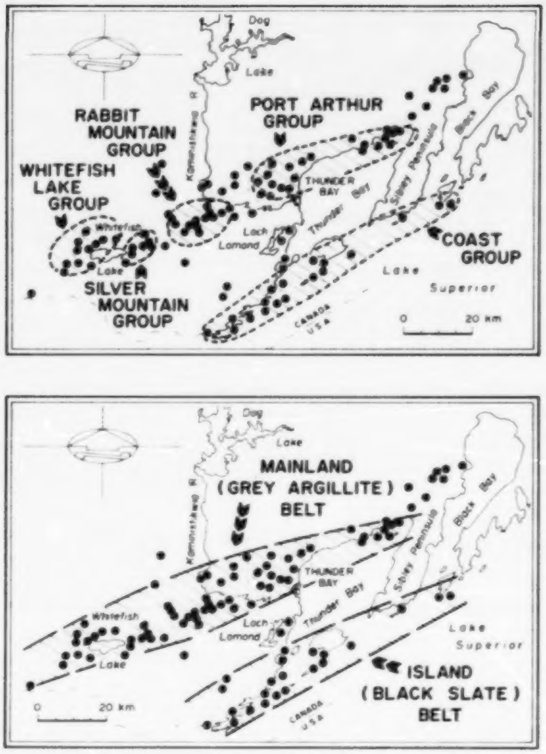

Figure 300.1. (a) Locations of groups of silver vein deposits in the Thunder Bay area according to Ingall (1888), with dots representing 98 localities described by Tanton (1931).
(b) The two belts of silver veins according to Oja (1967) and Bowen (1911, parentheses).

and the Island Belt (Oja 1967). The deposits within the Mainland Belt are broadly similar, with base-metal and silver mineralization, while those in the Island Belt show some diversity, ranging from fully developed five-element assemblages at Silver Islet to simple sulphide and silver assemblages elsewhere.

The mines studied here are shown in Figure 300.2. These were selected on the basis that they were generally producers or had especially good access and exposure. All groups from both belts are represented with the exception of the Whitefish Lake Group (Figure 300.1a), which has no producers and was judged to be of less significance. Active collection with the aim of determining the position of samples within the paragenetic sequence at a particular mine was undertaken. In addition, material collected in previous studies emanating from Lakehead University was used, as well as some material borrowed from the Thunder Bay District office of the Ontario Geological Survey, and the Royal Ontario Museum.

The paragenetic sequence of mineralization is highly significant for the interpretation of the results of fluid inclusion heating/freezing studies. The paragenetic sequences for the studied mines are described in detail by Jennings (1987), but can be roughly summarized by reference to Figure 300.3. The Mainland Belt veins, exemplified in Figures 300.3b, c, and d are characterized by early deposition of quartz, calcite, and green fluorite followed by a period of fracturing. Later quartz, calcite, and purple fluorite are then superceded by sulphide mineralization and native silver. The period of fracturing is not evident, however, in the Port Arthur Group of the Mainland Belt nor in the Island Belt deposits. Barite is generally absent in the Mainland Belt deposits; however, exceptions occur in the Port Arthur Group, Silver Mountain and one of the veins of the Porcupine Mine.

The paragenetic sequence in the Island Belt differs from that of the Mainland Belt in that assemblages vary from simple base metal sulphide+barite+minor silver to fully developed five-element assemblages at Silver Islet. The sequence at Spar Island (Figure 300.3a) is given here, as the vein is well exposed, and the most complete and reliable interpretation of its paragenesis is possible. Two periods of sulphide and silver deposition are noted, in conjunction with three phases of barite deposition, giving rise to a symmetrically zoned vein. In addition to the minerals noted in Figure 300.3a, Jennings (1987) noted the occurrence of minor safflorite late in the paragenesis, establishing links to the five-element type deposit.

FLUID INCLUSION STUDIES

Fluid inclusion freezing studies were carried out prior to heating studies in order to avoid stretching of the inclusions. The data show equivalent weight percent NaCl in solution ranging from 30.3 to 2.1. The very low salinities of some inclusions suggest that meteoric water has, to some extent, mixed with saline brines, yielding the observed range of salinities. Salinities appear to vary considerably in all deposits, although data are inadequate in some cases.

The fluid inclusion heating data are more extensive and show great variability. Inclusions homogenizing to both liquid and vapour in the same specimen occur sporadically, indicating that the fluid phase was not boiling continuously throughout ore deposition. This observation, combined with the absence of evidence of boiling in several deposits, suggests that veins were sporadically, at best, subjected to hydrostatic rather than lithostatic pressures.

The inclusions yield wide ranges of homogenization temperatures within individual deposits and even within single hand specimens. Clearly, position within the paragenetic sequence is of utmost importance in interpreting data of this sort, and detailed consideration of this factor has been made by Jennings (1987). However, for purposes of summarizing the results, it is useful to consider separately the temperatures obtained from inclusions in calcite, quartz, fluorite, and sphalerite.

Figure 300.4 illustrates fluid inclusion homogenization and decrepitation temperatures from calcite from all deposits. A peak at 100°C and small peaks at 300° and 400°C are present with considerable scatter at higher temperatures. Homogenization to vapour, indicating boiling, occurs at high and low temperatures, suggesting opening and closing of veins to the surface during precipitation of vein minerals.

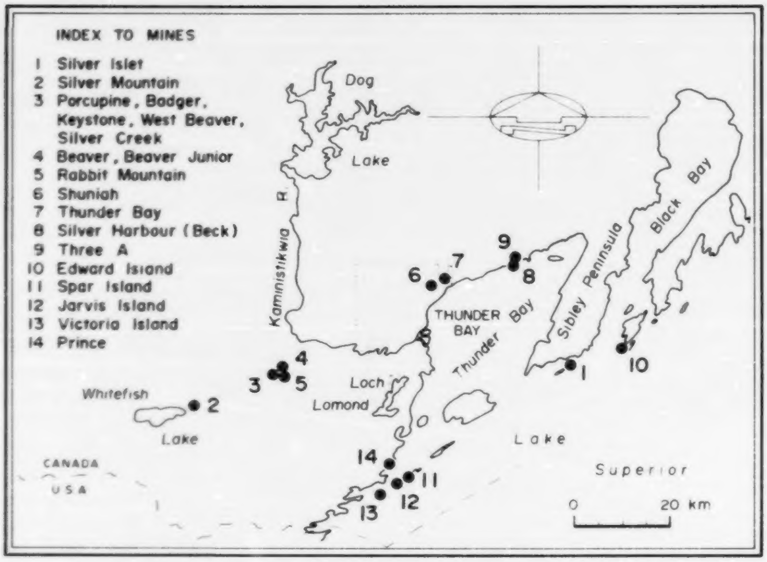

Figure 300.2. *Mines selected for study of fluid inclusions and sulphur isotopes.*

The heating data from quartz and fluorite are illustrated in Figure 300.5. Peaks occur at 100°, 250°, and 350°C in quartz and at the similar temperatures of 125°, 325°, and 425°C in fluorite. Only in sphalerite (Figure 300.6) is the distribution of homogenization temperatures rather tight with all within the range 80° to 120°C.

The detailed consideration of the position of the fluid inclusion-containing sample in its paragenetic sequence reveals a distinctive pattern in all of the Mainland Belt deposits except for the Port Arthur Group. This pattern, illustrated schematically in Figure 300.7. Early calcite, quartz, and green fluorite, accompanied by minor base-metal sulphides at most, were followed by a marked decline in temperature. A fracturing episode was healed in a renewed episode of high-temperature deposition of calcite, quartz, and green and purple fluorite accompanied by base-metal sulphides and argentite/native silver as the temperature decreased. The late, vug-filling phase is also accompanied by precipitation of base-metal sulphides and argentite. Sphalerite, thus, was generally precipitated at low temperature phases of the paragenetic history.

The paragenetic sequence in relation to temperature at Spar Island is shown in Figure 300.8. Ore deposition occurred both early and late in the sequence, both periods occurring at relatively low temperatures. No distinct fracturing event is evident, and sulphide mineralization was also deposited in the final vug-filling phases. This schematic sequence applies generally to all of the deposits of the Island Belt and the Port Arthur Group of the Mainland Belt.

No trend is apparent in paired freezing point depression versus homogenization temperature data. In various examples in the literature, linear trends are used as evidence of mixing (for example, a cool, low-salinity fluid mixing with a hot, high-salinity fluid). However, such a linear trend would emerge only in the case of a simple, single-stage mixing process. As noted previously, the wide range of salinities determined is strongly suggestive of mixing of fluids, but the process must have been considerably more complex than single-stage mixing of two fluids.

SULPHUR ISOTOPIC STUDIES

Sulphide minerals and barite were analyzed for sulphur isotopic content in order to determine such things as the source of sulphur in vein sulphide mineralization, the stage in isotopic equilibrium of the sulphide mineralization, and, if possible, the temperature of precipitation of sulphide minerals by means of isotopic partitioning. Sphalerite proved to be the most widespread and abundant sulphide mineral, and it was sought as the primary mineral for analysis. In mine cases, galena was in close contact with sphalerite and was also analyzed, potentially yielding information on isotopic partitioning. In two cases galena-pyrite pairs were analyzed.

The results of these analyses (Table 300.1) yield a fairly tight clustering of sulphur isotopic compositions. Barite from the Island Belt has $\delta^{34}S$ between +8.3 and +6.5‰, with similar values from Silver Mountain and Silver Harbour. Sample SM30, however, has $\delta^{34}S = +30.9$‰, but inspection of the sample revealed signs of supergene dissolution of calcite. Such supergene processes seem also to have affected the isotopic composition of the barite.

Sulphur isotopic-composition of galena from the Island Belt is tightly grouped between +3.6 and +4.1‰. Sphalerite is slightly more variable with $\delta^{34}S$ ranging from +4.2 to +10.9‰. Sphalerite sample SI-05 yielded a much more positive $\delta^{34}S$; however, examination of a polished surface revealed the presence of secondary marcasite in the sphalerite. Again, supergene processes seem to have affected the specimen.

Sulphur isotopic compositions within the Mainland Belt are much more variable, particularly at Rabbit Mountain. The observed range of -1.2 to +9.9‰ in sphalerite includes all other values for

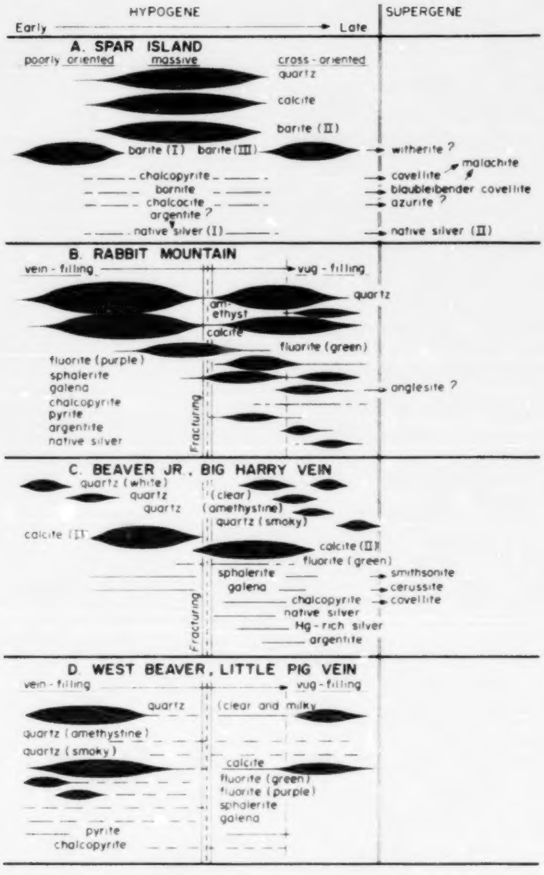

Figure 300.3. *Paragenetic sequences at representative mines in the Mainland and Island Belts. Diagrams are modified after the following: Spar Island (Smyk 1984); Rabbit Mountain Mines (Mosely 1977); Big Harry Vein, Beaver Jr. Mine (Cole 1978); Little Pig Vein, West Beaver Mines (Manunula 1979).*

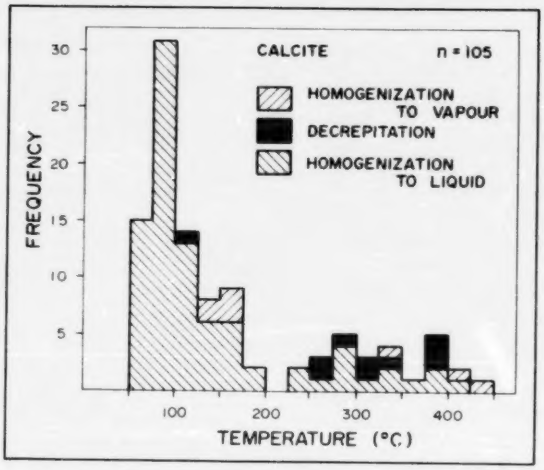

Figure 300.4. *Fluid inclusion homogenization and decrepitation temperatures in calcite from all mines.*

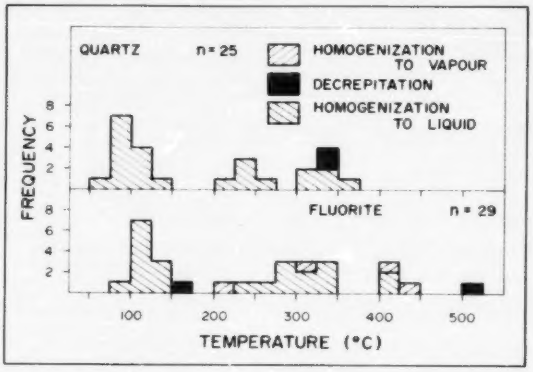

Figure 300.5. *Fluid inclusion homogenization and decrepitation temperatures in quartz and fluorite from all mines.*

Mainland Belt deposits. Galenas vary from -9.3‰ at Rabbit Mountain to +3.6‰ at the Keystone Mine. Two analyses of pyrite give +4.3‰ at Silver Mountain and +0.7‰ at the Shuniah Mine.

The wide variation in sulphur isotopic composition in a single mineral, even from a single mine, suggests a lack of isotopic equilibrium among the various mineral phases. Use of a formulae given by Ohmoto and Rye (1979) permits the calculation of temperatures based on partitioning of $\delta^{34}S$ in the pairs sphalerite-galena and pyrite-galena. Although the sphalerite-galena pairs EA6, TB3, SM600, SI4, and M9170 yield temperatures compatible with fluid inclusion data in the range of 50° to 200°C, the lack of equilibrium in each of these deposits prevents the drawing of much significance for these results.

Pinckney and Rafter (1972) showed that a plot of $\ln\alpha \equiv \Delta$(sphalerite-galena) versus the $\delta^{34}S$ of the individual phases, where α is the distribution coefficient and Δ is the difference in $\delta^{34}S$, will give an indication of the isotopic composition of the sulphur source, provided that the pairs are in isotopic equilibrium and that the system is closed with respect to sulphur. That the five pairs listed above yielded reasonable temperatures can be taken as evidence that these pairs, at least, are in equilibrium. Although they come from five different mines, they may be products of a single source of sulphur (that is, a closed system). The plot of $\delta^{34}S$ versus Δ in Figure 300.9 implies a sulphur source composition of $\delta^{34}S = +4.7$‰.

The implied source composition is close to values typically obtained for magmatic sulphur, rather than the sedimentary sulphide mineralization of the Aphebian black shales of the Rove Formation, as had been anticipated. Unpublished data from 15 samples from four localities give a mean $\delta^{34}S = +17.7 \pm 4.4$‰ ranging from +12.1 to +25.3‰ (E.N. Cameron, Research Officer, Geological Survey of Canada, Ottawa, personal communication, 1986), all distinctly heavier

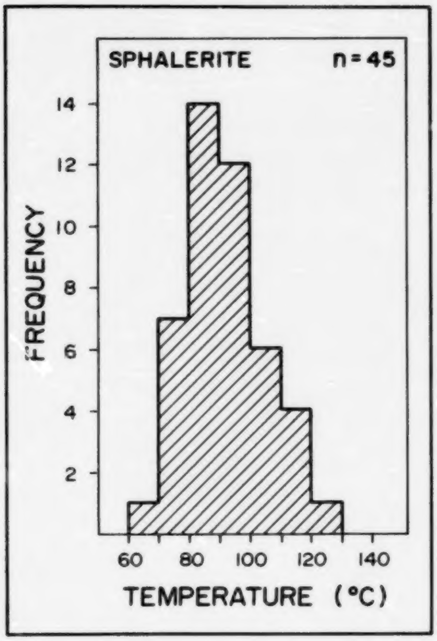

Figure 300.6. *Fluid inclusion homogenization temperatures in sphalerite.*

than any of the vein sulphide mineralization. Two pyrite samples from the Rove Formation near Gunflint Lake in Cook County, Minnesota, analyzed in this study, have $\delta^{34}S = +15.8$ and $+15.2$‰. The Gunflint Formation also contains sulphide mineralization, which, in the Kakabeka Falls area, yields a mean $\delta^{34}S = +3.5 \pm 1.3$‰ (s.d., n=22) according to Cameron (1983). R.J. Shegelski (Geologist, Esso Minerals Canada, Timmins, personal communication, 1986) found a mean $\delta^{34}S = +8.9 \pm 2.1$‰ for 26 samples from various localities, which ranged from -4.1 to +15.7‰.

The source value of +4.7‰ is therefore within the range of values for sedimentary sulphide mineralization in the Gunflint Formation. However, all of the deposits, with the exception of those in the Port Arthur Group, are remote from Gunflint rocks. The source sulphur is possibly of magmatic origin although some fractionation is required in order to obtain most of the values present in the silver veins. Episodes of boiling would liberate SO_2, which preferentially fractionates ^{32}S. The residual fluid would

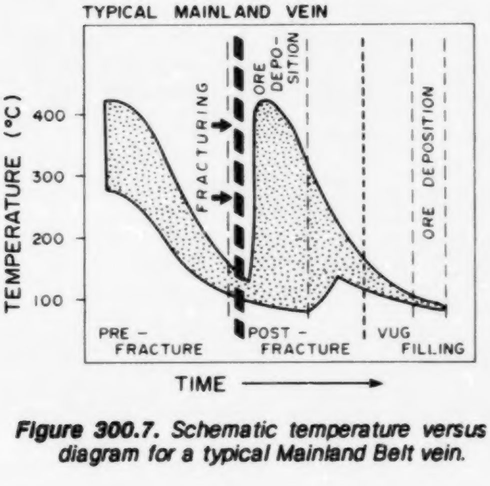

Figure 300.7. *Schematic temperature versus time diagram for a typical Mainland Belt vein.*

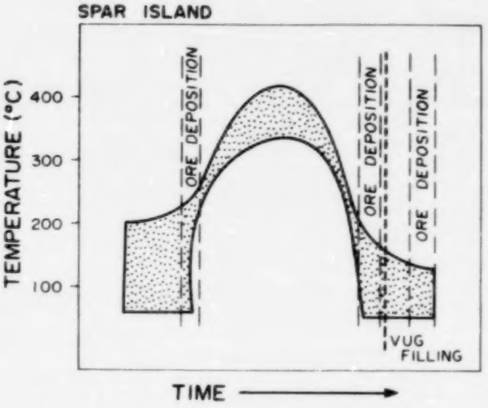

Figure 300.8. *Schematic temperature versus time diagram Aor the Spar Island vein.*

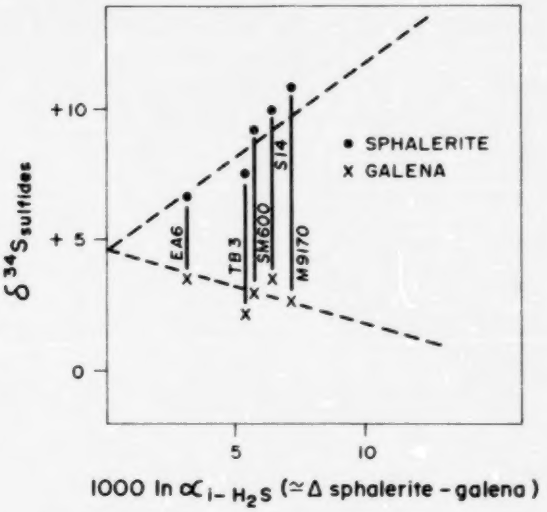

Figure 300.9. *Plot of sulphur isotopic composition of sphalerite-galena pairs versus $\ln\alpha$ – Δ(sphalerite-galena) for five selected samples.*

TABLE 300.1. SULPHUR ISOTOPIC ANALYSES.

Sample	Location	δ^{34}S Mineral			
		Sphalerite	Galena	Pyrite	Barite
EA 15	Victoria Island				+ 8.3
EA 32	Jarvis Island				+ 7.7
EA 39	Spar Island				+ 8.3
EA 41	Spar Island				+ 6.5
SI 4	Silver Islet	+10.0	+3.6		
SI 5	Silver Islet	+25.6			
SI 7	Silver Islet	+ 4.2	+4.1		
SI 17	Silver Islet	+ 9.8			
SI A	Silver Islet	+ 9.7	duplicate		
SI A	Silver Islet	+ 9.9			
M 9170	Edward Island	+10.9	+3.8		
BLC 1	Big Harry	+ 4.7			
BLC 3	Big Harry	+ 6.3			
BLC 5	Big Harry	+ 7.1			
BLC 7	Big Harry	+ 6.3			
RM 1	Rabbit Mountain	- 1.2			
RM 3	Rabbit Mountain	+ 3.5	-9.3		
RM 6	Rabbit Mountain	+ 9.9			
RM 8	Rabbit Mountain	+ 9.3			
SM 30	Silver Mountain				+30.9
SM 51	Silver Mountain	+ 6.4			
SM501	Silver Mountain				+ 7.0
SM514	Silver Mountain				+ 8.7
SM600	Silver Mountain	+ 9.2	+3.0	+4.3	
EA 1	Keystone	+ 5.7			
EA 6	Keystone	+ 6.8	+3.6		
EA 50	Keystone	+ 6.7			
EA 52	West Beaver	+12.2	-0.4		
EA 56	Keystone	+ 3.5			
EA 61	Porcupine	+ 6.7			
EA 95	Silver Harbour	+ 3.4			
EA 98	Silver Harbour		-0.7		+ 6.6
EA101	3A	+ 2.2			
SH 11	Shuniah		-1.7	+0.7	
TB 3	Thunder Bay	+ 7.6	+2.2		

then be enriched in ^{34}S, possibly giving rise to the heavier sulphur isotopic values observed.

The composition of the source sulphur is open to some question, particularly as to whether the system was actually closed to sulphur. Analysis of additional sphalerite-galena pairs from the same mines should help to resolve questions of isotopic equilibrium and sulphur source.

A portion of the mineralogical study undertaken was the analysis of sphalerite from the various deposits (Table 300.2). The iron-content of sphalerite will permit the calculation of activity of sulphur when combined with independent information from fluid inclusion studies on the temperature of deposition. All sphalerites analyzed have iron-contents ranging from 2.47 to 0.02 weight percent, although most yielded values of less than 1 weight percent. Minor element content is also low, except for Cd, which is fairly high at the Keystone Mine and very high at the native As and Bi deposits of Edward Island. Calculated a_{S2} (activity of S_2) at fluid inclusion homogenization temperatures indicates a range of a_{S2} from 10^{-13} to 10^{21}. Comparison with sulphurization curves given by Barton and Skinner (1979) indicates that ore deposition occurred in a region of a log a_{S2} versus 1/T diagram about the argentite-native silver sulphurization curve and close, as well, to the realgar-native arsenic curve. Thus, the presence of argentite or native silver was controlled by small fluctuations in a_{S2}. The presence of native arsenic at Silver Islet and Edward Island is partly a function of a relatively low a_{S2} in these deposits, but, as realgar is not found elsewhere, a much higher availability of arsenic must also have been a factor.

DISCUSSION

The foregoing results seem to have devastated the original hypothesis of the temperature dependence of the mineral assemblage. The fluid inclusion homogenization results show no systematic differences in temperatures in adequately sampled deposits ranging from barren (for example Little Pig Vein) to simple (for example, Keystone) to five-element type (for example, Silver Islet). All seem to have reached peak temperatures in the 350° to 450°C range. As well, the two thermal peaks separated by a period of fracturing, observed in most of the Mainland Belt deposits,

TABLE 300.2. MICROPROBE ANALYSES OF SPHALERITE COMPOSITION

Sample[2]	Zn	Fe	Cd	Cu	Ag	S	Total	FeS[1]
MAINLAND BELT								
Little Pig Vein								
LP25	66.70	0.33	–	–	–	32.23	99.26	0.57
LP25	66.64	0.44	–	–	–	31.83	98.91	0.77
Big Harry Vein								
BLC4	66.84	0.40	–	–	–	31.62	98.86	0.69
BLC4	67.05	0.26	–	–	–	31.88	99.21	0.46
BLC5	67.94	0.25	0.35	–	–	33.16	101.72	0.43
BLC5	68.15	0.37	–	–	–	32.96	101.48	0.63
BLC5	67.47	0.97	–	–	–	33.17	101.60	1.66
Rabbit Mountain								
RM 1	66.38	0.53	–	–	–	31.95	98.86	0.92
RM 1	67.44	0.18	0.51	–	–	31.84	99.97	0.31
Badger								
BAD1	64.95	0.48	–	–	–	30.41	95.84	0.86
BAD1	66.22	1.12	0.31	–	–	32.01	99.66	1.94
BAD1	67.03	0.34	0.36	–	–	31.88	99.61	0.56
BAD4	63.60	2.09	–	–	–	31.60	97.29	3.70
BAD4	64.57	2.26	–	–	–	32.22	99.05	3.94
EA68	66.51	0.28	–	–	–	32.20	98.99	0.49
EA68	64.69	0.68	–	–	–	32.62	97.99	1.22
West Beaver								
EA52	66.19	0.90	–	–	–	33.30	100.39	1.57
EA52	65.72	0.21	–	–	–	33.38	99.31	0.38
EA52	65.52	0.37	–	–	–	33.38	100.27	0.65
EA52	67.07	0.23	–	–	–	33.63	100.93	0.40
EA52	66.61	0.27	–	–	–	33.90	100.78	0.47
EA53	63.25	0.31	–	–	–	32.10	95.66	0.58
EA53	63.49	0.14	–	–	–	32.31	95.94	0.26
EA53	64.36	0.27	–	–	–	32.18	96.81	0.49
EA53	65.55	0.60	0.25	–	–	32.65	99.05	1.05
EA53	64.79	1.10	–	–	–	32.60	98.49	1.95

[1] mol % FeS in sphalerite

[2] detectability limits - Fe:0.01 wt.%; Cd:0.02 wt.%; Ag:0.03 wt.%; Cu:0.02 wt.%; Mn:0.01 wt.%.

TABLE 300.2. (cont'd.)

Sample	Zn	Fe	Cd	Cu	Ag	S	Total	FeS[1]
Silver Creek								
EA10	65.79	0.34	–	–	–	32.37	98.50	0.60
EA10	65.60	0.27	–	–	–	32.49	98.36	0.48
Porcupine								
EA67	63.73	2.16	–	–	–	32.04	97.93	3.82
EA67	65.12	1.57	–	–	–	32.71	99.40	2.74
Keystone								
EA 1	63.00	0.39	–	–	–	32.74	96.13	0.72
EA 1	66.62	0.42	–	–	–	33.48	100.52	0.73
EA 1	66.32	0.39	–	–	–	33.66	100.37	0.65
EA 1	66.31	0.28	–	–	–	33.78	100.37	0.49
EA 1	66.78	0.22	–	–	–	33.59	100.59	0.38
EA 1	65.27	0.32	0.59	–	–	31.55	97.73	0.56
EA 1	66.77	0.37	–	–	–	32.44	99.58	0.64
EA 2	64.35	0.32	–	–	–	31.81	96.48	0.58
EA 2	63.82	0.23	–	–	–	31.13	95.18	0.42
EA 2	67.68	0.25	–	–	–	31.86	99.79	0.43
EA 6	65.75	0.47	–	–	–	32.44	98.67	0.83
EA 6	65.33	0.59	–	–	–	32.50	98.42	1.04
EA 6	65.55	0.12	0.33	–	–	31.60	97.60	0.21
EA 6	64.28	0.35	–	–	–	31.75	96.38	0.64
EA56	65.64	0.13	1.50	–	–	32.37	99.64	0.23
EA56	66.76	0.13	0.79	–	–	32.70	100.38	0.22
EA56	67.14	0.24	0.62	–	–	28.15	96.15	0.41
EA57	67.03	0.28	–	–	–	32.31	99.62	0.48
EA57	66.63	–	0.34	–	–	32.39	99.36	0.00
EA57	67.94	0.19	–	–	–	28.09	96.22	0.33
Silver Mountain								
SM51	65.95	0.13	0.32	–	–	32.19	98.59	0.21
SM51	67.06	0.26	–	–	–	32.20	99.52	0.46
SM51	66.79	0.40	–	–	–	32.22	99.41	0.70
ISLAND BELT								
Silver Islet								
SI17	66.21	0.47	–	–	–	32.82	99.50	0.82
SI17	64.03	2.33	–	–	–	32.98	99.34	4.08
SI17	65.57	0.45	–	–	–	32.95	98.97	0.78
SI17	64.90	0.39	–	–	–	33.01	98.30	0.70
SI17B	64.36	1.77	–	–	–	31.94	98.07	3.12
SI-B	64.81	0.36	–	–	–	31.87	97.04	0.64

TABLE 300.2. (cont'd.)

Sample	Zn	Fe	Cd	Cu	Ag	S	Total	FeS[1]
Silver Islet (cont'd.)								
SI-B	63.81	0.52	–	–	–	32.45	96.78	0.94
SI-A	66.52	0.48	–	–	–	33.07	100.07	0.83
SI-A	63.44	0.86	–	–	–	32.27	96.57	1.56
SI-A	64.84	0.41	–	–	–	31.97	97.22	0.73
SI-A	66.03	0.73	–	–	–	33.37	100.13	1.26
SI-A	66.67	1.18	–	–	–	31.35	99.20	1.88
SI-A	63.90	0.33	–	–	–	31.94	96.17	0.60
SI-A	61.38	1.65	–	–	–	31.74	94.77	3.05
SI19	60.63	1.99	–	0.36	–	31.99	94.97	3.68
SI19	63.90	1.76	–	0.42	–	32.43	98.51	3.10
SI22	64.75	0.27	–	–	–	31.93	96.95	0.48
SI22	65.80	–	–	–	–	32.08	97.88	0.00
SI22	66.56	0.29	–	–	–	32.52	99.37	0.51
M12460	66.93	1.82	–	–	–	32.37	101.51	3.09
M12460	64.61	1.85	–	–	–	31.91	98.37	3.24
M12460	65.55	2.47	–	–	–	33.10	101.12	4.22
Prince Location								
PR10	66.45	0.33	–	–	–	32.19	98.97	0.58
PR10	66.43	0.29	–	–	0.33	31.99	99.04	0.51
PR10	67.04	0.50	–	–	–	32.56	100.10	0.87
PR 2	63.58	1.17	–	–	–	31.80	96.55	2.10
PR 2	65.48	0.63	–	–	–	31.82	97.93	1.15
PR 3	64.14	0.22	–	–	–	31.30	95.66	0.40
PR 3	65.82	1.43	–	–	–	32.20	99.45	2.48
Edward Island								
9170A3	62.03	–	2.09	–	–	31.92	96.04	0.00
9170A3	65.91	0.38	0.87	–	–	32.32	99.49	0.66
9170A3	65.66	–	3.44	–	–	32.19	101.29	0.00
9170A3	64.03	–	4.37	–	–	32.12	100.52	0.00
9170B	67.42	0.16	0.52	–	–	32.81	100.91	0.26
9170B	66.98	0.18	0.56	–	–	32.74	100.46	0.31
9170B	66.73	0.30	0.73	–	–	32.97	100.73	0.52

seem to preclude a cooling, single-stage heat source (that is, dikes or sills, as the mobilizer for hydrothermal solutions).

The sulphur isotopic data gathered to date suggest a rather more complex source of sulphur in the deposits than the Rove Shales alone. While more data are required, the lead isotopic data from Franklin *et al.* (1986) also suggest that local influences have modified leads derived from diverse sources.

Both of the above considerations imply that the ore-depositing solutions were derived from a much greater area than that immediately adjacent to Keweenawan intrusions. However, the Keweenawan intrusions clearly have played some role in localizing deposition of the ore. G.C. Patterson (Resident Geologist, Ministry of Northern Development and Mines, Thunder Bay, personal communication, 1986) has commented on the association of graphitic carbon with the ores and suggested that nucleation of minerals, particularly native silver, is related to "activation" of carbon in the contact aureoles of the intrusions. Similarly, carbon dispersed in sedimentary rocks could be recrystallized into a more chemically active form by the heat of the intrusions. The carbon may then have served as a reductant at the site of deposition.

The ore-bearing solution is still without an obvious source in the above scenarios. The high temperatures determined require heating well beyond that generated in a sedimentary basin under normal conditions. A conjecture at this point is that heating may be associated with high heat-flow associated with the Keweenawan rifting event. The ore-bearing solutions could then have circulated in the basement as well as the Proterozoic basin, deriving their compositions from diverse source rocks, but with important contributions from shaley sedimentary rocks.

CONCLUSIONS AND FUTURE OBJECTIVES

The results of the present year's work have led to the following conclusions:

1. The spectrum of deposit types in the Thunder Bay area is unrelated to differences in tempera-

ture at the site of deposition. Two thermal peaks in the Mainland Belt deposits, separated by a period of fracturing, indicate that a single cooling heat source could not be the heat engine driving circulation of hydrothermal solutions.

2. Sulphur isotopic data from various deposits and within single deposits show a considerable range. The source of the sulphur does not appear to correspond to sedimentary sulphide mineralization in the Rove shales, but to a more complex source.
3. Salinities of fluid inclusions show great variation, suggesting the mixing of meteoric and connate water, perhaps with limited effects due to boiling of the ore-depositing solutions.

FUTURE OBJECTIVES

Further work on the origin of sulphur in the veins seems to be of value. To this end, additional data, particularly for sphalerite-galena pairs, will be sought. As well, studies of carbon and oxygen isotopes in calcite and quartz will further help to characterize the origin of the solutions.

Knowledge of behaviour of the vein systems as a function of depth is also necessary in order to further constrain genetic mechanisms. Drill core from the Shuniah and Porcupine Mines has been obtained for this purpose, and samples from various levels of the Rabbit Mountain Mine has also been collected.

Finally, the Deadhorse Creek Veins (Patterson *et al.* 1984, 1985; Franklin *et al.* 1986), located much farther to the east, are believed to be related to the Thunder Bay veins. New discoveries in the Terrace Bay area (B.R. Schnieders, Staff Geologist, Ministry of Northern Development and Mines, Thunder Bay, personal communication, 1986) may also be of this type. With recent dramatic improvement in silver prices, study of this area may yield practical as well as scientific benefits.

ACKNOWLEDGMENTS

The following people at Lakehead University, Thunder Bay, provided invaluable assistance in various areas: R.L. Bennett and D. Crothers, polished section preparation; S.T. Spivak, drafting; and W.C. Bons, typing. Fluid inclusion studies were carried out at Queen's University, Kingston, through the courtesy of A.H. Clark and with the assistance of A.J. Anderson. Microprobe analyses were conducted at the University of Toronto with the assistance of C.M. Cermignani. G.C. Patterson (Resident Geologist, Ministry of Northern Development and Mines, Thunder Bay), and F.J. Wicks (Royal Ontario Museum) made valuable specimen material available.

REFERENCES

Barton, P.B., Jr., and Skinner, B.J.
1979: Sulfide Mineral Stabilities; p.236-333 *in* Geochemistry of Hydrothermal Ore Deposits, 2nd edition, edited by H.L. Barnes, John Wiley and Sons, Toronto, 798p.

Bowen, N.L.
1911: Silver in the Thunder Bay District; Ontario Bureau of Mines, Annual Report for 1911, Volume 20, Part 1, p.119-132. Accompanied by Map 20a, scale 1:63 360 or 1 inch to 1 mile.

Boyle, R.W., and Dass, A.S.
1971: Origin of the Native Silver Veins at Cobalt, Ontario; p.414-417 *in* The Silver-Arsenide Deposits of the Cobalt-Gowganda Region, Ontario, edited by W. Petruk and J.L. Jambor, Canadian Mineralogist, Volume 11, Part 1.

Cameron, E.M.
1983: Genesis of Proterozoic Iron-Formation: Sulphur Isotope Evidence; Geochimica et Cosmochimica Acta, Volume 47, p.1069-1074.

Cole, B.L.
1978: Geology and Mineralogy of the Beaver Junior Mines, Mainland Belt Silver Region, Thunder Bay District; Unpublished H.B.Sc. Thesis, Lakehead University, 54p.

Franklin, J.M.
1970: Metallogeny of the Proterozoic Rocks of the Thunder Bay District, Ontario; Unpublished Ph.D. Thesis, University of Western Ontario, 191p.

Franklin, J.M., and Mitchell, R.H.
1977: Lead-Zinc-Barite Veins of the Dorion Area, Thunder Bay District, Ontario; Canadian Journal of Earth Sciences, Volume 14, p.1963- 1979.

Franklin, J.M., Scott, S.D., Kissin, S.A., and Smyk, M.C.
1986: Silver Deposits Associated with the Proterozoic Rocks of the Thunder Bay District, Ontario; Canadian Journal of Earth Sciences, Volume 23, p.1576- 1591.

Geul, J.C.C.
1970: Geology of Devon and Pardee Townships and the Stuart Location, District of Thunder Bay; Ontario Department of Mines, Geological Report 87, 52p. Accompanied by Map 2207, scale 1:31 680 or 1 inch to 1/2 mile.
1973: Geology of Crooks Township, Jarvis and Prince Locations, and Offshore Islands, District of Thunder Bay; Ontario Division of Mines, Geological Report 102, 46p. Accompanied by Map 2250, scale 1:31 680 or 1 inch to 1/2 mile.

Guillet, G.R.
1963: Barite in Ontario; Ontario Department of Mines, Industrial Minerals Report 10, 42p.

Halls, C., and Stumpfl, E.F.
1972: The Five Element (Ag-Bi-Co-Ni-As) Vein Deposits—A Critical Appraisal of the Geological Environments in Which They Occur and of the Theories Affecting their Origin (Abstract); p.540 *in* Twenty-Fourth Session, International Geological Conference Proceedings, Section 4, 553p.

Ingall, E.D.
1888: Report of Mines and Mining on Lake Superior; Geological and Natural History Survey of Canada, Annual Report for 1887-88, New Series, Volume 3, Part H, p.1- 131.

Jennings, E.A.
1987: A Survey of the Mainland and Island Belts, Thunder Bay Silver District, Ontario: Fluid Inclusions, Mineralogy and Sulfur Isotopes; Unpublished M.Sc. Thesis, Lakehead University, 159p.

Manunula, T.L.
1979: Geology and Mineralogy of the Little Pig Vein, Mainland Belt Silver Region, Thunder Bay District; Unpublished H.B.Sc. Thesis, Lakehead University, 48p.

Mosley, E.B.
1977: Geology and Mineralogy of the Rabbit Mountain Mine, Mainland Belt Silver Region, Thunder Bay District; Unpublished H.B.Sc. Thesis, Lakehead University, 94p.

Ohmoto, H., and Rye, R.O.
1979: Isotopes of Sulfur and Carbon; p.509-567 *in* Geochemistry of Hydrothermal Ore Deposits, 2nd edition, edited by H.L. Barnes, John Wiley and Sons, Toronto, 798p.

Oja, R.V.
1967: Geochemical Investigations of the Lake Superior Silver Area; p.211-221 *in* Proceedings, Symposium on Geochemical Prospecting, edited by E.M. Cameron, Geological Survey of Canada Paper 66- 54, 282p.

Owsiacki, L.
1984: Geology and Silver Deposits of the Cobalt Area; p.1-75 *in* Geology, Silver, and Gold Deposits, Cobalt and Kirkland Lake, Field Trip 4, Geological Association of Canada Field Trip Guidebook, 1984, edited by L. Owsiacki and H. Lovell, 114p.

Patterson, G.C., Mason, J.K., and Schnieders, B.R.
1984: Report of Activities 1983, Thunder Bay Resident Geologist Area, North Central Region; p.47-106 *in* Report of Activities 1983, Regional and Resident Geologists, edited by C.R. Kustra, Ontario Geological Survey, Miscellaneous Paper 117, 275p.

1985: Thunder Bay Resident Geologist Area, North Central Region; p.56-133 *in* Report of Activities 1984, Regional and Resident Geologists, edited by C.R. Kustra, Ontario Geological Survey, Miscellaneous Paper 122, 297p.

Pinckney, P.M., and Rafter, T.A.
1972: Fractionation of Sulfur Isotopes During Ore Deposition in the Upper Mississippi Valley Zinc-Lead District; Economic Geology, Volume 67, p.315- 328.

Sergiades, A.O.
1968: Silver Cobalt Calcite Vein Deposits of Ontario; Ontario Department of Mines, Mineral Resources Circular 10, 498p.

Smyk, M.C.
1984: A Comparative Study of Silver Occurrences, Island Belt Silver Region, Thunder Bay District, Ontario; Unpublished H.B.Sc. Thesis, Lakehead University, 132p.

Stanton, R.L., and Russell, R.D.
1959: Anomalous Leads and the Emplacement of Lead Sulfide Ores; Economic Geology, Volume 54, p.588- 607.

Statham, P.J.
1976: A Comparative Study of Techniques for Quantitative Analysis of the X-Ray Spectra Obtained with a Si(Li) Detector; X-Ray Spectrometry, Volume 5, p.16-28.

Susak, N.J., and Crerar, D.A.
1985: Spectra and Coordination Changes of Transition Metals in Hydrothermal Solutions: Implications for Ore Genesis; Geochimica et Cosmochimica Acta, Volume 49, p.555- 564.

Tanton, T.L.
1931: Fort William and Port Arthur, and Thunder Cap Map-areas, Thunder Bay District, Ontario; Geological Survey of Canada, Memoir 167, 222p.